TECTONOSTRATIGRAPHIC EVOLUTION OF THE SWARTLAND REGION AND ASPECTS OF OROGENIC LODE-GOLD MINERALISATION IN THE PAN-AFRICAN SALDANIA BELT, WESTERN CAPE, SOUTH AFRICA.

Richard William Belcher

Dissertation presented for the Degree of Doctor of Philosophy at the University of Stellenbosch.

Promoters: A. Rozendaal

A.F.M. Kisters

December 2003

DECLARATION

I, the undersigned, hereby declare that the work contained in this dissertation is my own original work and that I have not previously in its entirety or in part submitted it at any university for a degree.

Signature: (12th November, 2003)

ABSTRACT

The Swartland region in the western Cape, South Africa, covers approximately 5000 km^2 and forms part of the Pan-African Saldania Belt that represents the southernmost extremity of the Pan-African orogenic belts in southern Africa. Regional mapping of the Swartland area shows that lithologies can be classified using predominantly structural and to a lesser extent lithological criteria. This led to the proposal of a new classification, were rocks of the previous classification of the Malmesbury Group are divided into two new groups, namely the Swartland and Malmesbury groups.

The Swartland group can be divided into the Berg River and Moorreesburg formations, a series of quartz-chlorite-muscovite-feldspar schists, quartz schists, graphitic schists and limestones; and the Bridgetown formation, a series of metavolcanic rocks with WPB-MORB affinities that possibly represent seafloor. Deposition of the sediments is suggested to have occurred concurrently with deformation in an accretionary prism/fore-arc and was initiated with the opening of the Iapetus Ocean at ca. 600 Ma. This early deformation event, D_1 (ca. 575 Ma), only affected the Swartland group and exhibits pervasive bedding transposition, thrusting and imbrication of units creating a tectonostratigraphic sequence. Where identified, kinematic indicators and fold vergence indicate a top-to-the-west transport direction during the early, low-angle D_1 deformation.

The Malmesbury group overlies the Swartland group, being locally separated by an unconformity. The Malmesbury group is a succession of conglomerates, grits and shales (Piketberg Formation), grading into greywackes, shales, siltstones, sandstones and minor limestones of the Tygerberg and Porterville formations. Sedimentation probably commenced after ca. 575 Ma and lasted until shortly after 560 Ma. Both the Swartland and Malmesbury groups were then deformed by the

deformation event, D_2 (ca. 552-545 Ma), and were intruded by the 552 to 510 Ma Cape Granite Suite. The Franschhoek Formation, formally part of the Malmesbury Group is now classified, along with the inferred ca. 535-510 Ma Magrug and Populierbos Formations of the previous Klipheuwel Group. The redefined Klipheuwel group documents a change in depositional environment from the continental slope/ocean trench, marine and flyschoid deposits of the Malmesbury group to continental, fluvial half-graben and graben deposits. Exhumation, extensive erosion and the formation of a peneplain, was followed by the deposition of the Table Mountain Sandstone Group around 550-510 Ma.

The Spitskop gold prospect, located 10 km south of Piketberg, represents the first identified occurrence of mesothermal gold mineralisation in the Saldania Belt. Metamorphic devolatilisation of the Swartland group during D_1 led to the scavenging and transportation of gold along shallow-dipping shear zones that are contained within the early, sub-horizontal S_0/S_1 tectonic fabric. Pervasive fluid movement in the Spitskop area led to elevated gold values compared to background values throughout the lithologies at Spitskop. The lack of any economic-grade gold mineralisation is probably related to the absence of suitably orientated structures, such as high-angle faults, that are commonly believed to represent the prerequisite for large fluid throughputs that could result in economic-grade gold deposits. The mineralisation at Spitskop, however, provides a genetic model for further exploration of gold in the Swartland group.

SAMEVATTING

Die Swartland streek in die Wes-Kaap, Suid-Afrika, beslaan ongeveer 5000 km^2 en vorm deel van die Pan-Afrikaanse Saldania-gordel wat die mees suidelike deel van die Pan-Afrikaanse orogene gordels in suidelike Afrika verteenwoordig. Regionale kartering van die Swartland streek dui aan dat die gesteentes geklassifiseer kan word deur oorwegend strukturele, en tot 'n mindere mate litologiese kriteria te gebruik. Gevolglik word 'n nuwe klassifikasie voorgestel, waar gesteentes volgens die vorige klassifikasie van die Malmesbury groep verdeel word in twee groepe, naamlik die Swartland en Malmesbury groepe.

Die Swartland groep kan verdeel word in die Bergrivier en Moorreesburg formasies, 'n reeks kwarts-chloriet-muskoviet-veldspaat skis, kwarts skis, grafitiese skis en kalksteen; en die Bridgetown formasie, 'n reeks metavulkaniese gesteentes met WPB-MORB affiniteite wat moontlik oseaanvloer verteenwoordig. Daar word voorgestel dat afsetting van die sedimente gelyktydig plaasgevind het saam met vervorming in 'n akkresionêre prisma/voorboog, geïnisieer deur die opening van die Iapetus Oseaan (ca. 600 Ma). Hierdie vroeë vervorming, D_1 (ca. 575 Ma), het slegs die Swartland groep geaffekteer en vertoon deurdringende verplasing van gelaagdheid, oorskuiwing en imbrikasie van eenhede en het 'n tektonostratigrafiese opeenvolging gevorm. Waar identifiseer, dui kinematiese aanwysers en plooi kanteling op 'n bokant-na-wes beweging gedurende die vroeë, lae hoek D_1 vervorming.

Die Malmesbury groep oordek die Swartland groep, plaaslik geskei deur 'n diskordansie. The Malmesbury groep bestaan uit 'n opeenvolging konglomeraat, grintsteen en skalie (Piketberg formasie), wat gradeer in grouwak, skalie, sliksteen, sandsteen en ondergeskikte kalksteen van die Tygerberg en Porterville formasies. Sedimentasie het waarskynlik begin na ca. 575 Ma en het voortgeduur tot kort na

560 Ma. Beide die Swartland en Malmesbury groepe is hierna vervorm deur D_2, (ca. 552-545 Ma) en daaropvolgend ingedring deur die 552 tot 510 Ma Kaap Graniet Suite. Die Franschhoek Formasie, voorheen deel van die Malmesbury Groep, word nou geklassifiseer tesame met die afgeleide ca. 535-510 Ma Magrug en Populierbos formasies as deel van die voorheen geklassifiseerde Klipheuwel groep. Die hergedefinieerde Klipheuwel groep dui op 'n verandering in afsettingsomgewing vanaf die kontinentale glooiing/oseaantrog, mariene en flyschoïede afsettings van die Malmesbury groep na kontinentale, fluviale half-graben en graben afsettings. Herblootstelling, omvattende erosie en die vorming van 'n skiervlakte is gevolg deur die afsetting van die Tafelberg Sandsteen Groep rondom 520-510 Ma.

Die Spitskop goudvoorkoms, 10 km suid van Piketberg, verteenwoordig die eerste identifiseerde voorkoms van mesotermale goudmineralisasie in die Saldania Gordel. Metamorfe ontvlugtiging van die Swartland groep gedurende D_1 het aanleiding gegee tot die roofuitruiling en vervoer van goud langs laaghellende skuifskeursones in die vroeë, subhorisontale S_0/S_1 tektoniese maaksel. Deurdringende vloeistofbeweging in die Spitskop omgewing het aanleiding gegee tot verhoogde goudwaardes in vergelyking met agtergrond waardes dwarsdeur die litologieë by Spitskop. Die gebrek aan ekonomiese graad goud mineralisasie is waarskynlik verwant aan die afwesigheid van geskikte georiënteerde strukture, soos hoë hoek verskuiwings, wat oor die algemeen beskou word as 'n voorvereiste vir die toevoer van groot hoeveelhede vloeistof wat kon aanleiding gegee het tot ekonomiese graad goudafsettings. Die mineralisasie by Spitskop verskaf egter 'n model vir verdere goud eksplorasie in die Swartland groep.

ACKNOWLEDGEMENTS

The author wishes to thank the many people who helped during the completion of this thesis, in particular to the following persons.

Prof. A. Rozendaal, for the introduction to the Spitskop project that formed the initial M.Sc. and for acting as promoter for the Ph.D. thesis.

Prof. A.F.M. Kisters for acting as co-promoter for the Ph.D., and for also being a friend and confidant for the last four years. For his guidance with the structural interpretation and controls on gold mineralisation that formed part of the Spitskop project and later for his help with the regional tectonic interpretation as part of the Ph.D. thesis. Furthermore, for always being available to discuss ideas and to go into the field.

Financial support for this project was provided by the Department of Geology, University of Stellenbosch and is gratefully acknowledged.

Mr Langenhoven (PPC Cement, Piketberg) for access to the limestone quarries at Piketberg and Riebeeck West.

Dr. L. Pretorius (Opaline Gold) for access to percussion drilling logs and company progress reports related to the Spitskop Project and for allowing the use and further analyses of the percussion drilling samples.

Dr. M. Roberts and Ms. S. Bramdeo (Rhodes University) for assistance with electron microprobe analyses.

Dr. W. Przybylowicz (iThemba Labs, South Africa) for microPIXE elemental mapping as part of the search for gold during the Spitskop project and the culmination of our efforts with a publication in the *Journal of X-Ray Spectrometry*.

Dr. A. Späth (University of Cape Town) for assistance with electron microprobe analysis and undertaking ICP-MS analysis.

Personnel at the Geology Department, University of Stellenbosch for analyses and sample preparation: Mrs. A. Uttley and Mrs. E. Spicer for XRF and XRD analyses;

Prof. G. Stevens, Mr. N. Steenkamp and Mrs E. Spicer (University of Stellenbsoch) for assistance with the Scanning electron microscope (SEM) analyses;

Mr. D. Hendriks for thin, thick and double polished sections;

Mr. J. Smit for XRF sample preparation;

Mr. S. Kruger for computer assistance and for the Afrikaans translation of the abstract;

Tannie Loxie for all the sweets and chocolates.

My parents and family for their continued support, guidance, and encouragement.

CONTENTS

SYMBOLS AND ABBREVIATIONS

Minerals

ab	albite
act	actinolite
alm	almandine
and	andalusite
als	aluminosilicate
bt	biotite
cc	calcite
chl	chlorite
dol	dolomite
ep	epidote
fspr	feldspar
jd	jadeite
ky	kyanite
kfs	K-feldspar
ms	muscovite
pa	paragonite
pl	plagioclase
qtz	quartz
ser	sericite
sil	sillimanite
tlc	talc

aspy	arsenopyrite
cpy	chalcopyrite
py	pyrite

XPL	crossed polars
PPL	Plane polarised light
T_f	temperature of freezing
T_h	temperature of homogenisation
T_m	temperature of melting

1 INTRODUCTION

1.1 Locality and geographic setting

Low-grade metamorphic sedimentary and subordinate volcanic rocks of the Malmesbury Group underlie much of the western branch of the Pan-African Saldania Belt, outcropping between the towns of Aurora and Porterville in the north and Stellenbosch and Franschhoek in the south (32° 00' S and 33° 45' S and between 18° 30' E and 19° 00' E; Fig. 1.1). Along the west coast the landscape is generally flat with extensive sand cover, to the east gentle rolling hills develop covered by a deeply weathered soil profile.

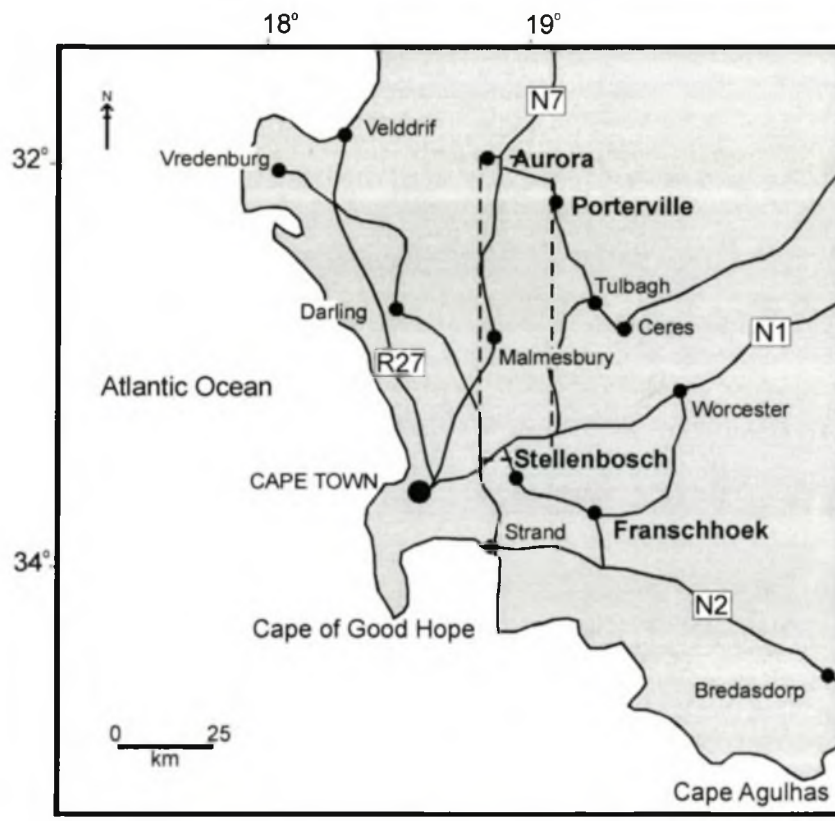

Figure 1.1. Map of the Western Cape highlighting the location of the field area (dashed box) with respect to major towns and national roads.

This area is known as the Swartland and is farmed for wheat on the more moderate slopes with the higher ground being covered with native vegetation known as 'fynbos'. Extensive weathering and farming, together with subdued topography means outcrop within the Malmesbury Group is less than 1%.

1.2 The project

The present study is an extension of an M.Sc. project on the Spitskop gold prospect, situated 10 km south of the town of Piketberg, along the N7 national road, in the Western Cape, RSA. This initial project involved a study of the geology and structure of the Spitskop area, with specific reference to gold mineralisation, in an attempt to understand the localisation of gold.

What became apparent from this early study was that the geology of the Spitskop area was difficult to explain in terms of the available regional geological framework (e.g. Hartnady et al., 1974; SACS, 1980; Theron et al., 1992). This suggested that the present understanding of the Malmesbury Group in terms of its classification and tectonic models was not capable of fully explaining all localities that fall within the present boundaries of the Malmesbury Group. A detailed literature review, highlighted many discrepancies within the current lithostratigraphic classification of the Neoproterozoic Malmesbury Group in the Swartland area where the prospect is situated (Chapter 3). The project was therefore expanded to include the whole of the Swartland, and the emphasis of the project moved away from the economic potential of gold mineralisation to a regional geological and structural mapping survey.

1.3 Present understanding of the Malmesbury Group

Poor exposure of Malmesbury Group rocks has inhibited geological mapping and interpretations. Although geological maps of the Malmesbury Group have been published (1:125 000, 3318 B and 3319A, compiled by Visser et al., 1975; 1:250 000, 3318, compiled by Theron, 1990), the distance between individual outcrops has required much extrapolation and inference. Similarly, the relatively monotonous succession of low-grade metamorphosed schists precludes any correlation over larger distances, despite the fact that such correlations are the basis for the present

classification (e.g. Hartnady et al., 1974; Rabie, 1974a; SACS, 1980; Theron et al., 1992). This has led to many discrepancies within the classification of the Malmesbury Group as discussed in detail in Chapter 3. With little advances in the understanding of the Malmesbury Group over the past three decades, the development of a comprehensive tectonostratigraphic framework and therefore a model for the evolution of the Saldania Belt has been inhibited. The early model presented by Hartnady et al. (1974) and Tankard et al. (1982), described the Malmesbury Group in terms of a geosyncline. Only minor modifications have been made to this model to date (Chapter 2). Correlations of the Malmesbury Group with the southern branch of the Saldania Belt and further north in the Gariep Belt (e.g. Dunlevey, 1992; Rozendaal et al., 1999) are only speculative at best.

1.4 Aims of the study

The aims of the study can be summarised as follows:

i) To describe and record the petrographic, structural, geochemical and metamorphic characteristics of the different lithologies of the Malmesbury Group;

ii) To determine the relationship of the different metavolcanic and metasedimentary rocks occurring within the Malmesbury Group;

iii) To produce a new classification of the Malmesbury Group based on the above findings that is capable of explaining current discrepancies in the existing tectonostratigraphic classification;

iv) To provide new insights into the tectonic evolution of the Saldania Belt;

v) To investigate the occurrence of gold mineralisation at Spitskop.

1.5 Methodology

Over two hundred outcrops were visited during the regional mapping, including the type localities for the formations of the present Malmesbury Group, but excluding the Brandwacht and Norree Formations, which fell outside the field area. The field area covers the present Swartland Terrane, as defined by Hartnady et al. (1974) and measures approximately 100 km by 30 km. At each locality, the lithologies were described and classified following distinct lithological, structural and metamorphic

criteria, as outlined in Chapters 4, 5 and 7. At well-exposed outcrops, e.g. road cuts and quarries, detailed mapping was undertaken, and these localities were then used in many instances as type localities for a new classification (Chapter 11). Some 156 hand specimens were collected and 259 thin sections made to allow the comparison and classification of the different lithologies. One hundred and twenty-one whole-rock geochemical analyses were performed for the geochemical description of the lithologies and to establish the protolith of the metasedimentary and metavolcanic rocks. The geochemistry of the metavolcanic rocks was also used to geochemically classify and to compare with the previously studied metavolcanic rocks of the Bridgetown Formation (Chapter 6). Microprobe (Rhodes University) and Scanning Electron Microscopy (Stellenbosch University) work on mineral compositions, specifically chlorite, biotite and garnet were carried out for temperature estimates of the metamorphic conditions.

The Spitskop area was mapped on a 1:10 000 scale and surface samples along with samples from the earlier percussion drilling programme performed by Swingler (1998) were used to investigate the gold mineralisation (Chapter 9). Due to the low gold grade and disseminated nature of the mineralisation, samples taken from the ore zones were subjected to heavy mineral separation using bromoform to concentrate the sulphide fraction. These samples (38 in total) were then investigated using optical microscopy. Microprobe, Scanning Electron Microscopy and micro-PIXE analyses were undertaken on the sulphides (specifically pyrite) to identify their compositions and to identify the location of gold and its relationship to the sulphide minerals. Fluid inclusion analyses were undertaken on veins to identify the source of the ore-bearing fluids and to classify the fluid with respect to other styles of gold mineralisation.

Additional information on sampling methods, analytical techniques, sample descriptions and locations are provided in Appendix B. The full data set of all the analyses is presented in Appendix C. The regional map of the Swartland area along with detailed maps of specific localities are provided in Appendix D.

2 THE SALDANIA BELT: A REVIEW OF THE REGIONAL GEOLOGICAL SETTING

This chapter provides a detailed review of the current understanding of the regional geology of the western branch of the Saldania Belt and its relationship to global tectonics up to and including the most recent work by Rozendaal et al. (1999).

The Saldania Belt consists of a series of Neoproterozoic supracrustal rocks located along the western and southern coasts of South Africa that were intruded by the syn- to post-tectonic Cape Granite Suite. The supracrustal rocks include the Malmesbury and Klipheuwel Groups in the western branch and the Kango, Kaaimans and Gamtoos Groups in the southern branch (Fig. 2.1). The rocks now known as the Malmesbury were first studied in the mid-nineteenth century by Bain (1856), who described the lithologies as a 'Clay Slate Series'. However, it was Dunn (1872) who first gave the name Malmesbury, then the Malmesbury Beds, to these rocks after the town in the area where outcrops are comparatively well developed. Additional work by Rogers (1903) and Rogers and Du Toit (1909) developed a basic classification (the Malmesbury Series) and later Rogers (1913) correlated these rocks with the Nama Group, which Du Toit (1926) later followed (Fig. 2.2a). However, Truter (1950) suggested that the Malmesbury Beds, the equivalent of the Malmesbury Series of Rogers (1913) were in fact Archaean in age and later related the Malmesbury Beds to the now Gariep Supergroup. The correlation of the Malmesbury Group to the Gariep Supergroup was later also followed by De Villiers (1956) and De Villiers et al. (1964). Mapping by Rabie in the late 1940's (map printed but not published; Rabie, 1948) provided the most detailed sedimentological and structural maps to date and subdivided the rocks into two 'systems' that are separated by a major fault (Rabie, 1974a, b). These systems were subsequently considered to have formation status by Verwoerd in the explanatory note to Rabie's maps (Rabie, 1974a, b) and in essence, are the basis for the subdivisions by later workers. Hartnady et al. (1974) suggested that the Malmesbury rocks should attain group status and divided the

a)

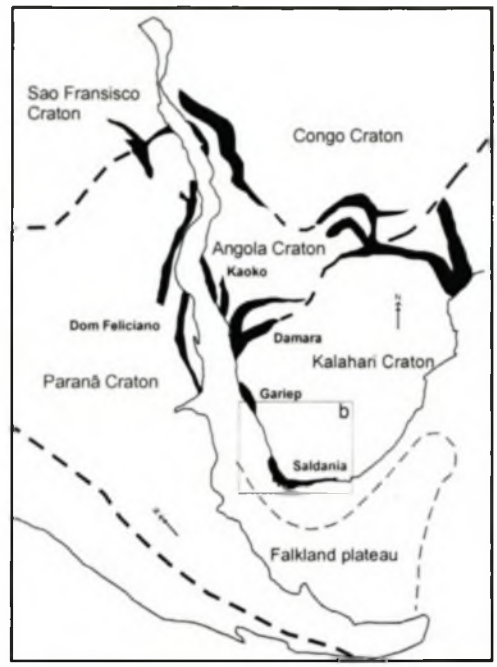

b)

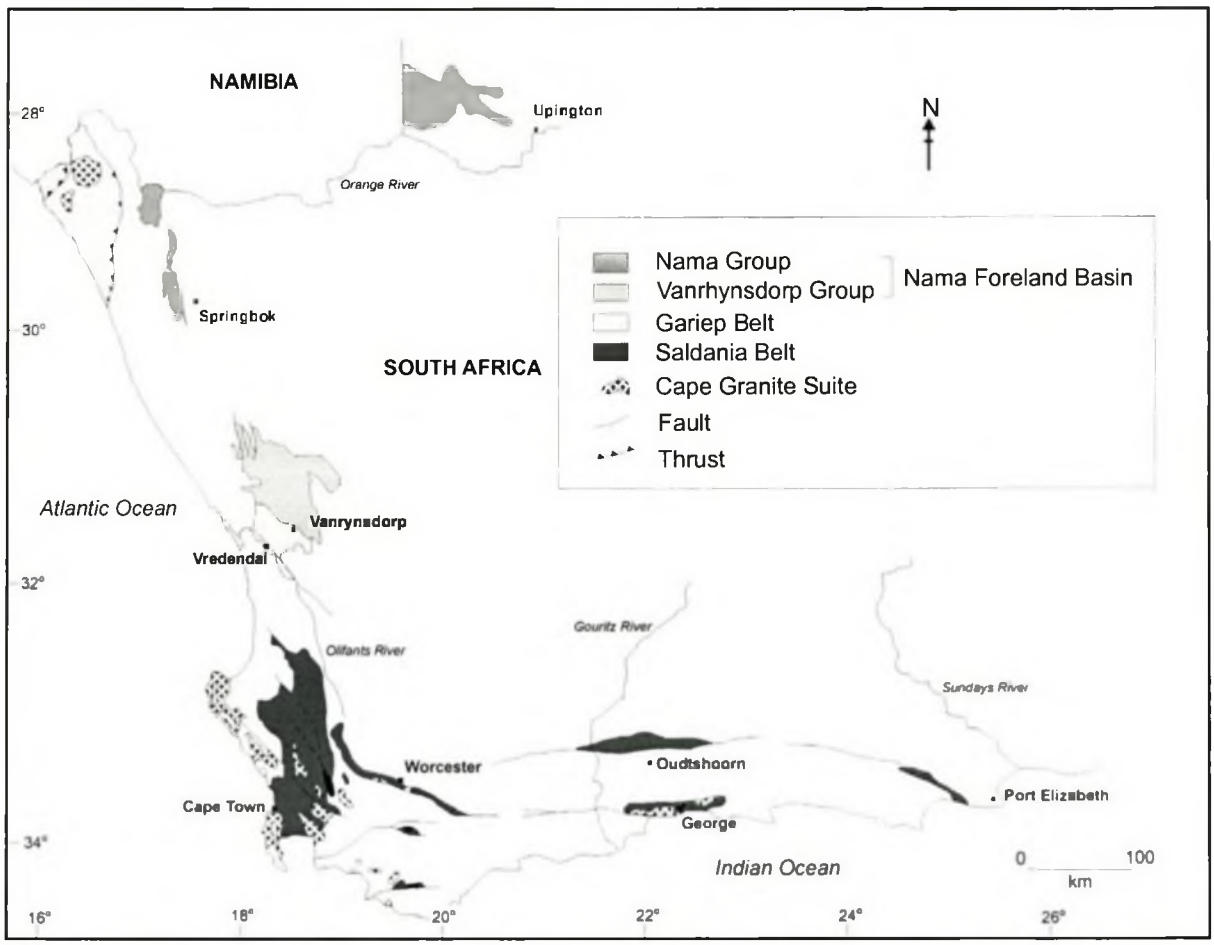

Figure 2.1.

a) The Late Precambrian-Early Palaeozoic distribution of the Pan-African belts of southern Africa and South America (Porada, 1989) based on Porada's (1985) reassembly. Note, the present-day continental outlines used in the figure are for reference only.

b) Distribution of Pan-African rocks in South Africa, after Rozendaal et al. (1999).

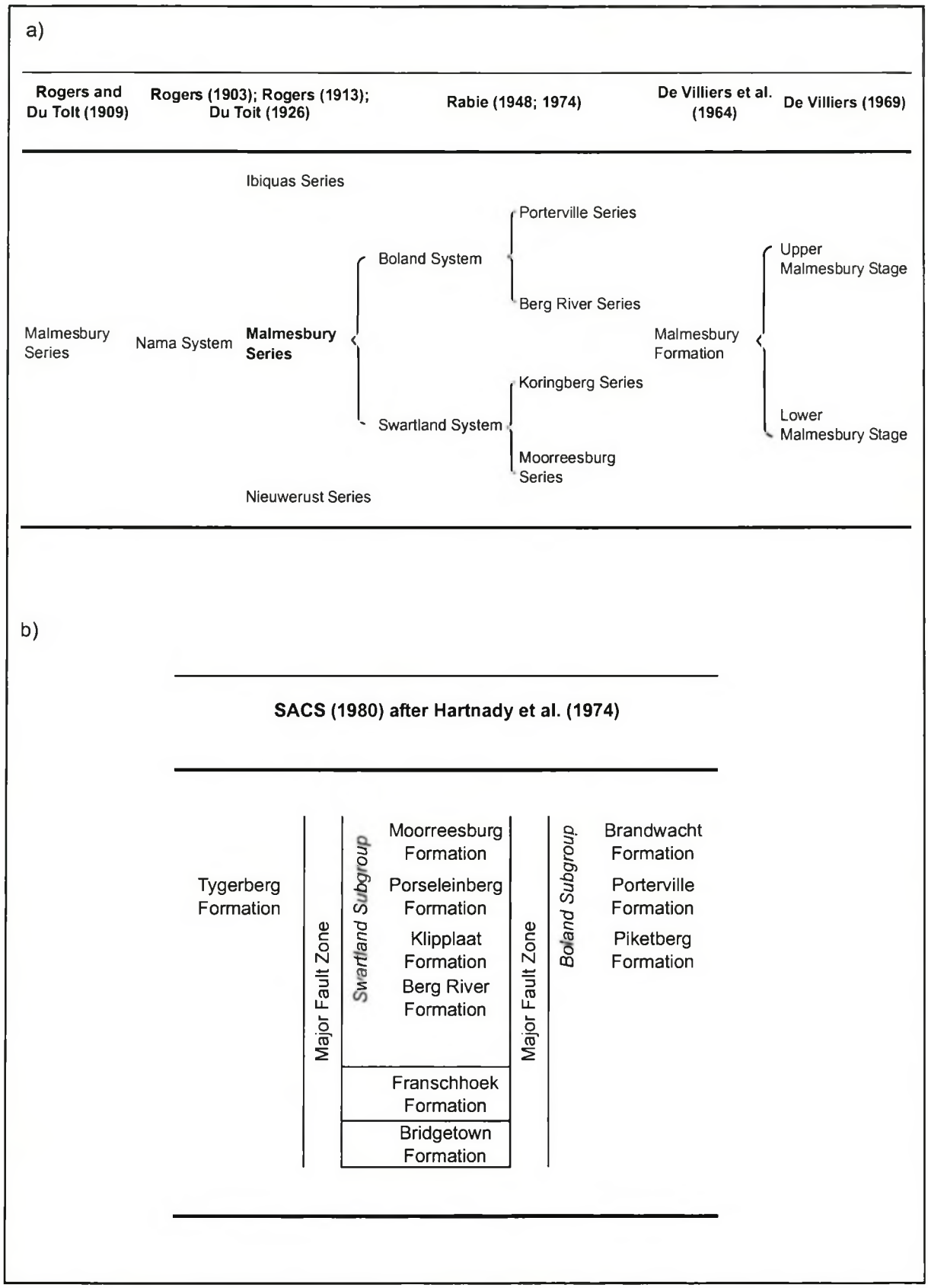

Figure 2.2. Summary of the past classifications of the Malmesbury Group. See text for further information on individual classifications. Figure modified from SACS (1980).
a) From Rogers and Du Toit (1909) up until De Villiers (1969).
b) Present classification according to SACS (1980) based on Hartnady et al. (1974).

rocks into ten formations within three subgroups characterised by contrasting lithological and structural properties.

The work of Rabie (1974a, b) and Hartnady et al. (1974) forms the basis of the currently accepted classification by the South African Committee for Stratigraphy (SACS, 1980; Fig. 2.2b). However, at the time not all the formations could be stratigraphically correlated and a correlation across subgroups was not possible, problems that are still unresolved today.

2.1 The Malmesbury Group

The Malmesbury Group represents the most extensive and best-studied group in the Saldania Belt being characterised by a series of metasedimentary and metavolcanic rocks (Fig. 2.3). These have been deformed and metamorphosed to lower greenschist facies during the Pan-African orogenic event (e.g. Rozendaal et al., 1999; Fig. 2.4). The Malmesbury Group in the western branch of the belt is divided into three distinctly different tectonostratigraphic terranes that are separated by two northwest-trending parallel fault zones (Fig. 2.5). These are the Colenso Fault Zone, separating the western Tygerberg Terrane from the central Swartland Terrane and the Piketberg-Wellington Fault Zone separating the Swartland Terrane from the eastern Boland Terrane (Hartnady et al., 1974).

The age of the Malmesbury Group is constrained by the presumed underlying Namaqua-Natal basement (ca. 1000 Ma; Burger and Coertze, 1973) and the base of the overlying Table Mountain Sandstone (TMS) Group (ca. 520 Ma; Armstrong et al., 1998). The Malmesbury Group is intruded by the granitoids of the Cape Granite Suite (ca. 550-510 Ma; Da Silva et al., 1997; 2000, Scheepers and Poujol, 2002). Although the base of the Malmesbury Group is nowhere exposed, Rozendaal et al. (1999) suggested, following work by Frimmel et al. (1996a) in the Gariep Belt to the north, that its deposition was on Meso- to Palaeoproterozoic basement during the break-up of Rodinia (780-750 Ma; Grunow et al., 1996). This assumption is corroborated by the identification of Kibaran (1.0-1.2 Ga) and possible Eburnean (1.7-2.0 Ga) zircon cores within the granitoids of the Cape Granite Suite (Da Silva et al., 1997, 2000).

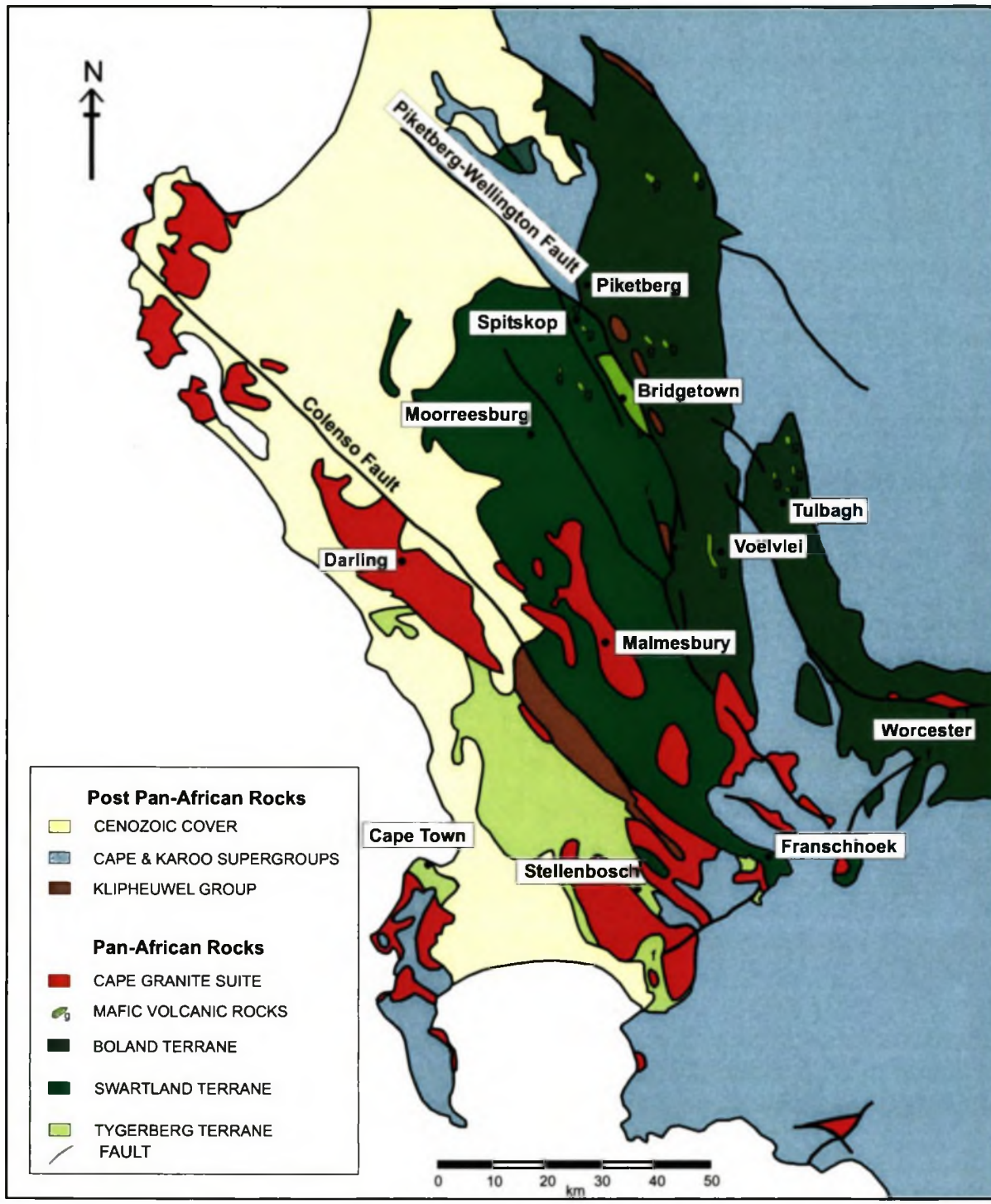

Figure 2.3. The tectonostratigraphic terranes of the western Saldania Belt, with the location of mafic volcanic rocks of the Swartland and Boland terranes. Map after Rozendaal and Scheepers (1994). Localities of the mafic volcanic rocks after Rabie (1974a).

However, Armstrong et al. (1998) have identified zircons with ages as young as 560 Ma from within the Tygerberg Formation, indicating that at least parts of the Malmesbury Group have a much younger age for deposition than previously thought. This, along with the discrepancies discussed later in Chapter 3, suggests that the present understanding of the Malmesbury Group is incomplete.

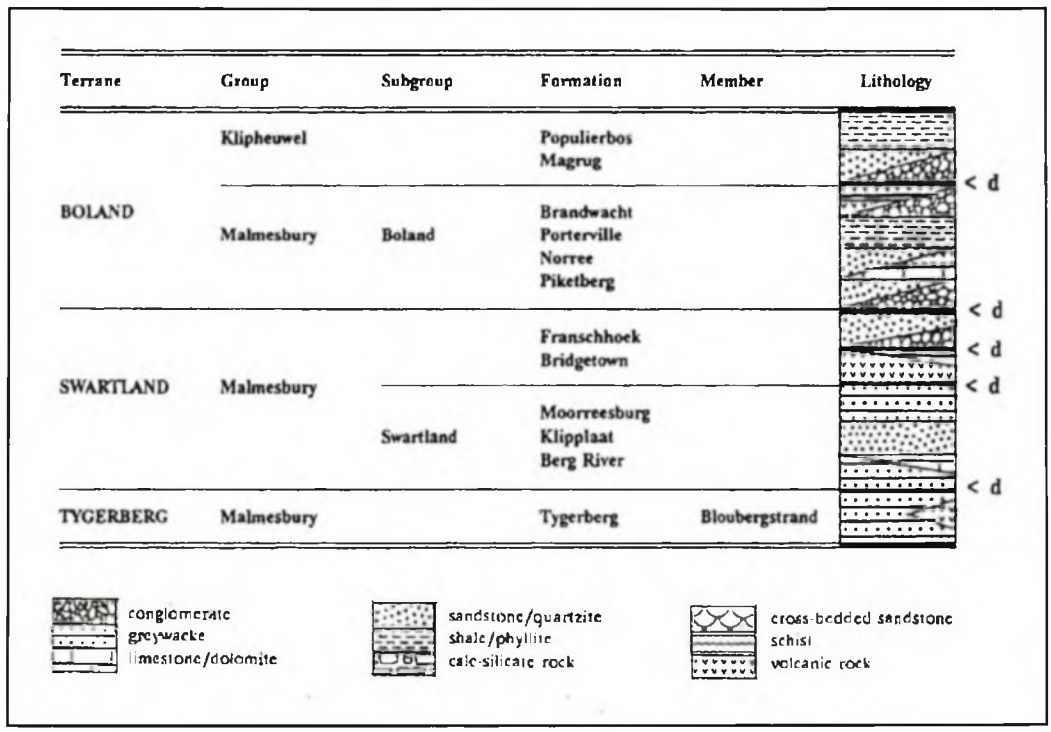

Figure 2.4. Stratigraphy of the Malmesbury Group of the Saldania Belt, Western Cape as proposed by Rozendaal et al. (1999). Note: 'd' denotes a discontinuity in the stratigraphy.

2.1.1 Tygerberg Terrane

The Tygerberg Terrane is the westernmost terrane of the exposed Saldania Belt (Fig. 2.3). The Tygerberg Formation (Figs. 2.4 & 2.5) is the only formation recognised in the Tygerberg Terrane consisting of predominantly pelitic and finely-bedded semi-pelitic rocks, containing zones of massively bedded, fine-grained greywackes and immature quartzites (Hartnady et al., 1974; Von Veh, 1983; Theron, 1984). The sediments are of turbiditic origin and accumulated in either a continental rise/ocean trench environment or possibly on a continental slope (Von Veh, 1983). The localised occurrence of a volcanic succession (tuff, conglomerate and altered calc-alkaline andesite) constitutes the Bloubergstrand Member (Von Veh, 1983).

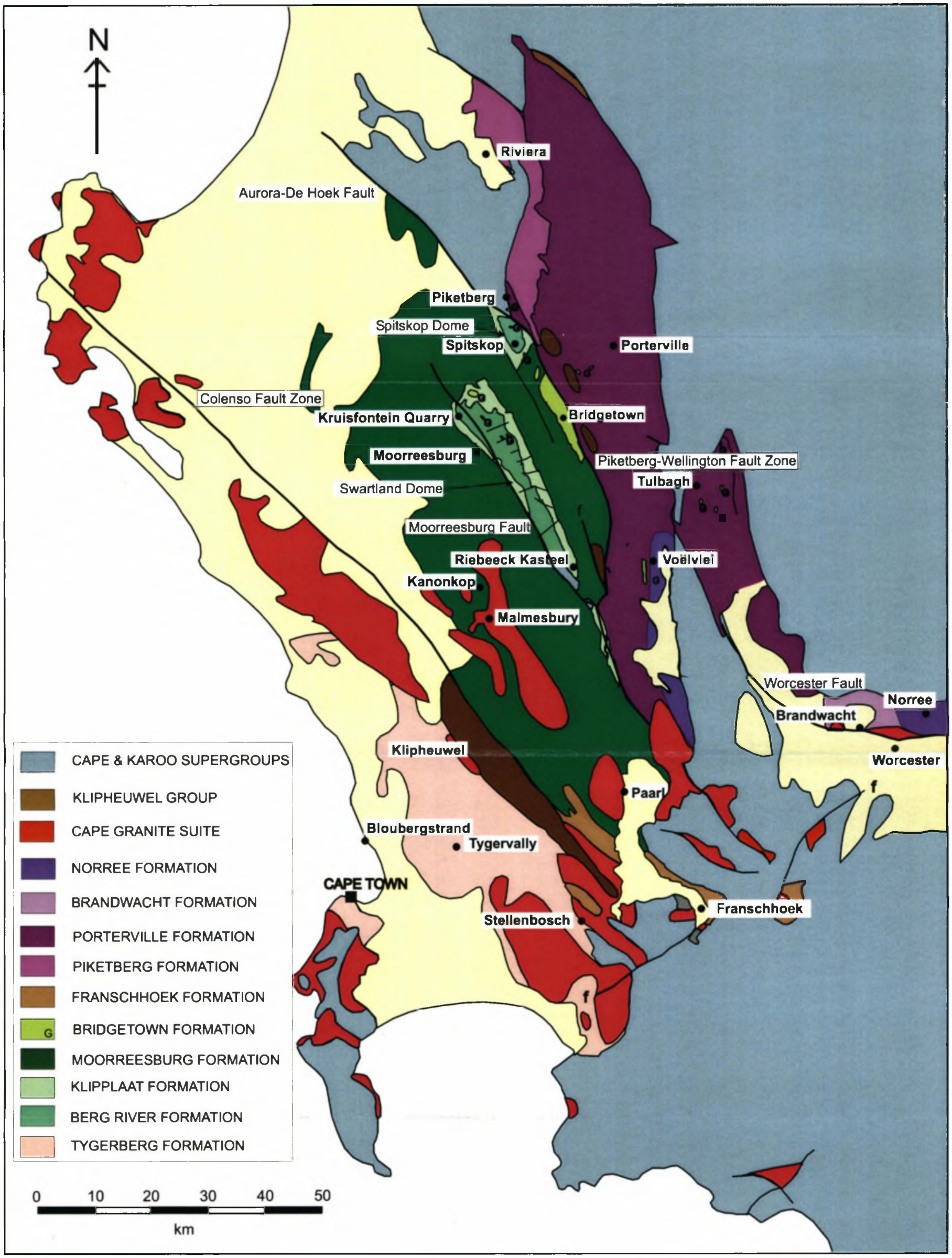

Figure 2.5. Geological map of the formations of the Malmesbury Group. Adapted from Rabie (1974a,b) & Hartnady et al. (1974).

Structurally, the Tygerberg Terrane is deformed into a series of tight, upright folds with axial planes striking northwest (Table 2.1). These folds are seen on a regional scale, with half wavelengths ranging between 500 and 1500 m (Hartnady et al., 1974). In certain localities, e.g. Robben Island and Melkbosstrand, open folding orientated north-northwest is seen (Von Veh, 1983). However, in Bloubergstrand, evidence of refolding in the form of minor later folds associated with the development of a fracture cleavage has been identified. These later folds appear to be related to faults with sinistral movement (Hartnady et al., 1974).

Table 2.1. Comparison of the deformation events recorded by different authors in the Malmesbury Group.

Deformation event	Hartnady (1969)	(Hartnady et al., 1974)		Rozendaal et al. (1994)
	Worcester area	Tygerberg & Boland Terranes	Swartland Terrane	Piketberg Formation
D_1			S_e fabric	
	Phase O (N-S folds)	F_1 folding (NNW-SSE)	S_e/S_m transposition fabric (NW-SE)	F_1 folding (NW-SE)
		S_1 axial planar cleavage	S_m fabric	S_1 axial planar cleavage
D_2	Phase M (NW-SE folds)	F_2 folding (NE-SW)	F_2 folding (NNW-SSE)	F_2 folding (NE-SW)
D_3	Phase X (NE-SW, NNW-SSE folds)		F_3 folding (NE-SW)	S_3 axial planar cleavage (Cape Orogney)
	Phase K, open crenulation (Cape Orogeny)			

2.1.2 Swartland Terrane

The Swartland Terrane is more intensely deformed than the Tygerberg and Boland Terranes and according to Theron et al. (1992) may be subdivided into five formations. These are, from the stratigraphic bottom to top, the Berg River, Klipplaat, Moorreesburg, Bridgetown and Franschhoek Formations (Fig. 2.5). The deposits of the Swartland Terrane consist of mica schists and fine-grained quartz-mica schists with limestone and dolomite lenses and, based on the type of lithologies and sedimentary features present are typical of an oceanic trench environment (Theron et al., 1992).

Berg River Formation

The Berg River Formation is stratigraphically the lowest formation within the terrane and only occurs in the cores of the Swartland and Spitskop domes that represent two kilometre-scale, northwest-southeast trending, doubly plunging antiforms (Figs. 2.3 & 2.4). The formation consists of mica schists and meta-greywackes, which contain impure limestone layers. The impure limestones vary in thickness, lateral extent and composition, but they become more prominent to the south and towards the top of the formation. The top of the succession is marked by the occurrence of a quartz schist. Also within the schists are small metamorphosed sills, which are difficult to distinguish from the surrounding schists due to their high chlorite content (Visser et al., 1981). The contact between the Berg River and the overlying Klipplaat Formation is considered to be a dark grey-blue/black, strongly lineated and foliated cherty horizon, containing ferruginous quartzite layers. Its origin is still enigmatic; Visser et al. (1981) suggest similarities to a Banded Iron Formation, although a later interpretation by Slabber (1995) suggests it is possibly derived from silica leaching of an underlying ultramafic body.

Klipplaat Formation

The Klipplaat Formation conformably overlies the Berg River Formation and is also located only in the Swartland and Spitskop domes. This formation differs from the other formations within this subgroup by its higher quartz content, and consists of a weathering-resistant grey, to yellowish quartz schist containing minor sericite and chlorite. Along the Berg River, the cherty rock of the Berg River Formation and the overlying quartz schist of the Klipplaat Formation are separated by a grey-green micaceous schist. To the south, the quartz schist becomes more deformed, being interbedded with thin lenses of phyllite, mica schist and limestone, which are parallel to the regional foliation. The interlayering of the quartz schist with the quartz-sericite schist is interpreted to represent the differing maturity of the sandstones (Theron et al., 1992).

Moorreesburg Formation

The Moorreesburg Formation underlies most of the Swartland Terrane. The contact between the Moorreesburg and the underlying Klipplaat Formation is not sharp and is observed in the field as the interfingering of the two formations (Theron et al., 1992). The lower units of the Moorreesburg Formation are compositionally more arenaceous and are typified by a well-laminated quartz-muscovite-biotite schist that is interbedded at the top and bottom of the succession with a phyllitic chlorite-muscovite schist (De Villiers, 1969). To the south of Riebeeck West (Fig. 2.4), the phyllites grade upwards into greywackes. The upper part of the Moorreesburg Formation consists of a series of greywackes and pelites (Theron et al., 1992).

Bridgetown Formation

The Bridgetown Formation consists of a north-northwest trending lensoidal body, 15 km by 3 km in extent, situated around the farm of Bridgetown (Hartnady et al., 1974). The formation consists of a succession of mafic metavolcanic units, chert, dolomite, minor graphitic schists and shales that are cross cut by a mafic dyke (Slabber, 1995). The Bridgetown Formation is interpreted to represent an obducted segment of oceanic crust (Hälbich and Hartnady, 1985; Slabber, 1995; Rozendaal et al., 1999). Geochemically, the greenstone units may be subdivided into alkaline and subalkaline metabasalts (Slabber, 1995). Both are LREE enriched and exhibit no Eu anomalies. Their LREE and HREE slopes are similar, indicating that they both originated from the same source material. Both groups are believed to have a basaltic origin, and compositions are similar to within-plate basalts, ocean island basalts, ocean-floor and island arc basalts (Slabber, 1995).

The Bridgetown Formation was metamorphosed and deformed with the surrounding lithologies, indicating that its emplacement was prior to, or during deformation (Slabber, 1995).

Franschhoek Formation

The Franschhoek Formation occurs as narrow, northwest trending fault-bounded outcrops, located to the south and west of Paarl Mountain and to the northeast of

Stellenbosch (Fig. 2.4). The formation is characterised by feldspathic and sericitic arenites with feldspathic conglomerates and grit horizons, and intermittent shale beds that have all undergone deformation (Theron et al., 1992). Clasts from the conglomerates are, in general, composed of vein quartz, quartzite, chert, shale, arkose, greywacke and granite (Theron et al., 1992). More rarely, quartz porphyry, jasper and possibly mafic lava clasts occur. These arenites, conglomerates and shales often show sedimentary structures, i.e. trough cross bedding, fining upward cycles and sediment coarsening, with beds usually dipping steeply (60 to 70°). At Helshoogte Pass, rocks of the Franschhoek Formation are composed of conglomerate layers and grits, being preserved within kilometre-scale graben structures (e.g. De Villiers et al., 1964). Near Knorhoek the conglomerate contains quartz veining and jasper clasts, with pebbles poorly to semi-rounded and elongated northwest-southeast (Hartnady, 1969).

Structure

Structurally, the Swartland Terrane is more complex than the adjacent Tygerberg and Boland Terranes. The reason for this is still unclear, although Rozendaal and Scheepers (1995) suggest this to be related to the relative degree of vertical displacement of the three terranes along terrane-bounding faults, as seen by the varying level of emplacement of intrusive granites (Fig. 2.6). The two most prominent structural features of the terrane are the Swartland and Spitskop domes, which are elongated in a north-northwest-south-southeast orientation (Fig. 2.5).

Three phases of deformation are identified in the Swartland Terrane (Hartnady et al., 1974). The degree of deformation of the different formations within the Swartland Terrane decreases towards the top. In the Moorreesburg Formation, there is very little evidence for the first two phases of deformation described below (Table 2.1). The first phase is represented by folding of bedding (S_e) and is now represented by tiny fold closures with sheared-off limbs. During this early phase of deformation a strong foliation (S_m) developed, defined by the orientation of phyllosilicate minerals, and quartzitic laminae. The second phase of deformation is characterised by the large-scale folding of the foliation (S_m) into open, northwest-southeast trending folds. Small-scale folds associated with the open folds are rounded to angular chevron

folds. The third phase is characterised by minor folding trending northeast-southwest (Hartnady et al., 1974).

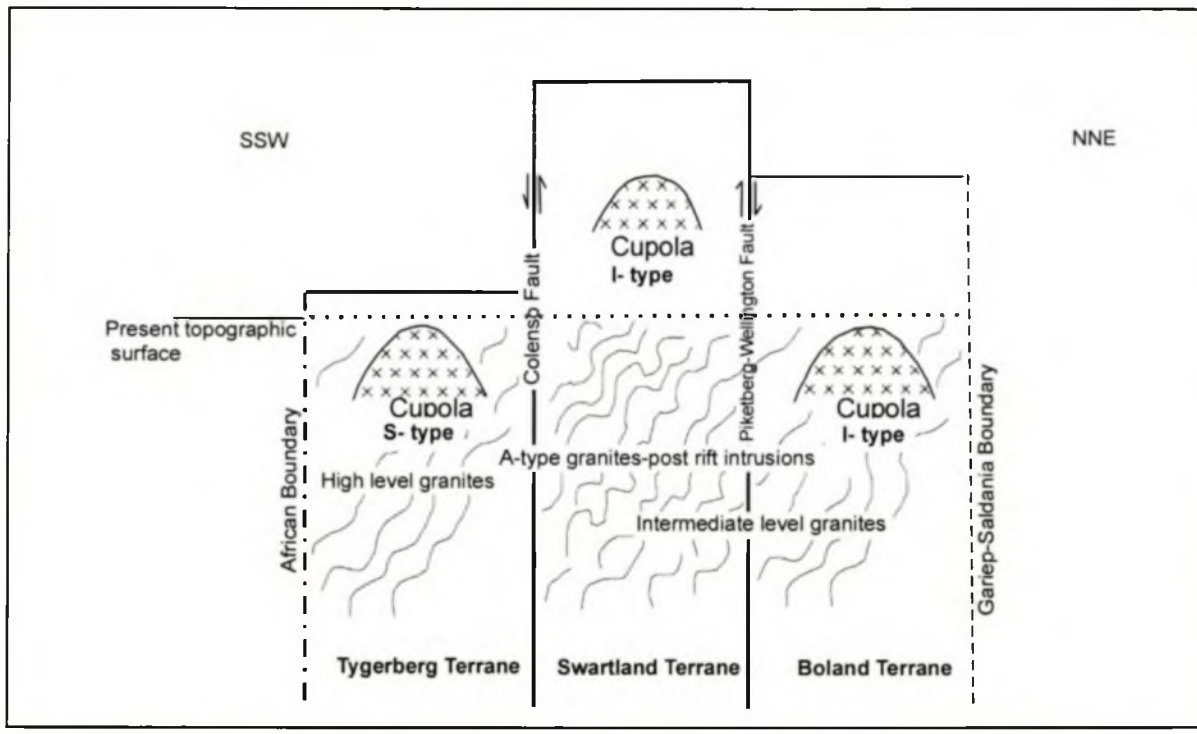

Figure 2.6. The relative displacement of the three terranes according to the level of granite emplacement, the preserved granite cupolas and the structural complexity of the metasedimentary rocks, modified from Rozendaal and Scheepers (1995).

2.1.3 Boland Terrane

The Boland Terrane is composed of four formations, namely the Piketberg, Norree, Porterville and Brandwacht Formations. Bedding is generally visible and the coarse, fluvio-marine, possible deltaic deposits within the Boland Terrane, suggest deposition in an evolving continental margin (Rozendaal et al., 1999).

Piketberg Formation

The Piketberg Formation is located around the eastern and northeastern margins of the Piketberg inlier (Fig. 2.5) and in the southern-most occurrences, interfingers with the lower portions of the Porterville Formation (Theron et al., 1992). The Piketberg Formation is composed of strongly foliated and lineated feldspathic quartzites,

greywackes, sericite schists, feldspathic grits and conglomerates, and minor impure marly limestones (Hartnady et al., 1974).

Norree Formation

The Norree Formation is located to the north of the Worcester Fault in the Nuy and Swellendam area (Fig. 2.5). It is composed of phyllite, medium-grained to gritty greywacke, feldspathic and sericitic quartzite, limestone, dolomite and feldspathic and calcareous grits (Gresse and Theron, 1992). Compositionally, the Norree Formation resembles the Piketberg and Franschhoek Formations with the exception of the limestone units. For this reason, Gresse and Theron (1992) have suggested a facies relationship between the Norree, Piketberg and Franschhoek Formations.

Porterville Formation

The Porterville Formation represents the mostly widely distributed formation of the Boland Terrane (Fig. 2.5). The formation is composed of phyllitic shale, schist and fine- to medium-grained greywacke. Minor limestone, quartzitic sandstone and conglomerate occur in places. The base of the Porterville Formation is composed of limestone (De Hoek Member) that wedges out southwards into arenite and shale, which also becomes coarser and better sorted to the south (Theron et al, 1992). This coarsening is marked by the presence of a conglomerate composed of angular to rounded pebbles of shale, greywacke, quartzite and vein quartz, within a phyllitic matrix.

Brandwacht Formation

The Brandwacht Formation only occurs in the area around Worcester, and is composed of green-grey greywacke and pelites (Fig. 2.5). The greywackes range from ruditic to arenaceous to fine-grained types, interbedded with poorly-sorted conglomerates. Volcanic rocks within the formation occur as concordant greenstone bodies (Hälbich and Hartnady, 1985), although in the past they have been described as a biotite-eucrite (De Villiers et al., 1964), a diorite (De Bruyn et al., 1974), a metabasalt (Hartnady et al., 1974) and a meta-andesite (Hoal, 1978). Rozendaal et

al. (1999) stratigraphically placed the Brandwacht Formation above the Porterville Formation.

Structure

Bedding is generally preserved and is folded into near-upright, tight to isoclinal folds striking north-northwest. Only one prominent cleavage is developed within the Boland Terrane, which is axial planar to the folding (Table 2.1). These structural features are similar to features observed in the Tygerberg Terrane (Hartnady et al., 1974). Evidence of late refolding is again seen, with the occurrence of kink-banding, similar to that observed in the Tygerberg Terrane.

2.1.4 Metamorphism

Limited research has been conducted on the metamorphism of the Malmesbury Group. This is most probably due to the very low grade of metamorphism, the simple mineralogy (quartz, chlorite, white mica, feldspar, actinolite and epidote), and the poor exposure of rocks in the area. In general, the Malmesbury Group was metamorphosed to lower greenschist facies, with some localities exhibiting very little evidence of metamorphism (Hartnady et al., 1974). The most in-depth study was undertaken by Newton (1966), who divided the Malmesbury Group into two units based on the differing degrees of metamorphism, which he believed were separated by a major break (fault?). Newton (1966) indicated that the less deformed and metamorphosed unit could possibly represent a younger unit overlying the more deformed/metamorphosed rocks. More recently, chlorite thermometry on samples from the Worcester area has indicated a temperature of 325± 12 °C for Pan-African metamorphism in this area (Frimmel et al., 2001).

2.1.5 Terrane-boundary fault zones

The three tectonostratigraphic terranes are separated by two major northeast-southwest trending vertical fault zones, known as the Colenso Fault Zone in the southwest and the Piketberg-Wellington Fault Zone in the northeast (Hartnady et al., 1974; Fig. 2.5).

Colenso Fault Zone

The Colenso Fault Zone separates the Tygerberg and Swartland tectonostratigraphic Terranes and shows evidence of ductile shearing, brecciation and cataclasis (Hartnady et al., 1974; Figs. 2.3 & 2.5). The fault zone is orientated northwest-southeast and can be traced for some 100 km from Franschhoek to Darling, and beyond to Trekoskraal along the west coast. The fault zone contains minor (<4 km long) fault splays, as indicated by the occurrence of breccia in the Darling area (Schoch, 1975). Within the Darling Pluton and along the west coast there is evidence of ultramylonites and mylonites (Visser and Schoch, 1973), and in the Franschhoek area, evidence for cataclasites (De Villiers et al., 1964).

Recent studies by Kisters et al. (2002) have revealed that both sinistral and dextral movement have occurred along the Colenso Fault Zone. This movement can be temporally constrained. Shear sense indicators point to a sinistral sense of shear within the ca. 547 ± 6 Ma (U-Pb SHRIMP dating, Da Silva et al., 2000) Darling batholith, that was intruded syn-kinematically into the fault zone. The syn-kinematic intrusion of aplites (ca. 539 ± 4 Ma; U-Pb single zircon dating, Kisters et al., 2002) into dextral strike-slip mylonites in the Trekoskraal area in the northwest, indicates a reversal from sinistral to dextral movement (Kisters et al., 2002). The intrusion of the undeformed Klipberg granite into the fault around 510 ±4 Ma (Da Silva et al., 2000) indicates that movement by this time had largely ceased (Kisters et al., 2002).

Piketberg-Wellington Fault Zone

The Piketberg-Wellington Fault Zone is described as a near vertical zone of faulting, which separates the Swartland and Boland Terranes (Hartnady et al., 1974; Figs. 2.3 & 2.5). To the west of the Piketberg inlier the Mesozoic Aurora-De Hoek fault (Fig. 2.5) has a downthrow to the northeast. The fault trends northwest-southeast and strikes for approximately 40 km from Aurora in the north to Piketberg in the south. Between Piketberg and Riebeeck Kasteel the location of the fault is controversial (e.g. Rabie, 1974b; Hartnady et al., 1974; De Villiers, 1979; Slabber, 1995). The Moorreesburg Fault (Fig. 2.5), can be identified in the Riebeeck Kasteel area and trends northwest-southeast with downthrow to the east. This fault is suggested to be

a bifurcation of the Piketberg-Wellington Fault Zone based on scattered occurrences of quartz veins and springs (Hartnady et al., 1974). The tracing of the Piketberg Fault further to the south of Riebeeck Kasteel is made more complicated by the occurrence of extensive post-Cape faulting in and surrounding the town of Worcester. The age of movement along this fault is still unresolved and has been suggested to be Pan-African in age (e.g. Rozendaal et al., 1999) but a much younger, Mesozoic component is clearly evident (Rozendaal et al., 1994).

2.1.6 Cape Granite Suite

The Cape Granite Suite (CGS) is intrusive into the Malmesbury Group and post-dates the volcanism and sedimentation of all the known lithological units except the Franschhoek Formation (Fig. 2.7). The granites can be divided into four main groups based on their composition (Scheepers, 1995; Scheepers and Poujol, 2002), as depicted in Table 2.2. The oldest S-type granites, are dated at 555-540 Ma (U-Pb SHRIMP dating, Da Silva et al., 1997; 2000; Scheepers and Armstrong, 2002), while the I-type granites are slightly younger (540-520 Ma, U-Pb SHRIMP dating; Da Silva et al., 1997; 2000), with the youngest granites (A-type) being intruded around 520-510 Ma (U-Pb SHRIMP dating, Scheepers and Poujol, 2002).

Table 2.2. Classification of the Cape Granite Suite into four phases of magmatism (Rozendaal et al., 1999).

Magmatism	Association	Rock Type	Examples
Phase IV (515 Ma)	Volcanic	Ignimbrites, tuffisite, quartz porphyry.	Postberg ignimbrite, Saldanha quartz porphyry.
Phase III	Aa	Alkali feldspar granite, quartz syenite.	Klipberg granite.
(520 Ma)	Ab	Alkali feldspar granite.	Cape Columbine granite.
Phase II	Ib	Granite, alkali feldspar granite.	Paarl fine-grained granite, Slippers Bay granite.
(540-520 Ma)	Ia	Monzogranite, granite, alkali feldspar granite.	Paarl coarse- and medium-grained granite, Vredenburg quartz monzonite, Greyton pluton.
Phase I	Sb	Granite.	Trekoskraal granite, Karnberg granite, Rondeberg granite, Coarse porphyritic Darling granite.
(555-540 Ma)	Sa2	Granite, alkali feldspar granite.	Stellenbosch fine-grained granite. Contreberg granite, Olifantskop granite.
	Sa1	Granite.	Pennisula granite, Hoedjiespunt granite, Seeberg granite.

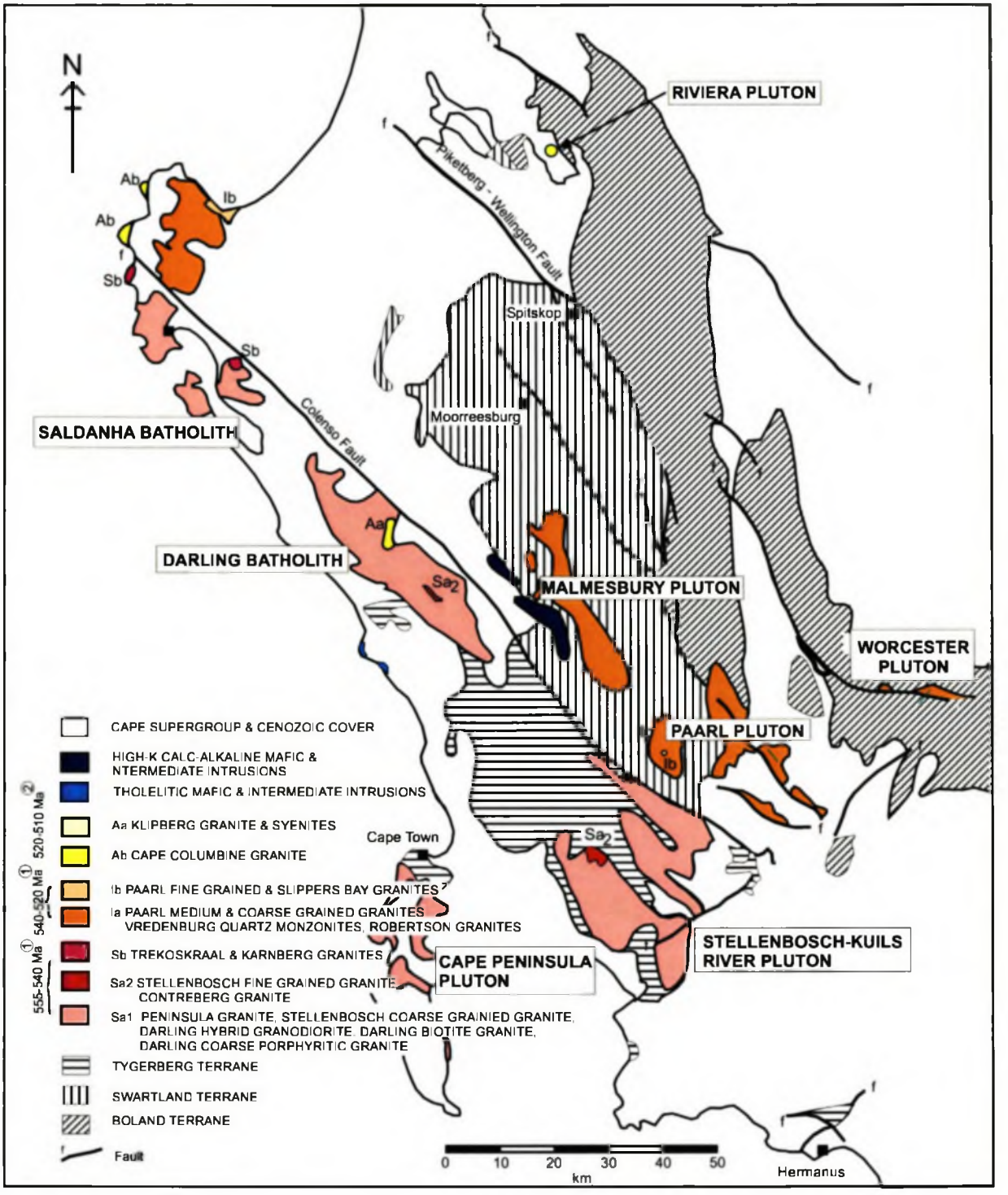

Figure 2.7. Location of the Cape Granite Suite in the western branch of the Saldania Belt (after Scheepers, 1995). Radiometric ages are from (1) Da Silva et al. (1997, 2000) and Scheepers and Armstrong (2000), and (2) Chemale et al. (in press) and Scheepers and Poujol (2002).

2.2 Klipheuwel Group

The Klipheuwel Group lies stratigraphically between the Malmesbury Group and the Table Mountain Sandstone (TMS) Group and is subdivided into two formations, the lower Magrug and upper Populierbos Formations. It currently has the status of a 'group' (SACS, 1980), although earlier workers (e.g. Rogers, 1897; Du Toit, 1926; Hall, 1929) suggested that the Klipheuwel Group should actually be part of the TMS Group. However, this was refuted by later workers (e.g. Theron et al., 1992; Rozendaal et al., 1999).

Magrug Formation

The Magrug Formation is composed of conglomerate, grit and coarse sandstone beds and reaches a maximum thickness of in excess of 1000 m (Visser et al., 1981). The conglomerates are composed of pebble- to cobble-sized clasts of quartz, quartzite (white and red), chert, shale and arenite, all of Malmesbury derivation (Theron et al., 1992). Less common are granite, granite porphyry, quartz porphyry and red jasper clasts varying in size from 6 mm (well-rounded) to 100 mm (angular). The conglomerates are matrix-supported and alternate with grit and coarse sandstone beds. The sandstones beds are on average less than 1 m thick, exhibiting bedding features such as laminar cross-bedding (northwest and southeast palaeocurrents) and current ripple marks (Theron et al., 1992).

Populierbos Formation

This formation rests conformably on top of the Magrug Formation, being composed of reddish-purple mudstone, shale and thin sandstone beds and having a stratigraphic thickness of in excess of 600 m. The transition zone between the two formations is seen as interbedded red shales, grits and greywackes (Theron et al., 1992).

Contacts between the Klipheuwel Group and the underlying lithologies are rare, although Visser (1967) has identified the Magrug Formation unconformably overlying rocks of the Malmesbury Group approximately 3 km to the north of Klipheuwel. In the Klipheuwel Quarry, an angular unconformity is seen between Malmesbury hornfels intruded by granitic dykes and the Magrug Formation (Theron et al., 1992). The

contact between the TMS Group and the Klipheuwel Group is locally both conformable and unconformable (Rust, 1967; SACS, 1980; Broquet, 1992; Thamm, 1993).

The morphology and size of the clasts of the Magrug Formation, the fault-bounded contacts between the Klipheuwel Group and the underlying Malmesbury Group, suggest accumulation in subsiding fault blocks (grabens) with little sediment transport (e.g. Theron et al., 1992). Rust (1973) and Tankard et al. (1982) suggested the formation of subsiding fault blocks was related to the closing stages of Pan-African collisional tectonics. The upward fining deposits of the two formations suggest a subdued topography in the provenance area or a more distal depositional environment.

Although the Klipheuwel Group does not contain any fossils that would allow it to be dated, it is older than the TMS Group, whose basal units contain detrital zircons that are dated at 510-520 Ma (U-Pb SHRIMP dating, Armstrong et al., 1998).

2.3 The Saldania orogenic event

The Saldania Belt forms the southernmost extent of the Pan-African belts in southern Africa. The orogenic history of the Saldania Belt is poorly understood and numerous different tectonic models have been proposed (e.g. Dunlevey, 1992; Gresse and Scheepers, 1993; Rozendaal and Scheepers, 1994). These are discussed in Chapter 3.4. The most recent review of the Saldania Orogeny was provided by Rozendaal et al. (1999) and is outlined below.

Sedimentation of the Malmesbury, Kango, Kaaimans and Gamtoos Groups commenced in rift basins along the then southern African coast after the break-up of the Rodinia supercontinent at approximately 780 to 750 Ma (Dalziel et al., 1994). These sediments were deposited into stepped pull-apart basins, which were defined by northwest trending, dextral transtensional margins (Rozendaal et al., 1999). Rifting occurred along the northern margin of these troughs, and ocean-floor spreading is evidenced by the presence of alkaline oceanic crust of the Bridgetown Formation. During this time, deep-water sediments were deposited into continental margin

basins, producing the turbidite successions of the Tygerberg Terrane (Rozendaal et al., 1999). However, Rozendaal et al. (1999) also suggest that the Tygerberg and Swartland Terranes represent part of a series of micro-plates that were accreted to the Kalahari Craton.

This period of rifting after the break-up of Rodinia was followed by the closure of the Adamastor Ocean, possibly related to the opening of the Iapetus Ocean (Grunow et al., 1996). As a consequence, sinistral transpression resulted from the oblique subduction/collision (Rozendaal et al., 1999) associated with S-, I- and A-type granites of the Cape Granite Suite (Scheepers, 1995). The development of syn- to post-orogenic marginal pull-apart basins allowed deposition of molassic sediments (Kansa Subgroup of the Kango Group and Franschhoek Formation of the Malmesbury Group) at approximately 510 Ma (Rozendaal et al., 1999).

3 DISCREPANCIES IN THE CLASSIFICATION OF THE MALMESBURY GROUP

The currently accepted classification of the Malmesbury Group (SACS, 1980), and the more recently modified lithostratigraphies by Theron et al. (1992) and Rozendaal et al. (1999) were presented in detail in the previous chapter. In this scenario, the Malmesbury Group can be subdivided into three lithologically and structurally distinct tectonostratigraphic terranes, which are separated by two major fault zones representing the terrane boundaries. Controversy surrounding the practicality and effectiveness of the subdivision of the western branch of the Saldania Belt into three tectonostratigraphic terranes has continued since its inception by Hartnady et al. (1974).

3.1 Classification

The subdivision of the western branch of the Saldania Belt into three distinct terranes to be underlain by only the Malmesbury Group is at variance with stratigraphic principles. A group is defined as "...an assemblage of two or more successive formations with significant unifying lithological features in common" (SACS, 1980, page 649). A terrane can be defined as a "Piece of exotic crust that has been attached to the margin of a larger continent as a consequence of collision." (Van der Pluijm and Marshak, 1997, page 357). Therefore, it is not correct to use the term Malmesbury Group to describe the stratigraphy of three supposedly distinct terranes. Either the Malmesbury Group encompasses all the formations and thus precludes the presence of three distinct lithological and structural terranes, or, if three terranes are present, three distinct lithological and structural successions must be distinguished.

3.2 Similarities across the terranes

Subdivision of the three terranes is based on lithological and structural variations. The Swartland Terrane is described as exhibiting an earlier deformation event to that seen in the other two terranes (Hartnady et al., 1974). However, this earlier deformation event is not seen within all the formations of the Swartland Terrane (Chapter 2.1.2). The Moorreesburg Formation, which incidentally forms the major surface expression of the Swartland Terrane, does not exhibit this early fabric (Hartnady et al., 1974; Theron et al., 1992) and thus is not only structurally dissimilar to the rest of the Swartland Terrane, but is actually lithologically similar to the Tygerberg and Boland Terranes. This alone has caused problems with the positioning of the boundaries between each terrane, especially when similarities have been identified in the rocks of supposedly separate terranes as outlined below.

De Villiers (1979) and later Theron et al. (1992) identified compositionally similar lithologies between sediments in the Tygerberg Formation of the Tygerberg Terrane and the Moorreesburg Formation of the Swartland Terrane. De Villiers (1979) reported that south of Piketberg no distinct differences in appearance or composition occur within the rocks on either side of the Piketberg-Wellington Fault Zone.

Metavolcanic rocks of the Riviera area of the Piketberg Formation in the Boland Terrane are suggested by Slabber (1995) to be similar to metavolcanic rocks of the Bridgetown Formation in the Swartland Terrane, although this was based on appearance alone. Rozendaal et al. (1999) identified that metavolcanic rocks from both areas have similar incompatiable trace element chemistries. Rozendaal et al. (1994) reported lithologically very similar rocks from core during the drilling of the Riviera area in the Piketberg Formation of the Boland Terrane with outcrops from the Spitskop area that is hosted within the Berg River Formation of the Swartland Terrane.

3.3 Stratigraphic position of the formations

Following the accepted classification by SACS (1980), it is still not possible to place some of the formations stratigraphically within the Malmesbury Group. The presently

accepted stratigraphic position of the formations of the Swartland Terrane is based on Hartnady et al. (1974), who managed to place all but the Bridgetown and Franschhoek Formations stratigraphically (Fig. 2.2). Hartnady et al. (1974) were the first to subdivide the Malmesbury Group, and based the currently accepted classification on the prerequisite: "Provided no major recumbent folding is present, these units are probably in correct stratigraphic sequence..." (Hartnady et al., 1974, page 198). However, bedding transposition was recorded by numerous authors in the lower formations of the Swartland Terrane (e.g. Theron, 1984; Theron et al., 1992; Belcher et al., 2000), and even by Hartnady et al. (1974), therefore casting doubts on the stratigraphic position of even these formations.

3.3.1 The Franschhoek Formation

SACS (1980) placed the Franschhoek Formation within the Swartland Terrane (Fig. 2.2). However, Gresse and Theron (1992) suggested that it actually represents, along with the Piketberg and Norree Formations of the Boland Terrane, facies variations of the same sedimentary succession. Theron et al. (1992), in contrast, suggest that the Franschhoek Formation, due to the presence of abundant autochthonous clasts and granite clasts, the latter of which bear resemblance to the Cape Granite Suite (CGS), in fact post-dates the intrusion of the CGS. Since the Piketberg Formation is intruded by the CGS and the Franschhoek Formation post-dates the CGS, the two formations cannot be facies variations. Most recently, Rozendaal at al. (1999) placed the Franschhoek Formation at the top of the Swartland Terrane in the Malmesbury Group. However, the occurrence of the Franschhoek Formation within all three terranes (Fig. 2.5), adds further to the confusion of the positioning of this formation within one particular terrane.

3.3.2 The Brandwacht Formation

Although the Brandwacht Formation is stratigraphically placed as the topmost of the formations of the Boland Terrane (SACS, 1980), it represents a distinct lithological succession to that of the other formations (Hartnady et al., 1974). The basal conglomerates of this formation are suggested to represent a tectonic mélange (Hartnady, 1969), therefore creating a tectonic boundary between the Brandwacht

and Porterville Formations. It has also been suggested that the formation represents a thrusted section of the Swartland Terrane (Hartnady et al., 1985). Slabber (1995) proposed that the (andesitic) metavolcanic rocks in the upper part of the Brandwacht Formation could represent the high-level gabbroic complex of an ophiolite succession, already identified in the Swartland Terrane (Bridgetown Formation), further strengthening the possible connection of the Brandwacht Formation with the Swartland Terrane.

3.3.3 The Bridgetown Formation

Although the origin of the Bridgetown Formation appears now well constrained (Slabber, 1995), its stratigraphic position within the Malmesbury Group is still debatable (Fig. 2.2). This is mainly due to its position adjacent to the Piketberg-Wellington Fault Zone, and the exact location of the fault being undecided. Rabie (1974a) originally placed the Bridgetown Formation within the Boland Terrane. Following Hartnady et al. (1974), SACS (1980) classified the Bridgetown Formation as part of the Swartland Terrane. More recently Slabber (1995) relocated the Piketberg-Wellington Fault Zone approximately 5 km to the west, making the Bridgetown Formation again part of the Boland Terrane. The inclusion of the Bridgetown Formation into the Boland Terrane is based on the following points (Slabber, 1995, page 35):

i) There is little evidence for a fault at the eastern border of the greenstone unit, except for a 15-20 m wide silicified schist zone;
ii) The phyllites that border both sides of the position of the fault as proposed by Hartnady et al. (1974) are similar;
iii) The greenstone units show only one prominent near vertical cleavage, trending north-northwest, which is characteristic of the Boland Terrane;
iv) Lithological similarities exist between the Bridgetown Formation and the metavolcanics of Riviera and Voëlvlei, both located in the Boland Terrane.

Most recently, the Bridgetown Formation was again placed in the Swartland Terrane (Rozendaal et al., 1999). The position of the Bridgetown Formation in the Swartland or Boland Terranes is therefore still uncertain.

The discrepancies with the currently accepted classification (SACS, 1980, Theron et al., 1992; Rozendaal et al., 1999) suggests that the present model requires either refining or replacing, and that the present lithological criteria on which the model is based are not capable of producing a classification that adequately explains the geology of the Malmesbury Group. The occurrence of rocks with similar lithologies and structure across the current terrane-bounding faults also suggests that the proposed boundaries between the terranes are incorrect.

3.4 Tectonic model

Hartnady et al. (1974) suggested deposition of the Malmesbury Group on a continental margin, with the different lithologies representing differing environments of deposition. The variation in the intensity of deformation between the three terranes was attributed by Hartnady et al. (1974) to reflect large-scale differences in the intensity or character of the strain. Dunlevey (1992) suggested that the metasedimentary rocks of the three tectonostratigraphic terranes are comparable to those seen along a classic continental margin. However, this was deemed to be an oversimplification and Rozendaal and Scheepers (1994; 1995) suggested, on account of the difference in structural intensity and granite emplacement, that considerable vertical displacement along the major fault zones had occurred. Gresse and Theron (1992) suggested that the Colenso and Piketberg-Wellington Fault Zones possible represent geosutures.

Geochemical characteristics of the Cape Granite Suite (CGS) and their areal extent in the Western Cape has been related to major subduction tectonics (Scheepers, 1990; 1995). The difference in structural intensity across the Malmesbury Group was attributed to vertical displacement of the domains relative to one another (Rozendaal and Scheepers, 1994; 1995; Rozendaal et al., 1999).

However, the structural intensity and metamorphic grade of the Malmesbury Group is uncharacteristic of a well-developed collision orogen. It has therefore been envisaged, that either a poorly developed oblique collision or strike-slip transpression occurred (Hälbich, 1988; Dunlevey, 1992; Rozendaal et al., 1999). The direction of

subduction, either beneath the South America or the South African plates has been disputed since the early models of the Saldania Orogeny were proposed, e.g. westward subduction (Rozendaal and Scheepers, 1994; Slabber, 1995; Rozendaal et al., 1999), or eastward subduction (Dunlevey, 1992; Scheepers, 1990; Siegfried, 1993).

As reviewed in Chapter 2.3, the three terranes possible represent allochthonous micro-plates accreted together during sinistral transpressional tectonics (Rozendaal et al., 1999).

3.5 Summary of the discrepancies

The discrepancies related to the classification of the Malmesbury Group may be summarised as follows:

i) The term 'Malmesbury Group' cannot be used to classify the rocks of the western branch of the Saldania Belt if the belt is supposedly underlain by three distinct tectonostratigraphic terranes;
ii) Lithological and structural similarities exist across the purported terrane boundaries;
iii) The actual location and existence of the terrane boundaries are disputed;
iv) The stratigraphic positioning of all the formations is currently not possible;
v) The direction of subduction during the Saldania Orogeny is disputed.

4 LITHOLOGY AND FIELD RELATIONSHIPS

Primary sedimentary features are preserved in nearly all the lithologies identified in the field area, except where the schistosity is very strong. Therefore, the rocks of the Malmesbury Group can be subdivided into two groups; schistose and non-schistose rocks depending on the presence or absence of a strong schistosity. As reference is made in this chapter to the various fabrics and deformation events presented in Chapter 5, a summary of the structural data is presented below in Table 4.1.

Table 4.1. Summary of the structural fabrics and deformation events identified during this study and explained in detail in Chapter 5.

Deformation event	Summary of fabrics and fold axes	
D_1	S_0	Bedding.
	F_1	Intrafolial, isoclinal folds.
	S_1	Planar fabric, axial planar to F_1.
	S_0/S_1	Transposition fabric (NW-SE).
	L_1	Stretching lineation.
D_2	F_2	Upright NNW-SSE folds.
	S_2	Axial planar cleavage.
	L_2	Stretching lineation (clasts) and crenulation lineation related to F_2.
D_3	F_3	NE-trending cross folds.
	L_3	Crenulation lineation related to F_3 .

4.1 Schistose lithologies

The schistose lithologies all have a penetrative foliation, which is characteristically developed as a schistosity and in some localities, where the grain size is smaller (e.g. Zoutkloof Quarry), as phyllitic cleavage (Fig. 4.1). These lithologies vary from dark

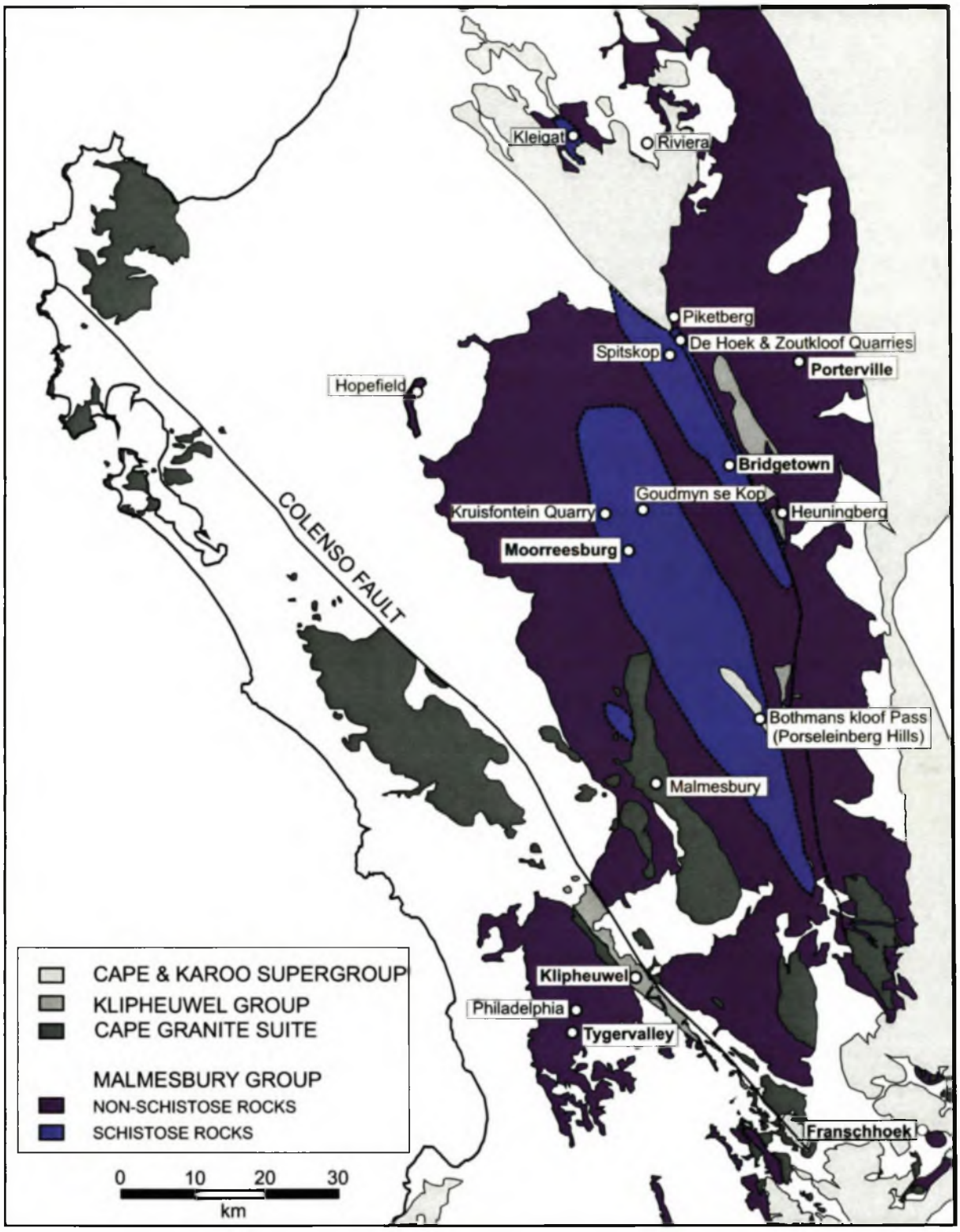

Figure 4.1. Simplified geological map of the Malmesbury Group, subdivided into schistose and non-schistose lithologies. Boundary between the schistose and non-schistose units is marked as a dashed line. Indicated on the map are the major towns and localities described in the text as well as the type localities of the present formations according to SACS (1980). Boundaries of the Cape Granite Suite, Klipheuwel Group, and Cape and Karoo Supergroups from Theron et al. (1992). See Appendix D, Map 4 for a detailed version of this map.

green, grey-green through to yellow-cream. All the rocks exhibit a sheen or lustre related to the phyllosilicate content. The schistose rocks may be subdivided based on their composition as described below.

4.1.1 Quartz-chlorite-muscovite-feldspar schists

The majority of the rocks of the schistose zone (Fig. 4.1) can be described as either quartz-chlorite-muscovite or quartz-muscovite-feldspar schist. These schists are mentioned in detail below and are located, from north to south, at Riviera, Spitskop, Kruisfontein Quarry, Goudmyn se Kop and in the Porseleinberg hills (Bothmaskloof Pass). Their localities are shown on Figure 4.1.

From the petrographic study of the schists at Spitskop, that typifies this lithology, it was possible to divide the schists into two units depending on their quartz content (Table 4.2). Schists that contain predominantly quartz (i.e. ≥50%) are classified as quartz-rich. They are composed of quartz, chlorite, muscovite, plagioclase and calcite, with accessory apatite, tourmaline, zircon and epidote. Schists that contain less than 50% quartz are classed as quartz-poor, and are mainly composed of chlorite and muscovite, with variable amounts of quartz and plagioclase.

Table 4.2. Classification of the quartz-chlorite-muscovite-feldspar schists at Spitskop and the surrounding area. Composition of differing schists based on modal analyses from thin section work.

Quartz-chlorite-muscovite-feldspar schists	
Quartz-rich (>50%)	**Quartz-poor (<50%)**
Quartz-chlorite-muscovite schist >60% qtz, 10-30% chl, 10-30% ms, 2-3% fspr	Muscovite-chlorite schist <20% qtz, <45% ms, 35% chl
Quartz-feldspar-muscovite schist 50-60% qtz, 20% fspr, 10-15% ms, <10% chl	Chlorite-muscovite schist 20-25% qtz, <40% chl, <35% ms

Further subdivisions were created for the quartz-rich schists depending on their variable feldspar content and for the quartz-poor schist depending on the dominance of chlorite and/or muscovite. In the majority of the quartz-poor schists, feldspar was

absent and they were, therefore, classified as muscovite-chlorite-quartz or chlorite-muscovite-quartz schists depending on the dominance of chlorite or muscovite.

In the Spitskop area (Appendix D, Map 2), the outcrops are composed of a monotonous series of quartz-chlorite-muscovite schists (Plate 4.1). The schists are green to olive-brown and exhibit a high lustre due to the presence of muscovite. These schists are predominantly composed of quartz (on average >60%), with varying amounts of chlorite and muscovite (Plate 4.2), the latter of which defines a pervasive foliation. Microscopically the P (phyllosilicate) domains are 0.2 mm to 0.6 mm wide. They are composed of chlorite and muscovite and are separated by Q (quartz) domains. Most of the schists contain only minor plagioclase (2-3% by volume) identified as albite (An_{01}; Table 4.3), thus distinguishing it from the quartz-feldspar-muscovite schist. The quartz-chlorite-muscovite schist forms layers within the quartz-feldspar-muscovite schist and varies in thickness from tens of centimetres to a few metres. Contacts between the two schists are irregular and do not appear to be sedimentological but tectonic. This feature is discussed further in Chapter 8. Similar schists to that identified in the Spitskop area are also found to the north-northwest, directly north of the Piketberg inlier in the vicinity of the farm Kleigat and to the south-southeast in the vicinity of the farm Bridgetown and the area in between the two farms (Appendix D, Map 4).

Additional outcrops of the quartz-chlorite-muscovite schists are also located to the north of Moorreesburg at Kruisfontein Quarry and Goudmyn se Kop (Fig. 4.1). Here the schist is less quartzitic in nature, containing predominantly chlorite (approx. 50%), white mica (< 25%), and varying amounts of quartz, which rarely exceeds 20-25%. The schist contains a strong penetrative foliation, is dark green and in places lime green related to weathering of sulphides. In such localities, the schists are often graphitic. Extensive veining ranging from a few millimetres to decimetres in thickness, are commonplace in these localities. The veins are laterally continuous and occur parallel to the main foliation. Occasionally the veins crosscut the foliation at angles less than 45°. Compositionally, the veins are dominated by quartz but the carbonate content can locally be high (up to 50%). Minor veins (both quartz- and carbonate

Plate 4.1. Typical example of the monotonous sequence of quartz-chlorite-muscovite-feldspar schists identified in the Spitskop area. Few sedimentary features within the schists can be identified apart from minor compositional changes seen as colour variations. Photograph taken looking northwest along the fold axes of F_2 kink folding.

a)

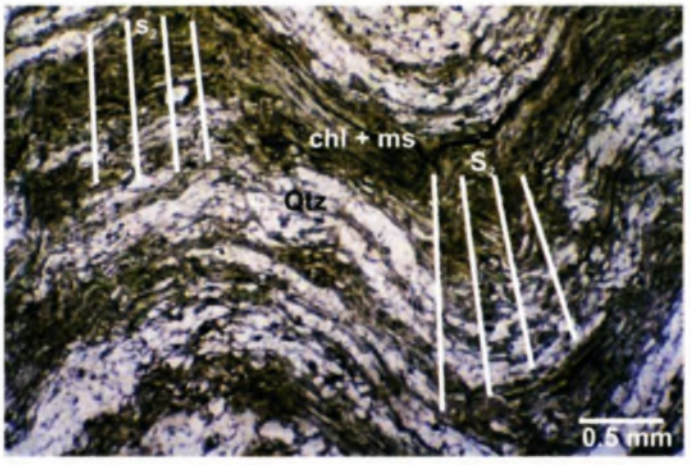

b)

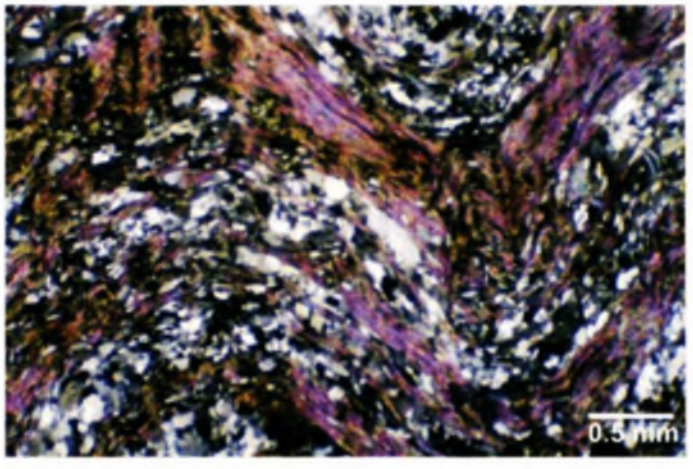

Plate 4.2. Quartz-chlorite-muscovite schist from Spitskop. Thin section orientated at right angles to F_2.
a) Folding of S_0/S_1 fabric by F_2 folding. Note the weak S_2 axial planar crenulation cleavage. Photomicrograph taken in PPL.
b) The same slide as in 4.2a but taken in XPL.

Table 4.3. The average composition of probed minerals from selected lithologies excluding chlorite (see Chapter 7.3). The analyses were undertaken at Rhodes University. Note, sd = standard deviation, n= number of analyses. Full data set presented in Appendix C, 1 to 4.

	Spitskop				Kruisfontein Quarry		Bridgetown Formation				Kanonkop			
	Plagioclase		Muscovite		Plagioclase		Plagioclase		Epidote		Plagioclase		Biotite	
	n=20	sd	n=37	sd	n=14	sd	n=11	sd	n=11	sd	n=13	sd	n=12	sd
MgO	0.05	0.09	1.38	0.65	0.01	0.02	0.30	0.62	0.06	0.14	0.01	0.01	9.04	0.30
SiO_2	68.19	1.11	46.43	2.03	67.78	2.95	68.16	2.96	43.28	18.79	62.69	2.39	34.40	0.84
Na_2O	11.69	0.48	0.59	0.24	11.72	0.66	11.67	0.69	0.02	0.02	9.31	1.22	0.17	0.06
Al_2O_3	20.08	0.44	35.02	1.77	19.56	0.89	19.38	0.88	19.53	6.20	22.53	1.81	18.63	0.65
K_2O	0.17	0.41	8.77	0.83	0.06	0.02	0.13	0.20	0.00	0.00	0.20	0.13	8.90	0.42
CaO	0.05	0.06	0.04	0.03	0.15	0.05	0.14	0.15	21.55	6.82	3.99	1.75	0.03	0.02
TiO_2	0.01	0.01	0.23	0.05	0.02	0.02	0.01	0.02	0.07	0.03	0.01	0.02	3.10	0.36
Fe_2O_3T	0.12	0.20	4.52	1.60	0.10	0.05	0.40	0.73	12.02	3.79	0.06	0.04	18.84	0.91
MnO	0.01	0.02	0.05	0.06	0.08	0.28	0.11	0.28	0.19	0.13	0.08	0.26	0.20	0.04
Cr_2O_3	0.02	0.02	-	-	0.02	0.02	0.03	0.03	0.02	0.02	0.01	0.01	0.03	0.03
O	0.00	0.00	-	-	0.00	0.00	0.00	0.00	0.00	0.00	0.00	0.00	0.00	0.00
Total	100.39	1.07	97.03	2.40	99.50	2.91	100.32	2.72	96.74	2.14	98.87	2.10	93.34	1.02
Mg	0.01	0.02	-	-	0.00	0.01	0.08	0.16	0.01	0.02	0.00	0.00	34.40	0.84
Si	11.89	0.09	-	-	11.92	0.20	11.91	0.22	3.54	0.93	11.22	0.33	0.17	0.06
Na	3.95	0.15	-	-	4.00	0.25	3.96	0.29	0.00	0.00	3.24	0.48	18.63	0.65
Al	4.13	0.10	-	-	4.06	0.20	4.00	0.19	2.00	0.63	4.75	0.36	8.90	0.42
K	0.04	0.09	-	-	0.01	0.00	0.03	0.04	0.00	0.00	0.04	0.03	0.03	0.02
Ca	0.01	0.01	-	-	0.03	0.01	0.03	0.03	2.01	0.64	0.76	0.34	3.10	0.36
Ti	0.00	0.00	-	-	0.00	0.00	0.00	0.00	0.00	0.00	0.00	0.00	18.84	0.91
Fe^{2+}	0.02	0.03	-	-	0.01	0.01	0.06	0.11	0.87	0.28	0.01	0.01	0.20	0.04
Mn	0.00	0.00	-	-	0.01	0.04	0.02	0.05	0.01	0.01	0.01	0.04	0.03	0.03
Cr	0.00	0.00	-	-	0.00	0.00	0.00	0.00	0.00	0.00	0.00	0.00	0.00	0.00
Cation Total	20.04	0.05	-	-	20.05	0.23	20.08	0.23	8.45	0.62	20.04	0.21	-	-
X (Si+Al)	16.01	0.02	-	-	15.98	0.07	15.91	0.11	-	-	15.97	0.05	-	-
Z (rest)	4.03	0.05	-	-	4.08	0.28	4.17	0.28	-	-	4.07	0.25	-	-
An	0.24	0.25	-	-	0.68	0.22	0.64	0.71	-	-	19.06	8.37	-	-
Ab	98.78	2.41	-	-	99.01	0.23	98.65	1.82	-	-	79.83	8.67	-	-
Or	0.98	2.44	-	-	0.31	0.09	0.71	1.14	-	-	1.11	0.74	-	-

Plate 4.3. Highly foliated quartz-chlorite-muscovite schist located in road cutting approximately 2 km west of the farm Goudmyn se Kop, near Moorreesburg. The schist contains abundant layer-parallel quartz veins associated with extensive chlorite alteration haloes, which make up to 30% of the rock volume. The boudinaged quartz veins identifies the deformation this rock has undergone during D_1. A later, boudinaged quartz vein crosscuts the fabric at an angle of approximately 40°. Photograph taken looking south, note hammer for scale in the centre of photograph.

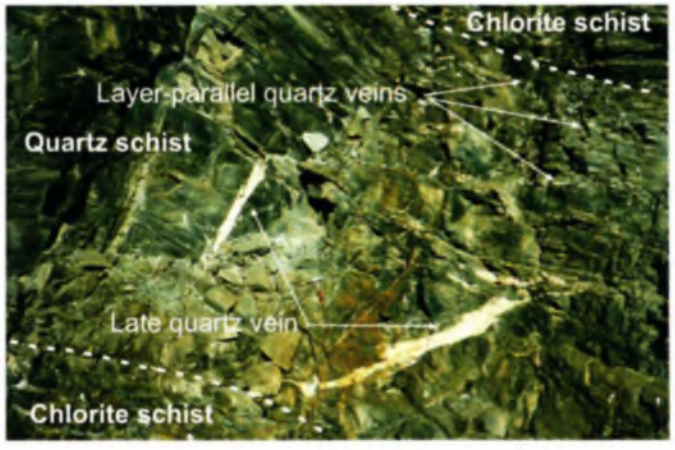

Plate 4.4. Section of the southern wall of Kruisfontein Quarry showing the interlayering of the quartz schist and the chlorite schist. Note the layer-parallel veining associated with the quartz schist. Further crosscutting veins are later extension fractures. Photograph taken looking to the south, rocks dipping approximately 45° to the southwest.

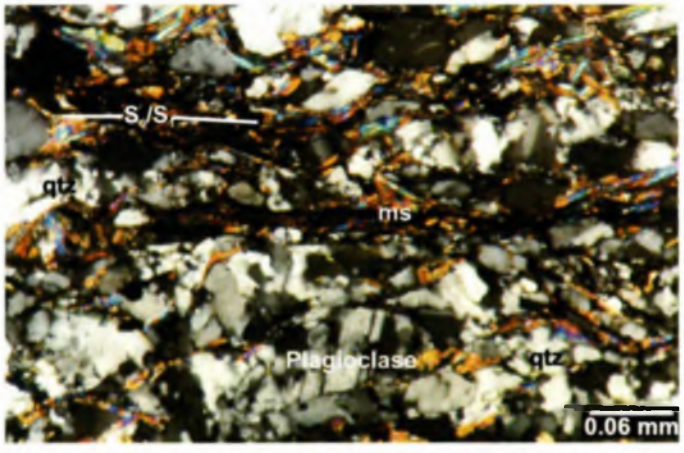

Plate 4.5. Quartz-feldspar-muscovite schist from 3 km north of Moorreesburg. Note muscovite defining the S_0/S_1 regional fabric and the extensive recrystallisation of quartz. Photomicrograph taken in XPL.

are surrounded by chlorite-rich haloes that are composed predominantly of chlorite (70%), muscovite (approx. 25%) and minor quartz defining a strong schistosity.

All schists described above are compositionally very similar, despite minor petrographic differences and characterise a wide spectrum of quartz-chlorite-muscovite-feldspar schists, rather than individually distinct mappable units across the present Swartland Terrane. This is emphasised in the Kruisfontein Quarry, where individual units have a varying thickness and are laterally discontinuous, and where contacts between lithological units are tectonic, not sedimentary. Plate 4.4 shows a section from the base of the quarry upwards. At the bottom a coarse-grained chlorite-muscovite schist (similar to that identified at Spitskop and as described above) is overlain by a grey-green quartz schist, approximately 3-4 m thick (see Chapter 4.1.2). The contact between the two units is sharp. Above the quartz schist is a chlorite schist containing an approximately 3 m thick zone containing bands (<15-20 cm) of grey to off-white quartzite alternating with bands of the chlorite-muscovite schist (<8 cm thick). The contact between the chlorite schist and the underlying quartz schist is sharp. In general, the chlorite schist is highly inhomogeneous becoming either more muscovite-rich and thus appears similar to the chlorite-muscovite schist described above or more graphitic. Where the chlorite schist is graphitic, it takes on a very dark green colour and contains abundant disseminated pyrite. A strong schistosity is present throughout this unit, but becomes more pronounced within the more muscovite-rich units of the chlorite schist.

Another chlorite schist is identified at the Riebeeck West Quarry, being composed of approximately 40% chlorite, 40% white mica and 20% quartz. Veining is prominent in this schist and occurs parallel to the main foliation. In general, the schist is dark green, but becomes lime green with red (iron) staining where weathering has taken place. In these localities the schist is similar to the chlorite schists identified at the Kruisfontein Quarry and described above. The grain size of the schist varies and some units can be described as phyllites rather than schists. Their colour is much lighter (green-silver) and is similar in appearance to the phyllites described below at the Zoutkloof Quarry (Fig. 4.1). Veining is extensive within these phyllites and occurs parallel to the foliation, composed of colourless quartz and quartz-carbonates, where

the phyllites occur in the vicinity of limestone units. The thickness of phyllite units varies from a few centimetres to decimetres, although the units always pinch out laterally over distances of 3-10 m.

To the north of Moorreesburg, the schists are more feldspathic. They are composed predominantly of quartz, plagioclase and muscovite, with only minor chlorite. The rocks are olive-green to brown, with a high lustre and more 'blocky' appearance. They differ from the schist in the Spitskop area mainly due to their slightly smaller grain size and the higher plagioclase (Albite- An_{02}) content that occurs as anhedral grains, or as part of the fine-grained matrix (Plate 4.5). The matrix consists of quartz, minute albite and muscovite, which occur in muscovite-rich domains with all the laths orientated in the same direction defining the foliation. The schist contains approximately 50-60% quartz and 20% albite, 10-15% muscovite and minor chlorite (<10%). Back-scatter electron SEM analysis of the quartz-feldspar-muscovite schists revealed the phosphates monazite (Ce, La, Th)PO_4 and xenotime (Y, Dy, Gd)PO_4. These two phosphates commonly occur as detrital minerals in sedimentary rocks (Overstreet, 1967).

The quartz-feldspar-muscovite schist is commonly associated with the muscovite-chlorite-quartz schist. The latter is particularly developed in zones of quartz veining (Plate 4.6) and exhibits a stronger foliation and lustre due to the increased white mica content. The colour is generally olive-green depending on the chlorite content. Compositionally, the schist is composed of muscovite (approx. 60%), chlorite (20-30%) and quartz (10-20%). The quartz-feldspar-muscovite schist is located across the Swartland Terrane, but is difficult to trace laterally across the field area. In outcrop, it often tapers out along strike within short distances. Contacts between the quartz-chlorite-muscovite and the quartz-feldspar-muscovite schists are irregular and do not appear to be sedimentological in nature (Chapter 8).

Two types of phyllites are observed in the Zoutkloof Quarry and can be distinguished from one another by their colour (Appendix D, Map 1). The first is a yellow-brown to silvery-green, highly foliated rock. It is often devoid of veins, but in places contains extensive veining parallel to and refolded within the main foliation. Within this

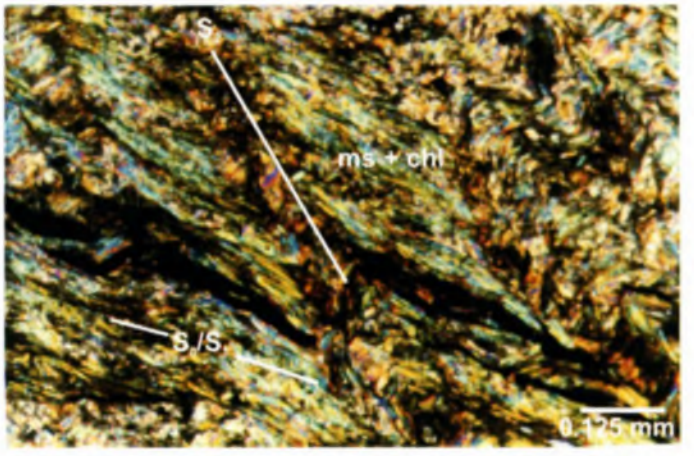

Plate 4.6. A typical example of a muscovite-chlorite schist located to the north of Moorreesburg. The muscovite and minor chlorite define the regional fabric (S_0/S_1) which has been folded during D_2. Photomicrograph taken in XPL.

Plate 4.7. Example of the quartz schist that characterises the Klipplaat Formation (Figure 4.2). The colour variation within the schist denotes bedding, that was folded during D_1. Photograph taken at Goudmyn se Kop.

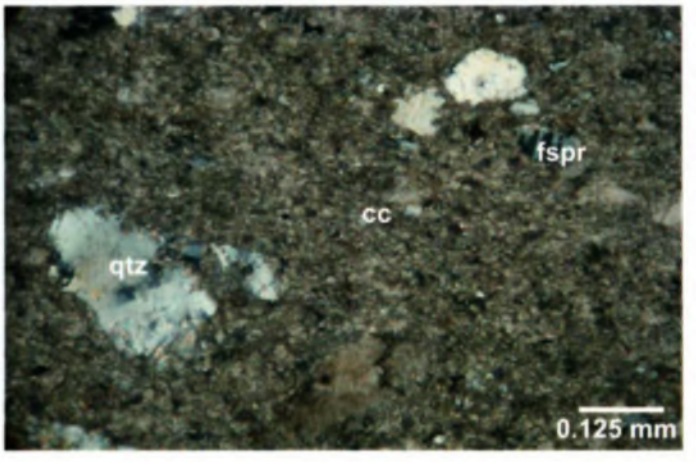

Plate 4.8. Limestone from the Zoutkloof Quarry, near Piketberg. The limestone consists of very fine-grained calcite with accessory quartz (showing undulose extinction) and plagioclase. Photomicrograph taken in XPL.

succession of phyllites, minor colour and grain-size variations can be discerned, identifying primary bedding features. The second phyllite is dark-green with some purple and lime-green staining, and is of a slightly larger grain size than the first phyllite. Ignoring the smaller grain size, the phyllite displays a prominent schistosity and, discounting the different grain size, it is very similar in appearance to the chloritic schists that characterises both the Kruisfontein and the Riebeeck West Quarries. Both of the phyllites occur as lenses up to 5 m long and 1-2 m wide within the limestones, parallel to and enclosed by the regional fabric. Contacts between the phyllite lenses and the surrounding schists are sharp and limestones adjacent to the contacts are often mylonitised. Quartz veining is also present within some units, and always occurs parallel to the regional foliation. Where veining occurs, the phyllite is very similar in appearance to the schists described in the Spitskop area. To the south, in the vicinity of the Porseleinberg Hills and Bothmaskloof Pass, a monotonous succession of grey-green quartz-chlorite schists occurs. Compositionally, only minor variations in the chlorite and muscovite content can be identified within these. Compositional variations are often associated with the occurrence of quartz veins, where an increase in chlorite and muscovite is related to an increase in veining.

Mineralogically, the schists are simple, being composed of quartz, muscovite and minor chlorite. Quartz grains (approx. 70%) are on average less than 0.5 mm long. All the quartz grains are elongated, and show preferred orientation, undulose extinction and subgrain formation. Muscovite is very fine-grained and its preferred orientation defines the main foliation in the schist. Both quartz and muscovite form Q and P layers respectively.

Although several different schists/phyllites can be described from across the Swartland Terrane, they are all similar in their mineralogical composition and appearance. Contacts between the schists are generally tectonic and units not only change dramatically in thickness but also taper-out along strike over short distances. Some contacts appear to be neither tectonic nor sedimentary and these are discussed further in Chapter 8. Outside the type localities described above, it is difficult to 'pigeon-hole' the schists into one of the stratotypes as the schists vary compositionally and fall between the compositions of the two main schists.

4.1.2 Quartz schists

Two types of quartz schist can be identified, distinguished by their colour; the first exhibits a greenish tint, the second is off-white to cream/yellow. The first type of quartz schist mainly occurs in Kruisfontein Quarry associated with the quartz-chlorite-muscovite and chlorite-muscovite schists and in the Riebeeck West Quarry associated with the chlorite schist. The schist is green-grey, with a sugary texture, composed predominantly of quartz (> 90%), muscovite (approx. 5%), and chlorite (approx. 5%).

Petrographically, the quartz grains (0.2 mm in diameter) are elongated, exhibit undulose extinction and have irregular grain boundaries. Minor muscovite and chlorite show a preferred orientation and together with elongated quartz grains define the foliation. Accessory minerals are carbonate, plagioclase (albite, An_{01}; Table 4.3) and pyrite. Minor quartz veins crosscut the fabric being composed of quartz showing straight grain boundaries and triple point junctions, indicating static recrystallisation. The schist forms a distinct unit within the succession of rocks identified at Kruisfontein Quarry. Contacts with the other schists are sharp and the thickness of the quartz schist units vary from a couple of centimetres to metres. All units are parallel to the main regional foliation.

Another quartz schist occurs at Spitskop, where it underlies a chert unit (Chapter 4.1.7). Although outcrops are scarce, this schist appears to grade over a vertical distance of 15-20 m into the quartz-chlorite-muscovite schist that characterises the Spitskop area, suggesting that this schist is a quartz-rich variety of the quartz-chlorite-muscovite schist. To the south, at Riebeeck West Quarry, more quartz schists are identified. These are off-white to grey in colour with an occasional greenish tint. The quartz schist shows minor colour variations representing primary sedimentary features that have been folded within the main foliation during regional-scale folding (Chapter 5). The schist is similar to the quartz schist at Kruisfontein Quarry and is even associated with a chlorite schist as identified in the Kruisfontein Quarry. Contacts between the different lithologies are sharp.

The second quartz schist forms a distinct lithology in the schistose zone. This schist unit was classified as the Klipplaat Formation (SACS, 1980). The schist varies from pale yellow-cream when fresh, to more of a dirty-brown when weathered (Plate 4.7). The quartz schist is texturally distinct from the other schists described above and for this reason was used as a marker horizon by earlier workers (e.g. Hartnady et al., 1974; Rabie, 1974a; Theron et al., 1992). However, due to the sporadic occurrence of outcrops and the laterally discontinuous nature of the units, its use as a stratigraphic marker appears limited. It can, however, be distinguished from the quartz schist of the Berg River Formation by its colour. In the Spitskop area, the quartz schist is a cream/yellow to light grey, highly foliated schist that often shows grain-size variation. It has a sugary texture and is resistant to weathering, forming positive ridges in the subdued topography of the Swartland.

To the northeast of Spitskop on the farm Klipplaat 219, the type locality of the Klipplaat Formation (SACS, 1980), the schist is well-developed and pale yellow, containing minor brown/black bands and grain-size variations, both denoting primary bedding. The quartz schist is well foliated and contains a strong layer-parallel cleavage as seen throughout all the schistose rocks. The quartz schist lies above the grey-green chlorite-muscovite schist, which varies in thickness between 1-2 m. Directly beneath this schist is a grey-blue, chert-like lithology. All contacts between the three units are sharp and the schists are highly foliated. An increase in veining within the quartz schists is accompanied by an increase in the muscovite (± chlorite) content, which imparts a greenish hue to the rocks. In these localities, the schist starts to take on an appearance similar to the muscovite and chlorite schists described in the Moorreesburg area.

4.1.3 Graphitic schists

The main occurrence of the graphitic schist is in the Zoutkloof and De Hoek Quarries (Fig. 4.1), although further lens-like occurrences of graphitic schists are identified to the north at Riviera and in the south at Spitskop (Fig. 4.1). In the Zoutkloof Quarry (Appendix D, Map 1), the schist is dark-grey to black, fine-grained and highly foliated. In thin section, it consists almost exclusively of graphite and minor pyrite (approx. 1 vol.%). Veining is extensive, being composed of quartz and carbonates, occurring

parallel to and crosscutting the main foliation. The schist is primarily located at the southern end of the quarry and is approximately 20 m thick. It occurs directly below the limestone unit (see section 4.1.4) and the contact between the two units is gradational, with the graphite content of the limestone increasing towards the graphitic schist lenses. The limestone often contains veining (quartz-carbonate) and is pervasively recrystallised with a mylonitic texture. However, the lateral thickness of the units varies greatly and can change in thickness from several metres to centimetres over a strike length of 10 m or so. Thin graphitic lenses between 10-30 cm thick also occur in the limestone unit, exhibiting a very strong foliation and being laterally continuous over only 1-2 m.

Graphitic schists are only intersected in the drill core in the Spitskop area. They occur as silver-grey, highly foliated schists, often containing visible pyrite mineralisation up to approximately 1 vol.%. The graphitic schist shows a maximum thickness with a maximum of 8 m, although, it is on average, only 2 m thick. Although the schist was intersected in numerous boreholes it occurred at different stratigraphic levels and could not be correlated from one borehole to another. This suggests that the schist possible occurs as isolated lenses throughout the stratigraphic column. Due to the character of the percussion drilling the actual nature of the contacts between the graphitic schist and the surrounding schists could not be determined. The graphitic schist is always located within approximately 10 m of the metavolcanic lithologies (section 4.1.5).

Further graphitic schists were identified to the southeast of Spitskop, associated with metavolcanic rocks of the Bridgetown Formation. These schists were described from drill core by Slabber (1995), as highly foliated, grey to dark-grey, with abundant quartz lenses and pyrite mineralisation. The light-grey graphitic schist contains quartz, graphite, muscovite, chlorite and actinolite. Further away from the metavolcanic rocks the schists become more graphite-rich (Slabber, 1995). Highly weathered, medium-grey graphitic schists were also located in outcrop. They contain a strong foliation and occur as laterally discontinuous (less than 3 m) minor lenses ranging in thickness from a few cm to 1-2 m. This graphitic schist is similar in appearance to the graphitic schist identified along strike to the northwest at Spitskop

and at the Zoutkloof and De Hoek Quarries. The contact between the graphitic schist and the surrounding highly foliated metavolcanic rocks is also sharp.

Graphitic schists were also located during drilling at Riviera, occurring as lenses varying in thickness between 1-4 m (Rozendaal et al., 1994). These lenses occur together in a horizon between 20-30 m thick. The schists are dark-grey to black, medium-grained with a strong foliation, containing visible pyrite mineralisation. Contacts between the graphitic schist lenses and the surrounding metasedimentary rocks (quartz-chlorite schists) are sharp and occur parallel to the main foliation. The graphitic schists at Riviera are similar in appearance and composition to the graphitic schists at Zoutkloof and De Hoek Quarries, located 25 km to the south.

4.1.4 Limestones

The main occurrence of limestone is at the Zoutkloof and De Hoek Quarries and further south at the Riebeeck West Quarry. Minor occurrences were also intersected during drilling at Riviera, approximately 30 km north of De Hoek and at Spitskop, approximately 5 km south of De Hoek (Fig. 4.1).

The limestone at the Zoutkloof and De Hoek Quarries is known as the De Hoek Member, being grey to dark-grey in colour, fine-grained and forming beds up to 40 cm thick parallel to the regional foliation (Appendix D, Map 1). It is composed predominantly of calcite, with minor quartz and plagioclase (Plate 4.8). The average chemistry of the limestone is presented in Table 4.4 and is geochemically very similar to the limestone at Riebeeck West Quarry. The present thickness of the limestones within the Zoutkloof Quarry is 60-70 m. Commonly the beds are not laterally continuous and can only be traced for up to approximately 30 m along strike. The bed thickness also varies significantly from 30 cm to 2 cm over a 1 m strike. Beds are often boudinaged and numerous examples show isoclinal folding within the regional foliation identifying bedding transposition. Thin (<10 cm), grey shale units are often intercalated with thinly bedded limestone units. These shales are strongly foliated.

At numerous localities, these schist units occur as metre-scale boudins, separated by quartz-carbonate necks and surrounded by limestone. In highly strained zones, the

Table 4.4. Average chemistry of the limestone mined at the De Hoek/Zoutkloof Quarries near Piketberg and the Riebeeck West Quarry, and the dolomite at the Bridgetown Quarry. Chemistry is kindly provided for the limestone by PPC Cement (Langenhoven, pers. comm., 2002) and for the dolomite by Bridgetown Quarry (Katzeff, pers. comm., 2002).

	De Hoek & Zoutkloof Quarry	**Riebeeck West Quarry**	**Bridgetown Quarry**
	Limestone	Limestone	Dolomite
SiO_2	7.3	6.2	0.1
TiO_2	0.1	0.1	-
Al_2O_3	1.8	1.3	0.2
Fe_2O_3T	0.8	0.8	0.4
MnO	0.0	0.0	-
MgO	0.8	0.6	21
CaO	48.5	50.0	31
Na_2O	0.2	0.1	0
K_2O	0.4	0.2	0
P_2O^5	-	0.1	0
H_2O-	-	-	-
LOI	39.9	40.0	46.5
Total	99.8	99.4	99.2

limestone is fine-grained with a very strong foliation defined by elongated and orientated recrystallised calcite. The well-foliated limestone contains abundant veins parallel to the foliation, which have been deformed to produce intrafolial folds within the main regional fabric (Chapter 5.2). In places, the limestones are developed as mylonites. Where the limestone forms a succession of beds containing few or no shale units, only a weak foliation is observed. These beds are often thick (up to 50 cm) and characterised by extensive en-échelon and crosscutting veins. These veins reduce in number with an increase in shale units. Contacts between the limestone and the schists are predominantly sharp, though some intercalations are locally developed. The limestone is laterally continuous along strike and is quarried approximately 2 km to the southeast of Zoutkloof Quarry. Further along strike, the limestone sporadically crops out for the next 2-3 km and has also been intersected during drilling (Langenhoven, pers. comm., 2002).

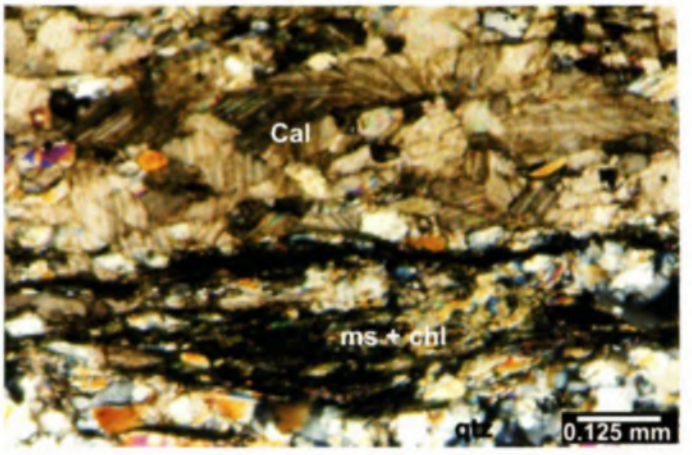

Plate 4.9. Marly limestone from Spitskop intersected during drilling at a depth of approximately 80 m below the peak of Spitskop Hill. Muscovite and chlorite define the strong foliation (S_0/S_1) and calcite occurs as elongated and orientated grains. Photomicrograph taken in XPL.

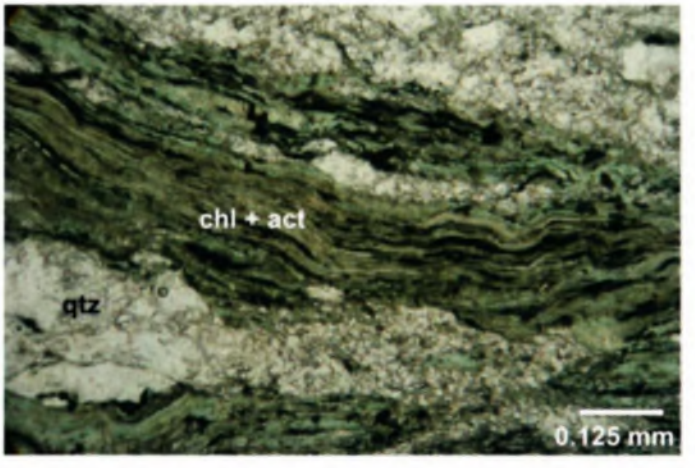

Plate 4.10. Metavolcanic unit from the Bridgetown Formation, 3 km to the east of the farm Bridgetown. The metavolcanic rock is composed of chlorite, epidote, quartz, actinolite, and albite. All the metavolcanic rocks of the Bridgetown Formation exhibit a strong schistosity. Photomicrograph taken in PPL.

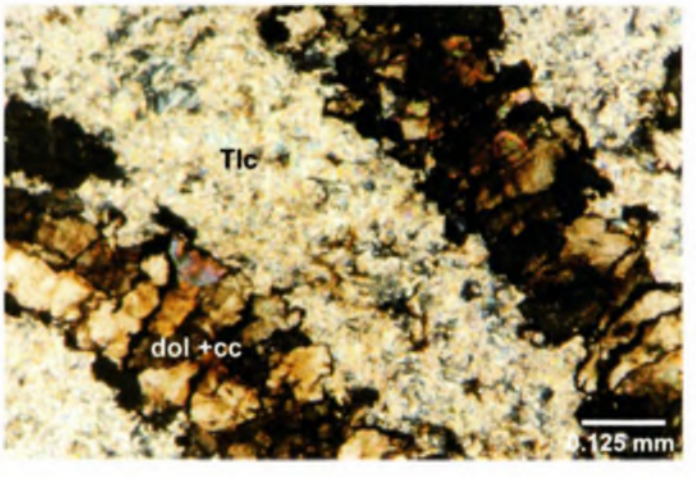

Plate 4.11. Talc-carbonate schist from the Spitskop area, showing randomly orientated talc crystals cross cut by dolomite and calcite veins. Photomicrograph taken in XPL.

A grey marly limestone unit was intersected by drilling at a depth of approximately 80 m below the peak of Spitskop, situated approximately 5 km south of the De Hoek Quarry. The thickness of the limestone layer is approximately 10 m, although it varies greatly from 5 to 1 m over a strike of 10 m, and can be traced laterally across boreholes for 150 m. The contact of the limestone and the surrounding schist was not observed, due to the nature of the percussion drilling. The limestone consists of mainly recrystallised calcite with minor quartz and euhedral pyrite. The calcite crystals vary in size, shape, and orientation and exhibit prominent twinning (Plate 4.9). The crystals are interlocked, occasionally producing triple point contacts, suggesting static recrystallisation. Tiny pyrite grains (<0.1 mm across) are located throughout the limestones and are predominantly euhedral in shape. In thin section, muscovite and chlorite occasionally occur and define the foliation. Calcite situated between the microlithons has a grain-shape preferred orientation parallel to the chlorite and muscovite. The chemical composition of the limestone at Spitskop is discussed in Chapter 6.

Other major limestone units are exposed some 35 km along the regional strike to the southeast of Zoutkloof. Here the limestone (see Table 4.4 for chemistry) is currently being quarried at the Riebeeck West Quarry. Two types of limestone can again be identified: the first is a more massive limestone occurring in beds up to 2 m thick. The limestone is light- to medium-grey and contains calcite veins crosscutting the beds in variable orientations. Even in the more massive beds, the limestone has a foliation identified by elongated and orientated calcite crystals. The second is a highly foliated medium- to dark-grey limestone often intercalated with schist units. Veining within this limestone is often layer parallel and shows evidence of isoclinal, intrafolial folding. In both limestone types, bed thickness varies and beds cannot be traced laterally over long distances. The contact between the limestone and the overlying schist is sharp, dm-wide and mylonites are developed in the limestones beneath the contact. At these localities, evidence of duplexing and thrusting is seen in the limestones (Chapter 5.2). The limestones identified at Riebeeck West Quarry are macroscopically similar to those at the Zoutkloof and De Hoek Quarries some 60 km to the north-northwest.

4.1.5 Metavolcanic rocks

The main metavolcanic occurrence is located in the area surrounding the farm Bridgetown (Fig. 4.1), and was studied in detail by Slabber (1995) and for this reason will only be mentioned briefly here. The main outcrop at Bridgetown was classified as the Bridgetown Formation (e.g. SACS, 1980). The metavolcanic rocks are represented by a series of dark-green to olive-green/brown chlorite-epidote-actinolite-quartz-albite (An_{01}) schists (Table 4.3). All schists are strongly foliated in core and thin section. Outcrops are generally highly weathered and primary minerals are altered to clays. Chlorite and actinolite define the foliation and quartz and albite are often elongated and orientated with the main foliation (Plate 4.10). Calcite exhibits grain-boundary migration-recrystallisation and deformation lamellae evidenced by the fine and tapering lamellae. Epidote may form porphyroblasts and is wrapped around by the foliation, indicating that many of these units underwent shearing. In general, sulphides are elongated in the direction of the foliation. Dolomite (oolitic, massive) with jasper and chert units, are associated with the metavolcanic rocks (Slabber, 1995). The massive dolomite at the Bridgetown Quarry and surrounding area is very pure (see Table 4.4; Katzeff, pers. comm., 2002). The stratigraphic thickness of the metavolcanic units is unknown, but drilling documented by Slabber (1995) indicating a minimum thickness of 30 m.

Directly along strike to the northwest of the main metavolcanic body, small metavolcanic lenses are exposed at Spitskop. The metavolcanic units include talc-carbonate schists and chlorite-feldspar-quartz schists that occur as lenses within the quartz-chlorite-muscovite schist. From drilling, the metavolcanic rocks appear to occur as 1-2 m thick lenses, which cannot be traced between more than two boreholes (50 m apart). In some boreholes (e.g. SK47), several lenses are intersected over approximately 10 m or less. The talc-carbonate schist (Plate 4.11) was only intersected during drilling, although Slabber (1995) correlated this schist in outcrop with the chlorite-feldspar-quartz schist. However, because of the high degree of weathering, this could not be confirmed. The talc-carbonate schist is composed of talc (up to 60%) that occurs either as fine-grained radiating or sometimes randomly orientated crystals. The dolomite (<40%) occurs either as veins or as patches within

the talc. Minor chlorite (<10%) occurs as laths throughout the schist and pyrite is preferentially concentrated in the carbonates.

The chlorite-feldspar-quartz schist is exposed to the southeast of Spitskop (Plate 4.12). It occurs within the quartz-chlorite-muscovite schist, but the deep weathering of the rocks does not allow for further stratigraphic positioning. It is highly weathered, dark-green in appearance and strongly foliated. Plagioclase is common and occurs as porphyroblasts that are altered to muscovite, epidote and carbonates. The plagioclase occurs as albite, which varies in appearance from unaltered to highly altered and fragmented crystals, with minor euhedral alkali feldspar inclusions. Albite porphyroblasts occur in a matrix of chlorite and fine-grained plagioclase. Several highly-weathered outcrops of carbonate-bearing rocks were also identified in the Spitskop area. Their protolith could not be discerned due to the intense weathering, but could represent additional talc-carbonate bodies.

Numerous metavolcanic bodies were intersected during drilling of Riviera some 30 km to the north of Spitskop. These bodies intersected during drilling vary in thickness from 1 to 20 m. A correlation of the metavolcanic units between boreholes was not possible. The metavolcanic units are composed of chlorite, quartz, calcite, epidote, hornblende and opaques (Plate 4.13). All these minerals define the strong foliation and epidote often occurs as porphyroblasts that have been rotated within the foliation. Hornblende, however is randomly orientated, and only occurs in drill core samples in close proximity to the Riviera pluton. This suggests that the occurrence of hornblende is related to contact metamorphism and not to regional metamorphism. The opaques (pyrite and graphite) are euhedral to sub-euhedral and are elongated in the direction of the fabric. Contacts between different metavolcanic bodies and also between the metavolcanic units and metasedimentary schists are sharp and occur parallel to the main foliation. The metavolcanic bodies are mineralogically similar to the metavolcanic rocks of the Bridgetown area.

4.1.6 Biotite-feldspar schist

An isolated outcrop of a biotite-feldspar schist occurs next to the farm Kanonkop along the R45. The presence of biotite in this schist makes this unit quite unique

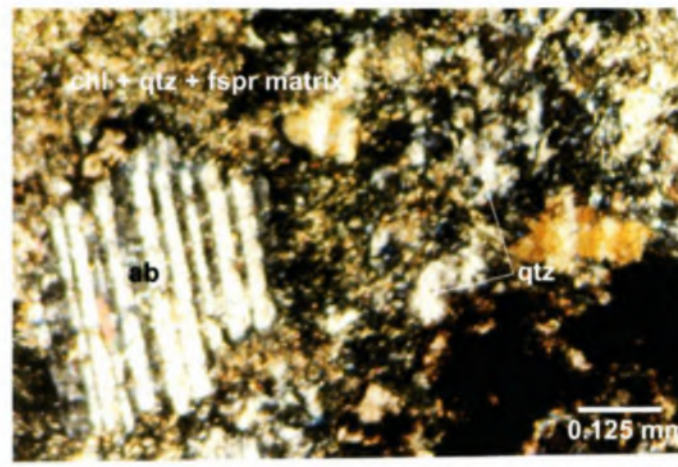

Plate 4.12. Chlorite-feldspar-quartz schist from Spitskop, composed of a fine-grained chlorite and feldspar matrix, with large euhedral albite crystals showing minor alteration to sericite. Photomicrograph taken in XPL.

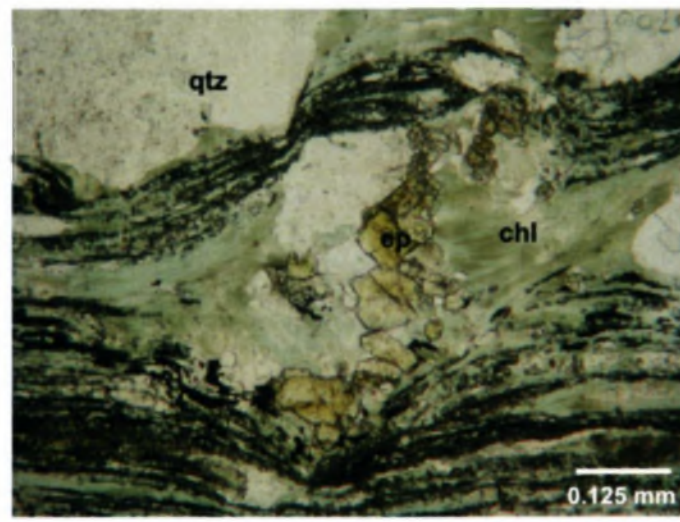

Plate 4.13. Quartz-chlorite-epidote schist from Riviera intersected during drilling. All the metavolcanic units exhibit a strong schistosity (S_0/S_1) which characterises the rocks of the schistose zone. Opaques along the foliation planes emphasise the mylonitic foliation. Photomicrograph taken in PPL.

Plate 4.14. Biotite-feldspar schist from near the farm Kanonkop, northwest of Malmesbury. Strong banding of the minerals into biotite and muscovite (dark bands) and plagioclase and quartz (light bands) is evident and defines the S_0/S_1 foliation of the rock. F_2 folds verge towards the southwest. Photograph taken looking towards the southeast.

within the chlorite-muscovite-dominated schists of the Saldania Belt. The schist is light to medium purple-brown, depending on weathering, and exhibits a high lustre. It is composed of biotite, plagioclase, muscovite and quartz. The schist contains a strong foliation defined by the banding of the minerals into P (biotite and muscovite) and Q (quartz and plagioclase) dominated layers (Plate 4.14). The quartz grains vary in size, with a marked decrease in grain size in zones where there is an increase in biotite. All quartz grains show evidence of preferred orientation and elongation, as well as grain-size reduction, deformation lamellae and the formation of subgrains. The biotite varies in colour from pale brown to very dark brown related to its varying TiO_2 content (2-3.5 wt.%, Table 4.3). Laths vary in size and are up to 2-3 mm long, showing preferred orientation and defining the strong foliation of the rocks. The plagioclase content is variable and ranges from only a few percent up to 30%. The anorthite composition of plagioclase varies from An_{01} to An_{22}. This differs markedly from the almost pure albite compositions of the quartz-chlorite-muscovite schists and an anorthite-rich composition of plagioclase is indicative of a higher metamorphic grade compared to the other schists (see Chapter 7.1). Many of the plagioclase grains have been severely saussuritised and can now only be distinguished by the 'cloudy' appearance in plane-polarised light (Plate 4.15).

4.1.7 Banded Chert

A 'banded chert' unit occurs on top of Spitskop and is at its maximum approximately 5 m thick. The bands within the chert are approximately 1 cm wide consisting of alternating bands of light- and dark-grey quartz interlayered with fine-grained magnetite bands giving the red-brown colour to the chert (Plate 4.16). A very strong foliation in the chert is defined by the preferred grain orientation of quartz crystals showing evidence of ductile deformation and dynamic recrystallisation. A strong lineation is defined by quartz rodding. Fine-grained muscovite, biotite and extensive iron-hydroxide staining along fractures is also present. Slabber (1995) identified subhedral to euhedral chromitic spinel grains consisting of a red-brown core surrounded by a black opaque rim. The contact between the chert and the underlying quartz-rich schist is sharp, and this schist grades over 15-20 m into the quartz-feldspar-muscovite schist that characterises the Spitskop area. Cross-cutting

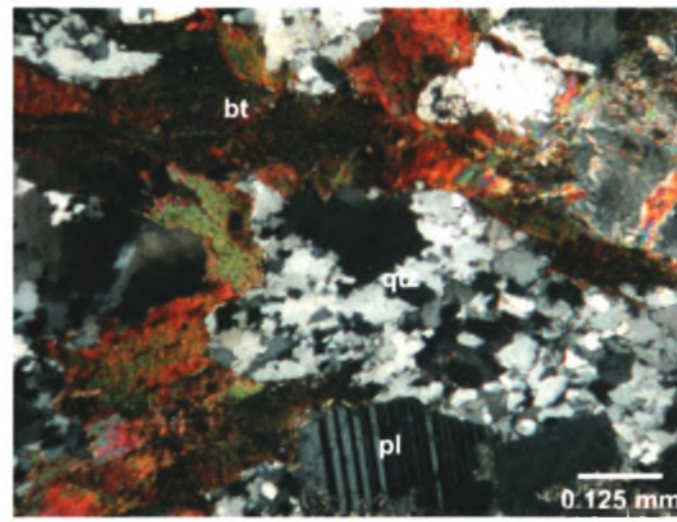

Plate 4.15. Biotite-feldspar schist from the road cutting along the R45 outside the farm Kanonkop. The schist is composed of biotite, plagioclase and quartz, all defining the foliation in the rock. Photomicrograph taken in XPL.

Plate 4.16. Strongly foliated iron-rich 'chert' outcrop located on the southwestern slope of Spitskop Hill. Steeply dipping milky-white, northeast-southwest trending quartz veins crosscut the foliation. Photograph taken looking towards the northwest.

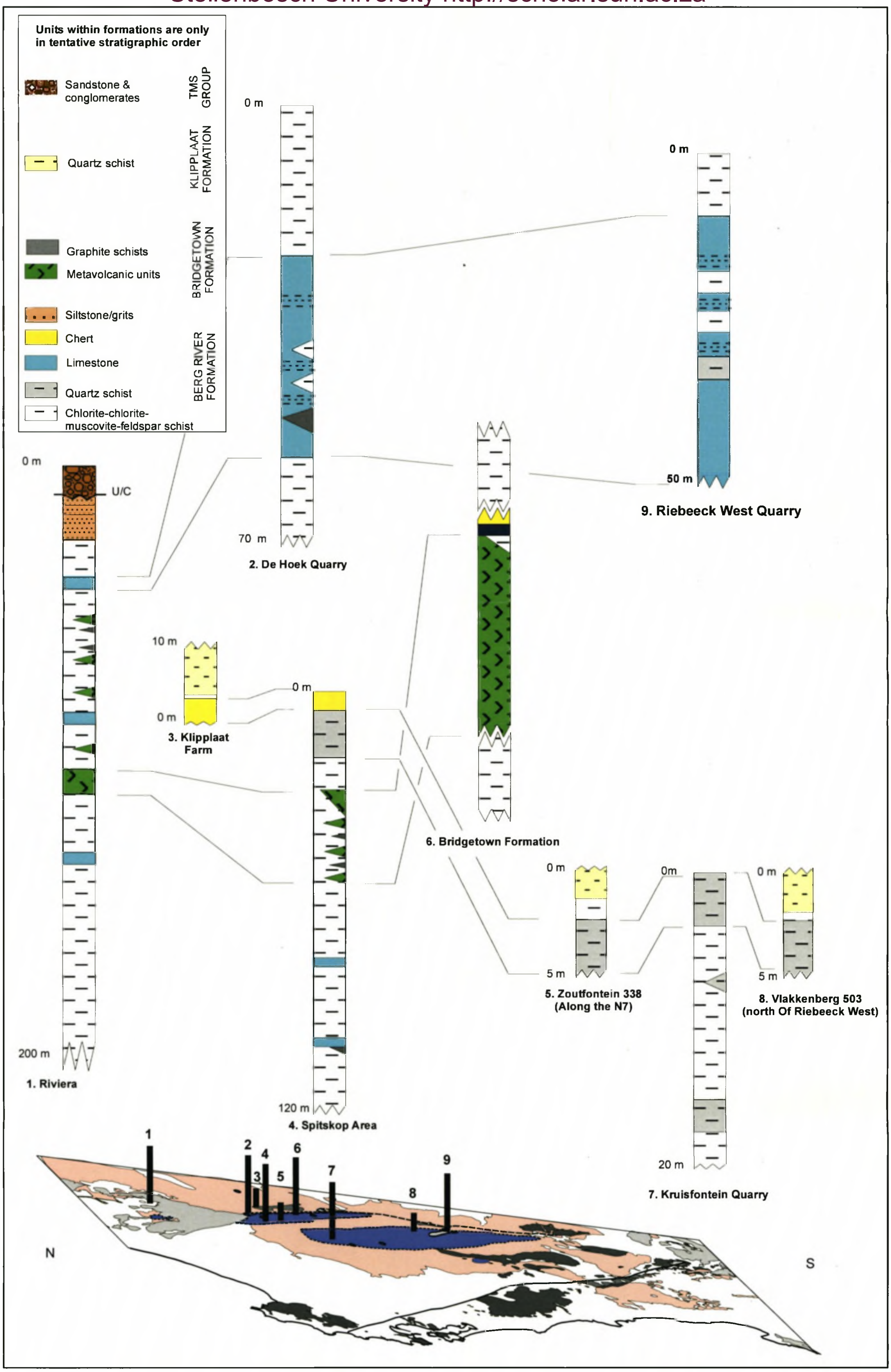

Figure 4.2. Simplified stratigraphic columns for the major outcrops described in the schistose rocks, based on field observations and where available, drilling information. Note that although similar (possibly the same) lithologies occur at different localities, the thickness of the units varies considerably, making correlations only tentative at best.

the strong foliation are milky white quartz veins varying in size from a few millimetres to centimetres, though most veins are laterally discontinuous.

4.1.8 Stratigraphic correlations

A stratigraphic correlation of individual units between outcrops located over 20 m apart is very difficult due to two main reasons. Firstly, on the outcrop scale the majority of the lithologies are similar. Secondly, where the distinct lithological units are present, individual units varying in thickness and units taper-out over only a few metres, making the units difficult to trace (Fig 4.2). The different lithologies described above are commonly lensoidal in shape and contacts between different units are tectonic and not sedimentary.

The presence of tectonic contacts between lithologies is also manifested on a regional scale. The location of the graphitic schists, limestones and metavolcanic rocks identifies a linear northwest-southeast feature. All three lithological units are enveloped by and orientated parallel to the main fabric in the Malmesbury Group. Comparison of the thickness of different lithologies described from the major outcrops situated along strike from one another highlights the considerable thickness variation (Fig. 4.2). Therefore, large-scale correlation between outcrops located kilometres apart is near impossible and impractical. Stratigraphic correlation is further complicated by the isolated nature of the major exposures. Finally, since the lithologies are relatively monotonous with often only minor compositional contrasts, the tracing of lithologies along strike and the comparison with each other have to be tentative at best, suggesting that a lithostratigraphic subdivision is unsuitable.

4.2 Non-schistose lithologies

The non-schistose units, in general, can be described as a series of greywackes, shales, siltstones, quartzites and conglomerates, which vary in colour, grain size, and composition both laterally across the region and through the stratigraphic column. The non-schistose lithologies identified lying directly above the schistose lithologies are characterised by conglomerates and quartzitic grits interbedded with shales. These shales become more dominant further up in the succession. A simplified

stratigraphic column is presented in Figure 4.3 highlighting the general correlations of units between Moorreesburg and Piketberg areas.

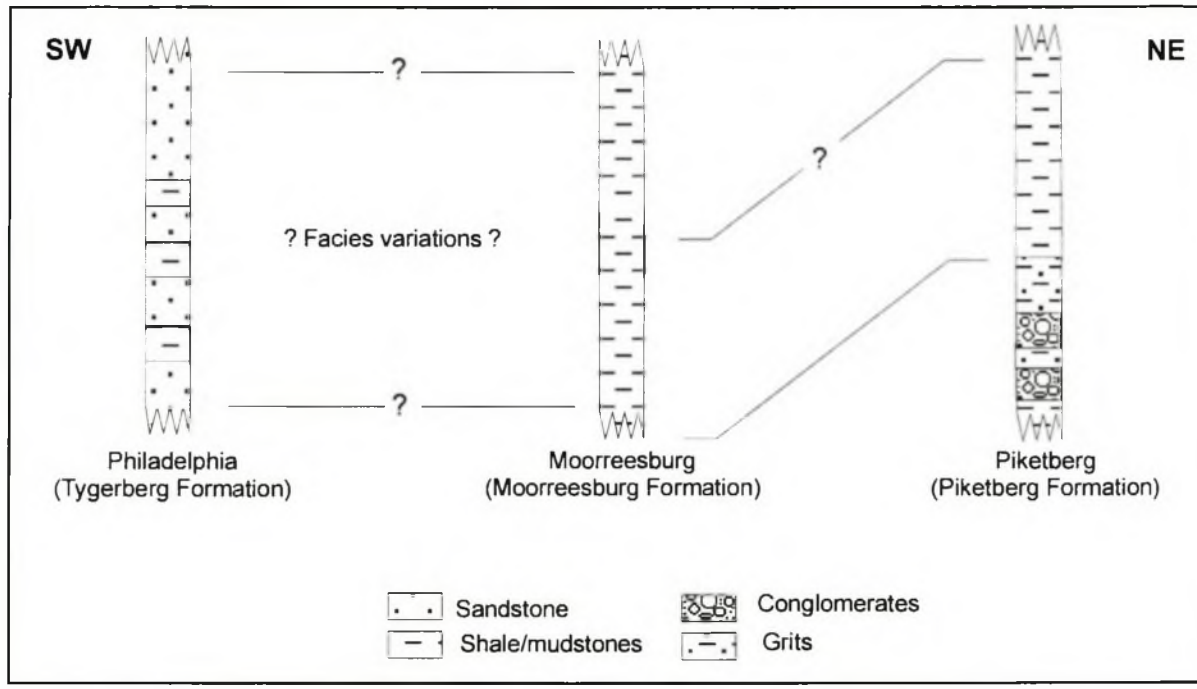

Figure 4.3. Simplified stratigraphic columns (not to scale) of the non-schistose rocks showing the approximate correlation of the different sedimentary units across the field area. Stratigraphic columns based on Von Veh (1983) and recent fieldwork (Appendix D, Map 4).

Due to poor outcrop, the contact between the non-schistose and schistose rocks is nowhere exposed in the field area. However, where outcrops allows the location of the contact can be narrowed-down to an approximately 200 m wide zone, e.g. along the N7, approximately 3 km south of Piketberg. Around the farm Spitskop and the town Piketberg, the first outcrops of the non-schistose rocks lying spatially above the contact zone are composed of conglomerates and grits.

The greywackes and shales vary in grain size both laterally across the field area and up through the stratigraphic column. Towards the west, in the Tygerberg Terrane, greywacke and sandstone beds are more pronounced, identifying a marked contrast in sedimentary style to the shales and mudstones of the Swartland and Boland areas.

4.2.1 Conglomerates and grits

The main occurrence of conglomerates and grits is in the vicinity of Piketberg (Piketberg Formation; SACS, 1980). Here a series of quartzitic grits, shales and minor conglomerates can be identified (Fig. 4.4; Appendix D, Figs. 1 & 2). To the north of Piketberg along the N7, grit beds vary in thickness from 30 cm up to approximately 2 m, containing quartz clasts ranging in size from 1 mm to 40 mm.

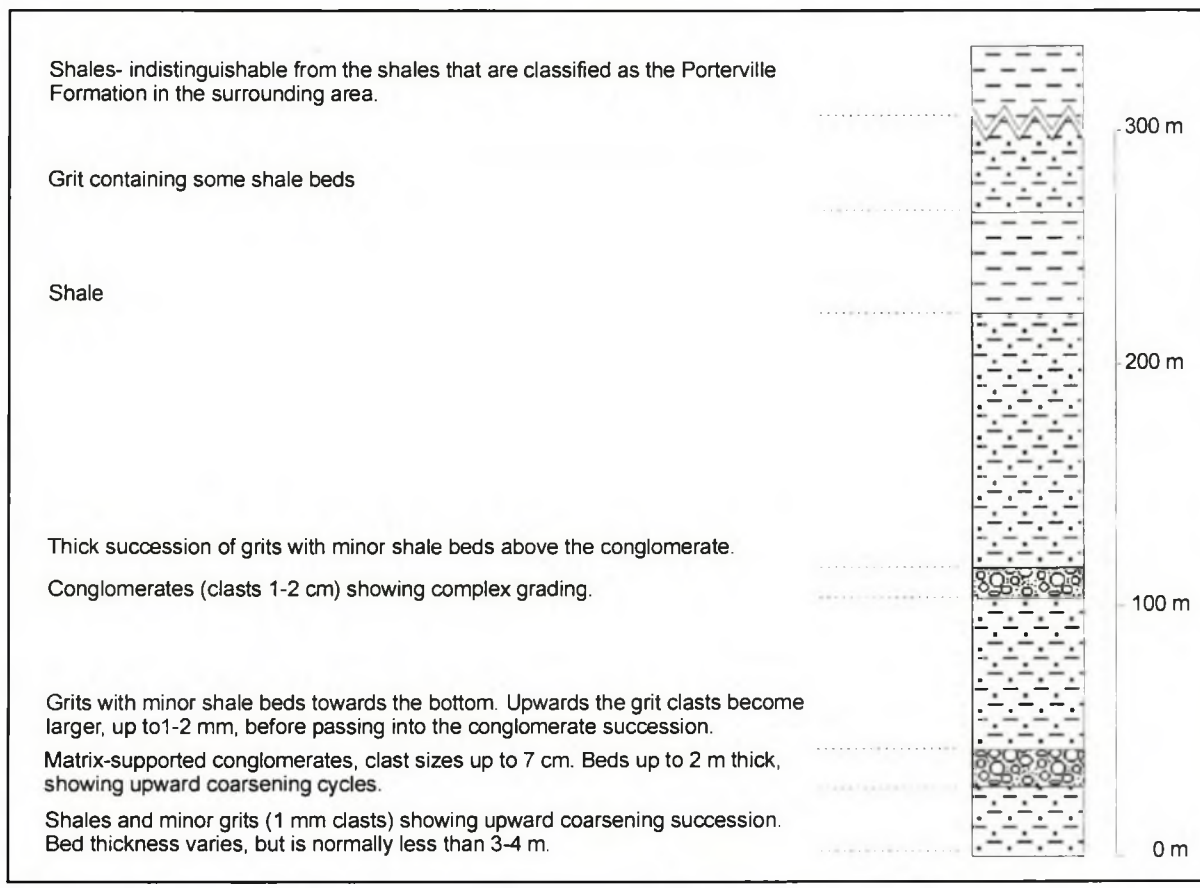

Figure 4.4. Simplified stratigraphic column of the Piketberg Formation, based on road cuttings around the town of Piketberg (type locality). Road cuttings are presented in Appendix D, Figures 1 and 2.

Clast shapes vary and range from angular to rounded, though generally, the larger the clasts the greater the angularity. Sorting within beds also varies significantly from poorly sorted to sorted, and both normal and reverse grading is developed. Shale units are generally fine grained and show a sharp contact with the overlying bed, but gradually become coarser grained over 20 to 30 cm, where they pass into a fine-grained (<2 mm) grit. Shale beds vary in thickness and may reach up to 0.5 m,

although often showing grain-size grading as described above. The thicker shale units (>40 cm) are often separated by minor grit beds (1-5 cm thick).

Conglomerate beds are up to 50 cm thick. They contain sub-rounded to rounded, up to 6 cm long quartz clasts. The clasts are elongated in shape and are all orientated northwest-southeast parallel to the sub-vertical bedding (Plates 4.17 & 4.18). The conglomerates are well sorted, matrix supported, and show both normal and reverse graded bedding. Towards the northeast around the train station Pools, shale/greywacke beds become more dominant and eventually no more grit or conglomerate beds occur. The lithologies around Pools are similar in appearance to the greywackes described further to the east around Porterville, indicating that the conglomerates/grits grade upwards and laterally into the greywackes/shales described earlier.

North of Piketberg, near the farm Dezenhoek and west of the road cutting profiles described above, grit beds supported in a pale-green shaly matrix contain sub-rounded to angular quartz clasts up to 2 cm long. Beds vary in thickness between 20-50 cm. Contacts between beds are sharp and often separated by 6-7 cm thick green shales.

Approximately 5 km to the north of Dezenhoek, the shale units become more dominant. To the north-northeast of the Piketberg Inlier in the area around Duikerfontein, up to 30 cm thick feldspathic grit beds with clasts up to 15 mm long (average 4-5 mm) are interbedded with minor, 2-3 cm thick shale units. Conglomerate beds become more dominant towards the south of Duikerfontein. Clasts are predominantly quartz, either milky white vein quartz or smoky grey. Due to the weathered nature of the outcrops, it is difficult to identify the original protolith of the other clasts. They are now represented by a series of clays ranging from white to red-brown, the red colour being due to limonitic staining. In some beds the clay pellets can become prominent and represent approximately 50% of the clasts. Detailed cross sections of the Piketberg Formation are presented in Appendix D, Figure 2. More outcrops of grit beds are located to the south of Piketberg for approximately 20 km. The grits are similar in appearance to those identified around

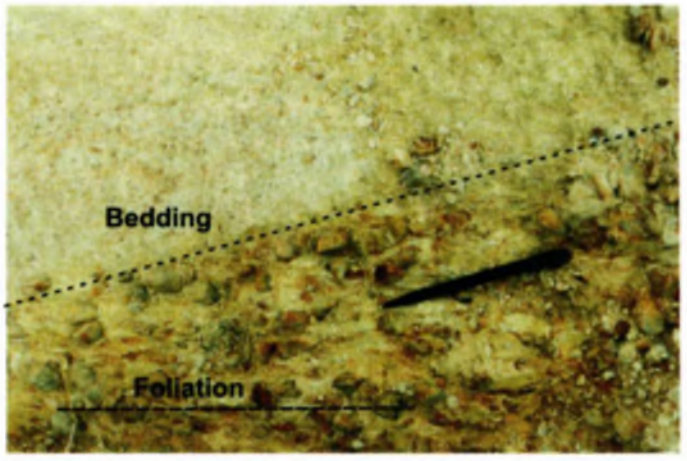

Plate 4.17. Matrix-supported conglomerate grading over 2-3 cm into a quartz grit. Beds located in road cuttings along the N7 national road approximately 3-4 km north of Piketberg. These lithologies are ascribed to the Piketberg Formation (e.g. SACS, 1980). Photograph taken looking east. Note the alignment of quartz clasts in the conglomerates (northwest-southeast) imparts a foliation on the rock.

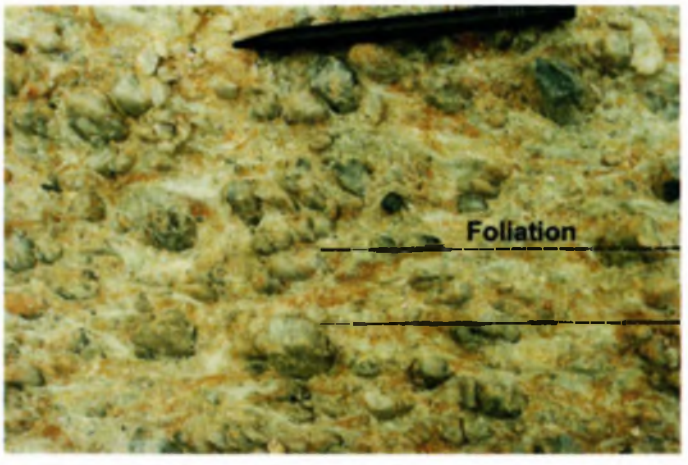

Plate 4.18. Example of matrix-supported conglomerate from the same location as pictured above. Clasts are semi-rounded and composed of smoky-grey and milky-white quartz, indicating a quartz-rich local source for the clasts (probably derived from quartz veins). The clasts are elongated defining the lineation, L_2.

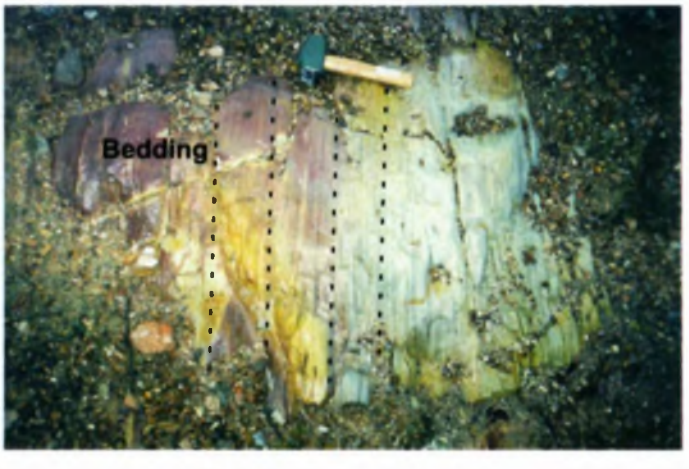

Plate 4.19. An example of a highly weathered outcrop of shale, approximately 10 km west of Porterville. This outcrop typifies the quality of the outcrops in much of the field area. Colour and grain-size variations identify the original bedding, and weathering of the surface allows strike and dips of bedding to be established. Photograph taken looking northwest.

Piketberg, although clasts size is commonly smaller, being less than 1 cm long. Conglomerate beds are only minor, being less than 20 cm thick. Other occurrences of grits and conglomerates were not identified across the Swartland area.

Further outcrops of conglomerates occur around the town of Franschhoek, where conglomeratic outcrops are assigned to the Franschhoek Formation (SACS, 1980). Although this formation does not fall within the study area, a brief summary is included to allow comparison with the other conglomerates that occur within the field area. The better outcrops of the formation occur in the Franschhoek Pass, although most exposures are deeply weathered. Here, conglomerates prevail, with clasts ranging in size from a few mm (grits) up to 3-4 cm. The clasts are orientated and elongated, and supported within the now clay matrix. The quantity of clasts also varies significantly from only minor (1-2 per m^2) to tens of clasts per m^2. Quartzitic beds contain angular to sub-angular quartz grains (2-3 mm) occurring within a clay matrix that shows varying degrees of orientation. These conglomerates are visually distinct from those described in the area around Piketberg due to the larger size of the clasts and their varying composition.

4.2.2 Greywackes and shales

The majority of the rocks within the Swartland and Boland Terranes represented by the Moorreesburg and Porterville Formations, can be classed as greywackes ranging from off-white-grey to grey-green when fresh, to yellow-brown when weathered. The greywackes are composed of quartz, muscovite and feldspar. Variations in grain size can be seen on a centimetre- to metre-scale (Plate 4.19). A weak foliation (S_1) is identified in the greywackes and shales, identified by the orientation and elongation of quartz. The greywackes and shales are described from south to north.

In the area around Philadelphia, located 10 km west of the farm Klipheuwel (Fig. 4.1), the greywackes are composed of sub-rounded to angular quartz (up to 70%), and angular to sub-angular feldspar (plagioclase and minor microcline, approx. 10%) within a muscovite-clay matrix (approx. 20%) depending on the degree of weathering (Plate 4.20a). Grain size varies, but is on average less than 1 mm in diameter. Greywackes are interbedded with up to 2 m thick shales and sandstone

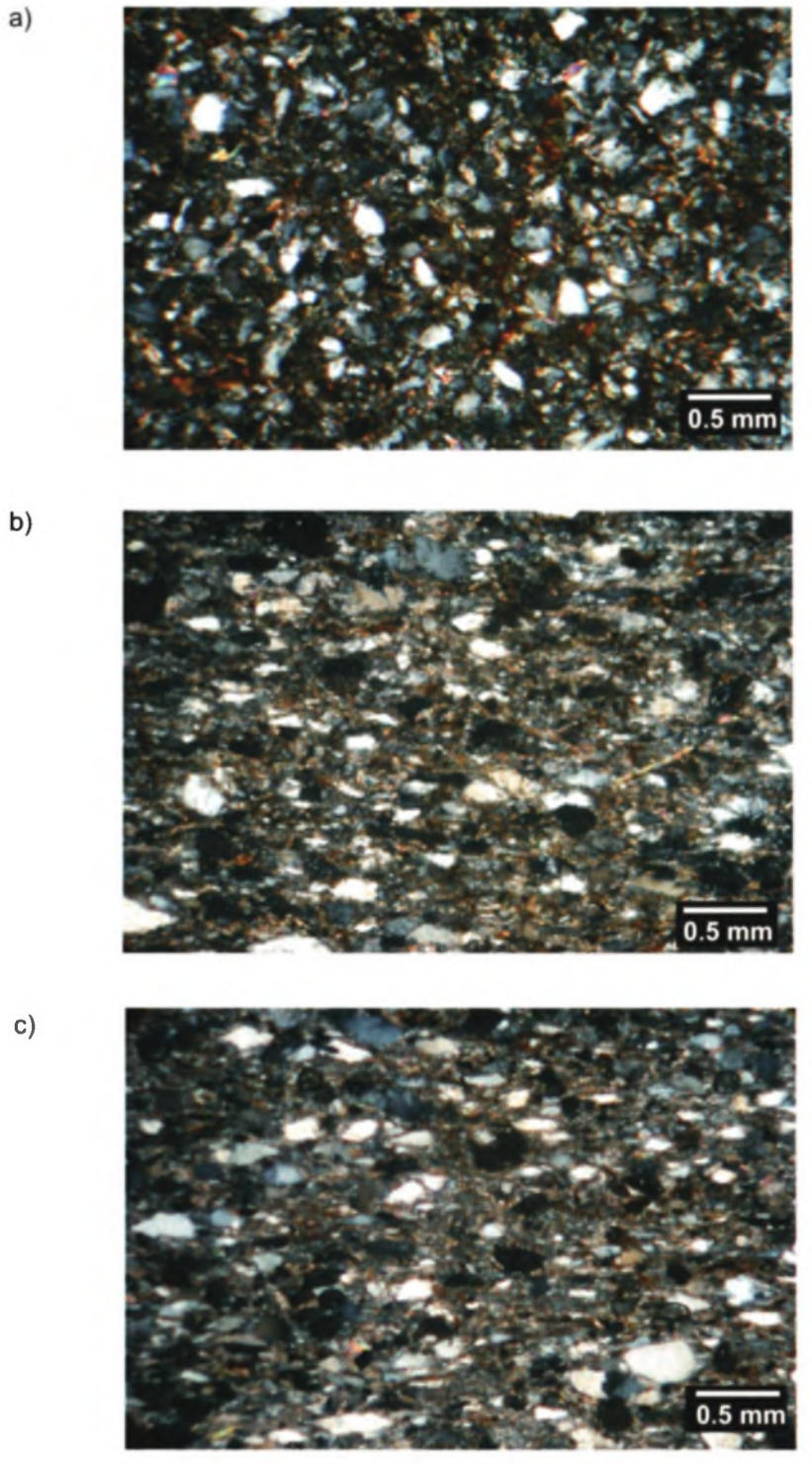

Plate 4.20. Typical examples of greywackes from the non-schistose rocks composed of quartz and feldspar in a fine-grained sericite and feldspar matrix. Note the elongation and orientation of quartz grains defining a weak fabric (S_1) and the similarity of all three deposits located throughout the Malmesbury Group. All plates XPL.

a) Philadelphia (Tygerberg Formation, Tygerberg Terrane).
b) 2 km northwest of Moorreesburg (Moorreesburg Formation, Swartland Terrane).
c) 5 km west of the town Porterville (Porterville Formation, Boland Terrane).

beds, and are compositionally similar to greywackes in the east described above. Bedding is prominent, with minor shale units (<5 cm thick) often occurring between the greywacke beds. To the south of Philadelphia, in the area around Tygervalley, greywacke, sandstone and mud/siltstones are interbedded, with beds on average 0.5 m thick. Compositionally, the greywackes in the present Tygerberg Terrane closely resemble those to the north and east in the Swartland and Boland Terranes, although individual beds in the latter terranes are thinner. In the Tygerberg Terrane, sandstone beds are more common.

Around Paarl, the sedimentary rocks are very fine grained, off-white in colour and can be described as mudstones. Little evidence of primary bedding exists, except for colour and grain size variations, where minor grit beds occur. These deposits show no evidence of regional metamorphism and deformation was only mild as indicated by the lack of a strong tectonic foliation in the rocks. Due to the fine-grained nature of the lithology, little petrographic information could be discerned from the thin sections.

Although only limited outcrops are exposed adjacent to the Colenso Fault Zone, there appears to be a marked contrast in the lithologies on either side of the fault. Very few sandstone beds are observed to the east of the Colenso Fault Zone, but in the west, sandstone forms a major lithological unit in the Tygervalley and Philadelphia areas (Von Veh, 1983). The Tygerberg Formation is resistant to weathering, whereas the other non-schistose rocks located to the east of the Colenso Fault Zone weather easily and are often decomposed to clays.

To the southwest of Malmesbury where outcrops are better, the boundary of the Swartland and Tygerberg Terranes is marked by the occurrence of the Klipheuwel Group (Fig. 4.1). Around the farms Klipheuwel and Prospect Hill, outcrops of Malmesbury Group rocks are very weathered, but are similar to outcrops seen further north between Malmesbury, Moorreesburg and Hopefield.

To the west of Moorreesburg around the town of Hopefield (Fig. 4.1), outcrops are again highly weathered and are quarried for kaolinite. On the farm Maatjesfontein, fine-grained clays vary in colour from white to pale greens, yellows, reds and browns.

These are similar in appearance to the highly weathered shales identified across the Moorreesburg area. The clays are largely devoid of veining, except for occasional veins that occur parallel to the bedding or crosscut at high angles. In areas of veining, the clays often exhibit minor faulting and localised folding. To the west of the farm Maatjesfontein, the lithologies become medium-grained and are more resistant to weathering and exhibit extensive iron staining.

In the vicinity of Porterville (Fig. 4.1), greywackes are composed of, on average, 75-80% quartz grains (<0.2 mm) (Plate 4.20b). Grains are elongated parallel to bedding. Quartz grains are bounded by muscovite laths (7-10 vol.%), which define the foliation and also make up the matrix. Feldspar occurs as albite (An_{02}) and minor microcline, both occurring as angular, orientated grains making up to 10% of the rock composition. Quartz grains occasionally exhibit weak undulose extinction. To the south, between Porterville and Heuningberg (Fig. 4.1), greywacke beds alternate with more shaly beds, ranging in thickness from 0.4 to 2-3 m. The grain size of the greywackes in this area is smaller. Directly to the east of Heuningberg, quartz-rich units can be identified consisting of up to 90% quartz. Further south, towards Hermon, the greywackes are again medium grained. Apart from minor grain size and compositional differences, and the occurrence of more shaly units, there is very little to discern between these deposits between Porterville and Hermon and those identified to the north at Porterville some 70 km away.

In the area west and south of Hopefield, outcrops become increasingly poor and scarce, with no outcrops occurring in the vicinity of the Colenso Fault Zone. In the vicinity of Moorreesburg, the greywackes are medium- to fine-grained, yellow-brown in colour, but more greenish when fresh. Petrographically (Plate 4.20c), little information may be deduced because of the small grain size of many of the lithologies (<0.2 mm). The greywackes are composed of sub-angular quartz grains (50 to 80%), exhibiting weak undulose extinction and elongation, with a preferred orientation. Muscovite is fine-grained, occurring as laths with preferred orientation and within the matrix. Alkali feldspar (approx. 10%) occurs as albite (An_{02}). It is sub-angular to sub-rounded, also with a preferred orientation. Both the feldspar and quartz exhibit fracturing. Further west and to the north, there is little change in

composition or grain size, except around the area of Koringberg, where deposits are more arenitic. To the north of Koringberg, the outcrops again become poorer and mineral components have undergone pervasive alteration to clay minerals. Outcrops along the Boesmans River between the farms Sauer and Sterkfontein (approximately 20 km north of Koringberg), are represented by a series of alternating pale-green, yellow and purple clay beds. The colour variations identify original bedding, along with slight grain-size variations, some beds are coarser grained and are similar in appearance to outcrops of weathered shales near Moorreesburg.

4.3 Conclusion

The lithologies of the Malmesbury Group can be provisionally subdivided in the field and from thin section studies into schistose and non-schistose rocks (Table 4.5). The schistose rocks correlate to the Berg River, Klipplaat, Porseleinberg and Bridgetown Formations and De Hoek Member of the Porterville Formation of the classification of SACS (1980). The schistose rocks are composed of a series of quartz-chlorite-muscovite-feldspar schists, quartz schists, metavolcanic rocks, limestones and graphitic schists. Although lithological correlations within and between outcrops are not possible, lithologically similar rocks do occur along the regional trend (northwest-southeast) between outcrops. For example, the occurrence of limestone units within the schistose rocks occurring along the regional strike from one another.

Table 4.5. Summary of the differences between the schistose and non-schistose rocks as identified during fieldwork.

	Schistose	**Non-schistose**
Sedimentary features	Minor colour & grain size variations	Numerous; bedding, cross-bedding and grain size variations
Lithological contacts	Predominantly tectonic	Sedimentary
Lateral extent of units within outcrop	Limited	Extensive
Tracing of units between outcrops	Speculative	Possible
Transposition folding	Yes	No
Foliation	3 (1 sub-horizontal, 2 sub-vertical)	2 (sub-vertical)
Quartz veining	Extensive	Subordinate

The contacts between individual units in the schistose rocks are predominantly tectonic, not sedimentary. Overlying the schistose rocks are the non-schistose rocks. The non-schistose rocks correlate to the Tygerberg, Piketberg, Porterville (excluding the De Hoek Member), Moorreesburg, and Franschhoek Formations of the classification of SACS (1980). These are from base to top, a series of conglomerate, grits and shales overlain by greywackes and shales, with sandstones becoming dominant to the west in the Tygerberg Formation. Sedimentary features are common throughout the lithologies and contacts between individual beds and lithologies are sedimentary. The contact between the schistose and non-schistose rocks cannot be directly identified in the field but constrained to a two hundred metre wide zone. However, the conglomeratic nature of the deposits directly overlying the boundary between the schistose and non-schistose rocks suggests that the boundary between the two groups is at least locally, sedimentological, and possibly an unconformity. The lack of conglomerates and grits at the boundary between the schistose and non-schistose rocks in the west of the field area indicates that in places the contact maybe conformable.

From field observations, the contact between the two units is subhorizontal, and not two vertical contacts (terrane-bounding faults) as suggested in the present model. Furthermore, similar lithological units were identified across the terrane bounding faults. These two observations are at variance with the present model and provide the motivation for the revision of the classification.

5 STRUCTURAL GEOLOGY

Up to three deformation events are identified in the Malmesbury Group (Table 4.1). The first deformation event (D_1) only affected the schistose rocks and is identified by the regional fabric S_0/S_1. This fabric contains isoclinal, intrafolial folds (F_1). D_2 affected all the rocks in the Malmesbury Group and folded the S_0/S_1 fabric in the schistose rocks and bedding (S_0) in the non-schistose rocks. These folds (F_2) are orientated northwest-southeast and can be observed on millimetre- to kilometre-scale. D_3 was a minor folding event that affected the whole of the Malmesbury Group, creating minor, centimetre- to metre-scale northeast-southwest orientated folds (F_3).

5.1 S_0

The presence of primary sedimentary features within the rocks varies greatly across the Malmesbury Group as described in Chapter 4. In the Philadelphia and Tygervalley areas (Tygerberg Terrane), bedding of the different lithologies is most prominent compared to further north and east within the Swartland and parts of the Boland Terranes. Across the Swartland and Boland Terranes, bedding is locally observed. The presence of bedding is in general, confined to the Tygerberg, Piketberg, Moorreesburg, and Porterville Formations, which equates to the non-schistose rocks described in the previous chapter.

In the schistose rocks, evidence of primary sedimentary features is generally restricted to grain-size and colour variations in the monotonous lithologies, e.g. at Spitskop and Goudmyn se Kop areas, as the strong foliation has, in many cases, obliterated any primary bedding features. In the Zoutkloof Quarry, bedding within the limestones is prominent, however, individual beds are laterally discontinuous and pinch out against or are truncated by mylonites or foliation zones (Plate 5.1). Where beds can be traced over 10-50 m across the outcrops, the bed thickness varies

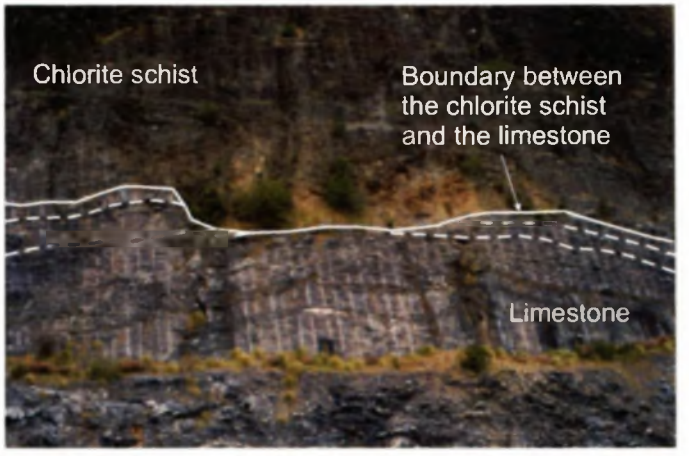

Plate 5.1. Example of the laterally discontinuous nature, varying bed thickness and the truncation of the limestone beds at the Zoutkloof Quarry, Piketberg. This is also observed in the other limestone quarries at De Hoek, 2 km to the south, and Riebeeck West, approximately 40 km to the south. Photograph taken looking northeast.

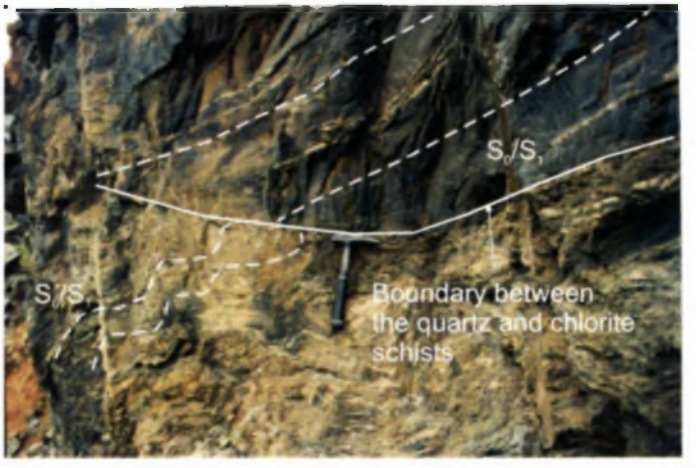

Plate 5.2. Truncation of quartz schists against the underlying chlorite schists at the Kruisfontein Quarry, Moorreesburg. This relationship implies that the schists represents a tectonic and not a sedimentary package.

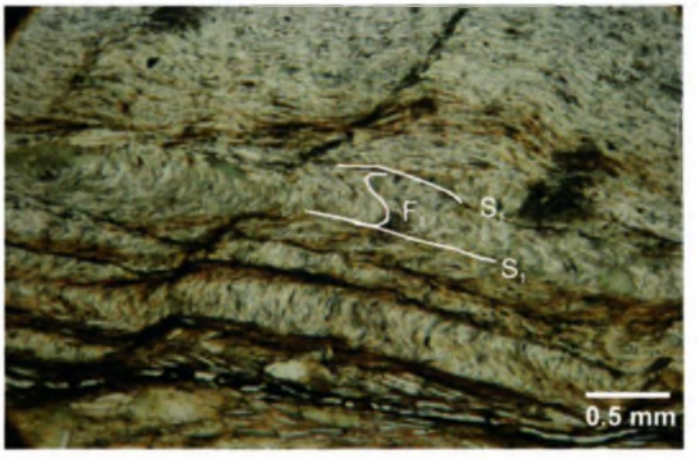

Plate 5.3. Microscopic, intrafolial F_1 folding within a chlorite-muscovite schist. Due to the monotonous nature of the lithology it was impossible to identify intrafolial folding on an outcrop scale. However, this folding could be identified in thin section confirming the presence of bedding transposition. Photomicrograph taken in PPL.

considerably between 1-2 cm and 1 m. The graphitic schist is a case in point. The thickness of the schist varies from only a few centimetres to approximately 20 m, over a lateral distance of 10-20 m. The same features are also identified in the limestone quarry at Riebeeck West, some 35 km along strike to the south. Here limestone and schist beds are truncated against one another, beds are laterally discontinuous and bed thickness varies greatly.

In the Kruisfontein Quarry, where a series of quartz-chlorite-muscovite schists and quartz schists are identified, the same features described above are also observed in these lithologies. The quartz schists can be used as a marker horizon in the Kruisfontein Quarry hosted by the monotonous quartz-chlorite-muscovite schists. The quartz schist beds vary from 1-2 cm to approximately 30 cm thick, and these variations in bed thickness occur over 1-2 m. Individual beds are laterally discontinuous and are often truncated by a sub-horizontal foliation (Plate 5.2). Such variations in bed thickness are hard to conceive in terms of mere sedimentary processes when considering the most likely low energy and deepwater environment. As discussed in Chapter 4.3, correlation of units within outcrops, e.g. at the De Hoek, Zoutkloof and Riebeeck West Quarries, and between outcrops, e.g. between Spitskop, Riviera and the Kruisfontein Quarry, is rather speculative.

5.2 D_1

Folding of bedding (S_0) during D_1 produced a series of dismembered, recumbent, isoclinal intrafolial folds, occurring on millimetre- to metre-scale (Plates 5.3 & 5.4). Where bedding could not be unequivocally identified, F_1 folding is expressed by folds of early quartz veins occurring parallel to the original bedding. This is exemplified in the limestones and schists/phyllites in the Zoutkloof Quarry and 50 km to the south-southwest in the Riebeeck West Quarry, in the Kruisfontein Quarry and around the town of Moorreesburg (Plate 5.5). The F_1 folds have an axial planar foliation, hereto referred to as S_1. Owing to the tight to isoclinal nature of the F_1 folding, the S_1 fabric is sub-parallel to bedding (S_0). The poles to S_1 (Fig. 5.1) lie on partial great circles that indicate later refolding by folds orientated northwest-southeast (Chapter 5.3). These recumbent intrafolial F_1 folds with an axial planar S_1 fabric sub-parallel to S_0 are evidence for bedding transposition. The interplay between S_0 and S_1, which will

(a)

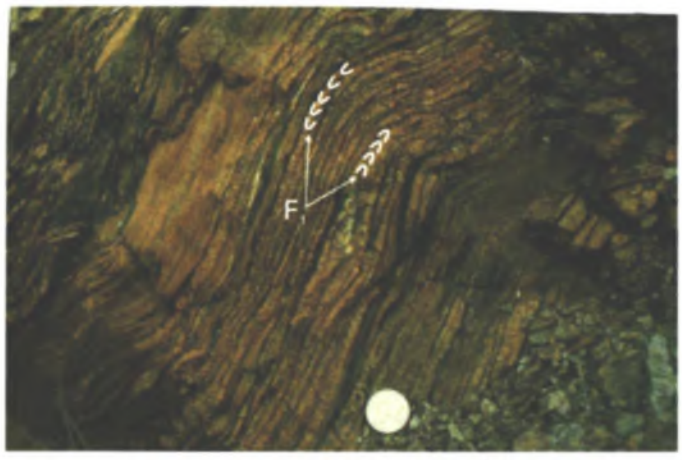

a) Small-scale (<1 cm) intrafolial F_1 folding in cross section within quartz-rich schists at Bothmaskloof Pass, Riebeeck Kasteel. Photograph taken looking south.

(b)

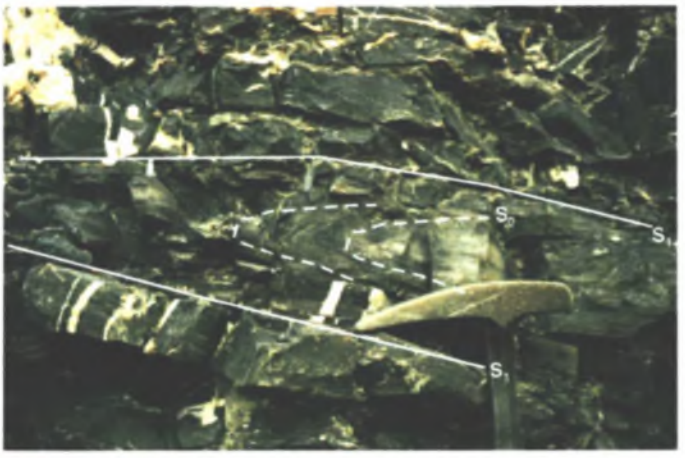

b) Intrafolial folding (10-15 cm scale) of limestone beds in cross section at the Zoutkloof Quarry, south of Piketberg. Looking east.

(c)

c) Tight to isoclinal intrafolial folding of quartzite beds (<50 cm), within strong S_0/S_1 fabric in schists at the Kruisfontein Quarry, north of Moorreesburg. Folding photographed in cross section looking south.

(d)

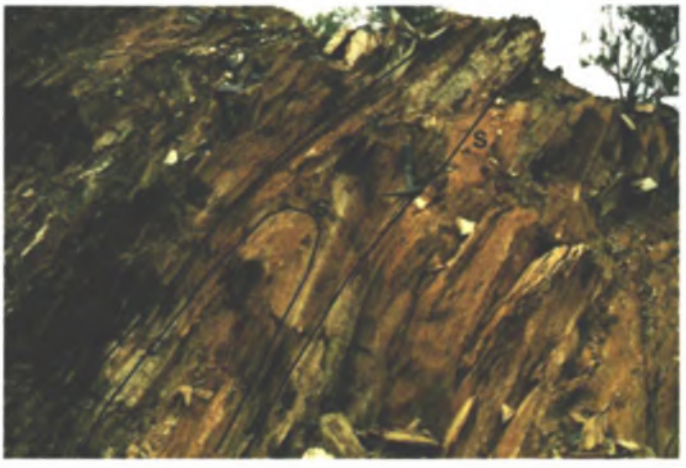

d) Transposition of bedding (1-2 m scale) within quartz-chlorite-muscovite phyllites at the De Hoek Quarry, producing recumbent tight to isoclinal intrafolial F_1 folding. Photograph looking towards the southeast along the strike of S_0/S_1.

Plate 5.4. Examples of intrafolial folding (F_1) at various outcrops across the Malmesbury Group, showing folding of bedding from mm- to m-scale. Bedding transposition has destroyed any original stratigraphic succession and juxtaposed unrelated lithologies against one another, creating a pseudo-stratigraphy.

a)

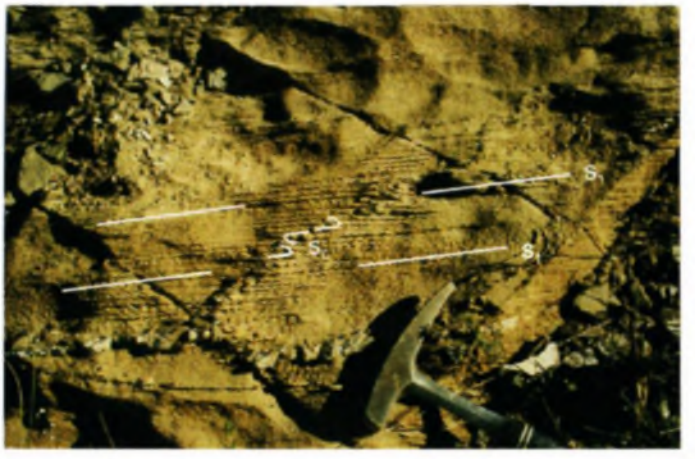

b)

Plate 5.5. Example of tight isoclinal folding of a quartz vein within a medium-grained feldspathic lithology in the Moorreesburg area. Without the presence of the veining, it would not be possible to identify the deformation the lithology has undergone.

a) Note the well developed S_1 axial planar fabric to the F_1 folds.

b) Close-up photograph of F_1 folding at the same locality.

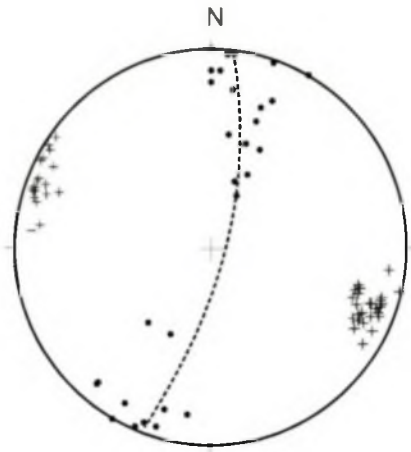

a) Bothmaskloof Pass and Porseleinberg Hills (F_1, n=38; S_1, n=27)

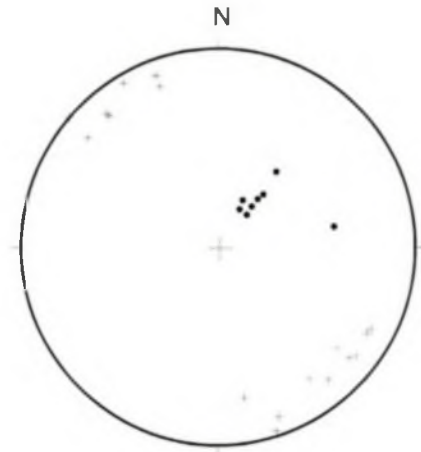

b) Kruisfontein Quarry (Berg River Formation) (F_1, n = 17; S_1, n=8).

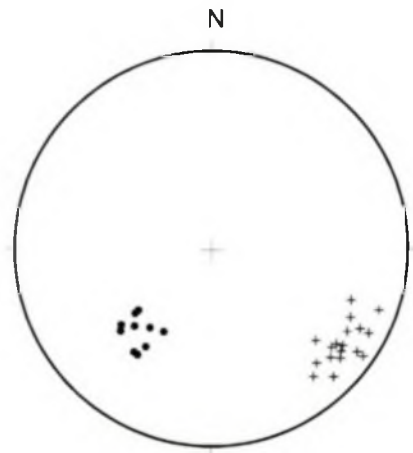

c) Riebeeck West Quarry (F_1, n=18; S_1, n=10)

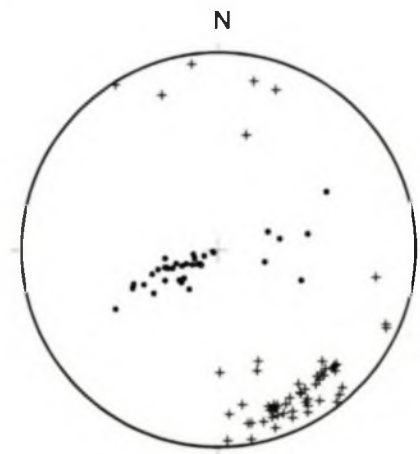

d) Biotite-feldspar schist, Kanonkop, north of Malmesbury. (F_1, n=94; S_1, n=36).

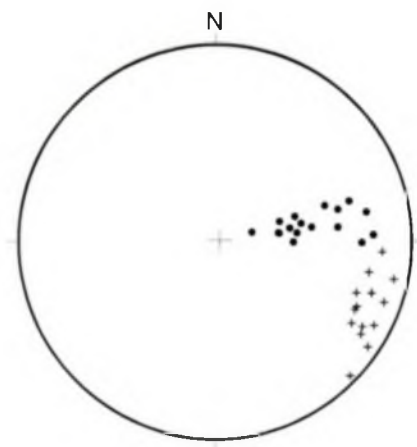

e) Zoutkloof Quarry (F_1, n=14; S_1, n=16)

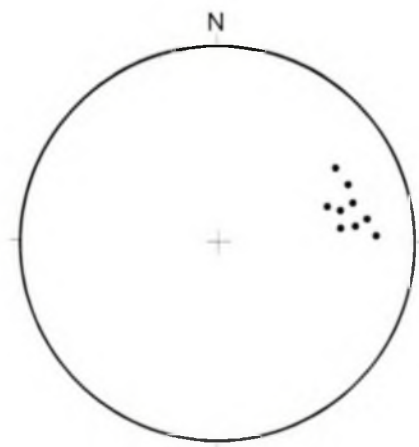

f) Zoutkloof Quarry (S_1 (mylonites), n=9)

Figure 5.1. Lower hemisphere equal-area projections of the plunge and plunge direction of fold axes of F_1. Note that poles to S_1 lie on a great circle indicating refolding around a northwest-southeast axis. Crosses denotes F_1 fold axes, and circles denote poles to S_1 axial planar fabric.

from henceforth be referred to as the S_0/S_1 fabric, is described in detail for each of the main outcrops. Transposed quartz veining and microscopic intrafolial folds can also be used to identify this transposition fabric. As this fabric is associated with F_1 folding, it is also only identified within the schistose rocks.

Due to the orientation of outcrop surfaces, measurements were often not possible at all the outcrops. Fold axes taken from the Kruisfontein Quarry, Porseleinberg hills and Riebeeck West Quarry trend northwest-southeast and plunge 25° or less (Fig. 5.1). No F_1 folds were identified in any of the non-schistose rocks. These outcrops are from north to south, Zoutkloof Quarry, Spitskop, Goudmyn se Kop, Kruisfontein Quarry, Riebeeck West Quarry and Porseleinberg hills. A form line map of the S_0/S_1 fabric (Fig. 5.2) clearly indicates the extent of the fabric. The curved nature of the form lines is related to F_2 folding during D_2. The occurrence of bedding transposition within the schistose rocks means that distinct lithological units that were previously interpreted to represent beds (e.g. Rabie, 1974a; Hartnady et al., 1974; Theron et al., 1992) are in fact tectonic layers, and will henceforth be referred to as layers not beds.

In the Zoutkloof Quarry, the transposition fabric is well preserved due to the alternation of original lithologies (limestone and shale). Here, isoclinal folding can be seen on a scale of 1-2 cm in limestones and shales and up to 5 m in the overlying phyllites. F_1 folding is seen throughout the rocks in the quarry, from the base to the top, a vertical distance of 70 m, indicating the pervasive nature of the bedding transposition. Strain within the rocks of the Zoutkloof Quarry is not homogeneous, and the strain was partitioned into mylonitic high strain zones (Plate 5.6; Figure 5.1). The foliation within the mylonites is well defined, containing small (<7 mm) elongated and rotated calcite porphyroclasts often exhibiting recrystallised tails. This foliation is parallel to the regional S_0/S_1 foliation and S-C fabrics and σ-type porphyroclasts in the mylonites identify a top-to-the-northwest movement (Plate 5.7). Associated with these high-strain zones are duplexes (Plate 5.8). Duplexing is fairly discrete and often composed of single horses ranging in length from 0.5-2 m, also indicating a transport direction to the northwest. The fold axes of the horses are orientated northeast-southwest, at right-angles to the F_1 fold axes. This feature can be attributed

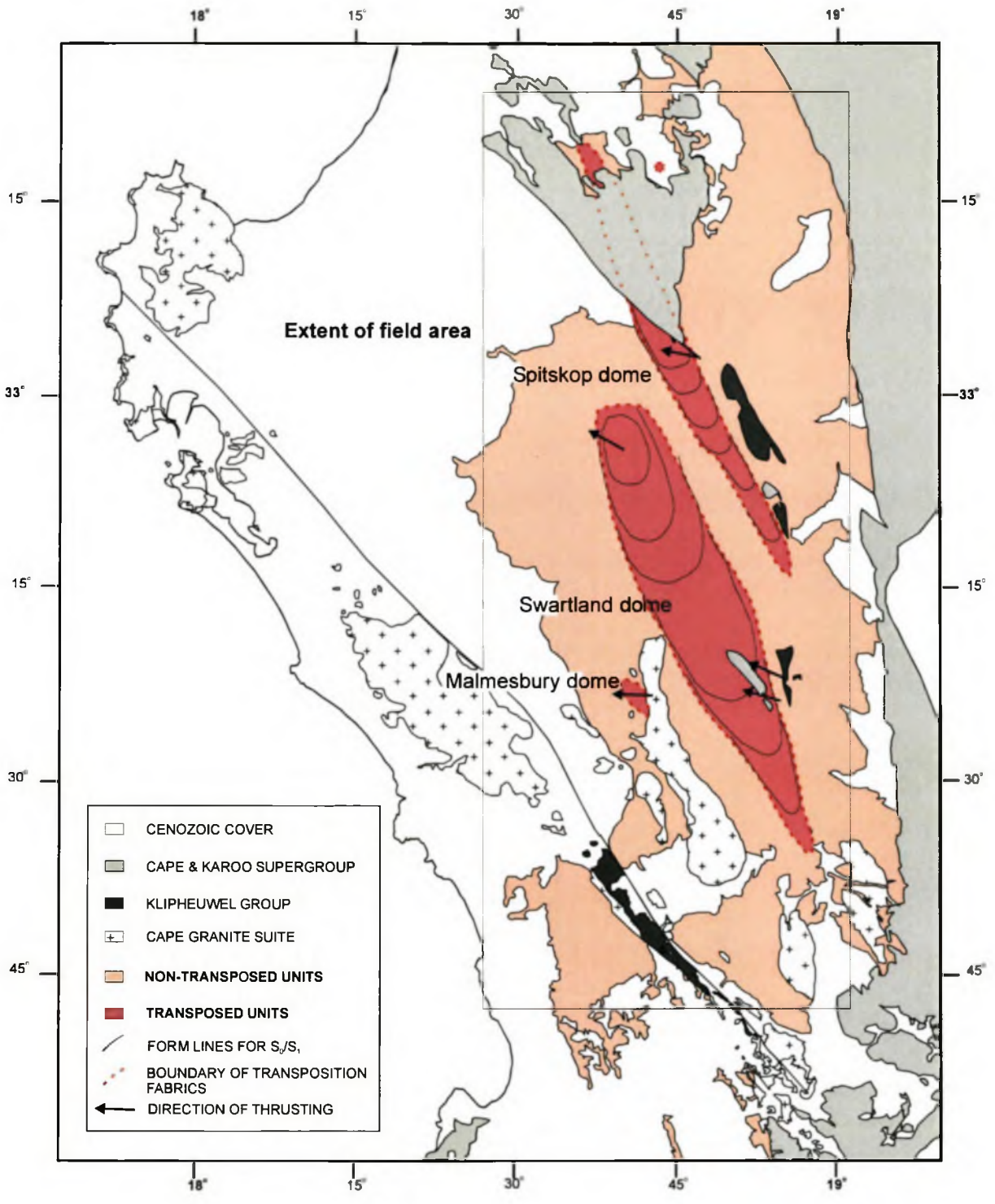

Figure 5.2. Foliation formlines for the S_0/S_1 transposition fabric related to the F_1 folding. Arrows indicate transport direction as identified from shear sense indicators (see text for further information on individual localities. Note the consistent top-to-the-northwest/west transport direction within the

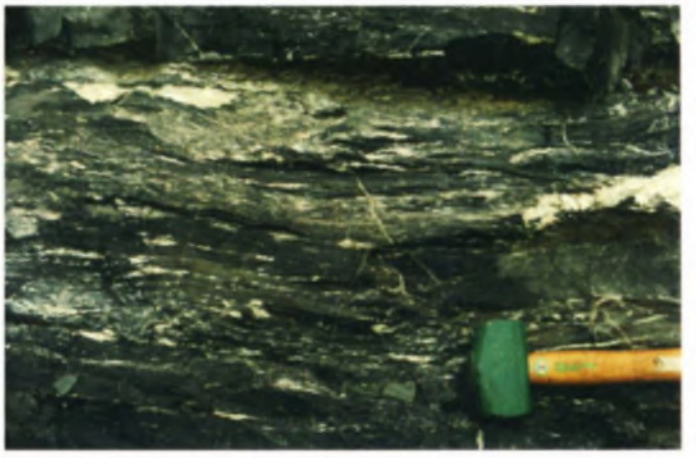

Plate 5.6. Example of limestone mylonites in the Zoutkloof Quarry, south of Piketberg. Photograph taken looking east. S-C fabrics and σ-type porphyroclasts of calcite identify a transport direction of top-to-the-northwest.

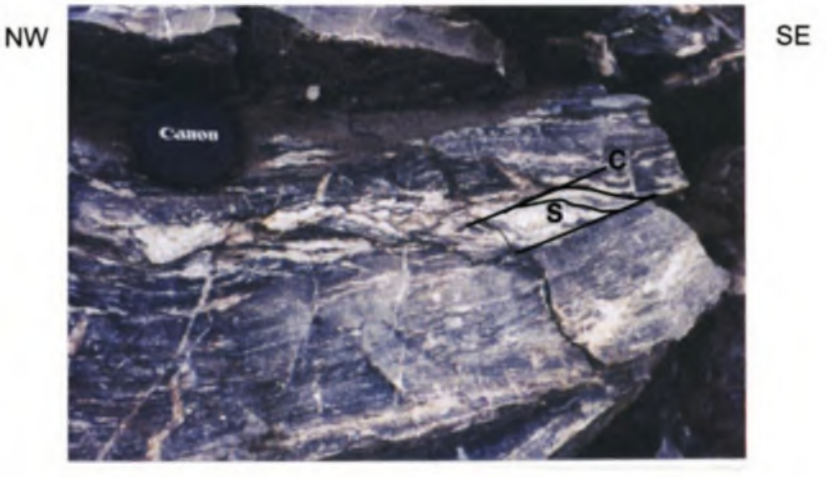

Plate 5.7. Highly deformed limestone layer from Zoutkloof Quarry. S-C fabrics within the limestone indicate top-to-the-northwest movement.

Plate 5.8. Example of duplexing at the Zoutkloof Quarry. Duplexes are situated above major zones of detachment and are composed of thin limestone units interlayered with graphitic schists. Note that the limestone below the duplex is relatively homogeneous, while the limestone above is highly strained. Photograph taken looking to the east, S-C fabrics identify top-to-the-northwest thrusting.

to the passive rotation of the F_1 fold axes during progressive deformation and explains the varying orientation of fold axes seen in many outcrops (e.g. Kruisfontein and Zoutkloof Quarries, and Kanonkop, Fig. 5.1). Minor schistose layers, only a few centimetres thick, often occur between the limestone layers and in the high strain zones, and form the horizons for thrusting and detachment. Such detachments can be traced along the quarry walls for 20-30 m, with detachment folding above the detachment. Thrusting along the detachment zones has caused intricate folding (e.g. box folding; Plate 5.9). This records top-to-the-northwest movement (Plate 5.10; Fig. 5.3).

Lineations are difficult to observe in the field. At the Zoutkloof Quarry, mineral lineations along the limestone layers were identified (Plate 5.11). They are composed of quartz-carbonate aggregates and show a consistent plunge direction and plunge of 135/25° (Fig. 5.4a). At Spitskop, the highly-foliated chert contains quartz rodding up to 2 cm long (stretching ratio of 10:1) plunging approximately 145/15° (Fig. 5.4b). Further to the south at the Riebeeck West Quarry stretching lineations within the highly foliated quartz-chlorite schist and also from the limestones near mylonites plunge direction and plunge of approximately 110/15° (Fig. 5.4c). L_1 is consistently orientated in the same direction across the schistose rocks and indicates stretching orientated northwest-southeast. Within the limestone quarries at Zoutkloof, De Hoek and Riebeeck West, boudins within the limestone layers are common. Boudinage is developed in the phyllites/schists at the Zoutkloof Quarry (Plates 5.12, 5.13 & 5.14) on a variety of scales from a few centimetres to tens of metres.

In the Spitskop and Goudmyn se Kop area, lithologies are monotonous so that compositional contrasts between individual beds are poorly developed. This makes the identification of F_1 intrafolial folding problematic, but the transposition fabric is evidenced by the isoclinal intrafolial folding of early quartz veins contained within S_1.

The lithological variations in the Kruisfontein Quarry accounts for the identification of bedding transposition on a variety of scales, from centimetre up to 1 m within the different units and also between them. Bedding transposition as seen throughout the quarry, both laterally and vertically, indicates the pervasive nature of

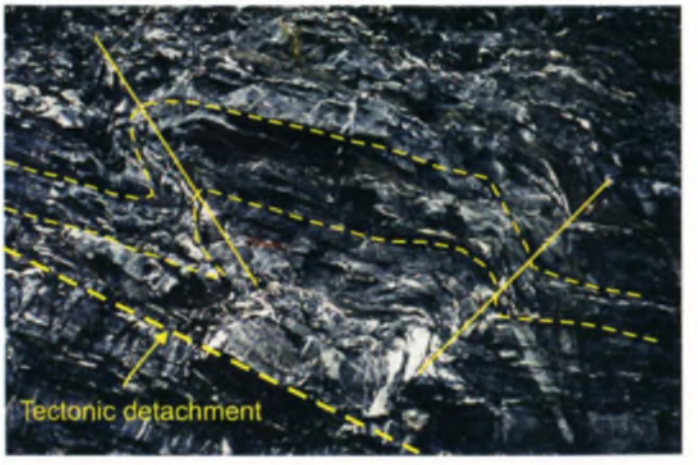

Plate 5.9. Box folding above a detachment in limestone layers at the De Hoek Quarry. Pencil, centre left for scale. Photograph taken looking northeast

Plate 5.10. Highly deformed limestone layers from De Hoek Quarry. Note the detachments occuring parallel to the bedding and therefore also parallel to S_1. Photograph taken looking northeast. Illustrated in Figure 5.3.

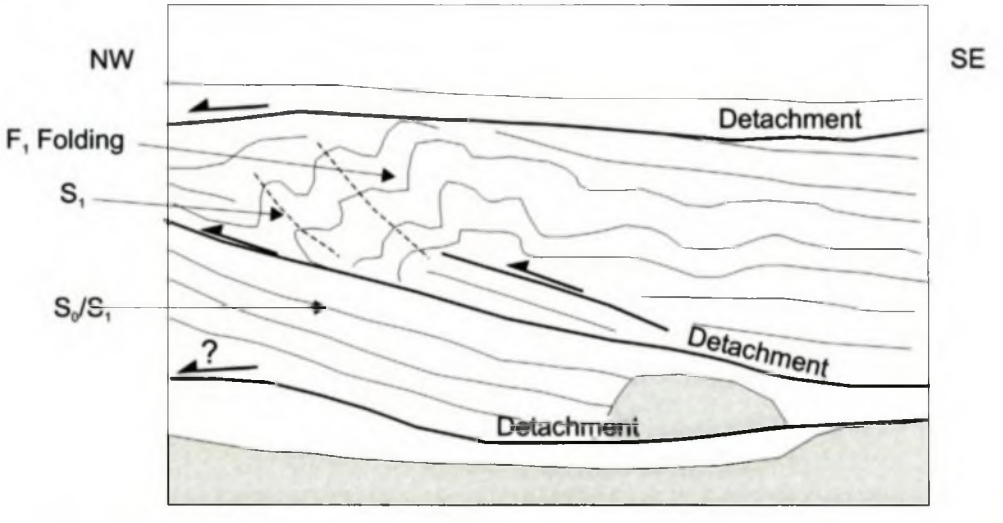

Figure 5.3. Schematic diagram from Plate 5.11 showing the location of the detachments and folding related to thrusting. Lower limestone layers are truncated against the lower detachment. Beds above lower detachment are folded during top-to-the-northwest thrusting. Layers above the upper detachment are relatively undeformed.

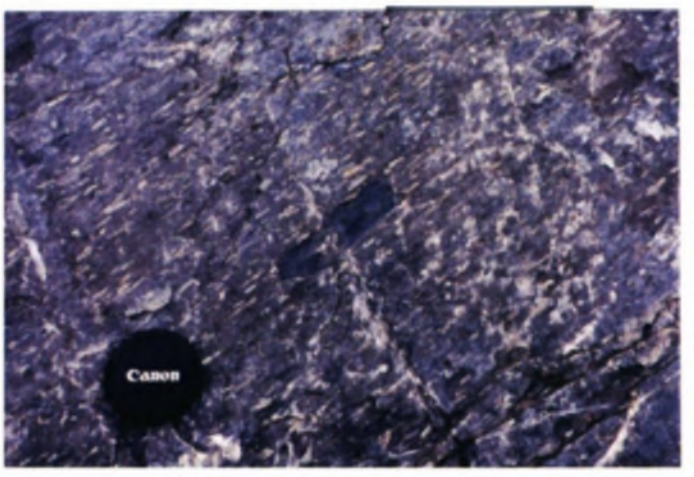

Plate 5.11. Example of mineral lineation in limestone from the Zoutkloof Quarry. Lineations plunge on average 25° to the southeast (135°). See Figure 5.4a.

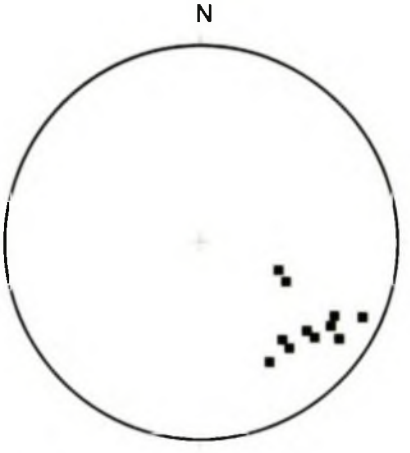

a) Mineral lineation, L_1 in limestones at Zoutkloof Quarry (n= 12)

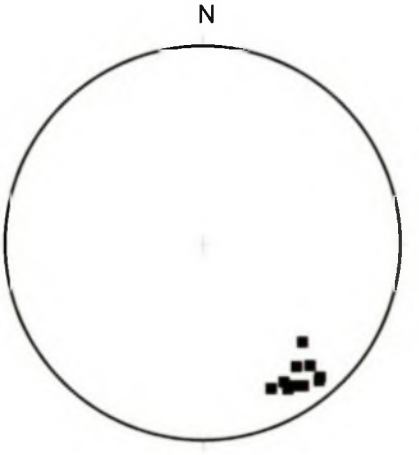

b) L_1: quartz rodding in 'chert' at Spitskop (n= 10)

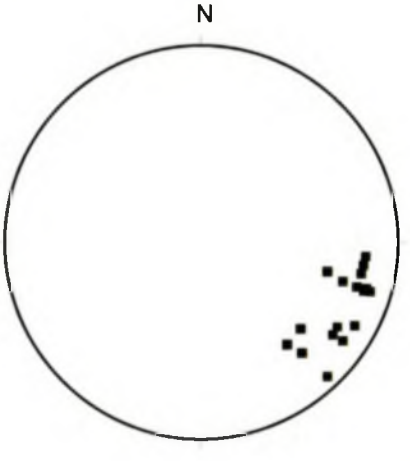

c) Mineral stretching lineation, L_1 in limestones at Riebeeck West Quarry (n= 16)

Figure 5.4. Lower hemisphere equal-area projections of L_1 lineations. Note all the lineations are plunging to the southeast.

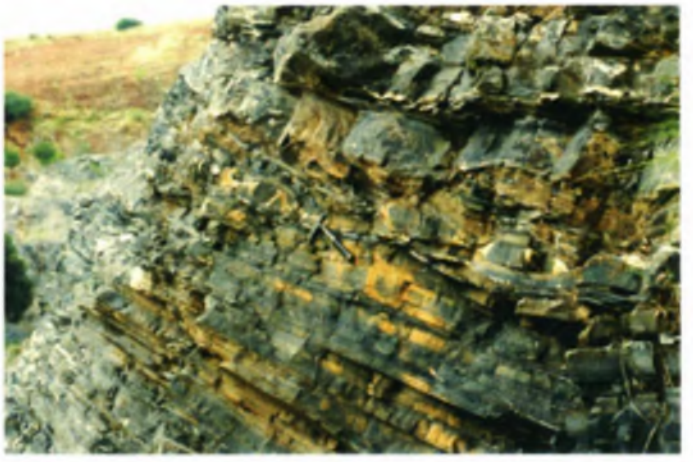

Plate 5.12. Limestone layers at the Zoutkloof Quarry, Piketberg. Directly above the hammer is a boudinaged limestone layer indicating rheological contrasts between limestone layers. Photograph taken looking northwards.

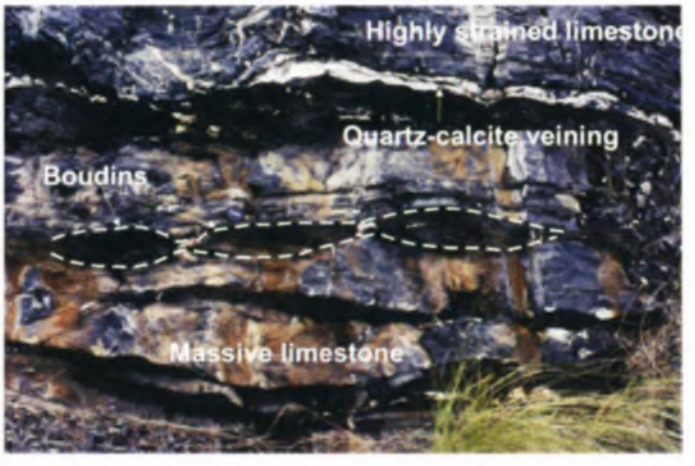

Plate 5.13. Boudins of graphitic schist occurring within limestone layers at the Zoutkloof Quarry. Contact between the massive limestone layers and the thin, highly strained limestone layers is an approximately 10 cm wide zone of quartz-calcite veining. Photograph taken looking towards the east.

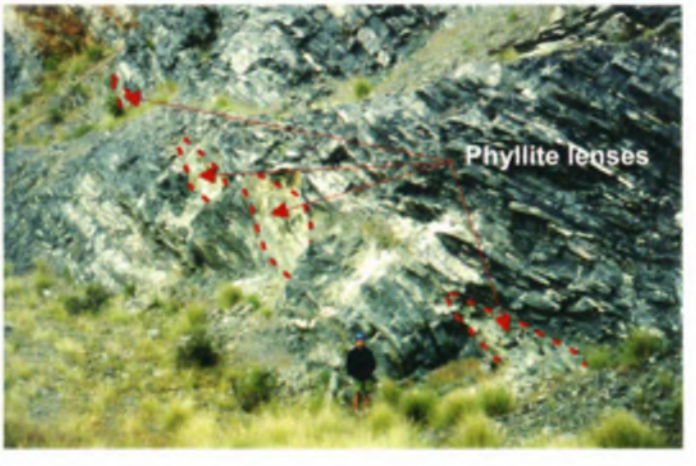

Plate 5.14. Isolated phyllite lenses occurring along strike from one another within the highly foliated and often mylonitised limestone beds (005°/35°). The phyllite lenses are all situated in the same stratigraphic position and represent a single phyllite unit that was dismembered during intense shearing. Photograph taken looking north at the eastern face of the Zoutkloof Quarry, Piketberg. This limestone is known as the De Hoek Member and is currently incorporated within the Porterville Formation (e.g. Theron et al., 1992).

transposition in the area. Bedding is still apparent, but beds are truncated, laterally discontinuous and bed thickness varies greatly, as is recorded in the quartz schist (Plate 5.15). S-C fabrics in foliation domains that envelope the intrafolial folds consistently indicate top-to-the-northwest movement.

In the Riebeeck West Quarry a similar structural style is portrayed to that seen in the De Hoek and the Zoutkloof Quarries. Intrafolial F_1 folding is identified in all the lithologies in the quarry and is very prominent within the quartz-chlorite schists and within high strain zones in the limestones. Intrafolial F_1 folding is identified from the base to the top of the quarry, which is approximately 50 m high, indicating again the pervasive nature of the transposition. These high strain mylonites zones are developed in limestone units containing extensive veining, varying in thickness from 0.2 m to 1.5 m (Plates 5.16, 5.17 & 5.18). F_1 folds are predominantly defined by quartz veining and fold axes plunge gently to the southeast. Quartz veins often have a sigmoidal shape, indicating a transport direction of top-to-the-northwest. The contact of the mylonites with the surrounding schists is sharp.

Duplexes are common in the thrust zones of the quarries, ranging in size from 1 m up to 5 m. They typically occur in the vicinity of the high strain zones associated with the strongly foliated limestone layers, directly above the detachment horizons. Individual limestone units within the duplexes rarely exceed 10 cm in thickness and show sharp contacts with one another and the surrounding limestones.

At Porseleinberg and in the Bothmaskloof Pass area, the schists are quartz rich, with only minor chlorite and muscovite. For a detailed structural map of the Porseleinberg area see Appendix D, Map 3. The S_0/S_1 fabric is well preserved within this quartzitic schist, creating spectacular small-scale, isoclinal folding (wavelengths <2 cm) in which bedding is transposed into the subhorizontal S_1 fabric (Plate 5.19). This S_0/S_1 fabric is clearly seen within metasedimentary rocks to the northeast around Riebeeck Kasteel (approx. 1 km away) and to the south along the Porseleinberg hills for approximately 1 km. On initial observation this tectonic fabric could be mistaken for a well developed sedimentary fabric (herring bone cross-lamination). However, on

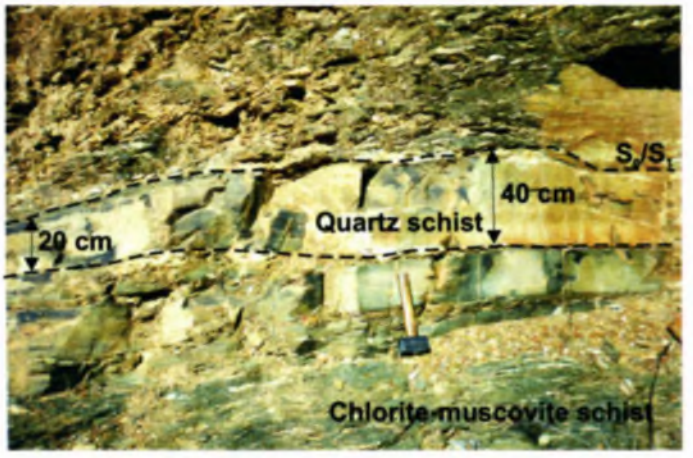

Plate 5.15. Quartz schist located in Kruisfontein Quarry occurring as layers within a succession of quartz-chlorite-muscovite schists. The upper quartz layer (annotated) varies in thickness from centre of photograph to the edge over only a few metres. This is also seen along the outcrop over 10-20 m. Photograph taken looking west, note hammer in foreground for scale.

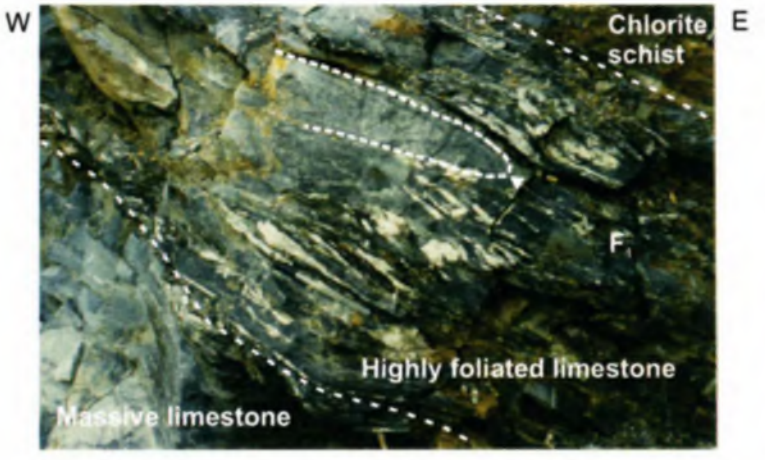

Plate 5.16. Mylonitic limestone showing bedding transposition and shearing. σ-type calcite porphyroclasts and S-C fabrics indicate top-to-the-west transport. The mylonite marks the boundary between the massive limestone (bottom left of photograph) and the chlorite schist (top right). Contacts between the different lithologies throughout the quarry are sharp and tectonic in origin. Photograph from Riebeeck West Quarry taken looking to the north.

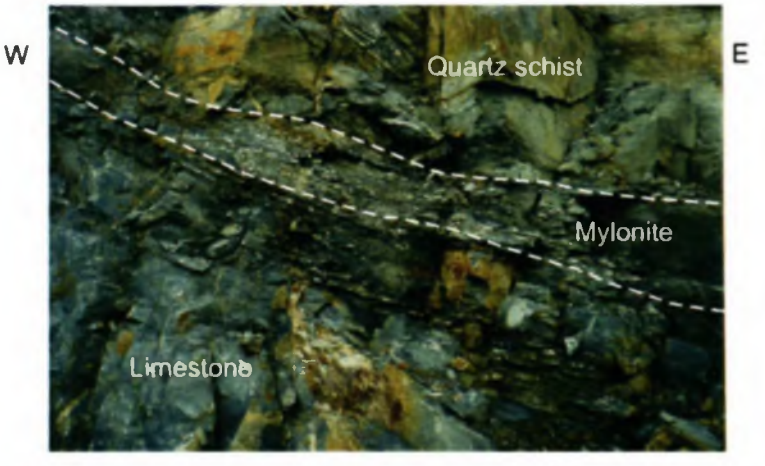

Plate 5.17. Limestone mylonite at the boundary between the limestone and quartz schist at Riebeeck West Quarry. Photograph taken looking north. S-C fabrics in the high strain zone indicate top-to-the-northwest transport. Such highly strained units occur at the contact between different lithological units, identifying the contact as tectonic, and not of sedimentary origin.

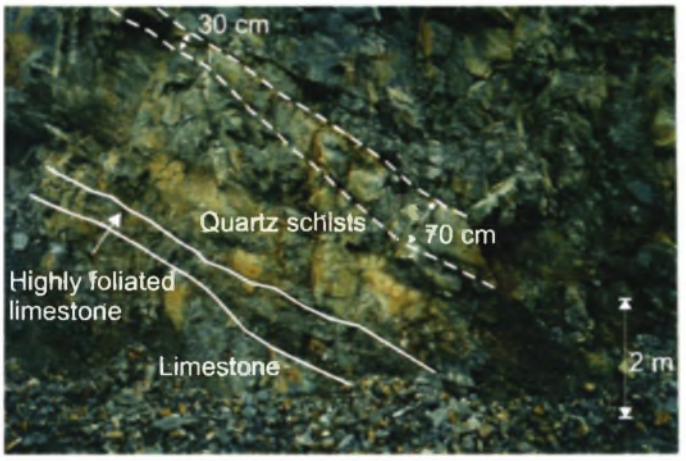

Plate 5.18. Typical contact between limestone and overlying quartz schist at Riebeeck West Quarry. The boundary between the two units is tectonic and often defined by mylonites. S-C fabrics within the mylonites indicate a top-to-the-west transport direction. Photograph taken looking north. Note, the lateral change in bed thickness over only a few metres (annotated).

a)

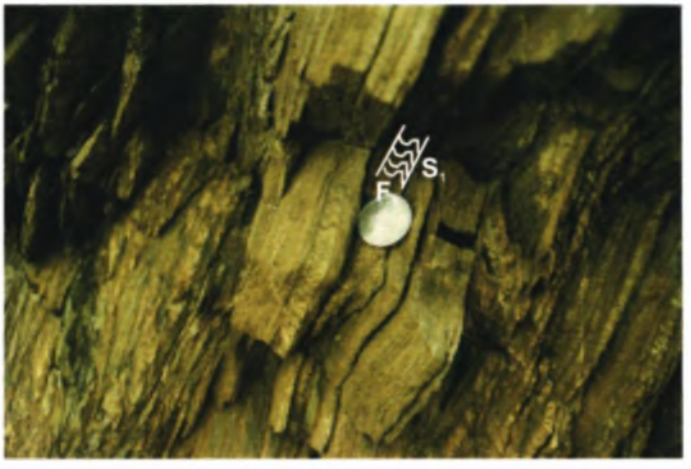

b)

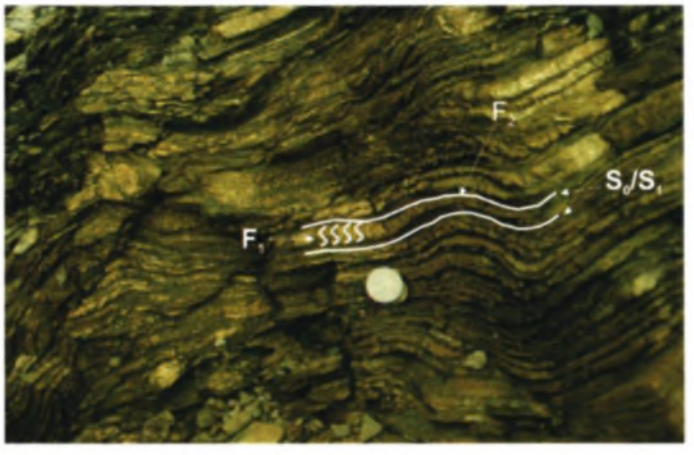

Plate 5.19. Example of the quartz-rich schist at Bothmaskloof Pass, near Riebeeck Kasteel. Both photographs taken looking to the southeast.

a) Note the minute intrafolial folding (F_1) and the well developed S_1 axial planar fabric to the F_1 folds.

b) The S_0/S_1 fabric was refolded during D_2 into near-upright folds (F_2).

closer observation and in thin section, the alignment and elongation of quartz grains and the orientation of phyllosilicate minerals show that this fabric is indeed tectonic.

Transposed bedding is seen as far north as the farm Kleigat and as far south as the Porseleinberg hills, some 85 km apart. Where outcrops permit, and vertical sections through the rocks are exposed, e.g. in the quarries, transposed bedding is seen over a vertical distance of approximately 70 m. This exemplifies the widespread occurrence of bedding transposition, not only laterally but also vertically throughout the schistose rocks. Mylonites and the S_0/S_1 fabric are parallel and orientated in a similar direction as the majority of F_1 fold axes and the L_1 lineations. Shear sense indicators, both S-C fabrics and σ type porphyroclasts, also indicate a top-to-the-north sense of movement, suggesting that F_1 folding, thrusting and duplexing were all part of the same event.

5.3 D_2

D_2 folding affected all rocks, i.e. both the schistose and non-schistose lithologies. Folding of the S_0/S_1 fabric in the schistose rocks and the S_0 fabric in the non-schistose rocks during D_2 produced a series of folds, with fold axes orientated approximately northwest-southeast being co-axial to F_1 (Fig. 5.5). However, as transposition is confined to the schistose rocks, previous authors (e.g. Theron et al., 1992) recorded this event as the earliest folding event in the non-schistose rocks, i.e. in the Tygerberg and Boland Terranes as F_1 with an axial planar cleavage, S_1.

Within the schistose rocks of the Berg River and Klipplaat Formations, F_2 folds are seen on a variety of scales. On a microscopic scale, the S_0/S_1 schistosity is crenulated with a wavelength of 0.5-1 mm (Plate 5.20). Kink folds, with wavelengths of 2-3 cm, are seen in outcrop and are a larger expression of the crenulation folding seen on a microscopic scale (Plates 5.21 & 5.22). Gentler folding is also seen on an outcrop scale, with interlimb angles varying from 90 to 70° (Plate 5.23). On a mesoscale (< 1m), tightly folded, similar F_2 folds can be observed.

Over 2 to 10 m along strike, gentle sigmoidally shaped folds (Plates 5.24 & 5.25) are observed. These are separated from each other by steep zones, dipping greater than

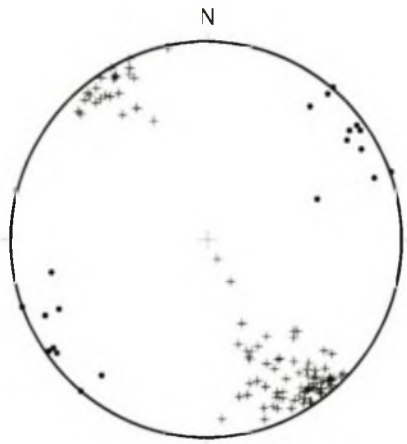

a) Spitskop area (F_2, n= 105; poles to S_2,n= 18).

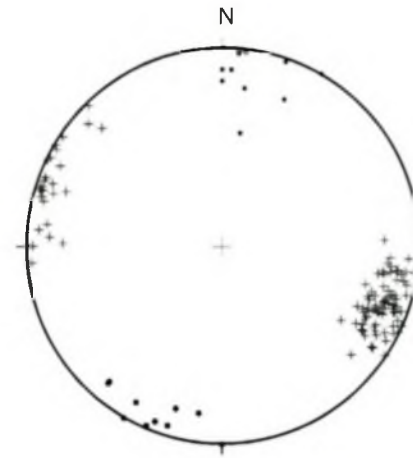

b) Porseleinberg hills and Bothmaskloof Pass (F_2, n= 106; poles to S_2, n= 18).

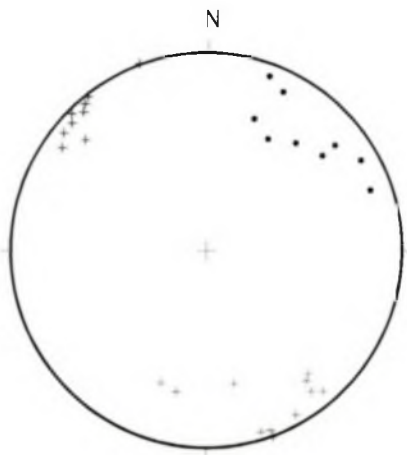

c) Kruisfontein Quarry (F_2, n= 20; poles to S_2, n= 9).

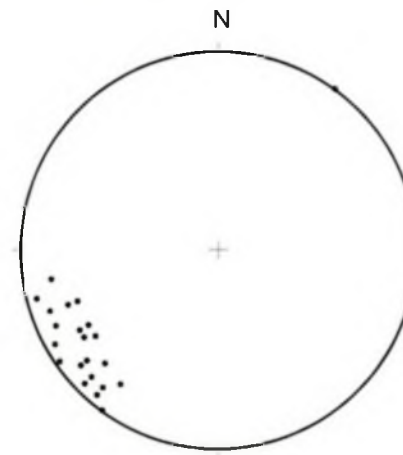

d) Hopefield, shales (poles to S_2, n= 21).

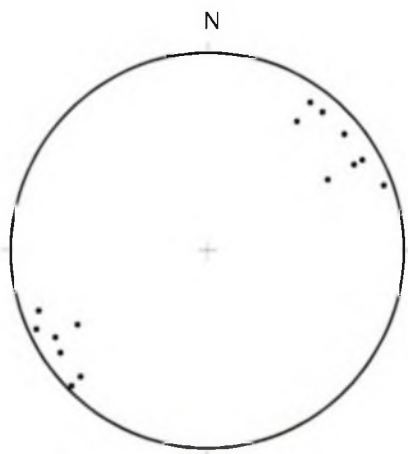

e) Philidelphia, greywackes and shales (Poles to S_2).

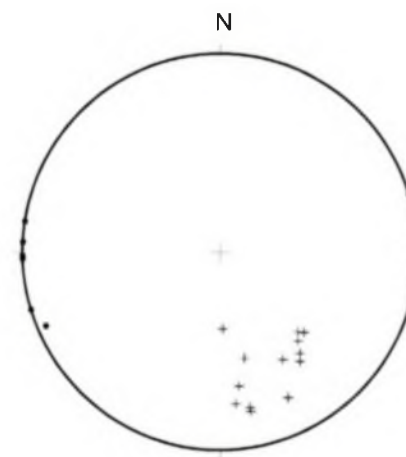

f) Malmesbury, greywackes (non-schistose rocks) (F_2, n=13; poles to S_2, n= 7).

Figure 5.5. Lower hemisphere equal-area projections of the orientation of F_2 folds and associated axial planar foliations (S_2). Note: + plunge and plunge direction of fold axes (F_2) and • poles of S_2 planar fabric.

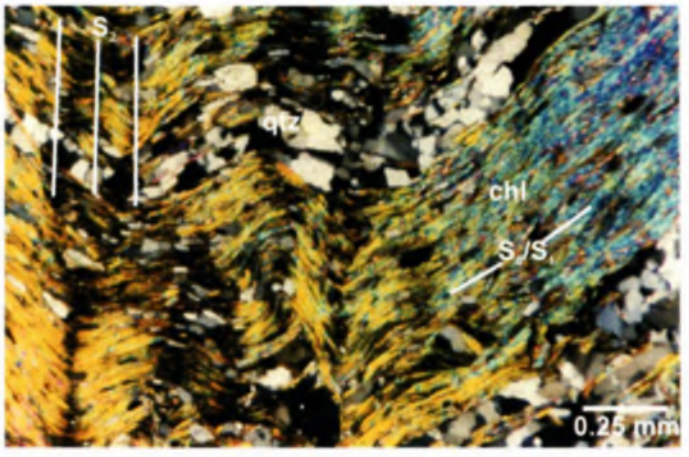

Plate 5.20. An example of F_2 crenulation/ kink folding on a microscopic scale, from a chlorite-muscovite schist at Spitskop.

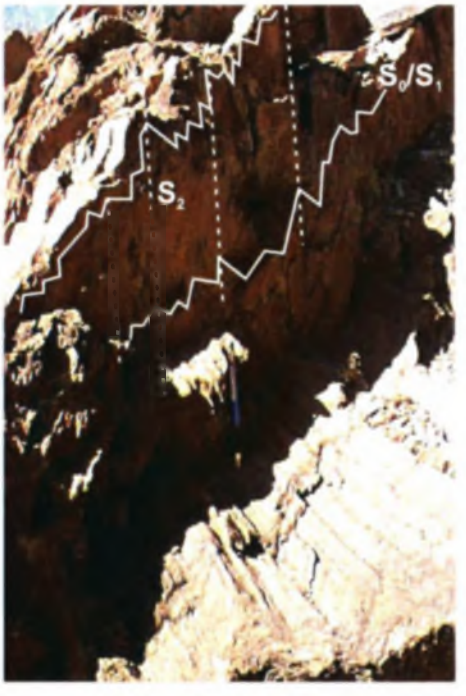

Plate 5.21. F_2 crenulation/ kink folding occurring within the quartz-chlorite-muscovite schist located in the Spitskop area. Photograph taken looking towards the southeast.

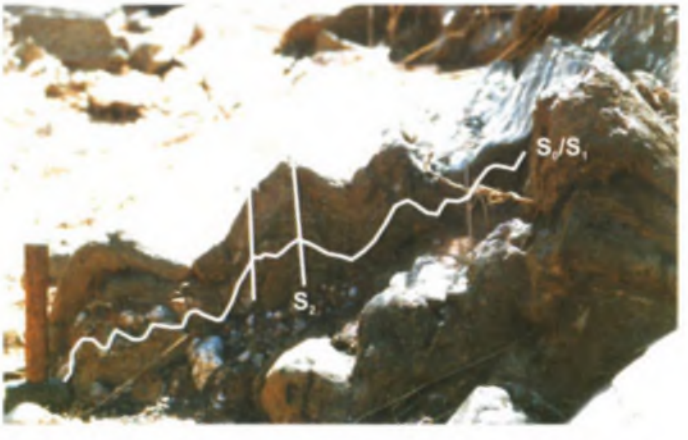

Plate 5.22. An example of crenulation/ kink folding (F_2) seen in quartz-chlorite-muscovite schists in the Goudmyn se Kop area. Photograph taken looking towards the northwest.

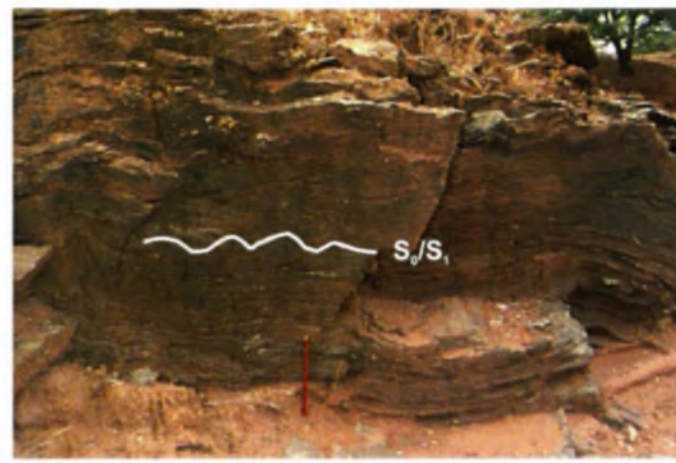

Plate 5.23. Gentle F_2 folding of the S_0/S_1 fabric (see annotation) within the quartz-feldspar-muscovite schist in the Spitskop area. Photograph taken looking to the southeast. Note pencil for scale.

Plate 5.24. An example of a "steep zone", looking along the strike (south-southeast) in quartz-chlorite-muscovite schists in the Spitskop area. The steep zone is more susceptible to weathering and erosion, and often controls the location of stream beds and *dongas*.

a)

b)

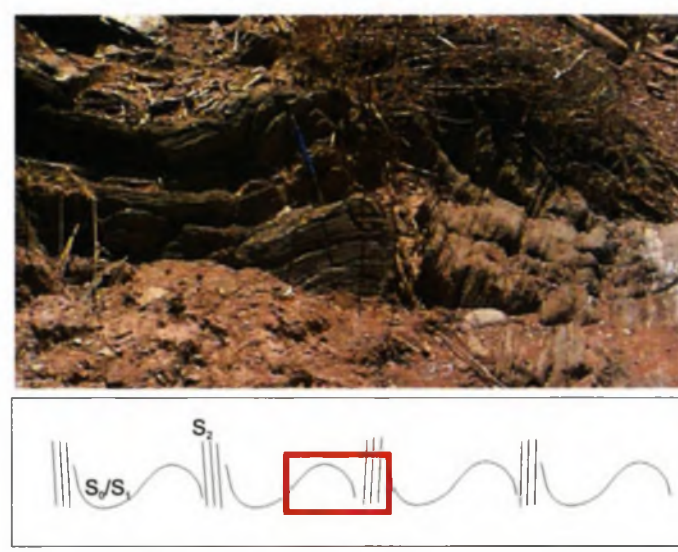

Plate 5.25.

a) Open folding (F_2) of quartz-feldspar-muscovite schist in the Spitskop area. Steeper fabric to the right of the photograph represents S_2 (Figure 5.5). Photograph taken looking towards the northwest. Note pen for scale.

b) Schematic diagram of the above relationship between the folded S_0/S_1 fabric and S_2 axial planar cleavage. Open sigmoidal folding of S_0/S_1 by F_2, separated by steep zones (S_2) S_2 in the schistose rocks is axial planar to the large scale folds (10 to 100 m). The red box represents folding in the photograph above.

70°. The steep limb zones are axial planar in orientation to the F_2 folds and therefore represent the S_2 axial planar cleavage in these rocks (Fig. 5.5a).

Large-scale F_2 folding is best seen within the Tygerberg Formation where outcrops are better. Here folding is upright, tight- to isoclinal, with limbs dipping greater than 60° with a penetrative axial planar cleavage (S_2). Folding in the Tygerberg Formation is consistently orientated northwest-southeast. Similar folding to that seen in the Tygerberg Formation is identified in the non-schistose rocks throughout the area, especially to the east around the town of Hermon, and north between the towns of Hermon and Porterville, where folding is orientated north-northwest-south-southeast. To the north of Tygervalley and Philadelphia, around the town of Hopefield and to the north of Moorreesburg, the F_2 folding is also orientated northwest-southeast.

The S_2 axial planar fabric, defined by chlorite and muscovite is axial planar to F_2 folds. The strike of the S_2 fabric on a regional scale is fairly consistent, varying from northwest-southwest to north-northwest-south-southeast (Figs. 5.5 & 5.6). The dip of S_2 varies in the non-schistose rocks, although it is always greater than approximately 70° and commonly near vertical (Figs. 5.5a, b & c). This fabric is best developed on an outcrop scale in the non-schistose rocks (e.g. the area around Philadelphia, Tygervalley, Hopefield and Porterville) as explained above. An S_2 foliation formline map (Fig. 5.6, based on data presented in Appendix D, Map 4) emphasises the relative consistent trend of the S_2 axial planar foliation, which is in marked contrast to the curved nature of the S_0/S_1 form lines shown in Figure 5.2 (See also Appendix D, Map 4).

Clasts within conglomerates and coarse-grained lithologies of the Piketberg Formation define a stretching lineation, L_{2a}, in the non-schistose rocks. The oval clasts are elongated and show axial ratios of, on average approximately 2:1. The long axes of the clasts consistently trend northwest-southeast throughout the Piketberg Formation. Approximately 2 km to the north of Piketberg, orientated clasts plunge less than 20° on a bearing of 320° (Fig. 5.7a).

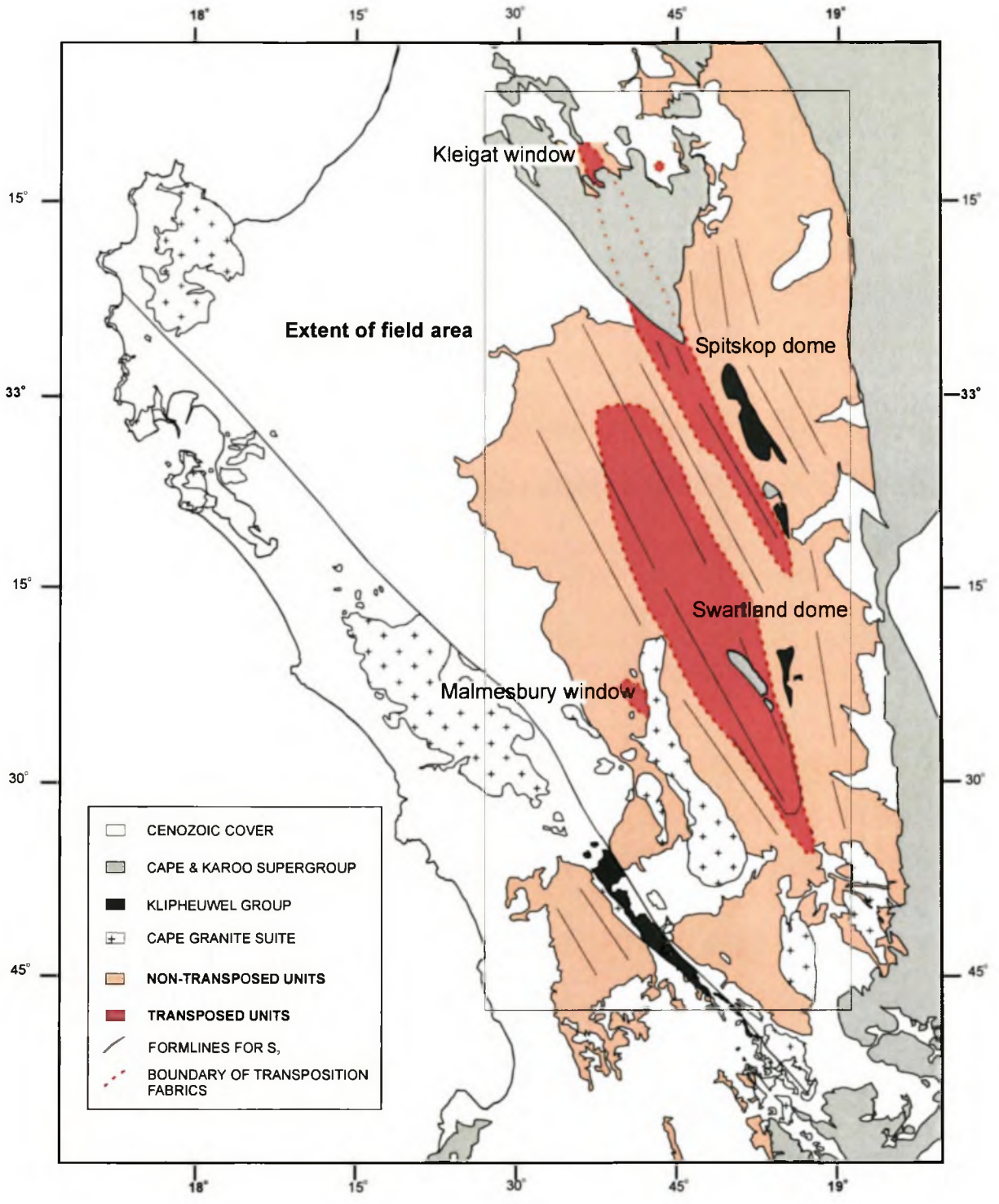

Figure 5.6. Foliation formline for the S_2 axial planar cleavage to the F_2 folds. S_2 has a consistent trend (northwest-southeast) in both the transposed and non-transposed units.

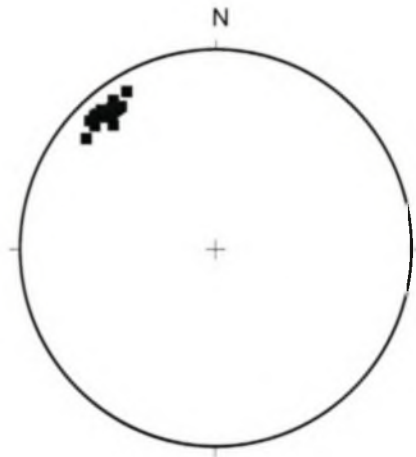

a) L_{2a} of clasts within conglomerates near Piketberg (n= 26)

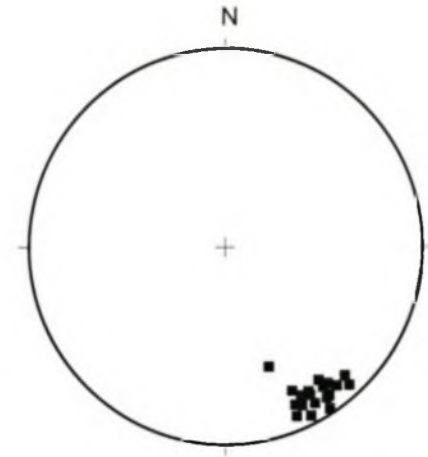

b) L_{2b}: Crenulation lineation of schists at Spitskop (n= 21)

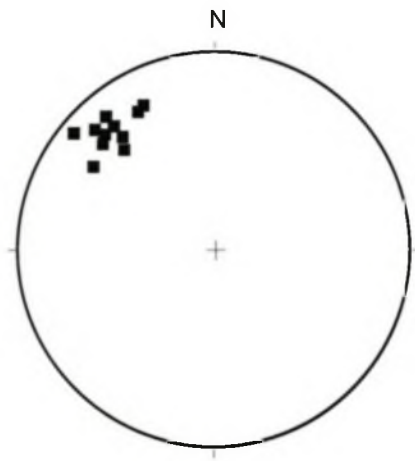

c) L_{2b}: Crenulation lineation within schists at Riebeeck West Quarry (n= 11)

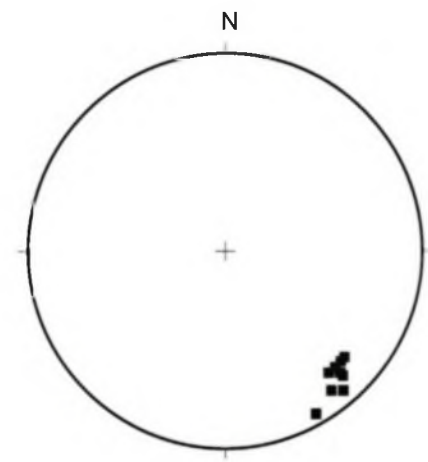

d) L_{2b}: Crenulation lineation within schists at Kruisfontein Quarry (n= 9)

Figure 5.7. Lower hemisphere equal-area projections of L_2 lineations. Note the lineations plunge both to the northwest and southeast, most likely a result of later F_3 folding orientated northeast-southwest.

At Spitskop, the S_0/S_1 lineation within the quartz-chlorite-muscovite-feldspar schists are crenulated by F_2 folds, from a microscopic scale up to approximately 5 cm. The small-scale crenulation folds (F_2) are parallel to the larger F_2 folds and define L_{2b} (Fig. 5.7b). The same crenulation lineation is identified in the quartz-chlorite schists at Riebeeck West and Kruisfontein Quarries (Fig. 5.7c & d).

5.4 D_3

Gentle refolding of the F_2 folds, seen in the periclinal northwest-southeast plunge of F_2 fold axes and L_2 lineations, produced a series of minor cross folds (F_3) whose axes are orientated northeast-southwest. F_3 folds are seen throughout the Malmesbury Group (Fig. 5.8). In the Spitskop area, these folds are open folds. Since F_3 folds are perpendicular to the F_2 fold axes, F_3 folding produces a gentle dome and basin morphology, classified as type-1 interference folds by Ramsay (1967).

F_3 kink folds were also identified in Kruisfontein Quarry. Here the fold wavelength rarely exceeds 5 cm and F_3 folds describe a consistent orientation of approximately 240/20° (Fig. 5.8b). Similar kink folding can be recorded approximately 10 km to the north in the Riebeeck West Quarry (Figs. 5.8c & d) identifying a orientation of approximately 045/45°, indicating a regional northeast-southwest trend for the F_3 folds.

Crenulation folds related to F_3 folding are seen in the schistose rocks. F_3 folding in general was gentle to open. Crenulation folding was only locally developed, specifically at the Kruisfontein and Riebeeck West Quarries. The doubly plunging nature of the L_2 lineations (Fig. 5.7) is most likely a result of the later F_3 folding.

5.5 Cross sections

Six cross sections, labelled A to F, were drawn across the Swartland Terrane running approximately northeast-southwest, perpendicular to the trend of the regional fabric (Appendix D, Map 4). The cross sections reveal two regional antiforms, orientated north-northwest-south-southeast. Hartnady et al. (1974) originally identified the two antiforms and referred to them as the Swartland and Spitskop domes. The Swartland

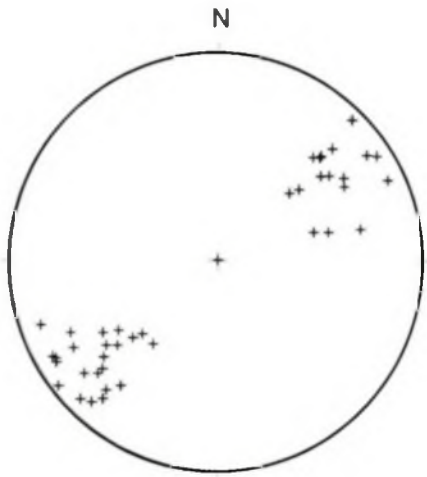

a) F_3 fold axes of the quartz-chlorite-feldspar schist in the Spitskop area, n=41

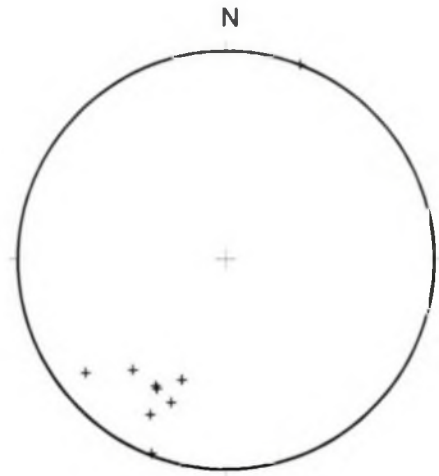

b) F_3 fold axes of the quartz-chlorite schists at the Kruisfontein Quarry, n=8.

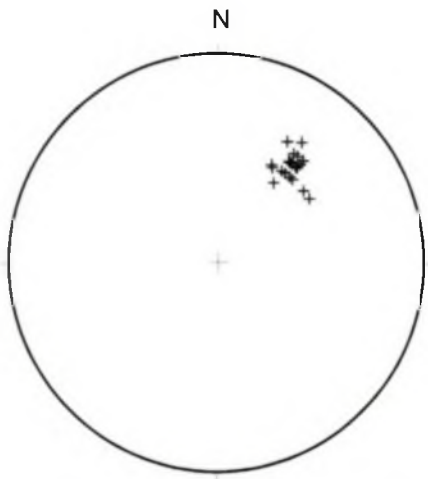

c) F_3 fold axes of the quartz-chlorite schists at Riebeeck West Quarry, n=19.

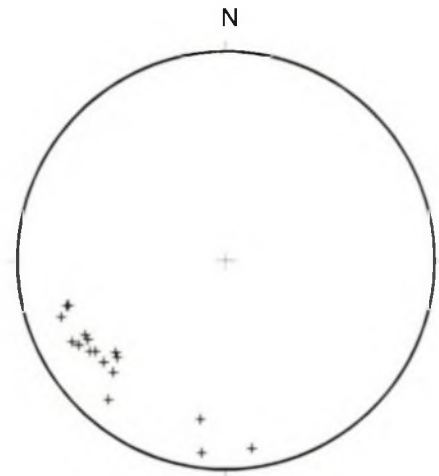

d) F_3 fold axes of the quartz schists at Porseleinberg and Bothmaskloof Pass, n=17.

Figure 5.8. Lower hemisphere equal-area projections of the orientation of F_3 fold axes throughout the Swartland Terrane.

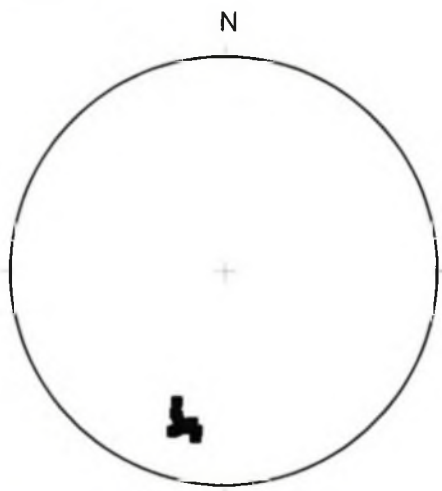

L_3: Crenulation lineation of schists at Kruisfontein Quarry (n= 12).

Figure 5.9. Lower hemisphere equal-area projection of the L_3 crenulation lineations.

dome is doubly-plunging and asymmetrical with generally steep dipping limbs (<60°). In the north, the plunge of the Swartland dome is approximately 50° to the northwest and in the south the plunge is approximately 30° to the southeast. The Spitskop dome is asymmetrical, with the western limb dipping generally 70-80° to the south-southwest, while the eastern limb dips shallower at 40-50° to the north-northeast. The Spitskop dome is also non-cylindrical with the axial trace of the antiform undulating, most notable to the south of Spitskop. The dome is doubly-plunging with plunges varying from sub-horizontal to approximately 50° along the strike of the antiform (Fig. 5.10).

5.6 Summary

The subdivision of the study area based on structural criteria alone, i.e. the presence or absence of the early transposition fabric, allows the identification of two major units. The occurrence of rocks exhibiting evidence of the early deformation event, D_1, corresponds to the distribution of schistose rocks, whereas the non-schistose rocks do not contain evidence of the early D_1 deformation event. The schistose rocks occur as isolated windows within the non-schistose rocks. These windows coincide with the regional F_2 antiforms (Fig. 5.10). The boundary between the two subgroups cannot be located in the field due to poor outcrops, but regional mapping suggests that the boundary can be constrained to a 200-300m wide zone (Appendix D, Map 4). Hereafter, the schistose rocks containing D_1 will be referred to as the lower unit and the non-schistose rocks devoid of D_1 deformation, as the upper unit.

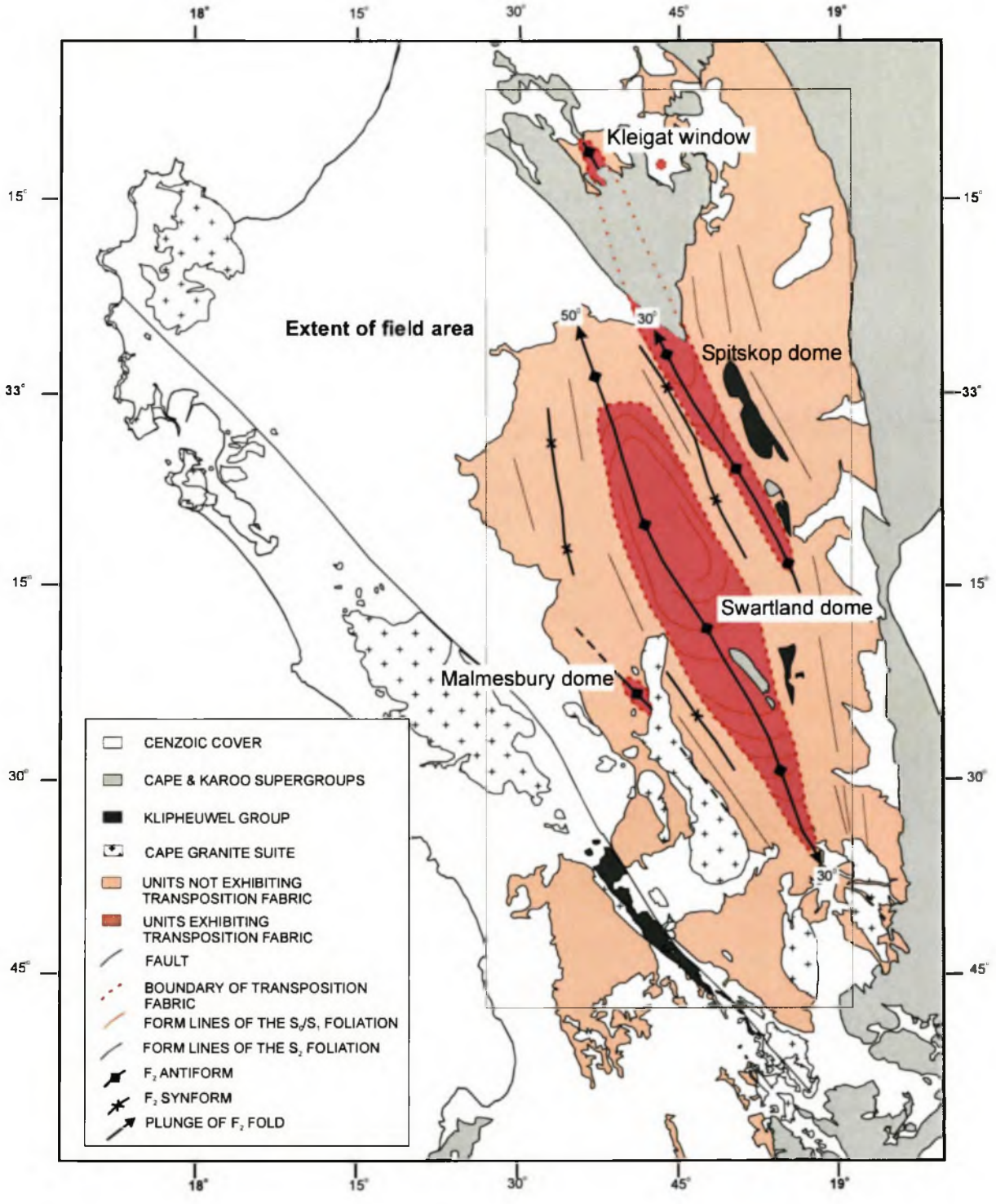

Figure 5.10. Summary of the structural information and the location of the rocks exhibiting the transposition fabric. The boundary between the rocks containing the tight-to-isoclinal intrafolial folds and those that do not, clearly correlates with the boundary between the schistose and non-schistose rocks described in Chapter 4 (Figure 4.1).

6 GEOCHEMISTRY

Whole-rock geochemical analysis (major and trace elements) was undertaken on a total of 121 samples. Ninety samples of the schistose rocks were analysed, including both the metasedimentary and metavolcanic rocks in the Spitskop area and at Kruisfontein Quarry (Fig. 4.1). The metavolcanic rocks of the Spitskop area were analysed to identify their protolith and also for geochemical comparison with metavolcanic rocks mapped along strike to the southeast (Bridgetown Formation) and in the northwest (Riviera area). This was undertaken in an attempt to establish a possible relationship between the three metavolcanic rock occurrences. The remaining thirty-one samples were taken from across the non-schistose rocks and represent lithologies of the Tygerberg, Moorreesburg and Porterville Formations.

Many of the discrimination diagrams used below are based on the of use elements interpreted to have been immobile during metamorphism, e.g. Winchester and Floyd (1977). However, the effect fluid alteration has on the mobility of the supposed immobile elements is still not fully understood (Rollinson, 1996). Even the REE, which are suggested to be immobile, have been recorded as being mobile in certain environments where fluid alteration was evident (e.g. Humphries, 1984; Vocke et al., 1987). Mass transfer calculations using the supposedly immobile elements Ti, Mg, Al, Mn, Zr, Y and P (Winchester and Max, 1984; Glazner and Batley, 1991; Selverstone et al., 1991) were carried out following the method of Grant (1986) and Baumgartner and Olsen (1995). Following the initial calculations, the elements Ti, Mg, Mn, Zr, Y and P, and in certain instances Al, were identified to be mobile in the metasedimentary and metavolcanic rocks. This introduces a possible uncertainty in the classification proposed below in the metasedimentary and metavolcanic rocks investigated here.

6.1 Metasedimentary rocks

Field and petrographic studies allow for the subdivision of the schists at Spitskop and Kruisfontein Quarry based on their quartz, chlorite, muscovite and feldspar contents (Chapter 4.1). Schists in the Spitskop and Kruisfontein areas typify the schist units throughout the Berg River Formation (lower unit), where they form the majority of outcrops. Although primary sedimentary features are rare, grain size and colour variations and occasionally bedding can be distinguished at certain localities, indicating that these schists were originally sediments.

The schists of the Berg River Formation have been subdivided based on their petrography and show slight variations in their geochemistries that reflect this compositional difference (Table 6.1). The quartz-chlorite-muscovite and quartz-feldspar-muscovite schists are composed, on average, of 66% SiO_2, 14% Al_2O_3, and 5% total alkalis. The lower quartz content of the quartz-poor schists is reflected in the lower SiO_2 content of approximately 55%. The quartz schist is composed predominantly of SiO_2 (86%), minor Al_2O_3 (4%), total iron (3%), MgO (1%) and 2% total alkalis. This reflects the petrology of the schist, being composed mainly of quartz and minor chlorite.

The quartz-chlorite-muscovite schists are geochemically characterised by their low CaO (< 1%), high Al_2O_3 (> 14%) and total iron (> 6%) content. According to Bucher and Frey (1994), this composition is characteristic of a metamorphosed pelitic rock, with the relatively high SiO_2, Al_2O_3, and K_2O typical of chemically mature argillaceous sediments (Garrels and Mackenzie, 1971). The composition of the schists is similar to the North American Shales Composite (NASC; Gromet et al., 1984) and the 'average' pelitic rock composition of Shaw (1956) (Fig. 6.1).

Shales and greywackes from the Porterville, Moorreesburg and Tygerberg Formations (upper units) were also plotted on Figure 6.1 for comparison against the schists. Geochemically the greywackes/shales from the Moorreesburg Formation are comparable to the Tygerberg Formation greywackes with very similar compositions (Table 6.2). The Porterville Formation greywackes differ geochemically from the other

Table 6.1. Summary of the geochemistry of the quartz-chlorite-muscovite-feldspar schists in the Spitskop area. Full data set presented in Appendix D, 5 & 6.

		Quartz-feidspar-muscovite schist		Quartz-chlorite-muscovite schist		Chlorite-muscovite schist		Muscovite-chlorite schist	
		n=16	sd	n=22	sd	n=9	sd	n=6	sd
wt.%	SiO_2	65.5	4.7	65.5	4.2	54.6	1.8	55.7	7.6
	TiO_2	0.8	0.1	0.8	0.1	0.9	0.0	0.8	0.2
	Ai_2O_3	13.6	2.8	14.3	2.4	21.1	1.1	19.9	4.2
	Fe_2O_3T	6.2	1.3	6.4	1.1	9.2	0.6	8.7	1.8
	MnO	0.2	0.1	0.1	0.0	0.1	0.1	0.2	0.1
	MgO	2.3	0.5	2.4	0.6	2.1	0.2	2.8	0.7
	CaO	0.9	0.7	0.9	0.7	0.1	0.4	0.6	1.0
	Na_2O	1.3	0.4	0.9	0.8	0.0	0.3	0.2	0.4
	K_2O	2.5	0.8	2.9	0.5	5.1	0.8	4.1	1.2
	P_2O_5	0.2	0.0	0.2	0.0	0.1	0.0	0.1	0.0
	H_2O-	0.4	0.3	0.3	0.1	0.3	0.1	0.3	0.2
	LOI	3.8	0.8	3.6	0.5	4.4	0.2	4.6	0.9
	TOTAL	97.7	0.6	98.4	1.4	98.0	0.3	98.0	1.0
ppm	Mo	1	1	1	1	1	0	1	1
	Nb	12	1	11	1	14	1	12	2
	Zr	196	28	197	32	175	10	157	19
	Y	33	3	33	3	37	2	34	5
	Sr	90	30	81	21	53	29	113	27
	U	3	1	3	1	2	1	2	1
	Rb	112	28	122	25	186	24	176	31
	Th	13	2	13	3	16	1	16	2
	Pb	19	5	22	6	37	4	23	9
	Ga	19	3	19	3	26	1	25	3
	Zn	114	34	106	14	134	10	130	31
	Cu	25	11	30	12	36	14	43	16
	Ni	42	17	47	20	53	3	58	29
	Cr	117	43	111	31	125	2	123	30
	Nd	35	5	37	7	43	3	44	6
	V	128	26	125	17	169	9	131	24
	Ce	74	7	75	11	88	4	89	12
	La	36	6	38	10	44	4	50	9
	Ba	513	47	507	59	572	78	486	83
	Sc	19	3	20	3	25	1	24	3

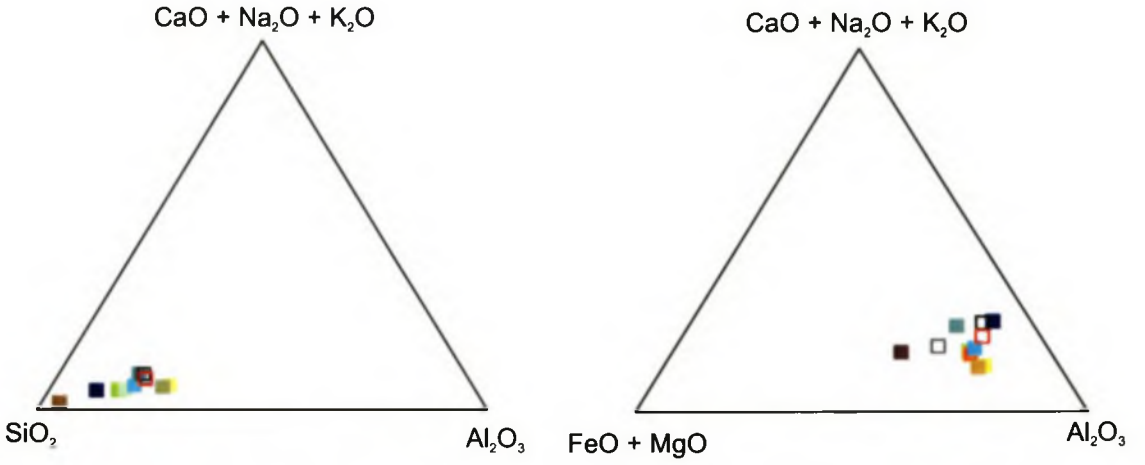

Figure 6.1. Al_2O_3 - $CaO+Na_2O+K_2O$ - SiO_2 and Al_2O_3- $CaO+Na_2O+K_2O$- $FeO+MgO$ ternary diagrams of the average geochemistry of the different metasedimentary rocks compared to the average shale geochemistry as defined by Gromet et al. (1984) and Shaw (1956). All the metasedimentary units plot close to the average shales compositions.

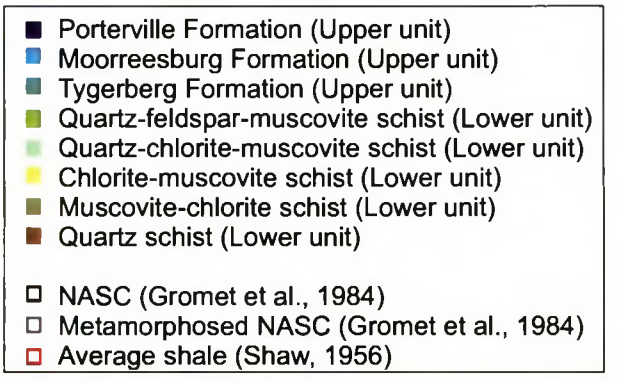

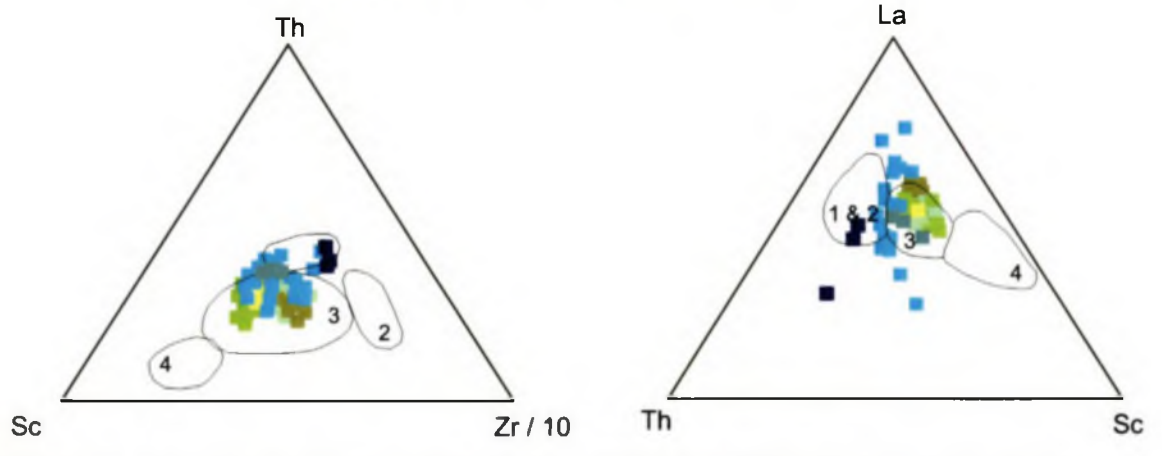

Figure 6.2. Discrimination diagrams from Bhatia and Crook (1986) for the different tectonic environments of deposition for greywackes and shales.The metasedimentary rocks generally plot within the "Continental Island Arc" tectonic environment. For further information see text.

(1) Active continental margin. (2) Passive margin. (3) Continental island arc. (4) Oceanic island arc.

Table 6.2. Summary of the geochemistry of the chert, quartz schist and marly limestone from the Spitskop area. Full data set presented in Appendix C, 5 & 6. For the location of individual lithological units, see Appendix D, Map 2.

		Chert		Quartz schist		Marly Limestone	
		n=10	sd	n=2	sd	n=7	sd
wt.%	SiO_2	83.4	2.3	85.7	0.5	44.8	9.6
	TiO_2	0.0	0.0	0.3	0.0	0.4	0.1
	Al_2O_3	1.1	0.5	3.7	0.5	8.6	2.2
	Fe_2O_3T	8.4	2.8	3.4	1.8	4.1	1.2
	MnO	0.3	0.0	0.0	0.0	0.6	0.1
	MgO	1.4	0.0	1.4	0.0	3.1	1.3
	CaO	0.1	0.1	1.6	0.1	17.3	8.4
	Na_2O	0.0	0.0	0.0	0.0	1.3	0.6
	K_2O	0.0	0.0	0.2	0.0	1.8	0.6
	P_2O_5	0.0	0.0	0.0	0.0	0.1	0.0
	H_2O-	0.8	0.3	0.2	0.3	0.1	0.1
	LOI	2.4	0.2	2.4	0.2	16.4	5.8
	TOTAL	97.9	0.7	99.1	0.3	98.7	0.9
ppm	Mo	1	0	-	0	2	0
	Nb	2	0	-	0	8	2
	Zr	46	17	89	10	129	31
	Y	21	13	9	4	24	3
	Sr	8	8	26	8	337	138
	U	1	0	2	0	4	1
	Rb	7	5	5	2	73	27
	Th	2	1	2	1	8	2
	Pb	2	1	1	1	15	3
	Ga	1	0	2	0	12	3
	Zn	111	61	22	4	56	16
	Cu	4	4	2	4	30	12
	Nl	3063	480	12	4	29	8
	Cr	3011	560	130	17	62	15
	Nd	6	3	7	3	22	5
	V	63	5	12	5	74	16
	Ce	9	6	15	6	55	11
	La	11	10	3	1	25	6
	Ba	162	115	8	3	432	134
	Sc	14	0	-	-	12	-

greywackes/shales due to the higher SiO_2 content and lower total iron and MgO. Geochemically the greywackes and shales of the three formations fall within the compositional range of greywackes and shales suggested by Carmichael (1989). The greywackes and shales of the non-schistose rocks are geochemically similar to the schistose rocks (Table 6.2; Fig. 6.1). The quartz schist, due to its high SiO_2 content was probably an impure sandstone before regional metamorphism. Minor clay minerals present in the protolith were converted into chlorite and muscovite during metamorphism (Table 6.2).

At Spitskop, the marly limestone layer intersected during drilling is interlayered with quartz-muscovite schist. This is reflected in its geochemistry, with the higher than expected SiO_2 and Al_2O_3 contents (Table 6.3). The chert at Spitskop is composed predominantly of quartz and minor magnetite layers (Chapter 4.1.7) and this is reflected in its geochemistry (Table 6.3). The SiO_2 content of cherts may vary significantly, depending on purity and associated mineralisation (Pettijohn, 1975). In general, the chert at Spitskop falls within the geochemical composition range of the average chert of Pettijohn (1975). The chert also has high Ni (3066 ppm) and Cr (3011 ppm) values. This was interpreted as related to hydrothermal alteration (Slabber, 1995).

6.1.1 Tectonic setting

The assumption used in geochemical discrimination diagrams for establishing tectonic environments for sedimentary rocks, is that differing tectonic environments have certain provenance characteristics, and this variation in provenance will be reflected in the whole-rock geochemistry of the sediments (e.g. Bhatia and Crook, 1986). Rollinson (1996), however, stated that this provenance classification is more applicable to immature sediments with high lithic contents and becomes less reliable with more mature sedimentary rocks.

Two discrimination diagrams of Bhatia and Crook (1986) were used (Th-Sc-Zr/10 and La-Th-Sc), which discriminate between different tectonic environments for greywacke-shale lithologies (Fig. 6.2). From both these discrimination diagrams the schists (lower unit) plot within the 'continental island-arc' field which, according to

Table 6.3. Summary of the geochemistry of the greywackes and shales from the Porterville, Moorreesburg, and Tygerberg Formations (Upper unit). For the location of the formations see Figure 2.5. Full data set presented in Appendix C, 5 & 6.

		Greywacke (Porterville Formation)		Greywackes/shales (Moorreesburg Formation)		Greywackes (Tygerberg Formation)	
		n=3	sd	n=23	sd	n=5	sd
wt.%	SiO_2	78.3	2.3	63.0	5.5	60.8	0.7
	TiO_2	0.6	0.1	0.9	0.2	0.8	0.0
	Al_2O_3	9.8	0.8	15.4	3.2	14.9	1.7
	Fe_2O_3T	3.2	0.0	6.3	3.5	6.3	0.7
	MnO	0.0	0.0	0.1	0.1	0.2	0.0
	MgO	1.0	0.2	2.6	1.4	4.0	0.7
	CaO	0.0	0.0	0.1	0.1	2.4	1.8
	Na_2O	1.5	1.0	1.8	0.9	2.0	0.6
	K_2O	3.3	0.4	3.6	1.1	3.7	0.4
	P_20_5	0.1	0.0	0.1	0.1	0.1	0.0
	H_2O-	0.3	0.0	1.0	1.1	0.1	0.0
	LOI	1.6	0.2	4.5	1.9	4.2	1.6
	TOTAL	99.7	0.9	99.5	0.2	99.7	0.4
ppm	Mo	-	-	-	-	-	-
	Nb	21	2	21	3	20	1
	Zr	307	19	214	38	184	4
	Y	33	6	50	13	35	1
	Sr	46	1	61	28	91	29
	U	11	3	7	3	10	5
	Rb	184	46	167	51	163	7
	Th	33	5	25	5	24	5
	Pb	40	10	27	8	20	8
	Ga	15	3	23	6	23	4
	Zn	30	17	92	78	107	12
	Cu	30	1	20	11	15	1
	Ni	20	1	46	20	49	2
	Cr	118	6	109	27	108	24
	Nd	36	5	46	18	36	7
	V	40	6	112	34	115	20
	Ce	100	12	118	40	102	20
	La	33	10	58	20	46	10
	Ba	590	87	635	269	540	112
	Sc	15	1	24	4	24	3

Bhatia and Crook (1986), describes sediments deposited in fore-, inter-, or back-arc settings on continental crust or thin continental margins. The greywackes/shales from the Tygerberg Formation also fall within the same field as the schists. The greywackes/shales from the Porterville Formation plot within the active continental margin and passive margin fields of Bhatia and Crook (1986). The Moorreesburg Formation plots across several different fields, plotting in both the continental island arc field with the schists and the Tygerberg Formation and the active continental margin and passive margin fields along with the Porterville Formation.

6.2 Metavolcanic rocks of the Spitskop area

As described in Chapter 4.1.5, two different metavolcanic rocks have been identified in the Spitskop area, namely a chlorite-feldspar-quartz and a talc-carbonate schist. Geochemically, the chlorite-feldspar-quartz schist is composed of 60% SiO_2, 16.5% Al_2O_3, 3.5% MgO and 6% total alkalis. Trace element geochemistry reveals unusually high Ni (475 ppm), Cr (381 ppm) and V (144 ppm) values (Table 6.4). The talc-carbonate schist is composed of 44% SiO_2, 2% Al_2O_3, 8% total iron, 28% MgO and 4% total alkalis. The talc-carbonate schist also shows very high Ni (2302 ppm) and Cr (2830 ppm) values. The high MgO and the low values for the other major elements are due to the dominance of talc in the schist. The CaO content of 3% is explained by the carbonate (calcite and minor dolomite) veining within this unit.

The identification of the protolith of the talc-carbonate and chlorite-feldspar-quartz schist is impeded by the chemical changes the rocks have undergone during metamorphism and alteration. The elements (normally silica and the alkalis) used to classify fresh or only slightly altered volcanic rocks (e.g. the classifications of Le Maitre et al., 1989) are all known to be highly mobile during metamorphism (Pearce, 1976).

For this reason the classification of the metavolcanic rocks following conventional classification diagrams was deemed inappropriate. Both the metavolcanic rocks are rich in magnesium, reflected in the abundance of mafic minerals. The high Ni and Cr contents are also characteristic of ultramafic rocks (e.g. Halberg, 1985; Redman and Keays, 1985; Naldrett and Cabri, 1976).

Table 6.4. Summary of the geochemistry of the metavolcanic rocks from the Spitskop area (Lower unit). Full data set presented in Appendix C, 5 & 6. For the location of individual lithological units see Appendix D, Map 2.

		Talc-carbonate schist		Chlorite-feldspar-quartz schist	
		n=8	sd	n=10	sd
wt.%	SiO_2	43.6	11.5	60.0	5.7
	TiO_2	0.1	0.1	0.8	0.2
	Al_2O_3	1.8	1.0	16.5	4.1
	Fe_2O_3T	7.7	2.2	8.4	1.9
	MnO	0.1	0.1	0.2	0.1
	MgO	27.7	6.2	3.5	1.1
	CaO	3.0	2.1	0.9	0.8
	Na_2O	0.5	0.4	2.0	1.0
	K_2O	0.0	0.0	3.1	1.1
	P_20_5	0.0	0.0	0.1	0.1
	H_2O-	0.5	0.3	0.5	0.5
	LOI	15.2	7.2	5.0	1.4
	TOTAL	100.3	0.8	101.1	0.5
ppm	Mo	1	1	1	0
	Nb	2	1	11	3
	Zr	26	27	157	65
	Y	11	8	35	9
	Sr	50	37	80	19
	U	3	1	4	1
	Rb	3	5	131	51
	Th	3	0	11	4
	Pb	3	2	16	8
	Ga	3	1	21	5
	Zn	149	205	133	40
	Cu	3	1	35	57
	Ni	2302	785	475	916
	Cr	2831	939	381	804
	Nd	8	2	36	12
	V	54	26	144	35
	Ce	9	5	81	23
	La	9	4	41	15
	Ba	100	228	523	141
	Sc	-	-	-	-

The identification of the talc-carbonate schist located close to the chlorite-feldspar-quartz and graphitic schists within regionally metamorphosed sedimentary rocks, is similar to that described by Pearton (1980) and Sanford (1982). Here the ultramafic rocks reacted with the surrounding metasedimentary country rocks during regional low-grade metamorphism and fluid metasomatism to produce chloritic and talc-carbonate schists, and where the metasedimentary rocks were graphitic, graphite schists (Pearton, 1980; Sanford, 1982).

6.2.1 Tectonic setting

The TiO_2-MnO-P_2O_5 ternary diagram of Mullen (1983) discriminates between tectonic settings of basalts and andesites of oceanic regions (Fig. 6.3a). On this diagram, both metavolcanic rocks plot across several fields, including those of calc-alkaline basalts, MORB and island arc tholeiites. Neither of the two metavolcanic rocks plotted within any of the defined fields of the widely used diagrams of Pearce and Cann (1973), except in one diagram shown in Figure 6.3b, where the chlorite-feldspar-quartz schist plots within the calc-alkaline field.

Additional discrimination diagrams are provided by Pearce and Norry (1979) and Meschede (1986) who plotted Zr-Zr/Y (Fig. 6.3c) and Zr-Nb-Y (Fig. 6.3d) respectively. In both these diagrams the chlorite-feldspar-quartz schist plots within the within-plate basalt field, while the talc-carbonate schist plots within the MORB fields.

6.3 Geochemical comparison of the metavolcanic rocks

Geochemical comparison of the metavolcanic rocks in the Spitskop area and those of the Riviera area (data from Busch, 1998) and the Bridgetown Formation (data from Slabber, 1995) were undertaken to ascertain whether these metavolcanic units are geochemically related. The discriminations diagrams of Winchester and Floyd (1977) were used to compare the different metavolcanic rocks (Fig. 6.4). The metavolcanic rocks of the Bridgetown Formation and the Riviera area plot in the same fields, while the Spitskop chlorite-feldspar-quartz schist and talc-carbonate schist plot separately, but close to the metavolcanic rocks of the Bridgetown Formation.

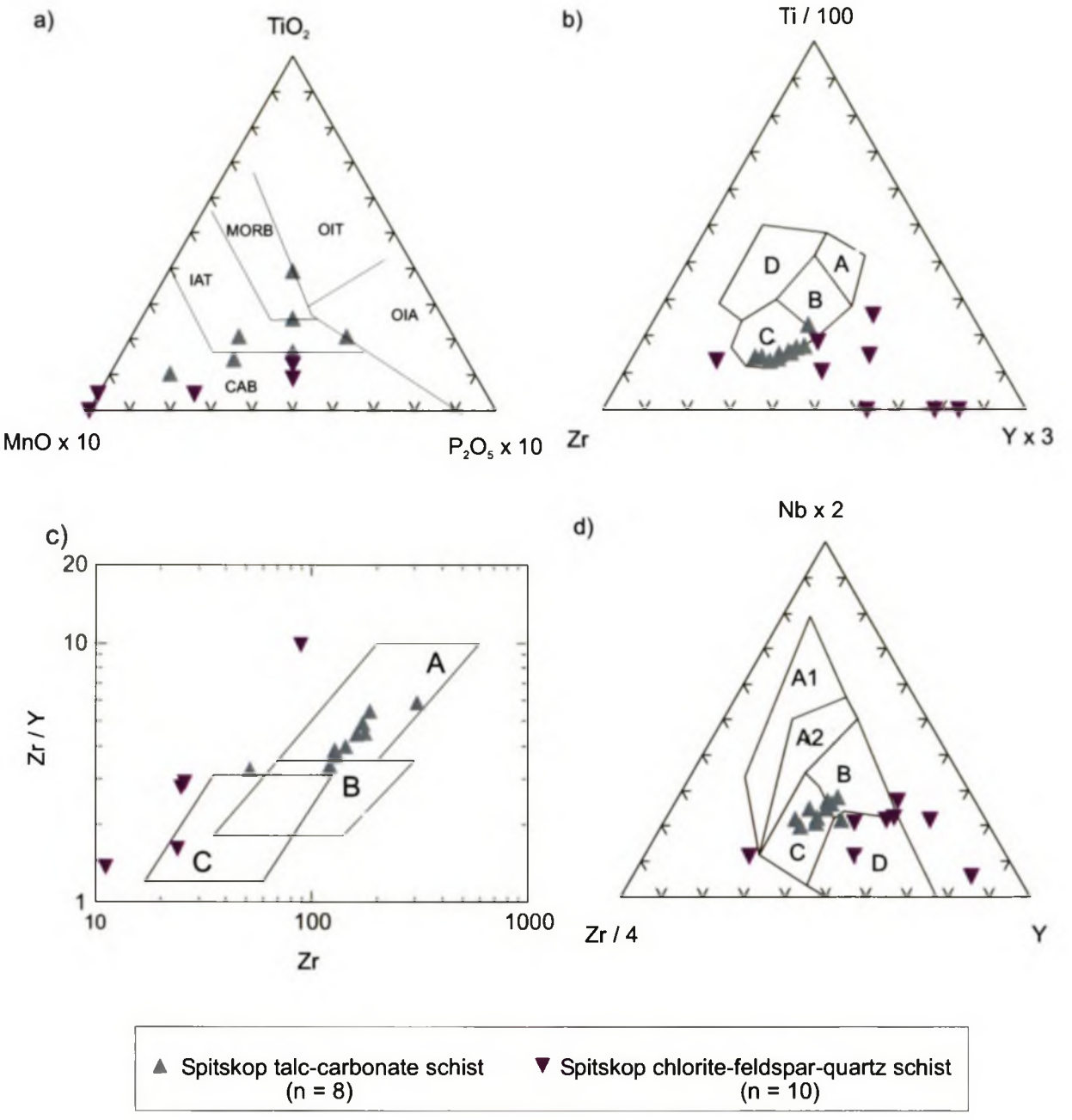

Figure 6.3. Discrimination diagrams for different tectonic environments.

a) After Mullen (1983).
b) After Pearce & Cann (1977); A- Island arc tholeiites, B- MORB, C- Calc-alkali basalt, D- within-plate basalt.
c) Pearce & Norry (1979); A- Within plate basalt, B- Island arc basalts, C-mid-ocean ridge basalts.
d) Meschede (1986); A1- Within-plate basalt, A2- Within-plate basalts & tholeiites, B- E-type MORB, C- Within-plate tholeiites & volcanic arc basalts, D- N-type MORB & volcanic-arc basalts.

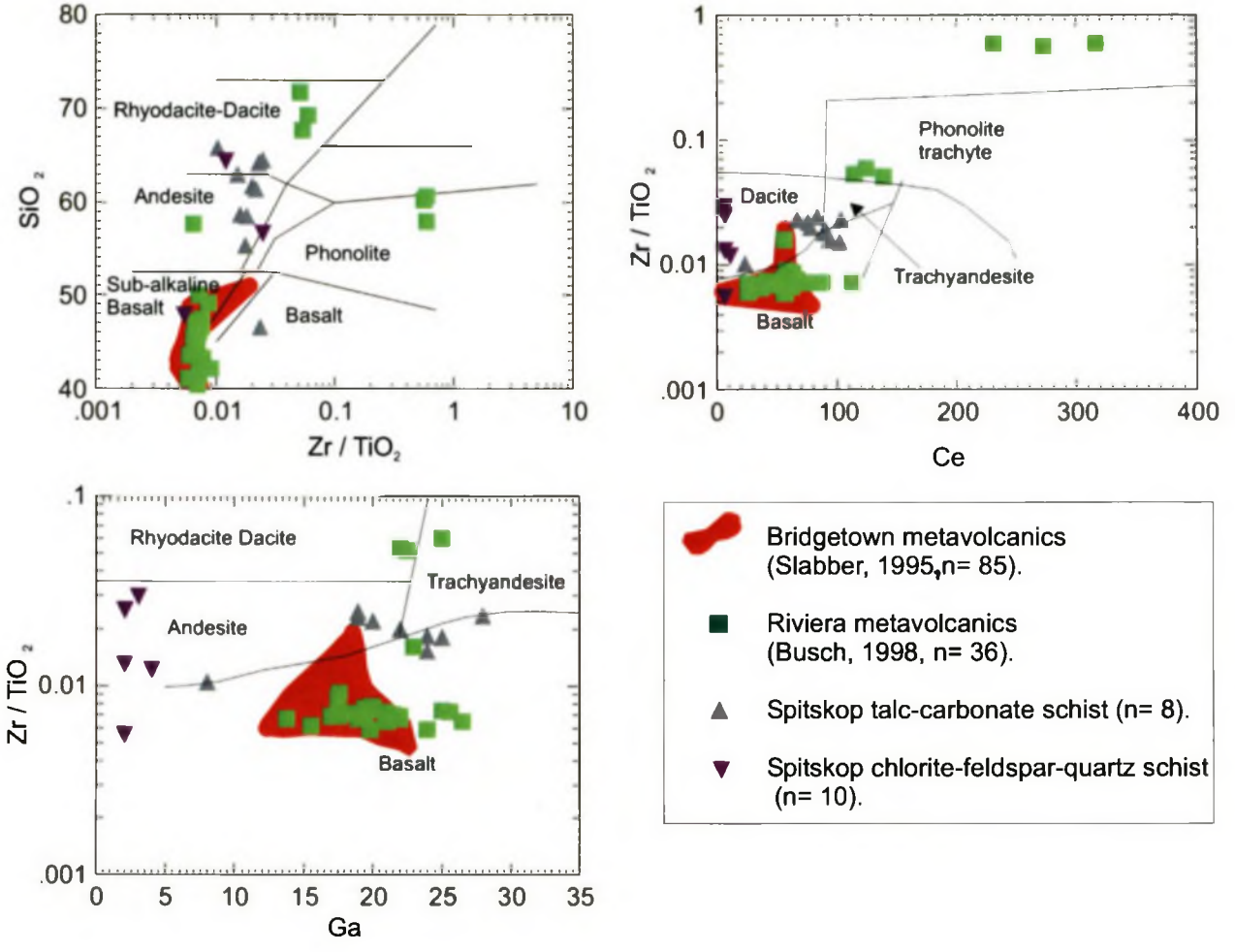

Figure 6.4. Classification of the metavolcanic rocks of the lower unit based on the discrimination diagrams for different igneous rocks by Winchester and Floyd (1977).

The geochemical similarities between the metavolcanic rocks of the Riviera area and the Bridgetown Formation are also indicated on the discrimination diagrams of Halberg (1985), as illustrated in Figure 6.5. From the classification of ultramafic rocks, a clear chemical difference exists between the Spitskop metavolcanic rocks and the Riviera area and Bridgetown Formation metavolcanic rocks because of the anomalously high Ni and Cr values of the talc-carbonate schist (Fig. 6.5). Comparison of the MgO content (Figs. 6.5d & e) of the metavolcanic rocks shows that the chlorite-feldspar-quartz schist (Spitskop) is similar to the Bridgetown and Riviera metavolcanic rocks, while the talc-carbonate schist with its unusually high MgO content always plots in a separate field. The metavolcanic rocks of Riviera and the Bridgetown Formation are geochemically classified as tholeiites, while the Spitskop metavolcanic units classify as komatiitic (Fig. 6.5d). In Figure 6.5e, the Bridgetown Formation and the Riviera metavolcanic rocks again plot together on the boundary between low- and high-magnesium basalts. Here, due to the varying MgO content, a clear separation in the metavolcanic rocks of Riviera can be seen.

6.4 Summary

The quartz-chlorite-muscovite-feldspar schists (lower unit) were originally mudstones and shales that were deposited in a continental island arc setting according to their trace element geochemistry. The greywackes and shales of the Tygerberg, Moorreesburg and Porterville Formations (upper unit) are geochemically similar to one another and classifying as sediments deposited in an active continental margin/continental island arc setting.

The chlorite-feldspar-quartz schist and talc-carbonate schist were originally mafic volcanics. The geochemistry of the rocks points to their origin as tholeiitic basalts and a high-magnesium basalt, respectively. The metavolcanic rocks at Riviera and the Bridgetown Formation are geochemically very similar, and are comparable to the two metavolcanic units from the Spitskop area, possibly suggesting that they may be part of the same magmatic suite.

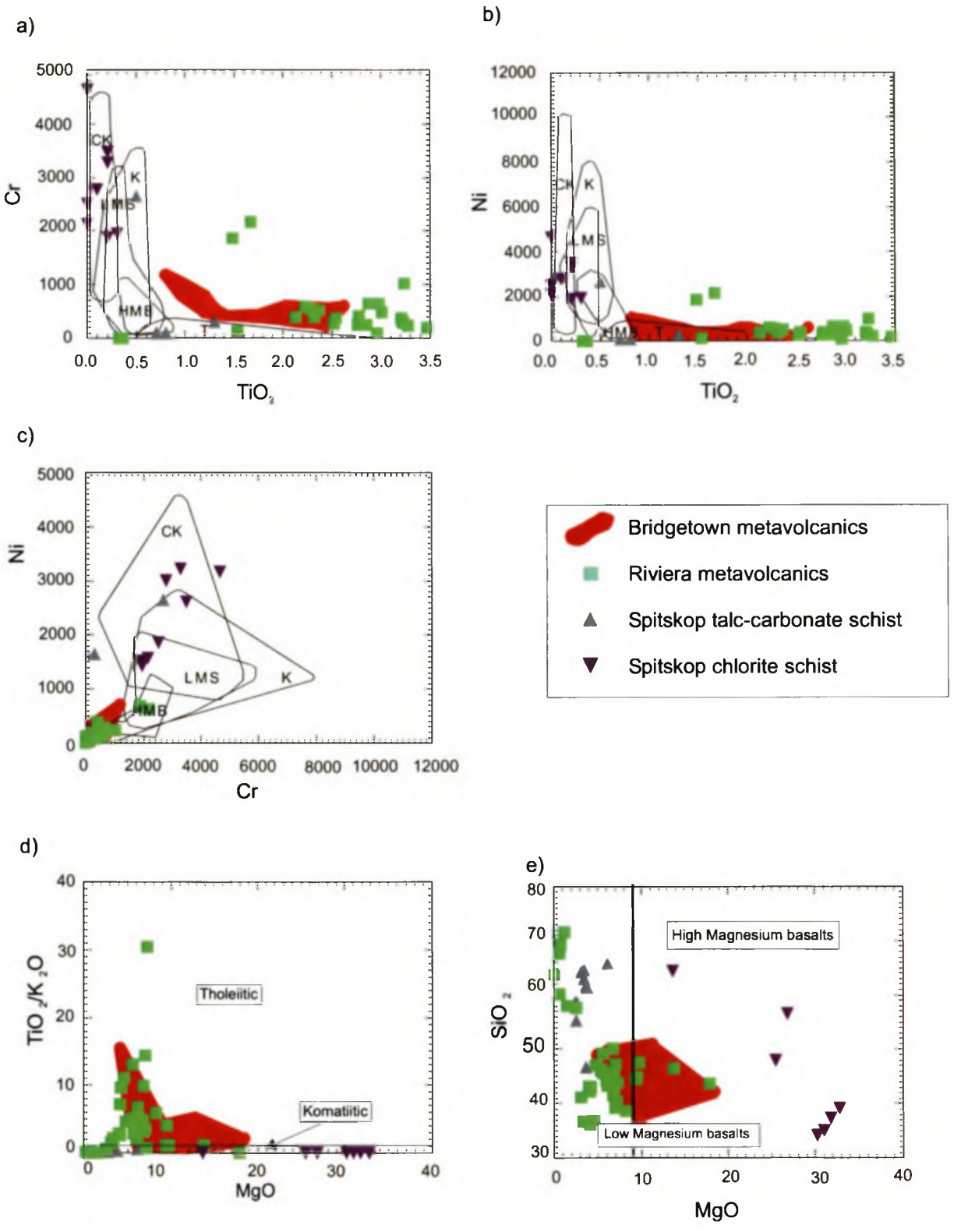

Figure 6.5. Classification diagrams for Mg-rich basalt, komatiite and tholeiites.
a) Cr- TiO_2; CK- cumulative komatiite, K- komatiite, HMB- high-magnesium basalt, LMS- layered high-magnesium basalt, T- tholeiitic basalt. Field boundaries from Halberg (1985).
b) Ni-TiO_2, field boundaries the same as above.
c) Ni-Cr, field boundaries the same as above.
d) TiO_2/K_2O- MgO, after Naldrett & Cabri (1976)
e) SiO_2- MgO, after Redman & Keays (1985)

7 METAMORPHISM

The Malmesbury Group has undergone regional, low-grade metamorphism during the Saldanian Orogeny (e.g. Theron et al., 1992; Rozendaal et al., 1999). However, very little work has been done to constrain the conditions of metamorphism of the lithologies. The monotonous nature and the low grades of metamorphism of the lithologies have made such constraints difficult. Recent work by Frimmel et al. (2001) has provided the only information on the metamorphism of the Malmesbury Group. A temperature of approximately 325 °C is indicated for greywackes of the Brandwacht and Norree Formation of the Boland Terrane in the Worcester area (for locations see Fig. 2.5).

As described in Chapter 4 and 5, both the S_0/S_1 and S_2 are defined by the metamorphic minerals chlorite and muscovite. Depending on whether D_1 and D_2 represent two temporally distinct or one progressive deformation event(s), the Malmesbury Group rocks could have undergone two metamorphic events during the Saldanian Orogeny. The earlier event (D_1), did not affect the non-schistose rocks (upper unit), as they do not contain the S_0/S_1 fabric. During the later Cape Orogeny, a temperature of approximately 300 °C indicating lower greenschist facies was reached (Hälbich and Cornell, 1983; Frimmel et al., 2001). The possibility of two metamorphic events related to the Saldanian Orogeny and the later overprint of the Cape Orogeny are further discussed in Chapter 10.3.3.

7.1 Metapelites

The metapelites of the lower unit are all composed of the mineral assemblage quartz-chlorite-muscovite ±albite (An_{01}) and accessory rutile (Plate 7.1; 7.2). Chlorite and muscovite define the folded S_0/S_1 fabric in the metapelites. The greywackes and shales of the upper unit are composed predominantly of quartz, feldspar, muscovite and minor chlorite. Quartz and feldspar (albite and microcline) are generally angular

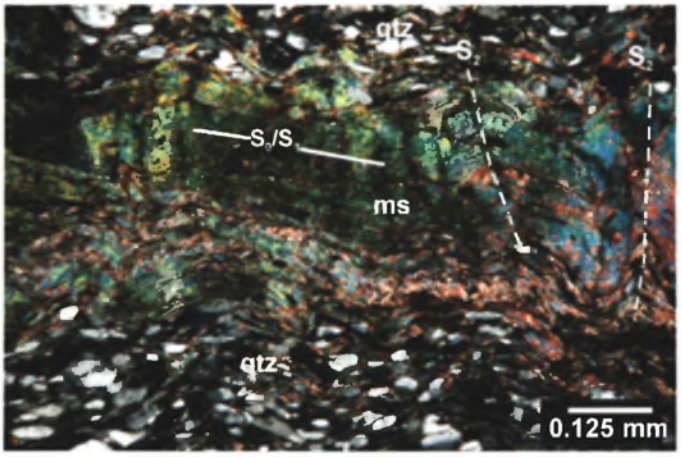

Plate 7.1. Muscovite-quartz schist. Sample from road cutting north of Moorreesburg described in Chapter 4.1.1 (Figure 4.1). Photomicrograph taken in XPL. Lithology is classified as part of the Berg River Formation (Theron et al., 1992).

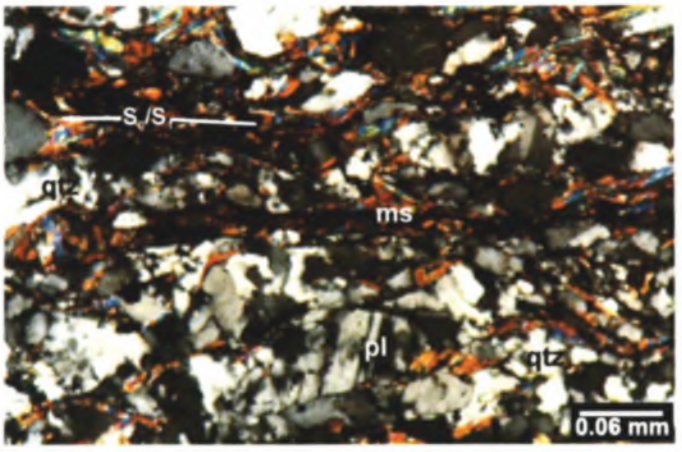

Plate 7.2. Quartz-muscovite-feldspar schist from east of the Moorreesburg (Figure 4.1). Classified as part of the Berg River Formation (Theron et al., 1992). Photomicrograph taken in XPL.

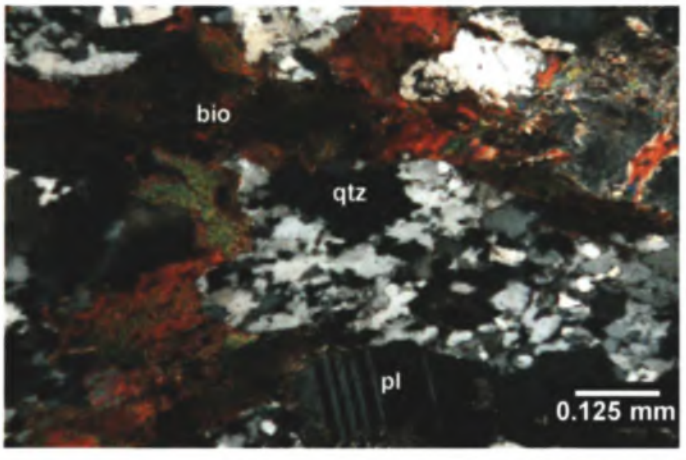

Plate 7.3. Biotite-feldspar schist from the road cutting next to the farm Kanonkop (Figure 4.1). The schist is described in detail in Chapter 4.1.6. Photomicrograph taken in XPL. Classified as part of the Moorreesburg Formation (Theron et al., 1992).

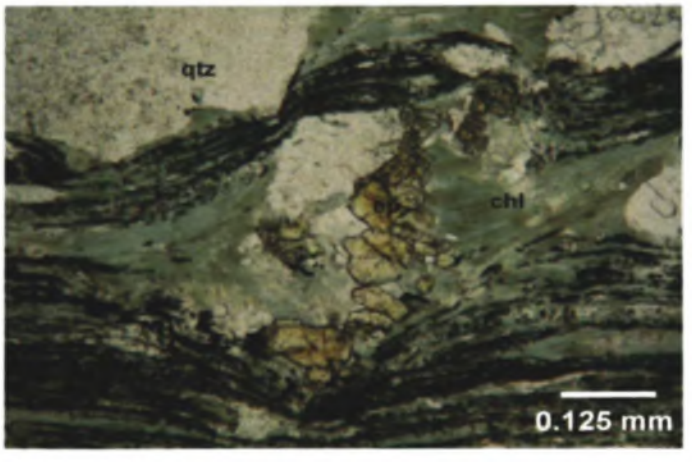

Plate 7.4. Quartz-chlorite-epidote schist (metavolcanic rock) from Riviera (Figure 4.1). Photomicrograph taken in PPL. Classified as part of the Bridgetown Formation.

to sub-angular, fractured and show little or no evidence of a preferred orientation. Muscovite forms laths that are often orientated, thus defining a weak fabric. The matrix is composed of kaolinite (from weathering) and chlorite, the latter of which occurs as small laths associated with muscovite. The mineral assemblage of the non-schistose rocks is not suited for any detailed geothermobarometric work and these minerals occur in a wide range of P-T conditions (e.g. Frey, 1987).

Figure 7.1 shows the AFM projection of the metasedimentary rocks of both the schistose and the non-schistose units compared to the average pelite and shale compositions of Shaw (1956), Gromet et al. (1984) and Carmichael (1989). The composition of the metasedimentary rocks is very similar to that of the average compositions plotted on the diagram.

The first prograde biotite appears in metapelites at a temperature of approximately 400 °C (420 °C at 3.5 kbar; Bucher and Frey, 1994). The lack of any biotite within the schists thus provides an upper limit for the maximum metamorphic temperature obtained in the schists (Fig. 7.2). The temperature of metamorphism can thus be constrained between approximately 200 °C (the first occurrence of chlorite and muscovite; Spear, 1995) and 400 °C. This temperature range characterises the lower greenschist facies (e.g. Bucher and Frey, 1994).

7.2 Biotite-feldspar schist (lower unit)

This schist is unique in the Malmesbury Group in that it is the only metasedimentary lithology containing biotite. This places the schist within a slightly higher grade of metamorphism than the other metapelites of the lower unit. The schist is composed of the mineral assemblage: biotite-feldspar-muscovite-quartz (Plate 7.3). The presence of biotite indicates a minimum temperature of 400 °C (Bucher and Frey, 1994) and is suggested to have formed at the expense of K-feldspar and chlorite or muscovite and chlorite following the equations (Spear, 1995):

$$Chl + Kfs = Bio + Ms + Qtz + H_2O \quad (7.1)$$

$$Chl + Ms = Bio + Al\text{-richer } Chl + Qtz \quad (7.2)$$

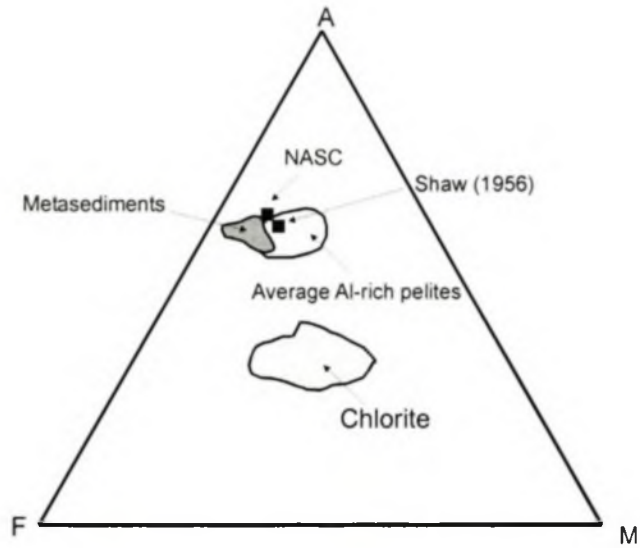

Figure 7.1. AFM projection diagram for shales and pelites (Bucher and Fry, 1994). Plotted on the diagram along with the whole rock compositions of the metasedimentary rocks of this study (see Table 6.1 & 6.3) are the average compositions of shales and pelites as discussed in the text. Also plotted are the chlorite compositions from the metasedimentary rocks as discussed later in the chapter (Table 7.1).

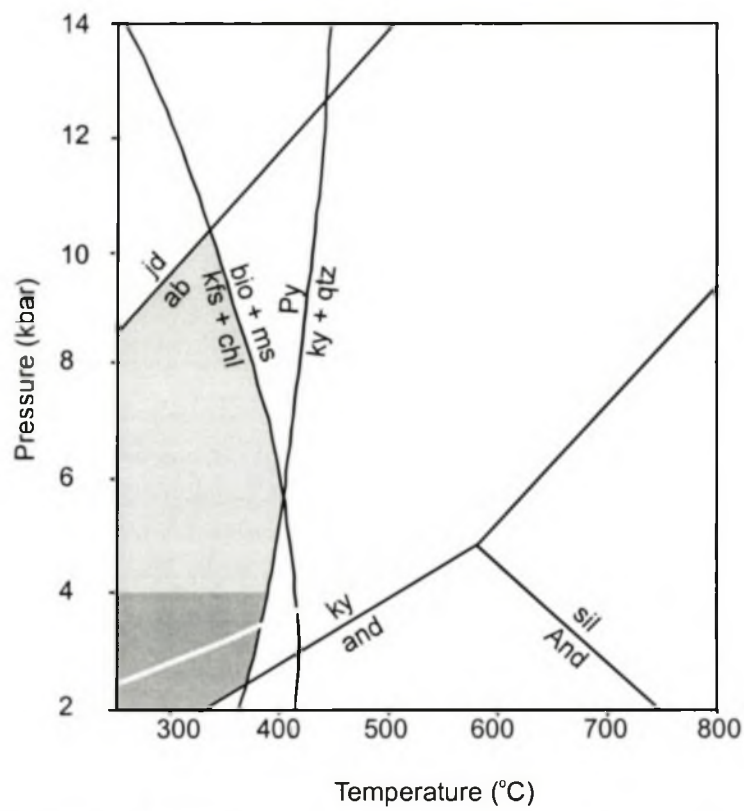

Figure 7.2. Petrogenetic grid for muscovite-bearing pelitic rocks (Bucher and Fry, 1994). Light grey area indicates the possible pressure-temperature conditions for the quartz-chlorite-muscovite-feldspar metasedimentary rocks. The dark grey area indicates the more probable, low-pressure conditions, when taking into consideration the proposed tectonic setting of the rocks (Chapter 2.3)

The plagioclase composition in the biotite-feldspar schist differs to that observed in the other metasedimentary rocks, where the plagioclase composition is An_{01} (Chapter 4.1). The plagioclase in the biotite-feldspar schist has a composition of An_{0-5} and An_{10-22}. This gap in the anorthite content is known as the peristerite gap and is characteristic of low to medium grade (greenschist- to amphibolite-facies) metamorphism (Spear, 1995). The presence of low temperature albite can thus be used to constrain the metamorphic temperature and following Smith (1974), a temperature of below approximately 600 °C can be established. The presence of biotite and a temperature of greater than approximately 400 °C and below approximately 600 °C characterises upper greenschist-facies (e.g. Bucher and Frey, 1994) grade of metamorphism at this locality.

7.3 Metavolcanic rocks (lower unit)

The Spitskop metavolcanic rocks (chlorite-feldspar-quartz schist and talc-carbonate schist) are composed of the mineral assemblage chlorite-talc-albite-carbonate-muscovite-quartz. The metavolcanic units of the Bridgetown Formation and the Riviera area are composed of the mineral assemblage chlorite-muscovite-epidote-actinolite-albite-calcite ±titanite ±magnetite ±ilmenite (Plate 7.4). The presence of the minerals actinolite, epidote, chlorite, and albite characterises the greenschist facies in mafic rocks indicating a temperature above 280 ±30 °C (Bucher and Frey, 1994) and is consistent with the metamorphic grade of the surrounding metasedimentary rocks of the lower unit. Again the absence of biotite limits the upper temperature to below 400 °C (Spear, 1995).

7.4 Graphitic schists (lower unit)

In the graphitic schists it was not possible to use the vitrinite reflectance (e.g. Burnham and Sweeny, 1989) to quantify the temperature of metamorphism. However, the presence of 'true' graphite in itself defines a minimum temperature of metamorphism. Numerous temperatures have been estimated for the formation of graphite (depending on pressure) between 255 °C at 3 kbar to 335 °C at 5.5 kbar (Diessel et al., 1978), 300 °C for the first formation of graphite to approximately 450 °C (2-6 kbar) according to Landis (1971), and between 300-500 °C (Grew, 1974).

This provides quite a wide range of possible temperatures for the formation of graphite; 200 to 500 °C. However, the graphitic schists are associated with other lithologies that are indicative of lower greenschist facies metamorphism, thus indicating that within the range suggested above it is highly unlikely that the graphitic schists were formed at temperatures above approximately 350 °C. Therefore, a temperature of approximately 300 °C for the formation of graphite in the graphitic schists is proposed based on Taylor's (1971) suggestions for the temperature of formation for graphite under shear stress, as the graphitic schists show evidence of high strain (Chapter 4.1.3).

7.5 Deformation textures

The presence of certain deformation structures within rock forming minerals can be used to approximate temperature conditions during deformation and metamorphism (e.g. Passchier and Trouw, 1996).

7.5.1 Schistose rocks (lower unit)

Quartz

Three mechanisms of dynamic recrystallisation were identified in the quartz grains from the schists and within quartz-bearing veins (pre-D_2). Quartz grains from within Q layers of the schists and the veins all have irregular grain boundaries, and some of the crystals bulge into the surrounding neighbours (Plate 7.5), thus providing evidence of grain boundary migration (Drury and Urai, 1990).

Subgrain rotation recrystallisation is identified by the formation of subgrains and new grains around larger older grains with differing angles of extinction (Plate 7.6; 7.7). Undulose extinction is common throughout all the quartz layers in the lithologies (Plate 7.8). The evidence of dynamic recrystallisation in the quartz indicates a minimum temperature of approximately 300 °C during deformation (Passchier and Trouw, 1996).

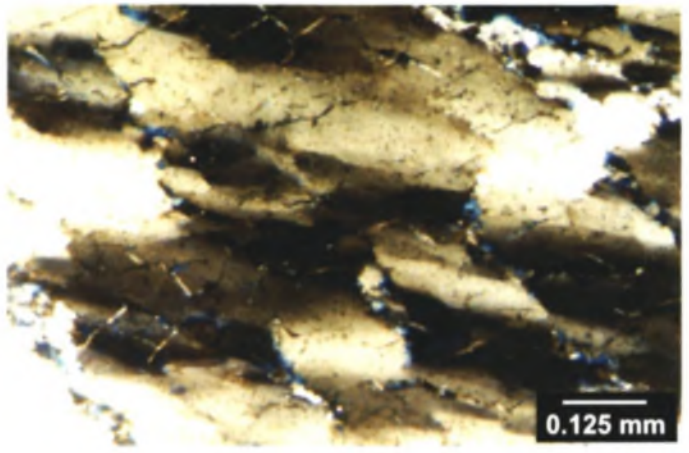

Plate 7.5. Undulose extinction within quartz grains and the formation of subgrains. Sample from quartz veins occurring within the S_0/S_1 foliation of the quartz-chlorite-muscovite schist at Spitskop. Photograph taken in XPL.

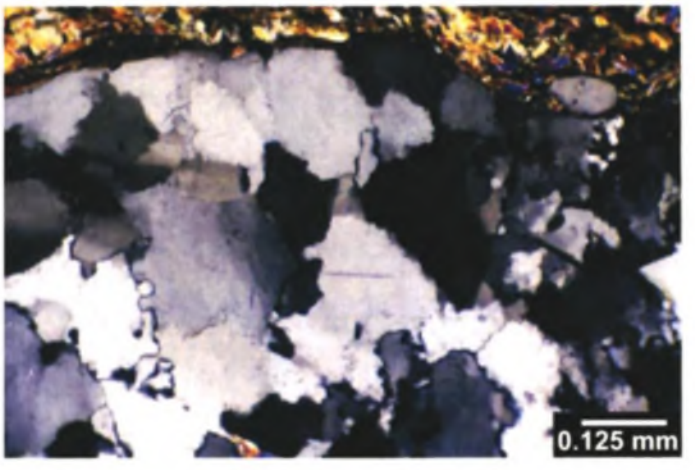

Plate 7.6. Polycrystalline quartz with irregular grain boundaries as a result of grain-boundary migration. Note the bulging of grain boundaries. Sample from quartz vein occurring within the S_0/S_1 foliation within quartz-chlorite-muscovite schist from Spitskop. Photograph taken in XPL.

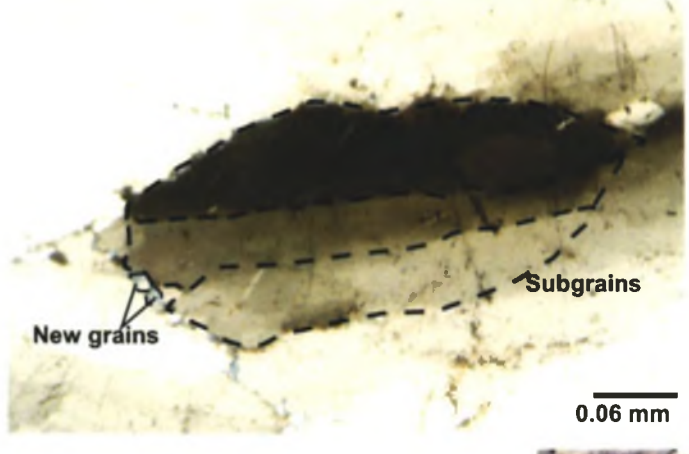

Plate 7.7. The formation of subgrains and new grains between larger, older undulose quartz grains. Sample from a quartz vein occurring within the S_0/S_1 foliation in the quartz-chlorite schist from Kruisfontein Quarry. Photomicrograph taken in XPL.

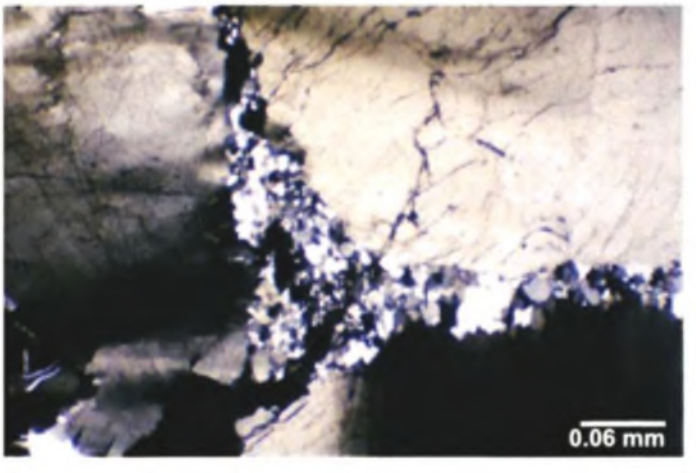

Plate 7.8. Evidence of dynamic recrystallisation by the formation of subgrains, producing undulose extinction and the formation of new grains. Quartz vein occurring within the S_0/S_1 foliation in the quartz-chlorite-muscovite schist from Spitskop. Photograph taken in XPL.

Feldspar

Plagioclase in the metasedimentary and metavolcanic units occurs as angular to semi-angular fragments, varying in size, but in general are less than 0.2 mm long. The plagioclase grains are often fractured and some grains exhibit undulose extinction. These features are characteristic of brittle fracture and cataclastic flow, indicating a temperature of approximately 300 °C (Passchier and Trouw, 1996).

7.5.2 Non-schistose rocks (upper unit)

Quartz

Quartz grains are generally angular and fragmented containing fractures and occasionally exhibiting undulose extinction. Deformation mainly occurred by brittle fracturing and pressure solution and indicates a temperature of less than 300 °C (Hobbs, 1985).

7.6 Chlorite thermometry

The simple and monotonous mineralogy of the lithologies in the Malmesbury Group precludes any detailed quantification of the P-T conditions during metamorphism. Chlorite is the main metamorphic mineral seen in lithologies of the lower unit and to some extent the upper unit as well, and it provides the only geothermometer available.

Matrix chlorite, which defines the S_0/S_1 foliation in the schistose rocks and the S_2 foliation in the non-schistose rocks, was deemed to best represent peak metamorphic conditions. In total, some 263 analyses were performed on samples from thirteen localities located in all three terranes of the Malmesbury Group, plus an additional 24 analyses from Slabber (1995) (Table 7.1).

Variation in the $^{[4]}Al$ content of chlorite has been related to changes in temperature (Cathelineau, 1988) and can therefore be used as a geothermometer. Numerous calibrations have been established for calculating the peak temperature such as Walshe (1986), Cathelineau (1988) and Zang and Fyfe (1995). Recently, Frimmel (1997) evaluated the reliability of a variety of methods for chlorite

Table 7.1. Summary of the average chlorite compositions from selected localities within the Malmesbury Group. See text for further details. Full data set presented in Appendix C, 8.

	Goudmyn se Kop		Spitskop		Kruisfontein Quarry		Porseleinberg		Bridgetown Formation #2		Bridgetown Formation #1		De Hoek Quarry	
	n=13	s.d.	n=18	s.d.	n=33	s.d.	n=15	s.d.	n=24	s.d.	n=53	s.d.	n=29	s.d.
Al_2O_3	21.65	0.34	21.68	1.03	21.33	0.62	19.08	0.23	19.84	0.79	18.26	0.42	20.79	0.60
CaO	0.04	0.03	0.03	0.01	0.02	0.02	0.04	0.02	0.04	0.05	0.11	0.35	0.01	0.01
Cr_2O_3	0.01	0.01	-	-	0.07	0.07	-	-	-	-	0.06	0.11	0.01	0.01
Fe_2O_3T	26.18	0.47	24.59	1.67	27.79	1.74	14.28	0.32	20.35	6.10	19.83	4.87	28.10	0.75
K_2O	0.00	0.00	0.01	0.02	0.00	0.00	0.00	0.00	0.00	0.00	0.03	0.13	0.00	0.00
MgO	12.75	0.40	15.33	1.81	13.76	0.70	24.13	0.40	21.01	4.76	20.21	3.45	13.72	0.49
MnO	0.31	0.05	0.62	0.06	0.21	0.03	0.13	0.03	0.21	0.14	0.19	0.05	0.21	0.03
Na_2O	0.03	0.02	0.02	0.02	0.01	0.02	0.02	0.01	0.00	0.01	0.05	0.06	0.01	0.01
O	0.00	0.00	-	-	0.00	0.00	-	-	-	-	0.00	0.00		
SiO_2	24.07	0.40	24.55	0.96	24.59	0.44	28.98	0.27	27.79	1.26	27.26	0.80	25.49	0.58
TiO_2	0.05	0.02	0.05	0.02	0.05	0.02	0.01	0.02	0.01	0.03	0.06	0.21	0.04	0.02
Total	85.08	0.75	86.86	2.34	87.84	1.90	86.71	0.54	89.24	1.12	86.07	1.56	88.37	1.04
Al	5.61	0.06	5.42	0.19	5.36	0.13	4.52	0.04	4.70	0.28	4.49	0.12	5.20	0.12
Ca	0.01	0.01	0.01	0.00	0.01	0.01	0.01	0.00	0.01	0.01	0.02	0.08	0.00	0.00
Fe2+	4.82	0.07	4.20	0.45	4.82	0.20	2.55	0.15	3.32	1.21	3.28	0.95	4.92	0.11
Fe3+	0.00	0.00	0.17	0.16	0.26	0.19	0.00	0.00	0.17	0.14	0.23	0.22	0.07	0.09
K_2O	0.00	0.00	0.00	0.00	0.00	0.00	0.00	0.00	0.00	0.00	0.01	0.04	0.00	0.00
Mg	4.18	0.14	4.86	0.50	4.37	0.20	7.22	0.09	6.25	1.27	6.26	0.94	4.34	0.16
Mn	0.06	0.01	0.11	0.01	0.04	0.01	0.02	0.00	0.03	0.02	0.03	0.01	0.04	0.01
Na	0.01	0.01	0.01	0.01	0.01	0.01	0.01	0.01	0.00	0.00	0.02	0.02	0.01	0.01
Si	5.30	0.07	5.21	0.08	5.24	0.10	5.82	0.07	5.57	0.12	5.68	0.13	5.41	0.09
Ti	0.01	0.00	0.01	0.00	0.01	0.00	0.00	0.00	0.00	0.00	0.01	0.03	0.01	0.00
$Al^{(4)}$	2.70	0.07	2.79	0.08	2.76	0.10	2.18	0.07	2.43	0.12	2.32	0.13	2.59	0.09
Xfe	0.54	0.01	0.46	0.05	0.52	0.02	0.26	0.01	0.35	0.13	0.34	0.10	0.53	0.01
T (°C)	286	8	302	10	293	10	256	8	275	8	264	16	274	11

Table 7.1 Continued.

	Bloubergstrand		Bridgetown Formation		Robben Island		Tygervalley		Riviera		Boland Terrane	
	n=17	s.d.	n=10	s.d.	n=27	s.d.	n=18	s.d.	n=30	s.d.	n=7	s.d.
Ai_2O_3	18.22	1.12	21.09	0.58	19.50	0.42	21.01	0.34	21.25	0.60	19.84	1.52
CaO	0.06	0.02	0.02	0.01	0.01	0.01	0.04	0.02	0.01	0.02	0.14	0.07
Cr_2O_3	0.01	0.02	0.04	0.01	0.01	0.02	0.03	0.02	0.03	0.03	0.02	0.03
Fe_2O_3T	25.86	0.70	28.20	0.44	29.27	0.68	26.15	0.52	18.64	0.42	24.54	0.29
K_2O	0.00	0.00	0.00	0.00	0.00	0.00	0.00	0.00	0.00	0.00	0.14	0.22
MgO	15.16	1.18	13.41	0.39	13.33	0.45	14.27	0.47	20.34	0.22	13.23	0.60
MnO	0.24	0.17	0.31	0.02	0.34	0.05	0.54	0.03	0.18	0.02	0.16	0.03
Na_2O	0.01	0.01	0.00	0.00	0.03	0.03	0.02	0.02	0.02	0.02	0.12	0.11
O											0.00	0.00
SiO_2	27.37	0.91	25.23	0.33	26.11	0.43	26.72	0.38	27.25	0.33	25.66	0.51
TiO_2	0.01	0.01	0.07	0.01	0.04	0.02	0.07	0.02	0.07	0.02	0.07	0.03
Total	86.94	0.59	88.38	0.47	88.65	0.86	88.85	0.92	87.80	0.80	83.94	1.64
Al	4.60	0.33	5.29	0.13	4.90	0.12	5.20	0.10	5.09	0.12	5.19	0.31
Ca	0.01	0.00	0.01	0.00	0.00	0.00	0.01	0.01	0.00	0.00	0.03	0.02
Fe2+	4.96	0.29	5.06	0.14	5.17	0.13	5.03	0.16	3.33	0.09	4.56	0.10
Fe3+	-0.33	0.20	-0.05	0.18	0.05	0.07	-0.44	0.17	-0.16	0.10	0.00	0.00
K_2O	0.00	0.00	0.00	0.00	0.00	0.00	0.00	0.00	0.00	0.00	0.04	0.06
Mg	4.84	0.34	4.25	0.13	4.23	0.11	4.47	0.11	6.16	0.07	4.38	0.21
Mn	0.04	0.03	0.06	0.00	0.06	0.01	0.10	0.00	0.03	0.00	0.03	0.01
Na	0.00	0.00	0.00	0.00	0.01	0.01	0.01	0.01	0.01	0.01	0.05	0.05
Si	5.86	0.15	5.37	0.06	5.56	0.07	5.61	0.07	5.54	0.05	5.70	0.17
Ti	0.00	0.00	0.01	0.00	0.01	0.00	0.01	0.00	0.01	0.00	0.01	0.00
$Ai^{(4)}$	2.14	0.15	2.63	0.06	2.44	0.07	2.39	0.07	2.46	0.05	2.30	0.17
Xfe	0.51	0.03	0.54	0.01	0.55	0.01	0.53	0.01	0.35	0.01	0.51	0.01
T (°C)	229	15	278	6	257	8	253	8	278	5	246	18

geothermometry of Witwatersrand lithologies and concluded that Zang and Fyfe's (1995) calibration was the most reliable for those lithologies. In this study, the latter-mentioned calibration (Zang and Fyfe, 1995); $T = 17.5 + 106.2\ [^{[4]}Al - 0.88(X_{Fe} - 0.34)]$, will be used, where $^{[4]}Al$ content is calculated by 8 minus the number of SiO_2, and X_{Fe} is the Fe^{2+}: Fe^{2+}+ Mg ratio. Chlorite compositions were determined using electron microprobe analysis at Rhodes University. Only matrix chlorite, defining the main foliation, was chosen for analysis.

The chlorite geothermometer is fallible as octahedral vacancies in chlorite and therefore $^{[4]}Al$ can be a result of submicroscopic inclusions or interlayering (Jiang et al., 1994). Such contamination should be identifiable by variable alkali (Ca, Na & K) contents. Therefore only chlorite containing none or very little alkalis was used in the geothermometer. The chlorites were recalculated on the basis of 20 oxygens and 16 OH anions, calculating to 28 oxygen equivalents (Deer et al., 1998). Fe^{3+} contents were calculated using the formula of Droop (1987). The geochemistry of the chlorites are presented in Table 7.1 and plotted in Figure 7.4 according to Fe^{2+} + Fe^{3+} versus Si content. The chlorites plot within the ripidolite and pycnochlorite fields according to the classification of Hey (1954). As can be seen from Figure 7.4, a scatter in the Si values is observed. As the formulae for calculating the temperature uses the $^{[4]}Al$ content, which is calculated using the Si value, this will create a spread in the temperature obtained. Although chlorite from different samples was analysed, they were all collected from close proximity to one another at the specific outcrop. One would expect the chlorite contents to be equibrilated at specific outcrops and therefore a consistency in the Si value. As stated above, contamination by interlayering of muscovite was identified by the variable alkali content and these analyses were discarded and therefore eliminating this as a possibility. The only other cause for the variable Si values could be tiny inclusions of quartz within the chlorite analysed, which would directly affect the Si value.

When plotting non-interlayering cations against Al_{tot} as defined by Robinson et al. (1993) (Fig. 7.5), the chlorites compositionally plot within the compositional range of the clinochlore end-member (defined by Bailey, 1988). Table 7.2 shows the results of the chlorite geothermometry. In the lower unit, temperatures range from

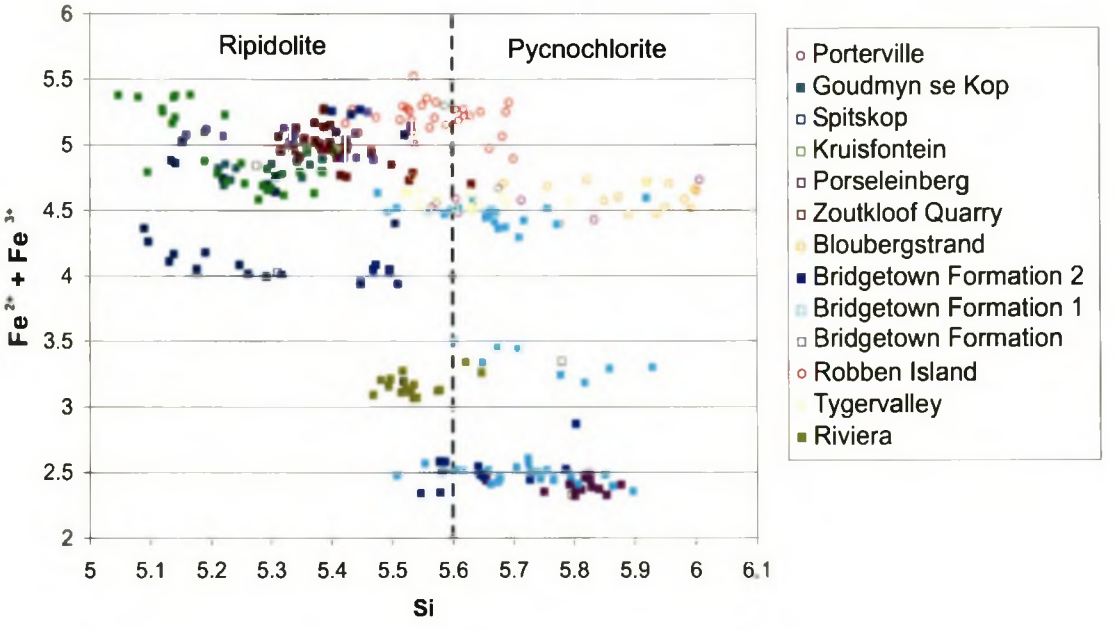

Figure 7.3. Plot of Si versus total iron for the different chlorites probed for the chlorite thermometry. Chlorite compositions are defined on the graph from Hey (1954).

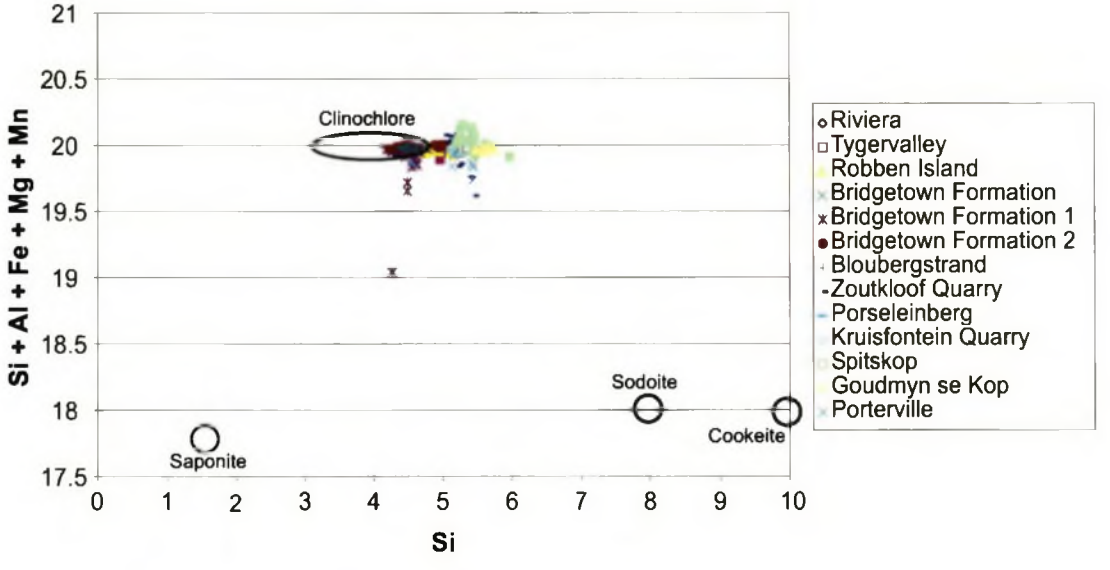

Figure 7.4. Plot of Si verses Si+Al+Fe+Mg+Mn for the different chlorites probed for the chlorite thermometry. Chlorite classification as defined by Robinson et al. (1993).

Table 7.2. Temperatures of prograde metamorphism across the Malmesbury Group based on chlorite thermometry undertaken on chlorite defining the matrix. Full data set presented in Appendix C, 8.

Location	Temperature range (°C)		Average temperature (°C)	Standard deviation
Robben Island	242	272	257	8
Tygergvalley	244	266	253	8
Bloubergstrand	213	243	226	11
Porterville	230	256	251	12
Goudmyn se Kop	275	296	286	8
Spitskop	287	318	302	10
Kruisfontein Quarry	278	312	293	10
Porseleinberg	246	280	256	8
Bridgetown Formation	268	283	278	6
Bridgetown Formation #1	250	301	267	12
Bridgetown Formation #2	257	290	275	8
Riviera	265	286	278	5
De Hoek Quarry	255	289	276	8

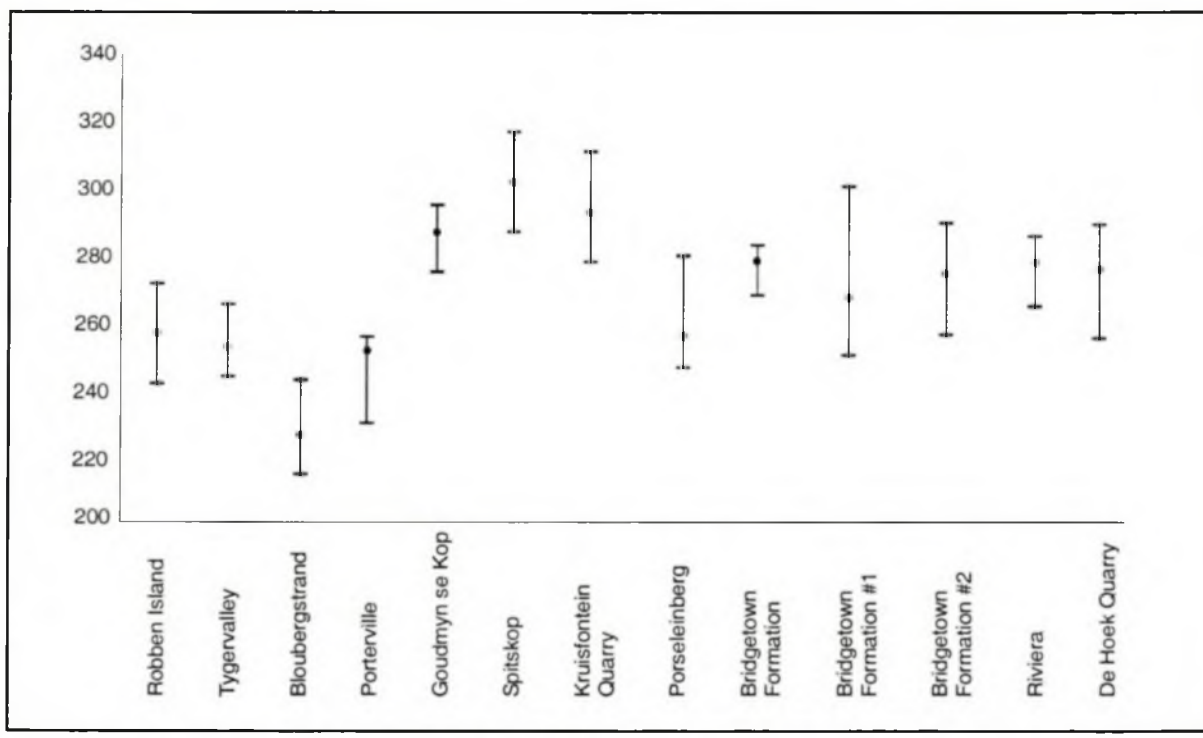

Figure 7.5. Temperature of prograde metamorphism based on chlorite thermometry showing averages and temperature range for each locality (Fig. 7.4 and Table 7.2). In general, the lower unit (schistose rocks exhibiting the transposition fabric) have a slightly higher temperature of metamorphism than the upper (non-schistose, not exhibiting the transposition fabric) unit.

246 to 318 °C. In the upper unit, temperatures range from 213 to 272 °C. These results indicate a slight but definite difference in metamorphic temperature between the upper and lower units (Fig. 7.6). However, two factors regarding the usefulness of the chlorite thermometer should be taken into consideration when interpreting these results. First, the errors associated with the thermometer generally can be a large and secondly, the accuracy of the thermometer below temperatures of 300 °C is questionable (Cathelineau, 1988). This suggests caution should be used when interpreting these results.

7.7 Malmesbury Group xenoliths

Xenoliths are common within the Darling batholith and were first described in detail by Schoch (1975), who identified them as metasedimentary rocks from the Malmesbury Group. In general, the xenoliths vary in size from a few centimetres to metres, although Schoch (1975) identified xenoliths up to 3 km long. Xenoliths are commonly made up of various amounts of quartz, biotite and plagioclase, with accessory pyroxene, apatite, muscovite, garnet, chlorite and magnetite (Schoch, 1975). This mineralogy is different to that seen in the remainder of the metasedimentary rocks of the Malmesbury Group. For this reason, the higher grade of metamorphism depicted by the mineral assemblage in the xenoliths was suggested to be related to contact metamorphism by the enveloping granite.

However, the xenoliths contain internal foliation and folding that is reminiscent of the fabric development identified in the lower unit rocks described in this study. The presence of internal D_1-related fabrics suggests, that at least texturally, the xenoliths did not equibrilate with the granite. Additionally, this study described the biotite-feldspar schist from near the farm Kanonkop (Chapter 4.1.6). This schist indicates that some metasedimentary rocks of the Malmesbury Group locally, underwent higher grades of regional metamorphism. Therefore, if the xenoliths did not chemically equilibrate with the granite, then they could provide information, about the P-T conditions of the regional metamorphism of the deeper parts of the Malmesbury Group. This, in turn, could be used to constrain the minimum thickness of the Malmesbury Group.

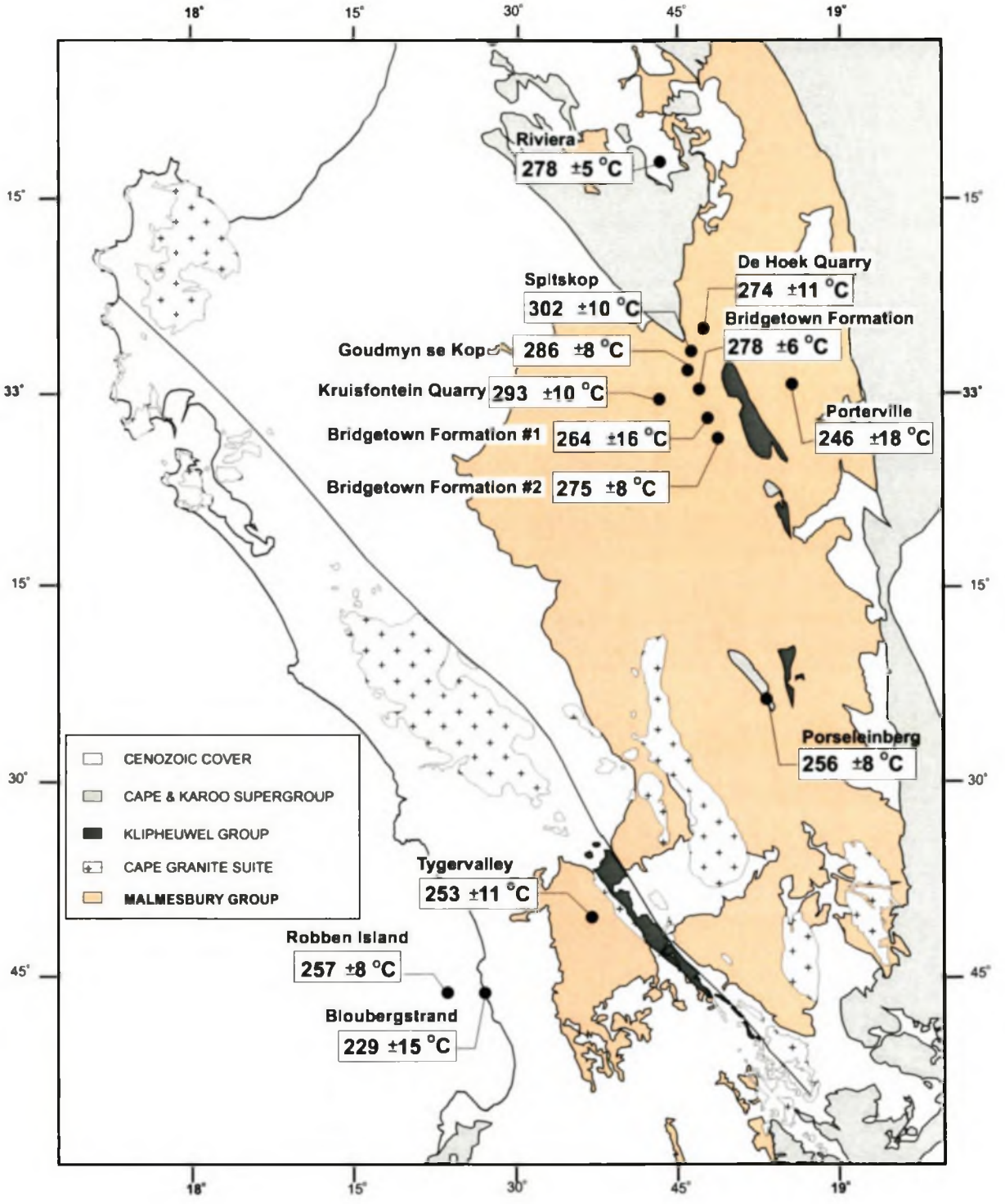

Figure 7.6. Temperatures of metamorphism for selected localities in the Malmesbury Group as derived from chlorite thermometry.

7.7.1 Petrography

Metasedimentary xenoliths in the Darling batholith are texturally similar to metasedimentary rocks of the Malmesbury Group identified during regional mapping, such as the biotite-feldspar schist at the Kanonkop road cutting. Xenoliths were collected from within the hybrid granodiorite of Schoch (1975) on the farm Rheboksfontein, 7 km west of Darling.

The xenoliths are composed of the mineral assemblage biotite-quartz-feldspar (An_{34-50} depending on the xenolith; Table 7.3), garnet and accessory orthoamphibole (Plate 7.9; Table 7.4). Garnet porphyroclasts are up to 5 mm long, are extensively fractured, subhedral and often elongated with the foliation and sometimes occur as highly fractured "slithers" within the foliation. Biotite (Table 7.5) is medium to dark brown and defines the tectonic fabric, wrapping around the garnets, indicating the garnets are pre- to syn-tectonic. The average garnet compositions are depicted in Table 7.6 for the different xenoliths studied, and are, in general, almandine-rich. The garnets are zoned showing a spessartine-rich core and a pyrope-rich rim (Plate 7.10; Fig. 7.7). Quartz is elongated and orientated with the foliation, exhibiting undulose extinction, new grain formation and irregular grain boundaries. Minor chlorite and muscovite are identified in some of the weathered xenoliths suggesting these two minerals are related to retrograde overprint.

The similar mineral assemblages and tectonic fabrics of the xenoliths and the biotite-feldspar schist outcrop at the farm Kanonkop, is suggestive that the xenoliths represent deeper parts of Malmesbury Group which did not chemically or texturally equilibrate in the granites and that were brought to the surface during granite ascent and emplacement. These xenoliths therefore represent samples of the deepest segments of the Malmesbury group to date, and thus can be used to estimate the thickness of the Malmesbury Group.

From the absence of chlorite and muscovite within the rocks a minimum temperature of 520 °C can be assumed following the reaction (after Bucher and Frey, 1994):

$$1Ms + 3Chl + 3Qtz = 4Alm + 1\ Bio + 12H_2O \qquad (7.2)$$

Table 7.3. Average plagioclase compositions from the four metasedimentary xenoliths from the farm Rheboksfontein, 7 km west of Darling. Quantitative EDS analysis, all data normalised. Full data set is presented in Appendix C, 9. s.d. = standard deviation.

	01-335a		01-335c		01-335d		X2	
	Average (n=17)	s.d.	Average (n=16)	s.d.	Average (n=14)	s.d.	Average (n=31)	s.d.
MgO	-	-	-	-	-	-	-	-
SiO_2	54.27	1.47	55.04	2.45	54.71	2.07	56.86	0.69
Na_2O	5.60	1.14	5.99	0.94	5.94	0.99	9.36	0.33
Al_2O_3	28.60	1.99	27.68	1.55	28.02	1.64	22.75	0.45
K_2O	0.81	2.53	0.52	0.61	0.28	0.07	0.71	0.12
CaO	10.75	2.84	10.83	1.98	11.10	1.51	7.18	0.54
TiO_2	-	-	-	-	-	-	-	-
FeO	0.00	0.05	0.00	0.05	0.00	0.10	0.00	0.05
MnO	-	-	-	-	-	-	-	-
Cr_2O_3	-	-	-	-	-	-	-	-
Total	100.03	0.01	100.06	0.01	100.05	0.01	96.86	0.01
Mg	0.00	0.00	0.00	0.00	0.00	0.00	0.65	0.00
Si	9.84	0.23	9.97	0.39	9.90	0.33	10.27	0.10
Na	1.97	0.40	2.10	0.32	2.08	0.34	3.05	0.11
Al	6.11	0.45	5.91	0.36	5.98	0.37	4.80	0.10
K	0.19	0.59	0.12	0.14	0.06	0.02	0.15	0.03
Ca	2.09	0.55	2.10	0.40	2.16	0.31	1.29	0.11
Ti	0.00	0.00	0.00	0.00	0.00	0.00	0.00	0.00
Fe^{2+}	-0.01	0.01	-0.01	0.01	-0.01	0.01	-0.01	0.01
Mn	0.00	0.00	0.00	0.00	0.00	0.00	0.00	0.00
Cr	0.00	0.00	0.00	0.00	0.00	0.00	0.00	0.00
Cation Total	20.18	0.05	20.19	0.10	20.18	0.12	20.20	0.05
X (Si+Al)	15.95	0.30	15.87	0.04	15.88	0.11	15.15	0.03
Z (rest)	4.24	0.28	4.31	0.12	4.30	0.23	4.35	0.07
An	48.51	12.70	48.55	8.26	50.14	7.00	33.75	2.39
Ab	45.98	8.19	48.65	7.59	48.34	7.06	62.93	2.38
Or	5.52	18.41	2.80	3.42	1.51	0.48	1.50	0.62

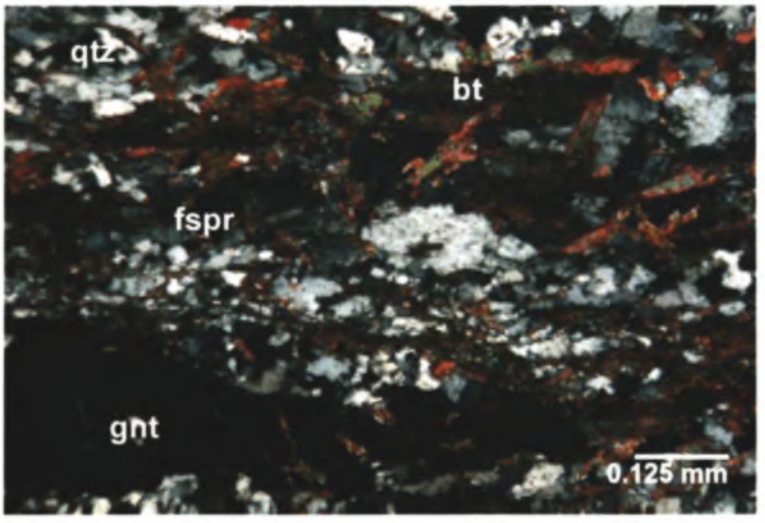

Plate 7.9. Biotite-quartz-feldspar-garnet assemblage from a schist xenolith from the Darling batholith. Garnets are often highly fractured and are aligned with the fabric. The xenoliths are interpreted to represent deep parts of the metasedimentary pile of the Malmesbury Group. Photomicrograph taken in XP.

Table 7.4. Average orthoamphibole (gedrite) composition from the xenolith 01-335c from the farm Rheboksfontein, 7 km west of Darling. Quantitative EDS analysis, all data normalised. Full data set presented in Appendix C, 10. s.d. = standard deviation.

	01-335c	
	Average (n=5)	s.d.
MgO	15.00	0.18
Al_2O_3	0.49	0.62
SiO_2	57.36	0.10
CaO	0.40	0.07
MnO	1.69	0.11
FeO	25.08	0.31
	100.00	1.38
Mg	3.06	0.04
Al	0.08	0.10
Si	7.85	0.03
Ca	0.06	0.01
Mn	0.20	0.01
Fe^{2+}	2.87	0.04

Table 7.5. Average biotite compositions from the four metasedimentary xenoliths from the farm Rheboksfontein, 7 km west of Darling. Quantitative EDS analysis, all data normalised. Full data set is presented in Appendix C, 11. s.d. = standard deviation.

	01-335a		01-335c		01-335d		X2	
	Average (n=19)	s.d.	Average (n=33)	s.d.	Average (n=28)	s.d.	Average (n=43)	s.d.
MgO	11.15	1.21	10.54	1.71	10.76	0.56	8.12	0.97
SiO_2	38.13	1.73	38.70	2.36	38.09	0.71	37.53	3.54
Na_2O	0.00	0.00	0.00	0.00	0.00	0.00	0.00	0.00
Al_2O_3	17.85	1.34	17.66	1.42	17.65	0.87	19.04	1.00
K_2O	9.91	2.48	9.80	1.65	10.02	0.53	10.15	1.54
CaO	-	-	-	-	-	-	-	-
TiO_2	2.73	1.05	2.68	0.81	3.24	0.51	1.80	0.64
FeO	20.01	2.52	20.39	2.64	20.02	1.12	23.10	2.34
MnO	0.24	0.11	0.23	0.08	0.21	0.10	0.27	0.13
Total	100.00	0.01	100.00	0.01	100.00	0.01	100.00	0.01
MgO	2.41	0.26	2.27	0.36	2.33	0.11	1.78	0.22
SiO2	5.53	0.25	5.60	0.25	5.53	0.07	5.51	0.36
Na2O	0.00	0.00	0.00	0.00	0.00	0.00	0.00	0.00
Al2O3	3.05	0.23	3.01	0.20	3.02	0.13	3.30	0.20
K2O	1.83	0.46	1.81	0.33	1.86	0.11	1.91	0.30
CaO	0.00	0.00	0.00	0.00	0.00	0.00	0.00	0.00
TiO2	0.30	0.11	0.29	0.09	0.35	0.06	0.20	0.07
FeO	2.43	0.31	2.48	0.37	2.43	0.16	2.85	0.32
MnO	0.03	0.01	0.03	0.01	0.03	0.01	0.03	0.02

Table 7.6. Average garnet compositions from the four metasedimentary xenoliths from the farm Rheboksfontein, 7 km west of Darling. Quantitative EDS analysis, all data normalised. Full data set is presented in Appendix C, 12. s.d. = standard deviation.

	01-335a		01-335c		01-335d		X2	
	Average (n=24)	s.d.	Average (n=29)	s.d.	Average (n=30)	s.d.	Average (n=44)	s.d.
Na_2O	-	-	-	-	-	-	-	-
K_2O	0.08	0.07	0.05	0.08	0.14	0.19	0.46	1.63
SiO_2	37.79	0.93	37.96	0.37	37.51	1.93	36.95	1.11
TiO_2	0.02	0.08	-0.04	0.10	0.06	0.14	0.25	0.95
Ai_2O_3	20.59	0.43	20.38	0.50	20.89	1.04	19.96	0.80
FeO	27.71	1.04	28.93	0.91	28.20	2.31	35.09	4.44
MnO	5.63	0.86	4.78	0.89	4.90	0.88	2.79	0.82
MgO	3.22	0.39	3.33	0.52	3.65	0.89	2.60	0.98
CaO	4.96	0.27	4.59	0.55	4.65	0.54	1.89	4.07
total	100.00	0.01	99.99	0.01	100.00	0.01	100.00	0.01
Na	0.00	0.00	0.00	0.00	0.00	0.00	0.00	0.00
K	0.02	0.01	0.01	0.02	0.03	0.04	0.09	0.33
Si	6.04	0.09	6.07	0.04	5.99	0.20	6.01	0.15
Ti	0.00	0.01	0.00	0.01	0.01	0.02	0.03	0.11
Al	3.88	0.05	3.84	0.08	3.93	0.13	3.83	0.17
Fe^{2+}	3.71	0.17	3.87	0.13	3.77	0.40	4.78	0.62
Fe^{3+}	0.07	0.31	0.05	0.17	0.15	0.73	0.26	0.37
Mn	0.76	0.12	0.65	0.12	0.66	0.13	0.38	0.12
Mg	0.77	0.09	0.79	0.12	0.87	0.21	0.63	0.23
Ca	0.85	0.05	0.79	0.10	0.80	0.10	0.33	0.70
Cation total	16.02	0.10	16.02	0.06	16.06	0.25	16.09	0.13
pyrope	12.65	1.66	13.01	1.89	14.27	3.10	10.47	4.88
almandine	60.87	1.12	63.47	2.13	61.75	1.91	78.07	9.22
spessartine	12.52	1.80	10.64	2.05	10.89	1.87	6.24	1.81
grossular	12.55	8.75	11.65	3.90	10.80	15.60	0.60	10.25
andradite	1.41	8.66	1.23	4.39	2.28	14.86	5.81	7.28
uvarovite	0.00	0.00	0.00	0.00	0.00	0.00	0.00	0.00

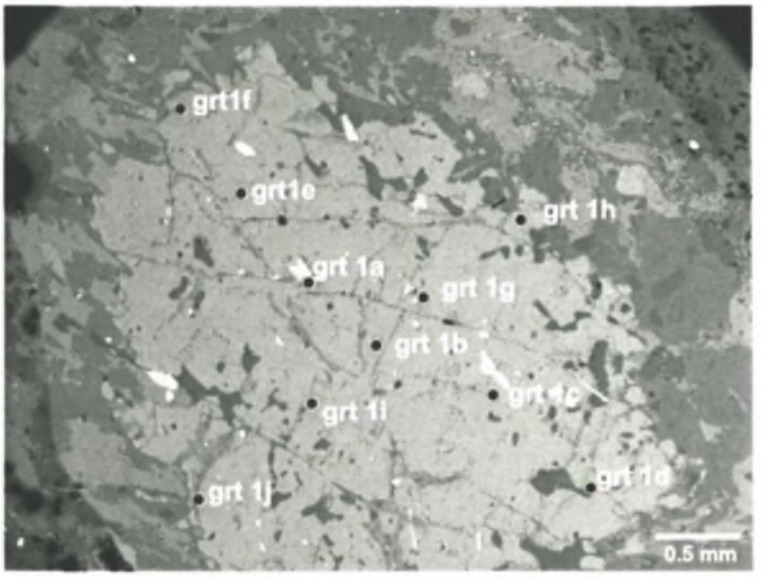

Plate 7.10. SEM image of a typical subhedral garnet within the metasedimentary xenoliths. The garnets are commonly fractured and elongated with the fabric. Locations where quantitative data was collected are marked on the image and identify that the garnets are compositionaly zoned. See Figure 7.7 below. Full data set presented in Appendix C, 9.

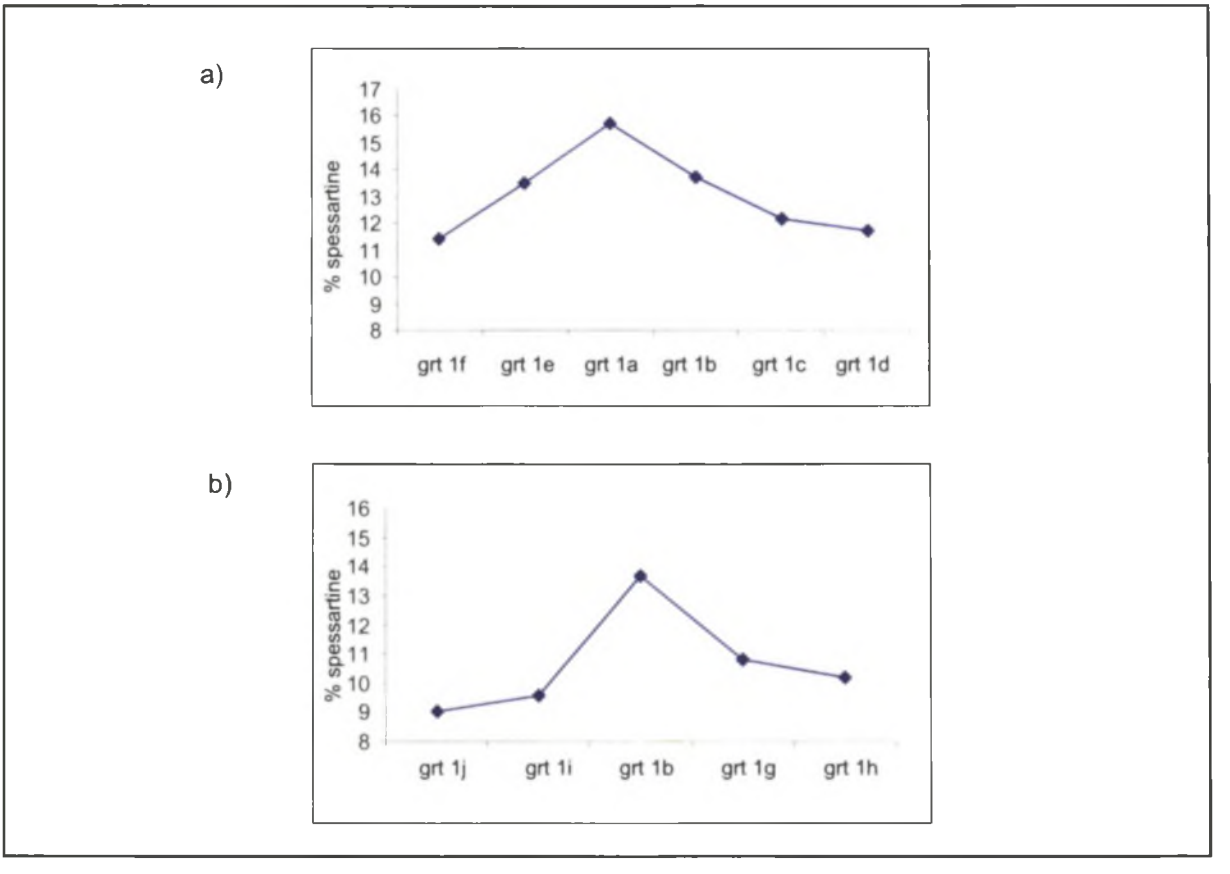

Figure 7.7. Graphs showing the varying spessartine composition across the garnet presented in Plate 7.10. Compositional zoning is common in the garnets identified in the metasedimentary xenoliths.
a) traverse from point grt 1f to grt 1d
b) traverse from point grt 1j to grt 1h.

The absence of white micas and the presence of feldspars indicate the following reactions to have taken place, representing the upper limit for the presence of muscovite:

$$Pa + Qtz = Ab + Als + H_2O \quad (7.3)$$

$$Ms + Qtz = Kfs + Als + H_2O \quad (7.4)$$

Reactions 7.3 and 7.4 results in the formation of albite and K- feldspar respectively, which indicates a temperature of above 600 °C (Bucher and Frey, 1994).

7.7.2 Quantitative temperature estimates

The presence of both garnet and biotite in the xenoliths allows the use of the garnet-biotite Fe-Mg exchange thermometer. Numerous version of this thermometer exist, at least eighteen according to Bucher and Frey (1994), and here five of the more commonly used calibrations are applied. Namely, the calibrations of Thompson (1976), Holdaway and Lee (1977), Ferry and Spear (1978), Perchuk and Lavrent'eva (1983) and Bhattacharya et al. (1988).

The Mn-Fe^{2+} zoning of the garnets, Mn-rich cores with Mn-poor rims is known as 'bell-shaped zoning' and is typical of growth zoning in regional metamorphosed pelitic sediments (Spear, 1995). Composition analyses of biotite inclusions from within the garnets were coupled with analyses of the Mn-rich core, and matrix biotite analyses were coupled with garnet analyses from the Fe^{2+}-rich rim to provide information on peak and prograde metamorphic temperatures respectively. The results of the geothermometry are represented in Table 7.7 and show that the five thermometers give consistently similar results to one another. In general, the temperature of prograde and peak metamorphism falls within the standard deviation of one another, so that a distinction between the two is not possible. A temperature of between 600 and 650 °C can be estimated from the geothermometers. This is consistent with the mineralogy of the xenoliths characterising mid-amphibolite-facies grades of metamorphism (e.g. Bucher and Frey, 1994).

Table 7.7. Results of the garnet-biotite thermometry for the four metasedimentary xenoliths analysed from the farm Rheboksfontein, 7 km west of Darling. The five geothermometers used are: 1) Thompson (1976), 2) Holdaway and Lee (1977), 3) Ferry and Spear (1978), 4) Perchuk and Lavrent'eva (1983) and 5) Bhattacharya et al. (1988). Full data set available in Appendix C, 9 & 10. s.d. = standard deviation.

		1		2		3		4		5		Average of the 5 geothermometers	
		Average	s.d.	Average	s.d.	Average	s.d.	Average	s.d.	Average	s.d.		s.d.
01-335a	Peak	639	30	616	25	634	40	613	20	622	23	**625**	**11**
	prograde	634	40	612	34	628	53	609	27	616	35	**620**	**11**
01-335c	Peak	638	64	615	55	635	86	612	44	620	51	**624**	**12**
	prograde	602	21	584	18	586	27	587	15	590	18	**590**	7
01-335d	Peak	662	14	635	12	665	18	628	9	643	11	**647**	**16**
	prograde	650	21	625	18	649	27	620	14	630	14	**635**	**14**
X2	Peak	669	18	642	15	676	24	633	12	630	12	**650**	**21**
	prograde	611	28	591	25	599	36	593	20	584	26	**596**	**10**

7.7.3 Thickness of the Malmesbury Group

The thickness of the Malmesbury Group is unknown. Based on metamorphic assemblages of the contact aureole around the Seapoint granite in Cape Town, Armstrong et al. (1998) estimation an intrusion depth of 8-10 km. Given the lower-greenschist facies metamorphism of the lower unit of the Malmesbury Group (approx. 300 °C), and assuming a normal geothermal gradient of approximately 35 °C/km (e.g. Best, 1982), approximately 9 km of rocks overlying the present level of the lower unit have been eroded before the deposition of the Klipheuwel and TMS Groups. This is in agreement with the above calculations of Armstrong et al. (1998). However, an estimate of the thickness of the lower unit and therefore the total thickness of the Malmesbury Group is unknown.

If we assume that the xenoliths represent deeper segments of the Malmesbury Group and that the textures have not been affected by the intrusion of the granites it is possible to estimate a minimum thickness for the lower unit of the Malmesbury Group using an estimated geothermal gradient from similar tectonic environments. Therefore based on the premise that a temperature of approximately 600-650 °C was achieved related to regional metamorphism, with a geothermal gradient of approximately 35 °C/ km. A thickness of between 17 and 19 km can be estimated for the Malmesbury Group (lower and upper units combined). The validity of such a thickness for the Malmesbury Group is discussed in Chapter 10.3.3.

7.8 Summary

In both the schistose and non-schistose rocks, lower greenschist-facies grades of metamorphism were achieved during regional metamorphism. The upper unit mainly shows deformation by brittle fracturing indicating a temperature below approximately 300 °C. The lower unit shows abundant evidence of recrystallisation and deformation by dislocation gliding indicating a temperature of at least approximately 300 °C. The metamorphic minerals chlorite and muscovite define the S_0/S_1 fabric in the schistose rocks related to D_1 and the S_2 fabric in the schistose and non-schistose rocks related to D_2 (Chapter 5). As these fabrics were formed by two separate deformation events, it implies that the rocks of the Malmesbury Group were affected by two metamorphic events: M_1 occurring synchronously with D_1 and M_2 occurring synchronously with D_2.

According to Frimmel et al. (2001) temperatures of approximately 300 °C would have been achieved in the Malmesbury Group rocks due to burial metamorphism by the overlying TMS Group. Further, during the Cape Orogeny (220-290 Ma, Hälbich et al., 1983) regional metamorphic temperatures of generally 300 °C were also reached. The Malmesbury Group was therefore affected by up to four low-grade metamorphic events. However, only near the Malmesbury Group-TMS Group contact is there evidence of metamorphic overprint on the Malmesbury Group rocks (Frimmel et al., 2001). Metamorphic minerals defining the D_1 and D_2 foliations are interpreted to be related to Pan-African tectonism and not the later Cape Orogeny. This indicates that in the Malmesbury Group, no new mineral growth occurred related to post Pan-African metamorphism and the latter two metamorphic events did not overprint onto M_1 and M_2.

8 FLUID-ROCK INTERACTION

During regional mapping, a clear correlation between the abundance of quartz veining and the volume of chlorite and/or muscovite in the surrounding rocks was identified in rocks of the lower unit. The chlorite and muscovite is predominantly confined to alteration haloes, but where veining is extensive, chlorite and muscovite is pervasive. This relationship suggests that metasomatic alteration is, at least partly, responsible for the present mineralogical compositions of certain lithological units, i.e. particularly the chlorite- and muscovite-rich lithologies of the lower unit. As the present stratigraphic classification of the Malmesbury Group is based on predominantly lithological criteria, the above observation will have repercussions on the present classification, namely, that a lithostratigraphic classification based on mineralogical compositions of the rocks is potentially invalid where veining is pervasive, and that correlations between lithologies should be made with caution.

8.1 Vein characteristics

Veining in rocks of the lower unit is abundant and is seen within all the lithologies, in particular in the metapelites. Two generations of veins can be distinguished based on vein orientation and their relationship to regional fabrics.

8.1.1 Type 1 veins

Type 1 veins represent the main type of quartz veining in the lower unit. They are laterally continuous and range in thickness from a few mm to 10's of cm. In general, the veins are milky-white and occasionally clear to smoky-grey in appearance. They are dominantly composed of quartz (80-95%), minor carbonates (calcite in the schists, rhodochrosite in the limestones, <5%), sulphides (mainly pyrite, with minor chalcopyrite and arsenopyrite, < 3%), chlorite and muscovite (<10%). Veins are contained within the regional fabric trend and the S_0/S_1 fabric, indicating that fluid movement was pre- to syn-D_1. Veining can become prominent in many localities,

forming up to 70 vol. % of the rocks, or can be only minor (1-2%) or even absent. Alteration envelopes associated with veins are composed of chlorite and muscovite and vary in thickness from 1 mm to 50 mm, depending on the size of the veins. Type 1 veins can be divided into two subtypes, namely Type 1a and 1b as explained below.

Type 1a veins represent the major type of veins. They are orientated north-northwest-south-southeast and developed early in the deformation history of the area and were affected by folding during D_1. The folds are isoclinal and the limbs of the folds are boudinaged, showing pinch-and-swell structures. Type 1a veins contain the majority of sulphide mineralisation seen in the field and also under the microscope. Details of the ore mineralogy are given in Chapter 9.3. Geochemically, the veins reflect their mineralogy, being dominated by silica, and minor alumina, total iron and alkalis reflecting the presence of chlorite and muscovite (Table 8.1).

Table 8.1. Average geochemistry of Type 1a quartz veins from the Spitskop area. Full data set presented in Appendix C, 13.

		Average of Type 1a vein	
		(n=5)	s.d.
wt.%	SiO_2	94.09	4.0
	TiO_2	0.03	0.0
	Ai_2O_3	1.80	1.9
	Fe_2O_3T	1.19	0.6
	MnO	0.01	0.0
	MgO	0.45	0.3
	CaO	0.12	0.1
	Na_2O	0.19	0.4
	K_2O	0.08	0.1
	P_20_5	0.09	0.1
	H_2O-	0.15	0.1
	LOI	0.62	0.3
	TOTAL	98.81	0.6

Fluid inclusion analysis on Type 1a veins presented later in Chapter 9.4 indicates a low salinity, H_2O-CO_2 fluid at approximately 300 °C. The temperature of the fluid is consistent with the temperature of regional metamorphism during fluid movement through the rocks.

Type 1b veins post-date 1a veins. The veins are similar to Type 1a in appearance, being milky-white to clear and of similar thickness, but they are not as abundant. These veins can be distinguished from later veins (Type 2), by the deflection of the S_0/S_1 foliation along the vein boundaries, and the alteration envelopes related to 1b veins is contained within the S_0/S_1 fabric.

8.1.2 Type 2 veins

Type 2 veins are younger than, and volumetrically subordinate compared to Type 1 veins. Lateral strikes are confined and never exceed 2-3 m in length. Type 2 veins are typically less than 1 cm wide and contain only minor, sporadic pyrite mineralisation. The veins are upright and trend northeast-southwest, parallel to the F_3 fold axes and classify as a-c joints of the F_2 folds.

Oxygen isotope ($\delta^{18}O$) analyses were undertaken on both Type 1 and Type 2 veins (Appendix C, 14). However, both vein types have very similar $\delta^{18}O$ values and it was not possible to differentiate different fluid sources for the two vein types.

8.2 Vein-wallrock relationship

At first glance, numerous compositionally different lithologies can be identified in the rocks of the lower unit (as described in Chapter 4.1). The contacts between the units are commonly regarded as bedding (e.g. Theron et al., 1992). However, as illustrated in Chapter 5, in the lower unit transposition of bedding has produced a pseudo-stratigraphy, and the sub-horizontal fabric (S_0/S_1) in the rock is clearly tectonic, and not sedimentary in nature. The tectonic nature of the contacts is exemplified in the Zoutkloof, De Hoek and Kruisfontein Quarries.

At many outcrops, e.g. the Kruisfontein Quarry and the road cuttings at Moorreesburg, a clear relationship between the chlorite and muscovite content of the rocks, and the volume of veining in individual rock-types can be noted. Individual veins are enveloped by centimetre-wide alteration haloes composed of muscovite and chlorite. Where veins are abundant and closely spaced, the alteration envelopes merge and thus the original composition of the rock is obliterated. As the majority of

veins in the lower unit are classified as Type 1a veins occurring parallel to the S_0/S_1 fabric and therefore are also sub-horizontal, the pervassive alteration envelopes appear as distinct lithological units related to original compositional differences. Lithologies that contain relatively little to no veining contain only minor chlorite and muscovite. The metasomatic alteration associated with quartz veining in these two lithologies is discussed below.

8.3 Alteration of quartz-muscovite-feldspar schist

The quartz-muscovite-feldspar schist is characteristic of the Berg River Formation and was described in Chapter 4.1. The schist is composed of mainly quartz, muscovite and feldspar and minor chlorite, with the muscovite and chlorite defining the main fabric (S_0/S_1). Associated with the quartz-muscovite-feldspar schist is a muscovite schist containing numerous quartz veins. These two types of schists have been identified as representing two distinct lithotypes within the Berg River Formation (e.g. Hartnady et al., 1974; Theron et al., 1992). The dominance of veining within the muscovite schist as apposed to the quartz-feldspar-muscovite schist could be explained by original compositional or grain size differences that favoured fluid movement through the protolith of the muscovite schist. However, as explained below there are certain outcrop features of the muscovite schist which are difficult to explain in terms of depositional processes.

Where veining passes through the feldspathic rocks, an increase in the muscovite (and minor chlorite) content is observed as alteration haloes normally up to a few centimetres in thickness around the vein. Where veins are located within a few centimetres from one another, the alteration envelopes merge and the original composition of the host rock between and directly surrounding the veins is overprinted. If the veining is volumetrically abundant, the merger of the alteration envelopes completely alters the composition of the quartz-muscovite-feldspar schist to a muscovite schist.

As the alteration envelopes are composed predominantly of muscovite, then sericitic alteration is the main type of alteration. The commonest form of sericitisation is the

alteration of potassium feldspar to white mica (e.g. Pirajno, 1992) and follows the reaction (MacKenzie, 1983; Faure, 1991):

$$\text{K-feldspar} + H^+ = \text{white mica} + \text{quartz} + K \qquad (8.1)$$

However, no potassium feldspar was identified in the quartz-muscovite-feldspar schist, only plagioclase (An_{01}), although minor potassium feldspar may occur within the fine-grained matrix. Sericitisation may also occur by the alteration of plagioclase if the fluid is potassium bearing (MacKenzie, 1983):

$$\text{Plagioclase} + H^+ + OH^- + K + C = \text{white mica} + \text{calcite or quartz} + Na \qquad (8.2)$$

These reactions are consistent with lower greenschist facies metamorphism (e.g. Spear, 1995), which occurred contemporaneous with D_1 deformation.

In these localities, the schists are indistinguishable from the muscovite schist, a supposedly distinct lithotype. When veining predominantly occurs parallel to the S_0/S_1 fabric, the boundary between the host rock and the altered rock is sub-horizontal and is thus reminiscent of bedding. However, these lithologies exhibit bedding transposition, so the main sub-horizontal fabric identified in these rocks is the S_0/S_1 fabric described in Chapter 5.2 and not bedding (S_0). Furthermore, where late Type 1 quartz veins crosscut the S_0/S_1 fabric (Plate 8.1a, b, c and d), the muscovite schist lenses are often connected by near-vertical units of muscovite schist. Such features are not possible to explain in terms of primary depositional features. This is exemplified in Plate 8.1e and 8.1f, where a late, Type 1 quartz vein crosscuts the S_0/S_1 foliation at right-angles within the quartz-muscovite-feldspar schist outcrop. The alteration halo associated with this vein is up to 50 cm wide and compositionally and in appearance wise almost identical to the muscovite schist described in Chapter 4.1.1. This locality was chosen as it identifies the two lithologies in question but clearly shows that the occurrence of units of muscovite schist is here related to fluid metasomatism and not primary compositional variations in the protolith. Therefore the fluid alteration has either partly or completely changed the composition of the original lithology.

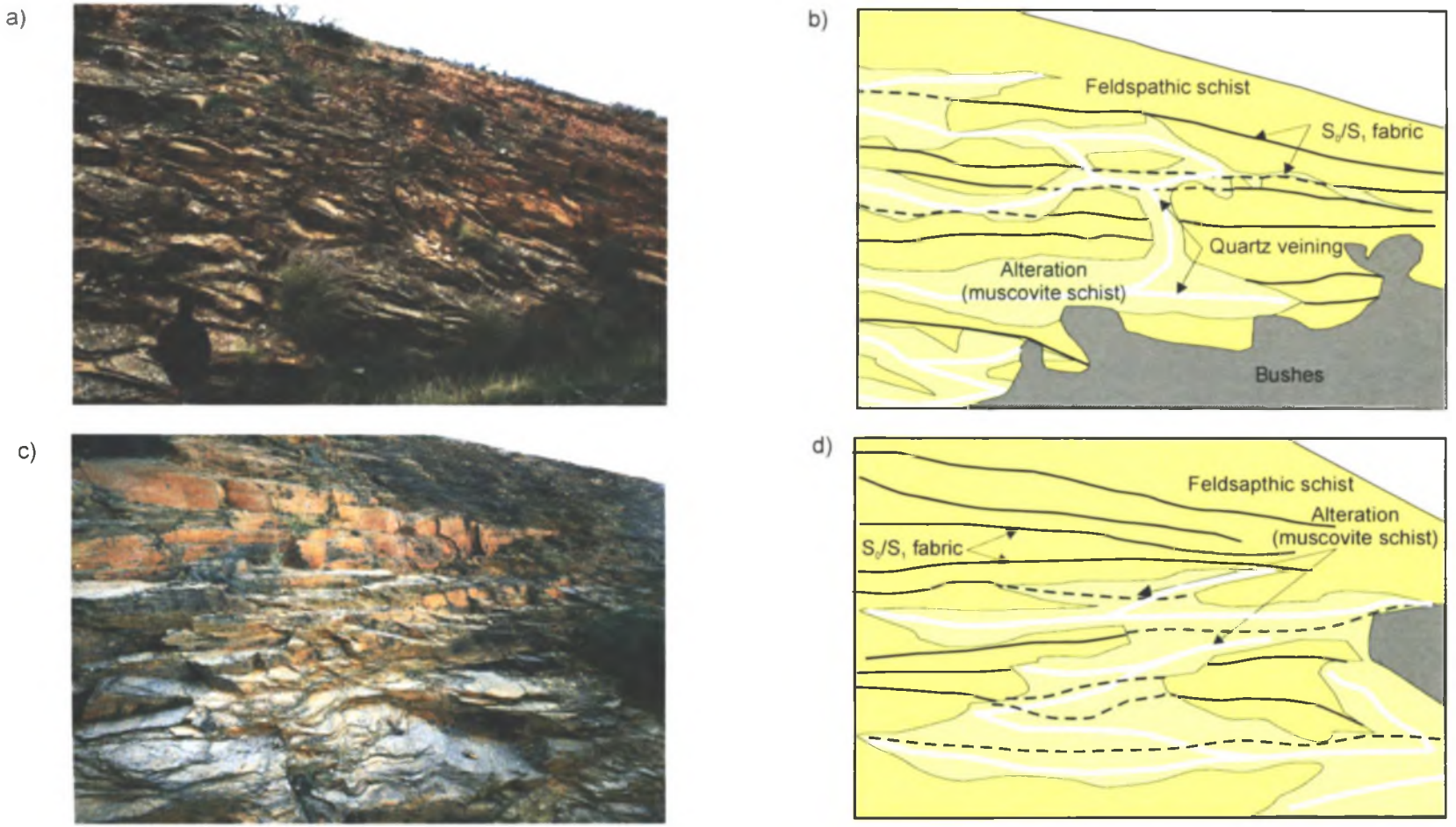

Plate 8.1. Quartz-feldspar-muscovite (sericite) schist along the N7 national road, 3 km north of Moorreesburg. Isoclinal folds located within the schist attest to the bedding transposition this lithology has undergone. Muscovite-rich schists occur as layers varying in thickness sub-parallel to the layering in the rocks (S_0/S_1 foliation).

a) Another example of the wide-spread alteration of the feldspathic schists into the muscovite schists on an outcrop scale.
b) Diagram showing the relationship of the two schists and veining in Plate 8.1a.
c) Extensive alteration of the feldspathic schists into the muscovite schists on an outcrop scale. This alteration is wide-spread Across the Swartland Terrane.
d) Diagram showing the relationship between the two schists and veining in Plate 8.1c.

e)

f)

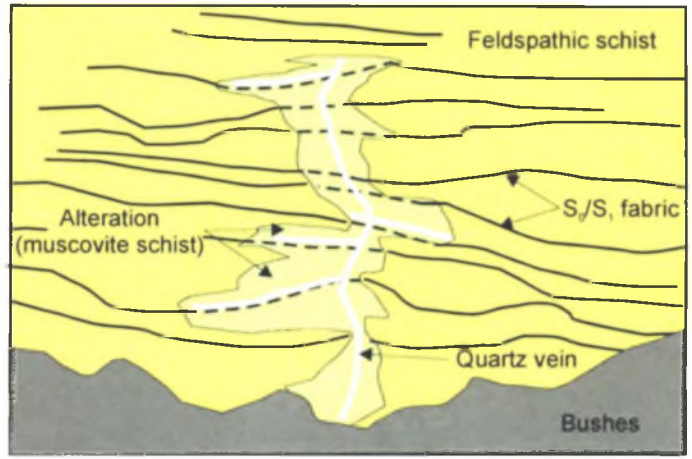

Plate 8.1. Continued.

e) Alteration of felspathic schist to sericite schist, but alteration is associated with a later crosscutting quartz vein. This shows the alteration of the feldspathic schist by the fluids, and thus indicating that the muscovite schist is related to fluid movement and not To differences in protolith composition.

f) Diagram showing the relationship of the two schists and veining in Plate 8.1e.

a)

b)

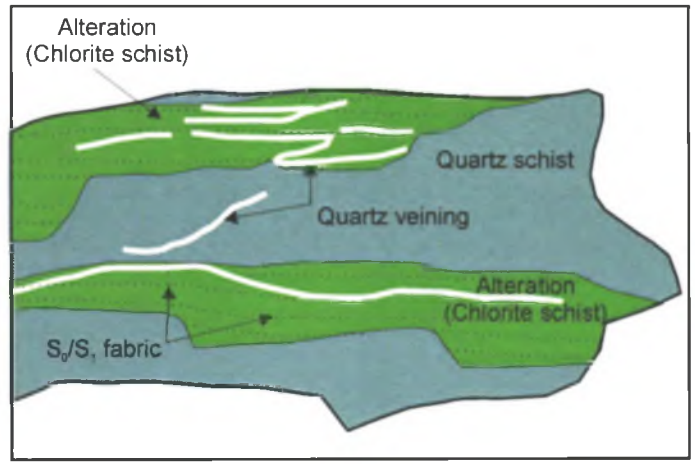

Plate 8.2.

a) Alteration of the quartz schist to the chlorite schist, quartz veining occurs parallel to and crosscuts the S_0/S_1 fabric, classifying the veins as Type 1a and 1b respectively (Chapter 8.1). Example from the Kruisfontein Quarry (Figure 4.1), but both these lithologies are wide-spread across the field area and characterise the Berg River Formation.

b) Diagram showing the relationship between the two schists and veining in Plate 8.2a.

8.4 Alteration of quartz-rich schists

At the Kruisfontein Quarry, the quartz schist and quartz-chlorite-muscovite schist described in Chapter 4.1.2 are prominent and are interlayered with a chlorite-muscovite schist. The chlorite-muscovite schist is described in Chapter 4.1.1 and occurs across the lower unit. These quartz-rich schists and chlorite-muscovite schists, as with the feldspathic and muscovite lithologies described above, are identified as representing distinct rock types (Plate. 8.2). The Kruisfontein Quarry shows the best examples of the relationship between these two rock types. Contacts are generally sharp and occur parallel to the main foliation (S_0/S_1), suggesting primary compositional differences. However, the contacts between the two rock types are tectonic, with the units along strike being laterally discontinuous. This in many instances is related to transposition of bedding, but is also on appearance, related to the volume of veining. The quartz schist is, in general, barren of veining, however where veining does occur, alteration envelopes of chlorite and minor muscovite are present. In the quartz-chlorite-muscovite schist, quartz veins are surrounding by chlorite alteration envelopes 2-30 mm wide. The width of the envelopes is directly proportional to the thickness of the quartz veins. In localities where veining in the quartz or quartz-chlorite-muscovite schists becomes dominant, the alteration envelopes merge and as a result the original composition of the unit between or immediately surrounding the veins is unidentifiable.

8.5 Summary

The abundant quartz veining occurs parallel to the early S_0/S_1 fabric and is, thus, restricted to the schistose, lower unit rocks. However, veining appears to be confined to certain packages, i.e. certain zones in outcrop are vein-rich while others barren. The above study of the fluid alteration of the quartz and feldspar schists to chlorite and muscovite schists respectively, indicates that many of the present compositional contrasts are related to fluid alteration and not to original (sedimentary) compositional contrasts.

The contemporaneous fluid production and regional deformation and metamorphism of the sedimentary pile, and the regional metamorphic grade, is suggestive of fluids

produced by metamorphic devolatilisation (e.g. Cox et al., 1995). This is common in wet sediments that are dewatered during deformation and regional metamorphism during collisional tectonics (e.g. Stephenson et al., 1994).

9 SPITSKOP GOLD PROSPECT

A regional exploration programme undertaken by Opaline Gold Pty Ltd in the 1980-1990's has identified the Spitskop prospect as a possible gold target. The Spitskop gold prospect is located at latitude 33°01'S and longitude 18°46'E, approximately 10 km to the south of the town of Piketberg, along the N7 national road, on the farms Spitskop and Die Brug (Fig. 9.1).

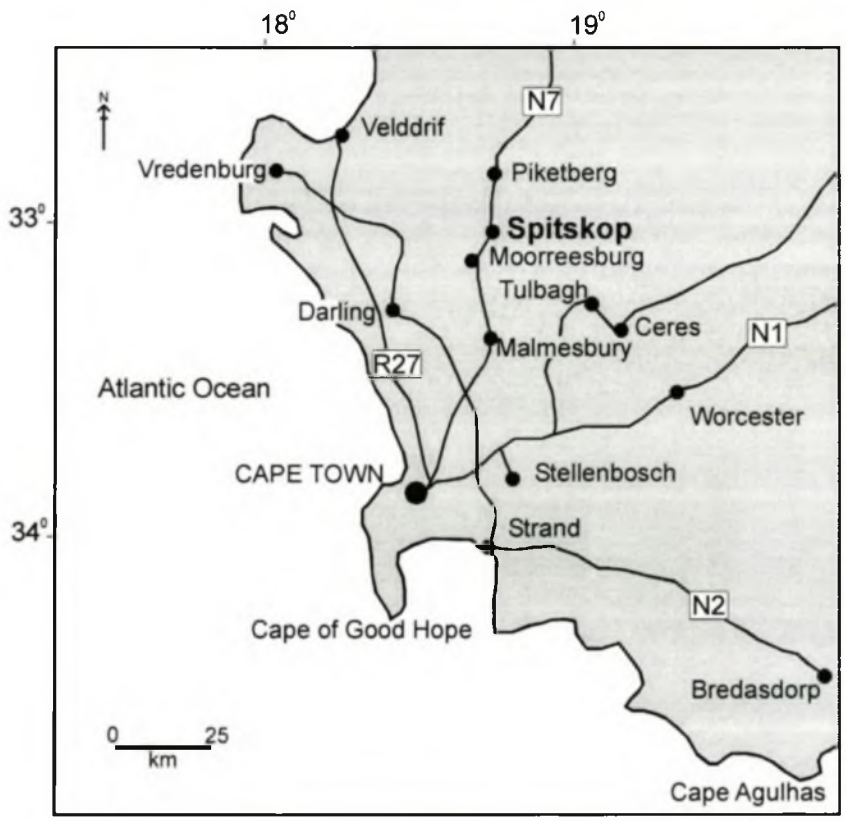

Figure 9.1. Map of the Western Cape showing the location of the Spitskop gold prospect, major national roads and towns.

Spitskop is named after the most prominent feature in the area, a small (635 m above SL), steep sided hill, in an otherwise subdued topography. The prospect area is extensively farmed for wheat and outcrops are restricted to the steeper slopes of

Spitskop and in streambeds. Although the outcrops are still very poor and highly weathered.

9.1 Geology and Structure

The Spitskop area was mapped on a 1:10000 scale (Appendix D, Map 2) and is underlain by the Berg River Formation that represents a monotonous series of quartz-chlorite-muscovite- and chlorite-muscovite-feldspar schists. Minor limestone and metavolcanic lenses occur within the schist package (Chapter 4). Three anomalies were identified by Swingler (1998), namely, Spitskop, Powerline, and Telecom. The Spitskop anomaly is situated within the chert-capped Spitskop, which is underlain by ultramafic slithers and silicified quartz-chlorite-muscovite schists. The chert has been interpreted to represent a silicified ultramafic rock that formed the locality for a major shear zone (Chapter 10). The Powerline and Telecom anomalies are situated within the quartz-chlorite-muscovite schists, stratigraphically below the chert horizon.

The rocks have undergone three phases of deformation (Chapter 5), and only limited original bedding (S_o) and/or sedimentary structures were identified within the schists. The early S_0/S_1 planar fabric is related to bedding transposition and the formation of isoclinal, intrafolial folds (F_1) during the early D_1 deformation event. The D_2 deformation event is responsible for the folding of the S_0/S_1 transposition fabric and produced north-northwest-south-southeast orientated folds that dominate the structure of the area. Folding varies from microscopic-scale folding e.g. crenulation folds, to folding on a macroscopic-scale e.g. kink- and sigmoidal-shaped folds, with wavelengths of up to 200 m. Steep zones related to the sigmoidal folds are also orientated north-northwest-south-southeast and represent the axial planar foliation of the F_2 folds (Chapter 5.2, Plate 5.20 to Plate 5.25).

A later deformation event D_3 is characterised by the refolding of the F_2 folds, with F_3 folds trending northeast-southwest, perpendicular to the F_2 fold axes. The plunge of the F_3 folds is on average 20-30°, producing a gentle dome-and-basin (type 1) interference pattern (Ramsay, 1967). Jointing is present throughout the field area. A

prominent set of joints is orientated perpendicular to the F_2 fold axes and parallel to the axes of F_3 folds.

9.2 Soil sampling and drilling programme

Swingler (1998) undertook detailed gold and arsenic soil sampling of the Spitskop area and identified three gold anomalies called Spitskop, Powerline and Telecom. The soil sampling revealed gold and arsenic values of up to 650 ppb Au and 1200 ppm As for the Spitskop anomaly, 240 ppb Au and 45 ppm for the Telecom anomaly and 530 ppb Au and 280 ppm As for the Powerline anomaly. The results of Swingler's (1998) soil sampling programme are presented in Figure 9.2. The results were overlain on the geological map produced during part of this study (Appendix D, Map 2) to identify any connections between the elevated gold and arsenic values recorded and the lithologies at Spitskop. When comparing the gold and arsenic values for the soil sampling programme at Spitskop there is limited correlation, with only minor overlap of peak gold and arsenic values, e.g. over the Spitskop anomaly. However, this can be explained by lateral dispersion of the anomalies by extensive ploughing (e.g. Rose et al., 1979).

The logging results from the percussion-drilling programme (Swingler, 1998) were plotted on the geological map of the Spitskop area (Appendix D, Map 2), and the lithological classification of the different lithologies of the Berg River Formation presented in Chapter 4 (Fig. 9.3). Only elevated gold readings (>50 ppb) were plotted and the results were inconclusive. Elevated gold values were recorded within the silicified ultramafic unit, the quartz-chlorite-muscovite and the quartz-feldspar-muscovite schists and the quartz vein-rich sections of the quartz-chlorite-muscovite schist. No elevated gold values were recorded related to the marly limestone.

9.3 Ore Mineralogy

Visible sulphides (mainly pyrite) occur both within Type 1a veins (<3%) and in the surrounding wall rocks (up to 15%), for up to 40 cm away from the nearest vein. Pyrite is the main sulphide mineral accompanied by minor chalcopyrite, galena, sphalerite and arsenopyrite. To identify whether the gold is related to the visible

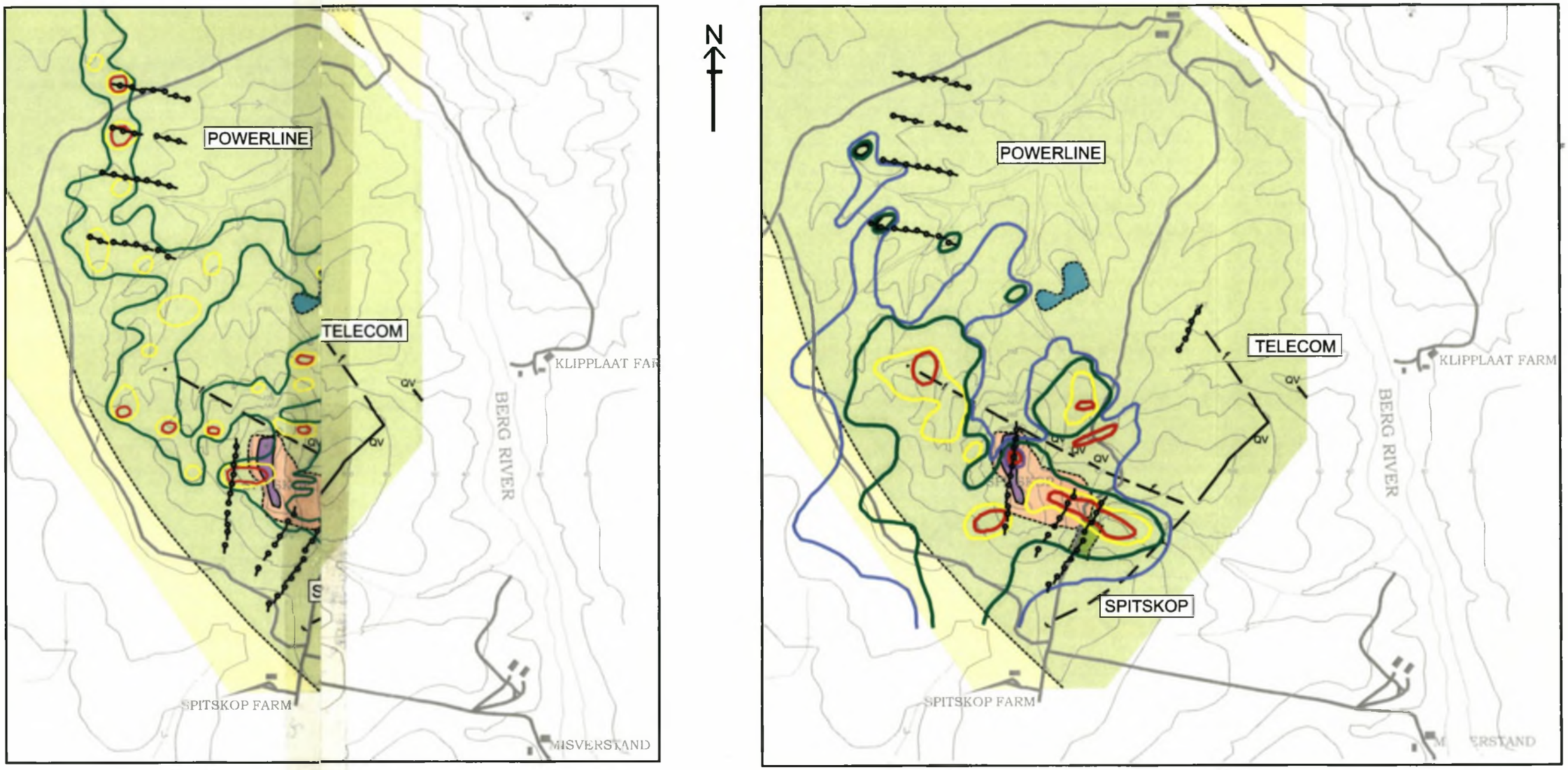

Figure 9.2. Soil sample (-40 mesh) anomaly mæsenic (Swingler, 1998), overlaid on the geological map of Spitskop (Appendix D, Map 2).

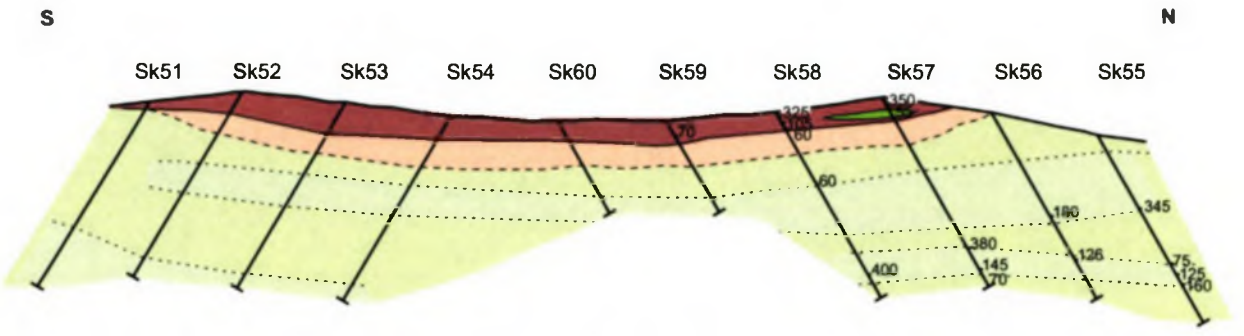

a) Cross section through the Spitskop anomaly, from borehole Sk51 to Sk60.

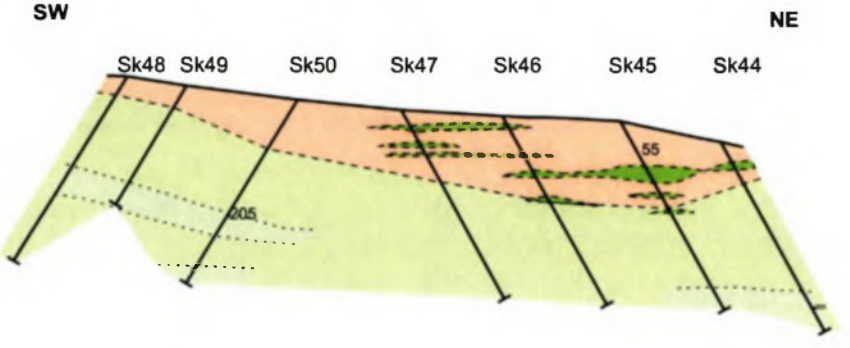

b) Cross section through the Spitskop anomaly, from borehole Sk44 to Sk50.

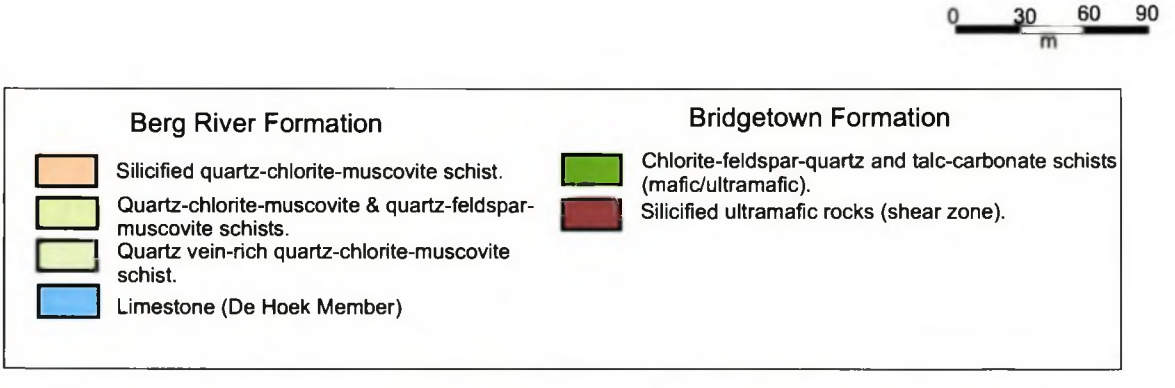

Figure 9.3. Cross sections across the Spitskop area from percussion drilling. A total of 6040 m were drilled over the three anomalies; Spitskop, Telecom and Powerline. The cross sections are based on logging results from Swingler (1998). Only gold values higher than 50 ppb intersected during drilling are shown on the diagrams. Gold analysed by fire assay (Swingler, 1998). Lithologies are based primarily on logging results and from field mapping for this thesis. The majority of the anomalous gold values are related to the quartz-chlorite-muscovite schist that contains abundant quartz veining.

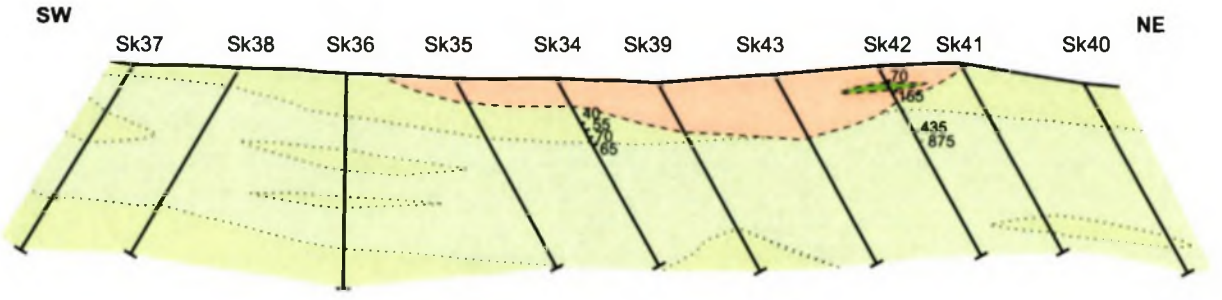

c) Cross section through the Spitskop anomaly, from borehole Sk35 to Sk43.

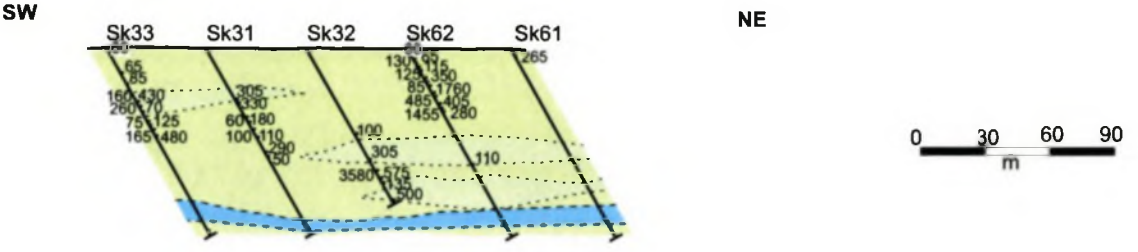

d) Cross section through the Telecom anomaly, from borehole SK31 to SK33 and SK61 and Sk62.

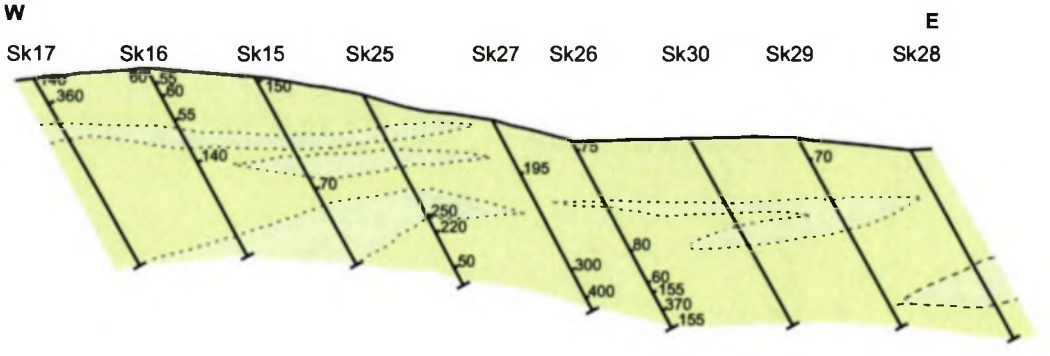

e) Cross section through the Powerline anomaly, from borehole Sk17 to Sk28.

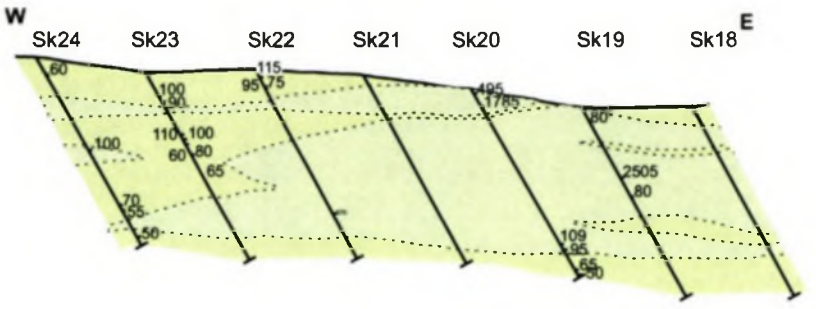

f) Cross section through the Powerline anomaly, from borehole Sk24 to Sk18.

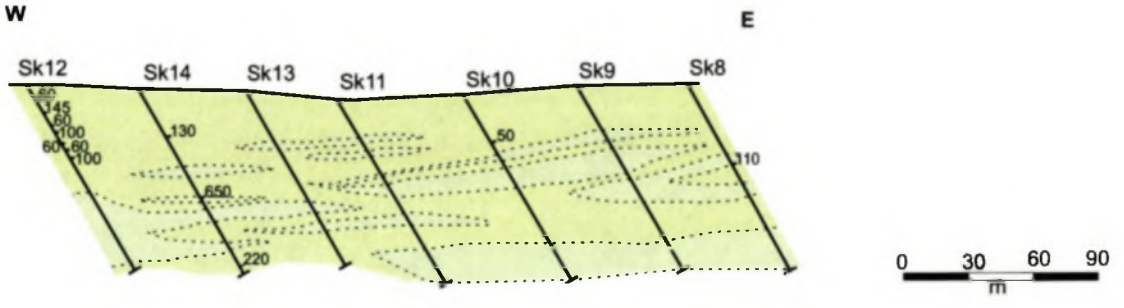

g) Cross section through the Powerline anomaly, from borehole Sk12 to Sk8.

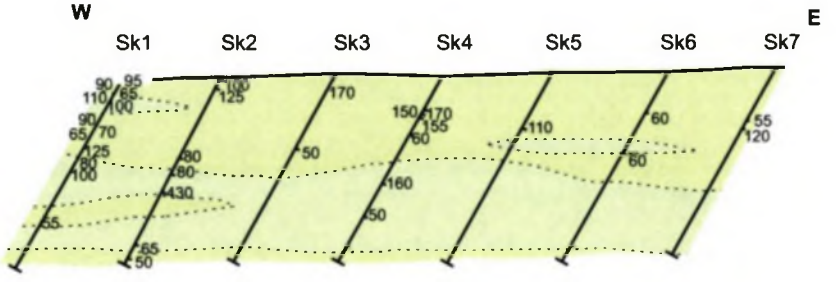

h) Cross section through the Powerline anomaly, from borehole Sk1 to Sk7.

sulphide mineralisation in the veins or surrounding wall rocks, a typical outcrop exhibiting extensive Type 1 quartz veins and visible sulphide mineralisation was chosen for geochemical analyses. The area chosen for sample collection is composed of quartz-feldspar-muscovite schist and contains an approximately 50 cm thick quartz-chlorite-muscovite schist layer representing the vein zone (Fig. 9.4). Type 1a veins make up approximately 70% of the volume of this zone. Many of the veins contain 'pock' marks that possibly represent the location of sulphide mineralisation before weathering. The hanging wall and footwall of the vein-rich layer are composed of quartz-feldspar-muscovite schists typical of that observed throughout the Spitskop area. This schist contains little to no quartz veining except that seen as part of the weak foliation. The schist is greenish-grey in colour, with a sugary texture.

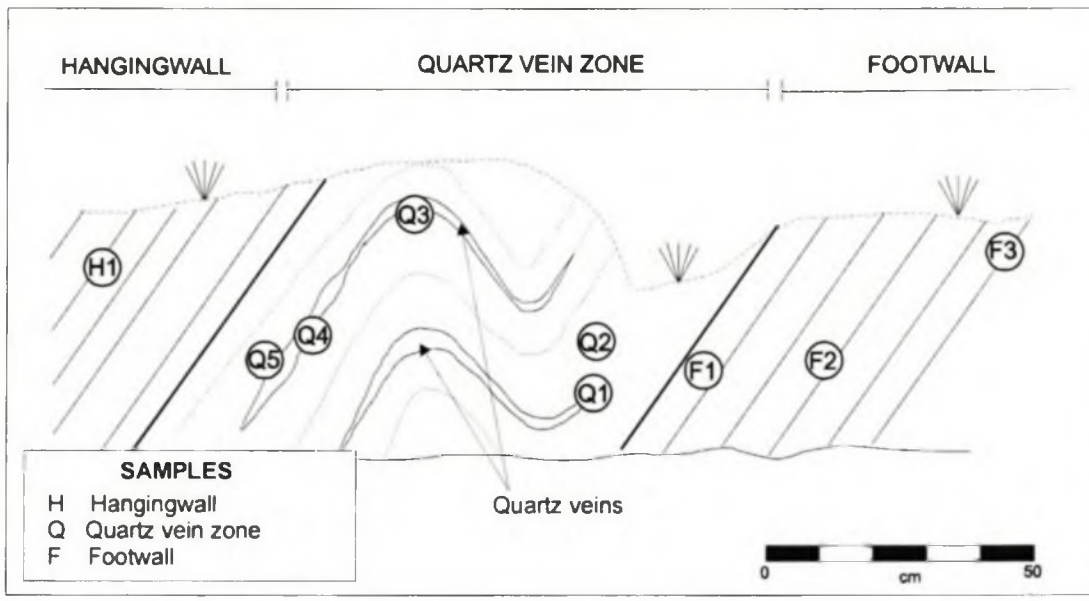

Figure 9.4. Location of samples from outcrop for gold analysis. For description of the hanging wall, footwall and vein zone see text.

Samples were taken from the hanging wall (one), vein zone (five) and the footwall (three). Geochemically the veins are composed of silica (95%), alumina (2%), total iron (1%) and magnesium (0.5%), in the form of quartz and minor chlorite and muscovite (Table 8.1, Appendix C, 13). The veins contain elevated levels of the metals Ni, Cr, As, Cu, Pb and Zn related to the sulphide mineralisation. Elevated gold values of 56, 45 and 58 ppb were identified in the hanging wall, vein zone and footwall respectively, indicating no definite distinction between gold values in the vein

zone compared to the hanging wall or footwall. However, compared to the average gold values of the Spitskop schist (<10 ppb; Swingler 1998), the quartz vein zone is significantly enriched. This is again indicative that the gold is related to Type 1a veins and surrounding wall rocks. All the elements except Pb show slightly higher values in the hanging wall and footwall compared to the veins themselves (Table 9.1), which can be explained by the majority of sulphides occurring in the surrounding rocks and not in the veins.

Table 9.1. Average concentration of ore-forming elements within the footwall, vein zone and hanging wall of the 'representative' outcrop. Au, Te and Sb values detected by ICP-MS (Appendix C, 15; University of Cape Town), the remaining elements by XRF (Stellenbosch University). All values are in ppm except gold in ppb.

	Footwall (n= 3)	**Vein Zone** (n= 5)	**Hangingwall** (n= 1)
Pb	9	27	3
Cu	27	17	19
Zn	88	70	130
Ni	39	27	54
Cr	75	9	101
As	56	41	21
Sb	0	0	0
Te	n.d.	n.d.	1
Au	56	45	58

Pyrites may be subdivided based on their different morphology, into two main groups: euhedral (undeformed) and cataclastic pyrites. The euhedral grains are larger than the anhedral grains although on average they do not exceed 3 mm in diameter. The euhedral pyrites can be subdivided into unzoned and zoned pyrites, the latter being described in more detail below (Plate 9.1).

The cataclastic pyrites have undergone extensive deformation, are much smaller in size than the first type (<1 mm across) and exhibit severe fracturing in the form of a cataclastic texture (Plate 9.2). These pyrites have overgrowths of late pyrite and are cracked with infilling and intergrowths indicating multiple pyrite generations (Plate 9.3).

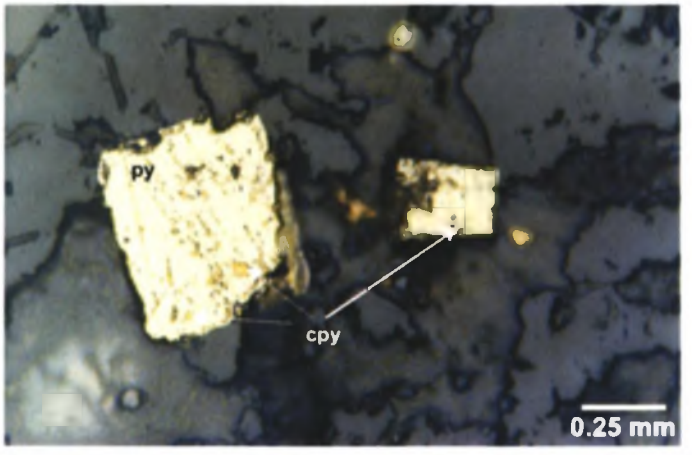

Plate 9.1. Euhedral crystals of pyrite, containing blebs of chalcopyrite. From a Type 1a quartz vein within the chlorite-muscovite schist.

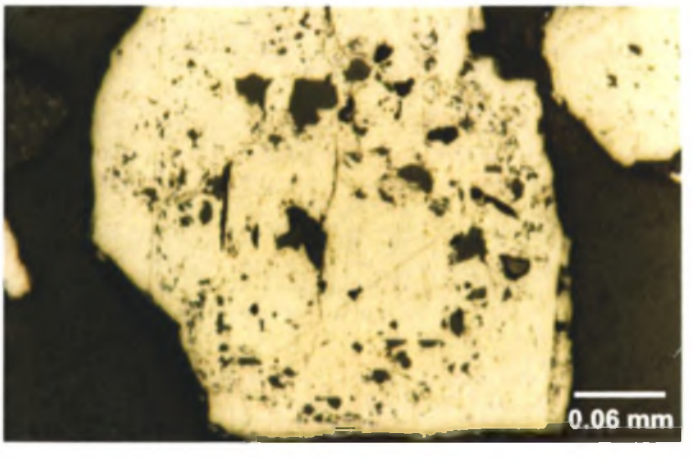

Plate 9.2. Example of an anhedral pyrite with numerous surface pits and cracks. From a Type 1a quartz vein within the chlorite-muscovite schist.

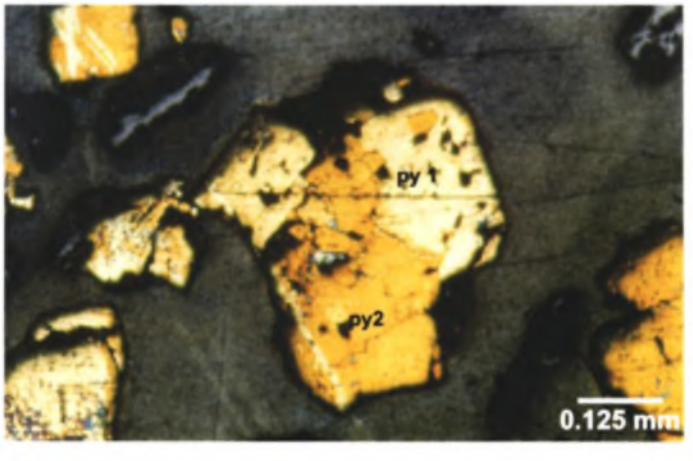

Plate 9.3. After staining with $KMnO_4$ solution as described in Chapter 9.3.1. Fractured pyrite grain (py1), with later pyrite growing in the fracture (py2). From a Type 1a quartz vein within the chlorite-muscovite schist.

Galena is predominantly located along the boundaries of the euhedral pyrite grains and also, to a minor extent, as isolated grains up to 10 μm in diameter. Chalcopyrite occurs as intergrowths with pyrite (Plate 9.4) or tiny grains (<0.5 mm) between quartz crystals. Its morphology is dependent on the surrounding quartz and occurs as 'bleb' -like structures within pyrite grains. Arsenopyrite and minor sphalerite are present as minute isolated grains. The arsenopyrite is also hosted by pyrite and occurs as inclusions of up to 0.1 mm in length, forming up to 25% of the surface area of the pyrites. The arsenopyrite only occurs in pyrites that have undergone very little deformation, with the surface of the pyrites having few or no cracks (Plate 9.5; 9.6).

9.3.1 Zoning of pyrite

Many of the euhedral pyrite grains contain visible zoning. Staining of pyrite grains was undertaken using a solution of $KMnO_4$ (2.5 g $KMnO_4$ in 100 cm^3 of water) and concentrated $H_2SO_{4\,(aq)}$ (Craig and Vaughan, 1981). Zoning and microstructures are revealed by colour contrasts (Plate 9.7), which, in air range from yellow/brown through to purple, blue and white. The change in colour is attributed to the elemental sulphur content on the surface of the analysed grain (Fleet et al., 1993). Thus the amount of elemental sulphur located on the surface of the pyrite grain is related to the proportion of sulphur substitution by other elements, e.g. As, and thus can be used to identify areas of possible high As content (Cameron, 1961; Fleet et al., 1989).

Quantitative SEM analysis for the elements Fe, S, As and Sb (Table 9.2) identified two different pyrite generations based on their As contents. The first are pure pyrites giving an average composition 32 wt.% Fe, 68 wt.% S with negligible As and Sb, and a S to Fe ratio of 2:1. The second population contains up to 0.4 wt.% As. These pyrites contain little to no visible arsenopyrite inclusions, suggesting that the As occurs in the crystal lattice. Sulphur isotope ($\delta^{34}S$) data for pyrites from Type 1a veins and Type 2 veins (Appendix C, 16) was inconclusive in identifying a source for the sulphur in the mineralisation.

The etching and staining revealed that nearly all the pyrites contain some form of

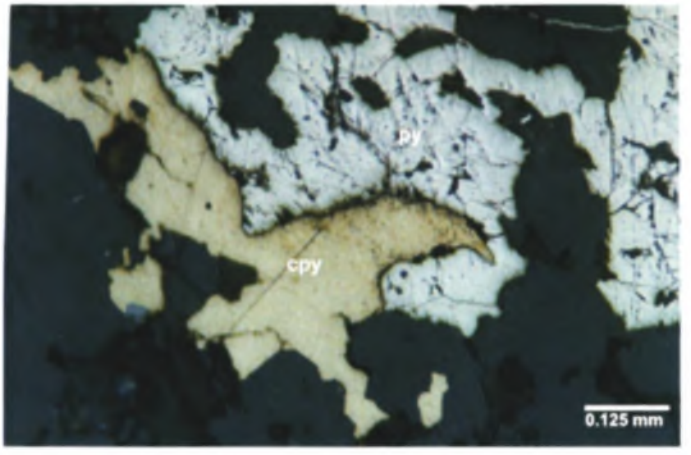

Plate 9.4. Intergrowth of pyrite with chalcopyrite, possibly representing chalcopyrite remobilisation into cracks within the pyrite.

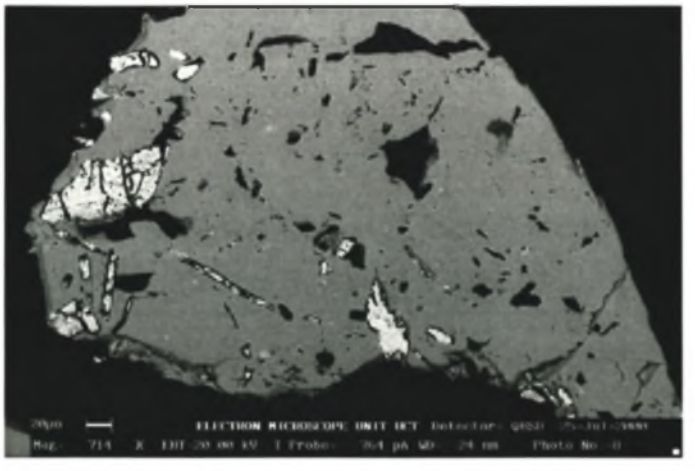

Plate 9.5. Arsenopyrite (bright mineral) occurring within a pyrite grain. The occurrence of arsenopyrite within the pyrite indicates that the pyrite and arsenopyrite formed synchronously.

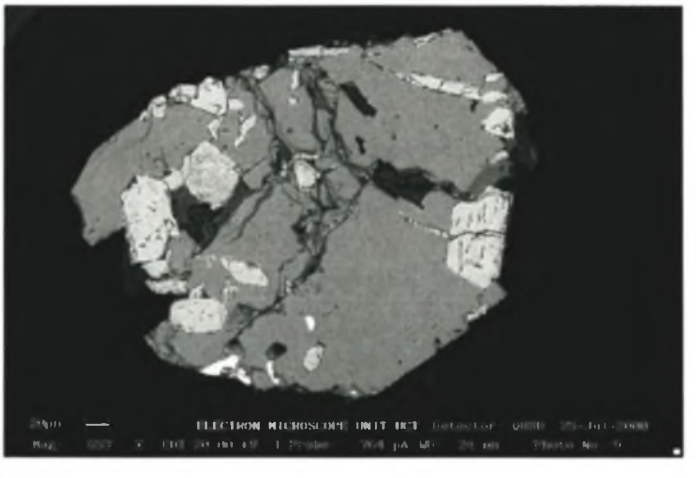

Plate 9.6. Euhedral arsenopyrite inclusions (light grey) within a pyrite grain. This grain is a typical example of the mode of occurrence of arsenopyrite in pyrite.

zoning that was not identified by microscopy. Although zoning is present, it was not possible to identify whether this zoning is related to arsenic or another ore-forming element (Plate 9.8; 9.9). For this reason elemental mapping by Proton Induced X-ray emission (PIXE) was undertaken.

Table 9.2. Selected electron microprobe analyses of pyrites from the mineralised zone at the Spitskop gold deposit. Analyses indicate that pyrites may be divided into two groups based on their arsenic content: As-rich (> 0.4%) and As-poor (< 0.4%).

			wt%		
Pyrite	**Fe**	**As**	**Sb**	**S**	**Total**
1	46.0	0.0	0.0	56.9	102.9
2	46.2	0.1	0.0	51.0	97.4
3	46.3	0.0	0.0	57.9	104.3
4	46.0	0.0	0.0	57.5	103.6
5	45.3	0.0	0.0	56.0	101.3
6	42.6	0.0	0.0	53.2	97.0
7	45.4	0.5	0.1	57.9	103.8
8	44.9	0.5	0.1	57.6	103.2
9	44.5	0.0	0.0	58.0	102.5
10	45.6	0.4	0.0	60.6	106.6
11	46.3	0.4	0.0	58.4	105.1
12	47.2	0.4	0.0	58.5	106.2
13	46.0	0.0	0.0	58.0	104.1
14	45.2	0.0	0.0	55.5	100.7

Measurements were made with a proton beam of 3.0 MeV energy and 0.5-1.5 nA beam current. The total accumulated charge varied between 0.2 and 0.9 μC for point analyses and between 0.8 and 44.5 μC for maps. PIXE spectra were registered using a Link-Pentafet Si (Li) X-ray detector, shielded with a 200 μm Al filter, and fitted using a DEC 2300 Alpha Server running VMS and the GeoPIXE software (Ryan et al., 1990a & b). A detailed description of the accuracy and the precision of the PIXE system was reported by Van Achterberg et al. (1995). Further information on the machine set up is provided in Appendix B, section 1.8.

Elemental maps were created by the use of dynamic analysis (DA), a rapid matrix transformation method, which is part of the GeoPIXE software (Ryan and Jamison, 1993; Ryan et al., 1995 and 1996). The elemental maps thus obtained are inherently overlap-resolved, background-subtracted and are generated on-line. Scanned

Plate 9.7. An example of a pyrite grain that contained no evidence of zoning before treatment and the enhancement of this zoning by etching and staining. The bright areas in the centre of the pyrite grain represents REE inclusions. Image created using the BSE- detector on the SEM (University of Cape Town.

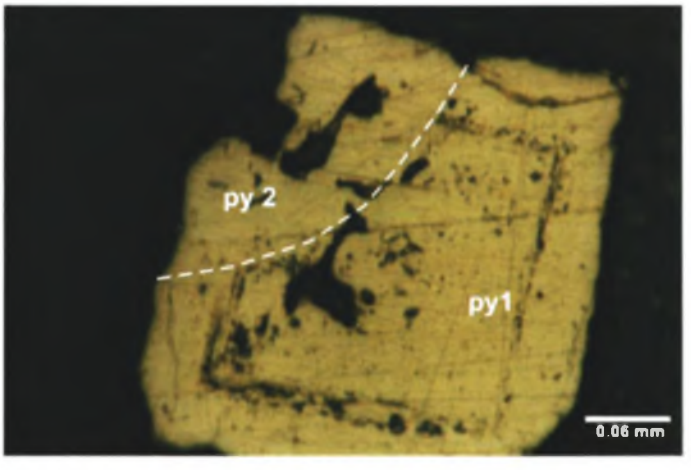

Plate 9.8. Zoned euhedral pyrite (py1) that appears to be fractured and overgrown by a later pyrite (py2) that does not exhibit any visible zoning (top left).

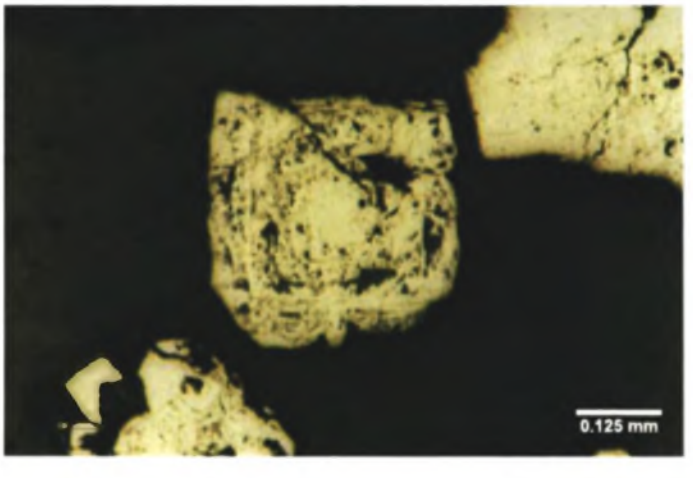

Plate 9.9. Typical zoned pyrite seen in the wall rock and Type 1a veins associated with elevated gold values.

regions were divided into 64 x 64 pixels. The final maps are quantitative, with the intensity in ppm, presented as contours linking pixels with the same values. This method has been thoroughly tested for geological applications (Ryan et al., 1996). Quantitative elemental mapping of pyrites was earlier reported by Przybylowicz et al. (1995).

Elemental mapping (PIXE) identified zoning both within the pyrites that exhibited zoning (after staining) and also from pyrites that were optically unzoned. Minor elemental zoning was also identified in the highly deformed grains. In fact, zoning to some degree was identified in the majority of pyrites analysed. A summary of the zoning seen is presented in Table 9.3 and shows that arsenic, lead, nickel and antimony elemental zones are present in both euhedral and deformed pyrites. The zoning can be subdivided into two groups, those with an arsenic-rich core and those with an arsenic-poor core.

Table 9.3. Summary of zoning in pyrites from PIXE elemental mapping. Pyrites obtained from heavy mineral fraction from Type 1a vein and immediately surrounding wall rock. Full data set provided in Appendix C, 17.

Sample	Classification	Zoning		As content of core
		Major	Minor	
pr2c0024	Euhedral-deformed	-	As, Ni	Low
pyr9006	Deformed	As	Ni, Pb	Low
pyr80010	Euhedral-deformed	As, Pb	-	Low
pyr40020	Euhedral	As, Pb, Sb, Ni	-	High
pyr30021	Euhedral	As, Ni	Pb	Low
pr2b0023	Deformed	As	Pb	Low
pyr70011	Euhedral	As	Ni, Pb	Low
pyr20022	Euhedral-deformed	As, Pb	Sb	High

Pyrite with arsenic-rich cores shows a systematic zonation of nickel, antimony and lead from the core to the rim and these pyrites are invariable euhedral. Only the pyrite grains with an arsenic-rich core also showed antimony zoning (Plate 9.10). High antimony and nickel values are restricted to zones of high lead, while lead was restricted to high arsenic zones, or occurs in the low arsenic areas between arsenic-rich zones. Pyrites with arsenic-poor cores, show irregularly shaped arsenic-rich zones and occasional nickel- and lead-rich zones associated with the

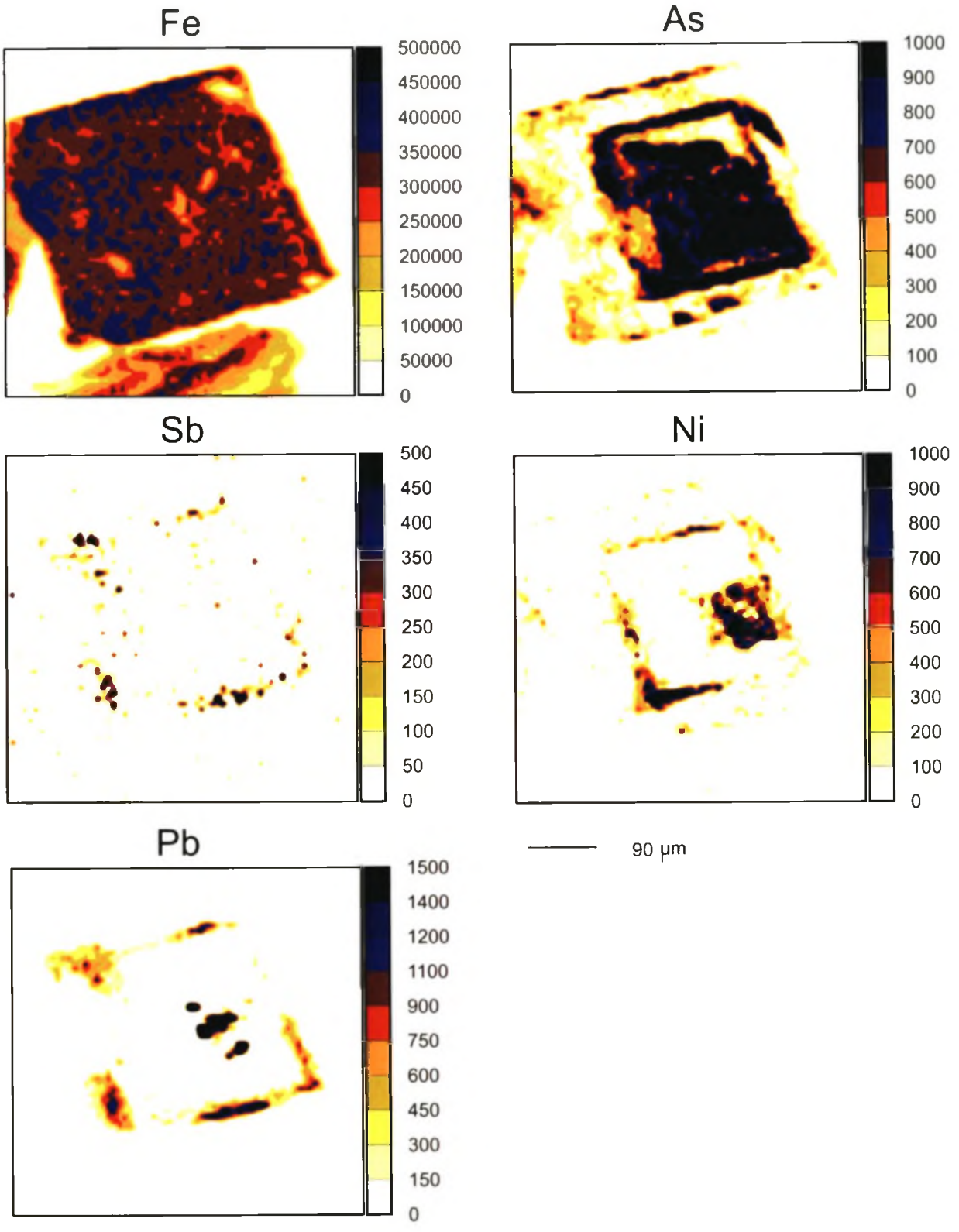

Plate 9.10. Elemental maps of an arsenic-rich pyrite grain with an As-rich core, using the micro-PIXE technique (see text for additional information). Full data set of elements analysed presented in Appendix C, 17.

arsenic-poor cores. No correlation between arsenic and antimony was identified (Plate 9.11). These As-rich zones often correlate with high lead and or nickel, in other cases the lead is located in As-poor areas between As-rich zones.

9.3.2 Gold Mineralogy

Samples from outcrops containing visible sulphides and from the percussion drilling samples that showed elevated gold showings (>1000 ppb) were taken to identify the location of gold and its possible association with other ore minerals. No free gold or gold occurring within secondary sites related to any of the sulphides was located by petrography. Both BSE-SEM and PIXE analysis were used in an attempt to identify the location of gold, but proved relatively unsuccessful, with only a few grains of gold being located within pyrite grains (Plate 9.12). These gold occurrences could not be unequivocally linked with any other ore mineral or element.

Due to the limited occurrence of sulphide minerals and gold, it was not possible to establish the paragenetic association of gold with sulphide minerals, although the majority of mineralisation is related to Type 1a veins.

9.4 Fluid inclusions of Type 1a veins

Type 1 veins are voluminous, laterally extensive and contain visible sulphide mineralisation seen in the field. While Type 2 veins are, in contrast, subordinate, laterally discontinuous and contain very little to no mineralisation (Chapter 8). For this reason it is suggested that the gold is probably associated with Type 1 veins.

Fluid inclusion studies were conducted on Type 1a veins in an attempt to establish the composition of the fluids responsible for veining. Type 1a veins are characterised by extremely small inclusions (predominantly less than 2 μm), with only a few (<10% of total) of the inclusions being greater than 5 μm in size making fluid inclusion studies extremely difficult. The inclusions occur along quartz grain boundaries and planes crosscutting the quartz crystals. Following the criteria of Roedder (1984), the

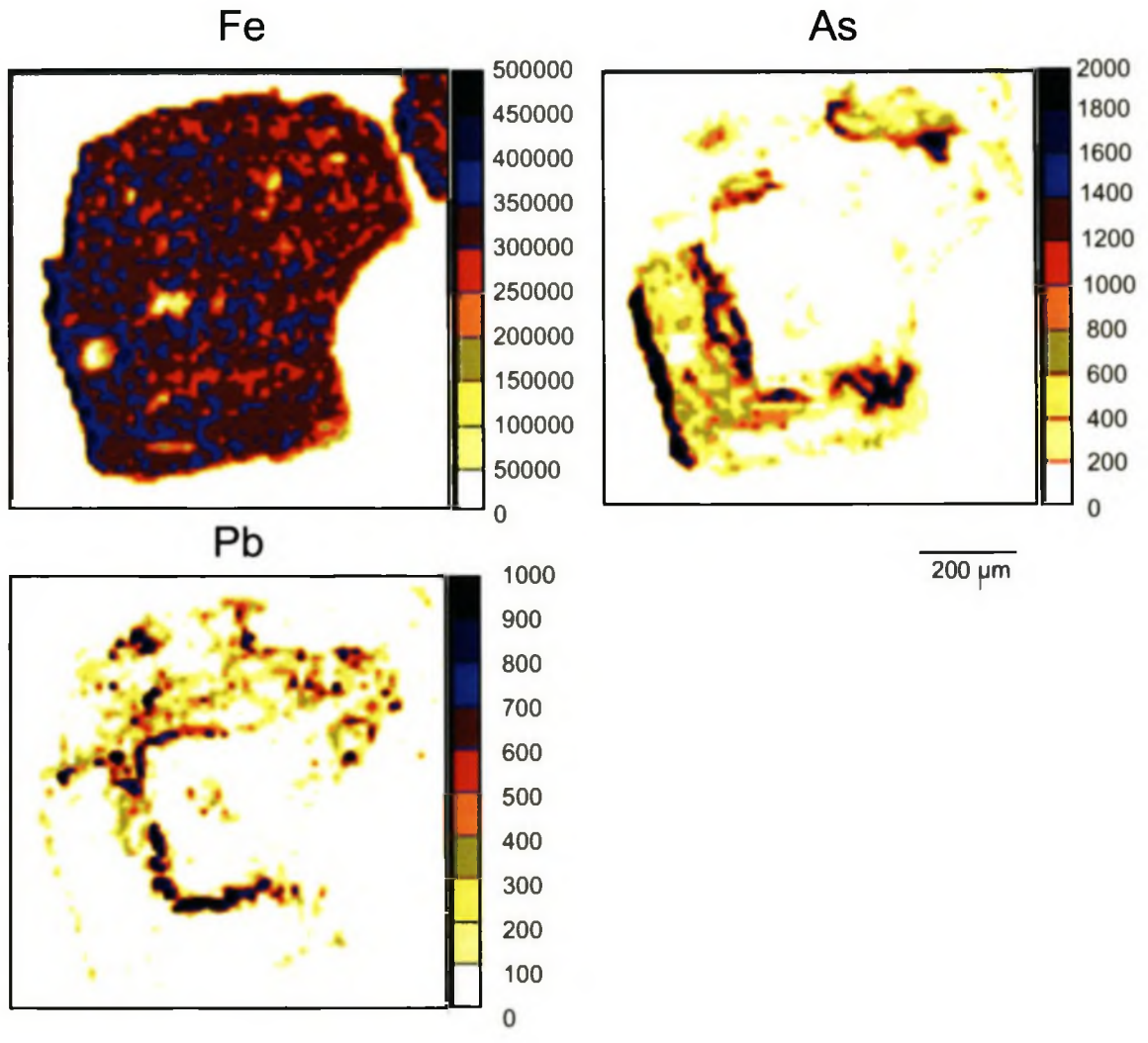

Plate 9.11. Elemental maps of a pyrite grain with an As-poor core, using the micro-PIXE technique (see text for additional information). Full data set available in Appendix C, 17.

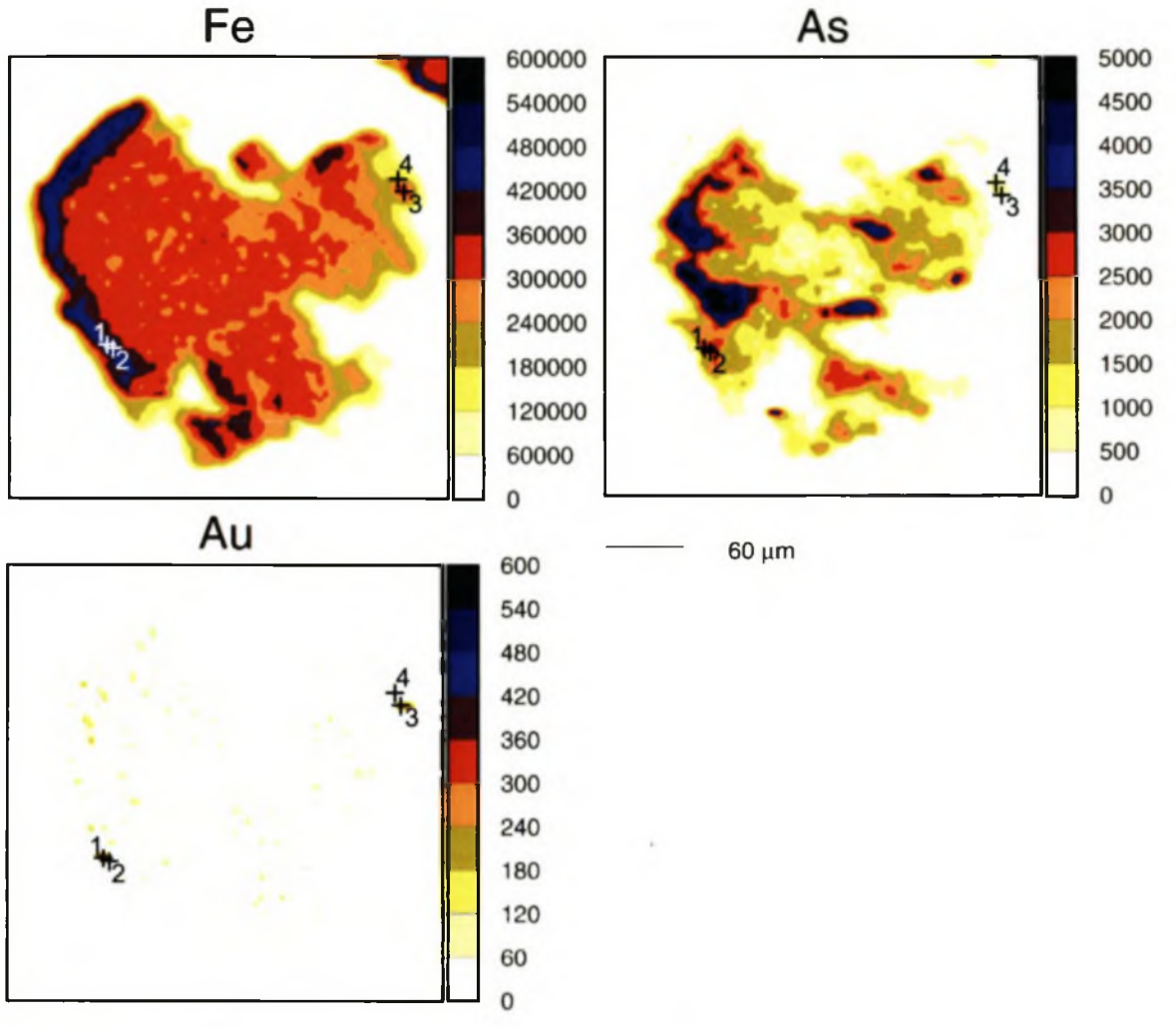

Plate 9.12. Elemental maps showing the location of gold on the surface of an arsenic-rich pyrite grain. Note that no positive correlation between the gold localities and the elevated arsenic values could be conclusively identified. Full data set available in Appendix C, 17.

Table 9.4. PIXE spot analyses of trace element concentrations in pyrite in Plate 9.12 above. Concentration of elements in ppm. Full data set available in Appendix C, 17.

Point Analysis	1	2	3	4
As	1800 (60)	1510 (54)	1130 (40)	610 (15)
Ni	460 (40)	500 (29)	220 (40)	66 (10)
Pb	930 (180)	790 (480)	330 (100)	140 (40)
Sb	78 (18)	40 (4)	< 35	28 (14)
Au	770 (60)	130 (13)	840 (60)	<14
Ag	25 (9)	10 (2)	21 (7)	17 (5)

inclusions studied in the quartz veins of Spitskop are secondary in origin. However, Walther & Orville (1982) suggested that fluids in metamorphic rocks are transported along fractures. Thus the healed fractures, which are associated with secondary inclusion trails in metamorphic rocks, in fact may represent the healed fluid conduits (Crawford & Hollister, 1986). Whether the inclusions identified in this study can provide the same information as those inclusions trapped during crystal growth is discussed below.

It was possible to group the inclusions into three populations using morphology, size, their general appearance at room temperature, and after minor heating and cooling. Inclusions that showed evidence of leakage were not examined in this study. A summary of the fluid inclusion analysis for the three inclusion types is represented in Table 9.5. Histograms for the T_m and T_h are represented in Figure 9.5 and 9.6 respectively.

9.4.1 Type 1- H_2O-NaCl

These are the most abundant inclusions. They are round to oval in shape, containing a small vapour bubble (F (degree of fill) = 0.95) at room temperature (25 °C). The fluid freezes at approximately -40 °C and melts on average at -2.6 °C, corresponding to a salinity of 4.6 wt.% NaCl eq. (Potter et al., 1978). The T_h ranges from 140 to 316 °C and two peaks can be identified, the first at 160-180 °C and the second at approximately 240 °C. This range in homogenisation temperatures could reflect either a variance in the trapping temperatures, or trapping pressures. From these temperatures it is possible to calculate the density using the graph of Roedder (1984); based on the data of Potter et al. (1977) and Khaibullin et al. (1980), and taking into account the degree of fill. This provides densities of 0.85 and 0.87 g/cm^3 for the two peaks respectively.

9.4.2 Type 2-H_2O-CO_2-NaCl

This population is oval in shape and consists of two phases at room temperature, which, on initial cooling, become three phases. T_f of the two bubbles is approximately

Table 9.5. Summary of the fluid inclusion study on the three types of inclusions identified within Type 1a quartz veins. Note, values marked with an asterisk were calculated using the computer programme Flincor (Brown, 1989), and the equations of Brown and Lamb (1989). Full data set available in Appendix C, 18.

Type	1 H_2O-NaCl	2 H_2O-CO_2-NaCl		3 CO_2
T_f°C	-40	-35	-100	-100
T_m°C	-2.6	9	-57	-57.2
T_h°C	150 & 240	271	16	12
wt% NaCl eq.	4.63	2-4		-
Density (g/cm^3)	0.85 & 0.87	0.97		0.82
T_t°C*	304 & 449	323		585
Vapour pressure*	-	-	-	47.3
Molar volume*	19.6	27.2		52.0
Molar NaCl*	0.83	0.35	-	-
Molar fraction*	0.02	0.00	-	-
Bulk molar volume*	19.59	20.94	-	-
Critical point °C*	416.9	-	-	-

-35° and -100 °C denoting a water and carbon dioxide component respectively. The T_m for the CO_2 bubble is -57 °C, and assuming that the slight depression in the CO_2 freezing point is related to the presence of CH_4. Then the X_{CH_4} can be estimated at 0.01-0.02% (Swanenberg, 1979). The T_h of the CO_2 bubble varies from 12° to 22 °C, with a median of 16 °C. Due to the "water" component melting above 0 °C, the presence of a clathrate can be surmised. The clathrate component melts between 6 ° and 12 °C, with a median of 9 °C, which is slightly lower than the pure clathrate melting temperature of 10 °C (Seitz and Pasteris, 1990). This slight depression of T_h for the clathrate is consistent with a CO_2 clathrate melting in the presence of an aqueous phase of approximately 2-4 wt.% NaCl eq. (Diamond, 1994). This is assuming that the depression in the melting temperature is not related to the counter-effect of CH_4. However, from the T_m of the CO_2-rich component, very little CH_4 is present and can thus be discarded. The salinity of these inclusions is similar to the salinity values recorded for H_2O-NaCl population (Type 1). The presence of an electrolyte in H_2O-CO_2 fluids affects the fluid phase equilibrium and thus the phase relationships (Bowers and Helgeson, 1983 and references therein). To estimate the

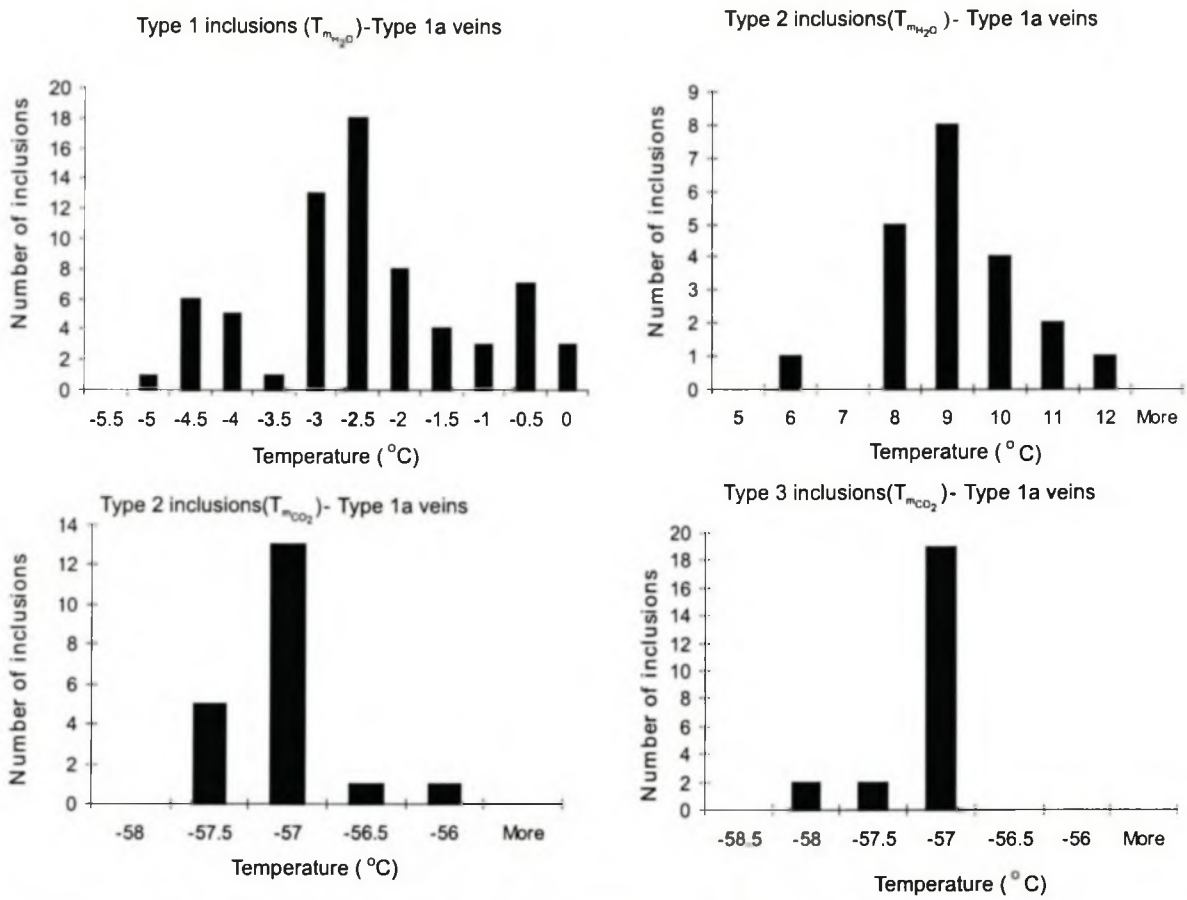

Figure 9.5. Temperature of melting (T_m) for the three types of inclusions seen within Type 1a veins at Spitskop. Full data set available in Appendix C, 18.

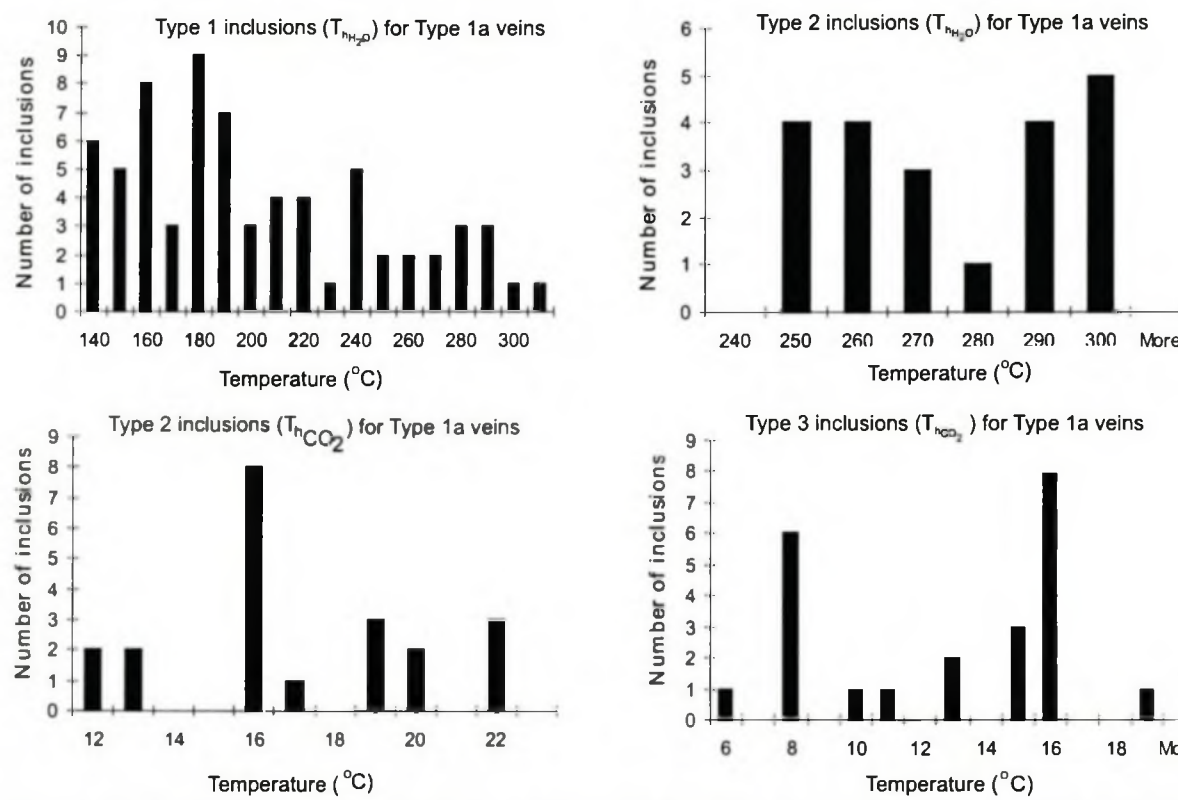

Figure 9.6. Temperature of homogenisation (T_h) for the three types of inclusions seen within Type 1a veins at Spitskop. Full data set available in Appendix C, 18.

CO_2 and bulk densities the programme *Flincor* (Brown, 1989) was used with the equations of Brown and Lamb (1989). This provided a CO_2 density of 0.81 g/cm^3 and a bulk density of 0.97 g/cm^3.

9.4.3 Type 3- CO_2

Type 3 inclusions are oval in shape, consisting of only one phase at room temperature that, on cooling, forms a small bubble that continues to grow until the degree of fill is between 0.75-0.95 at 0 °C. The bubble freezes at approximately -100 °C and melts at -57.2 °C, just below the melting temperature of pure CO_2, suggesting that another minor component is also present which is either CH_4, N_2, or SO_2 (Swanenberg, 1979). If we assume that the other component is methane, then following Swanenberg (1979) we can calculate the bulk X_{CH_4} as 0.02-0.03%, which is consistent for the values obtained for Type 2 inclusions. The T_h (into the liquid state) for this population is at 12 °C and from Brown and Lamb (1989) a density of 0.84 g/cm^3 for the CO_2 phase can be calculated. This agrees with the calculation of Swanenberg (1979), estimating the equivalent CO_2 density of 0.82 g/cm^3 and is similar to the density calculated for the CO_2 in the Type 2 inclusions.

9.4.4 Primary verses secondary inclusions

Walther and Orville (1982) have suggested that secondary inclusions may provide the same information as primary inclusions. The identification above of three types of fluids in the veins suggests that these secondary inclusions are related to the modification of primary fluid inclusions during decrepitation, or they represent fluids trapped during later fluid introduction (Roedder, 1984). However, as deformation was progressive during D_1, with fluid movement occurring throughout this deformation event, the primary inclusions would most likely have been modified as the veins were folded during D_1. This may well explain why no primary inclusions were identified and the inclusions observed could still be related to D_1, but were modified by the deformation event.

9.4.5 Estimation of the geothremal gradient

Whether the inclusions were produced early, during or post-D_1, the veining occurred during lower greenschist facies metamorphism (Chapter 7). From chlorite geothermometry a temperature of approximately 300 °C for regional metamorphism has been determined (Chapter 7). It is therefore possible to estimate the pressure of the fluid, if one assumes a temperature of approximately 300 °C. Following Roedder (1984), this indicates a pressure of between 0.8 and 1.75 kbars. In such environments, the fluid pressure is approximately equal to the lithostatic pressure. Given that the quartz-chlorite-muscovite schist and feldspathic schist give an average density of between 2.65 and 2.7 g/cm^3, the depth of formation of the inclusions can be estimated at between 3 and 6.5 km.

Following the estimation of the depth of the formation of the fluid inclusions and a temperature of approximately 300 °C, a geothermal gradient can therefore be estimated at between 100 ° and 46 °C/km. Such a high geothermal gradient of 100 °C/km in a collisional environment as envisaged for the Saldania Belt (Chapter 10.3.2) is very unlikely. However, an elevated geothermal gradient of 46 °C/km is possible in such a scenario and therefore a thickness of between 6-7 km is a reasonable estimate. The present thickness of the lower unit is unknown, as the underlying basement is nowhere exposed, nor has it been intersected during drilling. Also, thrusting and duplication occurred in the lower unit (Chapter 5.2), and therefore any thickness estimated will not give the original stratigraphic thickness, but only an estimate of the minimum tectonostratigraphic thickness for the lower unit.

9.5 Summary

Gold mineralisation is tentatively suggested to be associated with predominantly euhedral arsenic-rich pyrites occurring within Type 1 quartz veins. These quartz veins occurred early- to syn-D_1 and this therefore confines the gold mineralisation to early in the deformation history of the western branch of the Saldania Belt. Type 1 quartz veins were generated by a low salinity, H_2O-CO_2 fluid, which is characteristic of fluids generated by the devolatilisation of sedimentary rocks during regional metamorphism.

Fluid inclusion analyses of quartz veins in the Spitskop area by Slabber (1995) identified three populations: H_2O-NaCl, H_2O-NaCl-CO_2 and CO_2, with T_h of 160, 270 and 15 °C respectively. This is comparable to the results from this study. The T_h of 160 °C for the H_2O-NaCl population is suggested to represent a regional metamorphic overprint in the Malmesbury Group or later orogenesis related to the Cape Fold Belt (Slabber, 1995). Bruwer (1998) identified 200 and 350-300 °C populations in the Kuils River-Kuiperskraal area (Tygerberg Terrane) and suggested that these populations are wide-spread throughout the Tygerberg Terrane.

10 DISCUSSION

Regional mapping has shown that the metasedimentary and metavolcanic rocks of the Malmesbury Group can be divided into two units mainly based on their structural characteristics, namely the presence or absence of an early, refolded (S_0/S_1) schistosity and to a lesser extent, their lithology.

10.1 Schistose rocks

10.1.1 Bedding transposition and layer-parallel thrusting

The schistose rocks have been subjected to an early deformation event, D_1 that is manifested by the pervasive development of a strong fabric (S_0/S_1). In contrast, this early fabric is not developed in the non-schistose rocks. Isoclinal, intrafolial, and commonly dismembered folds within the S_0/S_1 fabric (Chapter 5.2) indicate that the schistose rocks have undergone layer-parallel folding and bedding transposition. The transposition fabric is found on a variety of scales and intrafolial fold wavelengths range from millimetres up to several metres (Fig. 5.4). It is likely that larger, regional-scale folding is also present in the schistose rocks, but due to the limited outcrop, the monotonous nature of the rocks, and the absence of any markers or horizons, the identification of this large-scale folding has been inhibited.

The tracing of individual units between outcrops is difficult as the layers are often not laterally continuous and their thickness varies considerably. Such dramatic changes in the thickness of units occur over only a few metres, as is identified in the graphitic schists and phyllites lenses in the Zoutkloof and De Hoek Quarries (Chapters 4.1.1 & 4.1.3). For example, where the graphitic schists are intersected during drilling (e.g. at Spitskop and Riviera), the schists occur as lenses at different stratigraphic heights that cannot be correlated across drill holes that are located 10 m or less apart. In the De Hoek, Zoutkloof and Riebeeck West Quarries, the limestone beds taper out over short strike extents and are often truncated against one another (Chapter 4.1.4). The

quartz schist identified in the Spitskop and Goudmyn se Kop areas and also at Kruisfontein Quarry shows a similar lensoidal and discontinuous character as the limestone beds, graphitic schists and phyllites described earlier (Chapter 4.1.2). Metavolcanic rocks intersected away from the main body at Bridgetown, occur as isolated lenses at Spitskop and Riviera rather than as continuous units, indicating a dramatic reduction in lithological thickness (Chapter 4.1.5).

The contacts between different lithological units are always sharp, often containing quartz veining, highly strained lithologies or even mylonites (Plates 5.13, 5.14, & 5.19). For example, the mylonites in the Zoutkloof and Riebeeck West Quarries, are parallel to bedding and to the S_0/S_1 fabric, and are, thus, probably related to the same deformation event responsible for the transposition of bedding described in Chapter 5. Also in these quarries, zones of major detachment have been identified occurring parallel to bedding in the limestone. Along these zones of detachment, detachment folds, small-scale thrusting, imbrication and duplexing are observed (Chapter 5.2; Plates 5.8, 5.9, & 5.10).

None of these features can be explained in terms of facies variations in sediment deposition, but rather points towards a tectonostratigraphic sequence.

10.1.2 Correlation of lithologies on an outcrop and regional scale

Hartnady et al. (1974) proposed the subdivision of the Malmesbury Group into the present formations accepted by SACS (1980) as discussed in Chapter 2. They were also the first to identify bedding transposition in the Berg River and Klipplaat Formations. When they proposed the stratigraphic succession of the Swartland Terrane, they stated "Provided no major recumbent folding is present, these units are probably in correct stratigraphic sequence..." (Hartnady et al., 1974, page 198). It is clear that the bedding transposition identified in this study equates to that earlier identified by Hartnady et al. (1974) and that this fabric is pervasive throughout the schistose rocks of the Berg River, Klipplaat and Bridgetown Formations (Chapters 5 & 10.1.1). The pervasive nature of the bedding transposition indicates that the 'lithostratigraphy' observed today in outcrop as well as in a regional context is tectonic. The present stratigraphic positions of the Berg River, Klipplaat and

Bridgetown Formations are tectonically induced and therefore do not represent their original stratigraphic positions, but a pseudostratigraphy.

Although no detailed correlation of lithologies can be carried out, there are some regional correlations, which have been noted. For example, similar graphitic schists are recorded at Riviera and 25 km to the southwest at the Zoutkloof and De Hoek Quarries, and 35 km to the southwest at Spitskop. Major limestone units occur at the De Hoek, Zoutkloof and Riebeeck West Quarries that are separated along strike from one another by some 65 km. Metavolcanic rocks occur at Spitskop and Riviera situated approximately 10 and 25 km respectively to the northwest of the main metavolcanic body at Bridgetown.

These lithologies all trend northwest-southeast. This orientation is the same orientation as the regional fabric S_0/S_1, the F_1 fold axes and L_1 lineation (Figs. 5.1 & 5.4). Shear sense indicators, northeast-southwest orientated horse structures, and northwest, west and southwest verging folds are also orientated with the regional northwest-southeast structural trend. This suggests that the present location of the lithologies is related to the early deformation event, D_1.

10.1.3 Thrust kinematics and vergence of structures

F_1 fold axes are parallel to L_1 lineations on the S_0/S_1 surfaces, and are co-axial to F_2 fold axes and F_2 lineations. A similar scenario is described from the Gifberg Group, the Gariep-aged rocks underlying the Vanrhynsdorp Group, and is interpreted to be a result of sinistral transpression (De Beer et al., 2002). The northeast-southwest dip of the S_2 axial planar fabric of the F_2 folds is related to the deformation event D_3, which is characterised by folding with fold axes orientated northwest-southeast. A consistent top-to-the-northwest or -west sense of movement is indicated by: kinematic indicators in mylonites (Plates 5.7 & 5.8) and small-scale thrust imbricates (Plate 5.9), the ubiquitous westerly (southwest to northwest) vergence of early F_1 folds, and the northwest-southeast orientation of L_1 (e.g. at the De Hoek, Kruisfontein and Riebeeck West Quarries, in the Porseleinberg Hills and the Kanonkop farm outcrop). This direction is in conflict with earlier suggestions (Chapter 3.4). Hälbich and Hartnady (1985) suggested that the cleavage pattern in the Swartland Terrane

reflects a major thrusting event, with the lithologies to the west transported over the lithologies in the east, indicating eastward vergence. Hälbich and Hartnady (1985) identified a distinct 'S' symmetry of the early microfolds in the Porseleinberg area and also postulated a top-to-the-east transport direction. However, no S-shaped folds could be identified at Bothmaskloof Pass that would indicate an easterly vergence. Further, the westerly vergence identified at this locality is in agreement with the vergence direction (also westerly) identified on a regional scale. Westerly verging folds described during this study in the Zoutkloof and Riebeeck West Quarries were also described earlier by Damp (1983).

This westward vergence of structures in the lower unit/schistose rocks is opposite to that identified further north in the Gariep Belt (transport direction to the southeast), where subduction beneath the South American plate has been proposed (e.g. Frimmel, 1995; Frimmel et al., 1996a). In the Gariep Belt, there is little evidence of granitic activity (e.g. Frimmel, 2002), although granitic intrusions are located in the equivalent sedimentary successions in South America (e.g. Chemale et al., 1995) also suggesting subduction beneath the South American plate in the north.

In the Saldania Belt, westward vergence of folds and top-to-the-northwest thrusting in the Malmesbury Group may indicate that subduction was beneath the South African plate. This is supported by the presence of the voluminous Cape Granite Suite (CGS), which are interpreted to be related to subduction beneath the South African plate (e.g. Rozendaal and Scheepers, 1994; Scheepers, 1995; Rozendaal et al., 1999). The presence of the CGS in the Saldania Belt was suggested (e.g. Frimmel, 2000) to be related to displacement along the Colenso Fault, and that the original position of the granites was next to the southern Gariep Belt and thus related to subduction beneath the South American plate. The granites were then transported to the south by this left-lateral displacement along the Colenso Fault (e.g. Frimmel, 2000). However, recently Kisters et al. (2002) concluded that left-lateral (sinistral) movement along the Colenso Fault only occurred until ca. 540 Ma, when a reversal to dextral strike-slip commenced. As the majority of the granites were intruded between 540 and 510 Ma after sinistral movement had ceased, faulting from the north to their present position could not have transported the granites.

To resolve the conflict in contrasting directions of subduction between the Gariep Belt to the north (westward directed subduction) and the Saldania Belt to the south (eastward directed subduction), a major transform fault connecting the two subduction systems would be required. For example, in New Zealand, east directed subduction beneath South Island and west directed subduction beneath North Island is connected by the approximately 400 km long strike-slip Alpine Fault (Sutherland et al., 2000; Barnes et al., 2001). It is commonly accepted that the Gariep Belt represents a foreland-fold-and-thrust belt (e.g. Frimmel, 2000). In such a tectonic scenario, the actual subduction margin is commonly located approximately 200-300 km away (e.g. Twiss and Moores, 1992). Therefore, the major strike-slip fault located between the two oppositely directed subduction zones of the Gariep and Saldania Belts, is most likely located on the South American continent. Large-scale transform faults have also been invoked in the tectonic evolution of the Gariep Belt and the Vanrhynsdorp Basin in southern Africa (e.g. Gresse, 1995; Frimmel, 2000) and in the South American equivalent (e.g. Cunningham et al., 1998; Aceñolaza et al., 2002).

10.1.4 Metasomatic alteration

The muscovite-chlorite content of the lithologies in the schistose rocks is proportional to the presence of quartz veining in rocks of the lower unit (Chapter 8.3 & 8.4). The occurrence of quartz veins and their associated alteration envelopes parallel to, and confined within the S_0/S_1 fabric, indicates that fluid movement was early- to syn-D_1. The formation of rock units with varying compositions parallel to bedding, created bedding-parallel compositional contrasts in lithologies that were initially identical in composition. The bedding-parallel (S_0/S_1) and selective alteration of lithologies by fluid movement through the rocks has therefore created a pseudo-stratigraphy on an outcrop and on a regional scale. The muscovite and chlorite alteration is consistent with the regional lower greenschist facies metamorphic grade. The syn-deformation and syn-metamorphic nature of the fluids (Chapter 9.5) suggests that the fluids were generated from dewatering of water-rich sediments (e.g. Stephenson et al., 1994).

The banded chert identified at Spitskop is interpreted to represent an example of extreme fluid alteration. The chert is situated between two lithological packages,

namely the Berg River and Klipplaat Formations. It is bedding-parallel and contains a strong linear fabric seen as quartz rodding related to the D_1 deformation event. The chert contains extensive quartz veining and the lithologies surrounding the chert are rich in quartz veins and exhibit extensive silicification (Chapter 4.1.7). The pervasive quartz rodding parallel to the regional L_1 fabric indicates that the chert has undergone intense shearing, and represents a D_1 high-strain zone. The extensive silicification of the surrounding rocks and the silica-rich nature of the chert, suggests that the shear zone represented a major fluid conduit. The identification of the chert protolith is inhibited by the extensive alteration that has occurred, but the high Cr and Ni values suggest a relationship between the chert and the surrounding ultramafics that are also high in both Ni and Cr. This correlation was also observed by Slabber (1995), who suggested the chert represents silica leaching from an underlying ultramafic body. However, the chert is here interpreted to represent an ultramafic body that has been silicified. The silicification of ultramafic rocks has been recorded from Archaean greenstone belts, such as the Barberton Greenstone Belt (e.g. Duchač and Hanor, 1987). Here the alteration was caused by metasomatism of the ultramafic units by shear-zone controlled silica-rich fluids (Hanor and Duchač, 1990).

In the Spitskop area, the following scenario is envisaged. Initial shearing was concentrated along lithological contacts between the metasedimentary and metavolcanic rocks, i.e. the quartz-chlorite-muscovite schist and the talc-carbonate and chlorite-feldspar-quartz schists of the Berg River Formation. The less competent quartz-chlorite-muscovite schist behaved in a ductile manner, whereas the more competent ultramafic rocks behaved in a brittle manner and fracture networks were developed within these rocks during deformation. These brittle fracture networks within the ultramafic rocks formed the fluid conduits during the layer-parallel, D_1 deformation event and therefore extensive vein-stockworks were developed. Fluids passing through the ultramafic rocks caused extensive metasomatic alteration and silicification of the ultramafic rocks and the immediately surrounding schists. Quartz veins within the silicified ultramafic rocks were transposed during D_1 and the strong rodding was developed. The alteration of an ultramafic rock to a silica-rich rock would require the majority of elements to be mobile and therefore requires a large volume of fluid (e.g. O'Hara and Blackburn, 1989). The extent of quartz veining within and

surrounding the chert and the siliceous nature of the chert itself, attests to the volume of fluid passing through the shear zone. Such a scenario explains why the silicified ultramafic rocks have a similar major element geochemistry to typical cherts but still contains high Ni and Cr values. Limited stable isotope analysis revealed values of $\delta^{18}O_{quartz}$ of 15.45 and 15.90 ‰ for the chert (Slabber, 1995). These are considerably lower than the average values expected for cherts, which are on average above 20 ‰ (Hoefs, 1987), further indicating that this lithology does not represent a chert of sedimentary origin.

10.1.5 Conclusion

The pervasive nature of the bedding transposition and associated bedding-parallel thrusting indicates that the schistose rocks are a tectonostratigraphic package. The presence of a tectonostratigraphy was first recognised by Hartnady et al. (1974). Individual units are tectonically juxtaposed, on both an outcrop and on a regional scale into their present stratigraphic positions making lithostratigraphic interpretations complicated. The extent of S_0/S_1-parallel fluid alteration caused the pervasive layer-parallel alteration of schist compositions, and further added to the complexity of the tectonostratigraphic package. The effect of both the early deformation event (D_1) and the fluid alteration on the schistose rocks has most likely created a pseudo-stratigraphy.

10.2 Non-schistose (upper unit)

The upper unit comprises, from base to top, conglomerates, grits and shales that are only locally developed in the north around Piketberg (Piketberg Formation). The shales of the Piketberg Formation are compositionally and visually the same as the shales in the surrounding area classified as the Porterville Formation, and the former passes into the latter. The compositions and morphologies of the clasts of the Piketberg Formation at the base of the upper unit, suggests erosion of local iron-rich lithologies containing abundant quartz veins. The conglomeratic and coarse-clastic nature of the basal beds is indicative of braided stream/alluvial fan deposition of locally eroded sediments in a high-energy environment (e.g. Tucker, 1986). Poor exposure inhibits the identification and exact location of the contact between the

upper and lower units in the field. The contact has, however, been located to within a approximate 200 m wide zone, and coincides in the north with the occurrence of the conglomerates and grits of the Piketberg Formation, and further south with quartz grits near Spitskop (Chapter 4.3.2, Appendix D, Map 4). It is here suggested that the contact between the upper and lower units is an unconformity; as the conglomerates of the Piketberg Formation occur directly above the contact and the clasts of the Piketberg Formation are composed of vein quartz and an originally iron-rich lithology (Chapter 4.3.2). The underlying lower unit is composed of chlorite and muscovite-rich schists that contain pervasive quartz veining, which could represent the source of the Piketberg Formation. In this scenario, the Piketberg Formation was derived from the erosion of the local underlying rocks.

No conglomerates or grits were located around the margin of the Swartland dome at the contact between the schistose and non-schistose rocks. The lack of the identification of these lithologies can be interpreted in two ways. First, the outcrop is simply too poor to identify conglomerates and grits, although they are present, or secondly, the upper unit in this area lies conformably on the lower unit, and for this reason, localised erosion and the deposition of coarse-grained units would not have occurred.

The idea that the lower and upper units are separated at least locally by a sedimentary contact or unconformity is supported by early observations by Von Veh (1983). Von Veh (1983) suggested that the sedimentary units of the Tygerberg Hills (eastern side of the Tygerberg Formation; Fig. 2.4) represent the feeder channels for the turbidite fans located to the west of the Tygerberg Terrane (Bloubergstrand area; Fig. 2.4). In such a scenario, he suggested that the sediments were sourced from further to the east, represented by the Swartland Terrane, with an unexposed depositional contact existing between the two. Applying Von Veh's (1983) observations in terms of the lower and upper units suggested in this study, the source for the Tygerberg Formation, which is part of the upper unit, would therefore be the rocks of the lower unit to the east. This concurs with the lower and upper unit subdivision, as rocks from the lower unit are located to the east in the Swartland and Spitskop domes that form the central area of the Swartland Terrane.

The conglomerates of the Piketberg Formation grade into grits and shales both laterally and vertically. The shales are widespread and occur throughout the present Swartland and Boland Terranes. Grain-size variations and slight compositional differences exist within the deposits across the field area, but these variations between the Boland and Swartland Terranes are no greater than differences in sediments from within each individual formation as described in Chapter 4. It is therefore suggested that the shales and greywackes of the Moorreesburg Formation (Swartland Terrane) and the Porterville Formation (Boland Terrane) are lithologically very similar and cannot be distinguished using lithological or structural criteria.

Limited samples from selected outcrops of the Tygerberg Formation were also studied as part of the project to allow comparison with the deposits from the field area (Chapter 4). It is clear that although compositionally the shales/greywackes are, in general, similar to the sedimentary rocks described above, the predominance of other lithologies such as sandstones, the greater bed thickness and the better preservation of rocks generally indicates that the Tygerberg Formation cannot be easily correlated with the other two formations. Sedimentary rocks of the Tygerberg Terrane were studied extensively by Von Veh (1983) and have been interpreted to be of turbiditic origin, deposited in a deepwater environment, possibly on a continental slope. This indicates a change in depositional environment from the west to the east, moving from deep water (continental slope) into shallower water (continental shelf/continental margin). This interpretation remains valid when considering the Malmesbury Group in terms of a lower and upper unit. For example, the upper unit is composed, from west to east, of the Tygerberg (deep-water turbidites), Moorreesburg (greywackes and pelites) and Porterville Formations (shales and minor limestones).

10.3 Deposition, deformation and metamorphism of the Malmesbury Group

The age of the Malmesbury Group has only been determined indirectly, through ages bracketed by the underlying basement and the intrusion of the Cape Granite Suite (CGS) and by comparison with the Gariep Belt to the north. Rozendaal et al. (1999) suggested deposition onto Meso- to Palaeoproterozoic basement, initiated by the break-up of Rodinia between ca. 780-750 Ma (Frimmel et al., 1996a). The oldest

phase of the CGS at ca. 552 Ma (Da Silva et al., 1997; 2000) provides a minimum age.

10.3.1 Deposition

Sedimentation in the Gariep Belt is suggested to have occurred between ca. 770 and 550 Ma (Frimmel et al., 2001), with rifting commencing ca. 741 Ma (Frimmel et al. 1996b). Following Porada's (1989) model, sedimentation in the Saldania Belt to the south commenced at approximately the same time. By inference, deposition of the Malmesbury Group commenced sometime between ca. 800 and ca. 750 Ma. However, similar deposits to that described in the Gariep Belt, e.g. feldspathic arkoses, diamictites and thick limestone successions of the Stinkfontein and Hilda Subgroups (Frimmel, 2000) are not present. Equivalent units to the lower part of the Port Nolloth Group could be located beneath what is considered to be the Malmesbury Group.

In the lower unit, the type of deformation identified (e.g. bedding transposition, low-angle thrusting), the tectonostratigraphic sequence of the metasedimentary and metavolcanic rocks, and the pervasive syn-D_1 fluid flow, suggests deposition and incorporation into an accretionary prism. Accretionary prisms form in convergent environments and therefore the switch from extensional to compressional tectonics along the present west coast of South Africa at ca. 600-570 Ma (Grunow et al., 1996) would have provided a suitable environment.

Armstrong et al. (1998) identified detrital zircons in the Tygerberg Formation of the Malmesbury Group rocks ranging in age from 2960 to 560 Ma, with the majority of zircons ranging in age between 900-1050 and 575-700 Ma, suggesting their source from the Namaqua-Natal Mobile Belt and Pan-African rocks respectively. Notably, the youngest zircons dated at 560 Ma indicate that deposition of the upper unit must have lasted until shortly after 560 Ma.

10.3.2 Deformation

Attempts at dating the deformation within the Malmesbury Group directly have been ambiguous. Gresse et al. (1992) dated an early sub-horizontal tectonic fabric within schists of the Swartland Terrane at ca. 484-505 Ma (Ar^{40}/Ar^{39} whole rock). This early S_0/S_1 fabric was later refolded by D_2 and D_3 events. D_1 and D_2 fabric generations are truncated by the oldest plutons of the CGS, the oldest of which are dated at ca. 552 Ma (552 ±4 Ma; Scheepers and Armstrong, 2002). This makes the fabric older than ca. 552 Ma. Since the S_0/S_1 fabric clearly represents the oldest fabric in the Saldania Belt, the younger age of ca. 500 Ma most likely represents a resetting age, as suggested by Kisters et al. (2002). Muscovite has a closure temperature of 300-430 °C (e.g. McDougall and Harrison, 1988), and therefore resetting is most likely related to a higher geothermal gradient during this time, related to crustal thinning, mantle upwelling and plutonism (Kisters et al., 2002). This ca. 500 Ma K/Ar and Ar/Ar age is widespread, not only across Africa, from which the term Pan-African originated (Kennedy, 1964), but also across large areas of Gondwana (e.g. Jackson and Ramsay, 1980; Veevers, 2003).

However, it is possible to date D_1 and D_2 indirectly due to the inferred ages of sedimentation of the two units, the intrusion of the CGS and comparison to the Gariep Belt directly to the north. Sedimentation and deformation are synchronous in an accretionary wedge, so D_1 would have commenced shortly after the initiation of collisional tectonics and sedimentation at ca. 600-575 Ma as stated above. The absence of D_1 in the upper unit rocks also provides a lower limit for the onset of sedimentation of the upper unit and a lower limit for the timing of D_2.

Although F_2 folding is coaxial with folding related to the later Cape Orogeny, e.g. Gresse et al. (1992), it can be identified as being 'Pan-African' and not related to the Cape Orogeny, as firstly, F_2 folds are truncated by the majority of the CGS, and secondly the Table Mountain Sandstone (TMS) Group lies on both the lower and upper unit rocks, the former being exposed in the cores of regional F_2 folds. Thirdly, the folding intensity of the Cape Orogeny decreases northwards from Worcester (e.g. Gresse et al., 1992), yet the F_2 folding intensity in the Malmesbury Group rocks stays consistent. The Darling batholith, which is syn-kinematic is dated at 547 ±6 Ma (Da

Silva et al., 2000). Thus D_2 was synchronous with the intrusion of the Darling batholith at ca. 545 Ma. The timing of the F_3 folding cannot be constrained.

In the Gariep Belt, $^{40}Ar/^{39}Ar$ dating of hornblende generations in the Chameis Complex at ca. 575 ±2 Ma and 545 ±2 Ma (Frimmel and Frank, 1998) are interpreted to indicate the formation of an accretionary wedge during the onset of crustal convergence related to subduction tectonics, and peak regional metamorphism and collision at ca. 545 Ma respectively (Frimmel and Frank, 1998). This is in agreement with the ages suggested for the western branch of the Saldania Belt. The different deformation events and their comparison with previous workers is summarised in Table 10.1.

Table 10.1. Summary of the three deformational events identified in this study correlated with other workers both regionally and locally. Note that the different events are essentially the same in all the studies, but the spatial distribution and relationship of these events differ.

Deformation event	Hartnady (1969)	(Hartnady et al., 1974)		Rozendaal et al. (1994)	This study
(according to this study)	Worcester	Tygerberg & Boland Terrane	Swartland Terrane	Piketberg Formation	Summary of structure
D_1				S_0 bedding.	S_0 bedding.
	Phase O (N-S folds).		Se fabric. S_e/S_m transposition fabric (NW-SE). S_m fabric.		S_0/S_1 transposition fabric (NW-SE), F_1 intrafolial folds, S_1 planar fabric.
D_2	Phase M (NW-SE folds).	F_1 folding (NNW-SSE). S_1 axial planar cleavage.	F_2 folding (NNW-SSE).	F_1 folding (NW-SE). S_1 axial planar cleavage.	F_2 folding (NW-SE). S_2 axial planar cleavage.
D_3	Phase X (NE-SW, NNW-SSE folds).	F_2 folding (NE-SW).	F_3 folding (NE-SW).	F_2 folding (NE-SW).	F_3 folding (NE-SW). Possible Cape Orogeny (?).
	Phase K, open crenulation. (Cape Orogeny).			S_3 axial planar cleavage. (Cape Orogeny).	

The change from collisional to extensional tectonics and subsequent uplift, is seen in the change of depositional style, to the deposition of rift-related sediments of the Franschhoek Formation in the Malmesbury Group, the reversal of strike-slip tectonics in the Saldania Belt (Kisters et al., 2002), and the molasse-type sediments in the Nama Group in the north (Gresse and Germs, 1993). The change from transpressional to transtensional tectonics can be temporally constrained by the identification of the 539 ±1 Ma synkinematic aplites that intrude dextral strike-slip mylonites in the Trekoskraal granite (Kisters et al., 2002).

10.3.3 Metamorphism

It is not possible to temporally constrain the metamorphic events using geochronology as explained in Chapter 10.3.2, but it is possible to constrain the M_1 and M_2 metamorphic events in terms of the three deformation events. The deformation event D_1 only affected the lower unit rocks and the metamorphic minerals define the early fabric (S_0/S_1), thus indicating that M_1 was synchronous with D_1. Chlorite and muscovite define the S_2 fabric of the upper unit, indicating that M_2 and D_2 were synchronous (Chapter 7.5).

M_1 affected only the rocks of the lower unit and occurred at temperatures of lower greenschist facies (approx. 260-300 °C) across the field area. The identification of the biotite-feldspar schist tectonic slither (approx. 400 °C), now located within rocks of lower greenschist facies, indicates considerable vertical transport of this unit into its present position. Assuming a geothermal gradient of between 35 and 45 °C in such an environment (e.g. Best, 1982 and Chapter 9.4) and a temperature difference of approximately 100 °C, a vertical throw of 2-3 km is indicated.

The temperature calculated from the metasedimentary xenoliths using the biotite-garnet thermometer is approximately 600-650°C, indicating an approximate thickness of the Malmesbury Group rocks between 14 and 19 km (Chapter 7.4). Such a thickness for the Malmesbury Group is difficult to comprehend when comparing to the Gariep Belt to the north, where thin-skinned tectonics were in evidence and where the Port Nolloth Group is estimated to be approximately 2 km thick (Frimmel, 2002).

The metasedimentary xenoliths were brought up to their present position by the intrusion of the Cape Granite Suite and represent rocks of the lower parts of the lower unit. Thus the estimated thickness above is the combined thickness of the lower unit (sedimentation and tectonic thickening due to transposition) and the upper unit (sedimentation) and possibly thickening of both units during the deformation event, D_2. The thickness of the upper unit has been estimated at between 8-12 km based on the intrusion depth of the Cape Point granite (Armstrong et al., 1998) and the regional metamorphism of the lower unit (Chapter 7.7.3). Assuming an average

thickness of 10 km for the upper unit, then the tectonically duplicated lower unit (due to thrusting and transposition related to D_1) must have been between 4 and 9 km thick. Depending on how much tectonic thickening occurred (less than 2 to 5 times original thickness) this could possible point to a different depositional environment to the Gariep Belt (thickness approx. 2 km, Frimmel, 2002).

10.3.4 Constraints on the tectonic setting for deposition and deformation

Two lithological associations can be established in the Malmesbury Group. The first are the Late Neoproterozoic sedimentary and minor volcanic rocks of oceanic affinity (lower unit). The second is the Late Neoproterozoic marine succession (upper unit). In the lower unit, development of an intense foliation (S_0/S_1) where early quartz veins (Type 1a) and sedimentary layers have been completely transposed related to D_1, marks a distinct contrast in the later deformation (D_2). Here deformation was characterised by open to tight, upright folding and associated low-grade metamorphism (M_2). Accretionary prism environments are typified by marine successions containing tectonic slithers of oceanic crust. The deformational style of accretionary prisms is indeed often characterised by early low-angle thrusting and bedding transposition that are refolded by later upright chevron-type folds, documenting the progressive shortening of the wedge (e.g. Miller and Gray, 1996; Şengör and Okuroğullari, 1991).

In general, the Malmesbury Group has many similarities to well recognised and studied accretionary wedges/fore-arc environments around the world, e.g. Shimanto Accretionary Complex, Japan (e.g. MacKenzie et al., 1987; Kimura and Mukai, 1991), the Kodiak Accretionary Complex, Alaska (e.g. Fisher and Byrne, 1987; Sample and Moore, 1987), and the Lachlan Orogen, Australia (e.g. Foster et al., 1998; Gray and Foster, 1997).

10.4 Colenso and Piketberg-Wellington Fault Zones

The Colenso and Piketberg-Wellington Fault Zones are suggested to represent the boundaries of three tectonostratigraphic terranes (Theron et al., 1992; Rozendaal and Scheepers, 1994, 1995; Rozendaal et al., 1999). The Colenso Fault Zone

represents the boundary between the Tygerberg and Swartland Terranes and the Piketberg-Wellington Fault Zone represents the boundary between the Swartland and Boland Terranes. The Piketberg Wellington Fault Zone has also been proposed to possibly represent a geosuture between the then Kalahari Craton margin and the accreted units (e.g. Rozendaal et al., 1999; Chapter 2.3).

10.4.1 Colenso Fault Zone

Following the definition of terranes (Chapter 3), the Tygerberg and Swartland Terranes should exhibit distinct lithological, structural, and metamorphic characteristics, as well as differing provenances and ages. Outcrops along the fault zone within the metasedimentary rocks are poor, and it is not possible to establish whether a marked contrast occurs in the lithologies directly on either side of the fault. However, on a regional scale (10-20 km), only minor compositional differences occur between the lithologies on either side of the fault represented by the present Moorreesburg Formation (Swartland Terrane) and eastern parts of the Tygerberg Formation (Tygerberg Terrane) (Chapter 4 and 10.2). Structurally, the rocks directly on either side of the fault (approx. 15 km) have both been affected by D_2 and D_3 (Chapter 5) and are structurally identical. Furthermore, there is no difference in the metamorphic grade on either side of the Colenso Fault Zone (Chapter 7).

The Colenso Fault Zone can only be positively identified in the field within the Cape Granite Suite (CGS) and its trace in the metasedimentary rocks of the Malmesbury Group has only been inferred. Therefore, the kinematic development of the Colenso Fault Zone can only be estimated between ca. 545 Ma (the age of the oldest plutons, e.g. the Darling batholith intruded along the Colenso Fault Zone) and 510 Ma (the youngest intrusion of the CGS, Kisters et al., 2002). It is therefore not possible to establish whether the Colenso Fault Zone was active before ca. 545 Ma, and whether the fault represents a terrane boundary that accommodated accretion tectonics during the main collisional phase.

10.4.2 Piketberg-Wellington Fault Zone

Unlike the Colenso Fault Zone, there is very little physical field evidence for the Piketberg-Wellington Fault Zone within the Malmesbury Group and its identification as well as its location were inferred by Rabie (1974a; 1974b) based on:

i) Distinct lithological variations in the area;
ii) On the change in structural style identified on his (Rabie, 1948) form line map.

Additional evidence includes:

iii) The occurrence of springs and extensive quartz veining (Hartnady et al., 1974);
iv) Localities where the TMS Group inliers (Piketberg and Riebeeck Kasteel inliers) have been down-faulted during the Mesozoic (e.g. Theron et al., 1992);
v) The location of the Bridgetown Formation, being accreted into its present position during terrane accretion (e.g. Rozendaal et al., 1999).

However, due to the circumstantial evidence for the fault, the exact location has been in dispute (Hartnady et al., 1974; Rabie, 1974b; Visser et al., 1981; Slabber, 1995; Rozendaal et al., 1999) and even its existence (De Villiers, 1979).

Lithological variations

There appears to be no lithological, (Chapter 4; 10.2) or metamorphic (Chapter 7) contrasts on either side of the Piketberg-Wellington Fault Zone in its present location, or the location proposed by Rabie (1974a), nor do the rocks on either side of the Piketberg-Wellington Fault Zone, belonging to the Moorreesburg and Porterville Formations, have different provenances (Chapter 10.2).

Structural variations

There is no structural difference directly on either side of the Piketberg-Wellington Fault Zone (Chapter 5). Figure 10.1 represents a simplified map produced by Rabie (1974b), showing that the foliation pattern across the Swartland and Boland Terranes is significantly different. In the Boland Terrane, the foliation is near-vertical and trends northwest-southeast (D_2 of this study). This foliation corresponds to the axial planar cleavage (S_2) to near upright isoclinal folding (F_2) of the bedding observed during

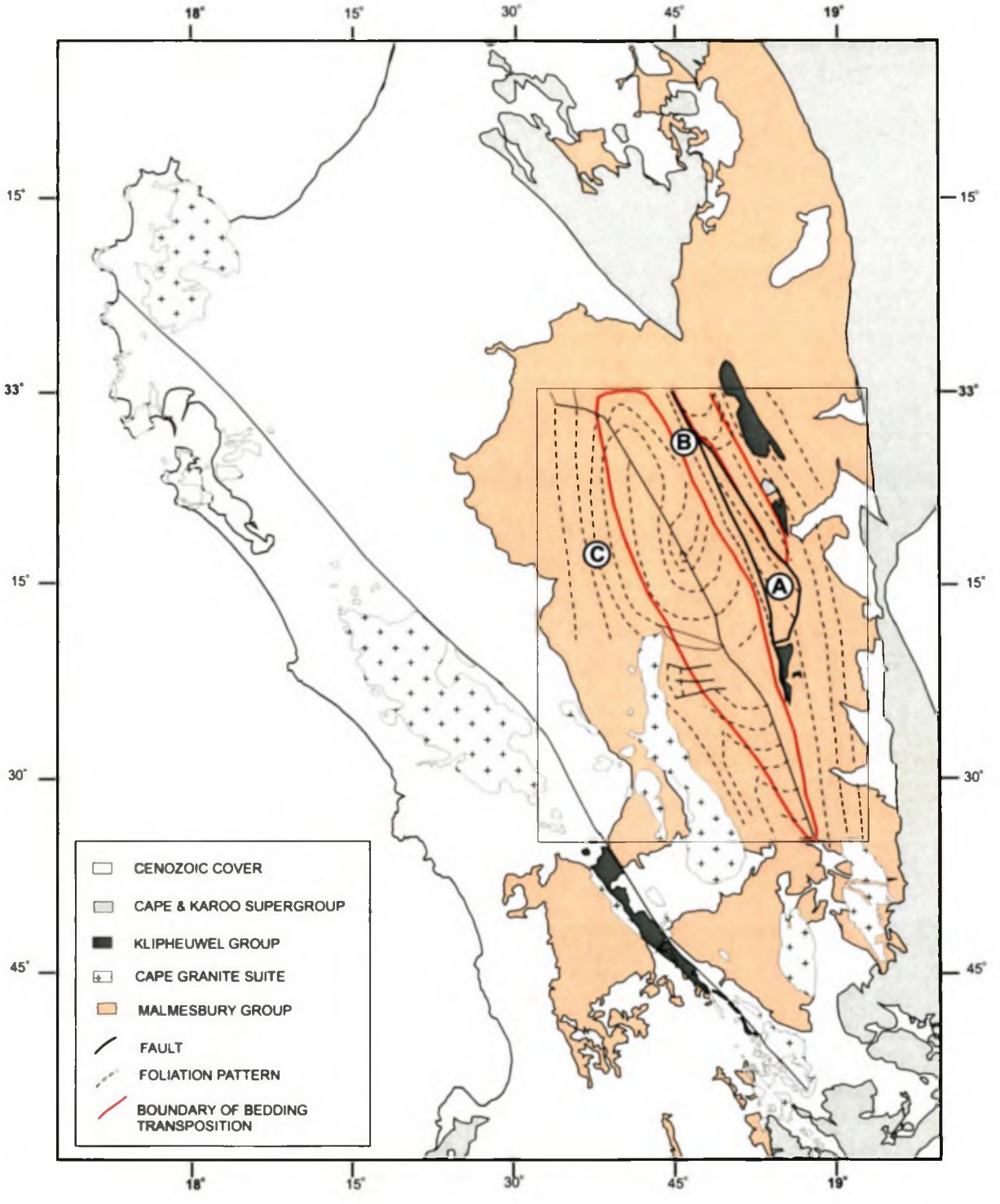

Figure 10.1. Simplified map of the regional structural fabrics of Rabie (1974b). The extent of the units containing the transposition fabric of this study, correlates to the curvilinear foliation pattern of Rabie (1974b).

recent mapping. In the Swartland Terrane, the dip and strike of the foliation largely varies, forming ovoid-shaped form line patterns related to the regional double-plunging-domal features. This foliation mapped by Rabie (1974b) is the S_0/S_1 fabric defined in this study, with the curvature of these domains being related to the later F_2 folding as described above. To define the boundary between these distinct zones, Rabie (1974b) identified several faults, which formed the basis for the later Piketberg-Wellington Fault Zone. However, as Figure 10.1 shows, the boundaries between the different fabrics identified by Rabie (1974b) correlate with the boundary between the upper and lower units identified in this study, and can thus be explained in terms of regional whale-back folding, without the use of major faulting. In fact, parts of Rabie's (1974b) Swartland Terrane have a similar structural style to the Boland Terrane (marked a, b and c on Figure 10.1). The use of this varying structural style for defining the terrane boundaries is thus obsolete.

Occurrence of springs and quartz veining

Whether the springs and quartz veining located across the Swartland represent specifically the location of the Piketberg-Wellington Fault Zone, is difficult to judge. Furthermore, whether the springs and quartz veining represent one major fault zone, i.e. the Piketberg-Wellington Fault Zone, or represent several smaller unrelated faults of different ages, i.e. they are not all Pan-African aged, is impossible to confirm and this point is therefore not constructive.

Faulting within the Table Mountain Sandstone (TMS) inliers

The displacement of the TMS Group only indicates that these faults were active during the Mesozoic (e.g. Theron et al., 1992). There is no evidence to indicate if these faults are Pan-African-aged, and were later reactivated during the Mesozoic, as suggested by Rozendaal et al. (1999). Hartnady et al. (1974) suggested that there are very few places along the fault that do not show evidence of post-Cape movement. For this reason it is not possible to use this point as evidence for a Pan-African aged fault zone.

The Bridgetown Formation

The Bridgetown Formation forms part of the tectonostratigraphic package of the lower unit (Chapter 10.1), whose present surface outcrop expression is related to regional, northwest-southeast orientated F_2 folding (Chapter 5.2). The subsequent erosion of the Malmesbury Group revealed the underlying units (Chapter 10.1; 10.3) occurring within the antiform cores (Chapter 5.5). Metavolcanic rocks related to the Bridgetown Formation, are identified along regional strike of the main body of metavolcanic rocks at Spitskop and at Riviera (e.g. Rozendaal et al., 1994). The latter lies to the north of Spitskop and approximately 25 km to the east of the Aurora-De Hoek Fault, the supposed continuation of the main fault. Rabie (1974a) also identified metavolcanic bodies, dyke-like in morphology, concordant with the regional foliation, ranging in size, up to approximately 7 km long around Moorreesburg, approximately 20-25 km to the west of the main fault. He correlated these metavolcanic rocks with the Bridgetown Formation in the area. The occurrence of these metavolcanic rocks in their present geographic positions can be explained in terms of the exposure of the lower unit in the core of one of the regional antiforms (Swartland dome). This is the same explanation as for the main occurrence of the metavolcanic rocks (Bridgetown Formation proper) in the core of the Spitskop dome. Furthermore, the present position of a geosuture does not explain the occurrence of the distal metavolcanic rocks located within the Swartland dome (approximately 15 km west of the fault) or in the Riviera area (20-25 km east of the fault). As the presence of the metavolcanics can be explained in terms of regional northwest-southeast trending domal structures, the use of their locations to identify the location or occurrence of the Piketberg-Wellington Fault Zone is, thus, circumstantial and speculative at best.

10.4.3 Summary

The regional geology of the Malmesbury Group is explained in the terms of a lower unit being overlain by an upper unit. The outcrops of the two units are related to regional folding during D_2 (Chapters 10.1 & 10.2) and subsequent erosion of the upper unit to reveal the lower unit in northwest-southeast orientated structural 'windows'. This explanation does not require three separate, allochthonous and/or

para-autochtonous terranes separated by terrane boundary faults (Chapters 10.1 & 10.2). For the faults to be terrane boundaries (e.g. Rozendaal et al., 1999) they would need to be of Pan-African age characterised by lithological, structural and/or metamorphic differences on either side of the Colenso and Piketberg-Wellington Fault Zones. This is not the case.

10.5 Mesothermal gold mineralisation

At the Spitskop gold prospect, it is suggested that mineralisation is related to Type 1 veins. These veins are parallel to the main fabric in the rocks, S_0/S_1, and were folded during the early deformation event D_1. This suggests that these veins were pre- to syn-tectonic with respect to D_1. From the crosscutting relationship of the Cape Granite Suite (CGS) and the early D_1 fabric, this fabric pre-dates the intrusion of the CGS, and, therefore, the fluid generation and movement also predates the intrusion of the CGS. Therefore it is highly unlikely that the CGS was the source for the fluids responsible for this early veining event.

The fluid that generated the Type 1 veins was a low salinity (4.6 wt.% NaCl eq.) H_2O-rich fluid with variable CO_2- and CH_4-content, with a temperature of approximately 300 °C, consistent with lower greenschist facies metamorphism (M_1). This is consistent with the composition of other fluids in greenschist facies terranes that are derived from metamorphic devolatilisation (e.g. Taylor, 1986; Foster, 1993; Cox et al., 1991; Cox et al., 1995). Alteration envelopes associated with the fluids responsible for Type 1 veins are composed of chlorite, muscovite, feldspar and minor calcite, which is consistent with the regional metamorphic grade (Chapter 8.3). The fact that fluid production and movement was synchronous with D_1 and M_1 is further evidence for a fluid derived from metamorphic devolatilisation (e.g. Ferry, 1994; Rumble, 1994; Oliver, 1986; Stuwe, 1998) of the hydrous sedimentary pile of the lower unit (Swartland group of Chapter 11).

As this fluid passed through the metapelitic and metavolcanic rocks of the Swartland Group it scavenged gold and other ore-forming elements. The chert at Spitskop is interpreted as representing a high strain zone with a high fluid throughput, as seen by

the alteration of the ultramafic lenses and the silicification of the underlying schists. This chert is thus suggested to represent the major fluid conduit in the Spitskop area. This is evident from the extent of Type 1 quartz veins in the vicinity of the chert in the area and the elevated, above background gold values. In similar low-grade metamorphic metasedimentary terranes, where gold mineralisation is at economical concentrations, e.g. Juneau (Alaska), Victoria (Australia), Nova Scotia, (Canada) and Otago (New Zealand), (e.g. Haynes, 1986; Kerrich and Wyman, 1990; Ramsay and VandenBerg, 1990; Teagle et al., 1990; Goldfarb et al., 2001), the occurrence of high-angle reverse, or reverse-oblique shear zones were identified as the host for the economic concentrations of gold (e.g. Sibson and Scott, 1998). Sibson et al. (1988) suggested that these shear zones acted as valves, promoting cyclic fluctuations in fluid pressure. As these faults are unfavourably orientated in the prevailing stress field, reactivation of these faults could only occur if fluid pressure exceeded lithostatic pressure, thus making these sites the loci for extensive fluid throughput (Sibson et al., 1988; Wilkinson and Johnston, 1996). Such high-angle reverse faults were not identified in the Spitskop area. The lack of these faults could be the main reason for the lack of fluid focussing and gold precipitation, and therefore economic concentrations of gold.

10.5.1 Implications for exploration

Spitskop is only at the "prospect" stage and percussion drilling, although intersecting elevated gold values, did not produce any incentives for the commencement of further exploration at this locality. Spitskop however, represents the first identification of mesothermal gold mineralisation in the Western Cape, a region where all other known occurrences of gold mineralisation, either major or accessory, have been interpreted to be related to the intrusion of the CGS (e.g. Theron et al., 1992; Rozendaal and Scheepers, 1995). Exploration for more prospects should therefore follow the established exploration programmes for mesothermal (orogenic) lode-gold mineralisation, specifically those hosted in metasediment-dominated successions, e.g. the turbidite-hosted lode-gold deposits mentioned above. However, the conclusion that the mineralisation took place early in the deformation history of the lower unit (Swartland group. Chapter 11) has some important implications for the

location of further gold prospects and local controls of gold mineralisation in the Western Cape.

As gold mineralisation is restricted to Type 1 veins that are syn-D_1 and M_1, mineralisation of a similar style, i.e. mesothermal lode-gold, will be restricted to the rocks of the lower unit (Swartland group). Exploration is therefore immediately restricted to the Spitskop and Swartland domes, the two northwest-southeast regional antiforms, that represent the surface exposure of the lower unit (Swartland group) (Appendix D, Map 4).

Secondly, as established earlier, gold mineralisation at Spitskop is related to low-angle thrusts and along Type 1 veins that are sub-parallel to the main foliation and thus these structures are suitably orientated for slip at low differential stress. High-angle reverse faults, as described by Sibson and Scott (1998) and Sibson et al., (1988), are the key to economical gold concentrations for this style of mineralisation.

Fluid flow through the lower units is concluded to have been pervasive, reflected by the existence of voluminous veining within the chlorite-muscovite schist package. Therefore exploration should focus on the identification of structures/mechanisms on a local scale that have been suggested to cause fluid focussing, such as in the turbidite-hosted mesothermal gold deposits of Australia, e.g. high-angle, reverse faults (Cox et al., 1995).

11 RECLASSIFICATION OF THE MALMESBURY GROUP

The current subdivision of the Malmesbury Group is based on lithostratigraphic criteria and follows Hartnady et al. (1974), who subdivided the Malmesbury Group into three subunits following the South African Code of Stratigraphy (SACS, 1971). Since then, the only change to the classification was the downgrading of the Porseleinberg Formation to a member within the Moorreesburg Formation (Theron et al., 1992). However, there are many discrepancies with this classification (Chapter 3), providing compelling evidence for its restructuring or modification.

Therefore, a new classification is presented below following primarily, structural criteria, i.e. the presence or absence of the D_1 transposition folding and to a lesser extent, general unifying lithological features. The classification is based on the 3rd edition of the South African Code of Stratigraphic Terminology and Nomenclature (SACS, 1980). As the classification proposed below is currently not approved by SACS, the terminology (e.g. group, formation, member) is informally used. Parts of the present classification of SACS (1980) that are retained without alteration are kept in the formal (e.g. Formation).

The lithologies of the present Malmesbury Group are divided into two distinct 'units'. The schistose or lower unit is called the Swartland group, after the area where the rocks are best developed, and the non-schistose or upper unit is called the Malmesbury group (Fig. 11.1). The latter allows the retention of the term 'Malmesbury Group', which is synonymous with the rocks in this geographical area.

11.1 Swartland group

The Swartland group comprises the former Berg River, Klipplaat, Bridgetown, and Porseleinberg Formations and the De Hoek Member of the Porterville Formation of SACS (1980). It is equivalent to the schistose/lower unit rocks described in this thesis

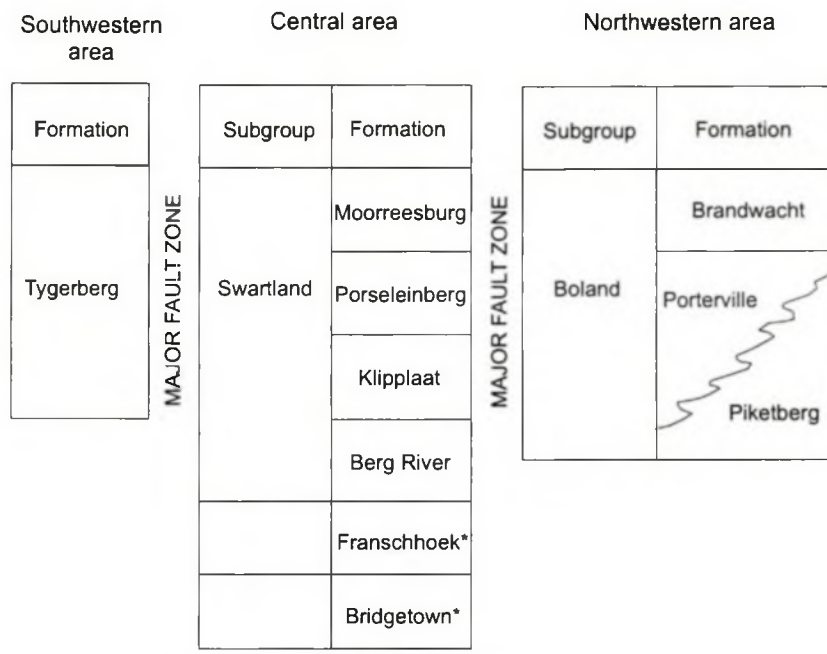

a) Distribution and relationship between the units of the Malmesbury Group, after SACS (1980). Formations denoted with an asterisk indicate unknown stratigraphic position.

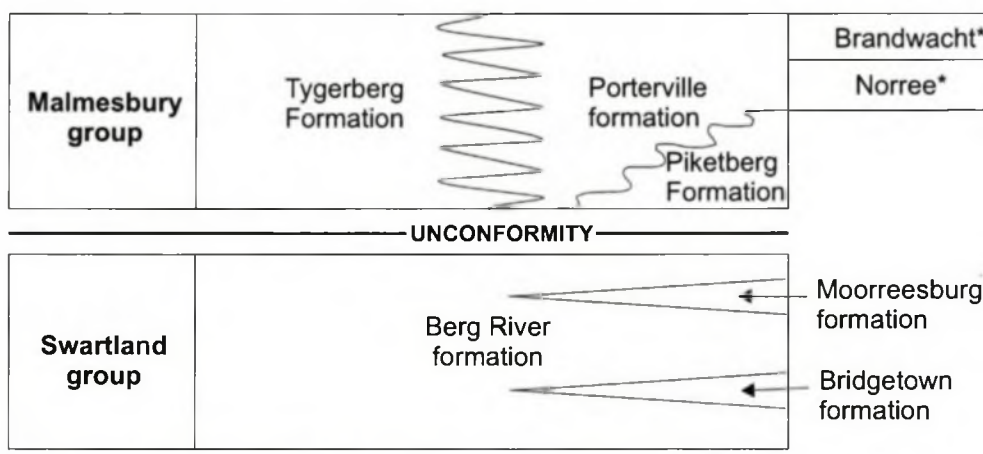

b) Distribution of the formations of the Swartland and Malmesbury groups following the new classification as outlined in this thesis. The Swartland group is composed of three tectonically bound formations and is unconformably overlain by the Malmesbury group. The Malmesbury group is composed of the Piketberg, Tygerberg and Porterville formations. Formations denoted with an asterisk indicates their stratigraphic position is unknown.

Figure 11.1. Distributions of the formations of the present Malmesbury Group according to SACS (1980) and the Swartland and Malmesbury froups according to this thesis.

from Chapter 4 onwards. The rocks have all undergone the early deformation event D_1, and this distinguishes these rocks from the overlying group described below. Due to the presence of D_1 the contacts between these formations and between different lithological units within these formations are tectonic; no clear sedimentological contacts are recorded in the field. The presence of isoclinal intrafolial folding (F_1) has created a pseudostratigraphy. As these rocks form a tectonostratigraphic package, the mapping on a 1:50 000 scale of lithological units previously considered to be marker horizons is no longer feasible. Furthermore, previously mapped lithological marker horizons, e.g. the quartz schist of the Klipplaat Formation, are not as widespread as previously indicated (e.g. Rabie, 1974). The Swartland group can be divided into three formations based on lithological differences (Table 11.1).

Due to the nature of the D_1 deformation and associated alteration, only minor differences in the metasedimentary lithologies can be identified, and the affect of fluid alteration on compositions means that further subdivision of the three formations as described below is presently deemed inappropriate.

11.1.1 Berg River formation

The Berg River formation contains the quartz-chlorite-muscovite-feldspar and quartz schists of the former Berg River and Moorreesburg Formations that contain the early transposition fabric. This is areally the most extensive formation of the Swartland group and contains all the metasedimentary rocks that do not classify within the Moorreesburg or Bridgetown formations below (Appendix B, section 5). Located within the Berg River formation are the transposed limestone units located at Spitskop, Riebeeck West and the De Hoek and Zoutkloof Quarries, near Piketberg.

The limestones located as the De Hoek and Zoutkloof Quarries were formally known as the De Hoek Member, though then grouped with the Porterville Formation (SACS, 1980). Although a thickness in excess of 50 m was observed in the limestone units, their thickness is not constant within and between outcrops and the thickness can be as little as a few centimetres. Therefore according to the criteria of SACS (1980) the limestone units are given the rank of member and the former name *De Hoek Member*

Table 11.1. Tectonostratigraphy of the Swartland group and the lithostratigraphy of the Malmesbury and Klipheuwel groups following the reclassification in this study. As the Swartland group represents a tectonostratigraphy the units are only in their recommended stratigraphic sequence. Additional information on type localities is provided in Appendix B, section 5.

	Unit	Rank	Lithology	Source of Name	Proposer	Type area
Klipheuwel group	Populierbos*	Formation	Red shale and mudstones.	Farm Populierbos, 13 km north-northwest of Klipheuwel.	Theron et al. (1992).	Klipheuwel Quarry and the farm Berg en Dal.
	Magnug*	Formation	Conglomerates and grits at base passing into sandstones.	Farm Magnug, northwest of Klipheuwel.	Theron et al. (1992).	Along the Mosselbank River around the farm Magnug, Klipheuwel Quarry, and the hills surrounding Klipheuwel.
	Franschhoek	Formation	Conglomerates and shales.	Valley and town to the east of Stellenbosch.	Rogers and Du Toit (1909); Hartnady (1969). Revised in this study.	Road cuts along the Franschhoek Pass directly north of the town.
Malmesbury group	Bloubergstrand*	Member	Fine red tuff, tuffaceous agglomerate and red-brown to green andesitic lava (part of the Tygerberg Formation).	Beach 12 km north of Cape Town.	SACS (1971).	Island and coastal outcrops at Bloubergstrand.
	Tygerberg*[1]	Formation	Pelitic and semipelitic, with massive fine-grained greywackes and impure quartzites.	Mountain immediately N of Bellville.	Hartnady et al. (1974).	Hilly terrain between Klipheuwel and Parow. Also exposed along the coast from Sea Point-Grainger Bay, Bloubergstrand-Melkbosstrand, and on Robben Island.
	Porterville[1]	formation	Greywackes and phyllitic shales.	Town, SW Cape Province.	Rabie (1974a); Hartnady et al. (1974). Revised in this study.	Around the town of Porterville along the Assegaaibos River, and south and southeast of Moorreesburg.
	Piketberg*	Formation	Conglomerates and grits at base, passing into arenites and shales.	Town, SW Cape Province.	Hartnady et al. (1974).	Versfeld Pass and farms Deeze Hoek and Klein Vogel Valley, 6 km due N of Piketberg.
Swartland group	Moorreesburg	formation	Dirty green-brown feldspathic schist, containing lenses and pods of khaki-green muscovite schist.	Town, SW Cape Province.	This study.	Road cuts along along N7, east of Moorreesburg.
	Klipplaat*[2]	member	Off-white quartz schist containing minor muscovite and chlorite (part of the Berg River Formation).	Farm Klipplaat.	Rabie (1974a); Hartnady et al. (1974).	Along the Berg River around the farm Klipplaat, approximately 10 km southeast of Piketberg.
	Bridgetown[2]	formation	Dark green metavolcanic rocks, dolomite and chert.	Farm Bridgetown (18 km east of Moorreesburg).	Rabie (1974a); Hartnady et al. (1974). Revised in this study.	Between Heuningberg and Viermuisdrift along Berg River.
	De Hoek[2]	member	Dark limestones containing graphitic schist (part of the Berg River Formation).	Quarry located to the south of Piketberg.	Rabie (1974a). Revised in this study.	The De Hoek and Zoutkloof Quarries located directly south of Piketberg. Riebeeck West Quarry.
	Berg River	formation	Quartz-chlorite-muscovite-feldspar schists, quartz and chlorite schists.	Principal river of southwest Cape Province.	Rabie (1974a); Hartnady et al. (1974). Revised in this study.	On the farms Spitskop and along the Berg River, Kruisfontein Quarry and Goudmyn se kop, directly north and east of Moorreesburg respectively.
	Kanonkop[2]	member	Biotite-feldspar-quartz schist (part of the Berg River Formation).	Farm Kanonkop (approx. 6 km northwest of Malmesbury).	This study.	Road cuts along the R45, approximately 6 km northwest of Malmesbury.

Footnote: Formations marked with an asterisk are unchanged from SACS (1980).
[1] represent the stratigraphic equivalents of one another.
[2] located within the Berg River Formation. Stratigraphic position inferred from field relationships (see text for further information).

is retained and is now used to describe all the transposed limestone units described during this study.

The quartz schist of the Klipplaat Formation of SACS (1980) is light yellow to cream, with a sugary texture, which makes it distinct from the quartz schists of the Berg River formation (Table 11.1). As stated above, this quartz schist is not as well developed as previously interpreted and for this reason, is reduced to the rank of member. The quartz schist is therefore called the *Klipplaat member* after the farm where it is best developed (Appendix B, section 5).

The biotite-feldspar schist located in the road cuttings near the farm Kanonkop (Chapter 4.1.6) forms a distinct lithological unit compared to the remaining metasedimentary rocks. Due to poor outcrop, the extent of this unit is unknown, and is therefore not presently given the status of formation. The biotite-feldspar schist has a similar structural fabric to the rest of the schist units of the Berg River formation, and possibly represents a higher grade equivalent (Chapter 10.1). For these reasons, the unit is currently called the *Kanonkop member* after the farm where it outcrops, and is included within the Berg River formation.

11.1.2 Moorreesburg formation

The Moorreesburg formation contains the feldspar and muscovite schists located predominantly around the Moorreesburg and Goudmyn se Kop area. These yellow to dirty brown, feldspar- and muscovite-rich schists are lithological distinct from the greenish chlorite-rich schists of the Berg River formation and form a mappable unit that can be traced for approximately 15 to 20 km. The Moorreesburg formation no longer includes the non-transposed greywackes and shales of the former Moorreesburg Formation of SACS (1980) that are now included within the Porterville formation of the Malmesbury group (Table 11.1).

11.1.3 Bridgetown formation

The Bridgetown formation is essentially the same as described by SACS (1980) and later by Slabber (1995). This formation consists of the metavolcanic rocks of the

former Bridgetown Formation (e.g. SACS, 1980; Theron et al., 1992) and the metavolcanic rocks containing the S_0/S_1 transposition fabric described from the Spitskop and Riviera areas (Appendix B, section 5). The metasedimentary rocks in contact with the metavolcanic rocks described by Slabber (1995) are identical to metasedimentary rocks of the Berg River formation and therefore are classified with this formation. The dolomite and different types of chert described by Slabber (1995) are retained within the Bridgetown formation (Table 11.1).

The metavolcanic rocks can be geochemically divided into separate units (Slabber, 1995), but they all have a geochemistry that is characteristic of WPB-MORB, indicating that the Bridgetown formation may represent oceanic crust (e.g. Hartnady et al., 1974; Hälbich and Hartnady, 1985; Slabber, 1995; Rozendaal et al., 1999). The identification of features indicative of an ophiolite succession, e.g. pillow lava and sheeted dykes, was not possible. These features were most probably destroyed due to the extent of bedding transposition and foliation development.

11. 2 Malmesbury group

The Malmesbury group is composed of the non-schistose upper unit described in the previous chapters. This includes the Tygerberg, Moorreesburg (non-schistose rocks only), Porterville (excluding the De Hoek Member) and Piketberg Formations of the classification according to SACS (1980). As these rocks have not undergone the D_1 deformation event (i.e. S_0/S_1 bedding transposition and thrusting), no major tectonic breaks or intricate refolding occur that characterise the rocks of the Swartland group. This indicates that their present stratigraphic relationship reflects their original stratigraphic position. Although poor outcrops inhibit the tracing of lithologies of the Malmesbury group across the field area, distinct lithological differences exist between these rocks as identified in the previous classification (Hartnady et al., 1974; SACS, 1980). This allows the rocks to be divided into three formations (SACS, 1980; 3.5, page 648).

Therefore, from base to top, the Malmesbury group is composed of the Piketberg Formation overlain by the Porterville formation. The latter formation represents the

proximal sediments, in terms of distance to the continental margin, to the distal Tygerberg Formation (Fig. 11.1).

11.2.1 Tygerberg Formation

It is proposed that the Tygerberg Formation be retained from the classification of SACS (1980). It forms a distinct lithological unit as mapped by numerous authors (e.g., Hartnady et al., 1974; Von Veh, 1983; Theron et al., 1992) (Appendix B, section 5). The *Bloubergstrand Member* is retained from the classification of SACS (1980) and consists of fine red tuffs and dark-red-brown to green amygdaloidal andesitic lavas outcropping on the beach near Bloubergstrand (Von Veh, 1983; Theron, 1984). In general, the units are highly weathered, and were deformed with the surrounding metasedimentary rocks. The Bloubergstrand Member forms an approximately 50 m thick succession, with sharp contacts with the surrounding metasedimentary rocks. The Tygerberg Formation is unchanged in the classification proposed here (Table 11.1).

11.2.2 Porterville formation

Compositional and/or lithological differences between the Moorreesburg and Porterville Formations of SACS (1980) as described in Chapter 4 and discussed in Chapter 10.2 are only minor. A distinct boundary between deposits placed in either of the two formations of SACS (1980) could not be established in the field, and for this reason it is suggested that the two formations be combined and be called the Porterville formation (Table 11.1). Although the town of Porterville is not geographically at the centre, the rocks surrounding the town represent the type area for the former Porterville Formation of SACS (1980) and it was deemed appropriate to retain the name.

11.2.3 Piketberg Formation

The Piketberg Formation forms a distinct mappable unit within the field area. The formation is composed of predominantly conglomerates and grits, and it is proposed that the formation is retained form the previous classification by SACS (1980) and is unchanged here (Appendix B, section 5).

11.3 Formations excluded from the new classification

Three formations of the classification of SACS (1980) are currently excluded from the new classification (either in the Swartland or Malmesbury groups) presented here, namely the Franschhoek, Brandwacht and Norree Formations.

11.3.1 Franschhoek Formation

The Franschhoek Formation lies unconformably on the Malmesbury group and also the Cape Granite Suite (CGS), thus indicating its deposition after the deposition and deformation of the Malmesbury group and the earliest phase of intrusion of the CGS (ca. 550-545 Ma; Da Silva et al., 2000). This separates it temporally from the Malmesbury group. Furthermore, the Franschhoek Formation does not contain evidence of D_1, D_2 or D_3 that characterise either the Swartland or Malmesbury groups. Clasts of the Franschhoek Formation are composed of vein quartz, shales and granite that reflect erosion of the local surrounding rocks (both the Malmesbury group and CGS). A minimum age for the Franschhoek Formation is provided by the later crosscutting quartz porphyry dykes that are dated at 522 ±15 Ma (Dunlevey, 1981). The Franschhoek Formation is composed of a series of conglomerate and grit beds interbedded with shales, and although it is lithologically similar to the Piketberg Formation, it was deposited within a series of narrow graben or half-graben structures. This is in contrast to the depositional environment of the Piketberg Formation. In fact, deposition within grabens and/or half-grabens marks a clear change in depositional environment from both the Swartland and Malmesbury groups. The Franschhoek Formation is lithological and structurally similar to the Klipheuwel Group; both are composed of a series of conglomerates grits and shales (e.g. Hartnady, 1969; Theron et al., 1992; Chapter 2). They were both deposited in similar depositional environments, i.e. graben/half-graben structures, and at approximately the same time (535-510 Ma; Chapter 10.3). Following this evidence, it is suggested here that the Franschhoek Formation should be grouped with the Magrug and Populierbos Formations of the present Klipheuwel Group of SACS (1980).

11.3.2 Brandwacht and Norree Formations

Both formations fall outside the study area. In general, both formations consist of grits, conglomerates, greywackes, quartzites and limestones (Gresse and Theron, 1992) and therefore are lithologically similar to the Piketberg and Franschhoek Formations. However, these two formations were extensively overprinted by the Cape Orogeny (e.g. Hartnady, 1969; De Bruyn et al., 1974; Toogood, 1976) and prevent the present inclusion of these formations either within the Swartland, Malmesbury or Klipheuwel groups.

11.4 Saldania Orogenic Event

Any tectonic model for the evolution of the Saldania Belt has to take the following geological constraints into account:

i) The western branch of the Saldania Belt is composed of three groups, the Swartland, Malmesbury and Klipheuwel groups that are separated by unconformities (Chapter 10.2);

ii) The Swartland group is composed of a series of metapelites and subordinate dark limestones and metavolcanic rocks (Chapter 4). Such a combination of lithologies is suggested to represent a marine, possibly deepwater environment, formed by turbidite currents (e.g. Reading, 1986). In this scenario, the limestones would have been deposited in a fore-arc basin. Similarly, the geochemistry of the metasedimentary rocks suggests a depositional environment associated with a continental volcanic arc (Chapter 6.5);

iii) The metavolcanic rocks that characterise the Bridgetown formation have WPB-MORB characteristics indicating their formation is possibly related to seafloor spreading (Slabber, 1995). Their association with metasedimentary rocks of marine origin further substantiates this. The Bridgetown formation is located with the metasedimentary rocks of the Berg River and Moorreesburg formations. These formations constitute a tectonostratigraphic package related to the D_1 folding and thrusting event associated with subduction (Chapter 10.1.2). This may indicate that the

Bridgetown formation represents oceanic crust that incorporated into the tectonostratigraphic package (accretionary prism; point 7) during this event;

iv) The identification of outcrop-scale thrusts and the isolated occurrence of the biotite-feldspar schist (Kanonkop member) containing the same tectonic fabric as the other schists of the Swartland group, but representing a higher grade of regional metamorphism suggests regional-scale thrusting;

v) The Swartland group was deformed and metamorphosed during the early D_1/M_1 event that is not identified within the Malmesbury group. Both the Swartland and Malmesbury groups were then deformed and metamorphosed together during deformation/metamorphic event, D_2/M_2, before the intrusion of the Cape Granite Suite (CGS). The time interval between deformation of the Swartland group (ca. 575 Ma), the deposition of the Malmesbury group (until ca. 560 Ma) and their deformation together (ca. 545 Ma), is only a narrow time interval of as short as ca. 30 Ma;

vi) The Malmesbury group consists from stratigraphic base to top, conglomerates and grits (Piketberg Formation) deposited in a braided stream/alluvial fan environment, related to localised erosion of the Swartland group (Chapter 10.2). The Piketberg Formation is overlain by a succession of shales and mudstones, indicating deepwater sedimentation along a continental margin. The westerly metasedimentary rocks (in today's coordinates) were deposited distal to the then Kalahari Craton (Dunlevey, 1992). The deposits of the Tygerberg Formation are characteristic of deepwater sediments deposited by turbidite currents or mass-flow (e.g. Reading, 1986), and are intercalated with sporadic volcanic rocks (i.e. the Bloubergstrand Member; Von Veh, 1983);

vii) The depositional environment of the Swartland and Malmesbury groups, the intense deformation associated with D_1, i.e. bedding transposition and thrusting, low-grade regional metamorphism, syn-tectonic fluid flow, and the rock association are characteristic of accretionary wedge environments (Chapter 10.3.4);

viii) The Gariep Belt to the north is regarded as a foreland fold-and-thrust belt (e.g. Frimmel, 2000). Based on rock association and structural style, Gray and Foster (1997) characterised both accretionary wedges and foreland

fold-and-thrust belts. However, the Swartland and Malmesbury groups do not have any of the characteristics of foreland fold-and-thrust belts and this suggests a different tectonic setting to that of the Gariep Belt;

ix) A generally westerly vergence of F_1 folds and thrusts in the Swartland group and the presence of the early syn-collisional S-type granites, suggests that subduction occurred beneath the South African plate (Chapter 10.1.2);

x) The abundant I- and A-type granites of the CGS were intruded between 540 to 510 Ma into an extensional tectonic regime, post-dating the collisional tectonic phase (Scheepers, 1995; Rozendaal et al., 1999; Kisters et al., 2002);

xi) During the extensional tectonic regime, deposition of the newly defined Klipheuwel group occurred into graben and half-graben structures. This was then overlain by the ca. 520-510 Ma Table Mountain Sandstone Group.

The depositional and deformation sequence of the Swartland and Malmesbury groups outlined above is tentatively explained within the tectonic evolutionary scheme of the Neoproterozoic Saldania Belt described below.

The break-up of the Mesoproterozoic Rodinian supercontinent was associated with the deposition of rift-type sediments along the newly formed craton margins at around 770 Ma, based on the single zircon dating of the pre-Gariep basement (Frimmel et al., 2002). Coarse clastic sediments were deposited in northwest-trending rifts in the Gariep Belt (e.g. Von Veh, 1992; Von Veh, 1993; Jasper et al., 1995; Frimmel et al., 1996a; Jasper et al., 2000) and, by inference similar sediments were deposited in the Saldania Belt (e.g. Frimmel and Frank, 1998; Rozendaal et al., 1999). The opening of the Proterozoic Adamastor Ocean is constrained by the ca. 717 Ma Gannakouriep dyke swarm (Onstott et al., 1986). As the Adamastor Ocean continued to open, the formation of oceanic crust began (Frimmel and Hartnady, 1992), attested to by the Chameis Complex in the Gariep Belt that has MORB geochemical characteristics (Hartnady et al., 1990; Frimmel et al., 1996a). The metavolcanic rocks of the Bridgetown Formation have WPB-MORB geochemistry and have been inferred to represent the equivalent of the Chameis Complex to the north (e.g. Slabber, 1995; Rozendaal et al., 1999). A timing for the occurrence of sea floor spreading in the

Gariep Belt has been suggested by Frimmel and Frank (1998) at 630-600 Ma from $^{40}Ar/^{39}Ar$ dating of the earliest generation of amphibole related to sea floor metamorphism. The rifting model of Porada (1989) indicates that the opening of the proto-Atlantic was diachronous, with opening initiated in the south. Thus, a similar and probably slightly older age can be inferred for ocean floor formation and the generation of the Bridgetown formation in the Saldania Belt.

The opening of the Iapetus Ocean between South America and Laurentia (600-570 Ma) is believed to be the controlling factor of the inversion from extensional to compressional tectonics and the closure of the Adamastor Ocean between South America and South Africa (Grunow, et al., 1996). Deposition of the Swartland group, the deformation event D_1, and metamorphism in an accretionary wedge/fore-arc environment commenced at this time (Fig. 11.2a & Chapter 10.3.1). The formation of an accretionary wedge in the Marmora Terrane in the Gariep Belt was initiated at ca. 575 Ma (Frimmel and Frank, 1998) and is thus comparable to the Saldania Belt. However, in this study subduction is interpreted to have occurred beneath the South African plate in the Saldania Belt (Chapter 10.1.3), which is in contrast to the Gariep Belt to the north, where subduction is interpreted to have been beneath the South American plate (e.g. Stanistreet et al., 1991; Frimmel et al., 1996a).

During this time, and as subduction continued, the Bridgetown Formation could have been accreted into the accretionary prism. Due to poor exposure and erosion of the basement rocks and the extent of TMS Group overlying the basement, the position of the subduction-related arc is not clear. The position of the arc may be related to many factors including the angle and rate of subduction and the age of the subducting lithosphere (e.g. Cross and Pilger, 1982; Van der Pluijm and Marshak, 1997). Typically the arc develops between 150-200 km from the trench axis (e.g. Maekawa et al., 1993; Keary and Vine, 1996), therefore the volcanic arc could be located further to the east and is now overlain by TMS Group rocks.

As convergence continued, the accretionary prism was deformed by west-verging thrusting and duplexing (Chapter 5.1), which suggests underplating (e.g. Shreve and Cloos, 1986) and uplift (Silver et al., 1985). At some point, the accretionary prism

a) Deposition and deformation of the Swartland group.
The opening of the Iapetus Ocean between South America and Laurentia at ca. 630 Ma initiated the reversal from extensional to compressional tectonics between South America and South Africa. The Swartland group, interpreted to represent deposits of an accretionary prism/fore-arc, was deposited and deformed during D_1 at ca. 575 Ma. As subduction continued a slither of oceanic crust was scraped off the down-going slab and was thrusted into the tectonostratigraphic package. The oceanic crust is now represented by the metavolcanic rocks of the Bridgetown formation. During D_1, the Swartland group was metamorphosed to low-grade greenschist facies (M_1). Early D_1-related thrusts and folds verge to the west.

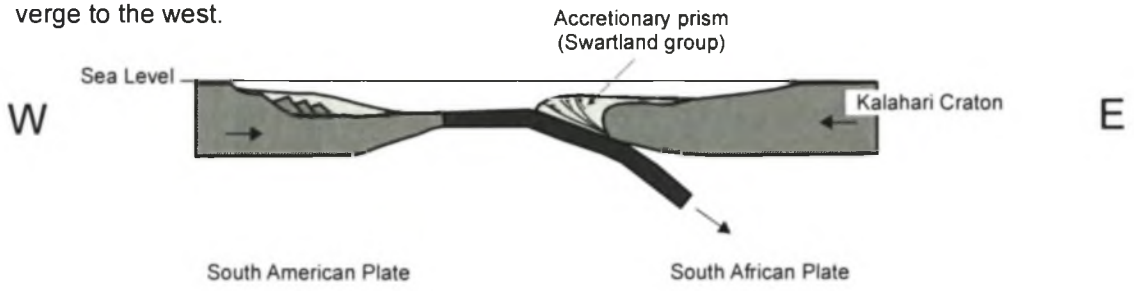

b) Uplift and erosion of the Swartland group.
As subduction and convergence continued, the Swartland group was uplifted and locally became subaerial. Erosion of the subaerial parts of the Swartland group and also the volcanic arc, provided the source for the sediments of the Malmesbury group

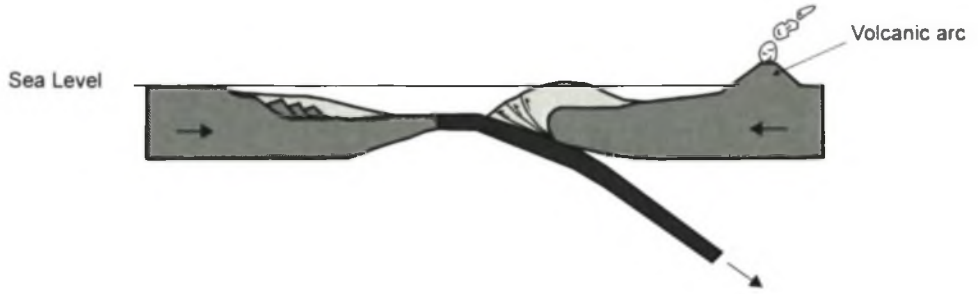

c) Deposition of the Malmesbury group
The coarse-grained grits and conglomerates of the Piketberg Formation were deposited locally, unconformably upon the Swartland group. Erosion of the Swartland group continued and the flysch-type sediments of the Tygerberg and Porterville formations were deposited on both the Swartland group and the Piketberg Formation. The Malmesbury group was deposited between ca. 575 and 560

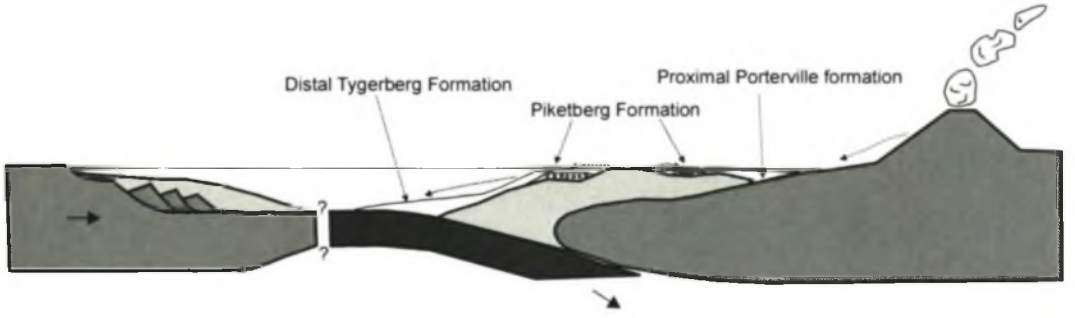

Figure 11.2. Tectonic evolution of the Neoproterozoic Saldania Belt. The ca. 600 to 540 Ma Swartland and Malmesbury groups are related to collisional tectonics. The overlying Klipheuwel group and Table Mountain Sandstone Group are related to extensional tectonics.

became subaerial as suggested by localised erosion of the Swartland group rocks and the deposition of the Piketberg Formation (Fig. 11.2b & Chapter 10.2). Additional sediments could have been derived either from the subducting slab, the volcanic arc or from the passive margin sediments from the South American plate. Deposition of these sediments would occur on top of and in front of the accretionary prism (Fig. 11.2b). The remainder of the Malmesbury group is composed of flysch-type, deepwater sediments, deposited by turbidity currents derived from the east (Von Veh, 1983) into the closing basin in front of the accretionary prism. Uplift and erosion of the accretionary wedge and the subsequent deposition of the overlying sediments occurred in a relatively short time span of 15 Ma (between D_1 and the deposition of the overlying sediments). The timing of the deposition of the Malmesbury group is similar to the time of sedimentation in the Nama Basin (between 600-540 Ma, Gresse & Germs, 1993; Grotzinger et al., 1995), in the Vanrhynsdorp Basin (ca. 570 Ma, Gresse & Germs, 1993) and in the Goegamma Subgroup (ca. 550 Ma, Fölling et al., 2000). The Bloubergstrand Member in the Tygerberg Formation is composed of tuffs, tuffaceous agglomerate and andesitic lava (Von Veh, 1983, Theron et al., 1992) and may represent extrusives and volcanoclastics related to the volcanic arc.

The continued convergence led to further deformation and metamorphism that now affected both the Swartland and Malmesbury groups rocks (Fig. 11.2d), and culminated in D_2, M_2 and D_3, all being constrained between 560 and 545 Ma (Chapter 10.3.2). In the Gariep Belt, collisional tectonics is dated at 545 ±2 Ma (Frimmel and Frank, 1998), which, considering Porada's (1989) diachronous model (collision initiated in the south first), correlates well with the western branch of the Saldania Belt (ca. 552-545 Ma). The earliest, strongly gneissic, syn-orogenic granites could possibly represent the plutonic remnants of the now eroded volcanic arc, e.g. Darling batholith, 547 ±6 Ma (Da Silva et al., 2000). Sinistral transpressional tectonics is recorded within the earliest phase of granites related to movement along the Colenso Fault Zone, indicating sinistral strike-slip motion from at least ca. 550 to 540 Ma. These early granites are classified as S-type granites on the basis of their geochemistry and were generated by the melting of the underlying Namaqua-Natal crustal rocks (Scheepers, 1995).

d) Collision and deformation of the western branch of the Saldania Belt
As subduction continued both the Swartland and Malmesbury groups were deformed and metamorphosed during D_2 and M_2 respectively. D_2 deformation occurred at ca. 550-545 Ma and coincides with the early, syn-tectonic ca. 550-540 Ma S-type granites of the CGS.

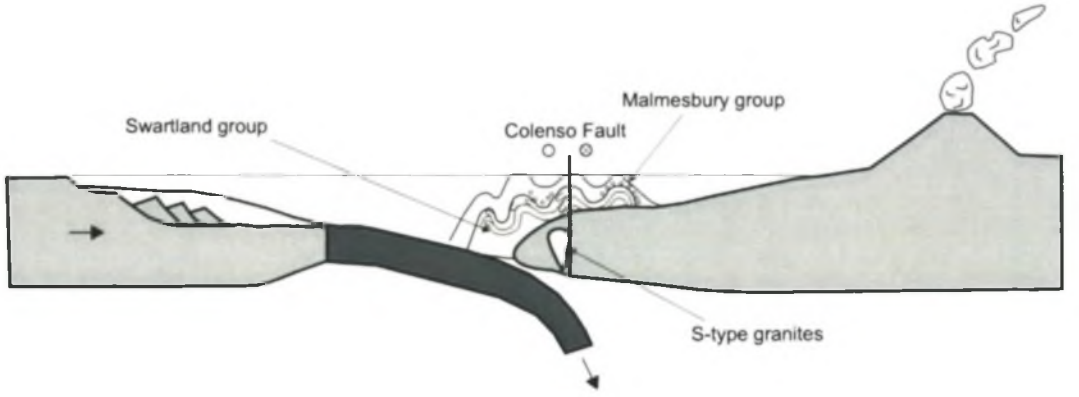

e) Cessation of collision and uplift of the western branch of the Saldania Belt.
Subduction ceased at ca. 540 Ma and the down-going slab broke away. This release of the down-going slab caused the uplift and eventually the erosion of the Malmesbury Group rocks overlying the South African Plate. Uplift and erosion of the South African plate continued until ca. 510 Ma.

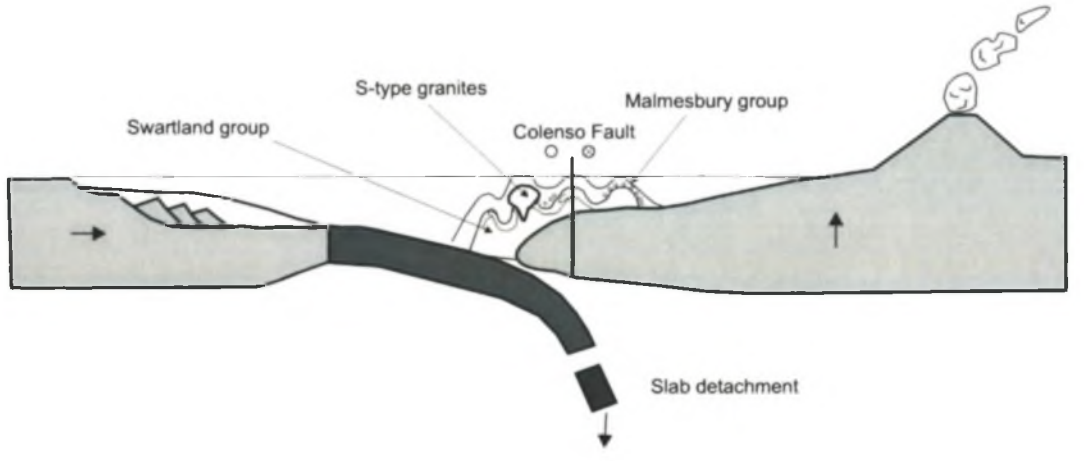

f) Extensional tectonics and the intrusion of the Cape Granite Suite.
Extensional tectonics commenced at ca. 540 Ma with the reversal from sinistral to dextral strike-slip movement along the Colenso Fault, and the onset of uplift. This was accompanied by first, the intrusion of the post-tectonic I-type granites (540-520 Ma) and the late A-type granites (ca. 520-510 Ma).

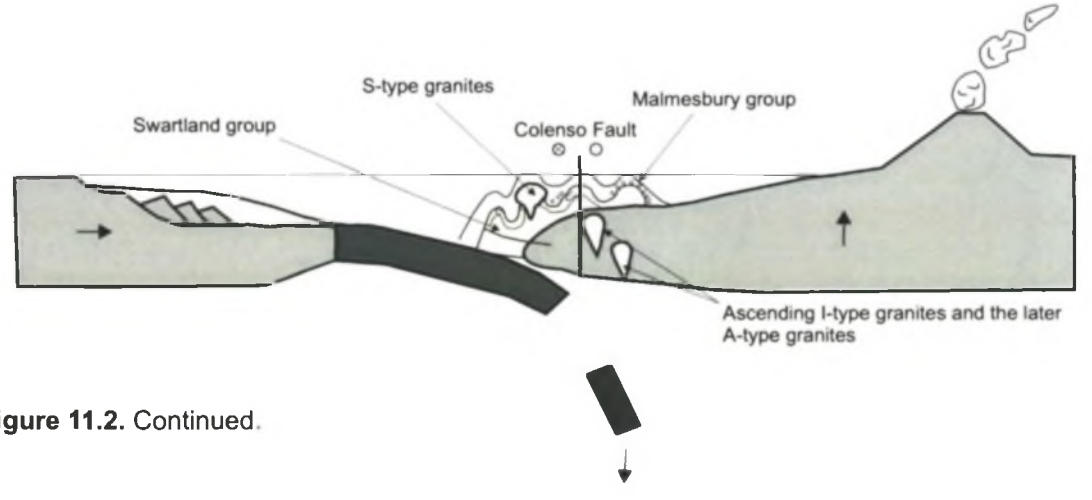

Figure 11.2. Continued.

Cessation of collisional tectonics can be temporally constrained at ca. 540 Ma (Fig. 11.2e & Chapter 10.3.2). The reversal of strike-slip motion along the Colenso Fault Zone coincided firstly with the intrusion of the I-type granites of the CGS into an extensional environment (Kisters et al., 2002), and secondly with the uplift of the rocks of the western branch of the Saldania Belt (Armstrong et al., 1998). If the direction of subduction suggested above is correct (Chapter 10.1.3), then magma generated from deeper segments of the subducting slab should be located further to the east (in today's coordinates), than the S-type granites, which is, in fact, the spatial distribution seen in the CGS (e.g. Rozendaal and Scheepers, 1994; Scheepers, 1995; Scheepers and Poujol, 2002).

The change from collisional to extensional tectonics is seen in the change in sedimentation style, to deposition in newly forming rift-related half-graben and graben structures, e.g. the conglomeratic nature of the Franschhoek Formation deposited after ca. 540 Ma (Fig. 11.2f & g). The newly defined Klipheuwel group rest unconformably on top of the CGS, indicating that considerable erosion of the Malmesbury Group rocks took place before sedimentation. The presence of CGS clasts in the Franschhoek Formation indicates that erosion of approximately 8-10 km of Malmesbury Group rocks overlying the granites must have already occurred (Armstrong et al., 1998). Therefore, to allow erosion of the granites, deposition of the Franschhoek Formation most probably occurred between ca. 530- 525 Ma. The remainder of the Klipheuwel group (Populierbos and Magrug Formations) being deposited after ca. 522 Ma (Chapter 11.3) and fine upwards indicating a more subdued topography in the provenance area (southwest in today's coordinates; Tankard et al., 1982). The extensive erosion of the Malmesbury group and formation of the peneplain by this time is further confirmed by the extrusion of the sub-aerial Langebaan volcanics at 515 ±3 Ma (Scheepers and Poujol, 2002) (Fig 11.2h).

Overlying the rift-deposited sediments both conformably and unconformably (Rust, 1967) is the Table Mountain Sandstone (TMS) Group (Fig. 11.2i). The onset of deposition of the TMS Group is suggested to be at ca. 520-510 Ma (Armstrong et al., 1998). According to some authors (e.g. Broquet, 1992; Armstrong et al., 1998), completion of the peneplain formation occurred before the deposition of the TMS

g) Deposition of the Klipheuwel group.
As extension tectonics continued, the eroded Malmesbury group sediments were deposited in developing graben/half-graben structures. These sediments formed the Klipheuwel group. The lowest formation is the Franschhoek Formation, was deposited between 530-525 Ma onwards, and then the overlying Magrug and Populierbos Formations.

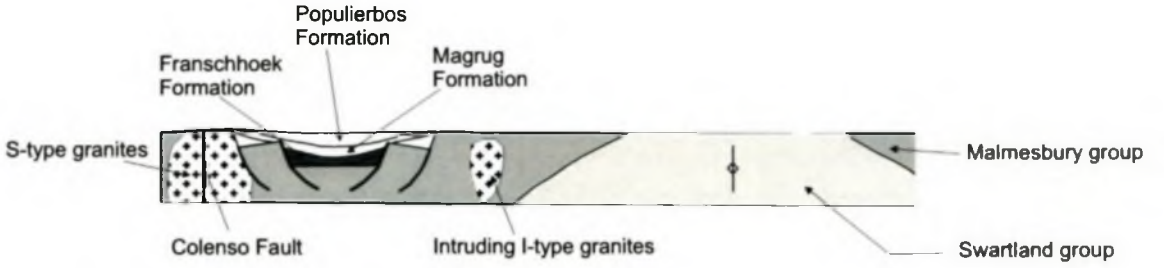

h) Intrusion of the shallow level I-type granites and volcanism.
Intrusion of I-type granites and the extrusion of the sub-aerial volcanics at Langebaan (ca 515 Ma) heralded in the end of exhumation of the basement rocks and the amalgamation of West

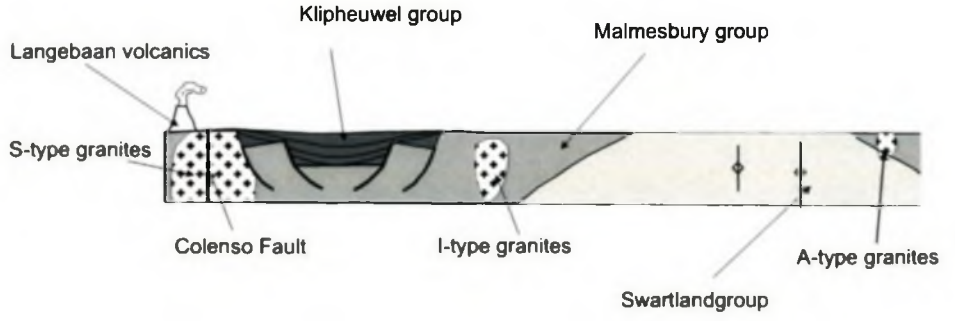

i) Deposition of the Table Mountain Sandstone (TMS) Group.
The TMS Group was deposited both conformably and unconformably on top of the Malmesbury and Klipheuwel groups. Commencement of deposition occurred ca. 510 Ma.

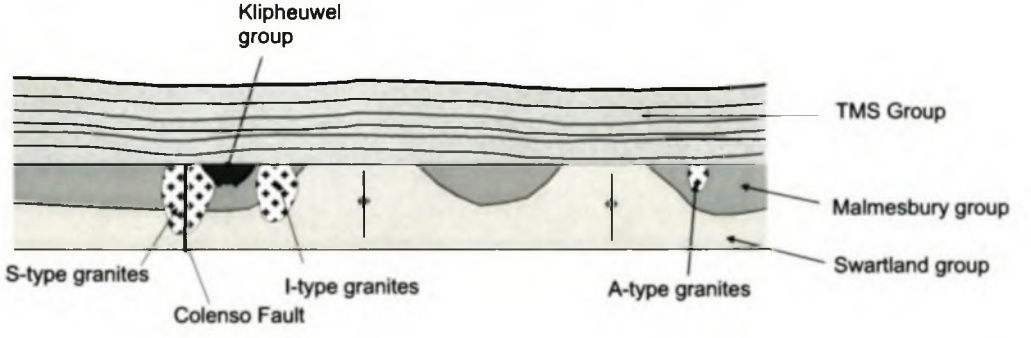

Figure 11.2. Continued.

Group and therefore erosion of the Malmesbury group occurred in a time interval of ca. 4-20 Ma, thus indicating a rate of uplift and erosion of approximately 0.4 -2 mm per year (Armstrong et al., 1998). More recently, Scheepers and Armstrong (2002) estimated a lower rate of uplift of 0.23 mm per year.

The present relationship between the Swartland, Malmesbury and Klipheuwel groups and the Table Mountain Sandstone Group as seen in cross section is presented in Figure 11.3.

11.5 Correlations between the Saldania and Gariep Belts

Following the new subdivision of the rocks of the western branch of the Saldania Belt into the unconformably separated Swartland, Malmesbury and Klipheuwel groups. It is possible to compare these groups with the other groups of the Saldania Belt and also the Gariep Belt and the deposits of the Nama and Vanrhynsdorp basins. Correlation between the Kaaimans, Kango, and Gamtoos Groups of the southern branch with the groups of the western branch of the Saldania Belt is impeded by poor outcrops, extensive overprinting of the Cape Orogeny, and limited age constraints on sedimentation, deformation and metamorphism. Traditionally, these groups are suggested to represent deposition in Pan-African ocean basins (e.g. Le Roux and Gresse, 1983; Frimmel and Van Achterbergh, 1995; Rozendaal et al., 1999). However, recent dating has revealed correlation of parts of the Saldania Belt with the younger Nama Group to the north (Frimmel et al., 2001). Also, other parts of the Saldania Belt are much younger than previously thought, e.g. the Kansa Subgroup (Barnett et al., 1997). This suggests that not all of the Saldania Belt is as old (ca. 750 Ma) as currently believed. A correlation of the groups of the Saldania Belt and the Gariep Supergroup and the Nama and Vanrhynsdorp Groups is shown in Figure 11.4. This is based on lithological and structural correlations and radiometric dating.

The Swartland group is characterised by the presence of transposition folding related to an early deformational event inferred at ca. 575 Ma (see above), therefore the equivalent rocks in the other groups of the Saldania Belt will most likely show a similar deformation style. The Kaaimans Group contains an early transposition fabric

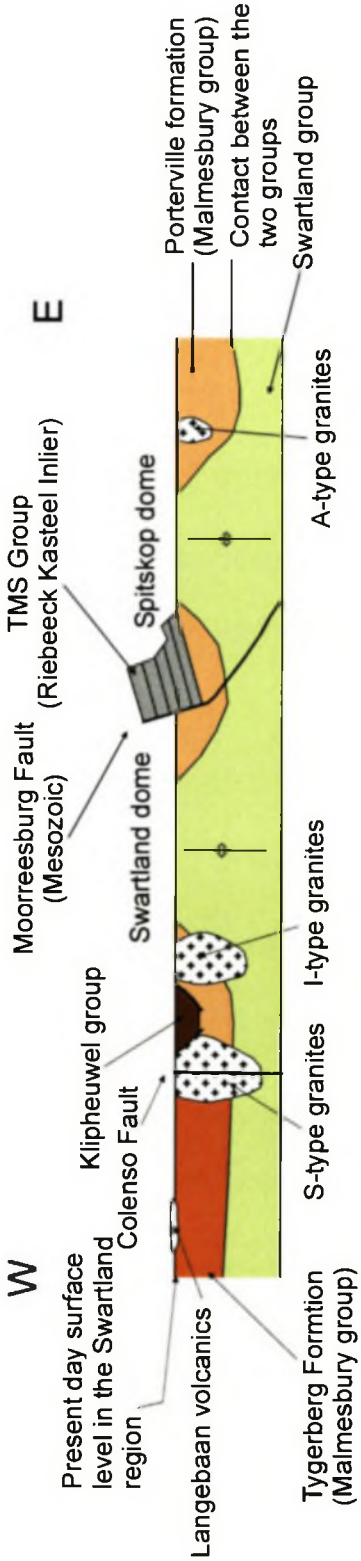

Figure 11.3 Schematic diagram showing the present-day relationships observed across the western branch of the Saldania Belt. Selective erosion of the TMS Group has led to the present topography now seen, where the Swartland group is only seen in the cores of the regional domal structures. The Klipheuwel group is also present in graben and half-graben structures where erosion has not completely removed these lithologies.

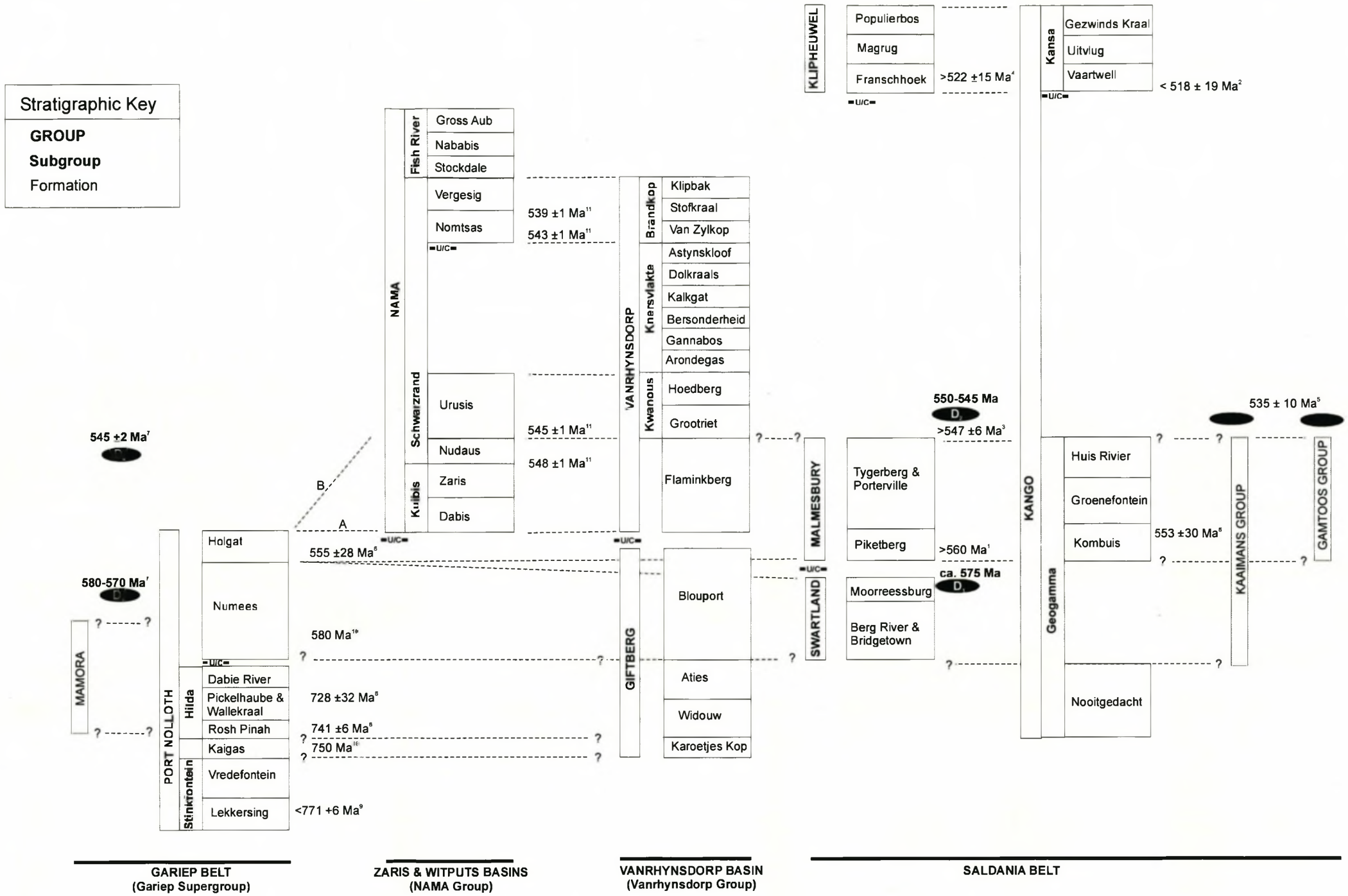

Figure 11.4. Proposed stratigraphic correlation between the groups of the Saldania Belt with the Gariep Supergroup and Nama and Vanrhynsdorp Groups to the north. Based on stratigraphic correlations of Gresse and Germs (1993), Frimmel et al. (2001) and De Beer et al. (2002). Depositional and metamorphic ages from (1) Armstrong et al. (1998), (2) Barnett et al. (1997), (3) Da Silva et al. (1997), (4) Dunlevey (1981), (5) Ferre and Ameglio (2000), (6) Folling et al. (2000), (7) Frimmel and Frank (1998), (8) Frimmel et al. (1996b), (9) Frimmel et al. (2001), (10) Frimmel et al. (2002). (11) Grotzinger et al. (1995). Major deformation/metamorphic events denoted by ●. U/C denotes an unconformable contact. A and B are two contrasting correlations; A (Germs, pers comm., 2003) and B (Frimmel et al., 2001).

(Gresse, 1983) related to top-to-the-north thrusting, but has been temporally constrained at 535 ±10 Ma (Ferré and Améglio, 2000). This is much younger than D_1 and also post-dates D_2 (ca. 545 Ma) and temporally corresponds to extension in the western branch. The Kaaimans Group is composed of quartzites, banded quartz schists, phyllites and impure limestones (Krynauw and Gresse, 1980) and was metamorphosed to upper greenschist facies during regional metamorphism (Frimmel and Van Achterbergh, 1995), indicating similar lithologies to that of the Swartland group. Therefore the Kaaimans Group may represent the temporal and spatial equivalent, in terms of sedimentation, to the Swartland group, but was unaffected by the same deformation events. Following recent subdivision of the Kango Group by Frimmel et al. (2001), the Nooitgedacht Formation represents the only equivalent of the 620-740 Ma Hilda Subgroup in the Gariep Supergroup (Frimmel et al., 1996b). As proposed in the tectonic model in this thesis (Chapter 11.4), deposition and deformation within an accretionary prism are synchronous. Therefore, the Swartland group is not likely to be much older than ca. 600 Ma and makes it significantly younger than the Nooitgedacht Formation (Kango Group). The Mamora Terrane (Gariep Supergroup) represents a complicated tectonic package composed of metasedimentary and metavolcanic rocks deposited and deformed in an accretionary wedge environment (Frimmel et al., 1996a; Frimmel, 2000). In general, this is a similar scenario as proposed for the Swartland group (Chapter 11.4) and therefore they are correlated here (Fig. 11.4). The Gifberg Group, originally part of the Vanrhynsdorp Group (Gresse, 1986), has been redefined and correlated to the Port Nolloth Group (e.g. Gresse and Germs, 1993; De Beer et al., 2002). In the Gifberg Group the extensive limestones and dolomites of the Widouw Formation are correlated to the extensive Stinkfontein and Hilda Subgroups (Gariep Supergroup) and by association the limestones of the Pickelhaube Formation (Fig. 11.4). This would make the Karoetjies Kop glaciogenic unit (e.g. Germs and Gresse, 1991; Gresse and Germs, 1993) the equivalent of the galciogenic unit of the Kaigas Formation of the Port Nolloth Group (e.g. Frimmel et al., 2001). The Numees Formation (Port Nolloth Group) and the Blouport Formation (Gifberg Group) both contains glaciogenic deposits correlated to the ca. 580 Ma Vandian glacial period, and therefore the approximate temporal equivalents of the Swartland group (Fig. 11.4).

Deposition of the overlying Malmesbury group continued at least until ca. 560 Ma (Chapter 10.3.1). The lithological equivalent to the Malmesbury group are the turbiditic sediments of the Holgat Subgroup (Gariep Supergroup), the coarse clastic and carbonate sediments, marine shales and siltstones of the Kuibis Subgroup and lower formations of the Schwarzrand Subgroup (Nama Group, Nama Basin) and the Flaminkberg Formation and the Kwanous Subgroup of the Vanrhynsdorp Group (Germs, 1972; 1974). Carbonates from within the Holgat Subgroup have been dated at 555± 28 Ma (Fölling et al., 2000) and this corresponds well to the likely age of the Malmesbury Group. Based on stratigraphic correlations and geochronology, Frimmel et al. (2001) concluded that the lower Nama Group, composed of the Kuibis Subgroup (≥548± 1 Ma), and the lower part of the Schwarzrand Subgroup (e.g. ≥545± 1 Ma; Grotzinger et al., 1995) is the equivalent of the Holgat Subgroup (Gariep Supergroup) and therefore by correlation is the equivalent of the Malmesbury group.

In the southern branch of the Saldania Belt, the Goegamma Subgroup (Kango Group) is composed of shales and wackes (Le Roux and Gresse, 1983) making it also lithologically comparable to the Malmesbury group. This is further confirmed by the Kombuis Formation (Goegamma Subgroup), which contains carbonates dated at 552± 27 Ma (Fölling et al., 2000), correlated to the Holgat Subgroup (Frimmel et al., 2002). Germs (1983) and Gresse (1986) suggested, based on similar lithologies including chemical sediments, that the Gamtoos Group is the correlative of the Nama Group. North-verging folding and thrusting related to Pan-African tectonics in the Gamtoos Group (Nolte, 1990) are possibly the equivalent of the 535 ±10 Ma thrusting event observed in the Kaaimans Group. The Gamtoos Group is tentatively correlated here with the Malmesbury group. However, the lack of geochronological constraints renders further correlation impossible. Therefore the Malmesbury group represents a possible stratigraphic and temporal equivalent of the Goegamma Subgroup (Kango Group), Holgat Subgroup (Gariep Supergroup), Gamtoos Group, lower Nama Group and the lower Vanrhynsdorp Group (Fig. 11.4).

As discussed in Chapter 11.4, the Klipheuwel group was deposited after ca. 540 Ma, most likely between 535 and 520 Ma in rift-related grabens and half-grabens. Due to the poor outcrops and the spatial relationships of the Franschhoek and Magrug

Formation, it is not possible to establish if one is older than the other. The Franschhoek Formation is cross cut by dykes dated at 522±15 Ma (Dunlevey, 1981), and thus this makes the Franschhoek Formation older than ca. 522 Ma. The Magrug Formation is composed of a series of conglomerates, grits and shales, and rests unconformably on the Malmesbury group, granites of the Cape Granite Suite, and granitic dykes (Visser, 1967; Theron et al., 1992) like the Franschhoek Formation. However, if these dykes are the temporal equivalent of the ca. 522 Ma dykes in the Franschhoek area, then the Magrug Formation would be younger and therefore lie stratigraphically above the Franschhoek Formation. However, until a better understanding of the formations of the Klipheuwel group can be understood, the Franschhoek Formation is temporally placed as the lower most formation. Barnett et al. (1997) have suggested that the Kansa Subgroup, which contains zircons as young as 518±19 Ma, is the lithological and temporal equivalent of the Klipheuwel group and this is also followed here.

12 CONCLUSIONS

The main findings of this study can be summarised as follows:

Based on lithostratigraphic and structural observations, it is suggested that the supracrustal rocks of the western branch of the Saldania Belt that were previously grouped under the Malmesbury Group are subdivided into three groups, namely the Swartland, Malmesbury and Klipheuwel groups. Contacts between the Swartland and Malmesbury groups appear to be unconformable and can be constrained to within approximately 200 m.

The new subdivision is based on lithological similarities of rocks within the Saldania Belt and across purported terrane boundaries, the uniformly developed lower-greenschist-facies grades of metamorphism, and the structural diversity of the Swartland and Malmesbury groups. These features were previously difficult to reconcile with the presence of three allochthonous or parautochtonous terranes underlying the Saldania Belt.

The penetrative D_1 deformation phase in the Swartland group is correlated with the D_1 deformations, for example, of the Kaoko and Gariep Belts to the north, where the formation of early fabrics is related to crustal convergence at ca. 580-575 Ma. The age of deposition of the Swartland group is not clear. However, a correlation with the Gifberg Group of the Vanrhynsdorp Basin and the Port Nolloth Group of the Gariep Supergroup in the Gariep Belt seems likely, based on structural similarities and the age of the D_1 deformation.

The overlying newly defined Malmesbury group does not contain evidence of the early D_1 deformation recorded in the Swartland group and therefore post-dates the D_1 deformation suggested to have occurred at ca. 575 Ma. A minimum age for the deposition and deformation of the Malmesbury group is provided by the intrusion of

the oldest phases of the CGS at ca. 552 Ma and is substantiated by ca. 560 Ma detrital zircons in the Tygerberg Formation. Thus, deposition and subsequent deformation of the Malmesbury group must have occurred over a relatively short time span of ca. 15-20 Ma. The Malmesbury group can be temporally and lithologically correlated with the Vanrhynsdorp and Nama Groups to the north.

The deposition of the Franschhoek Formation clearly post-dates the deposition and deformation of the Malmesbury group as well as the intrusion of the early phases of the CGS. Consequently, the Franschhoek Formation should be excluded from the newly defined Malmesbury group. Lithological and structural similarities rather suggest that the Franschhoek Formation should be correlated with the Klipheuwel Group of SACS (1980). The newly defined Klipheuwel group marks a contrast in deposition style to the underlying groups, being deposited in fault-bounded basins.

Exhumation of the Pan-African basement rocks and peneplain formation was achieved by ca. 510-520 Ma marked by subaerial volcanism, deposition of the coarse-clastic, fault-bounded sequence of the Klipheuwel group and sedimentation of the overlying, laterally extensive Cape Supergroup.

The Spitskop gold prospect represents the first identified occurrence of orogenic lode-gold mineralisation in the Saldania Belt. The prospect has many of the features, including tectonic environment, metamorphic grade, fluid composition and structural style, as world-renowned metasedimentary-hosted gold deposits, e.g. Lachlan Fold Belt. The lack of high-angle reverse faults at Spitskop are interpreted to be the main reason for the subeconomic grade.

REFERENCES

Aceñolaza, F.G., Millerm H., Toselli, A.J. (2002). Proterozoic-Early Paleozoic evolution in western South America- a discussion. *Tectonophysics*, **354**, 121-137.

Allsop, H.L., Köstlin, E.O., Welke, H.J., Burger, A.J., Kröner, A. and Blignault, H.J. (1979). Rb-Sr and U-Pb geochronology of Late Precambrian-Early Palaeozoic igneous activity in the Richtersveld (South Africa) and southern South West Africa. *Transactions Geological Society South Africa*, **82**, 185-204.

Armstrong, R., de Wit, M.J., Reid, D., York, D. and Zartman, R. (1998). Cape Town's Table Mountain reveals rapid Pan-African uplift of its basement rocks. *Journal of African Earth Sciences*, **27**, 1A, p10.

Bain, A.G. (1856). On the geology of Southern Africa. *Transaction of the Geological Society of London*, **Series 2**, 175-192.

Bailey, S.W. (1988). Chlorites: structures and crystal chemistry. *In:* Bailey, S.W. (Editor). *Hydrous phyllosilicates (exclusive of micas).* Reviews in Mineralogy, 19, 347-398.

Barnes, P.M, Sutherland, R., Davy, B. and Delteil, J. (2001). Rapid creation and destruction of sedimentary basins on mature strike-slip faults: an example from the offshore Alpine Fault, New Zealand. *Journal of Structural Geology*, **23**, 1727-1739.

Barnett, W., Armstrong, R.A. and De Wit, M.J. (1997). Stratigraphy of the upper Neoproterozoic Kango and Lower Palaeozoic Table Mountain Groups of the Cape Fold Belt, revisited. *South African Journal of Geology*, **100**, 237-250.

Baumgarter, L.P. and Olsen, S.N. (1995). A least-squares approach to mass transport calculations using the isocon method. *Economic Geology*, **90**, 1261-1270.

Belcher, R.W., Rozendaal, A. and Kisters, A.F.M. (2000). Quartz-vein hosted Au mineralisation in greenstones of the Neoproterozoic Bridgetown Formation, Saldania Belt, South Africa. *Journal of African Earth Sciences*. Special Abstract Issue GSSA 27: Geocongress 2000: A New Millennium on Ancient Crust, **31**, 1A, 7.

Best, M.G. (1982). *Igneous and Metamorphic Petrology*. W.H. Freeman and Company. 630 pp.

Bhatia, M.R. and Crook, K.A.W. (1986). Trace element characteristics of graywackes and tectonic discrimination of sedimentary basins. *Contribution to Mineralogy and Petrology*, **92**, 181-193.

Bhattacharya, A., Mazumdar, A.C. and Sen, S.K. (1988). Fe-Mg mixing in cordierite: constraints from natural data and implications for cordierite-garnet geothermometry in granulites. *American Mineralogist*, **73**, 338-344.

Bowers, T.S. and Helgeson, H.C. (1983). Calculation of the thermodynamic and geochemical consequences of non-ideal mixing in the system H_2O-CO_2-NaCl on phase relations in geological systems: Equation of state for H_2O-CO_2-NaCl fluids at high pressures and temperatures. *Geochimica et Cosmochimica Acta*, **47**, 1247-1275.

Broquet, C.A.M. (1992). The sedimentary record of the Cape Supergroup. *In:* De Wit, K. J. and Ransome, I. D. G. (Editors). *Inversion Tectonics of the Cape Fold Belt, Karoo and Cretaceous Basins of Southern Africa.* Balkema, Rotterdam, 239-248.

Brown, P.E. (1989). Flincor: a microcomputer program for the reduction and investigation of fluid inclusion data. *American Mineralogist*. **74**,1390-1393.

Brown, P.E. and Lamb, W.M. (1989). P-V-T properties of fluids in the system H_2O-CO_2-NaCl: New graphical presentations and implications for fluid inclusions studies. *Geochimica et Cosmochimica Acta*, **53**, 1209-1221.

Bruwer, L. (1998). *Petrology of the Neoproterozoic exo-granitic Kuiperskraal Sn-Zn-As deposit, Western Cape Province, South Africa.* M.Sc. thesis (unpublished), University of Stellenbsoch, pp.

Bucher, K. and Frey, M. (1994). *Petrogenesis of Metamorphic Rocks.* 6th Edition. Springer-Verlag, Berlin. 318 pp.

Burger, A.J. and Coertze, F. J., (1973). Radiometric age determinations on rocks from Southern Africa to the end of 1971. *Bulletin of the Geological Survey of South Africa,* **58,** 46pp.

Burnham, A.K. and Sweeney, J.J. (1989). A chemical kinetic model of vitrinite maturation and reflectance. *Geochimica et Cosmochimica Acta*, **53**, 2649-2657.

Busch, A. (1998). *The geochemistry and metamorphism of the Riviera W-Mo deposit, Western Cape, South Africa with references to the tectonic evolution of the Saldania Belt.* B.Sc. (Honours) thesis (unpublished), University of Stellenbosch.

Carmichael, R.S. (1989). *Practical handbook of physical properties of rocks and minerals.* CRC Press, Boca Raton.

Cameron, E.N. (1961). *Ore Microscopy.* John Wiley and Sons, New York, 293pp.

Cathelineau, M. (1988). Cation site occupancy in chlorites and illites as a function of temperature. *Clay Mineralogy*, **23**, 471-485.

Chemale, J.F., Hartman, L.A., and Da Silva, L.C. (1995). Stratigraphy and tectonism of Precambrian to early Paleozoic units in Southern Brazil and Uruguay. *Acta Geology Leopold.* **44**, 1-111.

Chemale, J.F., Van Schmus, W.R., Scheepers, R. and Gresse, P.G. (in press). Late Neoproterozoic to Cambrian evolution of the Saldania Belt, South Africa. *South American Journal of Earth Sciences.*

Churms, C.L., Pilcher, J.V., Springhorn, K.A. and Tapper, U.A.S. (1993). A VAX and PC-based data acquisition-system for MCA, scanning and list-mode analysis. *Nuclear Instruments and Methods,* **B77**, 56-61.

Cox, S.F., Etheridge, M.A., and Wall, V.J. (1991). Fluid pressure regimes and fluid dynamics during deformation of low-grade metamorphic terranes: Implications for the genesis of mesothermal gold deposits. *In:* Robert, F., Shahan, P.A., Green, S.B. (Editors). *Greenstone Gold and Crustal Evolution.* Geological Association of Canada, NUNA Conference Proceedings, Val d'Or, Quebec, May 24-27, 1990, 46-53.

Cox, S.F., Sun, S-S., Etheridge, M.A., Wall, V.J. and Potter, T.F. (1995). Structural and geochemical controls on the development of turbidite-hosted gold quartz vein deposits, Wattle Gully mine, Central Victoria, Australia. *Economic Geology,* **90**, 1722-1746.

Craig, J.R. and Vaughan, D.J. (1981). *Ore Microscopy and Ore Petrology.* J. Wiley and Sons, 406 pp.

Crawford, M.L. and Hollister, L.S. (1986). Metamorphic fluids: The evidence from fluid inclusions. *In:* Walther, J. V. and Wood, B. J. (Editors). *Fluid-rock Interactions during Metamorphism.* Springer-Verlag, Berlin. 1-35.

Cross, T.A and Pilger, R.H. Jr. (1982). Controls on subduction geometry, location of magmatic arcs, and tectonics of arc and back-arc regions. *Geological Society of America Bulletin*, **93**, 545-562.

Cunnigham, D., Alkmim, F.F., Marshak, S. (1998). A structural transect across the coastal mobile belt in Brazilian Highlands (latitude 20°S): the roots of a Precambrian transpressional orogen. *Precambrian research*, **92**, 251-275.

Damp, D.S. (1983). A comparison of the metamorphic grade and structural development between two terrains in the Malmesbury Group. B.Sc. (Honours) thesis (unpublished), University of Cape Town, 44pp.

Da Silva, L.C., Gresse, P.G., Scheepers, R., McNaughton, N.J., Hartmann, L.A. and Fletcher, I. (2000). U-Pb and Sm-Nd age constraints on the timing and sources of the Pan-African Cape Granite Suite, South Africa. *Journal of African Earth Sciences*, **30**, 795-815.

Da Silva, L.C., McNaughton, N.J., Hartmann, L.A., Fletcher, I.R., Gresse, P.G. and Scheepers, R. (1997). U-Pb (SHRIMP) isotopic constraints for the evolution of Southern Brazilian granitic

province, and some correlated South African, Pan-African plutons. *2nd International Symposium on Granites and Associated Mineralization, Salvador*, 24-29 August, 276-277.

Dalziel, I.W.D., Dalla Salda, L.H. and Gahagan, L.M. (1994). Paleaozoic Laurentuia-Gondwana interaction and the origin of the Appalachian-Andean mountain system. *Geological Society of America, Bulletin,* **109**, 243-252.

De Beer, C.H., Gresse, P.G., Theron, J.N. and Almond, J.E. (2002). *The Geology of the Calvinia Area.* Explanation of 1:250 000-scale 3118 Sheet. Council for Geoscience, South Africa, 92pp.

De Bruyn, P.L., De Jager, F.S.J., De Swardt, A.M.J. and Rabie, L.P. (1974). Geological map of the pre-Cape beds in the Worcester-Swellendam mountain foreland. *Annals of the University of Stellenbosch*, **49** (A4).

De Villiers, J. (1956). The three syntaxes in the southwestern Cape province (in Afrikaans). *Tegnikon*, **9**, 75-87.

De Villiers, J., Jansen, H., and Mulder, M. P. (1964). The geology of the area between Worcester and Hermanus: Explanatoin Sheet 3319C (Worcester) and 3419A (Caledon), and part of 3318D (Stellenbosch) and 3418B (Somerset West). (In Afrikaans). Geological Survey of South Africa, 69pp.

De Villiers, J.E. (1969). The geology of the country between Riebeeck-Kasteel and Moorreesburg. *Annals of the Geological Survey, South Africa*, **7**, 29-41.

De Villiers, J.E. (1979). Note on deformation and metasomatism in rocks of the Koringberg-Hermon area. *Transaction of the Geology Society, South Africa*, **82**, 179-181.

Deer, W.A., Howie, R.A. and Zussman, J. (1998). *An Introduction to Rock-forming Minerals.* 5th Edition. Longmans, Green and Co., London, 695pp.

Diamond, L.W. (1994). Salinity of multivolatile fluid inclusions determined from clathrate hydrate stability. *Geochimica et Cosmochimica Acta*, **58**, 19-41.

Diessel, C.F.K., Brothers, R.N. and Black, P.M. (1978). Coalification and graphitization in high-pressure schists in New Caledonia. *Contributions to Mineralogy and Petrology*, **68**, 63-78.

Droop, G.T.R. (1987). A general equation for estimating Fe^{3+} concentrations in ferromagnesian silicates and oxides from microscopic analyses, using stoichiometric criteria. *Mineral Magazine*, **51**, 431-435.

Drury, M.R. and Urai, J.L. (1990). Deformation-related recrystallisation processes. *Tectonophysics.* **172**, 235-253.

Du Toit, A.L. (1926). *The Geology of South Africa.* Oliver and Boyd, Edinburgh, 463pp.

Duchač, K.C. and Hanor, J.S. (1987). Origin and timing of the metasomatic silification on an early Archean komatiite sequence, Barberton Mountain Land, South Africa. *Precambrian. Research*, **37**, 125-146.

Dunlevey, J.N. (1981). The quartz-porphyry dykes of the Franschhoekberg tunnel. *Annals of the University of Stellenbosch*, Series **A1 (3)**, 349-426.

Dunlevey, J.N. (1992). Pan-African crustal evolution of south-western Africa. *Journal of African Earth Sciences*, **15**, 207-216.

Dunn, E.J. (1872). *Geological Sketch Map of Cape Colony.* E. Stratford, London.

Faure, G. (1991) *Principles and Applications of Inorganic Geochemistry: A Comprehensive Textbook for Geology Students.* Prentice-Hall, Inc. 626pp.

Ferré, E.C. and Améglio, L. (2000). Preserved magnetic fabrics vs. annealed microstructures in the syntectonic recrystallised George granite, South Africa. *Journal of Structural Geology*, **22**, 1199-1219.

Ferry, J.M. (1994). A historical review of metamorphic fluid flow. *Journal of Geophysical Research*, **99**, 15487-15498.

Ferry, J.M. and Spear, F.S. (1978). Experimental calibration of the partioning of Fe and Mg between biotite and garnet. *Contributions to Mineralogy and Petrology*, 66, 113-117.

Fisher, D. and Byrne, T. (1987). Structural evolution of underthrusted sediments, Kodiak Island, Alaska. *Tectonics*, **6**, 775-793.

Fleet, M.E., Chryssoulis, S.L., MacLean, P.J., Davidson, R. and Weisenier, C.G. (1993). Arsenian pyrite from gold deposits: Au and As distribution investigated by SIMS and EMP, and colour staining and surface oxidation by XPS and LIMS. *Canadian Mineralogist*, **31**, 1-17.

Fleet, M.E., MacLean, P.J., and Barbier, J. (1989). Oscillatory-zoned As-bearing pyrite from strata-bound and stratiform gold deposits: An indicator of ore fluid evolution. *In:* Keays, R. R., Ramsay, W. R. H. and Groves, D. I. (Editors.). *The Geology of Gold Deposits: The Perspective in 1988*. Economic Geology Monograph, 6, Economic Geology Publishing House, 356-362.

Fölling, P., Frimmel, H.E., and Zartman, R.E. (2000). A novel approach to double-spike Pb-Pb dating of carbonate rocks: examples from Neoproterozoic sequences in southern Africa. *Chemical Geology*, **171**, 97-122.

Foster, R.P. (1993). *Gold Metallogeney and Exploration.* Chapman and Hall, London, 432pp.

Foster, D.A., Gray, D.R., Kwak, T.A.P. and Bucher, M. (1998). Chronologic and orogenic framework of turbidite-hosted gold deposists in the western Lachlan Fold belt, Victoria. *Ore Geology Reviews*, **13**, 229-250.

Frey, M. (1987). *Low Temperature Metamorphism.* Blackie, London. 352pp.

Frimmel, H.E. (1995). Metamorphic evolution of the Gariep Belt. *South African Journal of Geology*, **98**, 176-190.

Frimmel, H.E. (1997). Chlorite thermometry in the Witwatersrand Basin: constraints on the Palaeoproterozoic geotherm in the Kaapvaal Craton, South Africa. *Journal of Geology*, **105**, 601-615.

Frimmel, H.E. (2000). The Pan-African Gariep Belt in the southwestern Namibia and western South Africa. *Communications of the Geological Survey of Namibia*, **12**, 197-209.

Frimmel, H.E. (2002). The glacial and interglacial record in the Gariep Belt: enigma of Neoproterozoic sedimentation rates. 11th IAGOD Quadrennial Symposium and Geocongress, Windhoek, Namibia. *Geological Survey of Namibia.*

Frimmel, H.E. and Frank, W. (1998). Neoproterozoic tectono-thermal evolution of the Gariep Belt and its basement, Namibia and South Africa. *Precambrian Research*, **90**, 1-28.

Frimmel, H.E. and Hartnady, C.J.H. (1992). Blue amphiboles and their significance for the metamorphic history of the Pan-African Gariep belt, Namibia. *Journal of Metamorphic Geology,* **10**, 651-669.

Frimmel, H.E. and Van Achterbergh, E. (1995). Metamorphism of calc-silicate and associated rocks in the Pan-African Kaaimans Group, Saldania Belt, South Africa. *Mineralogy and Petrology,* **53**, 75-102.

Frimmel, H.E., Fölling, P.G., and Diamond, R. (2001). Metamorphism of the Permo-Triassic Cape Fold Belt and its basement, South Africa. *Mineralogy and Petrology,* **73**, 325-346.

Frimmel, H.E., Hartnady, C.J.H. and Koller, F. (1996a). Geochemistry and tectonic setting of magmatic units in the Pan-African Gariep Belt, Namibia. *Chemical Geology*, **130**, 101-121.

Frimmel, H.E., Klötzli, U., Siegfried, P. (1996b). New Pb-Pb single zircon age constraints on the timing of Neoproterozoic glaciation and continetal break-up in Namibia. *Journal of Geology,* **104**, 459-469.

Frimmel, H.E., Fölling, P.G. and Eriksson, P.G. (2002). Neoproterozoic tectonic and climatic evolution recorded in the Gariep Belt, Namibia and South Africa. *Basin Research*, **14**, 1-18.

Garrels, R.M. and Mackenzie, F.T. (1971). *Evolution of Sedimentary Rocks.* Norton, New York, 397pp.

Germs, G.J.B. (1972). The stratigraphy and palaeontology of the lower Nama group, South West Africa. University of Cape Town, *Bulletin of the Precambrian Research Unit,* **12**, 250pp.

Germs, G.J.B. (1974). The Nama Group in South West Africa and its relationship to the Pan-African geosyncline. *Journal of Geology*, **82**, 301-317.

Germs, G.J.B. and Gresse, P.G. (1991). The foreland basin of the Damara and the Gariep Belt orogens in Namaqualand and southern Namibia: stratigraphic correlations and basin dynamics. *South African Journal of Geology*, **94**, 159-169.

Germs, G.J.B. (1983). Implications of a sedimentary facies and depositional environmental analysis of the Nama Group, SW Africa/Namibia. *Special Publication of the Geological Society of South Africa,* **11**, 89-114.

Glazner, A.F. and Bartley, J.M. (1991). Volume loss, fluid flow and state of strain in extensional mylonites from central Mojave Desert, California. *Journal of Structural Geology*, **13**, 587-594.

Goldfarb, R.J., Groves, D.I. and Gardoll, S. (2001). Orogenic gold and geological time: a global synthesis. *Ore Geology Reviews*, **18**, 1-75.

Grant, J.A. (1986). The isocon diagram- a simple solution to Gresens' equation for metasomatic alteration. *Economic Geology*, **81**, 1796-1982.

Gray, D.R. and Foster, D.A. (1997). Orogenic concepts- application and definition: Lachlan Fold Belt, eastern Australia. *American Journal of Science*, **297**, 859-891.

Gresse, P.G. (1983). Lithostratigraphy and structure of the Kaaimans Group. *Special Publication of the Geological Society of South Africa,* **12**, 17-19.

Gresse, P.G. (1986). *The tectonosedimentary history of the Vanryhnsdorp Group.* Ph.D. thesis (unpublished), University of Stellenbosch, 183pp.

Gresse, P.G. (1995). Transpression and transection in the late Pan-African Vanrhynsdorp foreland thrust-fold belt, South Africa. *Journal of African Earth Sciences*, **21**, 91-105.

Gresse, P.G. and Germs, G.J.B. (1993). The Nama foreland basin: sedimentation, major unconformity bounded sequences and multisided active margin advance. *Precambrian Research,* **63**, 247-272.

Gresse, P.G. and Theron, J.N. (1992). *The Geology of the Worcester Area.* Explanation sheet of 3319. Geological Survey. 79pp.

Gresse, P.G. and Scheepers, R. (1993). Neoproterozoic to Cambrian (Namibian) rocks of South Africa: a geochronological and geotectonic review. *Journal of South African Earth Sciences,* **16**, 375-393.

Gresse, P.G., Theron, J.N., Fitch, F.J. and Miller, J.A. (1992). Tectonic inversion and radiometric resetting of the basement in the Cape Fold Belt. *In:* De Wit, M.J. and Ransome, I.G.D. (Editors). *Inversion Tectonics in the Cape Fold belt, Karroo and Cretaceous Basins of Southern Africa.* Balkema, Rotterdam, 217-228.

Grew, E.S. (1974). Carbonaceous material in some metamorphic rocks of New England and other areas. *Journal of Geology*, **82**, 50-73.

Gromet, L.P., Dymek, R.F., Haskin, L.A. and Korotev, R.L. (1984). The "North American shale composite": Its compilation, major and trace element characteristics. *Geochimica et Cosmochimica Acta,* **48**, 2469-2428.

Grotzinger, J.P., Bowring, S.A., Saylor, B.Z. and Kaufman, A.J. (1995). Biostratigraphic and geochronologic constraints of early animal evolution. *Science*, **270**, 598-604.

Grunow, A., Hanson, R. and Wilson, T. (1996). Were aspects of Pan-African deformation linked to the Iapetus opening? *Geology,* **24**, 1063-1066.

Halberg, J.A. (1985). *Geology and Mineral Deposits of the Leonora-Laverton Area. Northeastern Yilgarn Block, Western Australia.* Hespirian Press, Perth. 140pp.

Hälbich, J.W. (1988). Progressive left lateral NW-SE slip movement along the West Coast of Southern Africa in Pan-African times. *Abstr. Geocongress '88,* Durban, South Africa.

Hälbich, I.W. and Cornell, D.H. (1983). Metamorphic history of the Cape Fold Belt. *In:* Sönghe, A. P. and Hälbich, I.W. (Editors). *Geodynamics of the Cape Fold Belt.* Special Publication of the Geological Society of South Africa, **12**, 131-148.

Hälbich, I.W. and Hartnady, C.J.H. (1985). *Structural Correlation on the Swartland Dome between Riebeeck Kasteel, Malmesbury and Moorreesburg.* Geological Society of South Africa, Western Cape Branch, Excursion Guide, 25th May, 1985.

Hälbich, I.W., Fitch, F.J. and Miller, J.A. (1983). *Dating the Cape Orogeny. In:* Sönghe, A. P. and Hälbich, I.W. (Editors). *Geodynamics of the Cape Fold Belt.* Special Publication of the Geological Society of South Africa, **12**, 165-175.

Hall, A.L. (1929). The Transvaal-Nama System. *In:* Steinmann, G and Wilckens, O (Editors). *Handbook of Regional Geology. Volume VII (7 Abt).* The Union of South Africa. University Press, Heidelberg, 72-95.

Hanor, J.S. and Duchac̆, K.C. (1990). Isovolumetric silification of early Archean komatiites: geochemical mass balances and constraints on origin. *Journal of Geology*, **98**, 863-877.

Hartnady, C.J.H. (1969). Structural analysis of some pre-Cape formations in the Western Province. *Bulletin of the Precambrian Research Unit, University of Cape Town*, **6**, 1-70.

Hartnady, C.J.H. and Hälbich, I.W. (1985). Structural correlation on the Swartland Dome between Riebeeck Kasteel, Malmesbury and Moorreesburg: Excursion guidebook of the Geological Society of South *Africa*, Western Cape Branch.

Hartnady, C.J.H., Joubert, P. and Stowe, C. (1985). Proterozoic crustal evolution in Southwestern Africa. *Episodes*, **8**, 236-244.

Hartnady, C.J.H., Newton, A.R. and Theron, J.N. (1974). The stratigraphy and structure of the Malmesbury Group in the southwestern Cape. *Bulletin Precambrian Research Unit, University Cape Town,* **15,** 193-213.

Hartnady, C.J.H., Ransome, I.G.D. and Frimmel, H.E. (1990). Accreted composite terranes- an example from the Gariep Orogenic Belt. *Extended Abstracts, Geocongress, 90*, Geological Society of South Africa, Cape Town, 218-221.

Haynes, S.J. (1986). Geology and chemistry of turbidite-hosted gold deposits, greenschist facies eastern Nova Scotia, Canada. *In:* Keppie, J.D., Boyle, R.W. and Haynes, S.J. (Editors).*Turbidite-hosted Gold Deposits.* Geological Association of Canada, Special Paper, **32**, 161-177.

Hey, M.H. (1954). A review of chlorites. *Mineral Magazine*, **30**, 277-292.

Hoal, B.G. (1978). *The pre-Cape Brewelskloof-Meiringsberg area north of Worcester: Structural analysis, petrography, geochemistry and application of white mica geothermometry and geobarometry.* B.Sc. (Honours) Project (unpublished), University of Cape Town, 86pp.

Hobbs, B.E. (1985). The geological significance of microfabric. *In:* Wenk, H.R. (Editor). *Preferred orientation in deformed metals and rocks.* Academic Press, New York,

Hoefs, J. (1987). *Stable Isotope Geochemistry.* 3rd Ed. Springer-Verlag, Berlin. 241pp.

Holdaway, M.J. and Lee, S.M. (1977). Fe-Mg cordierite stability in high-grade pelitic rocks based on experimental, theoretical, and natural observations. *Contributions to Mineralogy and Petrology*, **63**, 175-198.

Humphries, S.E. (1984). The mobility of the rare earth elements in the crust. *In:* Henderson, P., (Editor). *Rare Earth Element Geochemistry.* Elsevier, Amsterdam, pp 315-341.

Jackson, N.J. and Ramsay, C.R. (1980). What is the "Pan-African"? A consensus is needed. *Geology*, **8**, 210-211.

Jasper, M.J.U., Stanistreet, I.G., and Charlesworth, E.G. (1995). Opening and closure of the Adamastor Ocean: The Gariep Belt (southern Namibia) as a late Proterozoic/early Palaeozoic example of a Wilson Cycle. *Annales of Scientifique Musée royal l'Afrique centrale*, **101**, 143-161.

Jasper, M.J.U., Stanistreet, I.G., and Charlesworth, E.G. (2000). Neoproterozoic inversion tectonics, half-graben depositories and glacial controversies, Gariep fold-thrust belt, southern Namibia. *Communications of the geological survey of Namibia*, **12**, 187-196.

Jiang, W.T, Peacor, D.R. and Buseck, P.R. (1994). Chlorite geothermometry: contamination and apparent octahedral vacancies. *Clay Minerals*, **42**, 593-605.

Keary, P. and Vine, F.J. (1996). *Global Tectonics.* Blackwell Science, London, 333pp.

Kennedy, W.Q. (1964). The structural differentiation of Africa in the Pan-African (±500 m.y.) tectonic episode. *Leeds University Research Institute of African geology. 8th Annual Report of Scientific Results*, 48-49.

Kerrich, R. and Wyman, D. (1990). Geodynamic setting of mesothermal gold deposits: An association with accretionary tectonic regimes. *Geology*, **18**, 882-885.

Khaibullin, I.K.H., Novikov, B. Ye, Copeliovich, A.M. and Besedin, A.M. (1980). Phase diagrams for steam solutions and caloric properties of two-and three-component systems: H_2O-NaCl, H_2O-Na_2SO_4 and H_2O-NaCl-Na_2SO_4. *In:* Straub, J. and Scheffer, K. (Editors*). Water and Steam.* Pergamon Press, New York, pp 641-647.

Kimura, G. and Mukai, A. (1991). Underplated units in an accretionary complex: melange Shimanto Belt of Eastern Shikokuy, Southwest Japan. *AGU, Tectonics Series*, **10**, 31-50.

Kisters, A.F.M., Belcher, R.W., Armstrong, R.A., Scheepers, R., Rozendaal, A. and Jordaan, L.S. (2002). Timing and kinematics of the Colenso Fault; The Early-Paleozoic shift from collisional to extensional tectonics in the Pan-African Saldania Belt, South Africa. *South African Journal of Geology*, **105**, 257-270.

Kröner, A. (1981). *Precambrian Plate Tectonics*. Developments in Precambrian Geology, 4. Elsevier, Amsterdam, 781pp.

Krynauw, J.R. and Gresse, P.G. (1980). The Kaaimans Group in the George area, Cape Province: A model for the origin of deformation and metamorphism in the Southern Cape Fold Belt. *Transactions of the Geology Society of South Africa,* **83**, 23-38.

Landis, C.A. (1971). Graphitization of dispersed carbonaceous material in metamorphic rocks. *Contributions to Mineralogy and Petrology*, **30**, 34-45.

Le Maitre, R.W., Bateman, P., Dudek, A., Keller, J., Laymere Le Bas, M.J., Sabine, P.A., Scmid, R., Sorensen, H., Treckesien, A., Wolley, A.R. and Zanettin, B. (1989). A Classification of Igneous Rocks and Glossary of Terms. Blackwell. 193 pp.

Le Roux, J.P. and Gresse, P.G. (1983). The sedimentary-tectonic realm of the Kango Group. *In:* Sönghe, A.P. & Hälbich, I.W. (Editors). *Geodynamics of the Cape Fold Belt.* Special Publication, Geological Society of South Africa, **12**, 165-175.

MacKenzie, I.F. (1983). *Geology and geochemistry of tungsten mineralisation at Doctor Hill and Falls creek, Central Westland, New Zealand.* M.Sc. thesis (unplublished), University of Victoria, Wellington, 160pp.

MacKenzie, J.S., Needham, D.T., and Agar, S.M. (1987). Progressive deformation in an accretionary complex: an example from the Shimanto belt of eastern Kyushu, southwest Japan. *Geology*, **15**, 353-356.

Maekawa, H., Shozul,M., Ishii, T., Fryer, P. and Pearce, J.A. (1993). Blueschist metamorphism in an active subduction zone. *Nature*, **326**, 378-381.

McDougall, I. and Harrison, T.M. (1988). *Geochronology and Thermochronology by the $^{40}Ar/^{39}Ar$ Method.* Oxford University Press, New York, 212pp.

Meschede, M. (1986). A method of discriminating between different types of mid-ocean ridge basalts and continental tholeiites with the Nb-Zr-Y diagram. *Chemical Geology*, **56**, 207-218.

Miller, J. McL. and Gray, D.R. (1996). Structural signature of sediment accretion in a Palaeozoic accretionary complex, southeastern Australia. *Journal of Structural Geology*, **18**, 1245-1258.

Mullen, E.D. (1983). $MnO/TiO_2/P_2O_5$: A minor element discrimination for basaltic rocks of oceanic environments and its implications for petrogenesis. *Earth and Planetary Science Letters,* **62**, 53-62.

Naldrett, A.J. and Cabri, L.J. (1976). Ultramafic and related mafic rocks: Their classification and genesis with special reference to the concentration of nickel sulfides and Platinum-Group Elements. *Economic Geology,* **71**, 1131-1158.

Newton, A.R. (1966). *Preliminary Report on Work on Malmesbury Rocks.* 4th Annual Report, Precambrian Research Unit, University of Cape Town, 16-17.

Nolte, C.C. (1990). *Structural and tectonostratigraphy of the Gamtoos Belt between Tweewaters and Claassen Point, Eastern Cape Province, RSA.* M.Sc. thesis (unpublished), University of Port Elizabeth, 237pp.

Norrish, K. and Hutton, J.T. (1969). An accurate X-ray spectrographic method for the analysis of a wide range of geological samples. *Geochimica et Cosmochimica Acta,* **33**, 431-457.

O'Hara, K.D. and Blackburn, W.H. (1989). Volume loss model for trace element enrichments in mylonites. *Geology,* **17**, 524-527.

Oliver, J. (1986). Fluids expelled tectonically from orogenic belts: Their role in hydrocarbon migration and other geological phenomena. *Geology,* **14**, 99-102.

Overstreet, W.C. (1967). The Geological Occurrence of Monazite. *U.S. Geology Survey, Professional Paper,* **530**, 327pp.

Passchier, C.W. and Trouw, R.A.J. (1996). *Microtectonics.* Springer-Verlag, Berlin, 289pp.

Pearce, J. A. (1976). Statistical analysis of major element patterns in basalts. *Journal of Petrology*, **17**, 15-43.

Pearce, J.A, and Cann, J.R. (1973). Tectonic setting of basic volcanic rocks determined using trace element analysis. *Earth and Planetary Science Letters,* **19**, 290-300.

Pearce, J.A. and Norry, M.J. (1979). Petrogenetic implications of Ti, Zr, Y and Nb variations in volcanic rocks. *Contributions to Mineralogy and Petrology,* **69**, 33-47.

Pearton, T.N. (1980). *The geochemistry of the carbonate and related rocks of the antimony line, Murchison greenstone belt, with particular reference to their genesis and to the origin of stibnite mineralization.* Ph.D. thesis (unpublished). University of Witwatersrand.

Perchuk, L.L. and Lavrent'eva, I.V. (1983). Experimental investigations of exchange equilibria in the system cordierite-garnet-biotite. *In:* Saxena, S.K. (Editor) *Kinetics and Equilibrium in Mineral Reactions.* Springer-Verlag, New York, **3**, 199-239.

Pettijohn, F.J. (1975). *Sedimentary Rocks.* Harper and Row, 628pp.

Pirajno, F. (1992) *Hydrothermal Mineral Deposits: Principles and Fundamental Concepts for the Exploration Geologist.* Springer-Verlag, Berlin, 709pp.

Porada, H. (1985). Stratigraphy and facies in the Upper Proterozoic Damara Orogen, Namibia, based on a geodynamic model. *Precambrian Research*, **29**, 235-264.

Porada, H. (1989). Pan-African Rifting and Orogenesis in Southern to Equitorial Africa and Eastern Brazil. *Precambrian Research*, **44**, 103-136.

Potter, R.W. II, Babcock, R.S. and Brown, D.L. (1977). A new method for determining the solubility of salts in aqueous solutions at elevated temperatures, *U.S. Geological Survey, Research Paper,* **5, (3)** 389-395.

Potter, R.W. II, Clynne, M.A. and Brown, D.L. (1978). Freezing point depression of aqueous sodium chloride solutions. *Economic Geology*, **73**, 284-285.

Prozesky, V.M., Przybylowicz, W.J., van Achterbergh, E., Churms, C.L., Pineda, C.A., Springhorn, K.A., Pilcher, J.V., Ryan, C.G., Kritzinger, J., Schmitt, H. and Swart, T. (1995). The NAC nuclear microprobe facility. *Nuclear Instruments and Methods in Physics Research,* **B104**, 36-42.

Przybylowicz, W.J., Prozesky, V.M. and Meyer, F.M. (1995). True elemental imaging of pyrites from Witwatersrand reefs. *Nuclear Instruments and Methods in Physics Research,* **B104**, 450-455.

Rabie, L.P. (1948). *Geological map of the Moorreesburg-Wellington area.* Univ. Stellenbosch (printed but not issued).

Rabie, L.P. (1974a). Geological map of the Moorreesburg-Wellington area. *Annals of the University of Stellenbosch*, **49** A (5).

Rabie, L. P. (1974b). Structural map of the Moorreesburg-Wellington area. *Annals of the University of Stellenbosch,* **49** A (5).

Ramdohr, P., (1969). *The ore minerals and their intergrowths.* 3rd Edition. English. Pergamon Press, 1174pp.

Ramsay, J.G. (1967). *Folding and Fracturing of Rocks.* McGraw-Hill Book Company, New York, 562pp.

Ramsay, W.R.H. and VandenBerg, A.H.M. (1990). Lachlan Fold Belt in Victoria-regional geology and mineralisation. *In:* Hughes, F.E. (Editor). *Geology of the mineral deposits of Australia and Papua New Guinea. Vol. 2, Australasia.* Institute of Mining and Metallurgy, monograph, **14**, 1269-1273.

Reading, H. G. (1986). *Sedimentary Environments and Facies.* Blackwell Scientific Publications, Oxford, 615pp.

Redman, B.A. and Keays, R.R. (1985). Archean basic volcanism in the eastern goldfields province, Yilgarn Block, Western Australia. *Precambrian Research*, **30**, 113-152.

Robinson, D., Bevins, R.E. and Rowbotham, G. (1993). The characterization of mafic phyllosilicates in low-grade metabasalts from eastern North Greenland. *American Mineralogist*, **78**, 377-390.

Roedder, E. (1984). *Fluid Inclusions.* Reviews in Mineralogy, **12**. Mineralogical Society of America, 644pp.

Rogers, A.W. (1903). *Report of the Acting Geologist.* Annual Report of the Geological Commission of the Cape Good Hope, 3-10.

Rogers, A.W. (1913). The Nama System in the Cape Province. *Transactions of the Geological Society of South Africa*, **15**, 31-50.

Rogers, A.W. (1897). Survey of Stellenbosch District. *Annual Report, Geological Commission of the Cape of Good Hope*, 45-50.

Rogers, A.W. and Du Toit, A.L. (1909). *An introduction to the geology of the Cape Colony.* Longmans, Green and Co., London, 491 p.

Rollinson, H. R. (1996). *Using Geochemical Data: Evaluation, Presentation, Interpretation.* Longman Group, UK Ltd., 352pp.

Rose, A.W., Hawkes, H.E. and Webb, J.S. (1979). *Geochemistry in Mineral Exploration.* 2nd Ed. Academic Press, 657pp.

Rozendaal, A. and Scheepers, R. (1994). Metallogenesis and Exploration potential of the Neoproterozoic Saldania Belt in the southwestern Cape Province, South Africa. *Exploration and Mining Geology*, **3**, 419-438.

Rozendaal, A. and Scheepers, R. (1995). Magmatic and related mineral deposits of the Pan-African Saldania belt in the Western Cape Province, South Africa. *Journal of African Earth Sciences,* **21**, 107-126.

Rozendaal, A. Gresse, P. G. Scheepers, R. and De Beer, C. H. (1994). Structural setting of the Riviera W-Mo deposit, Western Cape, South Africa. *South African Journal of Geology*, **97**, 184-195.

Rozendaal, A. Gresse, P.G. Scheepers, R. and Le Roux, J.P. (1999). Neoproterozoic to early Cambrian crustal evolution of the Pan-African Saldania belt, South Africa. *Precambrian Research*, **97**, 303-323.

Rumble, D. III. (1994). Water circulations in metamorphism. *Journal of Geophysical Research*, **99**, 15,499-15,502.

Rust, I. (1967). *On the sedimentation of the Table Mountain Group in the Eestern Cape Province.* D.Sc. thesis (unpubl.), University of Stellenbosch, 110pp.

Rust, I. (1973). The evolution of the Palaeozoic Cape basin, southern margin of Africa in the ocean basins and margins, 1. *In:* Narin, A. E. M. and Stehli, F. G. (Editors) *The South Atlantic.* Plenum, New York, 583pp.

Ryan, C.G. and Jamieson, D.N. (1993). Dynamic analysis: on-line quantitative PIXE microanalysis and its use in overlap-resolved elemental mapping. *Nuclear Instruments and Methods in Physics research*, **B77**, 203-214.

Ryan, C.G., Cousens, D.R., Sie, S.H., Griffin, W.L., Suter, G.F. and Clayton, E. (1990a). Quantitative PIXE microanalysis of geological material using the CSIRO proton microprobe. *Nuclear Instruments and Methods*, **B47**, 55-71.

Ryan, C.G., Cousens, D.R., Sie, S.H. and Griffin, W.L. (1990b). Quantitative analysis of PIXE spectra in geoscience application. *Nuclear Instruments and Methods,* **B49**, 271-276.

Ryan, C.G., Jamieson, D.N., Churms, C.L. and Pilcher, J.V. (1995) A new method of online true-elemental imaging using PIXE and the proton microprobe. *Nuclear Instruments and Methods*, **B104**, 157-165.

Ryan, C.G., van Achterbergh, E., Jamieson, D.N. and Churms, C.L. (1996). Overlap corrected on-line PIXE imaging using the proton microprobe. *Nuclear Instruments and Methods in Physics Research,* **B109**, 154-160.

Sample, J.C and Moore, J.C. (1987). Structural style and kinematics of an underplated slate belt, Kodiak and adjacent islands, Alaska. *Bulletin of the Geological Society of America*, **99**, 7-20.

Sanford, R.F. (1982). Growth of ultramafic reaction zones in greenschist to amphibolite facies metamorphism. *American Journal of Science*, **282**, 543-616.

Scheepers, R. (1990). *Magmatic associations and radioelement geochemistry of selected Cape Granites, with special reference to subalkaline and leucogranitic phases.* (In Afrikaans). Ph.D. thesis (unpublished), University of Stellenbosch, 151pp.

Scheepers, R. (1995). Geology, geochemistry and petrogenesis of Late Precambrian S-, I-, and A-type granitoids in the Saldania Belt, Western Cape Province, South Africa. *Journal of African Earth Sciences*, **21**, 35-38.

Scheepers, R. and Armstrong, R. (2002). New U-Pb SHRIMP zircon ages of the Cape Granite Suite: implications for the magmatic evolution of the Saldania Belt. *South African Journal of Geology*, **105**, 241-256.

Scheepers, R. and Poujol, M. (2002) U-Pb zircon age of the Cape Granite Suite ignimbrites: characteristics of the last phase of the Saldania magmatism. *South African Journal of Geology*, **105**, 163-178.

Schoch, A.E. (1975). The Darling granite batholith. *Annals of the University of Stellenbosch.* **A1** (1), 1-104.

Şengör, A.M.C. and Okuroğullari, A.H. (1991). The role of accretionary wedges in the growth of continents:Asiatic examples from Argand to plate tectonics. *Eclogae Geolojica Helveticae*, **84**, 535-597.

Seitz, J.C. and Pasteris, J.D. (1990). Theoretical and practical aspects of differential partitioning of gases by clathrate hydrates in fluid inclusions. *Geochimica et Cosmochimica Acta*, **54**, 631-639.

Selverstone, J., Morteani, G. and Staude, J.M. (1991). Fluid channelling during ductile shearing: transformation of granodiorite into aluminous schist in the Tauern Window, Eastern Alps. *Journal of Metamorphic Geology*, **9**, 419-431.

Shaw, D.M. (1956). Geochemistry of pelitic rocks. Part III: major element and general geochemistry. *Bulletin of the Geological Society of America*, **67**, 919-934.

Shreve, R.L. and Cloos, M. (1986). Dynamics of sediment subduction melange formation and prism accretion. *Journal of Geophysical Research*, **91**, 10229-10245.

Sibson, R.H. and Scott, J. (1998). Stress/fault controls on the containment and release of overpressured fluids; Examples from gold-quartz vein systems in Juneau, Alaska; Victoria, Australia and Otago, New Zealand. *Ore Geology Reviews*, **13**, 292-306.

Sibson, R.H., Robert, F. and Poulsen, K.H. (1988). High-angle reverse faults, fluid-pressure cycling and mesothermal gold-quartz deposits. *Geology*, **16**, 551-555.

Siegfried, H. P. (1993). *The Malmesbury batholith and its relationship to granitic plutons in the Swartland tectonic domain.* Ph.D. thesis (unpublished), University of Stellenbosch, South Africa, 137pp.

Silver, E.A., Ellis, M.J., Breen, N.A. and Shipley, T.H. (1985). Comments on the growth of accretionary wedges. *Geology*, **13**, 6-9.

Slabber, N. (1995). *The geology and geochemistry of the Bridgetown Formation of the Malmesbury Group, Western Cape province.* M.Sc. thesis (unpublished), University of Stellenbosch, 99pp.

Smith, J.V. (1974). *Feldspar minerals, 1. Crystal Structure and Physical Analysis: Theory and Algorithms.* John Wiley and Sons, New York, 828pp.

South African Committee for Stratigraphy (SACS), (1971). South African Code of Stratigraphic Terminology and Nomenclature. *Transaction of the Geological Society of South Africa*, **74**, 111-131.

South African Committee for Stratigraphy (SACS). (1980). *Stratigraphy of South Africa. Part 1* (Comp. L. E. Kent). Lithostratigraphy of the Republic of South Africa, SW Africa/Namibia, and the Republics of Bophuthatswana, Transkei and Venda. *Handbook of the Geological Survey of South African*, **8**, 696pp.

Spear, F.S. (1995). *Metamorphic Phase Equilibria and Pressure-Temperature-time Paths*. 2nd Edition. Mineralogical Society of America. Monographs, Michigan, USA.

Stanistreet, I.G., Kukla, P.A. and Henry, G. (1991). Sedimentary basinal responses to a Late Precambrian Wilson Cycle: the Damara orogen and Nama foreland, Namibia. *Journal of African Earth Sciences*, **13**, 141-156.

Stephenson, E.L., Maltamn, A.J. and Knipe, R.J. (1994). Fluid flow in actively deforming sediments: 'dynamic permeability' in accretionary prisms. *In:* Parnell, J (Editor). *Geofluids: Origin, Migration and Evolution of Fluids in Sedimentary Basins.* Geological Society Special Publication, 78, pp 113-125.

Stuwe, K. (1998). Tectonic constraints on the timing relationships of metamorphism, fluid production and gold-bearing quartz vein emplacement. *Ore Geology Reviews,* **13**, 219-228.

Sutherland, R., Davey, F., Beavan, J. (2000). Plate boundary deformation in South Island, New Zealand, is rel;ated to inherited lithospheric structure. *Earth and Planetary Science Letters*, **177**, 141-151.

Swanenberg, H.E.C. (1979). Phase equilibria in carbonic systems, and their application to freezing studies of fluid inclusions. *Contributions to Mineralogy and Petrology,* **68**, 303-306.

Swingler, (1998). *Progress Report of the Spitskop Gold Prospect, Malmesbury Project, Swartland, Western Cape Province, Republic of South Africa.* Company Report (Unpublished),13pp.

Tankard, A.J., Jackson, M.P.A., Eriksson, K.A., Hobday, D.K., Hunter, D.R. and Minter, W.E.L. (1982). *Crustal evolution of Southern Africa.* Springer-Verlag, New York. 523pp.

Taylor, B.E. (1986). Origin and isotopic characteristics of mother Lode hydrothermal fluids and gold deposits with comparison to Archean analogues. *In:* Chapter, A. M. (Editor) *Gold `86. An Internatation Symposium on the Geology of Gold Deposits.* Toronto, 148-150.

Taylor, G.H. (1971). Carbonaceous matter: a guide to the genesis and history of ores. *Society of Mining Geology, Japan, Special Issue,* **3**, 283-288.

Teagle, D.A.H., Norris, R.J. and Craw, D. (1990). Structural controls on gold-bearing quartz mineralization in a duplex thrust system, Hyde-Macreas shear zone, Otago schist, New Zealand. *Economic Geology,* **85**, 1711-1719.

Thamm, A.G. (1993). Lithostratigraphy of the Piekenierskloof Formation (Table Mountain Group). *SACS Lithostratigraphy Series*, **27**, 1.

Theron, J.N. (1984). *The Geology of Cape Town and Environs.* Explanation Sheets 3318CD and DC, and 3418AB, AD and BA. Department of Mineral and Energy Affairs, Geological Survey, Pretoria. 77pp.

Theron, J.N. (1990). 1:250 000 Geological Series, 3318 Cape Town, Geological Survey, Pretoria.

Theron, J.N., Gresse, P.G., Siegfried, H.P. and Rogers, J. (1992). *The Geology of the Cape Town Area.* Explanation Sheet 3318. Department of Mineral and Energy Affairs, Geological Survey, Pretoria. 140pp.

Thompson, A.B. (1976). Mineral reaction in pelitic rocks: I. Prediction of P-T-X (Fe-Mg) phase relations. *American Journal of Science*, **276**, 401-424.

Toogood, D.J. (1976). The structural geology of De Wet and Vink, Cape Province. *Annals of the Geological Survey of South Africa.* **11**, 29-46.

Truter, F.C. (1950). A review of volcanism in the geological history of South Africa. *Proceedings of the Geological Society South Africa*, **52**, xxix-lxxxix.

Tucker, M.E. (1986). *The Field Description of Sedimentary Rocks*. Geological Society of London, Handbook. Open University Press, 112pp.

Twiss, R.J. and Moores, E.M. (1992). *Structural Geology*. Freeman and Company, New York, 532pp.

Van Achterberg, E., Ryan, C.G., Gurney, J.J. and Le Roex, A.P. (1995). PIXE profiling, imaging and analysis using the NAC proton microprobe-unravelling mantle eclogites. *Nuclear Instruments and Methods,* **B104**, 415-426.

Van der Pluijm, B.A. and Marsjak, S. (1997). *Earth Structure: An Introduction to Structural Geology and Tectonics*. McGraw-Hill, 495pp.

Veevers, J.J. (2003). Pan-African is Pan-Gondwanaland: Oblique convergence drives rotation during 650-500 Ma assembly. *Bulletin of the Geological Society of America*, **31**, 501-504.

Visser, H.N. (1967). Distribution and correlation of the Klipheuwel Formation in the Swartland and Sandveld. *Annals Geological Survey of South Africa,* **6** (2), 31-38.

Visser, H.N. and Schoch, A.E. (1973). The Geology and Mineral Resources of the Saldanha Bay Area. *South African Geological Survey, Pretoria, Memoir,* **63**, 150pp.

Visser, H.N. (1967). Distribution and correlation of the Klipheuwel Formation in the Swartland and Sandveld. *Annals of the Geological Survey of South Africa,* **6** (2), 31-38.

Visser, H.N., De Villiers, J.E., Theron, J.N. and Hill, R.S. (1975). 1:125 000 Geological Series, 3318B Malmesbury, and 3319A Ceres. Geological Survey, Pretoria.

Visser, H.N., De Villiers, J.E., Theron, J.N. and Hill, R.S. (1981). *The Geology of the Area between Ceres and Moorreesburg (In Afrikaans)*. Department of Mineral and Energy Affairs. Open File Report No. 1981-0024.

Vocke, R.D., Hanson, G.N. and Grunenfelder, M. (1987). Rare Earth element mobility in the Roffna Gneiss. *Contributions to Mineral Petrology*, **95**, 145-154.

Von Veh, M.W. (1983). Aspects of sedimentation, structure and tectonic evolution in the Tygerberg Terrane, southwestern Cape Province. *Bulletin of the Precambrian Research Unit, University of Cape Town,* **32**, 84pp.

Von Veh, M.W. (1992). Origin of the Gariep Arc. Abstracts Geocongress 1992. *Geological Society of South Africa*, Johannesburg.

Von Veh, M.W. (1993). The stratigraphy and structural evolution of the Late Proterozoic Gariep Belt in the Sendelingsdrift-Annisfontein area, northwestern Cape Province. *Bulletin of the Precambrian Research Unit, University of Cape Town,* **38**, 174pp.

Walshe, J.L. (1986). A six-component chlorite solid solution model and the conditions of chlorite formation in hydrothermal and geothermal systems. *Economic Geology,* **81**, 681-703.

Walther, J.V. and Orville, P.M. (1982). Volatile production and transport in regional metamorphism. *Contributions to Mineralogy and Petrology*, **79**, 252-257.

Winchester, J. A. and Floyd, P. A. (1977). Geochemical discrimination of different magma series and their differentiation products using immobile elements. *Chemical Geology*, **20**, 325-343.

Winchester, J.A and Max, M.D. (1984). Element mobility associated with syn-metamorphic shear zones near Scotchport, NW Mayo, Ireland. *Journal of Metamorphic Geology,* **2**, 1-11.

Wilkinson, J.J., and Johnston, J.D. (1996). Pressure fluctuations, phase separation and gold precipitation during seismic fracture propagation. *Geology*, **24**, 395-398.

Zang, W. and Fyfe, W.S. (1995). Chloritisation of the hydrothermally altered bedrock at the Igarape Bahia gold deposit, Carajas, Brazil. *Mineralium Deposita*, **30**, 30-38.

APPENDIX A

PUBLICATIONS

Below is a list of papers and abstracts from the thesis as of November 2003.

Papers

Belcher, R.W., Rozendaal, A. and Przybylowicz, W.J. (2003). Trace element zoning in pyrite determined by PIXE elemental mapping: evidence for varying ore-fluid composition and electrochemical precipitation of gold at the Spitskop deposit, Saldania Belt, South Africa. *Journal of X-Ray Spectrometry, in press.*

Belcher, R.W. and Kisters, A.F.M. (2003). Lithostratigraphic correlations in the western branch of the Pan-African Saldania belt, South Africa: the Malmesbury Group revisited. *South African Journal of Geology, in press.*

Kisters, A.F.M., **Belcher, R.W.**, Armstrong, R.A., Scheepers, R., Rozendaal, A and Jordaan, L.S. (2002). Timing and kinematics of the Colenso Fault; The Early-Paleozoic shift from collisional to extensional tectonic in the Pan-African Saldania Belt, South Africa. *South African Journal of Geology*, 105, 257-270.

Abstracts

Belcher, R.W., Rozendaal, A. and Kisters, A.F.M. (2000). Quartz-vein hosted Au mineralisation in greenstones of the Neoproterozoic Bridgetown Formation, Saldania Belt, South Africa. *J. African Earth Sciences*, 31. 1A. Special Abstract Issue GSSA 27: Geocongress 2000: A new Millennium on ancient crust.

Belcher, R.W. and Rozendaal, A. (2000). Epithermal Au mineralisation in the Neoproterozoic Malmesbury Group metasediments at Waaihoek, Saldania Belt, South Africa. *J. African Earth Sciences*, 31. 1A. Special Abstract Issue GSSA 27: Geocongress 2000: A new Millennium on ancient crust.

APPENDIX B

1 ANALYTICAL TECHNIQUES

1.1 X-ray fluorescence

Whole rock chemical analyses were done by XRFS on a Philips 1404 Wavelength Dispersive spectrometer, at the University of Stellenbosch. The spectrometer is fitted with a Rh tube, six analyzing crystals, namely: LIF200, LIF220, LIF420, PE, TLAP and PX1 and the detectors are a gas-flow proportional counter, scintillation detector or a combination of the two. The gas-flow proportional counter uses P10 gas, which is a mixture of 90% Argon and 10% Methane. Major elements were analysed on a fused glass bead at 50 kV and 50 mA tube operating conditions and trace elements were analysed on a powder briquette at 60 kV and 40 mA tube operating conditions. Matrix effects in the samples were corrected for by applying theoretical apha factors and measured line overlap factors to the raw intensities measured with the SuperQ Philips software.

1.1.1 Powder briquettes

Powder briquettes were made by mixing 8 g of powdered (300 mesh) sample with 1ml of Miwiol solution. This was allowed to dry in an oven (60°C), until almost dry. It was then removed and re-ground in an agate mortar and compressed in the steel pill-maker at 8 tons for 1 minute. The finished briquette was returned to the oven for final drying.

Detection limits (ppm) are as follows:

Mo	<8-10
Nb	<8-10
Zr	<8-10
Y	<2
Sr	<8-10
U	<4

Rb	<8-10
Th	<8-10
Pb	<8-10
Ga	<3-4
Zn	<3-4
Cu	<5
Ni	<7
Cr	<3-4
Ce	<13
Nd	<7
V	<3-4
Ba	<13
La	<7
Sc	<2
Co	<15

1.1.2 Fusion pennies

2g of the milled samples is heated to 110°C for four hours in a "vitreosil" crucible, to determine the H_2O^- content. The sample is then reweighed and ignited at 1000°C for a minimum of four hours to determine the loss of ignition (LOI). 0.53g of the ignited sample is then combined with 1.5g of the fusion mixture and heated to a minimum of 980°C for 15 minutes till the sample is completely mixed. The sample is then poured into a graphite holder and compressed with an Al-plunger to produce a glass disc.

Detection limits (ppm) are as follows:

SiO_2	0.059
TiO_2	0.015
Al_2O_3	0.049
$Fe_2O_{3(tot)}$	0.013
MnO	0.015
MgO	0.058
CaO	0.006

Na_2O	0.108
K_2O	0.006
P_2O_5	0.005

Additional major and trace element analyses were undertaken at the University of Natal.

1.2 Microprobe analyses

Microprobe analysis was undertaken at Rhodes University on a Joel Superprobe 733. Accelerating voltage was 15 kV, with a beam current of 20 nA , with a counting time of 10 seconds (peaks) and 5 seconds (background) for the elements Mg, Si, Na, Al, K, Ca and Fe, with 20 seconds (peaks) and 10 seconds (background) for the elements Cr, Ti and Ni. Dr. Malcom Roberts and Siska Bramdeo assisted with the analysis. Further microprobe analyses were undertaken at the University of Cape Town (UCT), on a Camebax Microbeam electron microprobe (model MBX). The accelerating voltage was 15 kV, beam current 40 nA, with a counting time of 10 seconds (peaks) and 5 seconds (background). Analysis was done with the assistance of Dr. A. Spath (UCT) and C. Philander (US).

1.3 Scanning electron microscope

Scanning electron microscopy (SEM) was undertaken at the University of Stellenbosch, University of Cape Town, UCT and the Council of Geoscience. Quantitative analyses was undertaken at the University of Stellenbosch on a Leo 1430 VP, with SED, Centaurus backscatter and cathodoluminescence detectors, and at UCT on a Cambridge Stereoscan 440, linked to an Oxford Link ISIS energy dispersive system. Conditions: 20 kV, 1.5 µA (probe current) with a working distance of 13 mm and spot size of 473.

1.4 X-ray defraction analyses

XRD analysis was undertaken at the Geology Department of the University of Stellenbosch, on Philips 1410 diffractometer with the software *Difftech 122*.

1.5 Fluid inclusion studies

Fluid inclusion analysis was undertaken in the microthermometry laboratory at the University of Stellenbosch,. Quartz veins from the different vein sets were chosen in the field and separated from the surrounding host rocks. Double-polished thick sections were made by Mr Hendrikse (US) for selected samples. Descriptions and classifications of inclusions were carried out following Roedder (1984).

1.6 ICP-MS

ICP-MS analysis was undertaken at the University of CapeTown by Dr. A. Spath.

1.7 Gold analyses

Samples for gold analysis were analysed by B & B Laboratories, Johannesburg. A minimum of 25 grams was submitted, which was first milled before analysis. Gold was analysed by fire assay with a minimum detection limit of 3 ppb.

1.8 PIXE microanalyses

Proton-induced X-ray emission (PIXE) micro-analysis was conducted using the nuclear microprobe at the iThemba LABS (previously National Accelerator Centre), Somerset West, South Africa. Both elemental mapping and point analysis were carried out. The facility is based on a 6 MV single-ended Van de Graaff accelerator with Oxford microprobe triplet lenses for beam focussing. Proton currents of the order of 10 nA result in beam spots not exceeding 10 μm. A more detailed description of the facility can be found elsewhere (Churms et al., 1993; Prozesky et al., 1995).

Symbols used for the outcrop descriptions

B	Bedding
c	coarse
diss	disseminated
dk	dark
f	fine
F	fresh
FA	fold axes
Fol	foliation
grn	grain(ed)
h	highly
l	light
Lst	limestone
m	medium
meta	metamorphism
mod	moderate
mst	mudstone
sst	sandstone
tr	trace
TRANS	transposition fabric, containing the
w	weathered
x-bedding	cross-bedding
x-c	cross-cutting

Colours

blk	black
brn	brown
gn	green
gry	grey
oran	orange
purp	purple
silv	silver

APPENDIX B, MAP 1

LOCATION MAP OF OUTCROPS VISITED

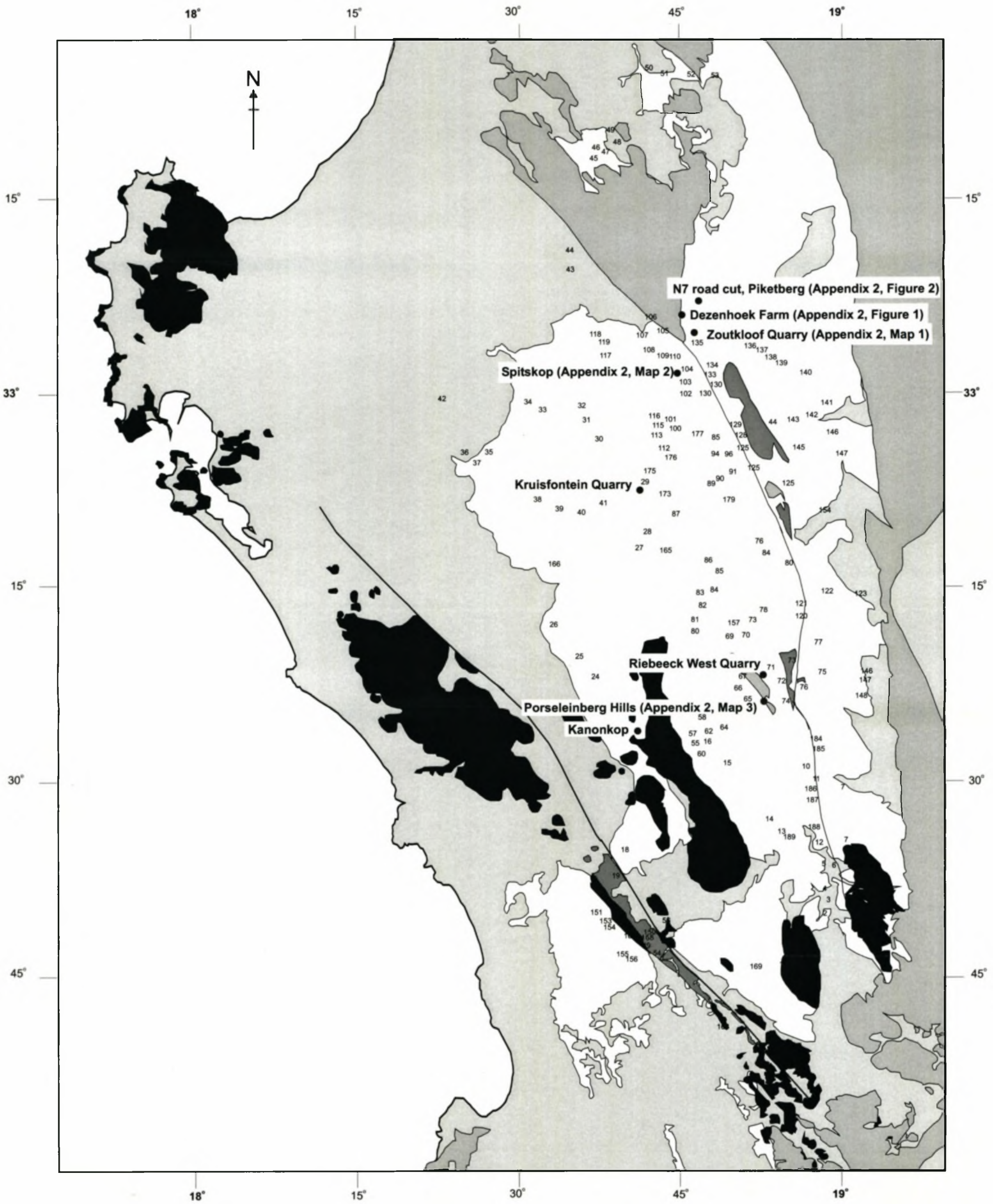

2 OUTCROP DESCRIPTIONS

LOCALITY No.	READINGS	LITHOLOGICAL DESCRIPTION
1	B 53/74°	mst- l. gy, f-grn, no evidence of meta
2	B 72/52°	h. weathered, y-br mst no evidence of meta
3	B 72/88° J 148/90°	mst y/br f-grn
4	B 76/89°	mst y/br (weathered) grn-gy when fresh
5	B 84/90° FA 174/40° AP 186/90°	mst, minor qtz veining, with ser. alt.
6	B 84/85° FA 170/10°	mst. minor veining
7	B 52/90°	mst y/br to red, grn size variation no meta.
8	B 70/90°	mst. bedding prominent
9	B 90/90°	mst. f-grn, red
10	B 106/63°	mst. m-gn minor qtz veining
11	B 102/88° FA 192/32°	mst. Containing fspr, highly weathered
12	Fol 148/28° FA 202/29°	qtz-rich mst, abundant sericite related to veining TRANS
13	B 62/75°	mst y/br, f-grn, highly weathered
14	B 79/30°	mst y/br with thin beds of gry, highly weathered
15	B 50/0°	same as above
16	B 67/50°	mst, f-grn same as above
17	No readings possible	same as above
18	B 82/90°	mst red, highly weathered
19	B 58/58°	Klipheuwel Formation- quartzites, evidence of bedding, x-bedding etc
20	B 44/02° AP 50/90°	mst, f-grn, y/br to r, colour changes denoting bedding, evidence of grain size variation
21	B 130/16°	mst gry, grain size variation, x-cutting qtz veins
22	Fol 230/30° FA 160/20°	Biotite-fsp schist, metamorphic fabric TRANS
23	No readings possible	Biotite-fsp schist, metamorphic fabric TRANS
24	B 66/78°	mst y/cream, f-grn, qtz veining-bedding parallel & x-cutting
25	No readings possible	Same as above
26	No readings possible	Qtz-rich schist, y to off-white, containing qtz fragments (recent cover).
27	J 200-020 28°W	Feldspathic schist, TRANS
28	J 132-312 69°W	Gry-gn feldspathic schist, containing extensive sericite alteration associated with veins.
29	See main thesis/ note books	Kruisfontein Quarry
30	No readings possible	Same lithol as 27
31	Fol 270/40°	f-grn, y-brn mst, strong fol.
32	Fol 262/22°	Mst same as 31
33	Fol 39/38°	y-brn mst (feldspar bearing).
34	Fol 026/50°	Gry-gn feldspathic rock.
35	016/80°	Gn-gry mst minor qtz veins
36	010/75°	Gn-y, m-grn schist
37	No readings possible	Same lithol as 36
38	058/40°	Gritty feldspathic schist, interbedded with gry-gn mst.
39	090/50°	p gn mst
40	042/08°	f-m gn y-brn-r clay?
41	286/40°	f-grn feldspathic, y-gn schist
42	See main thesis/ note books	Hopefield area- Maatjesfontein
43	054/36°	Similar lithology to 42.
44	050/62°	Poor outcrop-highly weathered
45	FA 172/30°	Silv-grn schist, abundant chl and ser. Possibly TRANS
46	FA 146/30°	Same lithology as 45
47	Fol 046/15°	Feldspathic rock, gn-gry when fresh, y-brn when

		weathered, minor qtz veining
48	FA 006/16°	Same as above (47)
49	Fol 048/59°	f-grn, y-brn mst.
50	B 086/80°	Grits/conglom (Piketberg Formation)
51	B 090/80°	Feldspathic & qtz-rich units, f-m grn
52	B 090/89°	Same as above
53	B 132/90°	Same as above
54	B 050/50°	m-grn, purple-orange mst, qtz-rich units
55	B 062/50°	Same as above but more gritty units
56	B 244/78°	Mst, y-brn, with red beds, no gritty beds as above localities
57	B 330/27°	Gry-gn-y, m-grn mst, interbedded with black-grey mst.
58	B 072/50°	f-m gn mst/slst, minor veining
59	Fol 284/48°	Fspr and qtz-rich schists TRANS
60	B 258/49°	Gn (F), y-brn (W) mst
61	Fol 155/20° FA 178/90°	Gn (F), y-brn (W) mst, upright chevron folding
62	FA 139/40°	m-grn feldspathic lithology, qtz veining
63	FA 172/32° AP 163/90°	Same lithology as above
64	B 270/90°	Same as above
65	Fol 228/22°	Fspr-ser schist, gn, TRANS
66	Fol 236/31°	Qtz-ser schist, strong fol. TRANS
67	No readings possible	Poor outcrop, ser-chl schist, TRANS
68	AP 150/42°	Poor outcrop
69	Fol 106/56°	Fspr-ser schist, TRANS
70	Fol 049/18° FA 018/06	Fspr-ser schist, TRANS
71	Fol 050/62° FA 016/32°	Red-brn, m-grn (h. W) TRANS
72	B 096/66°	Fspr-rich lithology
73	B 090/80°	Same as above
74	No readings	Red-brn c-grn, qtz-rich lithol, no deformation
75	B 134/90°	Ser-rich mst, some qtz veins
76	B 282/40°	Red c-grn lithology
77	B 284/76°	Blue-black mst
78	Fol 054/53°	y-brn, qtz-rich lithology
79	Fol 078/46°	Y quartzite
80	Fol 237/33°	Dk gry-gn phyllite, no veining
81	Fol 227/40°	Same as above
82	Fol 106/31°	Qtz-chl-ser schist, abundant boudinaged veins, possible TRANS
83	No readings	y-brn qtz schist passing into y quartzite
84	Fol 079/60°	Qtz schist
85	Fol 060/51°	Same as above
86	Fol 068/47°	Y-brn (W) schist
87	Fol 088/17°	Feldspathic schist
88	Fol 158/90°	y-brn (W) feldspathic rock, gn (F) qtz veining TRANS (90%) sure
89	Fol 166/90°	As above
90	B 166/90°	Mst
91	B 104/90°	y-red mst, colour variations identifying bedding
92	B 126/90°	Pale y-brn (W) feldspathic rock, m-grn
93	B 151/90°	y-brn (W) mst, pale gn (F)
94	B 235/80°	Mst (as above)
95	FA 028/12°	y-brn (W) sericitic schist, chevron folding
96	B 158/90°	-
97	FA 139/32	Qtz-chl-ser schist
98	FA 128/0° 297/36°	Qtz-chl-ser schist
99	FA 140/70, Fol 230/70	-
100	Fol 146/90°	y-brn mst with more feldspathic units, TRANS
101	B140/90°	-
102	B 078/63°	y-brn (W) mst containing sericitic units
103	B 160/90°	Feldspathic schist, m-grn, TRANS
104	FA 316/24°	Fol 060/70°
105	FA 309/10°, 134/9°	Qtz-chl-ser schist
106	FA 322/36°	m-grn, fspr-ser schist
107	Fol 055/79°	m-grn, y-brn mst
108	Fol 079/62°	Qtz-chl-ser schist, TRANS
109	FA 324/52°	Gry-grn schist
110	FA 314/32°	Fspr schist and qtz-chlr-ser schist

111	FA 316/28°	Qtz-chl-ser schist
112	FA 131/14°	Qtz-chl-ser schist
113	FA118/40°	Qtz-chl-ser schist, TRANS
114	Fol 058/56°	y-brn (h W) schist, TRANS
115	Fol 050/60°	Same as above
116	FA 122/18°	Same as above
117	Fol 011/46°	Gn-gry (F) y-brn (W), TRANS ?
118	Fol 026/39°	y-brn feldspathic schist
119	Fol 021/42° FA 044/30°	m-grn, gn lithology, interbedded with gn mst
120	Fol 202/60°	m-grn (h W) gry-blk, little deformation
121	Fol 037/65°	Same as above
122	Fol 270/85°	Same as above
123	Fol 290/86°	Same as above, not as blocky
124	Fol 248/48°	y-brn (W), f to m-grn, iron reach bands (leaching)
125	Fol 172/90°	v.f-grn, pale gn/cream, iron-rich units as above
126	Fol 070/36°	f-gm, dk gn metavolcanics
127	-	See notebook
128	Fol 196/90°	Gry-brn quartzite, f, m-grn mst units, iron-rich units as seen in 124
129	Fol 167/90°	Y, brn, red units, mst, iron-rich units
130	Fol 068/40°	Red-brn (W) sericitic schist, TRANS?
131	Fol 092/31°	y-brn (W) quartz schist containing minor grn mst
132	-	From day field trip last year
133	-	Quartz schist
134	Fol 102/20°	Fspr-ser schist
135	Fol 096/42°	Sericitic schist interbedded with fspr-rich units
136	Fol 070/33°	y-gn mst
137	Fol 080/70°	Mst
138	Fol 080/80°	Mst
139	Fol 351/90°	y-brn mst iron-rich lithology
140	Fol 070/35°	y-brn mst as above
141	Fol 014/90°	y-brn m-grn (similar to above)
142	Fol 002/90°	f-grn, gn
143	Fol 000/90°	Mst
144	Fol 358/90°	Same as above, y-brn, v. sericitic in places related to veins
145	006/90°	Same as above
146	000/90°	Same as above
147	007/90°	Same lithology pale gn (F), y-brn (W)
148	Fol 121/34°	m-grn, y-brn with iron-rich layers
149	-	Klipheuwel Quarry- see note book
150	B 299/64°	y-brn mst (Tygerberg Formation)
151	B 260/52°	Same as above
152	B 248/80°	Same as above
153	Fol 226/48°	r-brn mst, classic Moorreesburg Formation
154	-	Similar lithology to 152
155	B 108/90°	F to m-grn, y-brn lithol, well foliated (Tygerberg Formation)
156	B 354/90°	y-brn mst, with pale gn and red beds.
157	Fol 112/24°	y-brn (W) mst
158	Fol 267/48°	Varying colour, m to c-grn mst similar to above mst
159	Fol 130/30°	Same as above
160	Fol 120/42°	Fspr-ser lithology
161	Fol 134/22°	Fspr-ser lithology, qtz veins & ser alteration
162	Fol 140/20°	Same as above
163	Fol 134/12°	Same as above
164	Fol 131/40°	Same as above, qtz veining & ser alteration
165	Fol 040/0°	Ser alteration
166	Fol 32/80°	Pale gry/gn mst (F) y-brn (W)
167	-	m-grn mst, differs from other Tygerberg mst
168	B 238/80°	y-brn (W) mst, similar to mst above
169	B 246/85°	y-brn (W) pale grn (F), m-grn mst, minor qtz veins
170	Fol 260/10°	Gry/gn, m to c-grn mst, qtz-rich lithology, similar to fspr schist, TRANS
171	-	Fspr-ser schist, pale gn-cream, TRANS
172	FA 120/20°	Qtz schist, same as seen at Riebeek Kasteel
173	Fol 085/15°	Qtz-ser-chl schist (Spitskop schist)

174	Fol 076/80°	Same as 90
175	Fol 320/08°	y-brn quartz schists
176	Fol 074/35°	y-brn quartz schist (Klipplaat Formation)
177	Fol 078/70°	Pale gn (F), ser-rich, extensive qtz veining
178	Fol 225/40°	h. W f-grn mst, extensive qtz veining
179	B 222/74°	f-grn, gn-gry mst
180	B 198/76°	f-grn mst
181	B 202/84°	f-grn mst
182	B 237/80°	Poor outcrop- f-grn mst
183	Fol 280/14°	Qtz-rich schist
184	B 063/40°	m-grn lithology, sericite bearing
185	Fol 172/90°	y-brn qtz schist (Klipplaat Formation) TRANS
186	Fol 024/32°	Klipplaat Formation
187	Fol 036/24°, FA 126/20°	Qtz-rich schist
188	Fol 068/18°	Same as above, TRANS
189	Fol 254/14°, FA 160/40°	F to m-grn units, h W, TRANS?
190	-	h. W, clay outcrop
191	B 079/80°	Very poor outcrop
192	B 045/64°	Massive sandstone, Tygerberg Formation

3 SAMPLE DESCRIPTIONS (REGIONAL)

Sample No.	Description	Locality
T1	Quartz vein from metasedimentary (Tygerberg Terrane) Located within main foliation.	Tygerberg.
T2	Quartz vein from metasediment (Tygerberg Terrane) Located within main foliation.	Tygerberg.
T3	Mylonite (orientated).	Darling.
T4	Malmesbury hornfels.	Sea Point, Cape Town.
T5	Metasedimentary rock.	Mouille Point.
T6	Metasedimentary rock.	Tygervalley.
T7	Metasedimentary rock (Zone K).	Bloubergstrand.
T8	Metavolcanic rock (Zone J).	Bloubergstrand.
T9	Metasedimentary rock (Zone I).	Bloubergstrand.
T10	Metasedimentary rock.	Bloubergstrand.
T11	Metasedimentary rock.	Robbin Island.
B1	Qtz-muscovite schist.	Koornlandsdrift, S of Riebeeck Kasteel.
B2	Grit, Piketberg Formation.	south of Piketberg.
B3	Marble, Piketberg Formation.	South of Piketberg.
B4	Grit.	Piketberg Formation, south of Piketberg.
B5	Grit/ conglomerate.	Piketberg Formation, south of Piketberg.
B6	Grit/ conglomerate.	Piketberg Formation, south of Piketberg.
B7	Grit/ conglomerate.	Piketberg Formation, south of Piketberg.
B8	Grit/ conglomerate.	Piketberg Formation, south of Piketberg.
B9	Grit/ conglomerate.	Piketberg Formation, south of Piketberg.
B10	Grit/ conglomerate.	Piketberg Formation, south of Piketberg.
B11	Grit/ conglomerate.	Piketberg Formation, south of Piketberg.
B12	Grit/ conglomerate.	Piketberg Formation, south of Piketberg.
B13	Grit/ conglomerate.	Piketberg Formation, south of Piketberg.
B14	Grit/ conglomerate.	Piketberg Formation, south of Piketberg.
B15	Grit/ conglomerate.	Piketberg Formation, south of Piketberg.
SW1	Quartz vein located within foliation (Type 1).	Spitskop.
SW2	Quartz vein located within foliation (Type 1).	Spitskop.
SW3	Quartz vein located within foliation (Type 1).	Spitskop.
SW4	Quartz vein located within foliation (Type 1).	Spitskop.
SW5	Quartz vein from Chert at Spitskop.	Spitskop.
SW6	Chert at Spitskop.	Spitskop.
SW7	Chlorite schist.	Moorreesburg Quarry.
SW8	Chlorite schist.	Moorreesburg Quarry.
SW9	Chlorite schist.	Moorreesburg Quarry.
SW10	Chlorite schist.	Moorreesburg Quarry.

SW11	Chlorite schist.	Moorreesburg Quarry.
SW12	Quartz-rich chlorite schist.	Moorreesburg Quarry.
SW13	Quartz-rich chlorite schist.	Moorreesburg Quarry.
SW14	Quartz-rich lithology.	Riebeeck Kasteel.
SW15	Quartzite (Klipplaat Formation).	Botmansdrift.
SW16	Quartzite (Klipplaat Formation).	Botmansdrift.
SW17	Porseleinberg Formation.	
SW18	Porseleinberg Formation.	
SW19	Quartz veins.	Kersfontein.
SW20	Quartz veins.	Riebeeck Kasteel.
SW21	Chlorite schist (orientated).	Moorreesburg Quarry.
SW22	Chlorite schist (orientated).	Moorreesburg Quarry.
SW23	Chlorite schist (orientated).	Moorreesburg Quarry.
SW24	Chlorite schist (orientated).	Moorreesburg Quarry.
SW25	Chlorite schist (orientated).	Moorreesburg Quarry.
SW26	Quartz veins and chlorite alteration envelopes, Porseleinberg.	Porseleinberg Formation.
SW27	Quartz veins and chlorite alteration envelopes.	Riebeeck Kasteel.
SW28	Quartz veins and chlorite alteration envelopes.	De Hoek Quarry.
SW29	Quartz veins and chlorite alteration envelopes.	De Hoek Quarry.
SW30	Graphitic schist.	De Hoek Quarry.
SW31	Lst.	De Hoek Quarry.
SW32	Graphitic schist.	De Hoek Quarry.
SW33	Calcite.	De Hoek Quarry.
BS1	Quartz vein (type 1b) from biotite-feldspar schist.	Kanonkop farm.
BS2	Alteration associated with type 1b vein from BS1 schist.	Kanonkop farm.
BS3	Biotite-feldspar schist.	Kanonkop farm.
BS4	Biotite-feldspar schist.	Kanonkop farm.
Z1	Chlorite schist.	Kruisfontein Quarry.
Z2	Chlorite schist.	Kruisfontein Quarry.
Z3	Chlorite schist.	Kruisfontein Quarry.
Z4	Clay sample.	
Z5	Iron-rich alteration envelope Loc: 42.	42.
Z6	Iron staining from clays Loc: 43.	43.
Z7	f-m mudstone, sporadic veining Loc: 58.	58.
Z8	F mudstone Loc: 48.	48.
Z9	Cross-cutting dyke Loc: 68.	68.
Z10	Quartz schist (Klipplaat Formation).	
QS1	Qtz-fspr-ms schist 1.5m N of vein.	Goudmyn se Kop (outcrop 1).
QS2	Qtz-fspr-ms schist 0.5m N of vein.	Goudmyn se Kop (outcrop 1).
QS3	Transition zone between qtz-fspr-ser and sericite alteration.	Goudmyn se Kop (outcrop 1).
QS4	Qtz-fspr-ms schist 1.2m S of vein.	Goudmyn se Kop (outcrop 1).
QS5	Qtz-fspr-ms schist 2m S of vein.	Goudmyn se Kop (outcrop 1).
QS6	Qtz-fspr-ms schist.	Goudmyn se Kop (outcrop 2).
QS7	Qtz-fspr-ms schist.	Goudmyn se Kop (outcrop 2).
QS8	Qtz-fspr-ms schist.	Goudmyn se Kop (outcrop 2).
VS1	Sericite alteration around vein (Type 1b).	Goudmyn se Kop (outcrop 1).
VS2	Sericite alteration around vein (Type 1b).	Goudmyn se Kop (outcrop 1).

VS3	Sericite alteration around vein (Type 1b).	Goudmyn se Kop (outcrop 1).
VS4	Sericite alteration around vein (Type 1a).	Goudmyn se Kop (outcrop 2).
VS5	Sericite alteration around vein (Type 1a).	Goudmyn se Kop (outcrop 2).
VS6	Sericite alteration around vein (Type 1a).	Goudmyn se Kop (outcrop 2).
FL1	Qtz-rich schist with sugary texture.	Goudmyn se Kop (outcrop 2).
FL2	Qtz-rich schist with sugary texture.	Goudmyn se Kop.
FL3	Qtz-rich schist with sugary texture.	Goudmyn se Kop.
FL4	Sericitic schist.	Goudmyn se Kop.
FL5	Sericitic schist.	Goudmyn se Kop.
FL6	Highly weathered schist with powdery texture.	Goudmyn se Kop.
FL7	Feldspathic schist.	Goudmyn se Kop.
FL8	Arenaceous sedimentary lithology.	Goudmyn se Kop.
FL9	Sericite-chlorite schist (alteration envelope).	Goudmyn se Kop.
FL10	Major quartz vein with sericite and chlorite alteration.	Goudmyn se Kop.
FL11	Quartz vein within the foliation.	Goudmyn se Kop.
FL12	Milky/clear quartz vein.	Goudmyn se Kop.
FL13	Clear to smoky quartz vein.	Goudmyn se Kop.
FL14	Clear to smoky quartz vein.	Goudmyn se Kop.
FL15	Milky white quartz vein with sericite alteration.	Goudmyn se Kop.
FS1	Feldspathic schist.	Goudmyn se Kop.
FS2	Feldspathic schist.	Goudmyn se Kop.
FS3	Feldspathic schist.	Goudmyn se Kop.
FS4	Feldspathic schist.	Goudmyn se Kop.
S1	Sericitic schist.	Goudmyn se Kop.
S2	Sericitic schist.	Goudmyn se Kop.
S3	Sericitic schist.	Goudmyn se Kop.
T1	Transition zone between qtz-fspr-ser and sericite alteration.	Goudmyn se Kop.
KF1	Quartz schist (characteristic of the Berg River Formation.	Kruisfontein Quarry.
KF2	Quartz schist (characteristic of the Berg River Formation.	Kruisfontein Quarry.
KF3	Chlorite schist (characteristic of the Berg River Formation).	Kruisfontein Quarry.
KF4	Chlorite schist (characteristic of the Berg River Formation).	Kruisfontein Quarry.
KF5	Chlorite schist (characteristic of the Berg River Formation).	Kruisfontein Quarry.
MG1		Moorreesburg, south of Riebeek Kasteel, 74.
MG2	Grey clay.	Porterville, Blikhuis Station, 147.
MG3	Grey/green mst.	Porterville, Nooitgedacht, 123.
MG4	Yellow/brown clay (sericite).	Moorreesburg, turn off to Malansdam, 157.
MG5	Quartz-ser schist.	Moorreesburg, Kanonberg, 160/161.
MG6		Moorreesburg, Donkerskloof, 40.
MG7	Brown clay.	Moorreesburg, near Hopefield, 36.
MG8	Grey clay.	Moorreesburg, Matjiesfontein, 42.
MG9	Grey clay.	Moorreesburg, Koperfontein, 136/137.
MG10	Grey clay.	Moorreesburg, Eendrag, 166.
MG11	m-grained grey quartz rock.	Tygerberg, Goedommoeting, 155.
MG12	Purple/purple mst.	Tygerberg, west of Klipheuwel, 150.

MG13	Grey/yellow mst.	Tygerberg, se of Philadelphia, 167.
MG14	Yellow/purple clay (m-grained).	Tygerberg, se of Philadelphia, 168.
MG15	Yellow/purple clay (m-grained).	Tygerberg, Otterkuil, 169.
MG16	Pale yellow/grey mst.	Porterville, Ouitvlug, 181.
BT1	Metavolcanic rock (Bridgetown Formation).	Bridgetown Formation.
BT2	Graphitic(?) schist (Bridgetown Formation).	Bridgetown Formation.
BT3	Metavolcanic rock (Bridgetown Formation).	Bridgetown Formation.
BT4	Metavolcanic rock (Bridgetown Formation).	Bridgetown Formation.
BT5	Metavolcanic rock (Bridgetown Formation).	Bridgetown Formation.
MV1	Metavolcanic rock.	East of Moorreesburg.
X1	Metasedimentary xenolith from Darling granite.	Rheboksfontein, Darling.
X2	Metasedimentary xenolith from Darling granite.	Rheboksfontein, Darling.
X3	Metasedimentary xenolith from Darling granite.	Rheboksfontein, Darling.
X4	Metasedimentary xenolith from Darling granite.	Rheboksfontein, Darling.
X5	Metasedimentary xenolith from Darling granite.	Rheboksfontein, Darling.
X6	Metasedimentary xenolith from Darling granite.	Rheboksfontein, Darling.

Sample	Brief description
S1	Gry-grn mica schist (highly weathered) (Spitskop).
S2	Well-foliated gry-grn c-m schist (Spitskop).
S3	Boudinaged qtz vein within qtz-c-s- schist (Spitskop).
S4	2 m vertically above S3 (Spitskop).
S5	Qtz-c-m schist, very qtz-rich, just below chert, highly foliated (Spitskop).
S6	Qtz vein parallel to foliation, in an area of extensive qtz veining (Spitskop).
S7	Highly weathered grn-brn mica schist, containing qtz veins parallel to foliation (Spitskop).
S8	50 cm from S7, strongly foliated mica schist (Spitskop).
S9	Dark grn-gry schist, containing large qtz-veins (Spitskop).
S10	Grn-gry mica schist, strong foliation, taken form outcrop showing excellent refolding topography (Spitskop).
S11	Strong crenulation folding with jointing, d. grn schist, with no quartz veining (Spitskop).
S12	Highly feldspathic outcrop, which is highly weathered. Outcrop is a good example of steep zones (Spitskop).
S13	Taken 1m from S12, but with folded rock adjacent to steep zone, grn c-m schist with good foliation (Spitskop).
S14	Qtz vein parallel to foliation, within a grn schist. Vein is up to 25 mm thick (Spitskop).
S15	Same as above (S14) (Spitskop).
A1	Orientated thin section (Spitskop).
A2	Qtz vein, parallel to foliation, as part of fold, with extensive chlorite alteration (Spitskop).
A3	Qtz vein, parallel to foliation, as part of fold, with extensive chlorite alteration (Spitskop).
A4	Orientated thin section (Spitskop).
A5	Qtz vein, parallel to foliation (Spitskop).
A6	Qtz vein, parallel to foliation (Spitskop).
A7	x-cutting veins (1-3 mm wide), laterally discontinuous (Spitskop).
A8	Major qtz vein (8 cm wide), parallel to foliation + chlorite alteration (Spitskop).
A9	Qtz vein, parallel to foliation, as part of fold, with extensive chlorite alteration (Spitskop).
B1	Qtz vein parallel to the foliation (2cm wide) (Spitskop).
C1	Qtz vein, parallel to foliation (Spitskop).
C2	Qtz vein, parallel to foliation (Spitskop).
C3	Minor x-cutting vein (Spitskop).
C4	X-cutting vein (Spitskop).

C5	Qtz vein, parallel to foliation (Spitskop).
C6	X-cutting vein (Spitskop).
C7	X-cutting vein (Spitskop).
C8	X-cutting vein (Spitskop).
H1	Qtz vein, parallel to foliation (200/62) (Spitskop).
H2	Schist containing veins x-cutting the foliation + py and minor magnetite (Spitskop).
H3	Very little veining, outcrop appears to be resistant to weathering, very feldspathic (Spitskop).
H4	Feldspathic-rich sample (Spitskop).
H5	Qtz-chl-sericite-rich sample (Spitskop).
H6	Chlorite alteration from vein parallel to foliation. Alteration envelope approx. 5cm wide (Spitskop).
H7	Chlorite alteration from vein parallel to foliation. Alteration envelope approx. 3cm wide (Spitskop).
H8	Highly siliceous outcrop, on hill opposite Spitskop, to weathered for any measurements (Spitskop).
H9	Highly siliceous outcrop, on hill opposite Spitskop, possible marking fault (Spitskop).
H10	Silica-rich outcrop (220/15) marking fault? (Spitskop).
H11	Highly weathered greenschist from road cutting (Spitskop).
H12	Highly weathered greenschist from road cutting (Spitskop).

4

SAMPLE DESCRIPTIONS (SPITSKOP)

NB, SK00-00 =drill hole number from Swingler (1998) and depth down hole, e.g. SK14-10 is drill hole 14 at a depth of 10m.

Sample	Petrographic description	Quartz	Chlorite	Sericite	Feldspar	Carbonate	Talc
SK1-21	QTZ-FSPR-SER-SCHIST	80	2	8	10	-	-
SK1-43	CHL-SER SCHIST	20	45	35	-	-	-
SK1-53	CHL-SER SCHIST	25	40	35	-	-	-
SK1-55	SER-CHL SCHIST	20	30	50	-	-	-
SK2-01	SER-CHL SCHIST	20	25	55	-	-	-
SK2-31	SER-CHL SCHIST	20	30	40	-	-	-
SK3-12	QTZ-FSPR-SER-SCHIST	50	5	30	15	-	-
SK12-17	CHL-SER SCHIST	25	45	30	-	-	-
SK12-31	-	-	-	-	-	-	-
SK12-73	QTZ-FSPR-SER-SCHIST	55	10	20	15	-	-
SK14-11	-	-	-	-	-	-	-
SK14-43	QTZ-CHL-SER SCHIST	60	30	10	2	-	-
SK14-59	QTZ-CHL-SER SCHIST	70	25	5	Tr	-	-
SK16-25	-	-	-	-	-	-	-
SK16-51	SER-CHL SCHIST	25	30	45	-	-	-
SK16-61	SER-CHL SCHIST	15	35	50	-	-	-
SK17-13	QTZ-FSPR-SER-SCHIST	50	15	20	15	-	-
SK18-48	QTZ-FSPR-SER-SCHIST	45	10	25	20	-	-
SK18-65	-	-	-	-	-	-	-
SK18-77	-	-	-	-	-	-	-
SK19-19	QTZ-CHL-SER SCHIST	65	20	10	1	-	-
SK19-31	-	-	-	-	-	-	-
SK19-37	-	-	-	-	-	-	-
SK19-49	QTZ-CHL-SER SCHIST	65	20	15	Tr	-	-
SK20-10	QTZ-CHL-SER SCHIST	75	15	10	Tr	-	-
SK20-19	QTZ-CHL-SER SCHIST	70	20	10	Tr	-	-
SK21-67	QTZ-FSPR-SER-SCHIST	55	10	25	10	-	-
SK23-03	-	-	-	-	-	-	-
SK23-31	QTZ-FSPR-SER-SCHIST	50	10	20	20	-	-
SK23-79	SER-CHL SCHIST	20	30	50	-	-	-
SK23-61	-	-	-	-	-	-	-
SK24-31	QTZ-CHL-SER SCHIST	70	5	15	10	-	-
SK24-61	SER-CHL SCHIST	20	35	45	-	-	-
SK24-94	SER-CHL SCHIST	25	25	50	-	-	-
SK25-51	QTZ-CHL-SER SCHIST	60	20	15	5	-	-
SK25-63	CHL-SER SCHIST	35	40	35	-	-	-
SK25-77	CHL-SER SCHIST	20	45	30	-	-	-
SK31-27	QTZ-CHL-SER SCHIST	60	25	15	-	-	-
SK31-76	EQUAL CHL-SER SCHIST	25	35	35	-	5	-
SK32-29	QTZ-CHL-SER SCHIST	60	30	10	Tr	-	-

SK32-51	QTZ-CHL-SER SCHIST	70	20	30	Tr	-	-
SK32-65	QTZ-CHL-SER SCHIST	60	15	20	-	5	-
SK32-69	QTZ-CHL-SER SCHIST	70	20	10	2	-	-
SK32-79	-	-	-	-	-	-	-
SK33-07	-	-	-	-	-	-	-
SK33-51	CHL-SER SCHIST	20	45	25	-	5	-
SK43-21	IMPURE CHERT (CHERT/TALC)	60	20	-	-	-	20
SK43-39	QTZ-CHL-SER SCHIST	70	25	5	Tr	-	-
SK45-29	TALC	5	10	-	-	40	55
SK45-60	SER-CHL SCHIST	20	40	35	-	-	-
SK47-41	GRAPHITIC SCHIST	-	-	-	-	-	-
SK47-49	QTZ-CHL-SER SCHIST	65	20	15	Tr	-	-
SK47-61	QTZ-CHL-SER SCHIST	65	25	10	Tr	-	-
SK57-03	CHERT	90		5	-	-	-
SK60-03	CHERT	90		5	-	-	-
SK61-93	CARBONATE ZONE	5	5	5	85	-	-
SK62-05	-	-	-	-	-	-	-
SK62-23	QTZ-CHL-SER SCHIST	70	20	10	Tr	-	-
SK62-31	QTZ-CHL-SER SCHIST	60	30	10	-	-	-
SK62-49	QTZ-FSPR-SER-SCHIST	65	10	20	10	-	-

Samples from Spitskop (percussion drilling)

* denotes information taken from Swingler (1998).

Location*	Colour*	Alteration*	Au (ppb)*	General description*	Chip sample description
SK01-21	silv. gry, gry-rd-brn	hem.	40	Talc, c-m schist qtz veinlets	Foliation seen, mica layers, though the foliation is not as well formed as in other samples. The quartz veins are blocky, showing orange/brown staining. There is no sulphide mineralisation present.
SK01-43	silv. d. gry	mod. sil.	125	Sil c-m schist + qtz +/-cc veinlets. tr. py. (diss., cuts x-c veinlets.)	Well foliated, showing good layering of chlorite and mica. The foliation is deformed into folds of varying size and shape, (gentle to tight). Quartz veinlets (<1 mm thick) cross-cutting foliation and folds, bearing sulphide mineralisation, which is predominantly pyrite. These veinlets are not laterally continuous and stop abruptly or tail out. Some minor veining <1cm, which contains sulphide mineralisation. Mineralisation occurs in veins and at vein-wall rock boundary. Mineralisation is found in both vein sets. On a whole the sample contains abundant mineralisation in the form of pyrite, with possibly other sulphides. Showing two sets of veining.
SK01-53	silv. d. grn.	mod. sil.		Sil c-m schist + qtz veins.	Mica and chlorite occurring in layers (foliated). Crenulations are also seen on varying scales. Quartz veining occurs between the foliated layers, and is also foliated. There is only minor mineralisation located between the chlorite-mica layers. Possible the presence of bornite, some chalcopyrite, and pyrite.
SK01-55	silv. d gry	mod. sil.	<10	Sil c-m schist + qtz vs.	Description not possible

SK02-01	silv. oran. brn	None	100	W m schist + minor qtz veinlets + tr. MnO.	Little information can be obtained from the limited highly weathered samples. The samples are highly stained (orange), show good layering, and contain a large amount of quartz, found in veins 2-5mm thick.
SK02-31	oran. silv d. grn	None	15	c-m schist + minor qtz veinlets (lineations + crenulations)	Samples show well-formed layering. Some samples are deformed. Under high power tiny, tight folds are seen. Quartz veins occurring between layers varying in size from 3mm –5mm containing slithers of chlorite mica schist. There is no evidence of any mineralisation.
SK03-12	oran. brn	None	170	W. m schist + qtz veins	Highly-weathered. Description not possible.
SK12-17	silv. d gry-grn	mod. sil.	145	Fr silicified c-m-schist + qtz veinlets + tr. py.	Description not possible.
SK12-31	d. silv. grn-blk	mod. sil.	10	Fr silicified c-m-schist + qtz veinlets + tr. py.	Foliation present though poor in these samples. Samples contain extensive sulphide mineralisation, which is not necessarily confined to the quartz veins. The sulphides which are not within the quartz veins are aligned within the foliation.
SK12-73	silv. gry-grn	mod. sil.	<10	Sil. Qtz-c-m schist + vlets. Tr. Py.	Description not possible
SK14-11	Silv. olive grn	None	<10	W m-c schist	Highly-weathered. Description not possible
SK14-43	pale silv, grn-gry	mod. sil.	<10	Qtz-c-m schist + qtz veinlets	Strong foliation seen, contains high concentration of quartz crystals. Crenulation of foliation present. Mineralisation not present.
SK14-59	Silv d. grn gry	mod. sil.	950	Qtz-m-c schist. Qtz veinlets + tr. py.	Good foliation, with folding at right angles to foliation. Quart veins cross-cutting the foliation at right angles. Veins up to 2mm thick containing sulphide mineralisation (pyrite), quartz is opaque in colour.
SK16-25	silv. gry-grn	None	<10	W m-c schist	Highly weathered. Description not possible
SK16-51	silv-blk	mod. sil.	25	M-c schist in places micaceous shale + qtz veinlets.	Good foliation. The quartz veins are >5mm wide, opaque white and cloudy white. Minor veins are 1-2mm wide and crosscut the foliation at right angles. Mineralisation is abundant, located within quartz veins and is orientated at 90 degrees to the foliation. In the major veins the mineralisation is located at the quartz/schist contact.
SK16-61	purp. gry-grn	mod. sil.	<10	M-c schist in places micaceous shale	Description not possible.
SK17-13	silv-oran brn	None	380	W m-schist	Highly weathered but contains a strong foliation, no evidence of folding. Contains quartz veins 2-3mm wide, which occur within the foliation.
SK18-48	med-gry	mod. sil.	<10	Qtz-m schist/minor shale	Description not possible
SK18-65	silv-grn, gry, blk	mod. sil.		Py. micaeous shale + qtz-m schist	Description not possible

SK19-19	silv-grn gry	mod. sil.		Fresh qtz-m-c schist + qtz veinlets	Well-formed foliation, which has been folded at right angles to the foliation direction. Quartz veins 1-2mm wide running parallel to foliation, some sulphide mineralisation associated with veins. Sulphide mineralisation, contains pyrite, occurring within the mica-chlorite-schist, forming euhedral crystals. Sulphides are not associated with the quartz veins.
SK19-31	silv gry	mod. sil.	<10	qtz-m schist	Description not possible
SK19-37	silv-grn gry	mod. sil.	2505	Qtz-m-c schist	Shows very strong folding at right-angle to the foliation direction producing strong folds both on a large and small scale. Slight thickening towards fold hinges, with increase in deformation. The first vein set is folded within the foliation. There is extensive quartz veining up to 3mm thick, though on average less than 1mm thick. The second set cross-cuts the foliation, these veins are sparse and are only minor compared to the first set (<1mm). Mineralisation is seen associated with the quartz veins, sulphides, showing euhedral pyrite cubes, varying in size from 0.1mm upwards. There is also some disseminated pyrite throughout the samples, though predominantly at the vein/host rock boundary. Some of the veins are possibly calcite
SK19-49	med-d gry	mod. sil.	<10	Qtz-m schist	Description not possible.
SK20-10	silv. gry	None	20	Weathered qtz-m-c schist	Highly weathered. Description not possible.
SK20-19	oran, silv-grn d gry	None	<10	Weathered qtz-m-c schist	Highly weathered samples containing orange/brown staining. Good foliation. Extensive veins. The quartz itself is opaque, with orange staining.
SK20-20	oran, silv-grn, dark gry	None	<10	Weathered qtz-m-c schist	Highly weathered samples, which show good foliation. Samples contain a lot of quartz. The quartz veins are predominantly cross-cutting the foliation (2mm thick), veins are opaque white.
SK21-67	d silv gry-gm	mod. sil	<10	Qtz-m-c schist + py.	Description not possible.
SK23-03	oran. brn	None	20	W. m-qtz schist	Highly-weathered. Description not possible.
SK23-31	silv. gry-grn	mod. sil	30	c-m schist + py. diss. xc	Description not possible.
SK23-61	silv. gry-grn	mod. sil	10	m-c schist	Description not possible.
SK23-79	d silv. grn gry	mod. sil.	<10	Qtz-m schist/ c shale	Strong foliation seen, further deformation also seen on a microscopic scale, crenulations are both symmetrical and asymmetrical, from tight to gentle folding. Thickness of foliation appears to be related to the competence of the layers. Quartz veining occurs in many samples, cross-cutting foliation. Major quartz veins are parallel to foliation and are cross-cut by smaller veins. The mineralisation is in contact with the quartz/host rock boundary and within the veins. Some of the crosscutting veins have grown into the foliation as well.

SK24-31	silv, gry grn	mod. sil.		Qtz-m-c schist, rare limonitic staining.	Weak foliation due to the quartz content being high. Both the mica and chlorite are layered. Evidence of deformation of foliation producing S-shape folding. Limonitic staining occurs in patches across some samples. Quartz veining up to 4-5mm thick found within foliation layers. Minor staining (orange/yellow) of quartz veins in places. The second set of veins cross-cuts the foliation at an angle of 60 to 90 degrees. These veins are often stained orange. No mineralisation located.
SK24-61	silv. gry-grn	mod. sil	<10	m-c schist	Description not possible.
SK24-94	med. to l. silv. gry-grn	mod. sil.	55	c-m schist	Description not possible.
SK25-51	silv. gry-grn	mod. sil.	<10	py. qtz veining	Description not possible.
SK25-63	silv, grn bik	mod. sil.	200	c-m schist + qtz veinlets + py. diss., cts + x-c veins.	Shows very good foliation. Two sets of veins, one parallel to the foliation, the other cross-cutting it. Pyrite mineralisation is abundant, associated with the minor quartz veins within the foliation. The crosscutting veins are 1mm wide, containing pyrite. Quartz veins up to 6 mm wide, with foliation not extensive, mineralisation is extensive
SK25-77	silv, gry, bik	mod. sil.	<10	c-m-schist, + qtz veinlets + py.- diss. cts + x-c veins.	Well foliated. Quartz veins (up to 10mm) orientated with the foliation. These contain sulphide mineralisation. There are also veins (<1mm) which cross-cut the foliation at 90 degrees. The quartz is opaque white, containing extensive sulphide mineralisation (euhedral and disseminated). Mineralisation in cross-cutting veins is very high 50-60%. Many of the larger veins contain no mineralisation, but is associated with the smaller veins. The pyrite is well formed and is mostly located at the quartz/chlorite-mica-schist boundary.
SK31-27	silv. med. grn gry	Sil.	305	Crenulated c-m schist, + veinlets + tr. py.	Foliation present, gently folded. Mineralisation seen in the nose of many folds. There are also some cross-cutting veins. Pyrite occurring as well formed crystals. Containing some massive quartz (white/opaque) which is crosscutting earlier veins.
SK32-29	oran, silv-grn bik.	Sil. + chl.	<10	c-m schist, limonitic staining + qtz veins.	Shows strong layering and is well deformed. Quartz veins parallel to foliation. Many of the samples contain black MnO, occurring in the chlorite mica schist and the quartz veins. There are two sets of veins. The first is parallel to the foliation and does not cross-cut the foliation. This is the major set and is up to 6 mm thick. The only mineralisation present is some MnO. The second set crosscuts the foliation and contains mineralisation in the form of euhedral crystals of pyrite (1mm diameter), forming in contact with the quartz/mica schist boundary.
SK32-51	silv. d. gry-grn	mod. sil + chl.	<10	Qtz-c-m schist + m-c schist	Description not possible.

SK32-65	dark silv-grn blk	mod. sil.	3580	Qtz-c-m/Qtz-m-c schist + tr. Py	Strong foliation. Quartz veins, opaque white, 3-10mm wide. Mineralisation extensive within the samples, varying in colour, from purple/blue/turquoise, possible bornite, pyrite also present (euhedral crystals).
SK32-66	d silv, grn, blk	mod. sil.	3580	Qtz-c-m schist + tr. Py	Shows distinct layering, quartz veins, and slight crenulation cleavage and minor folding. Quartz veins (6-7mm wide) occur between the foliated layers No cross-cutting veins are seen in these samples. Main veins are opaque white, some of the larger veins containing slithers of chlorite mica schist. Extensive mineralisation in the veins are well formed euhedral pyrite crystals 1mm across forming at the quartz/chlorite-mica-schist boundary. The mineralisation is confined to the veins and is predominantly pyrite.
SK32-69	d silv. grn blk	mod. sil. + chi.	110	Qtz-c-m schist + tr. Py	Description not possible.
SK32-79	d silv. grn blk	mod. sil. + chl.	<10	Qtz-c-m schist	Description not possible.
SK33-07	oran. bom-silv.-grn-gry	None	15	c-m schist	Highly weathered. Description not possible.
SK33-51	silv. grn-blk	mod. sil. + chl.	<10	c-m schist	Description not possible
SK43-21	oran. brn	None	<10	Chert	Highly-weathered. Description not possible.
SK43-39	silv. grn-gry	sil.	<10	qtz-c-m schist	Description not possible.
SK45-29	oran. d. grn blk	strong chl.	<10	c-talc rock(soapstone?)	Patchy light and dark green rock, with brown staining. Possibly some layering/foliation. Very difficult to obtain any further information.
SK45-60	d. silv, grn blk	mod. sil.	<10	Qtz-c-m schist + tr. Py	Good foliation of mica and chlorite, folding of foliation also present, though mild. Quartz veins parallel to the foliation, and also cross-cutting, both containing extensive sulphide mineralisation. Mineralisation dominantly at the contact with the quartz and the chlorite-mica schist. The veins are 2-3mm wide an opaque in colour.
SK47-41	wh. mar. blk	None	<10	graphite chlorite hematite schist	Description not possible.
SK47-49	light- med. grey	None	<10	Qtz-m-c schist	Well foliated, distinct layering between qtz and phyllosilicates. Quartz veins cross-cutting foliation and occurring parallel to foliation (1-2mm thick), both vein sets opaque in colour.
SK47-61	med. to dark green grey	mod. sil.	<10	Qtz-c-m schist	Many samples contain strong foliation, while others have weaker foliation. The thickness of the veins varies from 1-2mm up to 7-8mm. In strongly foliated samples veins are parallel to the foliation. The quartz is white/opaque. Sulphide mineralisation (undistinguishable), mostly disseminated, not occurring in the veins. There is also limited mineralisation in the quartz veins, containing some euhedral pyrite crystals.

SK47-62	light- med. grey	None	<10	Qtz-m-c schist	Well foliated. The quartz veins occurring at right angles to the foliation (cross-cutting).Quartz veins are 1-2mm thick. No sulphide mineralisation is seen.
SK57-03	red brn	None	350	chert	Highly-weathered. Description not possible.
SK60-03	d. brn gry	None	35	Chert talc + qtz veinlets	Samples very poor, made up of orange/brown stained samples, up to 2cm across. No mineralisation is seen within the chert.
SK61-93	wh. silv. gry	chl. weak sil.	<10	marble	Description not possible.
SK62-05	oran. silv. grn-gry	None	60	m-c schist	Highly weathered. Description not possible.
SK62-23	oran. M. silv-grn-gry	none	1760	Qtz-c-m schist + qtz v. + c-m schist	Foliation seen. The veins are mostly cross-cutting veins at right angle to the foliation. The quartz varies in colour from white to orange; within quartz some highly weathered sulphide minerals. Vein width varies from 1-3mm. No mineralisation seen other than the staining and possibly highly weathered sections.
SK62-31	d. silv. grn-brn	mod. chl-sil.	1455	Qtz-m-c schist + qtz veinlets	The samples all contain orange brown colouration, similar seen in SK62-23, which is approximately 10m up the drillhole. The schists are highly foliated with gentle folding, and crenulations at right angles to the foliation. This has been deformed by cross-cutting quartz veins, which occur as tiny hair veins, up to 1mm wide, and cross-cut oblique to the foliation. There are other veins which are foliation parallel and these are up to 6mm thick. The quartz is predominantly opaque white with minor orange staining possibly related to Fe staining. Pyrite mineralisation is also present, in both euhedral and anhedral crystals occurring within the chlorite-mica-schist/quartz boundary
SK62-49	silv. blk	mod. chl-sil.	<10	c-m- schist + minor qtz-c-m schist	Description not possible.

Sample description Spitskop (quartz veins/alteration)

Sample	Description
F1	Qtz-fspr-s-schist.
	Located 5cm below the lower limit of the quartz zone.
F2	Qtz-fspr-s-schist.
	Located 30cm lower than the lower limit of the quartz zone
F3	Qtz-fspr-s-schist.
	Located 60-70cm lower than the lower limit of the quartz zone.
Q1	Qtz-c-s-schist
	5cm quartz vein, marking the lower limit of the quartz zone.
	Vein is milky white with chlorite alteration halo and extensive
	pits from sulphide weathering.
Q2	Qtz-c-s-schist
	Similar to Q1 in appearance, with iron staining and pock marks.
Q3	Qtz-c-s-schist

	Located in central part of quartz zone, where a series of mm
	thick veins occur in a chlorite-rich zone between the two
	main veins.
Q4	Qtz-c-s-schist
	Similar to above, though vein is greyish in colour with possible
	albite alteration.
Q5	Qtz-c-s-schist
	Top of quartz zone.
H1	Qtz-fspr-s-schist.
	Approximately 50cm above the quartz zone

5 TYPE LOCALITIES

1. Swartland group

1.1 Spitskop area (Berg River formation and Klipplaat member)

The Spitskop area is located on the farms Spitskop and Die Brug. The farms can be reached by following the N7 road, for approximately 20 km north of the town Moorreesburg to the sign indicating the Misverstand Dam Holiday Resort to the right (east). Following this road for approximately 5 km will lead to the farm Spitskop (18° 46' 00" E and 33° 00' 48" S), a further 4 km to the north is the farm De Brug. The Spitskop gold prospect is approximately 3.5 km^2 and is bounded to the east by the Berg River. Outcrops are mainly confined to seasonal streambeds and road cuttings. The rocks of this area are characteristic of the *Berg River formation* and also the *Klipplaat member*. The *Klipplaat member* is best exposed to the immediate east of the Spitskop on the farm Klipplaat (18° 47' 24" E and 33° 00' 33" S).

1.2 Bothmaskloof Pass and Porseleinberg Hills (Berg River formation)

Porseleinberg is situated to the south of Riebeek Kasteel, and forms a prominent N-S orientated range of low-lying hills. The northern extent of these hills is faulted out against Kasteelberg, a northwest-southeast orientated TMS inlier. The main road from Malmesbury to Riebeek Kasteel runs through the northern extremity of Porseleinberg, providing excellent outcrops in the form of road cuttings (Bothmaskloof Pass; 18° 53' 00" E and 33° 23' 50" S). Lithologies in this area are classified as part of the *Berg River formation*.

1.3 Kruisfontein Quarry (Berg River formation)

Kruisfontein Quarry (18°40' 18" E and 33° 06' 52" S) is located approximately 2km north of Moorreesburg, within the farm Biesiesfontein 340. The quarry is situated on

the northwestern slopes of the continuation of Goudmyn Mountains, and is approximately 300m by 75m in size. The quarry provides excellent fresh outcrops of the different lithologies and contact relationships of the Berg River formation, and shows an uninterrupted vertical section through the stratigraphic column.

1.4 De Hoek and Zoutkloof Quarries (De Hoek member)

De Hoek and Zoutkloof Quarries (18° 45' 40" E and 32° 56' 00" S) are located to the south of Piketberg along the N7 national road. Zoutkloof Quarry has been abandoned for numerous years, but mining for limestone continues just to the south at Zoutfontein Quarry. The quarry provides excellent outcrop of both the De Hoek limestone Member and a series of phyllites and graphitic schists classified within the Berg River Formation of SACS (1980). Both the quarries are owned by PPC Cement, and the quarry staff may be contacted by phoning PPC Cement (Piketberg) on 022 913 1100.

1.5 Kanonkop (Kanonkop member)

The farm Kanonkop (18° 40' 00" E and 32° 22' 55" S) is located approximately 10 km north of Malmesbury along the R45 road to Hopefield. Outcrops on this farm are restricted to a ca. 200m long road cutting along the R45. Only one lithology is present: a biotite-muscovite-quartz schist classified as the *Kanonkop member*, which is different in composition from all the other lithologies within the *Swartland group*.

1.6 Bridgetown area (Bridgetown Formation)

The main outcrops of the *Bridgetown formation* are located around the farm Bridgetown (18° 50' 13" E and 32° 06' 19" S) and along strike to the northwest and southeast. The locality has been described in detail by Slabber (1995). The farm Bridgetown can be reached by driving north along the N7 to Moorreesburg, then turning to the east to the farm Goudmyn se Kop (signs directing to the Bridgetown Quarry should be now visible). Follow this road east until it ends at the Berg River; the farm is situated just to the south. Approximately 1-2 km before the Bridgetown farm is reached, a sign to the left directing to the Bridgetown Quarry (contact: 0264

33008) is seen, the quarry provides excellent examples of the dolomites associated with the metavolcanics rocks.

Further localities for the *Bridgetown formation* are the Spitskop and Riviera areas, where rocks have been intersected during drilling. The Spitskop area is described in 1.1, the Riviera area is located to the north of the town Piketberg (approximately 100 km north of Stellenbosch) within the Moutonshoek Valley, on the farms Namaquasfontein 76 and Wilgenhoutdrift 48. Although no outcrops are present, core from the drilling programme of Anglo Gold in the late 1980's is stored by the University of Stellenbosch in the town of Piketberg (contact: Department of Geology; 021 808 3129).

2. Malmesbury Group

2.1 Tygervalley-Philadelphia area (Tygerberg Formation and Bloubergstrand Member)

The type locality for the Tygerberg Formation remains the same as defined by SACS (1980); the hilly terrain between the town of Klipheuwel and Parow. Other exposures are seen along the coast between Sea Point and Bloubergstrand and also on Robben Island. At Bloubergstrand (18° 27' 45" E and 33° 48' 10" S), red volcanic rocks representing the Bloubergstrand Member outcrop.

2.2 Piketberg (Piketberg Formation)

The type locality for this formation also remains the same and is located around the town of Piketberg, on the farms Deeze Hoek and Klein Vogel (6 km north of Piketberg) and in the Verfeld Pass (18° 44' 30" E and 32° 51' 40" S).

2.3 Porterville area (Porterville formation)

This formation is now much more extensive than previously classified. The type locality is still as defined for the Porterville Formation by SACS (1980), but also includes the area to the west, near Porterville along the Assegaaibos River and on the farms Breede Rivier, Pietersvlei and Vredehoek. It also occurs to the west in the hills to the north of Moorreesburg (Koringberg) and around the town of Hopefield.

APPENDIX C

APPENDIX C, 1. Feldspar compositions (Quartz-chlorite-muscovite schist), Spitskop.

	~31-1a	~31-1b	~31-1c	~31-2a	~31-2b	~31-2c	~31-3a	~31-3b	~31-3c	~31-3d	~31-4a	~31-4b	~31-4c	~31-4d	~31-4e	~31-4f	~31-5a	~31-5b	~31-5c	~31-5d
MgO	0.06	0.00	0.00	0.01	0.00	0.00	0.07	0.00	0.00	0.01	0.35	0.00	0.19	0.00	0.07	0.00	0.01	0.10	0.02	0.00
SiO2	69.11	2.96	68.11	68.52	69.51	68.21	67.07	69.13	69.63	67.80	65.42	68.15	68.29	67.71	70.06	68.20	66.24	68.27	68.06	68.19
Na2O	11.67	1.00	11.94	11.85	11.72	11.84	11.88	11.76	12.07	11.90	9.85	11.59	11.87	11.78	11.83	12.03	11.26	11.81	11.77	11.75
Al2O3	19.39	1.04	20.01	19.98	20.02	20.01	20.22	19.88	20.19	20.07	21.56	20.16	20.02	20.10	19.96	20.26	19.36	19.90	20.30	20.20
K2O	0.10	0.00	0.05	0.07	0.07	0.08	0.07	0.09	0.09	0.09	1.86	0.06	0.12	0.07	0.07	0.04	0.08	0.10	0.09	0.05
CaO	0.03	0.01	0.08	0.05	0.05	0.04	0.00	0.03	0.09	0.04	0.01	0.05	0.09	0.00	0.01	0.05	0.01	0.10	0.24	0.01
TiO2	0.05	0.00	0.00	0.00	0.00	0.02	0.00	0.00	0.00	0.00	0.04	0.00	0.01	0.01	0.02	0.00	0.00	0.00	0.00	0.00
Fe2O3	0.08	0.00	0.04	0.13	0.00	0.14	0.02	0.07	0.04	0.03	0.89	0.27	0.13	0.03	0.10	0.15	0.06	0.00	0.08	0.00
MnO	0.05	0.00	0.00	0.01	0.01	0.00	0.01	0.02	0.00	0.00	0.04	0.00	0.00	0.03	0.00	0.00	0.00	0.00	0.00	0.02
Cr2O3	0.01	0.00	0.05	0.04	0.00	0.01	0.07	0.00	0.00	0.00	0.00	0.00	0.00	0.02	0.00	0.00	0.00	0.06	0.02	0.00
O	0.00	8.00	0.00	0.00	0.00	0.00	0.00	0.00	0.00	0.00	0.00	0.00	0.00	0.00	0.00	0.00	0.00	0.00	0.00	0.00
Total	100.54	13.02	100.29	100.67	101.38	100.34	99.40	100.98	102.10	99.94	100.02	100.28	100.71	99.75	102.11	100.74	97.03	100.33	100.56	100.22
Mg	0.01	0.00	0.00	0.00	0.00	0.00	0.02	0.00	0.00	0.00	0.09	0.00	0.05	0.00	0.02	0.00	0.00	0.03	0.00	0.00
Si	12.01	10.84	11.88	11.91	11.97	11.89	11.82	11.96	11.93	11.87	11.56	11.88	11.87	11.87	11.98	11.86	11.92	11.90	11.85	11.89
Na	3.93	7.12	4.04	3.99	3.91	4.00	4.06	3.94	4.01	4.04	3.38	3.92	4.00	4.00	3.92	4.06	3.93	3.99	3.97	3.97
Al	3.97	4.48	4.12	4.09	4.06	4.11	4.20	4.05	4.08	4.14	4.49	4.14	4.10	4.15	4.02	4.15	4.11	4.09	4.16	4.15
K	0.02	0.02	0.01	0.02	0.01	0.02	0.01	0.02	0.02	0.02	0.42	0.01	0.03	0.01	0.01	0.01	0.02	0.02	0.02	0.01
Ca	0.01	0.02	0.01	0.01	0.01	0.01	0.00	0.01	0.02	0.01	0.00	0.01	0.02	0.00	0.00	0.01	0.00	0.02	0.04	0.00
Ti	0.01	0.00	0.00	0.00	0.00	0.00	0.00	0.00	0.00	0.00	0.01	0.00	0.00	0.00	0.00	0.00	0.00	0.00	0.00	0.00
Fe2+	0.01	0.00	0.01	0.02	0.00	0.02	0.00	0.01	0.01	0.00	0.13	0.04	0.02	0.00	0.01	0.02	0.01	0.00	0.01	0.00
Mn	0.01	0.00	0.00	0.00	0.00	0.00	0.00	0.00	0.00	0.00	0.01	0.00	0.00	0.00	0.00	0.00	0.00	0.00	0.00	0.00
Cr	0.00	0.00	0.01	0.01	0.00	0.00	0.01	0.00	0.00	0.00	0.00	0.00	0.00	0.00	0.00	0.00	0.00	0.01	0.00	0.00
Cation Total	19.98	22.49	20.08	20.05	19.97	20.06	20.12	19.99	20.05	20.09	20.09	20.01	20.09	20.06	19.97	20.10	20.00	20.06	20.06	20.03
X (Si+Al)	15.98	15.32	16.00	16.00	16.03	16.01	16.01	16.01	16.00	16.01	16.05	16.03	15.98	16.03	16.00	16.01	16.03	15.99	16.01	16.04
Z (rest)	4.00	7.16	4.08	4.05	3.94	4.05	4.10	3.98	4.05	4.07	4.03	3.98	4.11	4.03	3.97	4.10	3.96	4.07	4.05	3.99
An	0.1	0.3	0.4	0.2	0.2	0.2	0.0	0.1	0.4	0.2	0.0	0.3	0.4	0.0	0.0	0.2	0.1	0.4	1.1	0.1
Ab	99.3	99.5	99.4	99.4	99.4	99.4	99.6	99.4	99.1	99.3	88.9	99.4	99.0	99.6	99.6	99.5	99.5	99.0	98.4	99.6
Or	0.5	0.3	0.3	0.4	0.4	0.5	0.4	0.5	0.5	0.5	11.1	0.4	0.6	0.4	0.4	0.2	0.5	0.5	0.5	0.3

APPENDIX C, 1. Feldspar compositions (Quartz-chlorite-muscovite schist), Kruisfontein.

	01-273-1a	01-273-1b	01-273-1c	01-273-1d	01-273-2a	01-273-2b	01-273-2c	01-273-2e	01-273-3a	01-273-3b	01-273-3c	01-273-3d
MgO	0.00	0.00	0.00	0.08	0.00	0.00	0.01	0.00	0.00	0.00	0.00	0.00
SiO2	68.65	68.36	64.59	67.81	67.62	67.42	68.18	68.35	70.24	72.75	60.58	68.82
Na2O	11.90	12.10	10.07	11.86	12.12	12.09	11.99	12.32	11.71	10.72	12.09	11.72
Al2O3	20.08	19.99	19.54	19.60	20.01	20.16	20.43	20.54	18.98	17.45	18.45	19.56
K2O	0.07	0.04	0.06	0.07	0.05	0.07	0.06	0.08	0.03	0.02	0.06	0.07
CaO	0.18	0.23	0.09	0.11	0.19	0.17	0.18	0.11	0.08	0.15	0.08	0.19
TiO2	0.01	0.04	0.05	0.00	0.02	0.01	0.01	0.00	0.01	0.02	0.00	0.07
FeO	0.04	0.12	0.09	0.08	0.12	0.08	0.21	0.00	0.12	0.11	0.13	0.13
MnO	0.00	0.00	0.02	0.00	0.00	0.01	0.00	0.00	0.00	0.00	0.96	0.01
Cr2O3	0.00	0.05	0.00	0.01	0.01	0.07	0.01	0.00	0.05	0.00	0.03	0.01
O	0.00	0.00	0.00	0.00	0.00	0.00	0.00	0.00	0.00	0.00	0.00	0.00
Total	100.92	100.93	94.50	99.63	100.13	100.07	101.07	101.39	101.21	101.22	92.38	100.56
Mg	0.00	0.00	0.00	0.02	0.00	0.00	0.00	0.00	0.00	0.00	0.00	0.00
Si	11.90	11.87	11.89	11.91	11.84	11.82	11.82	11.82	12.11	12.45	11.64	11.97
Na	4.00	4.07	3.60	4.04	4.11	4.11	4.03	4.13	3.91	3.55	4.50	3.95
Al	4.10	4.09	4.24	4.06	4.13	4.16	4.17	4.18	3.85	3.52	4.18	4.01
K	0.01	0.01	0.01	0.02	0.01	0.02	0.01	0.02	0.01	0.00	0.02	0.02
Ca	0.03	0.04	0.02	0.02	0.03	0.03	0.03	0.02	0.02	0.03	0.02	0.04
Ti	0.00	0.01	0.01	0.00	0.00	0.00	0.00	0.00	0.00	0.00	0.00	0.01
Fe2+	0.01	0.02	0.01	0.01	0.02	0.01	0.03	0.00	0.02	0.02	0.02	0.02
Mn	0.00	0.00	0.00	0.00	0.00	0.00	0.00	0.00	0.00	0.00	0.16	0.00
Cr	0.00	0.01	0.00	0.00	0.00	0.01	0.00	0.00	0.01	0.00	0.00	0.00
Cation Total	20.06	20.12	19.78	20.08	20.15	20.16	20.11	20.17	19.92	19.57	20.53	20.01
X (Si+Al)	16.00	15.96	16.13	15.97	15.97	15.98	16.00	16.00	15.96	15.97	15.82	15.97
Z (rest)	4.06	4.16	3.65	4.11	4.18	4.18	4.11	4.17	3.96	3.61	4.71	4.03
An	0.8	1.0	0.5	0.5	0.8	0.8	0.8	0.5	0.4	0.8	0.4	0.9
Ab	98.8	98.7	99.1	99.1	98.9	98.9	98.8	99.1	99.4	99.1	99.3	98.7
Or	0.4	0.2	0.4	0.4	0.3	0.4	0.3	0.4	0.2	0.1	0.3	0.4

APPENDIX C, 1. Feldspar compositions (Biotite-feldspar schist), Kanonkop.

	01-231-1a	01-231-1b	01-231-1c	01-231-2a	01-231-2b	01-231-2c	01-231-2d	01-231-2e	01-231-4a	01-231-4b	01-231-5a	01-273-3c	01-273-3d
MgO	0.00	0.00	0.02	0.00	0.00	0.00	0.00	0.00	0.01	0.00	0.05	0.00	0.00
SiO2	61.20	61.29	61.67	63.22	61.43	62.66	62.50	61.49	61.26	62.19	66.65	60.58	68.82
Na2O	8.69	9.07	8.55	9.41	8.82	9.63	8.70	8.88	8.76	8.75	7.93	12.09	11.72
Al2O3	23.86	23.80	24.19	23.21	23.80	23.20	22.94	23.49	22.65	23.12	20.63	18.45	19.56
K2O	0.22	0.36	0.15	0.17	0.12	0.13	0.22	0.17	0.54	0.24	0.11	0.06	0.07
CaO	5.33	4.71	5.04	4.36	5.21	4.18	4.91	4.90	4.14	4.59	4.23	0.08	0.19
TiO2	0.01	0.00	0.00	0.01	0.00	0.01	0.03	0.00	0.00	0.00	0.00	0.00	0.07
Fe2O3	0.07	0.09	0.08	0.02	0.00	0.06	0.10	0.00	0.00	0.04	0.06	0.13	0.13
MnO	0.00	0.00	0.00	0.00	0.00	0.04	0.00	0.01	0.00	0.01	0.00	0.96	0.01
Cr2O3	0.00	0.02	0.00	0.00	0.00	0.00	0.00	0.05	0.00	0.00	0.00	0.03	0.01
O	0.00	0.00	0.00	0.00	0.00	0.00	0.00	0.00	0.00	0.00	0.00	0.00	0.00
Total	99.38	99.33	99.69	100.40	99.38	99.91	99.39	98.98	97.35	98.94	99.66	92.38	100.56
Mg	8.69	9.07	8.55	9.41	8.82	9.63	8.70	8.88	8.76	8.75	7.93	12.09	11.72
Si	11.93	11.90	12.09	11.61	11.90	11.60	11.47	11.74	11.33	11.56	10.32	9.23	9.78
Na	0.44	0.72	0.29	0.33	0.24	0.27	0.43	0.35	1.07	0.47	0.22	0.13	0.15
Al	3.55	3.14	3.36	2.90	3.48	2.79	3.28	3.26	2.76	3.06	2.82	0.05	0.13
K	0.03	0.01	0.00	0.02	0.01	0.01	0.06	0.00	0.00	0.00	0.00	0.01	0.13
Ca	0.07	0.09	0.08	0.02	0.00	0.06	0.10	0.00	0.00	0.04	0.06	0.13	0.13
Ti	0.00	0.00	0.00	0.00	0.00	0.02	0.00	0.01	0.00	0.01	0.00	0.48	0.01
Fe2+	0.00	0.02	0.00	0.00	0.00	0.00	0.00	0.05	0.00	0.00	0.00	0.03	0.01
Mn	0.00	0.00	0.00	0.00	0.00	0.00	0.00	0.00	0.00	0.00	0.00	0.00	0.00
Cr	66.25	66.22	66.46	66.93	66.25	66.61	66.26	65.99	64.90	65.96	66.44	61.59	67.04
Cation Total	90.97	91.16	90.84	91.23	90.69	90.98	90.29	90.27	88.82	89.85	87.78	83.72	89.08
X (Si+Al)	15.48	15.04	15.46	14.51	15.37	14.39	14.74	15.01	14.09	14.61	13.13	9.28	9.90
Z (rest)	75.48	76.12	75.38	76.72	75.32	76.60	75.55	75.27	74.73	75.24	74.64	74.44	79.18
An	13.3	11.1	21.2	6.3	0.0	17.6	16.5	0.0	0.0	8.1	21.7	48.5	31.5
Ab	81.9	88.2	78.8	87.8	97.5	78.2	73.6	100.0	100.0	91.9	78.3	48.5	36.2
Or	4.8	0.7	0.0	5.8	2.5	4.1	9.9	0.0	0.0	0.0	0.0	3.1	32.3

APPENDIX C, 1. Feldspar compositions (Chlorite-quartz-epidote-feldspar schist), Bridgetown

	01-279-1a	01-279-1d	01-279-5a	01-279-5b	01-279-5c	01-279-5d	01-273-2e	01-273-3a	01-273-3b	01-273-3c	01-273-3d
MgO	0.00	0.05	1.95	0.92	0.00	0.38	0.00	0.00	0.00	0.00	0.00
SiO2	67.82	68.51	66.45	68.68	68.83	68.72	68.35	70.24	72.75	60.58	68.82
Na2O	12.10	12.16	10.41	10.84	12.27	12.03	12.32	11.71	10.72	12.09	11.72
Al2O3	19.88	19.86	18.81	19.96	19.71	20.01	20.54	18.98	17.45	18.45	19.56
K2O	0.12	0.12	0.06	0.73	0.06	0.06	0.08	0.03	0.02	0.06	0.07
CaO	0.06	0.10	0.07	0.56	0.01	0.08	0.11	0.08	0.15	0.08	0.19
TiO2	0.02	0.03	0.00	0.02	0.00	0.00	0.00	0.01	0.02	0.00	0.07
Fe2O3	0.00	0.01	2.49	0.73	0.20	0.51	0.00	0.12	0.11	0.13	0.13
MnO	0.00	0.05	0.05	0.06	0.04	0.01	0.00	0.00	0.00	0.96	0.01
Cr2O3	0.03	0.02	0.04	0.10	0.00	0.01	0.00	0.05	0.00	0.03	0.01
O	0.00	0.00	0.00	0.00	0.00	0.00	0.00	0.00	0.00	0.00	0.00
Total	100.02	100.92	100.32	102.59	101.11	101.80	101.39	101.21	101.22	92.38	100.56
Mg	0.00	0.01	0.51	0.23	0.00	0.10	0.00	0.00	0.00	0.00	0.00
Si	11.88	11.90	11.72	11.79	11.93	11.85	11.82	12.11	12.45	11.64	11.97
Na	4.11	4.09	3.56	3.61	4.12	4.02	4.13	3.91	3.55	4.50	3.95
Al	4.10	4.06	3.91	4.04	4.03	4.07	4.18	3.85	3.52	4.18	4.01
K	0.03	0.03	0.01	0.16	0.01	0.01	0.02	0.01	0.00	0.02	0.02
Ca	0.01	0.02	0.01	0.10	0.00	0.01	0.02	0.02	0.03	0.02	0.04
Ti	0.00	0.00	0.00	0.00	0.00	0.00	0.00	0.00	0.00	0.00	0.01
Fe2+	0.00	0.00	0.37	0.10	0.03	0.07	0.00	0.02	0.02	0.02	0.02
Mn	0.00	0.01	0.01	0.01	0.01	0.00	0.00	0.00	0.00	0.16	0.00
Cr	0.00	0.00	0.01	0.01	0.00	0.00	0.00	0.01	0.00	0.00	0.00
Cation Total	20.13	20.13	20.11	20.06	20.13	20.14	20.17	19.92	19.57	20.53	20.01
X (Si+Al)	15.98	15.96	15.63	15.83	15.95	15.91	16.00	15.96	15.97	15.82	15.97
Z (rest)	4.15	4.17	4.48	4.23	4.17	4.22	4.17	3.96	3.61	4.71	4.03
An	0.27	0.46	0.38	2.67	0.04	0.34	0.47	0.38	0.79	0.35	0.88
Ab	99.10	98.88	99.22	93.22	99.64	99.35	99.14	99.45	99.09	99.31	98.71
Or	0.63	0.66	0.40	4.12	0.32	0.30	0.40	0.17	0.12	0.34	0.40

APPENDIX C, 2. Muscovite compositions (Quartz-chlorite-muscovite schist), Spitskop.

	A1	A2	A3	A4	A5	A6	A7	A8	A9	A10	A11	A12	C1	C2	C3	C4	C5	C6
Na2O	0.89	0.90	0.62	0.74	0.42	0.87	1.57	0.64	0.42	0.44	0.85	0.72	0.51	0.56	0.40	0.39	0.58	0.63
K2O	6.55	8.87	9.09	8.74	8.07	8.05	7.61	7.11	8.60	7.70	7.34	7.64	8.89	9.31	8.47	7.97	9.10	9.27
SiO2	40.44	47.41	46.94	46.43	45.50	45.07	47.35	43.09	48.29	44.94	43.93	48.79	47.16	49.34	46.28	44.89	48.44	47.32
TiO2	0.14	0.22	0.29	0.26	0.28	0.19	0.23	0.23	0.18	0.16	0.18	0.18	0.26	0.27	0.27	0.26	0.28	0.29
Al2O3	31.53	37.62	35.50	36.83	34.09	34.74	37.39	34.18	34.54	33.07	34.06	36.49	34.79	34.73	32.67	31.85	35.64	36.65
FeO	10.67	3.63	4.30	3.76	5.48	5.88	3.27	8.94	4.22	7.25	6.90	3.59	4.17	4.03	3.82	3.47	4.33	3.78
MnO	0.25	0.00	0.03	0.01	0.06	0.07	0.05	0.20	0.00	0.11	0.19	0.00	0.04	0.05	0.00	0.00	0.01	0.02
MgO	3.70	0.58	1.00	0.66	1.93	1.73	0.85	2.43	1.18	2.37	2.25	0.96	1.53	1.47	1.17	0.99	1.29	0.83
CaO	0.03	0.02	0.02	0.12	0.02	0.01	0.03	0.05	0.06	0.12	0.08	0.07	0.02	0.02	0.02	0.02	0.02	0.02
Total	94.18	99.25	97.79	97.55	95.84	96.61	98.35	96.85	97.49	96.17	95.79	98.43	97.39	99.78	93.10	89.85	99.69	98.61
Si	6.20	6.61	6.68	6.60	6.63	6.54	6.62	6.33	6.85	6.59	6.46	6.79	6.73	6.86	6.88	6.89	6.75	6.65
Al	1.80	1.39	1.32	1.40	1.37	1.46	1.38	1.67	1.15	1.41	1.54	1.21	1.27	1.14	1.12	1.11	1.25	1.35
Al	3.90	4.79	4.64	4.76	4.48	4.48	4.79	4.24	4.63	4.30	4.36	4.78	4.58	4.55	4.60	4.65	4.60	4.72
Ti	0.02	0.02	0.03	0.03	0.03	0.02	0.02	0.03	0.02	0.02	0.02	0.02	0.03	0.03	0.03	0.03	0.03	0.03
Fe	1.37	0.42	0.51	0.45	0.67	0.71	0.38	1.10	0.50	0.89	0.85	0.42	0.50	0.47	0.47	0.45	0.50	0.44
Fe	0.00	0.00	0.00	0.00	0.00	0.00	0.00	0.00	0.00	0.00	0.00	0.00	0.00	0.00	0.00	0.00	0.00	0.00
Mn	0.03	0.00	0.00	0.00	0.01	0.01	0.01	0.02	0.00	0.01	0.02	0.00	0.01	0.01	0.00	0.00	0.00	0.00
Mg	0.84	0.12	0.21	0.14	0.42	0.37	0.18	0.53	0.25	0.52	0.49	0.20	0.33	0.30	0.26	0.23	0.27	0.17
CaO	0.00	0.00	0.00	0.02	0.00	0.00	0.00	0.01	0.01	0.02	0.01	0.01	0.00	0.00	0.00	0.00	0.00	0.00
K	1.28	1.58	1.65	1.58	1.50	1.49	1.36	1.33	1.56	1.44	1.38	1.36	1.62	1.65	1.61	1.56	1.62	1.66
Na	0.26	0.24	0.17	0.20	0.12	0.24	0.43	0.18	0.11	0.13	0.24	0.19	0.14	0.15	0.12	0.12	0.16	0.17

APPENDIX C, 2. Muscovite compositions (Quartz-chlorite-muscovite schist), Spitskop.

	C7	C8	C9	C10	C11	C12	C13	C14	C15	D1	D2	D3	D4	D5	D6	D7	D8	D9	D10
Na2O	0.32	0.38	0.45	0.34	0.69	0.42	0.67	0.38	0.48	0.27	0.41	0.58	0.69	0.52	0.83	0.57	0.70	0.38	0.41
K2O	8.44	9.81	9.20	9.84	9.15	9.62	9.00	9.54	9.91	8.14	9.39	8.69	9.06	9.82	9.07	9.40	8.99	9.60	9.57
SiO2	47.53	48.30	48.66	48.23	47.57	47.91	49.64	48.44	47.53	43.41	45.59	44.52	45.67	44.91	43.28	43.96	46.33	47.47	47.37
TiO2	0.14	0.30	0.29	0.17	0.26	0.10	0.25	0.30	0.18	0.32	0.29	0.23	0.25	0.19	0.19	0.24	0.28	0.19	0.18
Al2O3	36.77	34.04	37.82	32.17	37.81	37.55	38.11	36.16	35.09	35.12	35.29	34.24	34.43	33.74	35.77	34.52	35.50	32.56	32.73
FeO	3.85	4.46	3.37	4.84	3.62	3.12	3.63	3.03	4.07	6.07	2.78	4.19	4.20	3.71	3.71	3.91	3.95	4.50	4.64
MnO	0.01	0.02	0.03	0.02	0.03	0.02	0.01	0.03	0.03	0.11	0.06	0.11	0.06	0.03	0.00	0.06	0.03	0.06	0.07
MgO	1.04	1.49	0.79	2.07	0.75	0.70	0.71	0.93	1.15	2.44	1.12	1.17	1.20	1.87	0.88	1.44	1.05	1.71	1.60
CaO	0.04	0.01	0.01	0.01	0.05	0.04	0.06	0.04	0.01	0.06	0.03	0.06	0.05	0.03	0.03	0.01	0.05	0.04	0.05
Total	98.14	98.81	100.63	97.69	99.94	99.47	102.10	98.85	98.45	95.94	94.95	93.81	95.60	94.83	93.75	94.09	96.87	96.51	96.61
Si	6.68	6.83	6.67	6.92	6.60	6.66	6.71	6.77	6.74	6.36	6.65	6.62	6.67	6.63	6.45	6.54	6.65	6.88	6.86
Al	1.32	1.17	1.33	1.08	1.40	1.34	1.29	1.23	1.26	1.64	1.35	1.38	1.33	1.37	1.55	1.46	1.35	1.12	1.14
Al	4.77	4.50	4.79	4.35	4.77	4.82	4.78	4.73	4.60	4.43	4.72	4.62	4.59	4.51	4.73	4.59	4.66	4.43	4.45
Ti	0.01	0.03	0.03	0.02	0.03	0.01	0.03	0.03	0.02	0.04	0.03	0.03	0.03	0.02	0.02	0.03	0.03	0.02	0.02
Fe	0.45	0.53	0.39	0.58	0.42	0.36	0.41	0.35	0.48	0.74	0.34	0.52	0.51	0.46	0.46	0.49	0.47	0.55	0.56
Fe	0.00	0.00	0.00	0.00	0.00	0.00	0.00	0.00	0.00	0.00	0.00	0.00	0.00	0.00	0.00	0.00	0.00	0.00	0.00
Mn	0.00	0.00	0.00	0.00	0.00	0.00	0.00	0.01	0.01	0.01	0.01	0.00	0.00	0.01	0.00	0.01	0.01	0.37	0.34
Mg	0.16	0.44	0.16	0.15	0.14	0.19	0.24	0.53	0.24	0.26	0.26	0.41	0.20	0.32	0.22	0.37	0.34	0.37	0.34
CaO	0.00	0.00	0.01	0.01	0.01	0.01	0.00	0.01	0.00	0.01	0.01	0.00	0.00	0.00	0.01	0.01	0.01	0.01	0.01
K	1.51	1.77	1.61	1.80	1.62	1.71	1.55	1.70	1.79	1.52	1.75	1.65	1.69	1.85	1.72	1.78	1.65	1.77	1.77
Na	0.09	0.10	0.12	0.09	0.19	0.11	0.18	0.10	0.13	0.08	0.12	0.17	0.19	0.15	0.24	0.17	0.19	0.11	0.11

APPENDIX C, 3. Biotite composition (Quartz-biotite schist), Kanonkop.

	01-231-2f	01-231-2g	01-231-3a	01-231-3b	01-231-3c	01-231-6a	01-231-8a	01-231-8b	01-231-8c	01-231-7a	01-231-7b	01-231-7c
MgO	8.88	9.38	9.30	8.91	8.91	8.36	9.26	8.87	8.83	9.32	9.31	9.10
SiO2	33.43	33.42	34.26	34.88	34.78	34.19	33.39	36.40	34.71	34.85	34.06	34.62
Na2O	0.23	0.18	0.04	0.26	0.25	0.18	0.14	0.15	0.18	0.10	0.14	0.16
Al2O3	17.32	17.62	18.83	18.60	19.02	18.91	19.74	19.10	18.68	18.90	18.46	18.45
K2O	8.61	7.76	8.91	8.85	8.97	9.09	9.34	9.09	8.80	9.39	8.94	9.10
CaO	0.07	0.03	0.03	0.01	0.02	0.02	0.02	0.01	0.06	0.02	0.07	0.03
TiO2	3.48	3.13	3.02	3.05	3.14	3.29	2.07	3.22	3.24	3.16	2.97	3.46
Fe2O3	19.77	21.16	19.29	17.89	18.53	18.53	18.32	18.42	17.82	18.68	18.66	18.96
MnO	0.16	0.18	0.14	0.20	0.24	0.15	0.24	0.19	0.20	0.22	0.24	0.22
Cr2O3	0.01	0.08	0.08	0.02	0.04	0.07	0.01	0.05	0.00	0.03	0.02	0.01
O	0.00	0.00	0.00	0.00	0.00	0.00	0.00	0.00	0.00	0.00	0.00	0.00
Total	91.96	92.94	93.89	92.65	93.90	92.80	92.54	95.49	92.50	94.47	92.87	94.11
MgO	2.10	2.20	2.14	2.06	2.05	1.95	2.17	1.99	2.05	2.13	2.17	2.09
SiO2	5.31	5.26	5.30	5.42	5.35	5.34	5.24	5.48	5.40	5.32	5.32	5.34
Na2O	0.07	0.05	0.01	0.08	0.08	0.05	0.04	0.04	0.05	0.03	0.04	0.05
Al2O3	3.24	3.27	3.43	3.41	3.45	3.48	3.65	3.39	3.42	3.42	3.40	3.35
K2O	1.75	1.56	1.76	1.75	1.76	1.81	1.87	1.75	1.75	1.84	1.78	1.79
CaO	0.01	0.01	0.00	0.00	0.00	0.00	0.00	0.00	0.01	0.00	0.01	0.00
TiO2	0.42	0.37	0.35	0.36	0.36	0.39	0.24	0.36	0.38	0.37	0.35	0.40
FeO	2.63	2.78	2.49	2.32	2.39	2.42	2.40	2.32	2.32	2.40	2.44	2.44
MnO	0.02	0.02	0.02	0.03	0.03	0.02	0.03	0.02	0.03	0.03	0.03	0.03
Cr2O3	0.00	0.01	0.01	0.00	0.01	0.01	0.00	0.01	0.00	0.00	0.00	0.00

APPENDIX C, 4. Epidote compositions (Chlorite-quartz-epidote-feldspar schist), Bridgetown Formation.

	01-279-2b	01-279-2c	01-279-2d	01-279-2e	01-279-3a	01-279-3b	01-279-3c	01-279-3d	01-279-3e	01-279-1b	01-279-2a
MgO	0.01	0.00	0.00	0.00	0.47	0.00	0.00	0.00	0.00	0.01	0.19
SiO2	37.27	37.42	36.82	37.69	37.10	102.70	37.51	37.12	38.48	37.27	36.73
Na2O	0.01	0.01	0.00	0.05	0.01	0.02	0.00	0.04	0.05	0.01	0.01
Al2O3	22.21	21.59	20.37	21.68	21.16	0.00	21.66	21.06	21.80	22.21	21.07
K2O	0.00	0.00	0.00	0.00	0.00	0.01	0.00	0.00	0.00	0.00	0.00
CaO	23.40	23.64	23.78	23.98	23.17	0.02	24.15	24.40	23.55	23.40	23.52
TiO2	0.06	0.05	0.08	0.08	0.05	0.00	0.09	0.10	0.12	0.06	0.11
Fe2O3	12.46	13.18	14.06	12.52	13.71	0.21	13.88	14.34	12.60	12.46	12.85
MnO	0.42	0.11	0.06	0.21	0.15	0.05	0.07	0.12	0.30	0.42	0.16
Cr2O3	0.03	0.01	0.00	0.00	0.02	0.04	0.00	0.00	0.00	0.03	0.06
O	0.00	0.00	0.00	0.00	0.00	0.00	0.00	0.00	0.00	0.00	0.00
Total	95.88	96.01	95.16	96.22	95.84	103.06	97.36	97.16	96.89	95.88	94.70
Mg	0.00	0.00	0.00	0.00	0.06	0.00	0.00	0.00	0.00	0.00	0.03
Si	3.23	3.25	3.26	3.26	3.24	6.49	3.23	3.22	3.30	3.23	3.24
Na	0.00	0.00	0.00	0.01	0.00	0.00	0.00	0.01	0.01	0.00	0.00
Al	2.27	2.21	2.12	2.21	2.18	0.00	2.20	2.15	2.20	2.27	2.19
K	0.00	0.00	0.00	0.00	0.00	0.00	0.00	0.00	0.00	0.00	0.00
Ca	2.18	2.20	2.25	2.22	2.17	0.00	2.23	2.27	2.16	2.18	2.22
Ti	0.00	0.00	0.01	0.01	0.00	0.00	0.01	0.01	0.01	0.00	0.01
Fe2+	0.90	0.96	1.04	0.91	1.00	0.01	1.00	1.04	0.90	0.90	0.95
Mn	0.03	0.01	0.00	0.02	0.01	0.00	0.01	0.01	0.02	0.03	0.01
Cr	0.00	0.00	0.00	0.00	0.00	0.00	0.00	0.00	0.00	0.00	0.00
Cation Total	8.6	8.6	8.7	8.6	8.7	6.5	8.7	8.7	8.6	8.6	8.7

APPENDIX C, 5. Whole rock geochemistry (University of Stellenbosch).

	Sample	SK1-20	SK1-21	SK1-43	SK1-53	SK1-55	SK2-01	SK2-31	SK2-96	SK2-97	SK3-12	SK3-83	SK3-84	SK4-52	SK4-54	SK12-17	SK12-31
Major elements (%)	SiO_2	64.48	64.61	54.24	55.82	53.15	52.69	54.60	61.28	63.01	65.94	61.72	64.29	55.26	58.65	56.30	57.72
	TiO_2	0.70	0.65	0.82	0.78	0.81	0.88	0.89	0.84	0.81	0.87	0.81	0.81	0.78	0.76	0.85	0.64
	Al_2O_3	15.25	13.26	20.77	20.33	21.04	21.34	21.13	15.86	14.84	13.87	15.80	13.84	18.86	19.51	19.80	17.07
	Fe_2O_3T	7.15	6.55	9.34	8.51	9.86	9.45	9.17	7.39	7.30	6.69	7.63	6.96	8.03	7.72	8.50	7.96
	MnO	0.49	0.54	0.19	0.18	0.20	0.23	0.13	0.17	0.11	0.17	0.10	0.12	0.25	0.22	0.28	0.35
	MgO	3.51	3.24	2.85	2.63	3.07	1.45	2.08	3.79	3.36	1.69	3.66	3.07	2.52	2.41	2.83	3.50
	CaO	0.19	0.15	0.54	0.41	0.35	0.01	0.13	1.57	1.79	0.26	1.32	2.25	0.85	0.50	0.81	1.77
	Na_2O	2.77	1.15	0.08	0.13	0.81	0.28	0.00	2.36	2.53	1.21	2.69	2.15	1.03	1.50	0.78	0.15
	K_2O	2.13	2.04	4.42	4.21	4.39	5.19	5.09	2.84	3.05	3.08	3.22	2.86	4.28	4.35	3.19	3.53
	P_2O_5	0.13	0.11	0.14	0.09	0.11	0.10	0.11	0.20	0.20	0.25	0.20	0.20	0.11	0.12	0.09	0.11
	H_2O^-	0.30	0.68	0.24	0.40	0.27	0.92	0.30	0.19	0.31	0.68	0.35	0.27	0.43	0.31	0.32	0.21
	LOI	3.82	3.98	4.72	4.24	4.61	6.09	4.36	4.53	4.11	3.23	3.84	4.37	8.51	5.71	4.38	5.22
	TOTAL	100.92	96.95	98.35	97.75	98.65	98.60	98.00	101.03	101.41	97.95	101.33	101.19	100.92	101.75	98.10	98.25
Trace elements (ppm)	Mo	2	3	0	1	1	0	1	1	1	1	1	1	1	1	1	0
	Nb	13	11	12	12	13	14	14	11	13	12	11	10	12	12	13	12
	Zr	172	182	137	159	144	172	175	176	121	211	160	185	144	129	167	127
	Y	35	28	35	31	37	37	37	39	36	36	36	34	36	35	37	31
	Sr	87	67	139	99	93	45	53	62	84	71	82	120	92	82	126	88
	U	4	2	3	3	3	4	2	5	3	3	4	3	3	3	1	2
	Rb	91	99	186	172	213	216	186	106	195	95	119	103	172	177	141	153
	Th	13	14	17	15	16	19	16	10	13	11	9	7	14	13	17	17
	Pb	30	28	21	28	17	25	37	19	19	11	9	8	16	17	29	24
	Ga	19	18	26	23	28	26	26	20	24	18	22	19	25	23	24	22
	Zn	113	111	146	131	163	187	134	122	118	105	123	114	105	106	130	119
	Cu	11	2	25	55	6	43	36	19	13	29	19	10	31	33	51	69
	Ni	48	46	62	53	70	131	53	50	67	45	50	43	59	59	56	52
	Cr	95	210	123	122	131	143	125	103	107	87	104	88	114	114	125	122
	Nd	33	35	45	40	47	43	43	30	50	36	34	26	47	44	43	44
	V	90	87	139	132	144	151	169	170	128	141	171	146	123	119	122	111
	Ce	84	78	92	83	100	84	88	76	103	74	78	67	91	94	88	93
	La	41	37	51	43	57	48	44	32	58	36	42	32	53	54	53	52
	Ba	477	537	472	501	549	669	572	483	725	542	537	562	491	513	379	438
	Sc		19	26	22	27	26	25			19					25	22
ppb	Au		40	125	10	<10	100	15			170					<10	10

APPENDIX C, 5. Whole rock geochemistry (University of Stellenbosch).

	Sample	SK20-19	SK21-67	SK23-03	SK23-31	SK23-79	SK23-61	SK24-31	SK24-61	SK24-94	SK25-51	SK25-63	SK25-77	SK28-15	SK31-27	SK31-76	SK32-29
Major elements (%)	SiO_2	74.85	66.03	62.46	56.87	60.13	57.97	71.18	57.50	54.84	65.50	53.20	56.32	58.47	64.35	59.48	61.62
	TiO_2	0.71	0.74	0.85	0.73	0.91	0.78	0.73	0.80	0.77	0.81	0.87	0.83	0.75	0.85	0.63	0.88
	Al_2O_3	10.57	12.22	15.47	18.72	15.73	18.51	10.86	18.88	20.74	13.66	21.18	19.26	19.69	15.86	12.27	16.53
	Fe_2O_3T	4.59	5.30	7.24	7.97	7.72	8.73	5.03	8.31	8.34	6.12	9.51	8.38	8.16	6.87	5.93	7.50
	MnO	0.07	0.09	0.13	0.28	0.12	0.18	0.12	0.22	0.25	0.10	0.11	0.16	0.15	0.14	0.62	0.17
	MgO	0.66	2.19	2.73	3.07	3.60	2.66	2.03	2.87	2.87	2.70	2.99	2.83	2.68	2.50	4.33	2.92
	CaO	0.17	1.72	0.09	0.95	1.31	0.47	1.39	0.56	0.52	1.40	0.22	0.29	0.80	0.21	4.19	0.21
	Na_2O	0.09	1.07	1.48	1.80	0.87	0.15	1.79	0.65	0.00	0.87	0.00	0.00	1.44	0.29	0.38	0.65
	K_2O	2.53	2.56	2.83	3.60	3.24	3.78	1.25	4.19	4.39	2.81	5.05	4.52	3.72	2.88	2.36	3.44
	P_2O_5	0.16	0.18	0.10	0.10	0.19	0.10	0.15	0.11	0.11	0.17	0.11	0.12	0.09	0.16	0.09	0.16
	H_2O-	0.49	0.20	0.85	0.18	0.10	0.14	0.12	0.18	0.23	0.29	0.20	0.08	0.11	0.47	0.19	0.37
	LOI	2.38	5.64	3.87	4.15	4.05	4.03	3.31	4.30	4.97	3.88	4.78	4.62	4.22	3.17	6.99	3.64
	TOTAL	97.25	97.95	98.10	98.40	98.00	97.50	97.95	98.60	98.05	98.30	98.20	97.45	100.26	97.75	97.45	98.05
Trace elements (ppm)	Mo	1	0	0	1	3	0	3	3	1	1	0	0	1	1	1	1
	Nb	11	12	12	13	11	12	10	11	13	12	13	13	12	12	11	12
	Zr	229	231	192	159	151	240	197	150	129	187	162	160	128	185	179	195
	Y	31	33	35	33	34	35	33	30	35	32	33	33	33	33	27	35
	Sr	44	79	67	98	93	118	59	84	95	66	64	109	83	51	133	53
	U	2	4	3	1	2	2	3	2	1	2	2	1	3	2	1	1
	Rb	98	109	124	165	158	96	87	172	205	127	213	180	167	130	104	145
	Th	12	13	13	16	16	12	12	17	18	12	18	16	14	14	13	15
	Pb	15	17	36	31	34	17	22	19	30	27	19	22	8	20	19	26
	Ga	15	17	20	23	23	17	17	23	25	19	26	24	24	19	15	21
	Zn	86	90	117	122	114	99	92	120	120	112	133	115	118	110	80	114
	Cu	21	20	32	26	30	22	27	43	1	26	39	59	15	34	2	41
	Ni	30	28	45	52	53	30	28	51	56	37	61	56	64	43	32	41
	Cr	84	85	100	107	153	103	133	179	116	116	126	122	115	100	76	103
	Nd	31	33	35	42	42	36	30	42	49	31	45	42	40	39	31	35
	V	101	117	144	127	122	142	133	129	126	156	144	129	133	134	66	146
	Ce	68	71	72	89	86	73	66	83	99	67	88	88	89	78	72	73
	La	32	34	33	46	47	32	30	46	56	31	51	49	47	39	34	37
	Ba	601	535	531	500	450	462	487	500	477	509	614	507	506	477	479	611
	Sc	13	14	20	23	24	19	17	24	25	20	25	25		21	15	22
ppb	Au	<10	<10	<10	30	<10	10	<10	<10	30	<10	200	<10		305	<10	<10

APPENDIX C, 5. Whole rock geochemistry (University of Stellenbosch).

	Sample	SK12-73	SK14-11	SK14-43	SK14-59	SK16-25	SK16-51	SK16-61	SK17-13	SK18-48	SK18-65	SK18-77	SK19-19	SK19-31	SK19-37	SK19-49	SK20-10
Major elements (%)	SiO_2	64.41	59.98	61.94	70.70	59.57	60.19	64.75	61.99	71.41	62.09	59.96	69.95	67.21	59.25	68.54	69.23
	TiO_2	0.91	0.74	0.86	0.66	0.72	0.75	0.79	0.92	0.69	0.76	0.79	0.73	0.64	0.73	0.86	0.68
	Al_2O_3	13.01	18.51	14.64	10.88	17.67	16.34	14.34	15.83	11.39	14.42	15.19	11.38	11.12	12.99	11.05	12.41
	Fe_2O_3T	6.39	7.40	6.80	4.79	7.32	6.60	6.29	7.33	4.65	5.82	6.65	4.80	5.55	5.98	5.09	5.38
	MnO	0.10	0.34	0.13	0.08	0.07	0.16	0.17	0.12	0.08	0.11	0.12	0.09	0.11	0.13	0.13	0.09
	MgO	2.70	2.56	3.08	1.83	2.24	2.32	2.62	2.02	1.87	2.34	2.69	1.94	2.12	2.39	1.98	1.78
	CaO	1.55	0.12	1.70	1.25	0.40	2.55	2.76	0.04	1.16	1.30	1.08	1.44	2.66	3.51	1.90	0.17
	Na_2O	1.86	0.00	0.88	0.89	0.74	0.72	1.15	1.74	1.40	0.09	0.45	0.15	0.14	0.09	0.73	0.35
	K_2O	2.26	3.93	2.95	2.11	4.64	4.28	2.90	3.87	1.89	3.70	3.94	2.55	2.21	3.24	2.30	3.09
	P_2O_5	0.18	0.07	0.18	0.14	0.31	0.08	0.22	0.15	0.15	0.18	0.16	0.16	0.15	0.16	0.18	0.19
	H_2O-	0.24	0.56	0.28	0.22	0.95	0.24	0.29	0.93	0.19	0.34	0.26	0.27	0.21	0.30	0.22	0.62
	LOI	3.56	3.81	4.59	3.31	3.95	4.66	4.78	3.89	2.88	7.05	5.85	4.25	5.17	8.95	4.04	2.86
	TOTAL	97.15	98.00	98.00	96.90	98.60	98.85	101.05	98.85	97.75	98.20	97.10	97.65	97.25	97.70	97.05	96.85
Trace elements (ppm)	Mo	1	0	1	1	1	0	1	1	0	2	2	0	1	0	0	1
	Nb	12	12	12	12	14	16	12	12	10	11	12	11	10	11	12	10
	Zr	206	133	219	168	150	157	179	193	215	178	194	227	197	187	284	183
	Y	36	33	35	34	35	31	37	36	29	28	30	31	29	31	35	29
	Sr	102	117	115	96	61	138	87	49	117	109	67	87	109	112	95	45
	U	1	1	3	2	1	0	3	5	4	1	1	4	2	5	4	4
	Rb	128	154	110	151	151	182	148	115	69	159	150	100	94	131	105	118
	Th	12	16	13	15	16	16	12	12	11	15	13	12	11	12	13	12
	Pb	15	24	16	25	17	25	10	22	16	335	39	31	18	20	18	19
	Ga	20	24	18	22	20	22	21	19	14	20	20	15	15	17	15	16
	Zn	126	124	105	128	128	92	123	199	70	256	114	99	86	104	85	96
	Cu	31	76	21	36	58	8	27	34	13	61	40	17	14	32	24	15
	Ni	41	63	30	56	54	40	38	77	19	28	28	21	22	25	21	40
	Cr	106	107	87	121	107	99	104	165	63	93	100	74	72	83	82	87
	Nd	36	47	37	41	46	40	36	35	29	35	34	30	28	35	38	33
	V	164	118	140	131	114	106	157	160	89	131	128	98	105	124	109	111
	Ce	75	95	71	83	89	87	74	74	62	69	72	66	63	66	72	65
	La	35	50	33	44	49	47	32	34	29	31	34	30	26	30	34	27
	Ba	556	451	503	506	473	501	570	584	444	540	527	421	440	479	463	478
	Sc	21	24	19	22	22	21	22	21	12	19	19	14	15	18	15	15
ppb	Au	<10	<10	<10	950	<10	25	<10	380	<10	<10	<10	<10	<10	2505	<10	20

APPENDIX C, 5. Whole rock geochemistry (University of Stellenbosch).

	Sample	SK32-51	SK32-65	SK32-69	SK32-79	SK33-07	SK33-51	SK42-11	SK42-15	SK43-21	SK43-27	SK44-3	SK44-3	SK43-39	SK44-11	SK45-29	SK45-31	SK45-60
Major elements (%)	SiO_2	60.02	60.32	62.57	58.37	61.55	58.47	56.60	64.36	66.79	47.87	34.12	34.12	63.44	39.12	35.06	37.45	76.70
	TiO_2	0.94	0.82	0.87	0.64	0.80	0.81	0.05	0.24	0.23	0.15	0.01	0.01	0.97	0.01	0.30	0.18	0.40
	Al_2O_3	16.61	17.13	16.33	12.57	17.24	18.14	1.74	3.34	8.01	1.99	0.68	0.68	14.83	1.04	2.89	2.12	8.91
	Fe_2O_3T	7.73	7.50	7.16	6.13	7.66	7.99	8.34	11.55	8.92	10.14	5.59	5.59	6.99	6.46	7.06	6.70	4.31
	MnO	0.23	0.18	0.18	0.51	0.14	0.31	0.18	0.32	0.25	0.12	0.07	0.07	0.10	0.10	0.10	0.08	0.13
	MgO	2.91	2.93	2.52	5.18	1.39	2.54	26.83	13.59	7.94	25.54	30.19	30.19	3.19	32.72	31.02	31.75	1.79
	CaO	1.38	0.77	0.94	4.27	0.01	1.41	0.00	0.05	0.04	3.53	5.41	5.41	0.55	3.01	2.78	3.77	0.75
	Na_2O	0.87	0.42	0.83	0.00	0.00	0.12	0.52	0.01	0.00	0.63	0.85	0.85	0.83	0.53	0.00	1.01	0.00
	K_2O	2.91	3.52	3.00	2.82	4.28	3.05	0.04	0.04	0.42	0.02	0.02	0.02	2.77	0.01	0.00	0.03	1.55
	P_2O_5	0.16	0.14	0.16	0.10	0.06	0.09	0.02	0.05	0.04	0.06	0.01	0.01	0.20	0.02	0.08	0.07	0.10
	H_2O-	0.24	0.24	0.20	0.23	0.71	0.30	0.73	0.96	0.57	0.18	0.49	0.49	0.34	0.59	0.26	0.31	0.12
	LOI	4.25	3.97	3.77	6.90	3.90	4.83	5.53	5.18	4.91	10.52	22.90	22.90	3.50	17.02	19.35	17.95	2.61
	TOTAL	98.20	97.95	98.55	97.70	97.75	98.05	100.58	99.67	98.15	100.73	100.33	100.33	97.75	100.61	98.90	101.43	97.35
Trace elements (ppm)	Mo	1	1	0	1	1	1	1	2	1	1	1	2	1	1	0	1	1
	Nb	13	12	12	11	12	12	2	3	0	2	1	1	12	1	2	1	9
	Zr	220	172	179	173	180	155	25	24	12	11	9	17	242	5	89	26	126
	Y	35	33	33	27	35	37	9	15	5	8	5	30	35	6	9	9	24
	Sr	74	61	77	125	72	141	1	17	13	39	116	49	76	52	41	86	86
	Li	2	3	1	1	3	2	3	4	1	3	3	4	2	3	1	3	1
	Rb	111	144	144	102	164	163	1	2	17	1	1	14	92	1	1	1	125
	Th	15	14	16	13	16	16	3	3	1	3	2	3	13	2	2	3	12
	Pb	20	23	25	17	22	19	3	3	37	3	3	7	19	3	1	3	19
	Ga	20	22	22	16	23	25	2	4	5	2	2	4	18	2	3	2	17
	Zn	115	113	104	84	113	128	63	439	100	44	31	518	100	29	33	31	91
	Cu	31	37	37	31	42	30	3	3	15	3	3	6	16	3	2	3	12
	Ni	42	46	41	34	68	57	3014	3223	2127	2612	1581	3178	92	1860	1428	1520	37
	Cr	103	108	106	86	109	120	2781	3273	2459	3475	2135	4643	159	2510	1947	1880	81
	Nd	40	39	41	31	51	47	8	9	4	9	8	10	37	8	2	8	30
	V	137	134	128	98	122	121	59	77	91	64	22	99	143	32	42	36	96
	Ce	80	82	79	70	89	94	7	11	2	6	6	20	70	6	6	7	60
	La	41	40	42	33	50	55	8	8	4	8	8	19	33	7	4	7	32
	Ba	456	561	499	562	482	444	53	54	126	7	7	661	565	6	3	7	382
	Sc	20	23	21	17	22	24			21				18		12		16
ppb	Au	<10	3580	575	<10	15	<10			<10				<10		<10		<10

APPENDIX C, 5. Whole rock geochemistry (University of Stellenbosch).

	Sample	SK47-19	SK47-41	SK47-49	SK47-61	SK57-03	SK57-17	SK60-03	SK61-93	SK62-05	SK62-23	SK62-31	SK62-49
Major elements (%)	SiO_2	65.79	68.39	66.06	65.59	83.09	46.58	83.78	38.05	64.99	62.41	65.04	56.80
	TiO_2	0.50	1.04	0.84	0.81	0.04	1.34	0.05	0.41	0.65	0.79	0.78	0.79
	Al_2O_3	8.05	16.72	13.54	14.02	0.79	22.91	1.45	7.78	16.17	16.98	15.49	20.25
	Fe_2O_3T	11.75	2.40	6.40	6.79	9.71	12.01	7.09	3.96	6.71	7.48	7.02	8.62
	MnO	0.23	0.01	0.14	0.11	0.24	0.07	0.27	0.49	0.20	0.19	0.14	0.15
	MgO	6.14	0.97	2.80	2.77	1.39	3.74	1.32	2.03	0.99	2.42	2.38	2.40
	CaO	0.12	0.02	0.57	0.55	0.00	0.08	0.12	22.62	0.00	0.17	0.22	0.24
	Na_2O	0.35	0.05	0.22	0.60	0.00	3.62	0.00	0.12	0.00	0.07	0.76	1.12
	K_2O	0.82	4.84	2.91	2.94	0.00	3.90	0.00	1.46	3.30	3.36	2.39	3.24
	P_2O_5	0.10	0.04	0.17	0.16	0.02	0.07	0.01	0.03	0.05	0.12	0.13	0.10
	H_2O-	1.34	0.37	0.20	0.31	0.58	1.59	0.99	0.21	0.84	0.30	0.13	0.20
	LOI	5.36	3.02	3.45	3.38	2.26	5.80	2.53	19.94	3.83	3.53	3.07	3.69
	TOTAL	100.54	97.85	97.30	98.05	98.10	101.71	97.65	97.10	97.75	97.85	97.55	97.60
Trace elements (ppm)	Mo	2	1	1	2	1	1	1	1	1	1	0	0
	Nb	4	14	11	11	1	18	2	8	11	13	12	12
	Zr	52	199	210	179	39	305	53	130	132	167	170	137
	Y	16	42	34	32	31	52	12	22	51	39	32	34
	Sr	61	72	82	95	3	52	14	264	90	86	98	143
	U	4	3	2	3	1	6	1	2	5	4	3	1
	Rb	27	204	116	134	11	156	3	99	159	161	134	161
	Th	3	17	12	14	3	14	2	11	16	17	16	17
	Pb	27	31	36	24	1	11	3	17	26	29	23	24
	Ga	8	25	18	20	1	28	1	14	22	23	21	24
	Zn	193	26	113	110	155	221	68	70	148	132	111	117
	Cu	196	11	26	28	7	3	2	35	59	49	48	38
	Ni	2653	9	63	88	3098	1659	3029	31	74	68	46	52
	Cr	2661	132	132	165	3132	307	2891	76	118	132	111	112
	Nd	9	44	34	35	8	45	4	29	97	58	40	44
	V	149	141	137	132	59	214	66	90	111	125	115	119
	Ce	23	89	68	76	13	104	5	60	172	111	79	82
	La	8	46	30	37	18	47	4	29	82	65	64	49
	Ba	219	551	560	518	81	721	244	454	475	551	438	439
	Sc		24	18	21	14		14	12	23	24	22	23
ppb	Au		<10	<10	<10	55		35	<10	60	1760	1455	<10

APPENDIX C, 5. Whole rock geochemistry (University of Stellenbosch).

	Sample	B1	B2	B3	MG-1	MG-10	MG-11	MG-12	MG-12B	MG-13	MG-13A	MG-14A	MG-14B	MG-15	MG-1A	MG-2	MG-2A	MG-3	MG-3A	MG-3B	MG-5	MG-8	MG-8A	MG-9
Major elements (%)	Al_2O_3	8.92	10.24	10.31	20.90	20.26	18.37	18.01	12.60	14.78	14.78	9.80	12.71	15.68	18.71	11.66	13.82	14.04	16.64	16.50	16.70	17.68	18.08	12.13
	CaO	0.04	0.03	0.02	0.03	0.01	0.04	0.02	0.25	0.27	0.42	0.20	0.06	0.06	0.11	0.31	0.23	0.29	0.17	0.18	0.22	0.04	0.04	0.04
	Cr_2O_3	0.01	0.01	0.01	0.01	0.01	0.01	0.01	0.01	0.01	0.01	0.01	0.01	0.01	0.01	0.01	0.01	0.01	0.01	0.01	0.01	0.01	0.01	0.01
	Fe_2O_3T	3.14	3.16	3.22	10.17	11.00	1.84	2.05	5.77	8.09	7.04	3.62	1.50	1.91	2.68	4.95	7.15	6.31	10.11	10.02	8.93	13.29	8.30	4.43
	K_2O	2.81	3.48	3.54	5.95	5.73	3.91	3.85	2.45	3.61	3.80	2.25	2.81	2.77	4.99	2.54	3.81	3.91	4.14	4.08	4.00	2.95	3.09	2.70
	MgO	0.83	1.10	1.11	1.32	1.39	2.19	1.86	3.07	5.18	4.45	1.18	1.51	1.63	2.23	2.55	3.68	4.01	4.26	4.18	4.90	1.62	1.56	1.54
	MnO	0.05	0.05	0.04	0.05	0.04	0.05	0.06	0.10	0.10	0.10	0.04	0.03	0.05	0.06	0.07	0.25	0.25	0.05	0.06	0.09	0.04	0.04	0.07
	Na2O	0.56	2.57	1.32	2.68	1.09	0.94	1.04	2.99	1.72	1.74	2.47	2.36	1.73	0.91	3.55	1.96	4.04	0.72	1.27	1.90	1.32	1.15	0.93
	NiO	0.00	0.00	0.00	0.00	0.00	0.00	0.01	0.01	0.00	0.00	0.00	0.00	0.00	0.00	0.00	0.00	0.01	0.01	0.00	0.01	0.00	0.00	0.00
	P_2O_5	0.07	0.05	0.06	0.07	0.06	0.03	0.02	0.13	0.15	0.23	0.12	0.03	0.03	0.03	0.12	0.14	0.14	0.14	0.14	0.14	0.07	0.06	0.05
	SiO_2	80.94	77.26	76.70	52.72	54.33	68.62	66.80	67.54	58.57	59.89	68.60	67.38	68.82	64.21	67.49	61.72	63.09	57.74	57.99	59.38	59.76	61.46	62.29
	TiO_2	0.51	0.62	0.65	0.99	1.00	1.09	1.06	0.58	0.86	0.92	0.65	0.73	0.89	1.00	0.62	0.85	0.87	0.89	0.92	0.89	0.97	0.98	0.75
	LOI	1.35	1.78	1.75	4.02	4.30	2.39	3.68	3.41	5.26	5.34	8.00	7.73	4.74	4.02	4.77	4.90	2.35	3.83	3.81	2.28	1.85	4.11	9.36
	H_2O-	0.25	0.33	0.31	0.44	0.50	0.33	0.79	0.58	1.02	1.02	2.45	2.56	1.05	0.44	0.85	0.94	0.35	0.66	0.74	0.33	0.24	0.61	4.93
	Total	99.48	100.69	99.04	99.35	99.72	99.80	99.25	99.48	99.63	99.74	99.39	99.41	99.36	99.41	99.49	99.45	99.66	99.39	99.90	99.78	99.84	99.48	99.25
Trace elements (ppm)	V	33	42	45	154	114	82	118	116	154	149	184	138	85	140	93	100	74	127	121	68	63	71	83
	Cr	124	112	117	165	84	103	100	92	109	110	164	127	118	175	80	82	101	105	90	105	119	81	87
	Co	6	7	7	26	6	12	19	16	26	25	33	19	12	28	3	4	14	21	17	10	9	3	4
	Ni	21	19	21	38	26	37	58	59	92	93	30	23	52	38	24	34	51	55	47	40	38	31	18
	Cu	31	29	30	5	32	25	17	19	10	8	0	18	25	2	35	33	23	14	16	30	28	35	37
	Zn	11	42	37	26	29	73	121	109	266	264	18	24	152	28	16	20	75	110	91	88	38	62	10
	Ga	12	17	15	35	30	19	21	21	25	27	27	24	17	31	25	26	15	27	22	14	13	22	23
	Rb	132	219	201	285	233	110	169	174	191	189	143	143	142	276	192	193	106	175	188	92	107	126	120
	Sr	45	47	45	91	55	101	46	56	36	39	45	43	48	86	45	44	103	58	64	65	58	152	27
	Y	27	35	38	49	53	32	43	39	53	50	37	41	72	48	48	44	66	70	83	52	45	35	35
	Zr	286	312	323	176	215	169	194	201	193	198	230	238	272	181	220	217	167	182	188	227	312	237	274
	Nb	19	21	23	22	24	18	21	21	21	20	24	26	21	19	24	25	15	17	21	15	18	21	23
	Ba	490	635	646	1360	716	455	464	516	617	616	871	616	884	1307	418	433	550	778	730	392	376	384	361
	La	39	22	38	65	53	34	56	54	63	70	28	18	78	68	59	45	85	84	76	96	36	40	37
	Ce	98	89	113	159	140	70	106	101	123	132	78	55	141	150	91	86	155	131	146	234	82	71	91
	Nd	40	30	37	48	46	24	41	38	42	48	21	14	63	46	47	38	62	56	66	102	36	27	40
	Pb	52	35	34	43	27	18	34	17	27	30	32	23	18	33	28	29	32	15	10	28	17	14	32
	Th	28	38	32	24	31	22	23	22	31	28	26	22	21	28	32	28	12	20	23	23	27	21	29
	U	9	15	10	8	7	10	4	3	8	13	4	13	9	8	11	4	4	10	10	10	1	11	5
	Sc	14	15	16	31	24	20	23	19	27	23	28	29	22	31	24	24	16	30	22	15	24	20	24

APPENDIX C, 6. Whole rock geochemistry (Rhodes University).

	SK	18-47	18-48	18-65	18-77	19-19	19-31	19-37	19-49	20-10.	20-19	23-03.	23-31	23-61	23-79	24-31	24-32	24-61	24-94
Major elements (%)	SiO_2	74.12	74.10	66.70	63.63	73.26	71.33	65.85	72.17	72.84	77.87	66.03	60.08	60.95	63.27	73.98	66.10	60.22	57.94
	Al_2O_3	11.41	11.71	15.36	15.98	11.96	11.65	14.26	11.50	12.94	10.92	16.33	19.65	19.40	16.40	11.39	15.92	20.03	21.35
	Fe_2O_3	4.49	4.75	6.25	7.00	4.98	5.80	6.52	5.30	5.58	4.77	7.58	8.33	9.02	8.03	5.26	7.08	8.54	8.65
	MnO	0.10	0.08	0.12	0.13	0.09	0.11	0.14	0.14	0.09	0.06	0.14	0.30	0.18	0.12	0.13	0.14	0.22	0.27
	MgO	1.96	2.09	2.62	2.98	2.20	2.46	2.91	2.22	2.00	0.87	2.94	3.43	2.93	3.87	2.28	3.73	3.08	3.18
	CaO	2.07	1.27	1.46	1.20	1.56	2.86	3.91	2.08	0.23	0.24	0.14	1.05	0.55	1.44	1.51	1.16	0.65	0.63
	Na_2O	2.20	2.25	0.95	1.22	1.28	1.25	0.32	1.65	1.34	1.36	1.98	2.08	1.21	1.96	2.59	1.81	0.94	1.05
	K_2O	2.07	2.07	3.91	4.21	2.72	2.41	3.64	2.53	3.38	2.75	3.09	3.69	4.01	3.43	1.44	2.85	4.17	4.85
	TiO_2	0.69	0.70	0.81	0.83	0.76	0.67	0.80	0.90	0.71	0.75	0.90	0.75	0.81	0.96	0.76	0.91	0.82	0.80
	P_2O_5	0.16	0.16	0.19	0.16	0.18	0.17	0.19	0.20	0.20	0.17	0.11	0.12	0.11	0.21	0.17	0.20	0.12	0.12
	TOTAL	99.26	99.18	98.38	97.33	99.00	98.72	98.54	98.69	99.31	99.76	99.25	99.47	99.18	99.70	99.50	99.89	98.80	98.84
Trace elements (ppm)	Nb	9	10	13	12	10	9	11	11	10	10	12	14	12	12	9	13	12	13
	Y	33	32	35	37	34	32	34	42	32	33	40	38	41	39	34	42	38	41
	Rb	70	71	143	166	103	93	132	92	120	89	120	165	171	130	60	117	172	211
	Zr	213	221	193	200	239	168	190	333	186	259	199	127	157	207	209	194	168	131
	Sr	130	105	78	70	77	121	112	106	44	40	46	156	80	109	66	53	109	97
	U	0	3	2	2	1	0	6	1	0	3	1	2	2	4	0	2	1	5
	Th	9	12	16	15	12	11	16	11	12	10	12	18	18	12	8	11	15	18
	Ba	466	480	505	554	441	395	495	494	496	597	587	461	499	508	367	643	518	488
	Sc	13	15	21	25	17	14	18	17	18	15	27	28	26	27	16	25	31	29
	Cr	55	60	82	101	62	67	77	71	75	62	98	101	107	99	60	194	111	110
	V	90	95	131	134	101	104	126	107	108	93	168	123	116	176	101	168	132	129
	La	47	33	23	24	29	18	30	44	31	34	22	51	41	40	26	27	53	260
	Zn	74	77	173	117	101	90	109	85	100	79	121	132	127	129	79	119	134	123
	Cu	7	8	22	34	12	9	21	13	9	9	23	59	13	17	10	25	28	0
	Ni	21	22	28	30	22	24	25	20	44	25	51	61	57	42	23	42	58	61
	Pb	17	11	147	68	31	22	27	11	18	17	33	34	12	21	16	37	22	44
	Ga	19	20	10	21	18	20	22	21	21	19	24	28	29	24	19	24	28	30
	Co	54	55	132	109	89	116	72	62	143	148	110	83	83	66	114	21	76	99
	Ce	67	60	54	62	68	50	38	101	54	60	58	95	81	57	47	66	70	85
	Nd	27	26	26	30	27	21	21	37	26	25	27	40	39	25	26	26	40	57
	As	10	10	73	88	47	12	139	27	42	23	22	10	15	9	2	9	24	13
	S	1152	996	7781	14138	4251	5582	6064	8666	106	45	96	1916	1244	324	803	81	3200	3303
	CL	6	11	17	0	11	81	42	227	127	168	64	1	8	5	75	78	0	0
(%)	F	0	0	0	0	0	0	0	0	0	0	0	0	0	0	0	0	0	0

APPENDIX C, 6. Whole rock geochemistry (Rhodes University).

	SK	31-27	31-75	32-51	32-52	32-65	32-69	32-79	33-07	33-51	61-93	62-05	62-23	62-31	62-32	62-49	62-50	62-85
Major elements (%)	SiO_2	67.06	61.55	62.95	67.07	62.93	64.90	63.14	65.18	62.03	48.61	69.01	65.38	67.92	66.28	59.75	63.19	64.84
	Al_2O_3	16.39	13.82	17.51	15.04	18.04	16.77	13.59	18.08	19.15	10.00	17.01	17.52	16.14	17.63	21.11	19.57	13.42
	Fe_2O_3	7.06	6.63	8.02	6.95	7.80	7.45	6.59	7.98	8.43	4.95	7.02	7.73	7.22	7.16	8.95	7.99	6.11
	MnO	0.15	0.74	0.24	0.24	0.19	0.19	0.56	0.14	0.34	0.63	0.21	0.19	0.15	0.12	0.16	0.12	0.53
	MgO	2.68	5.69	3.27	2.97	3.24	2.85	5.98	1.62	2.89	3.64	1.17	2.62	2.57	2.35	2.68	2.40	5.77
	CaO	0.29	6.08	1.52	1.74	0.90	1.01	4.72	0.05	1.55	28.37	0.04	0.23	0.28	0.31	0.33	0.30	3.98
	Na_2O	1.44	1.57	2.07	1.83	1.64	1.88	1.23	0.90	1.19	1.19	0.73	1.24	1.76	1.63	2.35	1.38	1.47
	K_2O	3.19	2.72	3.08	2.46	3.70	3.19	3.15	4.36	3.25	2.02	3.57	3.46	2.59	3.25	3.49	3.63	2.87
	TiO_2	0.88	0.68	0.97	0.89	0.85	0.89	0.69	0.84	0.85	0.54	0.69	0.81	0.81	0.77	0.83	0.75	0.67
	P_2O_5	0.18	0.12	0.18	0.19	0.15	0.16	0.13	0.07	0.11	0.11	0.07	0.13	0.13	0.13	0.11	0.12	0.11
	TOTAL	99.31	99.59	99.81	99.38	99.45	99.29	99.78	99.22	99.79	100.04	99.51	99.32	99.57	99.63	99.76	99.45	99.75
Trace elements (ppm)	Nb	13	11	15	12	13	13	12	12	12	6	10	12	12	12	13	11	11
	Y	39	31	42	38	39	40	31	39	42	21	55	41	37	36	43	37	32
	Rb	135	106	125	101	145	131	115	166	147	67	153	148	115	145	167	176	112
	Zr	198	173	222	228	185	204	178	174	182	107	122	173	186	161	137	125	174
	Sr	43	142	72	80	60	79	144	65	131	440	87	79	86	135	157	122	145
	U	2	2	3	0	2	3	3	0	0	3	2	1	4	0	2	1	2
	Th	16	13	18	13	15	16	14	14	18	8	15	15	18	16	15	17	12
	Ba	497	451	530	418	605	497	583	499	401	258	485	570	426	452	463	456	724
	Sc	25	18	28	21	27	26	20	27	25	8	28	26	25	25	30	28	18
	Cr	92	64	108	90	102	100	75	100	109	38	88	103	97	93	113	105	71
	V	130	76	153	129	146	128	92	123	112	50	107	126	120	106	132	117	105
	La	61	37	55	69	53	117	72	91	37	6	75	75	45	98	94	79	62
	Zn	110	87	128	114	120	107	90	120	127	55	142	118	116	112	131	118	88
	Cu	31	0	16	20	18	18	19	21	24	5	44	34	40	34	25	24	66
	Ni	43	33	47	40	48	44	35	74	55	18	68	55	45	52	57	55	37
	Pb	25	23	13	28	27	16	31	23	16	12	12	34	20	31	22	24	11
	Ga	25	21	28	21	27	26	21	27	25	14	26	26	22	26	31	28	21
	Co	99	46	67	105	69	67	57	168	86	26	218	136	66	83	96	106	51
	Ce	77	64	69	64	79	59	61	70	78	34	176	73	73	77	70	78	73
	Nd	29	25	33	30	38	35	23	40	34	14	108	34	39	43	40	39	31
	As	9	5	3	2	7	3	6	6	3	3	7	7	5	6	7	5	2
	S	358	1248	191	268	1182	1639	1136	66	31	1632	59	16	1979	401	18	32	246
	CL	5	0	0	0	12	0	5	61	0	7	20	16	13	8	16	11	8
(%)	F	0	0	0	0	0	0	0	0	0	0	0	0	0	0	0	0	0

APPENDIX C, 7. Whole rock geochemistry (Stellenbosch University).

	Sample	F1	F2	F3	H1	Q1	Q1A	Q1V	Q2	Q2A	Q2V	Q3	Q3A	Q3V	Q4	Q4A	Q4V	Q5	Q5A	Q5V
Major elements (%)	SiO_2	72.89	71.84	71.20	62.94	89.83	62.22	96.88	76.38	72.44	94.65	72.05	54.88	96.42	75.92	77.13	87.17	88.67	44.04	95.34
	TiO_2	0.84	0.79	0.82	0.92	0.11	0.79	0.01	0.25	0.42	0.05	0.69	1.32	0.02	0.45	0.27	0.08	0.24	0.82	0.02
	Al_2O_3	11.02	11.68	11.70	15.51	3.52	16.75	0.59	8.23	9.94	1.51	10.92	17.95	0.97	9.61	8.54	5.16	3.33	20.32	0.77
	Fe_2O_3t	5.41	5.45	5.56	7.30	2.57	6.35	0.66	5.74	6.40	1.22	5.98	9.41	0.59	4.61	4.94	2.06	2.86	14.52	1.40
	MnO	0.05	0.09	0.08	0.09	0.03	0.08	0.01	0.07	0.07	0.01	0.09	0.12	0.01	0.06	0.06	0.03	0.03	0.15	0.01
	MgO	2.12	1.88	1.85	3.45	1.07	2.82	0.23	2.11	2.52	0.45	2.58	4.23	0.20	2.07	2.21	0.94	1.31	7.21	0.44
	CaO	0.13	0.13	0.16	0.23	0.06	0.18	0.28	0.19	0.50	0.14	0.20	0.22	0.02	0.15	0.12	0.13	0.09	0.18	0.01
	Na_2O	1.22	1.31	1.40	1.32	0.04	1.74	0.00	0.86	1.12	0.00	0.30	0.72	0.00	1.24	1.12	0.93	0.00	0.87	0.00
	K_2O	1.76	1.99	1.82	2.69	0.45	2.78	0.02	0.65	0.96	0.08	2.34	3.83	0.05	1.08	0.62	0.19	0.33	2.88	0.05
	P_2O_5	0.12	0.11	0.15	0.19	0.05	0.15	0.21	0.14	0.39	0.12	0.18	0.21	0.02	0.13	0.09	0.09	0.06	0.14	0.01
	H_2O-	0.61	0.55	0.50	0.45	0.20	0.35	0.09	0.55	0.52	0.14	0.47	0.84	0.09	0.33	0.68	0.19	0.17	1.32	0.22
	LOI	2.39	2.44	2.53	3.52	1.10	3.33	0.44	2.31	2.83	0.56	2.92	4.76	0.33	2.21	2.02	0.96	1.28	6.19	0.79
	TOTAL	98.55	98.25	97.75	98.60	99.00	97.55	99.40	97.45	98.15	98.90	98.75	98.50	98.75	97.85	97.80	97.90	98.40	98.65	99.10
Trace elements (ppm)	Cr	81	74	70	101	30	62	10	44	102	11	85	140	7	55	38	13	21	99	4
	Nd	37	30	30	31	3	13	3	11	28	0	30	54	3	16	13	3	2	36	3
	V	106	113	105	159	33	76	9	61	157	9	124	194	6	72	56	21	26	181	11
	Ce	78	62	63	75	8	30	9	24	58	6	65	117	8	41	24	12	17	74	7
	La	44	31	33	34	3	16	6	12	30	3	32	58	3	20	10	0	9	39	7
	Ba	291	458	477	677	83	159	17	129	435	15	386	601	13	207	111	39	67	440	24
	Sc	15	16	15	23	4	12	3	9	22	1	16	26	1	11	6	1	1	23	1
	Zr	251	202	223	198	23	92	8	65	161	9	157	306	6	93	53	20	34	7	160
	Y	35	30	33	39	8	47	12	25	31	12	34	55	6	18	13	6	9	2	34
	Sr	36	49	53	55	8	46	12	29	48	11	28	39	3	32	27	22	15	1	54
	U	3	1	1	1	1	1	1	1	4	1	0	5	1	1	1	1	1	1	0
	Rb	70	84	76	104	19	37	1	28	117	2	93	155	2	43	25	7	12	2	107
	Th	11	9	9	11	1	7	0	6	11	1	9	17	1	6	4	3	0	1	11
	Pb	5	10	13	3	26	136	23	95	51	23	37	37	8	27	39	23	15	19	59
	Ga	13	16	15	21	5	12	1	9	21	0	15	25	0	11	10	5	4	2	27
	Zn	81	83	101	130	42	101	13	82	99	14	108	172	10	83	86	36	52	21	278
	Cu	23	36	22	19	26	67	22	47	42	23	36	42	5	27	30	7	15	20	29
	Ni	39	43	34	54	17	47	7	39	46	7	46	72	6	34	37	15	18	9	101

APPENDIX C, 8. Chlorite compositions (Riviera).

	C1	C2	C3	C4	C5	C6	C7	C8	C21	C22	C23	C24	C25	C26	C27	C28	C30
Na2O	0.06	0.04	0.02	0.01	0.06	0.05	0.00	0.01	0.00	0.00	0.03	0.03	0.01	0.02	0.01	0.03	0.03
K2O	0.00	0.00	0.00	0.00	0.00	0.00	0.00	0.00	0.00	0.00	0.00	0.00	0.00	0.00	0.00	0.00	0.00
SiO2	26.85	27.01	27.57	27.30	27.51	27.46	27.06	27.21	26.68	27.02	26.96	27.49	27.42	28.15	27.34	27.27	27.04
TiO2	0.07	0.05	0.07	0.07	0.09	0.09	0.06	0.12	0.04	0.04	0.08	0.07	0.07	0.06	0.08	0.07	0.05
Al2O3	20.85	21.48	21.45	21.43	21.65	21.81	21.42	19.06	21.12	21.08	21.29	21.53	21.69	20.98	21.48	21.65	21.25
Fe2O3	18.60	18.28	18.49	18.10	18.91	19.21	18.27	19.36	18.67	19.19	18.21	18.46	18.19	19.46	18.74	18.53	18.30
MnO	0.20	0.18	0.18	0.14	0.20	0.19	0.20	0.19	0.21	0.21	0.20	0.14	0.14	0.19	0.20	0.19	0.18
MgO	20.11	20.72	20.36	20.56	20.75	20.36	20.28	20.56	20.05	19.97	20.25	20.15	20.58	20.29	20.26	20.22	20.23
CaO	0.01	0.00	0.01	0.00	0.00	0.01	0.00	0.03	0.04	0.04	0.01	0.00	0.01	0.05	0.00	0.02	0.00
Cr2O3	0.03	0.02	0.00	0.06	0.00	0.01	0.00	0.02	0.06	0.09	0.06	0.04	0.00	0.00	0.01	0.02	0.02
Total	86.77	87.78	88.13	87.66	89.16	89.19	87.28	86.56	86.87	87.63	87.09	87.90	88.12	89.20	88.13	87.99	87.10
Na	0.03	0.01	0.01	0.00	0.02	0.02	0.00	0.00	0.00	0.00	0.01	0.01	0.00	0.01	0.00	0.01	0.01
K	0.00	0.00	0.00	0.00	0.00	0.00	0.00	0.00	0.00	0.00	0.00	0.00	0.00	0.00	0.00	0.00	0.00
Si	5.52	5.47	5.57	5.54	5.49	5.50	5.52	5.62	5.48	5.52	5.52	5.58	5.54	5.65	5.54	5.52	5.53
Ti	0.01	0.01	0.01	0.01	0.01	0.01	0.01	0.02	0.01	0.01	0.01	0.01	0.01	0.01	0.01	0.01	0.01
Al	5.05	5.13	5.11	5.13	5.10	5.15	5.15	4.64	5.11	5.07	5.13	5.15	5.16	4.96	5.13	5.17	5.12
Fe2+	3.20	3.16	3.40	3.30	3.25	3.37	3.33	3.26	3.30	3.40	3.29	3.45	3.32	3.53	3.39	3.37	3.31
Fe3+	0.00	-0.06	-0.27	-0.23	-0.09	-0.15	-0.21	0.08	-0.09	-0.12	-0.18	-0.32	-0.25	-0.26	-0.22	-0.23	-0.19
Mn	0.03	0.03	0.03	0.02	0.03	0.03	0.03	0.03	0.04	0.04	0.03	0.02	0.02	0.03	0.03	0.03	0.03
Mg	6.16	6.26	6.14	6.22	6.18	6.08	6.17	6.33	6.14	6.08	6.18	6.10	6.19	6.07	6.12	6.11	6.17
Ca	0.00	0.00	0.00	0.00	0.00	0.00	0.00	0.01	0.01	0.01	0.00	0.00	0.00	0.01	0.00	0.00	0.00
Xfe	0.34	0.34	0.36	0.35	0.34	0.36	0.35	0.34	0.35	0.36	0.35	0.36	0.35	0.37	0.36	0.36	0.35
Temperature (°C)	281	287	274	278	283	282	280	270	284	279	281	273	278	265	278	279	279

APPENDIX C, 8. Chlorite compositions (Tygervalley)/

	C1	C2	C3	C4	C5	C6	C7	C8	C9	C10	C11	C12	C13	C14	C15	C16	C17	C18
Na2O	0.04	0.03	0.02	0.04	0.03	0.05	0.01	0.00	0.02	0.01	0.01	0.04	0.01	0.01	0.01	0.05	0.01	0.04
K2O	0.00	0.00	0.00	0.00	0.00	0.00	0.00	0.00	0.00	0.00	0.00	0.20	0.00	0.00	0.00	0.00	0.00	0.00
SiO2	26.91	27.03	26.46	26.47	26.64	27.70	26.60	26.75	26.66	26.90	26.12	27.83	26.09	26.43	26.45	26.95	27.07	27.01
TiO2	0.08	0.07	0.07	0.06	0.08	0.12	0.09	0.06	0.06	0.07	0.07	0.14	0.08	0.05	0.06	0.05	0.07	0.09
Al2O3	21.14	20.75	21.14	21.12	21.56	20.42	21.05	21.76	21.37	21.21	20.90	19.81	20.81	21.05	20.48	20.80	20.84	20.83
Fe2O3	26.49	26.22	26.52	25.64	25.46	26.18	26.23	26.22	25.61	26.17	25.86	26.53	26.19	25.47	26.57	27.72	26.10	25.81
MnO	0.54	0.54	0.58	0.52	0.53	0.53	0.53	0.56	0.53	0.52	0.53	0.48	0.60	0.52	0.59	0.55	0.54	0.49
MgO	13.55	14.11	14.28	14.63	13.86	14.27	14.44	14.51	14.02	14.22	13.37	13.28	14.28	13.83	15.06	14.82	15.14	14.23
CaO	0.05	0.11	0.02	0.06	0.03	0.07	0.05	0.02	0.04	0.01	0.04	0.07	0.04	0.05	0.00	0.06	0.04	0.04
Cr2O3	0.04	0.01	0.00	0.01	0.07	0.04	0.00	0.02	0.02	0.00	0.03	0.08	0.08	0.03	0.01	0.03	0.01	0.03
Total	88.85	88.89	89.10	88.54	88.26	89.37	89.00	89.91	88.33	89.13	86.92	88.46	88.17	87.44	89.23	91.03	89.83	88.56
Na	0.02	0.01	0.01	0.02	0.01	0.02	0.00	0.00	0.01	0.01	0.00	0.01	0.00	0.01	0.00	0.02	0.00	0.01
K	0.00	0.00	0.00	0.00	0.00	0.00	0.00	0.00	0.00	0.00	0.00	0.05	0.00	0.00	0.00	0.00	0.00	0.00
Si	5.68	5.68	5.54	5.56	5.63	5.79	5.57	5.54	5.63	5.63	5.63	5.92	5.53	5.64	5.52	5.53	5.60	5.69
Ti	0.01	0.01	0.01	0.01	0.01	0.02	0.01	0.01	0.01	0.01	0.01	0.02	0.01	0.01	0.01	0.01	0.01	0.01
Al	5.25	5.14	5.22	5.23	5.37	5.03	5.20	5.32	5.32	5.23	5.30	4.96	5.20	5.29	5.04	5.03	5.09	5.17
Fe2+	5.29	5.12	4.97	4.85	5.15	5.21	4.96	4.97	5.11	5.10	5.23	5.49	4.91	5.13	4.74	4.86	4.83	5.11
Fe3+	-0.62	-0.52	-0.33	-0.35	-0.65	-0.64	-0.37	-0.42	-0.59	-0.52	-0.58	-0.78	-0.27	-0.59	-0.10	-0.10	-0.31	-0.57
Mn	0.10	0.10	0.10	0.09	0.10	0.09	0.09	0.10	0.10	0.09	0.10	0.09	0.11	0.09	0.10	0.09	0.09	0.09
Mg	4.26	4.42	4.46	4.58	4.37	4.45	4.51	4.48	4.41	4.44	4.29	4.21	4.51	4.40	4.69	4.54	4.67	4.47
Ca	0.01	0.02	0.00	0.01	0.01	0.01	0.01	0.00	0.01	0.00	0.01	0.02	0.01	0.01	0.00	0.01	0.01	0.01
Xfe	0.55	0.54	0.53	0.51	0.54	0.54	0.52	0.53	0.54	0.53	0.55	0.57	0.52	0.54	0.50	0.52	0.51	0.53
Temperature (°C)	244	245	261	260	250	233	258	261	251	251	250	217	263	250	266	263	256	245

APPENDIX C, 8. Chlorite compositions (Bridgetown Formation).

	C1	C2	C3	C4	C5	C6	C7	C8	C9	C10	C11	C12	C13	C15
Na2O	0.00	0.00	0.00	0.00	0.00	0.01	0.01	0.03	0.00	0.00	0.02	0.01	0.02	0.05
K2O	0.00	0.00	0.00	0.00	0.00	0.00	0.00	0.00	0.00	0.00	0.00	0.00	0.00	0.00
SiO2	25.07	25.19	25.20	25.71	25.00	24.32	24.17	24.28	24.76	25.69	25.41	26.14	25.57	25.57
TiO2	0.05	0.08	0.07	0.06	0.07	0.07	0.06	0.06	0.09	0.07	0.05	0.10	0.10	0.05
Al2O3	20.81	21.01	21.44	22.26	21.21	20.95	20.74	21.56	20.49	20.44	20.53	20.22	20.35	20.50
Fe2O3	28.20	28.56	28.75	27.71	28.17	28.69	28.08	28.58	28.56	27.47	27.49	29.06	28.62	29.42
MnO	0.32	0.29	0.34	0.30	0.30	0.31	0.31	0.32	0.31	0.31	0.32	0.35	0.34	0.33
MgO	13.81	13.57	13.08	12.77	13.31	13.64	13.55	13.51	13.35	13.99	13.95	13.31	13.48	12.66
CaO	0.02	0.03	0.03	0.03	0.03	0.01	0.00	0.01	0.02	0.00	0.02	0.01	0.04	0.03
Cr2O3	0.03	0.04	0.04	0.05	0.05	0.00	0.03	0.00	0.04	0.03	0.01	0.03	0.00	0.00
Total	88.31	88.77	88.95	88.88	88.12	87.98	86.94	88.34	87.62	88.00	87.79	89.22	88.50	88.60
Na	0.00	0.00	0.00	0.00	0.00	0.00	0.00	0.01	0.00	0.00	0.01	0.00	0.01	0.02
K	0.00	0.00	0.00	0.00	0.00	0.00	0.00	0.00	0.00	0.00	0.00	0.00	0.00	0.00
Si	5.33	5.34	5.34	5.44	5.33	5.19	5.22	5.16	5.32	5.47	5.42	5.53	5.44	5.46
Ti	0.01	0.01	0.01	0.01	0.01	0.01	0.01	0.01	0.01	0.01	0.01	0.02	0.02	0.01
Al	5.21	5.25	5.35	5.55	5.33	5.27	5.28	5.40	5.19	5.13	5.16	5.04	5.10	5.16
Fe2+	4.90	5.00	5.15	5.36	5.05	4.80	4.81	4.80	5.00	4.98	4.92	5.28	5.10	5.33
Fe3+	0.11	0.06	-0.05	-0.46	-0.02	0.32	0.26	0.28	0.14	-0.09	-0.01	-0.14	-0.01	-0.07
Mn	0.06	0.05	0.06	0.05	0.05	0.06	0.06	0.06	0.06	0.06	0.06	0.06	0.06	0.06
Mg	4.38	4.29	4.13	4.03	4.24	4.34	4.36	4.28	4.28	4.44	4.44	4.20	4.28	4.03
Ca	0.00	0.01	0.01	0.01	0.01	0.00	0.00	0.00	0.00	0.00	0.00	0.00	0.01	0.01
Temperature (°C)	283	282	280	268	282	298	296	302	283	269	274	259	270	266

APPENDIX C, 8. Chlorite compositions (Bridgetown Formation #1).

	93196-1a	93196-1d	93196-1g	93196-1h	93196-1i	93196-2b	93196-2c	93196-2e	93196-2h	93196-2i	01-232-1a	01-232-1b	01-232-1c	01-232-1d	01-232-1e	01-232-1f	01-232-1g	01-232-2a
MgO	18.67	19.25	19.19	19.19	19.41	19.18	20.31	19.00	18.96	18.35	16.21	16.63	17.01	13.45	16.97	16.63	16.55	17.17
SiO2	26.32	26.91	26.07	26.07	26.96	27.21	26.90	27.73	28.24	28.25	26.63	26.30	25.89	26.84	26.83	26.62	27.15	26.62
Na2O	0.05	0.09	0.17	0.17	0.07	0.07	0.08	0.07	0.01	0.28	0.02	0.00	0.01	0.01	0.02	0.02	0.01	0.00
Al2O3	17.41	18.24	18.34	18.34	18.63	17.91	18.63	18.59	18.27	17.47	18.48	18.48	18.67	18.12	18.17	17.16	18.00	18.25
K2O	0.79	0.07	0.00	0.00	0.07	0.42	0.00	0.01	0.32	0.00	0.00	0.00	0.00	0.00	0.00	0.00	0.00	0.00
CaO	0.04	0.07	0.08	0.08	0.06	0.50	0.08	0.06	0.11	2.61	0.06	0.06	0.04	0.03	0.05	0.04	0.07	0.07
TiO2	0.12	0.02	0.01	0.01	0.03	0.54	0.03	0.03	0.09	1.51	0.02	0.02	0.01	0.02	0.01	0.00	0.00	0.04
FeO	18.23	19.45	19.50	19.50	19.65	18.28	19.03	18.65	18.81	18.50	25.19	25.33	26.22	24.93	24.15	24.98	24.72	25.66
MnO	0.19	0.16	0.14	0.14	0.15	0.19	0.15	0.06	0.13	0.19	0.20	0.27	0.20	0.20	0.25	0.20	0.16	0.21
Cr2O3	0.08	0.54	0.36	0.36	0.41	0.03	0.06	0.04	0.00	0.19	0.02	0.00	0.04	0.06	0.00	0.00	0.00	0.01
O	0.00	0.00	0.00	0.00	0.00	0.00	0.00	0.00	0.00	0.00	0.00	0.00	0.00	0.00	0.00	0.00	0.00	0.00
Total	81.89	84.79	83.84	83.84	85.45	84.32	85.26	84.24	84.94	87.36	86.83	87.08	88.07	83.66	86.45	85.65	86.65	88.03
Mg	6.09	6.09	6.12	6.12	6.09	6.09	6.34	6.04	5.98	5.67	5.15	5.25	5.31	4.49	5.38	5.35	5.25	5.36
Si	5.76	5.71	5.58	5.58	5.67	5.79	5.63	5.91	5.98	5.86	5.67	5.58	5.42	6.01	5.71	5.74	5.78	5.58
Na	0.02	0.04	0.07	0.07	0.03	0.03	0.03	0.03	0.00	0.11	0.01	0.00	0.00	0.01	0.01	0.01	0.00	0.00
Al	4.49	4.56	4.63	4.63	4.62	4.49	4.60	4.67	4.56	4.27	4.64	4.62	4.61	4.78	4.55	4.36	4.52	4.50
K	0.22	0.02	0.00	0.00	0.02	0.11	0.00	0.00	0.09	0.00	0.00	0.00	0.00	0.00	0.00	0.00	0.00	0.00
Ca	0.01	0.02	0.02	0.02	0.01	0.11	0.02	0.01	0.03	0.58	0.01	0.01	0.01	0.01	0.01	0.01	0.02	0.02
Ti	0.02	0.00	0.00	0.00	0.00	0.09	0.01	0.00	0.01	0.23	0.00	0.00	0.00	0.00	0.00	0.00	0.00	0.01
Fe2+	3.16	3.45	3.27	3.27	3.45	3.25	3.19	3.32	3.33	3.21	4.46	4.26	4.06	5.46	4.26	4.33	4.40	4.17
Fe3+	0.17		0.22	0.22	0.01		0.15				0.02	0.23	0.53	0.80	0.04	0.17		0.33
Mn	0.03	0.03	0.02	0.02	0.03	0.03	0.03	0.01	0.02	0.03	0.04	0.05	0.04	0.04	0.05	0.04	0.03	0.04
Cr	0.01	0.09	0.06	0.06	0.07	0.01	0.01	0.01	0.00	0.03	0.00	0.00	0.01	0.01	0.00	0.00	0.00	0.00
Xfe	0.34	0.36	0.35	0.35	0.36	0.35	0.33	0.36	0.36	0.36	0.46	0.45	0.43	0.55	0.44	0.45	0.46	0.44
Temperature (°C)	255	259	274	274	263	251	269	238	231	243	253	265	282	210	252	248	242	266

APPENDIX C, 8. Chlorite compositions (Bridgetown Formation #1).

	01-232-2b	01-232-2c	01-232-2d	01-232-2e	01-232-2f	01-232-2g	01-232-2h	01-232-2i	01-232-3a	01-232-3b	01-232-3c	01-232-3d	01-232-3e	01-232-3f	01-279-4a	01-279-4b	01-279-4c	01-279-4d
MgO	17.28	17.34	17.65	16.73	16.97	17.48	16.98	16.70	16.64	17.16	16.97	17.44	16.87	17.48	23.52	23.98	23.79	23.70
SiO2	27.02	26.49	26.66	26.58	26.22	26.73	25.67	26.71	26.48	26.82	26.54	27.12	27.00	27.17	28.11	27.59	27.74	28.10
Na2O	0.03	0.04	0.00	0.00	0.00	0.00	0.00	0.00	0.00	0.01	0.03	0.06	0.01	0.01	0.03	0.03	0.04	0.06
Al2O3	18.21	18.50	17.59	18.00	18.98	18.46	18.57	18.32	18.14	18.18	17.81	18.22	18.36	17.70	18.62	18.68	18.42	18.68
K2O	0.00	0.00	0.00	0.00	0.00	0.00	0.00	0.00	0.00	0.00	0.00	0.00	0.00	0.00	0.00	0.00	0.00	0.00
CaO	0.02	0.08	0.02	0.04	0.05	0.07	0.09	0.07	0.06	0.04	0.04	0.03	0.10	0.06	0.06	0.04	0.08	0.02
TiO2	0.05	0.10	0.02	0.03	0.05	0.05	0.05	0.05	0.02	0.01	0.05	0.04	0.01	0.03	0.00	0.00	0.00	0.02
FeO	26.29	25.61	25.08	25.28	25.73	25.60	25.12	25.94	24.95	24.67	24.42	25.26	25.66	25.15	14.73	14.71	14.80	15.07
MnO	0.27	0.17	0.26	0.25	0.31	0.24	0.21	0.25	0.27	0.31	0.19	0.20	0.17	0.20	0.16	0.20	0.16	0.16
Cr2O3	0.00	0.02	0.03	0.05	0.04	0.03	0.00	0.00	0.04	0.00	0.05	0.04	0.06	0.02	0.00	0.02	0.00	0.04
O	0.00	0.00	0.00	0.00	0.00	0.00	0.00	0.00	0.00	0.00	0.00	0.00	0.00	0.00	0.00	0.00	0.00	0.00
Total	89.15	88.34	87.31	86.95	88.36	88.65	86.70	88.04	86.59	87.19	86.10	88.39	88.23	87.82	85.23	85.25	85.03	85.83
Mg	5.34	5.39	5.54	5.30	5.28	5.41	5.38	5.23	5.29	5.40	5.41	5.41	5.26	5.46	7.18	7.30	7.27	7.18
Si	5.60	5.52	5.62	5.64	5.47	5.55	5.45	5.61	5.64	5.66	5.67	5.65	5.65	5.69	5.75	5.63	5.69	5.71
Na	0.01	0.02	0.00	0.00	0.00	0.00	0.00	0.00	0.00	0.00	0.01	0.02	0.00	0.00	0.01	0.01	0.01	0.02
Al	4.44	4.54	4.37	4.50	4.67	4.52	4.65	4.54	4.55	4.52	4.49	4.47	4.53	4.37	4.49	4.50	4.45	4.48
K	0.00	0.00	0.00	0.00	0.00	0.00	0.00	0.00	0.00	0.00	0.00	0.00	0.00	0.00	0.00	0.00	0.00	0.00
Ca	0.00	0.02	0.00	0.01	0.01	0.01	0.02	0.02	0.01	0.01	0.01	0.01	0.02	0.01	0.01	0.01	0.02	0.00
Ti	0.01	0.02	0.00	0.00	0.01	0.01	0.01	0.01	0.00	0.00	0.01	0.01	0.00	0.00	0.00	0.00	0.00	0.00
Fe2+	4.20	4.07	4.02	4.30	4.13	4.09	4.03	4.33	4.30	4.19	4.21	4.15	4.33	4.18	2.51	2.27	2.34	2.46
Fe3+	0.36	0.40	0.39	0.19	0.36	0.36	0.44	0.23	0.15	0.16	0.16	0.24	0.16	0.23	0.01	0.24	0.19	0.10
Mn	0.05	0.03	0.05	0.04	0.06	0.04	0.04	0.04	0.05	0.06	0.03	0.03	0.03	0.04	0.03	0.03	0.03	0.03
Cr	0.00	0.00	0.01	0.01	0.01	0.00	0.00	0.00	0.01	0.00	0.01	0.01	0.01	0.00	0.00	0.00	0.00	0.01
Xfe	0.44	0.43	0.42	0.45	0.44	0.43	0.43	0.45	0.45	0.44	0.44	0.43	0.45	0.43	0.26	0.24	0.24	0.25
Temperature (°C)	263	272	263	258	277	269	280	261	258	257	256	259	257	254	264	278	272	268

APPENDIX C, 8. Chlorite compositions (Bridgetown Formation#1).

	01-279-4e	01-279-6a	01-279-6b	01-279-6c	01-279-6d	01-279-6e	01-279-6f	01-279-8a	01-279-8b	01-279-8c	01-279-8d	01-279-8e	01-279-9a	01-279-9b	01-279-9c	01-279-9d	01-279-9e
MgO	24.37	24.23	23.55	24.11	23.44	23.83	24.14	25.33	24.70	24.62	24.10	25.10	24.83	24.52	24.76	24.43	24.49
SiO2	28.39	28.98	28.44	28.90	27.59	27.99	27.74	28.43	28.02	28.45	28.03	27.69	27.44	28.07	26.91	27.69	27.59
Na2O	0.06	0.04	0.02	0.05	0.08	0.09	0.07	0.06	0.10	0.15	0.03	0.09	0.12	0.09	0.10	0.12	0.15
Al2O3	18.35	17.89	18.09	18.09	17.62	17.83	18.70	17.78	17.84	18.19	18.34	18.37	18.93	19.11	19.03	18.47	18.81
K2O	0.00	0.00	0.00	0.00	0.00	0.00	0.00	0.00	0.00	0.00	0.00	0.00	0.01	0.00	0.00	0.00	0.00
CaO	0.05	0.03	0.04	0.04	0.04	0.05	0.05	0.04	0.04	0.04	0.08	0.07	0.00	0.04	0.01	0.05	0.08
TiO2	0.00	0.00	0.00	0.00	0.02	0.00	0.01	0.00	0.01	0.00	0.00	0.01	0.01	0.01	0.02	0.01	0.01
FeO	15.49	13.85	13.90	14.70	13.72	14.28	14.33	14.86	14.63	14.41	14.34	14.82	15.19	14.31	14.49	14.18	14.84
MnO	0.21	0.19	0.15	0.15	0.16	0.15	0.18	0.16	0.17	0.16	0.11	0.22	0.13	0.13	0.19	0.17	0.16
Cr2O3	0.07	0.05	0.02	0.04	0.00	0.00	0.02	0.00	0.00	0.00	0.02	0.00	0.02	0.08	0.00	0.02	0.05
O	0.00	0.00	0.00	0.00	0.00	0.00	0.00	0.00	0.00	0.00	0.00	0.00	0.00	0.00	0.00	0.00	0.00
Total	86.99	85.27	84.19	86.07	82.67	84.22	85.24	86.65	85.51	86.02	85.05	86.36	86.67	86.35	85.52	85.11	86.18
Mg	7.29	7.36	7.26	7.28	7.35	7.34	7.34	7.56	7.48	7.41	7.34	7.52	7.42	7.35	7.48	7.42	7.36
Si	5.70	5.91	5.88	5.85	5.80	5.78	5.66	5.70	5.69	5.74	5.73	5.56	5.50	5.64	5.45	5.64	5.56
Na	0.02	0.02	0.01	0.02	0.03	0.03	0.03	0.02	0.04	0.06	0.01	0.03	0.05	0.03	0.04	0.05	0.06
Al	4.34	4.30	4.41	4.32	4.36	4.34	4.49	4.20	4.27	4.33	4.42	4.35	4.47	4.53	4.54	4.43	4.47
K	0.00	0.00	0.00	0.00	0.00	0.00	0.00	0.00	0.00	0.00	0.00	0.00	0.00	0.00	0.00	0.00	0.00
Ca	0.01	0.01	0.01	0.01	0.01	0.01	0.01	0.01	0.01	0.01	0.02	0.01	0.00	0.01	0.00	0.01	0.02
Ti	0.00	0.00	0.00	0.00	0.00	0.00	0.00	0.00	0.00	0.00	0.00	0.00	0.00	0.00	0.00	0.00	0.00
Fe2+	2.32	2.36	2.40	2.49	2.35	2.34	2.22	2.05	2.10	2.18	2.32	1.93	1.96	2.20	1.86	2.09	2.04
Fe3+	0.28	-	-	-	0.06	0.13	0.22	0.44	0.38	0.25	0.13	0.56	0.58	0.21	0.59	0.32	0.46
Mn	0.04	0.03	0.03	0.02	0.03	0.03	0.03	0.03	0.03	0.03	0.02	0.04	0.02	0.02	0.03	0.03	0.03
Cr	0.01	0.01	0.00	0.01	0.00	0.00	0.00	0.00	0.00	0.00	0.00	0.00	0.00	0.01	0.00	0.00	0.01
Xfe	0.24	0.24	0.25	0.25	0.24	0.24	0.23	0.21	0.22	0.23	0.24	0.20	0.21	0.23	0.20	0.22	0.22
Temperature (°C)	271	249	251	254	260	262	277	274	274	268	268	289	296	278	301	279	288

APPENDIX C, 8. Chlorite compositions (Bloubergstrand).

	C1	C2	C3	C4	C5	C7	C8	C9	C10	C11	C12	C13	C14	C15	C16	C17
Na2O	0.03	0.01	0.01	0.00	0.01	0.00	0.01	0.01	0.00	0.00	0.00	0.02	0.00	0.03	0.00	0.00
K2O	0.00	0.00	0.00	0.00	0.00	0.00	0.00	0.00	0.00	0.00	0.00	0.00	0.00	0.00	0.00	0.00
SiO2	27.43	26.32	27.35	26.64	24.58	27.86	27.22	27.80	27.89	28.11	28.11	27.20	27.62	28.12	27.51	28.14
TiO2	0.00	0.03	0.02	0.01	0.00	0.01	0.00	0.01	0.00	0.02	0.04	0.00	0.03	0.01	0.03	0.00
Al2O3	17.70	18.17	17.67	18.56	22.27	17.50	18.26	17.98	17.99	18.11	17.70	17.65	18.26	17.70	17.99	18.00
Fe2O3	24.98	26.09	25.64	25.93	27.82	25.14	25.47	26.50	25.31	25.33	26.12	26.46	25.10	26.06	25.99	25.80
MnO	0.70	0.25	0.30	0.25	0.06	0.34	0.51	0.14	0.24	0.21	0.11	0.14	0.25	0.13	0.17	0.09
MgO	16.82	15.26	15.55	14.81	11.26	16.11	15.10	15.12	16.19	15.39	15.24	15.48	15.03	15.21	14.54	15.42
CaO	0.05	0.08	0.05	0.06	0.02	0.04	0.04	0.06	0.09	0.04	0.06	0.08	0.06	0.09	0.07	0.08
Cr2O3	0.00	0.07	0.00	0.00	0.00	0.03	0.07	0.02	0.00	0.00	0.01	0.00	0.02	0.00	0.00	0.00
Total	87.72	86.27	86.58	86.25	86.03	87.05	86.69	87.64	87.71	87.23	87.39	87.03	86.37	87.34	86.31	87.52
Na	0.01	0.00	0.00	0.00	0.01	0.00	0.01	0.00	0.00	0.00	0.00	0.01	0.00	0.01	0.00	0.00
K	0.00	0.00	0.00	0.00	0.00	0.00	0.00	0.00	0.00	0.00	0.00	0.00	0.00	0.00	0.00	0.00
Si	5.78	5.68	5.87	5.76	5.40	5.94	5.85	5.92	5.89	5.99	6.00	5.82	5.95	6.00	5.96	5.98
Ti	0.00	0.00	0.00	0.00	0.00	0.00	0.00	0.00	0.00	0.00	0.01	0.00	0.00	0.00	0.00	0.00
Al	4.39	4.62	4.47	4.73	5.77	4.39	4.63	4.51	4.48	4.55	4.45	4.45	4.64	4.45	4.59	4.51
Fe2+	4.34	4.71	4.82	4.93	5.68	4.75	4.90	5.08	4.73	5.06	5.12	4.83	5.07	5.10	5.22	5.06
Fe3+	0.06	0.00	-0.22	-0.24	-0.57	-0.27	-0.32	-0.36	-0.26	-0.54	-0.46	-0.09	-0.54	-0.45	-0.51	-0.47
Mn	0.12	0.05	0.05	0.05	0.01	0.06	0.09	0.02	0.04	0.04	0.02	0.03	0.05	0.02	0.03	0.02
Mg	5.28	4.91	4.98	4.77	3.69	5.12	4.84	4.80	5.10	4.89	4.85	4.94	4.83	4.84	4.69	4.89
Ca	0.01	0.02	0.01	0.01	0.01	0.01	0.01	0.01	0.02	0.01	0.01	0.02	0.01	0.02	0.02	0.02
Xfe	0.45	0.49	0.49	0.51	0.61	0.48	0.50	0.51	0.48	0.51	0.51	0.49	0.51	0.51	0.53	0.51
Temperature (°C)	243	250	229	240	268	223	231	222	228	215	214	234	219	213	217	216

APPENDIX C, 8. Chlorite compositions (De Hoek Quarry).

	C1	C2	C3	C4	C5	C6	C7	C8	C9	C10	C11	C12	C13	C14	C15
Na2O	0.00	0.00	0.01	0.01	0.02	0.00	0.01	0.02	0.02	0.02	0.01	0.02	0.00	0.03	0.04
K2O	0.00	0.00	0.00	0.00	0.00	0.00	0.00	0.00	0.00	0.00	0.00	0.00	0.00	0.00	0.00
SiO2	24.86	24.86	25.38	25.17	25.35	25.27	25.66	25.18	25.18	25.19	24.82	25.37	25.14	25.47	25.47
TiO2	0.01	0.04	0.04	0.06	0.05	0.02	0.07	0.04	0.04	0.06	0.02	0.06	0.04	0.03	0.03
Al2O3	20.19	20.57	20.52	20.50	20.10	20.46	20.54	20.37	20.37	20.04	20.10	20.49	20.59	21.77	21.65
Fe2O3	29.14	28.55	26.74	28.19	29.66	29.10	29.31	28.72	28.72	26.43	27.63	27.52	27.62	28.40	28.33
MnO	0.23	0.16	0.26	0.22	0.22	0.23	0.26	0.22	0.22	0.16	0.17	0.22	0.22	0.24	0.19
MgO	12.89	13.52	14.44	13.91	13.70	13.70	13.82	13.54	13.54	14.66	13.88	14.10	14.49	13.89	13.69
CaO	0.00	0.00	0.01	0.00	0.00	0.02	0.00	0.00	0.00	0.00	0.01	0.00	0.01	0.00	0.02
Cr2O3	0.02	0.02	0.01	0.01	0.00	0.00	0.02	0.00	0.00	0.00	0.03	0.00	0.00	0.04	0.00
Total	87.35	87.71	87.41	88.08	89.10	88.79	89.70	88.10	88.10	86.55	86.68	87.79	88.12	89.85	89.42
Na	0.00	0.00	0.00	0.00	0.01	0.00	0.00	0.01	0.01	0.01	0.00	0.01	0.00	0.01	0.02
K	0.00	0.00	0.00	0.00	0.00	0.00	0.00	0.00	0.00	0.00	0.00	0.00	0.00	0.00	0.00
Si	5.38	5.33	5.42	5.36	5.36	5.36	5.39	5.38	5.38	5.42	5.37	5.41	5.33	5.31	5.34
Ti	0.00	0.01	0.01	0.01	0.01	0.00	0.01	0.01	0.01	0.01	0.00	0.01	0.01	0.00	0.00
Al	5.15	5.20	5.16	5.15	5.01	5.11	5.08	5.13	5.13	5.08	5.12	5.15	5.14	5.35	5.35
Fe2+	5.18	4.99	4.77	4.90	5.00	4.98	5.02	5.01	5.01	4.68	4.85	4.88	4.71	4.93	4.97
Fe3+	0.09	0.13	0.00	0.12	0.25	0.17	0.13	0.11	0.11	0.07	0.14	0.03	0.18	0.02	0.00
Mn	0.04	0.03	0.05	0.04	0.04	0.04	0.05	0.04	0.04	0.03	0.03	0.04	0.04	0.04	0.03
Mg	4.16	4.32	4.59	4.42	4.32	4.33	4.33	4.31	4.31	4.70	4.47	4.48	4.58	4.32	4.28
Ca	0.00	0.00	0.00	0.00	0.00	0.00	0.00	0.00	0.00	0.00	0.00	0.00	0.00	0.00	0.00
Xfe	0.55	0.54	0.51	0.53	0.54	0.54	0.54	0.54	0.54	0.50	0.52	0.52	0.51	0.53	0.54
Temperature (°C)	276	283	276	280	279	280	277	278	278	277	280	276	285	285	282

APPENDIX C, 8. Chlorite compositions (De Hoek Quarry).

	C16	C17	C18	C19	C20	C21	C22	C23	C24	C25	C26	C27	C28	C29
Na2O	0.03	0.00	0.03	0.04	0.00	0.01	0.03	0.00	0.00	0.00	0.00	0.00	0.00	0.01
K2O	0.00	0.00	0.00	0.00	0.00	0.00	0.00	0.00	0.00	0.00	0.00	0.00	0.00	0.00
SiO2	27.08	26.61	25.67	24.60	25.05	25.44	26.91	25.59	25.32	25.97	25.65	25.23	25.81	25.91
TiO2	0.05	0.04	0.02	0.05	0.03	0.02	0.03	0.03	0.04	0.03	0.05	0.02	0.05	0.03
Al2O3	22.26	21.28	20.74	19.88	20.72	21.08	22.25	20.82	20.63	21.03	21.09	20.91	20.91	20.99
Fe2O3	27.05	27.54	27.77	27.75	28.58	28.27	27.56	28.40	27.80	28.28	28.27	27.86	27.23	28.41
MnO	0.22	0.26	0.21	0.17	0.18	0.20	0.25	0.23	0.19	0.16	0.18	0.26	0.21	0.21
MgO	12.22	13.72	13.43	13.95	14.23	13.38	13.27	13.48	13.50	14.25	13.86	13.57	13.28	13.96
CaO	0.01	0.02	0.02	0.00	0.00	0.00	0.03	0.02	0.01	0.00	0.00	0.00	0.00	0.02
Cr2O3	0.00	0.00	0.01	0.00	0.00	0.00	0.02	0.01	0.01	0.03	0.00	0.00	0.00	0.00
Total	88.92	89.47	87.88	86.44	88.79	88.40	90.34	88.57	87.50	89.76	89.11	87.86	87.48	89.53
Na	0.01	0.00	0.01	0.02	0.00	0.00	0.01	0.00	0.00	0.00	0.00	0.00	0.00	0.00
K	0.00	0.00	0.00	0.00	0.00	0.00	0.00	0.00	0.00	0.00	0.00	0.00	0.00	0.00
Si	5.73	5.58	5.48	5.33	5.29	5.41	5.59	5.43	5.43	5.42	5.40	5.39	5.54	5.43
Ti	0.01	0.01	0.00	0.01	0.00	0.00	0.00	0.00	0.01	0.00	0.01	0.00	0.01	0.00
Al	5.56	5.25	5.22	5.08	5.15	5.28	5.45	5.21	5.22	5.17	5.23	5.26	5.29	5.18
Fe2+	4.79	4.83	4.96	4.77	4.78	5.03	4.79	5.04	4.99	4.94	4.98	4.98	4.88	4.98
Fe3+	0.00	0.00	0.00	0.26	0.26	0.00	0.00	0.00	0.00	0.00	0.00	0.00	0.00	0.00
Mn	0.04	0.05	0.04	0.03	0.03	0.04	0.04	0.04	0.03	0.03	0.03	0.05	0.04	0.04
Mg	3.86	4.29	4.28	4.51	4.48	4.24	4.11	4.27	4.32	4.44	4.35	4.32	4.25	4.36
Ca	0.00	0.00	0.00	0.00	0.00	0.00	0.01	0.00	0.00	0.00	0.00	0.00	0.00	0.00
Xfe	0.55	0.53	0.54	0.51	0.52	0.54	0.54	0.54	0.54	0.53	0.53	0.54	0.53	0.53
Temperature (°C)	238	257	266	285	289	274	255	271	272	274	276	277	261	272

APPENDIX C, 8. Chlorite compositions (Porseleinberg).

	C1	C2	C3	C4	C5	C6	C7	C8	C9	C10	C11	C12	C13	C14	C15
Na2O	0.01	0.02	0.01	0.01	0.02	0.01	0.06	0.03	0.04	0.01	0.03	0.00	0.02	0.03	0.03
K2O	0.00	0.00	0.00	0.00	0.00	0.00	0.00	0.00	0.00	0.00	0.00	0.00	0.00	0.00	0.00
SiO2	29.02	28.86	29.08	28.91	29.09	29.07	29.16	29.15	29.31	29.30	29.16	28.88	28.31	28.52	28.96
TiO2	0.06	0.04	0.00	0.01	0.01	0.02	0.02	0.01	0.00	0.00	0.03	0.02	0.01	0.00	0.00
Al2O3	19.13	19.17	18.93	18.87	19.41	19.22	19.13	18.74	19.42	18.98	19.31	18.66	19.07	18.92	19.18
Fe2O3	13.94	14.03	14.71	14.57	14.19	14.14	14.95	14.28	14.58	13.94	13.95	14.16	14.62	13.97	14.20
MnO	0.12	0.09	0.12	0.11	0.16	0.11	0.16	0.09	0.13	0.12	0.17	0.12	0.17	0.11	0.15
MgO	24.44	23.97	24.03	23.75	23.86	23.63	23.68	23.70	24.39	24.27	24.40	24.12	25.10	24.51	24.02
CaO	0.04	0.04	0.09	0.02	0.04	0.05	0.04	0.07	0.03	0.04	0.02	0.03	0.04	0.05	0.03
Cr2O3	0.03	0.06	0.01	0.09	0.02	0.08	0.01	0.06	0.07	0.06	0.05	0.07	0.00	0.00	0.00
Total	86.77	86.28	86.98	86.35	86.80	86.33	87.21	86.12	87.97	86.74	87.12	86.07	87.32	86.11	86.56
Na	0.00	0.01	0.00	0.00	0.01	0.00	0.02	0.01	0.02	0.00	0.01	0.00	0.01	0.01	0.01
K	0.00	0.00	0.00	0.00	0.00	0.00	0.00	0.00	0.00	0.00	0.00	0.00	0.00	0.00	0.00
Si	5.81	5.82	5.83	5.85	5.84	5.88	5.84	5.91	5.81	5.88	5.82	5.84	5.63	5.75	5.82
Ti	0.01	0.01	0.00	0.00	0.00	0.00	0.00	0.00	0.00	0.00	0.00	0.00	0.00	0.00	0.00
Al	4.52	4.56	4.47	4.50	4.59	4.58	4.52	4.47	4.53	4.49	4.54	4.45	4.47	4.49	4.54
Fe2+	2.49	2.58	2.60	2.65	2.65	2.72	2.69	2.69	2.54	2.58	2.51	2.54	2.14	2.33	2.57
Fe3+	-0.15	-0.21	-0.13	-0.19	-0.27	-0.33	-0.19	-0.27	-0.13	-0.24	-0.18	-0.14	0.29	0.02	-0.18
Mn	0.02	0.02	0.02	0.02	0.03	0.02	0.03	0.02	0.02	0.02	0.03	0.02	0.03	0.02	0.02
Mg	7.30	7.21	7.18	7.16	7.14	7.12	7.07	7.16	7.20	7.26	7.26	7.28	7.44	7.36	7.20
Ca	0.01	0.01	0.02	0.01	0.01	0.01	0.01	0.01	0.01	0.01	0.01	0.01	0.01	0.01	0.01
Xfe	0.25	0.26	0.27	0.27	0.27	0.28	0.28	0.27	0.26	0.26	0.26	0.26	0.22	0.24	0.26
Temperature (°C)	258	256	255	253	253	249	253	246	258	250	257	254	280	266	256

APPENDIX C, 8. Chlorite compositions (Porterville).

	01-267-1a	01-267-1b	01-267-1d	01-267-2a	01-267-2b	01-267-2c	01-267-2d
MgO	12.83	13.05	13.99	12.31	13.43	13.09	13.92
SiO2	24.98	25.55	25.34	26.64	25.77	25.79	25.58
Na2O	0.25	0.18	0.26	0.10	0.07	0.00	0.01
Al2O3	20.63	21.03	19.84	21.02	19.74	16.62	20.03
K2O	0.01	0.18	0.04	0.62	0.00	0.12	0.00
CaO	0.08	0.10	0.07	0.13	0.17	0.27	0.18
TiO2	0.07	0.07	0.09	0.12	0.05	0.08	0.04
Fe2O3	24.45	24.44	24.63	24.19	24.71	24.31	25.06
MnO	0.17	0.17	0.20	0.14	0.17	0.11	0.16
Cr2O3	0.00	0.01	0.02	0.02	0.00	0.08	0.03
O	0.00	0.00	0.00	0.00	0.00	0.00	0.00
Total	83.46	84.77	84.49	85.27	84.10	80.47	85.01
Mg	4.27	4.27	4.58	4.02	4.44	4.55	4.55
Si	5.57	5.61	5.57	5.83	5.71	6.01	5.61
Na	0.11	0.08	0.11	0.04	0.03	0.00	0.00
Al	5.42	5.44	5.13	5.43	5.16	4.56	5.17
K	0.00	0.05	0.01	0.17	0.00	0.04	0.00
Ca	0.02	0.02	0.02	0.03	0.04	0.07	0.04
Ti	0.01	0.01	0.01	0.02	0.01	0.01	0.01
Fe2+	4.56	4.49	4.52	4.43	4.58	4.73	4.59
Fe3+	-	-	-	-	-	-	-
Mn	0.03	0.03	0.04	0.03	0.03	0.02	0.03
Cr	0.00	0.00	0.00	0.00	0.00	0.01	0.01
Xfe	0.52	0.51	0.50	0.52	0.51	0.51	0.50
Temperature (°C)	259	255	261	230	245	213	257

APPENDIX C, 8. Chlorite compositions (Goudmyn se kop).

	01-158-2b	01-158-2c	01-158-2d	01-158-2f	01-158-2g	01-158-2h	01-158-2i	01-158-2j	01-158-1a	01-158-1b	01-158-1c	01-158-1d	01-158-1e
MgO	12.42	12.18	13.33	12.93	12.70	12.97	12.39	13.08	12.86	12.91	12.42	12.18	13.33
SiO2	24.48	24.36	23.56	23.81	23.60	24.60	24.43	23.77	23.79	24.10	24.48	24.36	23.56
Na2O	0.01	0.03	0.01	0.05	0.04	0.08	0.00	0.05	0.05	0.02	0.01	0.03	0.01
Al2O3	21.78	21.47	21.40	21.90	21.98	21.83	22.00	21.46	20.87	22.13	21.78	21.47	21.40
K2O	0.00	0.00	0.00	0.00	0.00	0.00	0.00	0.00	0.00	0.00	0.00	0.00	0.00
CaO	0.06	0.09	0.04	0.02	0.02	0.02	0.01	0.00	0.01	0.04	0.06	0.09	0.04
TiO2	0.06	0.07	0.04	0.05	0.07	0.02	0.07	0.02	0.04	0.06	0.06	0.07	0.04
Fe2O3	26.47	26.48	25.34	26.37	25.54	26.14	26.67	26.46	26.08	26.54	26.47	26.48	25.34
MnO	0.34	0.34	0.36	0.32	0.31	0.24	0.25	0.22	0.28	0.28	0.34	0.34	0.36
Cr2O3	0.02	0.00	0.02	0.00	0.00	0.01	0.02	0.03	0.02	0.00	0.02	0.00	0.02
O	0.00	0.00	0.00	0.00	0.00	0.00	0.00	0.00	0.00	0.00	0.00	0.00	0.00
Total	85.64	85.01	84.10	85.44	84.25	85.91	85.85	85.08	84.00	86.06	85.64	85.01	84.10
Mg	4.06	4.01	4.40	4.22	4.20	4.21	4.04	4.28	4.27	4.18	4.06	4.01	4.40
Si	5.37	5.39	5.22	5.21	5.23	5.35	5.34	5.22	5.30	5.24	5.37	5.39	5.22
Na	0.01	0.01	0.01	0.02	0.02	0.04	0.00	0.02	0.02	0.01	0.01	0.01	0.01
Al	5.63	5.59	5.59	5.65	5.74	5.60	5.67	5.56	5.48	5.67	5.63	5.59	5.59
k	0.00	0.00	0.00	0.00	0.00	0.00	0.00	0.00	0.00	0.00	0.00	0.00	0.00
Ca	0.01	0.02	0.01	0.00	0.01	0.01	0.00	0.00	0.00	0.01	0.01	0.02	0.01
Ti	0.01	0.01	0.01	0.01	0.01	0.00	0.01	0.00	0.01	0.01	0.01	0.01	0.01
Fe2+	4.85	4.90	4.69	4.83	4.74	4.76	4.88	4.86	4.86	4.83	4.85	4.90	4.69
Fe3+	-	-	-	-	-	-	-	0.00	-	-	-	-	-
Mn	0.06	0.06	0.07	0.06	0.06	0.04	0.05	0.04	0.05	0.05	0.06	0.06	0.07
Cr	0.00	0.00	0.00	0.00	0.00	0.00	0.00	0.01	0.00	0.00	0.00	0.00	0.00
Xfe	0.54	0.55	0.52	0.53	0.53	0.53	0.55	0.53	0.53	0.54	0.54	0.55	0.52
Temperature (°C)	278	276	296	295	294	281	280	294	286	292	278	276	296

APPENDIX C, 8. Chlorite compositions (Spitskop).

	CL1	CL2	CL3	CL4	CL5	CL6	CL7	CL8	CL9	CL10	CL11	CL12	CL13	CL14	CL15	CL16	CL17	CL18
Na2O	0.00	0.01	0.01	0.02	0.01	0.07	0.04	0.00	0.00	0.02	0.05	0.01	0.01	0.02	0.04	0.00	0.02	0.01
K2O	0.00	0.01	0.00	0.00	0.01	0.01	0.01	0.00	0.00	0.00	0.03	0.00	0.01	0.01	0.05	0.04	0.00	0.03
SiO2	25.39	25.66	23.18	24.57	24.79	25.79	25.40	25.44	24.18	23.92	24.03	25.12	24.68	25.13	22.64	24.50	22.65	24.87
TiO2	0.07	0.06	0.06	0.02	0.03	0.05	0.04	0.03	0.05	0.04	0.04	0.07	0.08	0.03	0.04	0.06	0.07	0.06
Al2O3	21.68	21.49	20.74	21.89	22.16	21.31	21.93	22.05	20.97	20.43	22.51	21.95	21.80	25.00	20.21	21.41	20.98	21.65
FeO	22.98	23.10	23.03	22.94	23.92	23.17	23.60	23.20	22.98	22.89	27.31	26.29	26.80	25.78	26.30	26.28	25.58	26.42
MnO	0.57	0.58	0.57	0.64	0.64	0.61	0.59	0.54	0.57	0.60	0.65	0.58	0.69	0.64	0.60	0.64	0.79	0.58
MgO	16.52	17.49	15.78	16.62	16.74	17.41	16.92	17.04	17.16	16.38	13.06	14.00	14.13	14.48	12.54	13.23	12.45	13.96
CaO	0.01	0.02	0.02	0.01	0.03	0.05	0.02	0.01	0.02	0.04	0.03	0.02	0.05	0.02	0.05	0.04	0.01	0.02
Total	87.21	88.42	83.38	86.72	88.33	88.47	88.54	88.32	85.93	84.31	87.72	88.04	88.24	91.12	82.46	86.20	82.55	87.60
Na	0.00	0.00	0.00	0.01	0.00	0.03	0.01	0.00	0.00	0.01	0.02	0.00	0.00	0.01	0.02	0.00	0.01	0.00
K	0.00	0.00	0.00	0.00	0.00	0.00	0.00	0.00	0.00	0.00	0.01	0.00	0.00	0.00	0.02	0.01	0.00	0.01
Si	5.31	5.29	5.10	5.18	5.14	5.32	5.25	5.26	5.13	5.19	5.13	5.31	5.22	5.09	5.15	5.31	5.14	5.29
Ti	0.01	0.01	0.01	0.00	0.00	0.01	0.01	0.00	0.01	0.01	0.01	0.01	0.01	0.00	0.01	0.01	0.01	0.01
Al	5.24	5.22	5.37	5.43	5.41	5.18	5.34	5.37	5.24	5.22	5.67	5.47	5.43	5.97	5.42	5.47	5.61	5.43
Fe2+	4.00	3.80	3.81	3.83	3.84	3.79	3.90	3.92	3.60	3.76	4.80	4.64	4.63	4.37	4.71	4.76	4.77	4.70
Fe3+	0.00	0.18	0.42	0.21	0.31	0.20	0.18	0.10	0.48	0.39	0.08	0.00	0.11	0.00	0.30	0.00	0.09	0.00
Mn	0.10	0.10	0.11	0.11	0.11	0.11	0.10	0.09	0.10	0.11	0.12	0.10	0.12	0.11	0.11	0.12	0.15	0.10
Mg	5.40	5.38	5.17	5.22	5.17	5.35	5.21	5.25	5.43	5.30	4.16	4.41	4.46	4.37	4.25	4.27	4.21	4.43
Ca	0.00	0.00	0.00	0.00	0.01	0.01	0.00	0.00	0.01	0.01	0.01	0.00	0.01	0.00	0.01	0.01	0.00	0.01
Xfe	0.43	0.41	0.42	0.42	0.43	0.41	0.43	0.43	0.40	0.42	0.54	0.51	0.51	0.50	0.53	0.53	0.53	0.51
Temperature (°C)	295	298	318	310	313	295	302	300	317	309	304	287	297	312	303	286	303	289

APPENDIX C, 8. Chlorite compositions (Kruisfontein Quarry).

	CL1	CL2	CL3	CL4	CL5	CL6	CL7	CL8	CL9	CL10	CL11	CL12	CL13	CL14	CL15	CL16	CL17	CL18
MgO	12.90	13.75	13.81	13.17	13.68	14.14	14.09	14.12	13.80	14.05	14.47	14.65	14.17	14.32	14.04	14.94	14.66	14.42
SiO2	24.23	24.76	24.27	23.68	24.69	24.88	24.84	24.67	24.34	23.47	25.11	25.05	24.59	25.04	24.58	24.79	25.38	24.62
Na2O	0.00	0.05	0.00	0.00	0.02	0.00	0.09	0.01	0.02	0.01	0.03	0.04	0.00	0.00	0.00	0.00	0.00	0.00
Al2O3	22.02	20.97	21.74	19.67	20.63	21.52	21.24	21.41	21.21	21.51	21.08	20.70	21.31	22.00	21.39	21.31	22.07	21.79
K2O	0.00	0.00	0.00	0.00	0.00	0.00	0.00	0.00	0.00	0.00	0.00	0.00	0.00	0.00	0.00	0.00	0.00	0.00
CaO	0.01	0.04	0.03	0.09	0.04	0.02	0.03	0.00	0.01	0.02	0.01	0.08	0.03	0.04	0.03	0.00	0.00	0.00
TiO2	0.03	0.06	0.03	0.05	0.02	0.05	0.06	0.05	0.07	0.07	0.06	0.05	0.03	0.04	0.03	0.07	0.07	0.03
Fe2O3	26.62	26.56	27.29	26.00	26.30	30.17	29.19	29.69	26.95	26.43	26.99	25.86	25.94	26.35	25.53	27.21	26.94	26.62
MnO	0.20	0.22	0.22	0.20	0.17	0.20	0.18	0.20	0.17	0.17	0.21	0.16	0.19	0.20	0.26	0.19	0.21	0.20
Cr2O3	0.00	0.07	0.00	0.05	0.07	0.00	0.05	0.05	0.01	0.06	0.04	0.01	0.04	0.02	0.05	0.00	0.02	0.00
O	0.00	0.00	0.00	0.00	0.00	0.00	0.00	0.00	0.00	0.00	0.00	0.00	0.00	0.00	0.00	0.00	0.00	0.00
Total	86.02	86.47	87.40	82.90	85.62	90.97	89.76	90.20	86.58	85.76	87.99	86.61	86.30	88.00	85.90	88.51	89.34	87.67
Mg	4.19	4.43	4.40	4.43	4.45	4.36	4.39	4.38	4.44	4.55	4.57	4.68	4.56	4.51	4.53	4.68	4.55	4.56
Si	5.27	5.35	5.19	5.35	5.39	5.14	5.19	5.14	5.25	5.09	5.32	5.37	5.30	5.29	5.32	5.21	5.29	5.22
Na	0.00	0.02	0.00	0.00	0.01	0.00	0.04	0.00	0.01	0.00	0.01	0.02	0.00	0.00	0.00	0.00	0.00	0.00
Al	5.65	5.34	5.48	5.23	5.30	5.24	5.23	5.25	5.39	5.50	5.26	5.23	5.41	5.48	5.46	5.28	5.42	5.45
K	0.00	0.00	0.00	0.00	0.00	0.00	0.00	0.00	0.00	0.00	0.00	0.00	0.00	0.00	0.00	0.00	0.00	0.00
Ca	0.00	0.01	0.01	0.02	0.01	0.00	0.01	0.00	0.00	0.00	0.00	0.02	0.01	0.01	0.01	0.00	0.00	0.00
Ti	0.01	0.01	0.00	0.01	0.00	0.01	0.01	0.01	0.01	0.01	0.01	0.01	0.01	0.01	0.01	0.01	0.01	0.00
Fe2+	4.85	4.80	4.74	4.91	4.80	5.21	4.70	4.71	4.77	4.52	4.78	4.61	4.68	4.66	4.62	4.51	4.69	4.63
Fe3+	-	-	0.13	0.05	-	0.46	0.40	0.46	0.09	0.28	0.08	0.02	-	-	-	0.28	-	0.09
Mn	0.04	0.04	0.04	0.04	0.03	0.04	0.03	0.04	0.03	0.03	0.04	0.03	0.03	0.04	0.05	0.03	0.04	0.04
Cr	0.00	0.01	0.00	0.01	0.01	0.00	0.01	0.01	0.00	0.01	0.01	0.00	0.01	0.00	0.01	0.00	0.00	0.00
Xfe	0.54	0.52	0.52	0.53	0.52	0.54	0.52	0.52	0.52	0.50	0.51	0.50	0.51	0.51	0.50	0.49	0.51	0.50
Temperature (°C)	289	282	299	282	278	302	299	305	293	311	286	282	289	289	287	300	290	297

APPENDIX C, 8. Chlorite compositions (Kruisfontein Quarry).

	CL19	CL20	CL21	CL22	CL23	CL24	CL25	CL26	CL27	CL28	CL29	CL30	CL31	CL32	CL33
MgO	15.22	14.53	12.80	13.01	12.96	12.89	12.19	13.84	13.71	13.47	13.32	13.65	13.10	13.36	12.95
SiO2	25.43	25.19	24.29	24.37	23.94	24.27	24.32	24.20	24.70	24.34	24.64	25.02	24.81	24.42	24.49
Na2O	0.02	0.00	0.00	0.00	0.03	0.00	0.04	0.03	0.00	0.00	0.03	0.01	0.00	0.00	0.01
Al2O3	21.75	22.38	21.60	22.09	21.78	22.00	21.94	20.79	20.74	20.70	20.74	20.72	20.63	20.46	22.08
K2O	0.00	0.00	0.00	0.00	0.00	0.00	0.01	0.00	0.00	0.00	0.00	0.00	0.00	0.00	0.00
CaO	0.01	0.03	0.01	0.01	0.02	0.00	0.04	0.00	0.00	0.01	0.02	0.04	0.06	0.01	0.02
TiO2	0.04	0.06	0.11	0.09	0.05	0.03	0.03	0.03	0.05	0.11	0.07	0.05	0.07	0.06	0.06
Fe2O3	27.24	26.17	30.33	30.81	30.54	29.93	29.14	29.69	30.80	30.47	27.58	27.62	27.23	26.07	26.67
MnO	0.18	0.20	0.24	0.32	0.20	0.21	0.19	0.19	0.19	0.26	0.18	0.27	0.21	0.24	0.21
Cr2O3	0.01	0.08	0.06	0.03	0.14	0.22	0.12	0.15	0.11	0.10	0.08	0.19	0.16	0.26	0.18
O	0.00	0.00	0.00	0.00	0.00	0.00	0.00	0.00	0.00	0.00	0.00	0.00	0.00	0.00	0.00
Total	89.89	88.64	89.44	90.73	89.65	89.55	88.01	88.92	90.30	89.45	86.64	87.56	86.26	84.88	86.66
Mg	4.69	4.54	4.04	4.04	4.07	4.05	3.90	4.36	4.28	4.24	4.30	4.36	4.25	4.39	4.17
Si	5.26	5.28	5.14	5.08	5.05	5.12	5.22	5.12	5.17	5.14	5.34	5.36	5.40	5.38	5.29
Na	0.01	0.00	0.00	0.00	0.01	0.00	0.01	0.01	0.00	0.00	0.01	0.00	0.00	0.00	0.00
Al	5.30	5.53	5.39	5.43	5.41	5.47	5.55	5.18	5.11	5.15	5.29	5.23	5.29	5.32	5.63
K	0.00	0.00	0.00	0.00	0.00	0.00	0.00	0.00	0.00	0.00	0.00	0.00	0.00	0.00	0.00
Ca	0.00	0.01	0.00	0.00	0.00	0.00	0.01	0.00	0.00	0.00	0.00	0.01	0.01	0.00	0.00
Ti	0.01	0.01	0.02	0.01	0.01	0.00	0.01	0.01	0.01	0.02	0.01	0.01	0.01	0.01	0.01
Fe2+	4.52	4.59	5.07	4.99	4.92	5.03	5.23	5.25	4.86	4.87	4.99	4.94	4.96	4.81	4.82
Fe3+	0.18		0.30	0.38	0.47	0.25		0.55	0.52	0.51	0.01	0.00			
Mn	0.03	0.03	0.04	0.06	0.04	0.04	0.04	0.03	0.03	0.05	0.03	0.05	0.04	0.04	0.04
Cr	0.00	0.01	0.01	0.00	0.02	0.04	0.02	0.03	0.02	0.02	0.01	0.03	0.03	0.05	0.03
Xfe	0.49	0.50	0.56	0.55	0.55	0.55	0.57	0.55	0.53	0.53	0.54	0.53	0.54	0.52	0.54
Temperature (°C)	295	291	301	308	312	303	291	304	300	303	282	280	275	278	287

APPENDIX C, 8. Chlorite compositions (Robben Island).

	650 G	649 G	648 G	647 G	646 G	644 G	643 G	642 G	641 G	640 G	639 G	638 G	637 G	636 G	635 G
Na2O	0.00	0.00	0.02	0.02	0.03	0.01	0.03	0.04	0.01	0.01	0.08	0.06	0.01	0.12	0.11
K2O	0.00	0.00	0.00	0.00	0.00	0.00	0.00	0.00	0.00	0.00	0.00	0.00	0.00	0.00	0.00
SiO2	26.30	25.89	26.12	26.38	26.39	26.74	26.46	26.38	26.46	26.57	25.28	25.50	26.45	27.18	26.54
TiO2	0.03	0.02	0.02	0.03	0.06	0.05	0.03	0.06	0.02	0.04	0.04	0.03	0.03	0.04	0.05
Al2O3	19.12	19.36	19.05	19.16	18.78	20.10	19.57	19.61	19.59	19.88	19.40	19.09	19.52	19.24	19.33
Fe2O3	29.85	30.05	29.87	29.14	29.71	27.47	29.19	29.31	29.72	28.34	28.79	30.47	29.36	30.03	30.34
MnO	0.38	0.33	0.38	0.40	0.45	0.23	0.32	0.37	0.37	0.30	0.28	0.39	0.35	0.38	0.39
MgO	13.42	14.16	13.82	14.16	13.64	13.52	13.68	13.05	13.04	13.08	13.20	12.20	13.14	13.41	13.65
CaO	0.02	0.03	0.00	0.03	0.01	0.00	0.00	0.00	0.02	0.02	0.03	0.00	0.03	0.03	0.03
Cr2O3	0.00	0.01	0.00	0.02	0.04	0.00	0.00	0.01	0.00	0.00	0.00	0.00	0.02	0.00	0.00
Total	89.11	89.84	89.29	89.34	89.10	88.12	89.29	88.83	89.23	88.24	87.10	87.74	88.91	90.42	90.43
Na	0.00	0.00	0.01	0.01	0.01	0.00	0.01	0.02	0.00	0.00	0.03	0.03	0.00	0.05	0.04
K	0.00	0.00	0.00	0.00	0.00	0.00	0.00	0.00	0.00	0.00	0.00	0.00	0.00	0.00	0.00
Si	5.59	5.44	5.53	5.56	5.60	5.70	5.59	5.62	5.62	5.68	5.47	5.54	5.63	5.69	5.55
Ti	0.00	0.00	0.00	0.00	0.01	0.01	0.00	0.01	0.00	0.01	0.01	0.00	0.00	0.01	0.01
Al	4.79	4.79	4.75	4.76	4.70	5.05	4.87	4.92	4.90	5.01	4.95	4.88	4.90	4.75	4.76
Fe2+	5.27	4.94	5.09	5.02	5.19	4.90	5.16	5.22	5.28	5.07	5.09	5.47	5.23	5.26	5.14
Fe3+	0.03	0.33	0.20	0.11	0.08	0.00	0.00	0.00	0.00	0.00	0.12	0.06	0.00	0.00	0.16
Mn	0.07	0.06	0.07	0.07	0.08	0.04	0.06	0.07	0.07	0.05	0.05	0.07	0.06	0.07	0.07
Mg	4.25	4.43	4.36	4.45	4.32	4.30	4.31	4.14	4.13	4.17	4.26	3.95	4.17	4.18	4.26
Ca	0.00	0.01	0.00	0.01	0.00	0.00	0.00	0.00	0.00	0.01	0.01	0.00	0.01	0.01	0.01
Xfe	0.55	0.53	0.54	0.53	0.55	0.53	0.54	0.56	0.56	0.55	0.54	0.58	0.56	0.56	0.55
Temperature (°C)	254	272	262	259	253	244	254	250	250	244	267	257	249	243	258

APPENDIX C, 8. Chlorite compositions (Robben Island).

	634 G	633 G	632 G	631 G	630 G	629 G	628 G	627 G	626 G	625 G	624 G	623 G	622 G	621 G	620 G
Na2O	0.03	0.08	0.00	0.04	0.01	0.09	0.13	0.06	0.01	0.03	0.02	0.06	0.04	0.02	0.05
K2O	0.00	0.00	0.00	0.00	0.00	0.00	0.00	0.00	0.00	0.14	0.00	0.00	0.00	0.00	0.00
SiO2	26.69	26.26	26.17	26.36	26.39	25.24	25.12	25.95	25.56	26.99	26.13	26.06	26.26	26.06	25.78
TiO2	0.01	0.04	0.05	0.04	0.01	0.05	0.08	0.04	0.02	0.08	0.03	0.01	0.04	0.02	0.04
Al2O3	18.71	19.75	20.30	19.73	19.23	20.33	20.23	19.78	19.27	20.65	19.57	19.64	19.29	19.22	19.31
Fe2O3	29.87	29.47	28.30	30.00	29.20	28.25	28.64	29.25	29.48	28.37	30.01	28.73	30.03	29.01	28.84
MnO	0.39	0.32	0.33	0.32	0.37	0.20	0.28	0.33	0.38	0.27	0.34	0.32	0.36	0.37	0.33
MgO	13.16	13.58	13.70	13.60	13.61	13.05	12.84	13.41	12.55	13.28	13.46	13.79	13.22	12.71	13.09
CaO	0.03	0.04	0.00	0.00	0.00	0.04	0.04	0.01	0.00	0.00	0.01	0.00	0.00	0.01	0.00
Cr2O3	0.06	0.01	0.03	0.00	0.01	0.00	0.00	0.00	0.00	0.00	0.01	0.01	0.01	0.04	0.00
Total	88.95	89.54	88.89	90.08	88.83	87.26	87.35	88.83	87.26	89.81	89.57	88.61	89.24	87.46	87.44
Na	0.01	0.03	0.00	0.02	0.00	0.04	0.05	0.02	0.00	0.01	0.01	0.02	0.02	0.01	0.02
K	0.00	0.00	0.00	0.00	0.00	0.00	0.00	0.00	0.00	0.04	0.00	0.00	0.00	0.00	0.00
Si	5.69	5.53	5.54	5.53	5.61	5.45	5.42	5.51	5.56	5.66	5.52	5.53	5.57	5.65	5.57
Ti	0.00	0.01	0.01	0.01	0.00	0.01	0.01	0.01	0.00	0.01	0.01	0.00	0.01	0.00	0.01
Al	4.70	4.90	5.06	4.88	4.82	5.17	5.15	4.95	4.94	5.10	4.87	4.92	4.83	4.91	4.92
Fe2+	5.33	5.14	5.01	5.19	5.19	5.10	5.13	5.17	5.36	4.98	5.21	5.07	5.30	5.26	5.21
Fe3+	0.00	0.05	0.00	0.07	0.00	0.00	0.04	0.03	0.00	0.00	0.09	0.03	0.03	0.00	0.00
Mn	0.07	0.06	0.06	0.06	0.07	0.04	0.05	0.06	0.07	0.05	0.06	0.06	0.06	0.07	0.06
Mg	4.18	4.27	4.32	4.25	4.31	4.20	4.13	4.25	4.07	4.15	4.24	4.37	4.18	4.11	4.22
Ca	0.01	0.01	0.00	0.00	0.00	0.01	0.01	0.00	0.00	0.00	0.00	0.00	0.00	0.00	0.00
Xfe	0.56	0.55	0.54	0.55	0.55	0.55	0.55	0.55	0.57	0.55	0.55	0.54	0.56	0.56	0.55
Temperature (°C)	242	260	261	260	252	269	271	262	255	247	261	261	255	247	256

APPENDIX C, 9. Feldspar compositions (Xenoliths).

	01-335c plag1a	01-335c plag1b	01-335c plag1c	01-335c plag1d	01-335c plag1e	01-335c plag1f	01-335c plag1g	01-335c plag2a	01-335c plag2b	01-335c plag2c	01-335c plag2d	01-335c plag3a
SiO2	55.45	56.57	55.36	54.76	52.97	56.75	49.28	56.14	54.98	54.29	52.69	55.41
Na2O	6.43	6.65	6.18	5.97	5.00	7.12	3.92	6.50	4.32	6.02	5.23	6.12
Al2O3	27.35	26.35	27.52	27.91	29.02	26.35	31.46	26.95	30.63	28.14	29.28	27.57
K2O	0.22	0.36	0.21	0.16	0.20	0.23	0.31	0.23	0.45	0.26	0.28	0.26
CaO	10.58	10.08	10.77	11.22	12.81	9.61	15.07	10.20	10.05	11.33	12.56	10.70
FeO	-0.03	-0.02	-0.04	-0.03	-0.01	-0.05	-0.04	-0.02	-0.42	-0.04	-0.04	-0.06
Si	10.03	10.22	10.01	9.91	9.63	10.24	9.05	10.13	9.83	9.85	9.59	10.01
Na	2.25	2.33	2.17	2.10	1.76	2.49	1.40	2.27	1.50	2.12	1.85	2.14
Al	5.83	5.61	5.86	5.96	6.22	5.60	6.81	5.73	6.45	6.01	6.28	5.87
K	0.05	0.08	0.05	0.04	0.05	0.05	0.07	0.05	0.10	0.06	0.07	0.06
Ca	2.05	1.95	2.09	2.18	2.50	1.86	2.96	1.97	1.92	2.20	2.45	2.07
Fe	0.00	0.00	-0.01	0.00	0.00	-0.01	-0.01	0.00	-0.06	-0.01	-0.01	-0.01
Cation Total	20.21	20.18	20.17	20.17	20.16	20.23	20.28	20.16	19.74	20.23	20.22	20.15
An	47.1	44.7	48.5	50.5	58.0	42.2	66.9	45.9	54.6	50.3	56.2	48.5
Ab	51.8	53.4	50.4	48.6	40.9	56.6	31.5	52.9	42.5	48.3	42.3	50.1
Or	1.2	1.9	1.1	0.9	1.1	1.2	1.6	1.2	2.9	1.4	1.5	1.4

	01-335c plag3b	01-335c plag3c	01-335c plag3d	01-335c plag3e	01-335a plag1a	01-335a plag1b	01-335a plag1c	01-335a plad1d	01-335a plag1e	01-335a plag1f	01-335a plag2a	01-335a plag2b
SiO2	51.93	56.19	57.16	55.40	56.67	53.23	54.64	54.23	55.33	53.08	55.18	51.56
Na2O	4.86	6.74	7.28	6.70	6.74	5.45	5.87	5.64	6.31	5.53	6.26	4.26
Al2O3	30.12	26.75	25.95	27.01	26.72	28.82	27.99	28.09	27.55	28.82	27.38	30.42
K2O	0.30	0.35	0.34	0.31	0.15	0.31	0.14	0.19	0.27	0.19	0.20	0.24
CaO	12.83	9.96	9.30	10.59	9.75	12.20	11.36	11.86	10.57	12.45	10.98	13.53
FeO	-0.05	0.01	-0.04	-0.01	-0.02	-0.02	0.00	-0.01	-0.02	-0.07	0.01	-0.01
Si	9.46	10.15	10.31	10.04	10.21	9.68	9.89	9.84	10.01	9.66	9.99	9.39
Na	1.72	2.36	2.55	2.35	2.35	1.92	2.06	1.98	2.21	1.95	2.20	1.50
Al	6.46	5.70	5.52	5.77	5.67	6.18	5.97	6.01	5.87	6.18	5.84	6.53
K	0.07	0.08	0.08	0.07	0.03	0.07	0.03	0.04	0.06	0.04	0.05	0.06
Ca	2.50	1.93	1.80	2.06	1.88	2.38	2.20	2.30	2.05	2.43	2.13	2.64
Fe	-0.01	0.00	-0.01	0.00	0.00	0.00	0.00	0.00	0.00	-0.01	0.00	0.00
Cation Total	20.20	20.22	20.24	20.29	20.15	20.23	20.17	20.17	20.20	20.25	20.21	20.12
An	58.4	44.1	40.6	45.9	44.07	54.39	51.29	53.20	47.38	54.89	48.70	62.86
Ab	40.0	54.0	57.6	52.5	55.13	43.97	47.96	45.78	51.18	44.12	50.24	35.81
Or	1.6	1.8	1.8	1.6	0.81	1.65	0.75	1.01	1.44	1.00	1.06	1.33

APPENDIX C, 9. Feldspar compositions (Xenoliths).

	01-335a plag2c	01-335a plag2d	01-335a plag2e	01-335a plag2f	01-335a plag2g	01-335a plag2h	01-335a plag2i	01-335a plag2j	01-335a plag2k	X2 plag3a	X2 plag3b	X2 plag3c
SiO2	54.14	55.16	55.01	51.79	54.02	56.00	55.56	52.20	54.86	59.67	59.58	59.66
Na2O	5.41	6.37	5.97	1.84	5.59	6.55	6.30	5.05	6.06	8.18	7.99	8.14
Al2O3	28.58	27.73	27.84	35.48	28.45	27.23	27.47	29.64	28.05	24.39	24.69	24.44
K2O	0.11	0.19	0.17	10.63	0.16	0.21	0.21	0.26	0.14	0.22	0.10	0.32
CaO	11.78	10.62	11.06	0.46	11.79	10.01	10.46	12.87	10.95	7.61	7.65	7.47
FeO	-0.03	-0.08	-0.04	-0.20	0.00	0.00	0.00	-0.02	-0.07	-0.06	-0.01	-0.03
Si	9.80	9.98	9.95	9.46	9.79	10.10	10.04	9.51	9.92	10.69	10.66	10.69
Na	1.90	2.23	2.09	0.65	1.97	2.29	2.21	1.78	2.12	2.84	2.77	2.83
Al	6.10	5.91	5.93	7.64	6.08	5.79	5.85	6.36	5.98	5.15	5.21	5.16
K	0.03	0.04	0.04	2.48	0.04	0.05	0.05	0.06	0.03	0.05	0.02	0.07
Ca	2.29	2.06	2.14	0.09	2.29	1.94	2.02	2.51	2.12	1.46	1.47	1.43
Fe	0.00	-0.01	-0.01	-0.03	0.00	0.00	0.00	0.00	-0.01	-0.01	0.00	0.00
Cation Total	20.11	20.21	20.15	20.29	20.17	20.17	20.17	20.23	20.17	20.18	20.13	20.18
An	54.28	47.47	50.12	2.80	53.36	45.27	47.31	57.67	49.59	33.56	34.42	33.08
Ab	45.11	51.52	48.96	20.25	45.78	53.60	51.56	40.95	49.66	65.28	65.05	65.23
Or	0.60	1.01	0.92	76.96	0.86	1.13	1.13	1.39	0.75	1.16	0.54	1.69

	x2 plag3d	x2 plag3e	X2 plag3f	X2 plag3g	X2 plag1a	X2 plag1b	X2 plag1c	X2 plag1d	X2 plag1e	X2 plag1f	X2 plag1g	X2 plag2a
SiO2	59.76	59.58	59.63	59.45	61.02	61.34	60.12	61.28	61.80	59.51	60.91	59.84
Na2O	8.32	8.05	7.86	8.26	8.27	8.54	8.64	8.84	8.83	8.25	9.08	8.16
Al2O3	24.25	24.34	24.62	24.64	24.03	23.35	23.95	23.29	23.01	24.44	23.53	24.23
K2O	0.30	0.20	0.23	0.26	0.25	0.19	0.26	0.30	0.27	0.21	0.22	0.17
CaO	7.43	7.86	7.69	7.40	6.50	6.65	7.08	6.33	6.12	7.65	6.30	7.65
FeO	-0.06	-0.04	-0.04	-0.01	-0.08	-0.06	-0.05	-0.04	-0.03	-0.07	-0.04	-0.05
Si	10.71	10.68	10.67	10.65	10.87	10.94	10.77	10.94	11.01	10.67	10.88	10.72
Na	2.89	2.80	2.73	2.87	2.86	2.95	3.00	3.06	3.05	2.87	3.15	2.83
Al	5.12	5.14	5.19	5.20	5.05	4.91	5.06	4.90	4.83	5.16	4.96	5.11
K	0.07	0.05	0.05	0.06	0.06	0.04	0.06	0.07	0.06	0.05	0.05	0.04
Ca	1.43	1.51	1.47	1.42	1.24	1.27	1.36	1.21	1.17	1.47	1.21	1.47
Fe	-0.01	-0.01	-0.01	0.00	-0.01	-0.01	-0.01	-0.01	0.00	-0.01	-0.01	-0.01
Cation Total	20.21	20.17	20.12	20.21	20.06	20.10	20.23	20.17	20.12	20.21	20.24	20.16
An	32.53	34.68	34.66	32.66	29.87	29.78	30.75	27.90	27.30	33.51	27.40	33.82
Ab	65.91	64.27	64.11	65.97	68.77	69.21	67.91	70.52	71.27	65.40	71.46	65.28
Or	1.56	1.05	1.23	1.37	1.37	1.01	1.34	1.57	1.43	1.10	1.14	0.89

APPENDIX C, 9. Feldspar compositions (Xenoliths).

	X2 plag2b	X2 plag2c	X2 plag2d	X2 plag2e	X2 plag2f	X2 plagf	X2 plag2g	X2 plag2h	X2 plag2i	X2 plag4a	X2 plag4b	X2 plag4c
SiO2	60.32	59.63	59.76	59.94	60.17	59.91	60.18	59.34	59.64	59.82	58.38	60.26
Na2O	8.46	8.57	8.44	9.02	8.74	8.68	8.59	8.32	8.12	8.39	7.71	8.67
Al2O3	23.84	24.45	24.11	24.60	24.07	24.06	24.15	24.33	24.53	24.35	25.21	23.86
K2O	0.25	0.18	0.24	0.25	0.26	0.58	0.29	0.44	0.27	0.31	0.32	0.40
CaO	7.18	7.15	7.48	6.21	6.77	6.83	6.77	7.58	7.43	7.20	8.40	6.88
FeO	-0.05	0.01	-0.03	-0.02	0.00	-0.06	0.01	-0.02	0.01	-0.06	-0.02	-0.06
Si	10.80	10.69	10.72	10.72	10.77	10.75	10.77	10.66	10.68	10.71	10.50	10.79
Na	2.94	2.98	2.93	3.13	3.03	3.02	2.98	2.90	2.82	2.91	2.69	3.01
Al	5.03	5.16	5.09	5.19	5.08	5.09	5.09	5.15	5.18	5.14	5.34	5.04
K	0.06	0.04	0.05	0.06	0.06	0.13	0.07	0.10	0.06	0.07	0.07	0.09
Ca	1.38	1.37	1.44	1.19	1.30	1.31	1.30	1.46	1.43	1.38	1.62	1.32
Fe	-0.01	0.00	0.00	0.00	0.00	-0.01	0.00	0.00	0.00	-0.01	0.00	-0.01
Cation Total	20.19	20.24	20.23	20.28	20.24	20.29	20.21	20.26	20.17	20.21	20.21	20.24
An	31.51	31.26	32.47	27.20	29.57	29.40	29.88	32.73	33.10	31.65	36.95	29.85
Ab	67.18	67.80	66.29	71.50	69.08	67.62	68.60	65.01	65.47	66.73	61.37	68.08
Or	1.31	0.94	1.24	1.30	1.35	2.97	1.52	2.26	1.43	1.62	1.68	2.07

	X2 plag4d	X2 plag4e	X2 plag6a	X2 plag6b	01-335d plag2a	01-335d plag2c	01-335d plag2d	01-335d plag2e	01-335d plag2f	01-335d plag2i	01-335d plag2g	01-335d plag3a
SiO2	59.75	59.31	59.73	60.25	55.20	55.83	55.23	57.75	56.41	55.48	59.24	53.05
Na2O	8.25	8.45	8.49	7.99	6.21	7.11	6.30	7.14	6.37	6.22	5.22	5.18
Al2O3	24.39	24.29	24.31	24.26	27.91	27.22	27.40	26.24	27.02	27.26	24.54	28.98
K2O	0.29	0.28	0.28	0.73	1.27	0.72	0.32	0.28	0.27	0.29	2.37	0.22
CaO	7.34	7.74	7.23	7.06	9.43	9.14	10.78	8.61	10.01	10.78	8.81	12.68
FeO	-0.01	-0.06	-0.03	-0.29	-0.02	-0.02	-0.03	-0.02	-0.08	-0.03	-0.18	-0.11
Si	10.70	10.65	10.70	10.78	10.00	10.10	10.00	10.37	10.16	10.04	10.67	9.65
Na	2.86	2.94	2.95	2.77	2.18	2.49	2.21	2.49	2.23	2.18	1.82	1.83
Al	5.15	5.14	5.13	5.11	5.96	5.80	5.85	5.55	5.74	5.81	5.21	6.21
K	0.07	0.06	0.06	0.17	0.29	0.17	0.07	0.06	0.06	0.07	0.54	0.05
Ca	1.41	1.49	1.39	1.35	1.83	1.77	2.09	1.66	1.93	2.09	1.70	2.47
Fe	0.00	-0.01	0.00	-0.04	0.00	0.00	0.00	0.00	-0.01	0.00	-0.03	-0.02
Cation Total	20.19	20.28	20.24	20.14	20.26	20.33	20.22	20.13	20.11	20.18	19.91	20.19
An	32.46	33.13	31.53	31.53	42.52	39.98	47.78	39.38	45.79	48.17	41.80	56.82
Ab	66.02	65.45	67.01	64.58	50.67	56.27	50.53	59.10	52.74	50.29	44.82	42.01
Or	1.53	1.43	1.45	3.88	6.82	3.75	1.69	1.52	1.47	1.54	13.39	1.17

APPENDIX C, 9. Feldspar compositions (Xenoliths).

	01-335d plag3b	01-335d plag3c	01-335d plag3d	01-335d plag3e	01-335d plag3f	01-335d plag5a
SiO2	48.43	54.14	55.01	54.56	54.25	56.04
Na2O	3.41	5.74	5.95	6.07	6.26	6.63
Al2O3	31.53	28.56	27.80	28.06	28.08	26.91
K2O	0.21	0.21	0.31	0.25	0.26	0.23
CaO	16.49	11.42	11.00	11.09	11.16	10.27
FeO	-0.07	-0.06	-0.07	-0.02	0.00	-0.07
Si	8.92	9.81	9.95	9.88	9.85	10.12
Na	1.22	2.02	2.09	2.13	2.20	2.32
Al	6.85	6.10	5.93	5.99	6.01	5.73
K	0.05	0.05	0.07	0.06	0.06	0.05
Ca	3.26	2.22	2.13	2.15	2.17	1.99
Fe	-0.01	-0.01	-0.01	0.00	0.00	-0.01
Cation Total	20.29	20.18	20.16	20.21	20.28	20.20
An	71.97	51.77	49.69	49.57	48.95	45.56
Ab	26.93	47.09	48.64	49.10	49.69	53.22
Or	1.09	1.13	1.67	1.33	1.36	1.21

APPENDIX C, 10. Orthoamphibole compositions (Xenoliths).

	3a	3b	3c	3d
MgO	14.82	14.88	15.20	15.08
Al2O3	0.83	0.84	0.71	-0.44
SiO2	57.30	57.31	57.32	57.50
CaO	0.36	0.34	0.38	0.50
MnO	1.63	1.66	1.61	1.85
FeO	25.07	24.97	24.78	25.51
Mg	3.02	3.03	3.10	3.09
Al	0.13	0.14	0.11	-0.07
Si	7.84	7.83	7.83	7.90
Ca	0.05	0.05	0.06	0.07
Mn	0.19	0.19	0.19	0.22
Fe	2.87	2.86	2.83	2.93

APPENDIX C, 11. Biotite compositions (Xenoliths).

	01-335d bio2a	01-335d bio2b	01-335d bio2c	01-335d bio2d	01-335d bio2e	01-335d bio2f	01-335d bio2g	01-335d bio2h	01-335d bio2i	01-335d bio2j	01-335d bio3a	01-335d bio3b	01-335d bio3c	01-335d bio3d	01-335d bio3e	01-335d bio3f	01-335d bio3h	01-335d bio3g
MgO	10.65	11.82	11.59	11.24	10.72	10.60	10.19	10.27	9.90	10.75	10.46	11.18	11.09	9.67	11.30	10.45	10.72	10.38
SiO2	37.87	39.78	38.82	39.21	37.36	38.42	37.31	37.89	36.44	38.45	37.61	38.58	38.68	37.64	37.74	38.04	39.11	38.15
Na2O	0.00	0.08	0.00	0.00	0.00	0.08	0.00	0.00	0.00	0.00	0.00	0.00	0.00	0.00	0.00	0.00	0.00	0.00
Al2O3	17.28	18.82	18.13	17.94	17.40	17.86	16.71	19.73	15.82	17.57	17.39	18.17	17.13	16.94	17.74	17.30	17.65	16.79
K2O	9.86	9.29	9.88	9.66	10.02	10.07	10.73	9.44	11.23	10.09	10.15	9.64	10.77	10.48	9.45	10.28	10.12	10.05
CaO	0.00	0.00	0.00	0.00	0.00	0.00	0.00	0.00	0.00	0.00	0.00	0.00	0.00	0.00	0.00	0.00	0.00	0.00
TiO2	3.46	2.70	2.47	3.33	3.41	3.08	3.22	3.07	3.90	3.45	3.40	3.29	3.23	3.44	2.44	3.18	2.96	3.74
FeO	20.65	17.48	18.86	18.44	20.91	19.72	21.66	19.30	22.75	19.67	20.78	18.83	19.06	21.51	21.11	20.51	19.33	20.49
MnO	0.22	0.12	0.25	0.18	0.18	0.25	0.19	0.32	-0.04	0.02	0.21	0.31	0.09	0.31	0.22	0.24	0.10	0.41
Mg	2.31	2.50	2.49	2.40	2.33	2.29	2.24	2.20	2.20	2.32	2.28	2.40	2.40	2.12	2.45	2.27	2.30	2.26
Si	5.51	5.84	5.58	5.61	5.46	5.56	5.50	5.45	5.43	5.56	5.49	5.55	5.60	5.53	5.49	5.54	5.64	5.56
Na	0.00	0.00	0.00	0.00	0.00	0.00	0.00	0.00	0.00	0.00	0.00	0.00	0.00	0.00	0.00	0.00	0.00	0.00
Al	2.96	3.14	3.07	3.03	3.00	3.05	2.90	3.34	2.78	3.00	2.99	3.08	2.93	2.93	3.04	2.97	3.00	2.88
K	1.89	1.68	1.81	1.76	1.87	1.86	2.02	1.73	2.13	1.86	1.89	1.77	1.99	1.96	1.75	1.91	1.86	1.87
Ca	0.00	0.00	0.00	0.00	0.00	0.00	0.00	0.00	0.00	0.00	0.00	0.00	0.00	0.00	0.00	0.00	0.00	0.00
Ti	0.38	0.29	0.27	0.36	0.37	0.34	0.36	0.33	0.44	0.38	0.37	0.36	0.35	0.38	0.27	0.35	0.32	0.41
Fe2+	2.51	2.07	2.27	2.21	2.55	2.39	2.67	2.32	2.83	2.38	2.54	2.26	2.31	2.64	2.57	2.50	2.33	2.50
Mn	0.03	0.01	0.03	0.02	0.02	0.03	0.02	0.04	-0.01	0.00	0.03	0.04	0.01	0.04	0.03	0.03	0.01	0.05

	01-335d bio4a	01-335d bio4b	01-335d bio4c	01-335d bio4d	01-335d bio4e	01-335d bio4f	01-335d bio4g	01-335d bio5a	01-335d bio5b	X2 bio3a	x2 bio3b	X2 bio3c	X2 bio3d	x2 bio3e	X2 bio3f	x2 bio3g	X2 bio1a	X2 bio1b
MgO	10.54	10.64	10.47	10.67	9.94	11.22	11.15	11.12	11.87	8.22	8.46	7.94	8.01	8.04	8.48	9.06	7.74	11.67
SiO2	38.11	37.28	36.33	38.09	37.82	38.72	38.10	37.44	37.44	36.51	35.28	36.78	36.90	37.58	36.70	36.93	35.78	31.96
Na2O	0.00	0.00	0.00	0.00	0.00	0.00	0.00	0.00	0.00	0.00	0.00	0.00	0.00	0.00	0.00	0.00	0.00	0.00
Al2O3	17.51	17.23	18.01	17.41	17.10	17.49	17.26	20.16	18.11	19.11	20.66	18.49	18.82	19.32	18.21	19.01	20.17	22.46
K2O	10.15	10.15	10.32	10.00	10.10	10.35	10.51	9.02	8.85	10.89	8.72	10.86	10.69	10.46	10.84	10.82	10.57	2.77
CaO	0.00	0.00	0.00	0.00	0.00	0.00	0.00	0.00	0.00	0.00	0.00	0.00	0.00	0.00	0.00	0.00	0.00	0.00
TiO2	3.24	4.33	3.59	3.27	4.29	2.80	3.39	2.24	2.45	1.00	1.04	2.03	1.47	1.62	2.22	2.08	0.96	0.23
FeO	20.14	20.07	19.09	20.23	20.50	19.22	19.46	19.79	21.03	24.31	25.47	23.65	23.86	22.87	23.21	22.05	24.38	30.62
MnO	0.31	0.30	0.20	0.33	0.25	0.21	0.13	0.24	0.25	-0.04	0.36	0.26	0.25	0.12	0.34	0.05	0.40	0.29
Mg	2.28	2.31	2.26	2.31	2.16	2.42	2.41	2.38	2.57	1.82	1.87	1.76	1.77	1.76	1.88	1.99	1.72	2.57
Si	5.54	5.43	5.54	5.54	5.51	5.60	5.53	5.38	5.43	5.43	5.23	5.47	5.48	5.53	5.45	5.44	5.33	4.72
Na	0.00	0.00	0.00	0.00	0.00	0.00	0.00	0.00	0.00	0.00	0.00	0.00	0.00	0.00	0.00	0.00	0.00	0.00
Al	3.00	2.96	3.07	2.98	2.94	2.98	2.95	3.42	3.09	3.35	3.61	3.24	3.29	3.35	3.19	3.30	3.54	3.91
K	1.88	1.89	1.90	1.85	1.88	1.91	1.95	1.65	1.64	2.07	1.65	2.06	2.02	1.96	2.05	2.03	2.01	0.52
Ca	0.00	0.00	0.00	0.00	0.00	0.00	0.00	0.00	0.00	0.00	0.00	0.00	0.00	0.00	0.00	0.00	0.00	0.00
Ti	0.35	0.47	0.39	0.36	0.47	0.30	0.37	0.24	0.27	0.11	0.12	0.23	0.16	0.18	0.25	0.23	0.11	0.03
Fe2+	2.45	2.45	2.31	2.46	2.50	2.32	2.36	2.38	2.55	3.03	3.16	2.94	2.96	2.81	2.88	2.71	3.04	3.78
Mn	0.04	0.04	0.02	0.04	0.03	0.03	0.02	0.03	0.03	-0.01	0.05	0.03	0.03	0.01	0.04	0.01	0.05	0.04

APPENDIX C, 11. Biotite compositions (Xenoliths).

	X2 bio1c	X2 bio1d	X2 bio1e	X2 bio1f	X2 bio1g	X2 bio2a	X2 bio2b	X2 bio2c	X2 bio2d	X2 bio2e	X2 bio2f	X2 bio2g	X2 bio2h	X2 bio2i	X2 bio4a	X2 bio4b	X2 bio4c	X2 bio4d
MgO	8.10	8.00	9.49	8.22	4.39	7.63	8.56	8.01	8.01	8.02	7.65	7.34	7.63	10.00	8.13	7.64	7.77	8.25
SiO2	37.83	37.48	34.32	36.88	59.11	36.96	37.72	37.38	37.34	36.49	37.45	37.07	37.01	38.49	37.22	36.96	36.77	37.43
Na2O	0.00	0.00	0.00	0.00	-0.01	0.00	0.00	0.00	0.00	0.00	0.00	0.00	0.00	0.00	0.00	0.00	0.00	0.00
Al2O3	18.91	19.56	21.91	19.60	16.71	19.16	18.64	18.69	19.56	19.51	18.75	18.62	18.99	19.73	17.93	20.37	18.96	18.26
K2O	10.42	10.49	6.41	10.86	6.01	10.64	10.36	10.71	10.38	10.40	11.05	10.84	10.56	9.26	11.04	10.50	10.68	10.45
CaO	0.00	0.00	0.00	0.00	0.00	0.00	0.00	0.00	0.00	0.00	0.00	0.00	0.00	0.00	0.00	0.00	0.00	0.00
TiO2	2.20	1.06	0.54	1.37	1.15	1.62	1.64	1.86	1.13	1.28	1.91	1.90	1.90	1.65	2.71	1.79	2.00	2.26
FeO	22.12	23.17	26.83	22.84	12.38	23.76	22.89	22.95	23.44	23.99	22.95	24.02	23.60	20.56	22.47	22.61	23.44	23.16
MnO	0.42	0.24	0.50	0.22	0.25	0.24	0.20	0.41	0.15	0.30	0.24	0.21	0.33	0.31	0.52	0.12	0.38	0.19
Mg	1.77	1.76	2.09	1.81	0.84	1.69	1.88	1.76	1.76	1.77	1.69	1.63	1.68	2.15	1.79	1.67	1.72	1.82
Si	5.55	5.52	5.06	5.45	7.63	5.48	5.55	5.52	5.50	5.41	5.54	5.51	5.48	5.55	5.51	5.43	5.45	5.53
Na	0.00	0.00	0.00	0.00	0.00	0.00	0.00	0.00	0.00	0.00	0.00	0.00	0.00	0.00	0.00	0.00	0.00	0.00
Al	3.27	3.40	3.81	3.41	2.54	3.35	3.23	3.25	3.40	3.41	3.27	3.26	3.31	3.35	3.13	3.53	3.31	3.18
K	1.95	1.97	1.21	2.05	0.99	2.01	1.94	2.02	1.95	1.97	2.08	2.05	1.99	1.70	2.08	1.97	2.02	1.97
Ca	0.00	0.00	0.00	0.00	0.00	0.00	0.00	0.00	0.00	0.00	0.00	0.00	0.00	0.00	0.00	0.00	0.00	0.00
Ti	0.24	0.12	0.06	0.15	0.11	0.18	0.18	0.21	0.13	0.14	0.21	0.21	0.21	0.18	0.30	0.20	0.22	0.25
Fe2+	2.71	2.85	3.31	2.82	1.34	2.94	2.82	2.84	2.89	2.98	2.84	2.98	2.92	2.48	2.78	2.78	2.91	2.86
Mn	0.05	0.03	0.06	0.03	0.03	0.03	0.02	0.05	0.02	0.04	0.03	0.03	0.04	0.04	0.07	0.01	0.05	0.02

	X2 bio4e	X2 bio4f	X2 bio4g	X2 bio4h	X2 bio4i	X2 bio4j	X2 bio5a	X2 bio5b	X2 bio5c	X2 bio5d	X2 bio5e	X2 bio5f	X2 bio5g	X2 bio5h	X2 bio5i	X2 bio6a	01-335a bio1a	01-335a bio1b
MgO	8.66	7.72	7.97	8.16	7.34	7.56	8.10	7.30	7.92	8.46	8.42	7.63	7.52	8.39	8.39	9.23	10.29	11.41
SiO2	36.46	37.41	36.25	37.25	36.94	37.65	37.96	37.26	37.33	37.80	37.90	37.81	37.75	37.31	37.82	38.41	38.38	38.65
Na2O	0.00	0.00	0.00	0.00	0.00	0.00	0.00	0.00	0.00	0.00	0.00	0.00	0.00	0.00	0.00	0.00	0.00	0.00
Al2O3	18.24	17.89	18.87	18.73	19.65	17.85	19.03	18.60	18.27	18.69	18.50	18.38	19.18	19.16	18.81	18.72	17.93	18.76
K2O	10.64	10.65	9.41	10.76	10.66	10.76	10.51	11.06	10.74	10.92	10.34	10.67	10.72	10.26	9.86	10.62	10.61	9.65
CaO	0.00	0.00	0.00	0.00	0.00	0.00	0.00	0.00	0.00	0.00	0.00	0.00	0.00	0.00	0.00	0.00		
TiO2	2.61	2.56	1.94	2.40	1.79	2.85	1.60	1.89	1.89	2.08	2.09	2.07	1.40	1.32	2.35	3.78	2.84	1.65
FeO	22.93	23.46	25.15	22.58	23.35	22.99	22.57	23.62	23.61	21.87	22.37	23.07	23.18	23.37	22.22	19.26	19.77	19.59
MnO	0.47	0.32	0.41	0.12	0.27	0.34	0.23	0.27	0.24	0.16	0.37	0.37	0.24	0.18	0.55	-0.03	0.18	0.29
Mg	1.91	1.71	1.77	1.79	1.62	1.67	1.77	1.62	1.75	1.85	1.84	1.68	1.65	1.84	1.83	1.99	2.23	2.45
Si	5.41	5.54	5.39	5.49	5.46	5.57	5.57	5.53	5.53	5.55	5.57	5.58	5.57	5.50	5.54	5.55	5.57	5.57
Na	0.00	0.00	0.00	0.00	0.00	0.00	0.00	0.00	0.00	0.00	0.00	0.00	0.00	0.00	0.00	0.00	0.00	0.00
Al	3.19	3.12	3.30	3.25	3.42	3.11	3.29	3.25	3.19	3.24	3.20	3.20	3.33	3.33	3.25	3.19	3.07	3.18
K	2.01	2.01	1.78	2.02	2.01	2.03	1.97	2.09	2.03	2.05	1.94	2.01	2.02	1.93	1.84	1.96	1.97	1.77
Ca	0.00	0.00	0.00	0.00	0.00	0.00	0.00	0.00	0.00	0.00	0.00	0.00	0.00	0.00	0.00	0.00	0.00	0.00
Ti	0.29	0.29	0.22	0.27	0.20	0.32	0.18	0.21	0.21	0.23	0.23	0.23	0.16	0.15	0.26	0.41	0.31	0.18
Fe2+	2.84	2.91	3.13	2.78	2.89	2.84	2.77	2.93	2.93	2.69	2.75	2.85	2.86	2.88	2.72	2.33	2.40	2.36
Mn	0.06	0.04	0.05	0.01	0.03	0.04	0.03	0.03	0.03	0.02	0.05	0.05	0.03	0.02	0.07	0.00	0.02	0.04

APPENDIX C, 11. Biotite compositions (Xenoliths).

	01-335a bio1d	01-335a bio1e	01-335a bio1f	01-335a bio1g	01-335a bio1i	01-335a bio1j	01-335a bio1k	01-335a bio2a	01-335a bio2b	01-335a bio2c	01-335a bio2d	01-335a bio2e	01-335a bio2f	01-335a bio2g	01-335a bio2h	01-335a bio2i	01-335a bio2j	01-335c bio1a
MgO	10.28	11.10	11.02	10.57	10.38	10.68	10.52	10.85	11.18	9.90	11.09	10.84	11.26	12.11	11.45	11.18	15.65	11.72
SiO2	38.92	38.73	38.91	38.36	38.38	37.68	37.52	38.92	38.64	37.96	37.96	38.76	38.77	38.94	38.69	39.00	31.21	38.43
Na2O	0.00	0.00	0.00	0.00	0.00	0.00	0.00	0.00	0.00	0.00	0.00	0.00	0.00	0.00	0.00	0.00	0.00	0.00
Al2O3	17.66	17.69	17.46	17.90	17.44	17.91	16.45	17.95	17.50	17.02	17.45	17.70	17.31	17.87	17.62	16.49	22.95	17.45
K2O	10.93	10.75	10.43	10.56	10.34	10.51	11.51	10.26	10.64	8.24	10.04	10.91	11.02	10.67	10.21	10.95	0.07	10.22
CaO																		0.00
TiO2	2.69	2.89	3.25	1.44	3.06	2.63	2.88	2.82	2.82	5.68	3.05	3.07	2.58	2.90	2.55	3.02	0.00	2.94
FeO	19.09	18.70	18.66	20.83	20.12	20.47	21.09	19.06	18.96	20.90	20.17	18.56	18.76	17.40	19.29	19.12	29.66	18.90
MnO	0.42	0.15	0.27	0.35	0.27	0.12	0.03	0.14	0.26	0.31	0.23	0.17	0.29	0.12	0.20	0.24	0.46	0.35
Mg	2.22	2.39	2.37	2.30	2.25	2.32	2.31	2.33	2.41	2.13	2.40	2.34	2.43	2.59	2.47	2.42	3.39	2.53
Si	5.64	5.60	5.61	5.60	5.58	5.50	5.53	5.61	5.59	5.48	5.52	5.60	5.62	5.59	5.59	5.66	4.53	5.55
Na	0.00	0.00	0.00	0.00	0.00	0.00	0.00	0.00	0.00	0.00	0.00	0.00	0.00	0.00	0.00	0.00	0.00	0.00
Al	3.02	3.01	2.97	3.08	2.99	3.08	2.86	3.05	2.99	2.90	2.99	3.01	2.96	3.02	3.00	2.82	3.93	2.97
K	2.02	1.98	1.92	1.97	1.92	1.96	2.17	1.89	1.96	1.52	1.86	2.01	2.04	1.95	1.88	2.03	0.01	1.88
Ca	0.00	0.00	0.00	0.00	0.00	0.00	0.00	0.00	0.00	0.00	0.00	0.00	0.00	0.00	0.00	0.00	0.00	0.00
Ti	0.29	0.31	0.35	0.16	0.33	0.29	0.32	0.31	0.31	0.62	0.33	0.33	0.28	0.31	0.28	0.33	0.00	0.32
Fe2+	2.31	2.26	2.25	2.54	2.45	2.50	2.60	2.30	2.29	2.52	2.45	2.24	2.27	2.09	2.33	2.32	3.60	2.28
Mn	0.05	0.02	0.03	0.04	0.03	0.01	0.00	0.02	0.03	0.04	0.03	0.02	0.04	0.01	0.02	0.03	0.06	0.04

	01-335c bio1b	01-335c bio1c	01-335c bio1d	01-335c bio1f	01-335c bio1g	01-335c bio 1h	01-335c bio1i	01-335c bio1j	01-335c bio1k	01-335c bio1l	01-335c bio1m	01-335c bio1n	01-335c bio1o	01-335c bio1p	01-335c bio1q	01-335c bio2a	01-335c bio2b	01-335c bio2c
MgO	11.08	16.00	8.23	10.46	11.58	6.90	10.49	10.19	9.98	10.90	10.39	11.20	10.84	11.66	10.74	10.25	9.00	9.57
SiO2	38.64	32.94	33.67	37.97	38.78	48.03	38.66	38.45	38.49	38.19	41.00	38.68	38.46	38.67	38.59	38.64	37.98	37.81
Na2O	0.00	0.00	0.00	0.00	0.00	-0.01	0.00	0.00	0.00	0.00	0.00	0.00	0.00	0.00	0.00	0.00	0.00	0.00
Al2O3	17.64	22.04	16.39	17.50	17.58	19.70	17.28	17.71	17.26	17.15	17.75	17.09	16.91	17.55	17.37	17.77	16.98	17.27
K2O	10.58	2.68	9.90	10.07	10.38	7.21	10.54	10.14	10.48	10.52	10.11	10.62	10.22	10.70	10.13	10.37	10.45	10.52
CaO	0.00	0.00	0.00	0.00	0.00	0.00	0.00	0.00	0.00	0.00	0.00	0.00	0.00	0.00	0.00	0.00	0.00	0.00
TiO2	2.67	0.88	3.55	2.88	3.02	2.10	2.78	2.53	3.37	3.35	2.77	2.65	3.12	2.66	2.85	1.71	3.13	2.93
FeO	19.13	25.22	27.90	20.78	18.49	15.85	19.94	20.67	20.05	19.80	17.81	19.41	20.27	18.47	20.10	21.19	22.24	21.68
MnO	0.27	0.25	0.35	0.34	0.18	0.22	0.31	0.31	0.36	0.09	0.15	0.34	0.19	0.28	0.23	0.09	0.23	0.22
Mg	2.39	3.43	1.88	2.27	2.49	1.39	2.27	2.21	2.16	2.36	2.21	2.42	2.35	2.51	2.32	2.23	1.97	2.09
Si	5.59	4.74	5.15	5.54	5.59	6.51	5.62	5.59	5.60	5.55	5.84	5.62	5.59	5.59	5.60	5.63	5.59	5.55
Na	0.00	0.00	0.00	0.00	0.00	0.00	0.00	0.00	0.00	0.00	0.00	0.00	0.00	0.00	0.00	0.00	0.00	0.00
Al	3.01	3.73	2.95	3.01	2.99	3.15	2.96	3.04	2.96	2.94	2.98	2.92	2.90	2.99	2.97	3.05	2.94	2.99
K	1.95	0.49	1.93	1.87	1.91	1.25	1.95	1.88	1.95	1.95	1.84	1.97	1.90	1.97	1.87	1.93	1.96	1.97
Ca	0.00	0.00	0.00	0.00	0.00	0.00	0.00	0.00	0.00	0.00	0.00	0.00	0.00	0.00	0.00	0.00	0.00	0.00
Ti	0.29	0.10	0.41	0.32	0.33	0.21	0.30	0.28	0.37	0.37	0.30	0.29	0.34	0.29	0.31	0.19	0.35	0.32
Fe2+	2.32	3.03	3.57	2.53	2.23	1.80	2.42	2.51	2.44	2.41	2.12	2.36	2.46	2.23	2.44	2.58	2.74	2.66
Mn	0.03	0.03	0.05	0.04	0.02	0.03	0.04	0.04	0.04	0.01	0.02	0.04	0.02	0.03	0.03	0.01	0.03	0.03

APPENDIX C, 11. Biotite compositions (Xenoliths).

	01-335c bio2d	01-335c bio2e	01-335c bio2f	01-335c bio2g	01-335c bio2h	01-335c bio2i	01-335c bio3a	01-335c bio3b	01-335c bio3c	01-335c bio3d	01-335c bio3e	01-335c bio3f	01-335c bio3h	01-335c bio3i
MgO	8.44	9.67	11.08	11.86	11.22	10.05	5.79	10.73	11.34	12.29	11.97	10.19	11.36	10.57
SiO2	37.04	38.60	38.83	42.46	39.21	39.68	37.33	38.13	39.42	37.73	38.97	40.53	38.74	38.51
Na2O	0.00	0.00	0.00	0.00	0.00	0.00	0.00	0.00	0.00	0.00	0.00	0.00	0.00	0.00
Al2O3	18.28	17.66	19.10	20.61	17.61	17.23	12.69	17.19	17.59	18.23	17.37	17.89	17.31	17.66
K2O	9.17	10.08	9.13	7.04	10.06	10.15	13.07	10.68	10.00	8.57	10.28	8.57	10.58	10.09
CaO	0.00	0.00	0.00	0.00	0.00	0.00	0.00	0.00	0.00	0.00	0.00	0.00	0.00	0.00
TiO2	3.16	2.28	2.09	1.46	2.50	2.60	3.46	2.75	1.75	0.57	2.53	4.96	2.83	3.47
FeO	23.73	21.54	19.60	16.44	19.07	20.18	27.51	20.28	19.67	22.20	18.68	17.68	19.05	19.44
MnO	0.17	0.17	0.19	0.13	0.32	0.11	0.15	0.24	0.24	0.41	0.21	0.17	0.14	0.26
Mg	1.85	2.10	2.37	2.44	2.41	2.17	1.33	2.33	2.44	2.67	2.57	2.15	2.45	2.28
Si	5.45	5.63	5.57	5.85	5.65	5.74	5.77	5.56	5.69	5.49	5.62	5.73	5.60	5.57
Na	0.00	0.00	0.00	0.00	0.00	0.00	0.00	0.00	0.00	0.00	0.00	0.00	0.00	0.00
Al	3.17	3.04	3.23	3.35	2.99	2.94	2.31	2.96	2.99	3.13	2.95	2.98	2.95	3.01
K	1.72	1.88	1.67	1.24	1.85	1.87	2.58	1.99	1.84	1.59	1.89	1.54	1.95	1.86
Ca	0.00	0.00	0.00	0.00	0.00	0.00	0.00	0.00	0.00	0.00	0.00	0.00	0.00	0.00
Ti	0.35	0.25	0.23	0.15	0.27	0.28	0.40	0.30	0.19	0.06	0.27	0.53	0.31	0.38
Fe2+	2.92	2.63	2.35	1.90	2.30	2.44	3.55	2.47	2.37	2.70	2.25	2.09	2.30	2.35
Mn	0.02	0.02	0.02	0.02	0.04	0.01	0.02	0.03	0.03	0.05	0.03	0.02	0.02	0.03

APPENDIX C, 12 Garnet compositions (Xenoliths).

	X2 grt3a	X2 grt3b	X2 grt3c	X2 grt3d	X2 grt3e	X2 grt3f	x2 grt3g	X2 grt3g	X2 grt1a	x2 grt1b	X2 grt1d	X2 grt1c	X2 grt1e	X2 grt1f	X2 grt1g	X2 grt2a	X2 grt2b	X2 grt2c
Na2O	0.00	0.00	0.00	0.00	0.00	0.00	0.00	0.00	0.00	0.00	0.00	0.00	0.00	0.00	0.00	0.00	0.00	0.00
K2O	2.03	0.00	0.05	0.12	-0.04	0.08	0.04	0.06	0.04	-0.04	0.01	0.02	0.09	0.04	-0.02	0.23	0.16	5.72
SiO2	34.16	37.24	36.47	36.27	36.10	36.20	36.66	36.46	36.18	35.60	36.22	36.66	36.38	36.31	37.20	36.22	37.31	36.68
TiO2	5.84	0.12	0.12	0.16	0.24	0.02	-0.07	0.01	-0.08	0.10	-0.04	0.01	0.01	-0.02	0.03	0.07	0.05	1.16
Al2O3	16.85	19.77	19.89	20.19	20.01	20.42	20.22	19.89	20.40	19.98	19.88	19.94	19.77	19.86	20.36	20.33	20.12	18.98
FeO	10.90	37.01	37.12	36.24	36.88	36.36	36.57	37.03	37.09	35.58	36.80	36.40	36.97	37.11	35.92	36.44	35.74	30.34
Fe2O3	1.96	2.60	2.64	2.72	2.50	2.99	2.27	2.89	3.64	6.35	3.77	3.60	3.98	3.60	2.91	1.99	2.10	1.60
MnO	0.37	2.02	2.40	3.12	3.02	2.69	3.04	2.29	1.75	1.38	2.11	2.22	1.75	1.93	2.35	3.56	3.20	5.09
MgO	27.88	1.22	1.30	1.17	1.29	1.23	1.27	1.36	0.99	1.05	1.23	1.15	1.06	1.17	1.25	1.16	1.33	0.43
CaO	0.00	0.00	0.00	0.00	0.00	0.00	0.00	0.00	0.00	0.00	0.00	0.00	0.00	0.00	0.00	0.00	0.00	0.00
Na	0.00	0.00	0.00	0.00	0.00	0.00	0.00	0.00	0.00	0.00	0.00	0.00	0.00	0.00	0.00	0.00	0.00	0.00
K	0.42	0.00	0.01	0.02	-0.01	0.02	0.01	0.01	0.01	-0.01	0.00	0.00	0.02	0.01	0.00	0.05	0.03	1.19
Si	5.49	6.08	5.97	5.92	5.90	5.92	5.97	5.98	5.94	5.89	5.96	6.00	5.99	5.97	6.04	5.90	6.04	5.99
Ti	0.71	0.01	0.01	0.02	0.03	0.00	-0.01	0.00	-0.01	0.01	0.00	0.00	0.00	0.00	0.00	0.01	0.01	0.14
Al	3.19	3.80	3.84	3.88	3.86	3.93	3.88	3.84	3.95	3.90	3.85	3.85	3.83	3.85	3.90	3.90	3.84	3.65
Fe2+	1.46	5.05	5.08	4.95	5.04	4.97	4.98	5.08	5.09	4.93	5.06	4.98	5.09	5.10	4.88	4.96	4.84	4.14
Fe3+	1.22	0.02	0.30	0.39	0.40	0.37	0.31	0.32	0.29	0.42	0.37	0.23	0.31	0.33	0.01	0.49	0.15	1.85
Mn	0.27	0.36	0.37	0.38	0.35	0.41	0.31	0.40	0.51	0.89	0.53	0.50	0.55	0.50	0.40	0.27	0.29	0.22
Mg	0.09	0.49	0.59	0.76	0.74	0.66	0.74	0.56	0.43	0.34	0.52	0.54	0.43	0.47	0.57	0.86	0.77	1.24
Ca	4.80	0.21	0.23	0.20	0.23	0.22	0.22	0.24	0.17	0.19	0.22	0.20	0.19	0.21	0.22	0.20	0.23	0.08
Cr	0.00	0.00	0.00	0.00	0.00	0.00	0.00	0.00	0.00	0.00	0.00	0.00	0.00	0.00	0.00	0.00	0.00	0.00
total	16.42	16.01	16.10	16.13	16.13	16.12	16.10	16.11	16.10	16.14	16.12	16.08	16.10	16.11	16.00	16.16	16.05	16.64
pyrope	1.34	8.04	9.36	12.08	11.59	10.48	11.80	8.92	6.91	5.37	8.19	8.70	6.86	7.53	9.38	13.71	12.60	21.82
almandine	22.13	82.60	81.16	78.69	79.40	79.46	79.65	80.88	82.12	77.66	80.08	80.04	81.29	81.21	80.43	78.72	78.94	72.96
spessartine	4.03	5.88	5.85	5.98	5.45	6.62	5.01	6.39	8.16	14.04	8.31	8.02	8.86	7.98	6.60	4.35	4.70	3.90
grossular	45.94	2.92	3.52	-6.07	-5.96	-5.22	-3.83	-3.93	-4.04	-6.92	-5.42	-2.40	-4.42	-4.66	3.30	-8.12	0.08	-31.59
andradite	26.57	0.57	7.16	9.32	9.52	8.66	7.37	7.74	6.85	9.85	8.85	5.64	7.41	7.94	0.28	11.33	3.68	32.91
uvarovite	0.00	0.00	0.00	0.00	0.00	0.00	0.00	0.00	0.00	0.00	0.00	0.00	0.00	0.00	0.00	0.00	0.00	0.00

APPENDIX C, 12 Garnet compositions (Xenoliths).

	X2 grt2d	X2 grt2e	X2 grt2f	X2 grt2g	X2 grt2h	X2 grt2i	X2 grt4a	X2 grt4b	X2 grt4c	X2 grt4d	X2 grt4e	X2 grt4f	X2 grt4g	X2 grt4h	X2 grt4i	X2 grt4j	X2 grt5a	X2 grt5b
Na2O	0.00	0.00	0.00	0.00	0.00	0.00	0.00	0.00	0.00	0.00	0.00	0.00	0.00	0.00	0.00	0.00	0.00	0.00
K2O	0.10	0.03	0.06	0.03	0.08	0.04	0.12	-0.01	-0.01	0.13	0.15	0.02	0.74	0.06	0.13	0.08	0.06	-0.02
SiO2	36.96	37.33	36.18	37.23	36.58	36.79	37.09	38.07	36.71	37.31	37.08	37.45	37.22	36.75	37.14	37.55	37.25	36.93
TiO2	0.07	-0.07	0.16	-0.02	-0.05	0.22	-0.05	0.05	0.02	0.08	0.05	0.03	0.07	0.03	0.01	0.03	0.02	0.05
Al2O3	19.98	20.42	19.61	20.30	20.22	20.00	19.98	19.68	20.25	20.15	20.35	20.02	20.17	20.53	20.24	20.36	20.57	20.39
FeO	37.12	35.96	37.53	36.51	36.54	36.36	36.00	35.86	35.95	34.59	35.83	35.32	34.36	35.28	34.76	35.23	35.46	35.82
Fe2O3	2.82	2.79	3.15	2.80	3.01	2.37	2.67	2.58	2.88	3.06	2.68	2.99	3.08	2.69	2.58	2.55	2.34	2.43
MnO	1.72	2.26	2.03	1.89	2.40	2.98	2.41	2.28	2.56	3.07	2.41	2.60	3.06	2.98	2.58	2.90	3.04	2.84
MgO	1.24	1.29	1.27	1.26	1.22	1.25	1.77	1.50	1.62	1.61	1.45	1.58	1.30	1.67	2.55	1.30	1.26	1.56
CaO	0.00	0.00	0.00	0.00	0.00	0.00	0.00	0.00	0.00	0.00	0.00	0.00	0.00	0.00	0.00	0.00	0.00	0.00
Na	0.00	0.00	0.00	0.00	0.00	0.00	0.00	0.00	0.00	0.00	0.00	0.00	0.00	0.00	0.00	0.00	0.00	0.00
K	0.02	0.01	0.01	0.01	0.02	0.01	0.02	0.00	0.00	0.03	0.03	0.00	0.15	0.01	0.03	0.02	0.01	0.00
Si	6.05	6.06	5.96	6.06	5.98	5.99	6.04	6.17	5.98	6.04	6.03	6.07	6.04	5.96	6.02	6.07	6.02	5.99
Ti	0.01	-0.01	0.02	0.00	-0.01	0.03	-0.01	0.01	0.00	0.01	0.01	0.00	0.01	0.00	0.00	0.00	0.00	0.01
Al	3.85	3.91	3.81	3.90	3.89	3.84	3.84	3.76	3.89	3.84	3.90	3.83	3.86	3.93	3.87	3.88	3.92	3.90
Fe2+	5.08	4.88	5.17	4.97	4.99	4.95	4.90	4.86	4.90	4.68	4.87	4.79	4.66	4.79	4.71	4.76	4.79	4.86
Fe3+	0.09	0.00	0.37	-0.01	0.27	0.22	0.18	-0.16	0.21	0.13	0.10	0.03	0.31	0.22	0.16	-0.01	0.07	0.15
Mn	0.39	0.38	0.44	0.39	0.42	0.33	0.37	0.35	0.40	0.42	0.37	0.41	0.42	0.37	0.35	0.35	0.32	0.33
Mg	0.42	0.55	0.50	0.46	0.58	0.72	0.59	0.55	0.62	0.74	0.58	0.63	0.74	0.72	0.62	0.70	0.73	0.69
Ca	0.22	0.22	0.22	0.22	0.21	0.22	0.31	0.26	0.28	0.28	0.25	0.27	0.23	0.29	0.44	0.23	0.22	0.27
Cr	0.00	0.00	0.00	0.00	0.00	0.00	0.00	0.00	0.00	0.00	0.00	0.00	0.00	0.00	0.00	0.00	0.00	0.00
total	16.03	16.00	16.13	16.00	16.09	16.07	16.06	15.95	16.07	16.04	16.03	16.01	16.10	16.08	16.05	16.00	16.02	16.05
pyrope	6.87	9.06	7.87	7.60	9.42	11.63	9.49	9.14	10.03	12.10	9.61	10.30	12.23	11.69	10.17	11.58	12.08	11.17
almandine	83.17	80.87	81.65	82.36	80.43	79.61	79.53	80.66	79.00	76.48	80.16	78.47	77.04	77.61	76.83	78.91	79.04	79.00
spessartine	6.40	6.35	6.94	6.40	6.71	5.26	5.97	5.88	6.41	6.85	6.07	6.73	6.99	5.99	5.78	5.78	5.28	5.43
grossular	1.26	3.79	-5.46	3.93	-3.05	1.83	0.57	8.44	-0.61	1.43	1.58	3.62	-3.58	0.75	3.18	3.87	1.98	0.82
andradite	2.30	-0.07	9.00	-0.29	6.49	5.34	4.44	-4.12	5.17	3.13	2.58	0.88	7.31	5.46	4.04	-0.14	1.62	3.59
uvarovite	0.00	0.00	0.00	0.00	0.00	0.00	0.00	0.00	0.00	0.00	0.00	0.00	0.00	0.00	0.00	0.00	0.00	0.00

APPENDIX C, 12 Garnet compositions (Xenoliths).

	X2 grt5c	X2 grt5d	X2 grt5e	X2 grt5f	X2 grt5g	X2 grt5h	X2 grt5i	01-335d grt2a	01-335d grt2b	01-335d grt2c	01-335d grt2h	01-335d grt2f	01-335d grt2g	01-335d grt2e	01-335d grt2i	01-335d grt3a	01-335d grt3b	01-335d grt3c
Na2O	0.00	0.00	0.00	0.00	0.00	0.00	0.00	0.00	0.00	0.00	0.00	0.00	0.00	0.00	0.00	0.00	0.00	0.00
K2O	0.07	0.10	0.11	0.02	9.08	0.01	0.00	0.25	0.07	0.09	0.14	0.10	0.14	0.20	0.81	0.10	0.22	0.06
SiO2	37.48	36.76	37.69	37.27	42.60	37.79	37.33	37.27	37.95	36.08	39.20	38.85	38.40	38.19	30.36	39.25	38.83	37.61
TiO2	0.14	0.13	-0.05	-0.03	2.26	-0.05	0.12	-0.02	-0.10	0.01	-0.09	-0.05	0.01	-0.07	0.62	0.03	0.17	-0.10
Al2O3	20.52	20.00	20.10	20.21	16.43	20.46	20.48	20.79	20.78	19.85	21.20	21.68	21.73	21.37	17.53	21.58	21.40	20.40
FeO	35.44	36.91	35.45	36.20	22.66	35.62	35.80	27.92	27.37	29.56	26.66	25.69	27.40	27.17	36.61	26.59	26.31	28.79
Fe2O3	2.45	2.92	2.36	2.88	0.30	2.86	2.45	5.55	5.56	5.76	5.16	5.11	4.67	4.89	5.39	3.90	4.50	4.73
MnO	2.66	1.99	2.95	2.27	6.96	2.13	2.52	3.12	3.54	3.43	2.76	3.87	3.44	3.57	3.83	3.68	4.03	3.62
MgO	1.23	1.19	1.40	1.18	-0.30	1.18	1.30	5.12	4.83	5.22	4.96	4.75	4.20	4.68	4.85	4.87	4.54	4.89
CaO	0.00	0.00	0.00	0.00	0.00	0.00	0.00	0.00	0.00	0.00	0.00	0.00	0.00	0.00	0.00	0.00	0.00	0.00
Na	0.00	0.00	0.00	0.00	0.00	0.00	0.00	0.00	0.00	0.00	0.00	0.00	0.00	0.00	0.00	0.00	0.00	0.00
K	0.01	0.02	0.02	0.00	1.82	0.00	0.00	0.05	0.01	0.02	0.03	0.02	0.03	0.04	0.18	0.02	0.04	0.01
Si	6.06	6.01	6.09	6.06	6.70	6.11	6.05	5.98	6.05	5.87	6.19	6.11	6.07	6.05	5.23	6.16	6.11	6.02
Ti	0.02	0.02	-0.01	0.00	0.27	-0.01	0.01	0.00	-0.01	0.00	-0.01	-0.01	0.00	-0.01	0.08	0.00	0.02	-0.01
Al	3.91	3.86	3.83	3.87	3.04	3.90	3.91	3.93	3.90	3.80	3.95	4.02	4.05	3.99	3.56	3.99	3.97	3.85
Fe2+	4.79	5.05	4.79	4.92	2.98	4.82	4.85	3.75	3.65	4.02	3.52	3.38	3.62	3.60	5.28	3.49	3.46	3.85
Fe3+	-0.07	0.16	0.03	0.03	1.24	-0.18	-0.04	0.25	0.06	0.71	-0.43	-0.30	-0.25	-0.07	2.81	-0.44	-0.27	0.21
Mn	0.34	0.40	0.32	0.40	0.04	0.39	0.34	0.75	0.75	0.79	0.69	0.68	0.63	0.66	0.79	0.52	0.60	0.64
Mg	0.64	0.49	0.71	0.55	1.63	0.51	0.61	0.75	0.84	0.83	0.65	0.91	0.81	0.84	0.98	0.86	0.95	0.86
Ca	0.21	0.21	0.24	0.21	-0.05	0.20	0.23	0.88	0.82	0.91	0.84	0.80	0.71	0.79	0.90	0.82	0.77	0.84
Cr	0.00	0.00	0.00	0.00	0.00	0.00	0.00	0.00	0.00	0.00	0.00	0.00	0.00	0.00	0.00	0.00	0.00	0.00
total	15.98	16.05	16.01	16.01	16.43	15.94	15.99	16.08	16.02	16.24	15.86	15.90	15.92	15.98	17.00	15.85	15.91	16.07
pyrope	10.72	7.89	11.72	9.06	35.47	8.67	10.11	12.18	13.87	12.69	11.40	15.73	14.05	14.31	12.39	15.14	16.38	13.94
almandine	80.11	82.13	78.96	81.03	64.76	81.28	80.56	61.14	60.15	61.33	61.77	58.58	62.78	61.08	66.43	61.35	59.97	62.18
spessartine	5.61	6.58	5.32	6.53	0.87	6.61	5.58	12.31	12.38	12.10	12.11	11.80	10.84	11.13	9.91	9.11	10.39	10.35
grossular	5.27	-0.54	3.31	2.72	-24.78	8.02	4.82	8.35	12.20	-2.37	26.28	21.71	18.71	15.20	-38.17	26.24	20.35	8.31
andradite	-1.71	3.93	0.69	0.66	23.69	-4.57	-1.07	6.01	1.40	16.24	-11.56	-7.83	-6.38	-1.72	49.45	-11.85	-7.09	5.22
uvarovite	0.00	0.00	0.00	0.00	0.00	0.00	0.00	0.00	0.00	0.00	0.00	0.00	0.00	0.00	0.00	0.00	0.00	0.00

APPENDIX C, 12 Garnet compositions (Xenoliths).

	01-335d grt3d	01-335d grt3e	01-335d grt3f	01-335d grt3g	01-335d grt3h	01-335d grt4a	01-335d grt4b	01-335d grt4c	01-335d grt4d	01-335d grt4e	01-335d grt4f	01-335d grt4g	01-335d grt4h	01-335d grt5a	01-335d grt5b	01-335d grt5c	01-335d grt5d	01-335d grt5f
Na2O	0.00	0.00	0.00	0.00	0.00	0.00	0.00	0.00	0.00	0.00	0.00	0.00	0.00	0.00	0.00	0.00	0.00	0.00
K2O	0.75	0.04	0.19	0.04	0.06	0.11	0.09	0.08	0.08	-0.01	0.08	0.00	0.05	0.03	0.14	0.04	0.12	0.09
SiO2	34.68	39.44	37.68	38.06	37.98	37.71	40.20	37.77	37.72	38.10	37.70	35.90	38.01	38.75	38.09	36.80	33.62	36.93
TiO2	0.06	0.01	0.03	-0.05	0.04	0.17	0.03	0.09	0.03	-0.02	0.10	0.02	0.09	0.16	0.08	0.21	0.10	0.16
Al2O3	20.89	21.93	20.44	21.05	21.62	20.83	22.41	20.85	21.11	21.14	21.15	20.27	20.83	21.46	22.75	20.49	18.42	19.94
FeO	30.00	25.83	29.55	27.78	27.45	28.31	25.21	28.78	28.54	28.80	28.78	30.70	28.82	25.43	25.13	27.61	32.54	29.33
Fe2O3	2.96	3.91	4.76	4.40	4.11	4.19	3.97	4.27	4.32	4.99	4.08	4.60	4.14	6.49	6.25	6.85	6.70	5.35
MnO	7.91	4.04	3.61	3.99	3.95	3.87	3.92	3.57	3.63	3.43	3.66	3.57	3.47	3.10	2.81	2.96	3.09	2.95
MgO	2.76	4.81	3.74	4.73	4.80	4.81	4.18	4.59	4.57	3.58	4.45	4.95	4.59	4.58	4.75	5.04	5.41	5.24
CaO	0.00	0.00	0.00	0.00	0.00	0.00	0.00	0.00	0.00	0.00	0.00	0.00	0.00	0.00	0.00	0.00	0.00	0.00
Na	0.00	0.00	0.00	0.00	0.00	0.00	0.00	0.00	0.00	0.00	0.00	0.00	0.00	0.00	0.00	0.00	0.00	0.00
K	0.15	0.01	0.04	0.01	0.01	0.02	0.02	0.02	0.02	0.00	0.02	0.00	0.01	0.01	0.03	0.01	0.03	0.02
Si	5.58	6.16	6.04	6.04	6.01	6.01	6.23	6.02	6.01	6.06	6.00	5.83	6.05	6.12	6.01	5.93	5.63	5.97
Ti	0.01	0.00	0.00	-0.01	0.00	0.02	0.00	0.01	0.00	0.00	0.01	0.00	0.01	0.02	0.01	0.03	0.01	0.02
Al	3.96	4.03	3.86	3.94	4.03	3.91	4.09	3.92	3.96	3.97	3.97	3.88	3.91	3.99	4.23	3.89	3.64	3.80
Fe2+	4.04	3.37	3.96	3.69	3.63	3.77	3.27	3.84	3.80	3.83	3.83	4.17	3.84	3.36	3.31	3.72	4.56	3.96
Fe3+	1.49	-0.51	0.15	0.01	-0.06	0.09	-0.82	0.05	0.05	-0.14	0.03	0.68	-0.04	-0.40	-0.35	0.30	1.60	0.36
Mn	0.40	0.52	0.65	0.59	0.55	0.57	0.52	0.58	0.58	0.67	0.55	0.63	0.56	0.87	0.83	0.94	0.95	0.73
Mg	1.90	0.94	0.86	0.94	0.93	0.92	0.91	0.85	0.86	0.81	0.87	0.86	0.82	0.73	0.66	0.71	0.77	0.71
Ca	0.48	0.80	0.64	0.80	0.81	0.82	0.69	0.78	0.78	0.61	0.76	0.86	0.78	0.77	0.80	0.87	0.97	0.91
Cr	0.00	0.00	0.00	0.00	0.00	0.00	0.00	0.00	0.00	0.00	0.00	0.00	0.00	0.00	0.00	0.00	0.00	0.00
total	16.51	15.83	16.05	16.00	15.98	16.03	15.73	16.02	16.02	15.95	16.01	16.23	15.99	15.87	15.88	16.10	16.55	16.12
pyrope	27.85	16.69	14.11	15.67	15.72	15.13	16.81	14.03	14.30	13.72	14.46	13.24	13.72	12.74	11.77	11.40	10.64	11.26
almandine	59.25	59.85	64.80	61.18	61.27	62.06	60.64	63.46	63.08	64.64	63.76	63.87	63.93	58.60	59.05	59.66	62.86	62.78
spessartine	5.92	9.18	10.57	9.81	9.29	9.30	9.67	9.54	9.67	11.34	9.15	9.69	9.30	15.15	14.87	14.99	13.11	11.60
grossular	-22.54	28.27	6.91	13.14	15.28	11.20	36.42	11.82	11.78	13.80	11.94	-2.39	14.08	24.21	23.31	6.82	-19.44	5.68
andradite	29.52	-13.99	3.60	0.20	-1.56	2.31	-23.54	1.15	1.16	-3.50	0.69	15.58	-1.03	-10.68	-9.01	7.13	32.83	8.69
uvarovite	0.00	0.00	0.00	0.00	0.00	0.00	0.00	0.00	0.00	0.00	0.00	0.00	0.00	0.00	0.00	0.00	0.00	0.00

APPENDIX C, 12 Garnet compositions (Xenoliths).

	01-335d grt5g	01-335c grt1a	01-335c grt1b	01-335c grt1c	01-335c grt1d	01-335c grt1e	01-335c grt1f	01-335c grt1g	01-335c grt1h	01-335c grt1i	01-335c grt1j	01-335c grt1k	01-335c grt1l	01-335c grt2a	01-335c grt2b	01-335c grt2c	01-335c grt2d	01-335c grt2e
Na2O	0.00	0.00	0.00	0.00	0.00	0.00	0.00	0.00	0.00	0.00	0.00	0.00	0.00	0.00	0.00	0.00	0.00	0.00
K2O	0.08	0.10	0.12	0.06	0.18	-0.03	0.03	0.01	-0.01	-0.03	-0.05	-0.07	-0.09	0.12	0.10	0.26	0.10	0.08
SiO2	38.24	37.52	37.82	38.09	37.70	37.68	37.82	37.84	37.86	37.88	37.90	37.92	37.94	37.84	38.18	38.24	38.13	38.50
TiO2	0.03	0.08	0.01	0.09	-0.07	-0.02	-0.07	-0.09	-0.12	-0.15	-0.18	-0.21	-0.23	0.07	0.08	-0.14	-0.10	0.00
Al2O3	20.94	20.64	20.86	20.34	20.61	20.15	20.15	20.03	19.91	19.78	19.66	19.54	19.41	20.09	20.73	20.31	20.20	20.72
FeO	27.21	26.90	26.90	27.62	27.96	27.92	28.39	28.70	29.01	29.32	29.63	29.94	30.25	29.58	28.72	29.13	29.17	28.28
Fe2O3	5.40	7.02	6.11	5.50	5.27	6.13	5.22	4.96	4.70	4.43	4.17	3.91	3.65	4.35	3.65	4.25	3.95	3.92
MnO	3.19	2.78	3.01	3.43	3.50	3.08	3.49	3.60	3.71	3.81	3.92	4.03	4.14	3.47	3.61	3.55	3.70	3.70
MgO	4.91	4.97	5.17	4.88	4.85	5.08	4.96	4.95	4.94	4.93	4.92	4.91	4.90	4.49	4.94	4.38	4.85	4.80
CaO	0.00	0.00	0.00	0.00	0.00	0.00	0.00	0.00	0.00	0.00	0.00	0.00	0.00	0.00	0.00	0.00	0.00	0.00
Na	0.00	0.00	0.00	0.00	0.00	0.00	0.00	0.00	0.00	0.00	0.00	0.00	0.00	0.00	0.00	0.00	0.00	0.00
K	0.02	0.02	0.02	0.01	0.04	-0.01	0.01	0.00	0.00	-0.01	-0.01	-0.02	-0.02	0.02	0.02	0.05	0.02	0.02
Si	6.08	6.02	6.04	6.08	6.03	6.05	6.06	6.06	6.07	6.07	6.08	6.08	6.09	6.06	6.07	6.11	6.09	6.11
Ti	0.00	0.01	0.00	0.01	-0.01	0.00	-0.01	-0.01	-0.01	-0.02	-0.02	-0.02	-0.03	0.01	0.01	-0.02	-0.01	0.00
Al	3.92	3.90	3.93	3.82	3.88	3.81	3.80	3.78	3.76	3.74	3.71	3.69	3.67	3.79	3.88	3.82	3.80	3.87
Fe2+	3.62	3.61	3.59	3.69	3.74	3.75	3.80	3.84	3.89	3.93	3.97	4.02	4.06	3.96	3.82	3.89	3.89	3.75
Fe3+	-0.11	0.09	0.03	0.01	0.17	0.13	0.15	0.18	0.20	0.22	0.24	0.27	0.29	0.13	-0.03	0.08	0.10	-0.11
Mn	0.73	0.95	0.83	0.74	0.71	0.83	0.71	0.67	0.64	0.60	0.57	0.53	0.50	0.59	0.49	0.57	0.53	0.53
Mg	0.76	0.66	0.72	0.82	0.83	0.74	0.83	0.86	0.89	0.91	0.94	0.96	0.99	0.83	0.86	0.85	0.88	0.87
Ca	0.84	0.85	0.88	0.83	0.83	0.87	0.85	0.85	0.85	0.85	0.85	0.84	0.84	0.77	0.84	0.75	0.83	0.82
Cr	0.00	0.00	0.00	0.00	0.00	0.00	0.00	0.00	0.00	0.00	0.00	0.00	0.00	0.00	0.00	0.00	0.00	0.00
total	15.96	16.03	16.01	16.00	16.06	16.04	16.05	16.06	16.07	16.07	16.08	16.09	16.10	16.04	15.99	16.03	16.03	15.96
pyrope	12.74	10.93	11.90	13.42	13.64	11.90	13.44	13.80	14.14	14.49	14.83	15.17	15.51	13.47	14.24	13.95	14.35	14.66
almandine	60.93	59.34	59.67	60.63	61.11	60.53	61.39	61.75	62.12	62.48	62.84	63.19	63.54	64.41	63.56	64.20	63.44	62.85
spessartine	12.25	15.68	13.73	12.23	11.67	13.46	11.43	10.80	10.18	9.57	8.96	8.36	7.76	9.59	8.18	9.49	8.70	8.82
grossular	17.02	11.73	14.00	13.36	9.40	10.78	9.89	9.24	8.60	7.96	7.31	6.67	6.04	9.27	14.84	10.48	10.92	16.42
andradite	-2.93	2.32	0.69	0.37	4.18	3.33	3.85	4.40	4.95	5.50	6.05	6.60	7.15	3.26	-0.83	1.88	2.60	-2.75
uvarovite	0.00	0.00	0.00	0.00	0.00	0.00	0.00	0.00	0.00	0.00	0.00	0.00	0.00	0.00	0.00	0.00	0.00	0.00

APPENDIX C, 12 Garnet compositions (Xenoliths).

	01-335c grt2f	01-335c grt2g	01-335c grt2h	01-335c grt2i	01-335c grt3a	01-335c grt3b	01-335c grt3c	01-335c grt3d	01-335c grt3e	01-335c grt3f	01-335c grt3g	01-335c grt3i	01-335a grt1a	01-335a grt1b	01-335a grt1c	01-335a grt1d	01-335a grt1e	01-335a grt1g
Na2O	0.00	0.00	0.00	0.00	0.00	0.00	0.00	0.00	0.00	0.00	0.00	0.00	0.00	0.00	0.00	0.00	0.00	0.00
K2O	0.10	0.06	0.04	-0.04	0.15	0.01	0.14	0.01	0.02	0.10	0.04	0.05	0.08	0.11	0.09	0.05	0.11	0.05
SiO2	37.85	38.31	38.18	37.80	38.17	39.35	37.21	37.93	38.06	37.87	37.70	37.61	37.83	38.17	37.92	41.10	38.24	38.19
TiO2	0.09	0.03	0.07	-0.03	-0.08	-0.10	0.02	0.05	-0.06	-0.11	0.01	0.07	-0.08	0.04	-0.13	0.05	0.08	0.01
Al2O3	20.21	20.06	20.21	20.34	20.76	21.71	20.42	20.84	20.99	20.99	20.77	20.66	20.64	20.63	20.58	22.43	20.80	20.11
FeO	30.35	29.24	28.91	30.23	28.82	28.11	29.46	28.69	28.88	29.17	29.55	30.11	27.89	27.90	28.63	23.94	28.21	28.27
Fe2O3	4.67	4.75	4.18	4.51	4.41	4.72	6.96	4.37	4.23	4.32	4.65	5.69	5.09	4.47	5.05	4.37	4.41	4.77
MnO	3.55	2.85	3.43	2.82	3.11	3.13	1.60	3.26	3.68	3.26	3.01	2.42	3.58	3.97	3.64	3.64	3.26	3.60
MgO	3.16	4.69	4.98	4.38	4.65	3.05	4.19	4.86	4.20	4.40	4.26	3.38	4.96	4.71	4.21	4.41	4.89	5.00
CaO	0.00	0.00	0.00	0.00	0.00	0.00	0.00	0.00	0.00	0.00	0.00	0.00	0.00	0.00	0.00	0.00	0.00	0.00
Na	0.00	0.00	0.00	0.00	0.00	0.00	0.00	0.00	0.00	0.00	0.00	0.00	0.00	0.00	0.00	0.00	0.00	0.00
K	0.02	0.01	0.01	-0.01	0.03	0.00	0.03	0.00	0.00	0.02	0.01	0.01	0.02	0.02	0.02	0.01	0.02	0.01
Si	6.07	6.13	6.09	6.07	6.09	6.20	6.03	6.05	6.05	6.04	6.04	6.05	6.04	6.07	6.06	6.33	6.08	6.10
Ti	0.01	0.00	0.01	0.00	-0.01	-0.01	0.00	0.01	-0.01	-0.01	0.00	0.01	-0.01	0.00	-0.02	0.01	0.01	0.00
Al	3.82	3.78	3.80	3.85	3.90	4.03	3.90	3.92	3.94	3.95	3.92	3.92	3.88	3.86	3.87	4.07	3.90	3.78
Fe2+	4.07	3.91	3.86	4.06	3.84	3.70	3.99	3.82	3.84	3.89	3.96	4.05	3.72	3.71	3.82	3.08	3.75	3.77
Fe3+	0.06	-0.07	0.01	0.02	-0.04	-0.61	0.09	-0.03	-0.04	0.01	0.01	-0.05	0.11	0.03	0.09	-1.13	-0.10	0.05
Mn	0.63	0.64	0.56	0.61	0.60	0.63	0.96	0.59	0.57	0.58	0.63	0.78	0.69	0.60	0.68	0.57	0.59	0.64
Mg	0.85	0.68	0.82	0.67	0.74	0.73	0.39	0.77	0.87	0.78	0.72	0.58	0.85	0.94	0.87	0.84	0.77	0.86
Ca	0.54	0.80	0.85	0.75	0.79	0.51	0.73	0.83	0.72	0.75	0.73	0.58	0.85	0.80	0.72	0.73	0.83	0.85
Cr	0.00	0.00	0.00	0.00	0.00	0.00	0.00	0.00	0.00	0.00	0.00	0.00	0.00	0.00	0.00	0.00	0.00	0.00
total	16.02	15.98	16.00	16.01	15.99	15.80	16.03	15.99	15.99	16.00	16.00	15.98	16.04	16.01	16.03	15.63	15.97	16.02
pyrope	13.92	11.26	13.40	11.07	12.38	13.17	6.38	12.87	14.55	12.92	11.90	9.69	13.94	15.54	14.22	16.02	12.99	13.98
almandine	66.77	64.77	63.34	66.53	64.35	66.33	65.86	63.54	64.03	64.83	65.54	67.64	60.92	61.27	62.75	59.10	63.03	61.56
spessartine	10.41	10.66	9.28	10.05	9.97	11.28	15.76	9.80	9.50	9.72	10.45	12.95	11.26	9.94	11.21	10.93	9.98	10.52
grossular	7.50	15.11	13.85	11.88	14.42	26.08	9.85	14.54	12.93	12.16	11.73	11.00	11.04	12.61	9.59	48.24	16.44	12.60
andradite	1.41	-1.80	0.13	0.47	-1.12	-16.86	2.15	-0.75	-1.00	0.37	0.38	-1.27	2.84	0.64	2.23	-34.29	-2.44	1.35
uvarovite	0.00	0.00	0.00	0.00	0.00	0.00	0.00	0.00	0.00	0.00	0.00	0.00	0.00	0.00	0.00	0.00	0.00	0.00

APPENDIX C, 12 Garnet compositions (Xenoliths).

	01-335a grt2a	01-335a grt2b	01-335a grt2c	01-335a grt2d	01-335a grt2e	01-335a grt2f	01-335a grt2g	01-335a grt2h	01-335a grt2i	01-335a grt2j	01-335a grt3a	01-335a grt3b	01-335a grt3c	01-335a grt3d	01-335a grt3e	01-335a grt3g	01-335a grt3h	01-335a grt3i
Na2O	0.00	0.00	0.00	0.00	0.00	0.00	0.00	0.00	0.00	0.00	0.00	0.00	0.00	0.00	0.00	0.00	0.00	0.00
K2O	-0.01	-0.02	0.02	0.02	0.20	0.21	0.14	0.12	0.12	0.01	-0.03	0.17	0.14	0.06	0.09	-0.01	0.10	0.03
SiO2	38.16	37.62	37.45	37.51	38.00	37.88	37.80	37.79	37.27	37.93	37.24	37.85	37.64	37.83	37.79	37.91	36.33	35.49
TiO2	-0.24	0.00	0.03	0.10	0.06	0.05	0.03	0.06	-0.04	-0.02	0.04	0.10	0.09	0.08	0.09	0.08	0.05	-0.05
Al2O3	20.52	20.47	20.33	20.53	20.51	20.78	20.28	20.51	20.59	20.75	20.46	20.52	20.62	20.59	20.64	20.39	20.41	20.14
FeO	28.81	28.01	27.78	27.18	27.84	27.66	27.02	27.32	27.38	27.10	27.49	26.91	27.80	27.52	28.28	27.32	29.09	29.57
Fe2O3	4.12	5.50	6.49	6.50	5.54	5.07	6.48	6.08	6.58	6.05	6.86	6.61	5.32	5.97	4.79	6.24	6.11	6.63
MnO	3.92	3.35	2.77	3.02	3.00	3.56	2.92	3.00	2.80	3.19	2.61	2.55	3.35	3.04	3.53	2.91	3.01	3.17
MgO	4.73	5.06	5.13	5.13	4.85	4.79	5.34	5.13	5.30	4.98	5.33	5.29	5.04	4.91	4.80	5.15	4.89	5.01
CaO	0.00	0.00	0.00	0.00	0.00	0.00	0.00	0.00	0.00	0.00	0.00	0.00	0.00	0.00	0.00	0.00	0.00	0.00
Na	0.00	0.00	0.00	0.00	0.00	0.00	0.00	0.00	0.00	0.00	0.00	0.00	0.00	0.00	0.00	0.00	0.00	0.00
K	0.00	0.00	0.00	0.00	0.04	0.04	0.03	0.02	0.02	0.00	-0.01	0.03	0.03	0.01	0.02	0.00	0.02	0.01
Si	6.08	6.02	6.02	6.01	6.08	6.04	6.06	6.05	5.99	6.05	5.99	6.06	6.02	6.05	6.03	6.07	5.89	5.80
Ti	-0.03	0.00	0.00	0.01	0.01	0.01	0.00	0.01	0.00	0.00	0.00	0.01	0.01	0.01	0.01	0.01	0.01	-0.01
Al	3.85	3.86	3.85	3.86	3.86	3.90	3.83	3.87	3.90	3.90	3.88	3.87	3.89	3.88	3.88	3.85	3.90	3.88
Fe2+	3.84	3.75	3.74	3.64	3.72	3.69	3.62	3.66	3.68	3.62	3.70	3.61	3.72	3.68	3.77	3.66	3.94	4.04
Fe3+	0.08	0.13	0.15	0.11	0.02	0.08	0.11	0.07	0.22	0.00	0.17	0.01	0.13	0.02	0.08	0.00	0.50	0.81
Mn	0.56	0.75	0.88	0.88	0.75	0.68	0.88	0.82	0.90	0.82	0.94	0.90	0.72	0.81	0.65	0.85	0.84	0.92
Mg	0.93	0.80	0.66	0.72	0.72	0.85	0.70	0.72	0.67	0.76	0.63	0.61	0.80	0.72	0.84	0.69	0.73	0.77
Ca	0.81	0.87	0.88	0.88	0.83	0.82	0.92	0.88	0.91	0.85	0.92	0.91	0.86	0.84	0.82	0.88	0.85	0.88
Cr	0.00	0.00	0.00	0.00	0.00	0.00	0.00	0.00	0.00	0.00	0.00	0.00	0.00	0.00	0.00	0.00	0.00	0.00
total	16.03	16.04	16.05	16.04	16.01	16.03	16.04	16.02	16.07	16.00	16.06	16.00	16.04	16.01	16.03	16.00	16.17	16.28
pyrope	15.18	12.97	10.77	11.78	11.88	14.02	11.41	11.78	10.89	12.56	10.13	10.12	13.09	11.97	13.81	11.42	11.44	11.69
almandine	62.59	60.84	60.57	59.45	61.85	61.09	59.21	60.18	59.75	59.83	59.86	59.89	60.94	60.78	62.05	60.14	62.01	61.15
spessartine	9.07	12.10	14.33	14.40	12.47	11.34	14.38	13.56	14.54	13.53	15.13	14.90	11.81	13.35	10.65	13.91	13.19	13.89
grossular	11.22	10.81	10.63	11.60	13.38	11.66	12.24	12.74	9.42	14.14	10.71	14.77	11.02	13.40	11.58	14.57	1.72	-4.86
andradite	1.94	3.27	3.70	2.77	0.42	1.90	2.76	1.73	5.40	-0.06	4.16	0.31	3.14	0.50	1.92	-0.04	11.64	18.14
uvarovite	0.00	0.00	0.00	0.00	0.00	0.00	0.00	0.00	0.00	0.00	0.00	0.00	0.00	0.00	0.00	0.00	0.00	0.00

APPENDIX C, 13. Whole rock geochemistry of quartz veins (Stellenbosch University).

		1	2	3	4	5
wt.%	SiO_2	96.88	94.65	96.42	87.17	95.34
	TiO_2	0.01	0.05	0.02	0.08	0.02
	Al_2O_3	0.59	1.51	0.97	5.16	0.77
	Fe_2O_3T	0.66	1.22	0.59	2.06	1.40
	MnO	0.01	0.01	0.01	0.03	0.01
	MgO	0.23	0.45	0.20	0.94	0.44
	CaO	0.28	0.14	0.02	0.13	0.01
	Na_2O	0.00	0.00	0.00	0.93	0.00
	K_2O	0.02	0.08	0.05	0.19	0.05
	P_2O_5	0.21	0.12	0.02	0.09	0.01
	H_2O-	0.09	0.14	0.09	0.19	0.22
	LOI	0.44	0.56	0.33	0.96	0.79
	TOTAL	99.40	98.90	98.75	97.90	99.10

APPENDIX C, 14. Oxygen Isotope analyses (Cape Town University).

	Sample	$\delta^{18}O$ (SMOW)
Vein set 1		
	A6	16.2
	Q2	15.5
	Q3	15.5
	Q5	15.2
	Q6	14.6
	Q7	15
	Q14	17.8
	C2	16.52
	B1	16.59
Vein set 2		
	A2	16
	Q8	15.14
	C8	16.01

APPENDIX C, 15. ICP-MS analyses for selected outcrop at Spitskop (Dr. C. Harris, Cape Town

		F 1	F 2	F 3	Q 1	Q 2	Q 3	Q 4	Q 5	H 1
ppm	As	49.0	67.3	50.7	21.2	64.1	57.6	37.7	23.1	21.4
	Sb	0.24	0.24	0.27	0.26	0.25	0.39	0.29	0.26	0.24
	Te	*n.d.*	*n.d.*	*n.d.*	*n.d.*	*n.d.*	*n.d.*	*n.d.*	*n.d.*	1.48
	Au	0.06	0.06	0.05	0.03	0.03	0.06	0.05	0.05	0.06

APPENDIX C, 16. Sulphur Isotope analyses from selected veins in the Spitskop area (Mr U. Horstmann, Council for Geoscience).

Sample	$\delta^{18}O$ (SMOW)
Vein set 1	
B	3.2
F	5.2
J	-4.3
K	2.8
L	2.7
M	6
N	2.4
Vein set 2	
C	7.9
D	4.4
E	8.3
G	9
H	2.2

APPENDIX C, 17. Results of microPIXE analysis.

Element (ppm)	PYR9_W120.5	PYR9_W120.6	PYR9_W120.7	PYR9_W120.8	PYR9_W120.9	PYR8_W120.10	PYR7_W120.11
Mn	1960.7	1927.8	816.2	0.0	3522.6	1627.8	1577.6
StD	151.2	163.9	399.3	0.0	297.1	136.9	127.1
MDL	46.6	53.9	147.7	89.8	150.1	37.3	35.7
Fe	170936.0	170758.0	278928.0	419993.0	365003.0	232436.0	202900.0
StD	9476.5	9451.8	15087.0	22800.0	20134.0	12707.0	10963.0
MDL	33.8	37.7	85.9	44.9	97.4	26.2	25.1
Ni	23.1	31.4	12.9	55.9	70.0	18.5	88.3
StD	6.8	6.2	11.3	19.1	22.4	7.7	5.2
MDL	9.9	10.9	29.4	21.0	36.1	8.2	7.8
Cu	34.9	40.5	80.0	0.0	67.3	10.4	154.9
StD	3.8	3.9	11.2	0.0	9.5	2.3	6.7
MDL	5.9	6.5	17.6	13.1	22.8	4.8	4.8
Zn	39.8	33.1	743.1	76400.0	33799.0	9.7	19.6
StD	1.9	2.0	21.3	2118.5	970.0	1.6	1.3
MDL	3.7	4.0	11.3	9.3	15.2	3.0	2.9
Ga	0.0	0.0	0.0	0.0	0.0	0.0	0.0
StD	0.0	0.0	0.0	0.0	0.0	0.0	0.0
MDL	0.0	0.0	0.0	0.0	0.0	0.0	0.0
As	552.0	552.5	2082.9	2577.7	3509.1	338.0	1103.4
StD	14.7	12.1	37.6	40.7	84.5	13.9	24.1
MDL	3.1	3.4	10.3	7.2	13.2	3.0	2.8
Se	3.3	4.1	6.2	6.8	11.4	4.8	6.2
StD	1.0	1.0	2.9	2.4	5.5	0.8	1.7
MDL	2.4	2.7	7.9	5.3	9.2	2.0	1.9
Sr	31.8	36.1	13.7	0.0	0.0	0.9	7.8
StD	1.6	3.1	2.9	0.0	0.0	2.0	0.7
MDL	2.2	2.5	6.2	3.7	6.3	1.8	1.6
Y	5.1	4.3	0.0	0.0	0.0	12.0	2.4
StD	1.2	1.0	0.0	0.0	0.0	1.0	1.0
MDL	2.2	2.5	6.4	7.8	9.3	1.8	1.7
Zr	10.4	9.2	0.9	0.0	0.0	4.9	24.9
StD	1.2	1.2	2.6	0.0	0.0	0.7	1.7
MDL	2.2	2.6	6.0	5.4	7.2	1.8	1.6
Nb	0.0	0.0	0.0	0.0	25.8	0.4	0.3
StD	0.0	0.0	0.0	0.0	3.3	0.8	0.7
MDL	0.0	0.0	0.0	0.0	6.9	1.8	1.7
Ag	0.0	2.9	0.0	6.8	9.5	2.5	2.9
StD	0.0	2.3	0.0	2.7	7.3	1.6	1.5
MDL	4.9	5.5	11.3	6.2	11.4	3.7	3.7
Cd	0.0	0.0	9.4	756.7	324.4	1.9	3.3
StD	0.0	0.0	9.5	17.4	18.4	2.0	1.8
MDL	0.0	0.0	13.2	8.1	15.8	5.2	4.5
Sn	100.0	117.0	360.1	13.3	894.1	10.5	20.0
StD	7.7	9.2	18.8	4.3	31.4	3.2	3.3
MDL	10.7	12.2	22.8	10.2	23.2	7.9	7.7
Sb	16.8	13.6	55.7	92.8	51.7	31.0	9.3
StD	7.6	6.2	13.5	9.4	17.4	4.3	3.9
MDL	13.3	15.2	28.2	15.7	29.5	9.8	9.6
Ba	0.0	0.0	0.0	0.0	0.0	0.0	0.0
StD	0.0	0.0	0.0	0.0	0.0	0.0	0.0
MDL	0.0	0.0	0.0	0.0	0.0	0.0	0.0
Au L	3.0	2.5	8.6	0.0	0.0	1.4	2.7
StD	2.5	4.3	11.5	0.0	0.0	2.3	3.5
MDL	6.8	7.4	29.1	1534.8	687.3	5.4	4.4
Pb L	50.6	42.0	169.6	278.4	449.8	116.7	117.5
StD	64.6	45.3	127.9	192.5	427.8	61.2	177.2
MDL	45.8	46.8	178.7	198.4	281.0	28.5	84.9

APPENDIX C, 17. Results of microPIXE analysis.

Element (ppm)	PR9B_W120.12	PR9B_W120.13	PR9B_W120.14	PR9C_W120.15	PR9C_W120.16	PR9C_W120.17	PR9C_W120.18
Mn	903.6	0.0	0.0	529.7	1121.8	0.0	0.0
StD	85.5	0.0	0.0	278.5	95.9	0.0	0.0
MDL	58.9	391.6	477.0	89.9	46.1	366.0	316.1
Fe	142232.0	371508.0	368705.0	237722.0	388593.0	360799.0	390189.0
StD	7890.2	20004.0	19840.0	12714.0	21737.0	19374.0	20965.0
MDL	32.3	180.5	211.2	50.8	26.0	163.2	172.2
Ni	83.5	488.4	296.8	140.6	389.9	642.0	949.0
StD	9.2	70.1	54.9	9.6	27.5	65.0	87.9
MDL	12.0	86.1	104.6	19.0	10.7	91.2	70.0
Cu	202.5	182.4	182.6	373.6	1106.4	194.3	153.8
StD	14.7	22.2	27.6	16.2	50.1	27.8	36.1
MDL	8.5	49.9	62.9	11.7	7.4	57.0	51.7
Zn	23.7	44.3	23.2	19.3	56.2	47.0	32.5
StD	8.0	44.5	46.3	3.7	14.2	49.1	43.2
MDL	6.2	38.4	57.3	7.1	4.3	43.5	38.2
Ga	0.0	0.0	0.0	0.0	0.0	0.0	0.0
StD	0.0	0.0	0.0	0.0	0.0	0.0	0.0
MDL	0.0	0.0	0.0	0.0	0.0	0.0	0.0
As	15124.0	456876.0	500978.0	7789.7	39554.0	482589.0	442570.0
StD	251.6	6162.8	6676.6	112.9	614.3	6623.6	6186.9
MDL	8.8	26.1	32.9	5.7	3.6	24.3	22.8
Se	41.3	0.0	0.0	0.0	0.0	0.0	0.0
StD	6.8	0.0	0.0	0.0	0.0	0.0	0.0
MDL	3.8	0.0	0.0	0.0	0.0	0.0	0.0
Sr	12.3	0.0	0.0	0.0	0.0	0.0	0.0
StD	5.8	0.0	0.0	0.0	0.0	0.0	0.0
MDL	2.7	0.0	0.0	3.8	0.0	0.0	0.0
Y	6.2	0.0	0.0	4.1	14.4	0.0	0.0
StD	6.8	0.0	0.0	2.0	2.7	0.0	0.0
MDL	3.7	0.0	0.0	3.8	2.0	0.0	0.0
Zr	6.6	0.0	0.0	32.6	3.5	0.0	0.0
StD	4.6	0.0	0.0	3.5	1.8	0.0	0.0
MDL	2.7	0.0	0.0	3.8	1.9	0.0	0.0
Nb	0.0	0.0	0.0	0.0	0.0	0.0	0.0
StD	0.0	0.0	0.0	0.0	0.0	0.0	0.0
MDL	3.1	0.0	0.0	0.0	0.0	0.0	0.0
Ag	0.0	0.0	0.0	0.0	0.0	0.0	0.0
StD	0.0	0.0	0.0	0.0	0.0	0.0	0.0
MDL	0.0	0.0	0.0	0.0	0.0	0.0	0.0
Cd	0.0	0.0	0.0	0.0	0.0	0.0	0.0
StD	0.0	0.0	0.0	0.0	0.0	0.0	0.0
MDL	0.0	0.0	0.0	0.0	0.0	0.0	0.0
Sn	0.0	0.0	0.0	0.0	13.2	0.0	0.0
StD	0.0	0.0	0.0	0.0	2.8	0.0	0.0
MDL	0.0	0.0	0.0	0.0	6.8	0.0	0.0
Sb	0.0	88.3	125.2	28.2	20.0	0.0	0.0
StD	0.0	25.0	35.6	8.9	3.9	0.0	0.0
MDL	0.0	51.6	72.6	15.0	8.3	0.0	0.0
Ba	0.0	0.0	0.0	0.0	0.0	0.0	0.0
StD	0.0	0.0	0.0	0.0	0.0	0.0	0.0
MDL	0.0	0.0	0.0	0.0	0.0	0.0	0.0
Au L	14.1	0.0	0.0	34.5	254.0	0.0	0.0
StD	11.1	0.0	0.0	18.7	98.2	0.0	0.0
MDL	9.2	72.7	91.8	10.9	7.8	67.9	58.0
Pb L	613.8	0.0	0.0	54.3	127.8	0.0	80.0
StD	3422.8	0.0	0.0	593.4	20728.0	0.0	107769.0
MDL	1114.5	0.0	0.0	589.9	2940.0	0.0	32670.0

APPENDIX C, 17. Results of microPIXE analysis.

Element (ppm)	PR9C_W120.19	PYR4_W120.20	PYR3_W120.21	PYR2_W120.22	PR2B_W120.23	PR2C_W120.24	PR2C_W120.25
Mn	0.0	2454.5	2394.1	2377.3	1798.4	2443.5	4250.9
SID	0.0	175.2	171.2	165.7	129.3	180.8	396.3
MDL	379.9	49.8	64.3	59.7	73.0	50.8	38.7
Fe	412059.0	248695.0	225947.0	234215.0	258345.0	196733.0	418588.0
SID	22367.0	13669.0	12427.0	12877.0	14204.0	10839.0	23889.0
MDL	200.0	28.9	34.5	33.2	36.7	30.7	39.3
Ni	1016.7	93.0	101.6	50.7	161.5	138.7	497.0
SID	84.9	5.2	9.9	3.8	13.6	10.3	29.0
MDL	81.4	6.9	8.8	8.5	10.7	7.3	9.4
Cu	204.6	31.2	33.7	19.7	25.2	17.5	90.1
SID	43.8	1.8	3.7	2.3	4.2	2.2	11.5
MDL	61.7	4.0	4.8	5.0	6.5	4.5	6.8
Zn	8685.6	26.6	36.0	30.4	33.0	22.6	109.9
SID	318.9	1.8	2.0	2.4	3.0	1.4	7.6
MDL	45.2	2.4	3.1	3.1	3.9	2.6	3.3
Ga	0.0	0.0	0.0	5.0	0.0	2.2	0.6
SID	0.0	0.0	0.0	1.6	0.0	0.9	2.3
MDL	0.0	0.0	0.0	2.8	3.0	2.4	2.9
As	410718.0	417.9	405.0	157.0	373.4	950.0	1508.7
SID	5756.1	16.6	14.2	8.6	15.4	24.5	54.0
MDL	27.6	2.4	2.8	3.0	4.2	3.0	8.5
Se	0.0	9.5	4.5	8.1	10.4	10.6	13.9
SID	0.0	1.0	0.8	0.9	2.0	1.3	1.1
MDL	0.0	1.6	2.0	2.0	2.5	1.7	2.3
Sr	0.0	2.9	0.9	0.0	0.0	0.0	0.0
SID	0.0	2.4	1.4	0.0	0.0	0.0	0.0
MDL	0.0	1.5	1.8	1.9	2.2	1.5	0.0
Y	0.0	13.5	2.5	11.3	5.3	13.4	0.0
SID	0.0	0.7	0.9	0.9	1.4	1.1	0.0
MDL	0.0	1.5	1.8	1.9	2.4	1.7	0.0
Zr	0.0	32.4	4.1	148.3	57.6	47.7	124.1
SID	0.0	2.4	0.7	8.3	3.6	1.9	3.5
MDL	0.0	1.4	1.7	1.8	2.2	1.6	1.5
Nb	0.0	0.0	1.0	5.4	2.1	13.9	0.0
SID	0.0	0.0	0.7	0.8	0.9	0.9	0.0
MDL	0.0	1.5	1.8	2.0	2.3	1.7	0.0
Ag	0.0	2.0	2.1	0.2	6.9	6.2	9.9
SID	0.0	1.2	1.6	1.4	1.8	1.4	1.7
MDL	0.0	2.9	4.0	3.5	4.2	3.4	3.2
Cd	0.0	1.8	1.4	2.8	0.0	3.6	0.0
SID	0.0	1.6	2.1	1.9	0.0	1.9	0.0
MDL	0.0	4.0	5.5	4.9	5.9	4.8	0.0
Sn	0.0	8.3	16.9	27.9	8.8	19.8	30.5
SID	0.0	2.5	3.9	4.5	3.7	3.1	3.1
MDL	0.0	6.2	8.4	7.6	9.0	7.4	6.8
Sb	0.0	24.3	22.7	37.8	67.4	40.4	39.6
SID	0.0	3.3	5.1	6.7	7.0	4.9	3.6
MDL	0.0	7.7	10.3	9.5	11.0	9.2	8.4
Ba	0.0	105.1	58.3	90.3	34.1	105.6	126.9
SID	0.0	14.1	17.2	12.6	17.2	12.2	15.4
MDL	0.0	22.5	29.7	27.6	31.1	26.8	24.2
Au L	12.0	1.3	0.9	0.0	0.0	5.1	128.4
SID	745.3	1.6	2.1	0.0	0.0	3.2	12.9
MDL	206.3	4.3	5.7	5.6	7.0	4.7	6.2
Pb L	25.6	106.0	79.2	117.3	192.0	155.9	786.4
SID	84645.0	100.5	67.7	27.3	60.2	190.7	478.6
MDL	30356.0	33.0	33.4	15.9	32.7	72.9	114.1

APPENDIX C, 17. Results of microPIXE analysis.

Element (ppm)	PR2C_W120.25	PR2C_W120.27	PR2C_W120.24	PR2C_W120.28	PR2C_W120.29	PR2C_W120.30
Mn	1458.3	2963.6	2279.2	3512.6	2611.2	2354.4
StD	402.7	211.3	191.0	313.7	212.3	175.6
MDL	238.0	16.1	33.8	226.0	116.3	26.9
Fe	562927.0	197245.0	196732.0	387038.0	197183.0	201616.0
StD	31584.0	10645.0	10836.0	21398.0	10580.0	11025.0
MDL	128.2	23.4	27.7	162.5	81.1	24.1
Ni	458.8	96.2	138.6	222.5	66.1	147.2
StD	40.9	6.0	10.3	40.9	10.4	6.5
MDL	56.0	3.4	7.3	63.7	24.8	5.7
Cu	71.3	19.7	17.5	35.4	18.9	16.2
StD	13.6	1.7	2.2	20.8	10.1	2.2
MDL	34.3	1.8	4.5	35.8	13.1	3.1
Zn	113.9	26.1	22.6	28.3	20.1	26.0
StD	10.3	1.0	1.4	9.2	6.4	1.5
MDL	19.9	1.2	2.6	22.4	8.7	2.1
Ga	0.0	1.5	2.2	0.5	0.0	2.2
StD	0.0	0.5	0.9	9.1	0.0	0.6
MDL	17.6	0.9	2.4	16.5	6.7	1.6
As	1798.2	636.3	949.8	1133.0	613.0	964.2
StD	56.0	21.2	24.5	39.0	14.6	22.8
MDL	22.6	2.1	3.0	20.0	7.6	2.5
Se	10.0	8.5	10.6	10.6	8.9	10.7
StD	6.0	0.4	1.2	7.0	2.7	1.0
MDL	16.0	0.9	1.7	18.6	5.9	1.4
Sr	0.0	0.0	0.0	0.0	0.0	0.0
StD	0.0	0.0	0.0	0.0	0.0	0.0
MDL	0.0	0.0	0.0	0.0	0.0	0.0
Y	0.0	0.0	13.4	10.2	3.1	12.7
StD	0.0	0.0	1.1	4.3	3.1	0.8
MDL	0.0	0.0	1.7	9.7	5.4	1.4
Zr	89.9	7.8	47.3	7.6	4.7	48.7
StD	5.6	0.5	1.8	3.4	2.1	2.2
MDL	8.8	0.7	1.6	8.0	5.2	1.2
Nb	0.0	0.0	13.9	0.0	0.0	13.9
StD	0.0	0.0	0.9	0.0	0.0	0.9
MDL	0.0	0.0	1.7	8.8	5.5	1.4
Ag	24.7	5.6	6.3	21.3	16.8	6.3
StD	9.1	0.7	1.4	6.9	5.1	2.0
MDL	14.4	1.6	3.4	12.2	11.1	2.9
Cd	0.0	0.0	3.6	5.4	7.2	2.6
StD	0.0	0.0	1.9	9.7	7.9	1.5
MDL	0.0	0.0	4.8	15.8	13.3	4.0
Sn	15.1	8.5	19.8	39.5	12.1	23.3
StD	13.0	1.7	3.1	17.1	10.4	2.7
MDL	30.9	3.5	7.4	28.0	25.2	6.1
Sb	77.7	25.5	40.4	26.2	27.6	40.6
StD	17.9	3.4	4.9	16.0	13.5	5.5
MDL	37.0	4.3	9.2	34.5	32.1	7.6
Ba	246.6	64.5	105.6	52.7	168.1	119.1
StD	53.7	5.5	12.2	44.5	43.0	12.5
MDL	100.5	12.7	26.8	92.6	74.5	22.3
Au L	774.0	55.5	5.2	836.7	7.6	5.3
StD	57.5	1.9	3.3	60.3	5.4	2.5
MDL	35.2	2.0	4.7	33.3	13.7	3.7
Pb L	928.8	178.1	156.4	327.9	136.7	158.0
StD	175.5	203.0	191.0	102.9	37.6	190.5
MDL	175.1	48.0	72.9	142.5	67.1	73.1

APPENDIX C, 18. Fluid Inclusion analyses from Type 1a quartz veins, Spitskop gold prospect..

Vein type	Inclusion type	Room Temperature (20oC)	Size	Fill	Tl(H2O)	Tl(CO2)	Te	Tm(H2O)	Tm(CO2)	Th(H2O)	Th(CO2)
1a	1	L+V	6.7	0.95	-35.6	-	-	-3.2	-	140	-
1a	1	L+V	2.83	0.9	-38.3	-	-	-3.3	-	140	-
1a	1	L+V	4.73	0.95	-34.8	-	-	-2.9	-	190	-
1a	1	L+V	5.12	0.95	-37.6	-	-	-2.2	-	190	-
1a	1	L+V	5.89	0.9	-39.2	-	-	-4.8	-	145	-
1a	1	L+V	7.58	0.9	-35.6	-	-	-1.9	-	140	-
1a	1	L+V	6.35	0.95	-37.2	-	-	-3.7	-	145	-
1a	1	L+V	4.3	0.95	-37.5	-	-	-3.1	-	140	-
1a	1	L+V	4.27	0.85	-41.2	-	-	-2.8	-	210	-
1a	1	L+V	3.01	0.9	-37	-	-	-3.3	-	210	-
1a	1	L+V	4.35	0.9	-36.9	-	-	-3.2	-	160	-
1a	1	L+V	5.34	0.9	-35	-	-	-4.1	-	160	-
1a	1	L+V	4.35	0.9	-37.4	-	-	-4	-	160	-
1a	1	L+V	6.71	0.9	-33.5	-	-	-2.8	-	160	-
1a	1	L+V	7.73	0.95	-33.7	-	-	-3.3	-	160	-
1a	1	L+V	9.11	0.95	-28.6	-	-	-0.6	-	180	-
1a	1	L+V	5.55	0.95	-33.2	-	-	-2.9	-	190	-
1a	1	L+V	3.84	0.95	-32.5	-	-	-0.5	-	190	-
1a	1	L+V	4.78	0.95	-28.3	-	-	-4.5	-	190	-
1a	1	L+V	5.22	0.95	-37.4	-	-	-2.2	-	240	-
1a	1	L+V	10.51	0.9	-37.5	-	-	-4.5	-	230	-
1a	1	L+V	9.92	0.95	-39.7	-	-	-4.7	-	235	-
1a	1	L+V	4.45	0.95	-22.5	-	-	-1	-	240	-
1a	1	L+V	2.43	0.75	-38.4	-	-	-2.5	-	240	-
1a	1	L+V	12.27	0.95	-31.9	-	-	-0.7	-	240	-
1a	1	L+V	4.73	0.95	-31.4	-	-	-0.9	-	180	-
1a	1	L+V	2.91	0.95	-32.8	-	-	-0.8	-	180	-
1a	1	L+V	4.87	0.95	-33.2	-	-	-3.1	-	180	-
1a	1	L+V	4.78	0.95	-33.1	-	-	-1.6	-	175	-
1a	1	L+V	3.19	0.9	-32.8	-	-	-3.2	-	215	-
1a	1	L+V	11.55	0.95	-33.7	-	-	-2.2	-	215	-
1a	1	L+V	5.59	0.95	-31.9	-	-	-0.4	-	218	-
1a	1	L+V	4.98	0.95	?	-	-	-2.2	-	270	-
1a	1	L+V	5.18	0.9	?	-	-	-1.9	-	268	-
1a	1	L+V	5.67	0.9	?	-	-	-1.8	-	280	-
1a	1	L+V	10.79	0.85	?	-	-	-3.3	-	284	-
1a	1	L+V	10.69	0.85	?	-	-	-3.1	-	291	-
1a	1	L+V	4.01	0.95	?	-	-	-0.1	-	275	-
1a	1	L+V	6.6	0.95	?	-	-	-1.1	-	274	-
1a	1	L+V	3.17	0.95	?	-	-	-0.8	-	260	-
1a	1	L+V	3.45	0.95	-35.5	-	-	-4.7	-	250	-
1a	1	L+V	3.01	0.95	-34.9	-	-	L	-	-	-
1a	1	L+V	12.84	0.95	-31.1	-	-	-0.7	-	200	-
1a	1	L+V	4.61	0.95	-32.7	-	-	-2.4	-	210	-
1a	1	L+V	3.37	0.95	-32.1	-	-	-2.9	-	210	-
1a	1	L+V	5.14	0.95	-32.9	-	-	-2.4	-	215	-
1a	1	L+V	4.1	0.95	-33.4	-	-	-2.7	-	160	-
1a	1	L+V	5.12	0.95	-33.7	-	-	-2.5	-	150	-
1a	1	L+V	2.3	0.95	-33.1	-	-	-2.6	-	140	-
1a	1	L+V	4.09	0.95	-34	-	-	-2.9	-	170	-
1a	1	L+V	4.36	0.95	-39.9	-	-	0	-	284	-
1a	1	L+V	2.43	0.95	-35.1	-	-	-2.7	-	316	-

APPENDIX C, 18. Fluid Inclusion analyses from Type 1a quartz veins, Spitskop gold prospect..

Vein type	Inclusion type	Room Temperature (20oC)	Size	Fill	Tf(H2O)	Tf(CO2)	Te	Tm(H2O)	Tm(CO2)	Th(H2O)	Th(CO2)
1a	1	L+V	8.45	0.9	-34.4	-	-	-2.6	-	177	-
1a	1	L+V	5.35	0.95	?	-	-	-2.7	-	260	-
1a	1	L+V	14.86	0.95	-36.3	-	-	-5.1	-	140	-
1a	1	L+V	4.5	0.95	?	-	-	-4.8	-	283	-
1b	1	L+V	18.35	0.95	-38.4	-	-11	-0.9	-	160	-
1b	1	L+V	4.49	0.95	-38.9	-	-	-3	-	178	-
1b	1	L+V	8.91	0.95	-35.7	-	-13	-2.5	-	180	-
1b	1	L+V	4.01	0.95	-34.4	-	-	-2.7	-	195	-
1b	1	L+V		0.95	-	-	-	-2.9	-	196	-
1b	1	L+V	3.5	0.95	-	-	-	-2.7	-	182	-
1b	1	L+V	3.48	0.95	-	-	-	-1.1	-	145	-
1b	1	L+V	4.1	0.95	-39	-	-	-3.3	-	154	-
1b	1	L+V	8.2	0.95	-	-	-	-2.9	-	153	-
1b	1	L+V	11.54	0.95	-38.2	-	-	-4	-	178	-
1b	1	L+V	4.01	0.95	-	-	-	-3.2	-	144	-
1b	1	L+V	7.36	0.95	-38	-	-	-4	-	166	-
1b	1	L+V	6.35	0.95	-36	-	-	-4	-	241	-
1a	2	L+V	8.94	0.8	-39.9	-99	-	-56.8	7.7	300	7.7
1b	1	L+V	11.08	0.95	-40.1	-	-	-2.2	-	166	-
1b	1	L+V	12.01	0.95	-35.5	-	-	-2.2	-	185	-
1a	2	L+V	8.36	0.8	-31.2	-99.3	-	-57.3	7.4	287	16.2
1a	2	L+V	7.1	0.8	-34	-101	-	-57.7	7.9	294	15.1
1a	2	L+V	6.2	0.8	-35	-99.8	-	-57.4	5.5	263	15.3
1b	1	L+V	6.17	0.95	-38	-	-	1.2	-	210	-
1b	1	L+V	5.2	0.95	-	-	-	-4	-	221	-
1b	1	L+V	4.63	0.95	-	-	-	-4	-	208	-
1b	1	L+V	6.54	0.95	-	-	-	-4	-	201	-
1b	1	L+V	11.03	0.95	-36.1	-	-	-2.5	-	206	-
1b	1	L+V	9.4	0.95	-39.2	-	-	-3.1	-	237	-
1b	1	L+V	3.78	0.95	-39.3	-	-5	-2.5	-	229	-
1b	1	L+V	4.42	0.9	-38.1	-	-	-2.9	-	215	-
1b	1	L+V	4.42	0.95	-36.5	-	-	-3.4	-	233	-
1b	1	L+V	14.41	0.85	?	-	-6	-3.6	-	268	-
1b	1	L+V	11.87	0.95	?	-	-	-3.4	-	275	-
1b	2	L+V	14.69	0.9	-31.4	-100	-	-3.7	11	245	21.3
1b	2	L+V	6.98	0.65	-28.9	-101.5	-	-55	9	292	19.1
1b	2	L+V	18.64	0.9	-	-99.4	-	-57.5	8.7	260	18.2
1a	3	L	11.43	0.8	-	-99.5	-	-57.1	-	-	15
1a	3	L	7.95	0.7	-	-99.7	-	-57.1	-	-	15
1b	3	L	9.32	0.75	-	-99.7	-	-57.3	-	-	10.9
1b	3	L	6.45	0.8	-	-99.9	-	-57.1	-	-	18.8
1b	3	L	3.5	0.9	-	-99.9	-	-58.2	-	-	7.1
1b	3	L	5.04	0.85	-	-99.7	-	-57	-	-	6
1b	3	L	4.73	0.85	-	-99.7	-	-57	-	-	9.6
1b	3	L	5.67	0.85	-	-100.2	-	-57	-	-	15.8
1b	2	L+V	5.53	0.85	-33.9	-96.8	-	-56.9	6	297	22.7
1b	3	L	3.8	0.9	-	-99.9	-	-58.2	-	-	7.5
1b	3	L	4.73	0.85	-	-99.7	-	-57	-	-	7.8
1b	3	L	5.04	0.85	-	-99.7	-	-57.1	-	-	8
1b	3	L	6.32	0.85	-	-99.4	-	-57	-	-	15.8
1b	3	L	7.45	0.8	-	-99.9	-	-57.1	-	-	14.9
1a	3	L	7.95	0.85	-	-99.8	-	-57.5	-	-	15.6

APPENDIX C, 18. Fluid Inclusion analyses from Type 1a quartz veins, Spitskop gold prospect..

Vein type	Inclusion type	Room Temperature (20oC)	Size	Fill	Tf(H2O)	Tf(CO2)	Te	Tm(H2O)	Tm(CO2)	Th(H2O)	Th(CO2)
1b	3	L	9.33	0.75	-	-99.9	-	-57.3	-	-	12.2
1a	3	L	9.65	0.8	-	-100.5	-	-57.1	-	-	16
1a	3	L	4.25	0.95	-	-99.8	-	-57.5	-	-	15.6
1a	3	L	4.68	0.95	-	-99.9	-	-57.3	-	-	12.7
1a	3	L	5.02	0.8	-	-100.5	-	-57.1	-	-	15.8
1a	3	L	5.8	0.95	-	-99.7	-	-57.1	-	-	7.6
1a	3	L	6.3	0.95	-	-99.7	-	-57	-	-	7.5
1a	3	L	6.74	0.85	-	-99.4	-	-57	-	-	15.6
1a	3	L	8.74	0.8	-	-99.9	-	-57.1	-	-	15.3
1a	2	L+V	14.69	0.9	-31.4	-99.9	-	-57.5	11	245	21.3
1a	2	L+V	6.98	0.65	-28.9	-101.3	-	-57.3	9.4	292	19.1
1a	2	L+V	18.64	0.9	-	-99.2	-	-57.1	8.2	260	18.2
1a	2	L+V	14.69	0.9	-31.4	-99.8	-	-57.5	10	244	21.3
1a	2	L+V	6.98	0.65	-28.9	-97.9	-	-57.3	9.6	292	15.6
1a	2	L+V	18.64	0.9	-	-98.8	-	-57.1	8.3	266	12.2
1b	2	L+V	14.69	0.9	-31.4	-99.4	-	-57.1	11.2	243	16
1b	2	L+V	6.98	0.65	-28.9	-100.5	-	-57	8.8	292	15.6
1b	2	L+V	18.64	0.9	-	-99.8	-	-57	7.9	260	12.7
1b	2	L+V	14.69	0.9	-31.4	-100.3	-	-57.1	8.6	256	15.8
1b	2	L+V	6.98	0.65	-28.9	-101.5	-	-55	7.6	284	7.6
1b	2	L+V	18.64	0.9	-	-99.4	-	-57.5	8.7	287	7.5
1b	2	L+V	14.69	0.9	-31.4	-100	-	-3.7	9.6	290	15.6
1b	2	L+V	6.98	0.65	-28.9	-99.8	-	-55	8.7	269	15.3
1b	2	L+V	18.64	0.9	-	-99.4	-	-57.5	7.9	277	18.2

APPENDIX D

APPENDIX D, Figure 1. Piketberg Formation, near Dezenhoek Farm, north of Piketberg. A series of matrix-supported quartzitic grits (varying grain size) interbedded with shale units. Grits are in generally angular to sub-rounded, with clasts orientated NW-SE within the regional foliation. For location see Appendix A, Map 1. Section line orientated NE-SW.

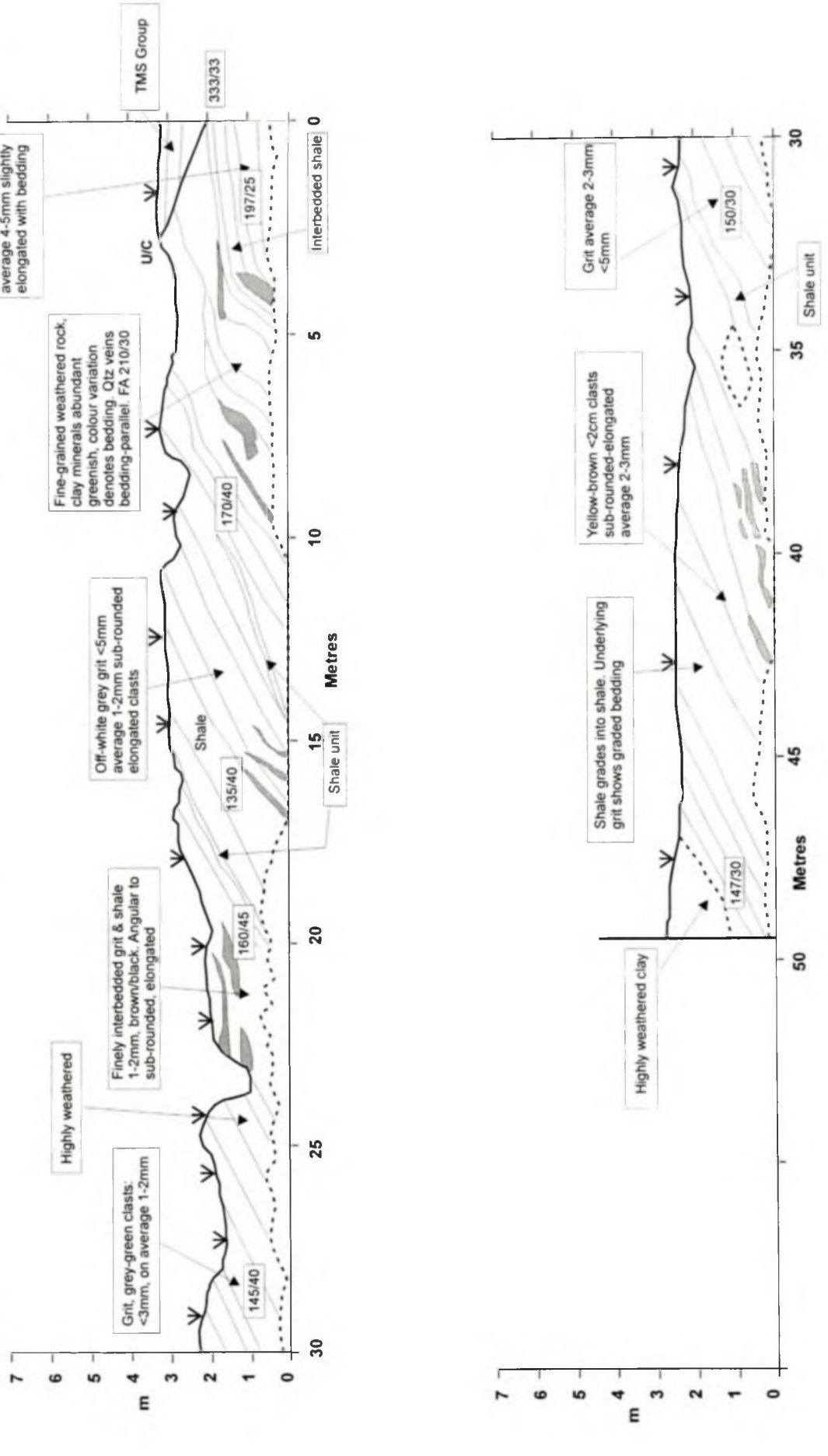

APPENDIX D, Figure 2. Cross section of the Piketberg Formation. Road cutting on the N7 national road, approximately 3 km north of the town Piketberg. For location see locality map in Appendix A, Figure 1. Section orientated N-S.

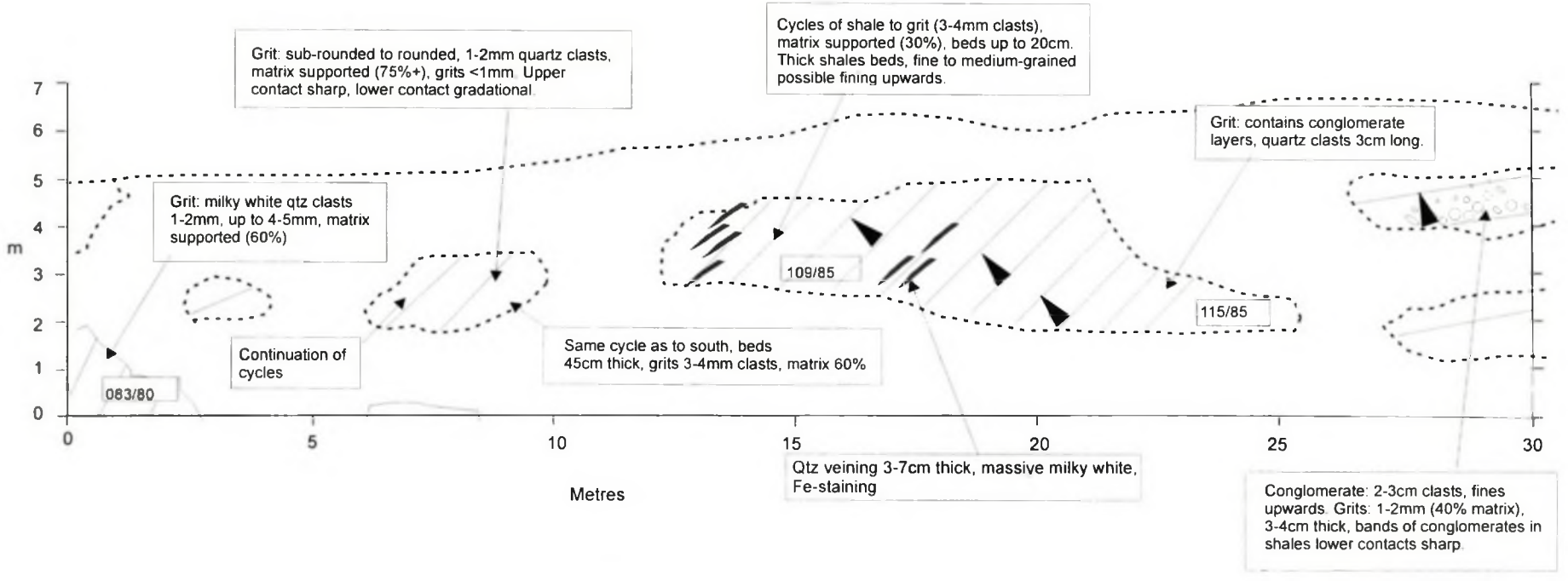

APPENDIX D, Figure 2. continued.

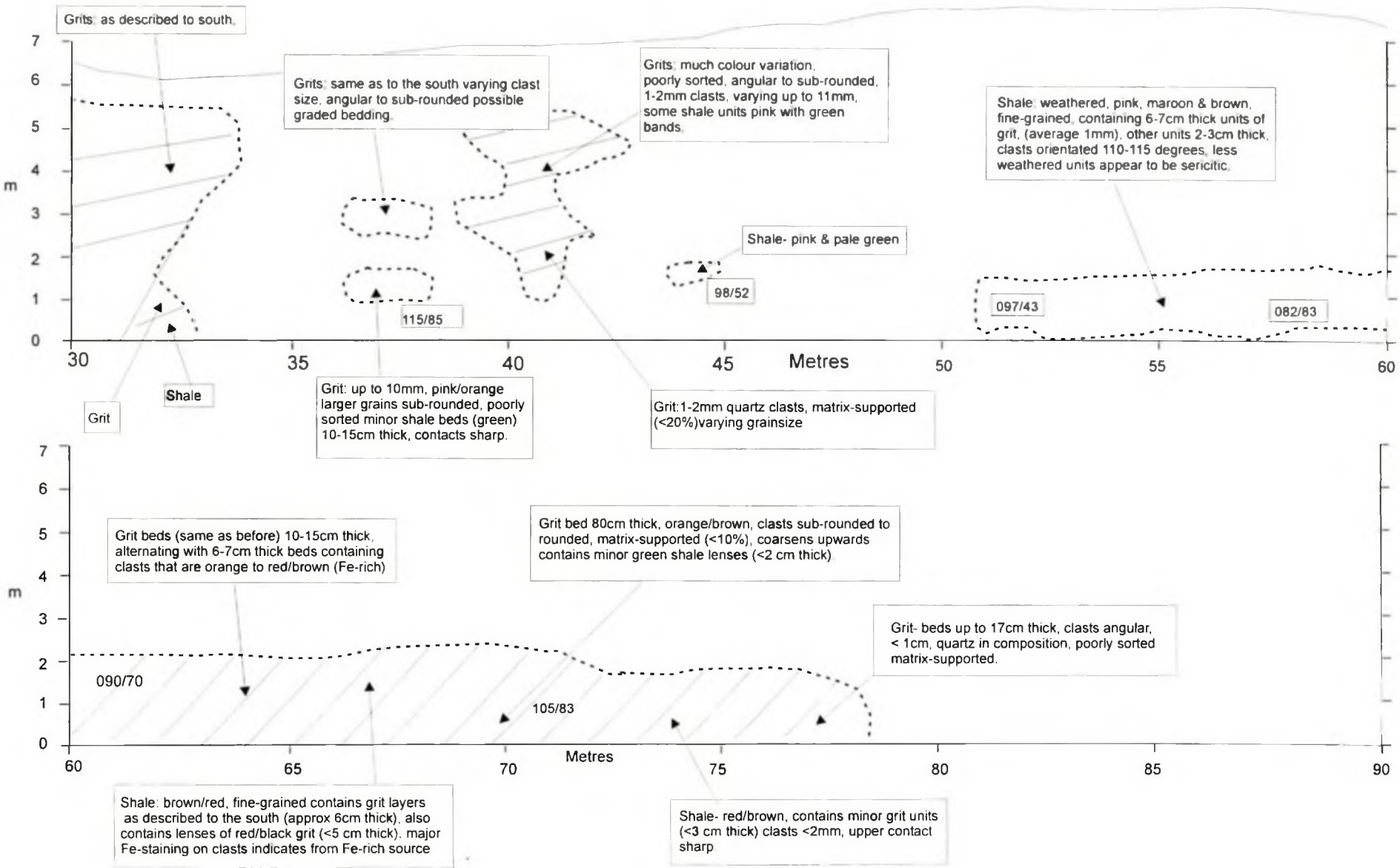

APPENDIX D, Figure 2. continued.

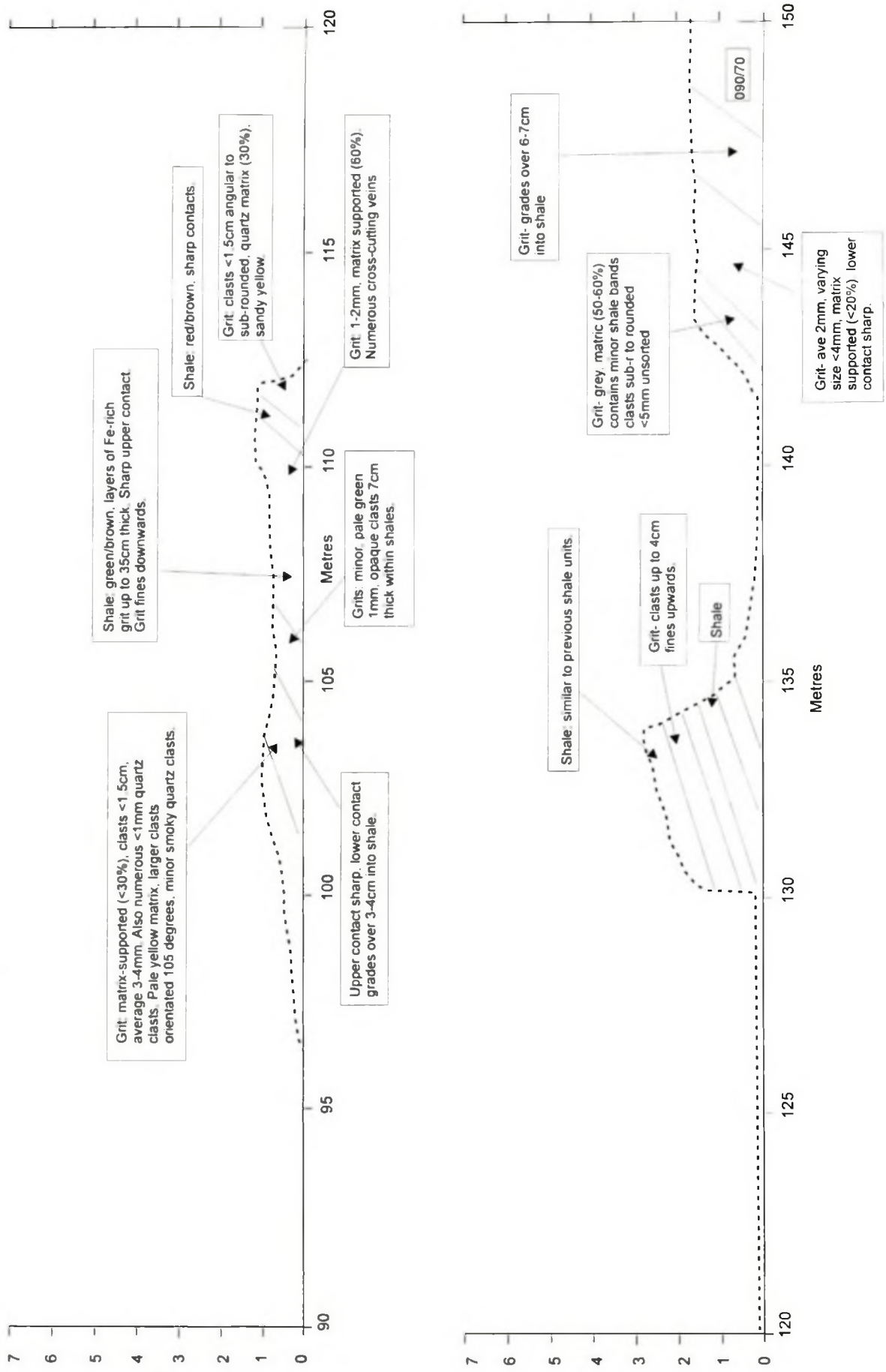

APPENDIX D, Figure 2. continued.

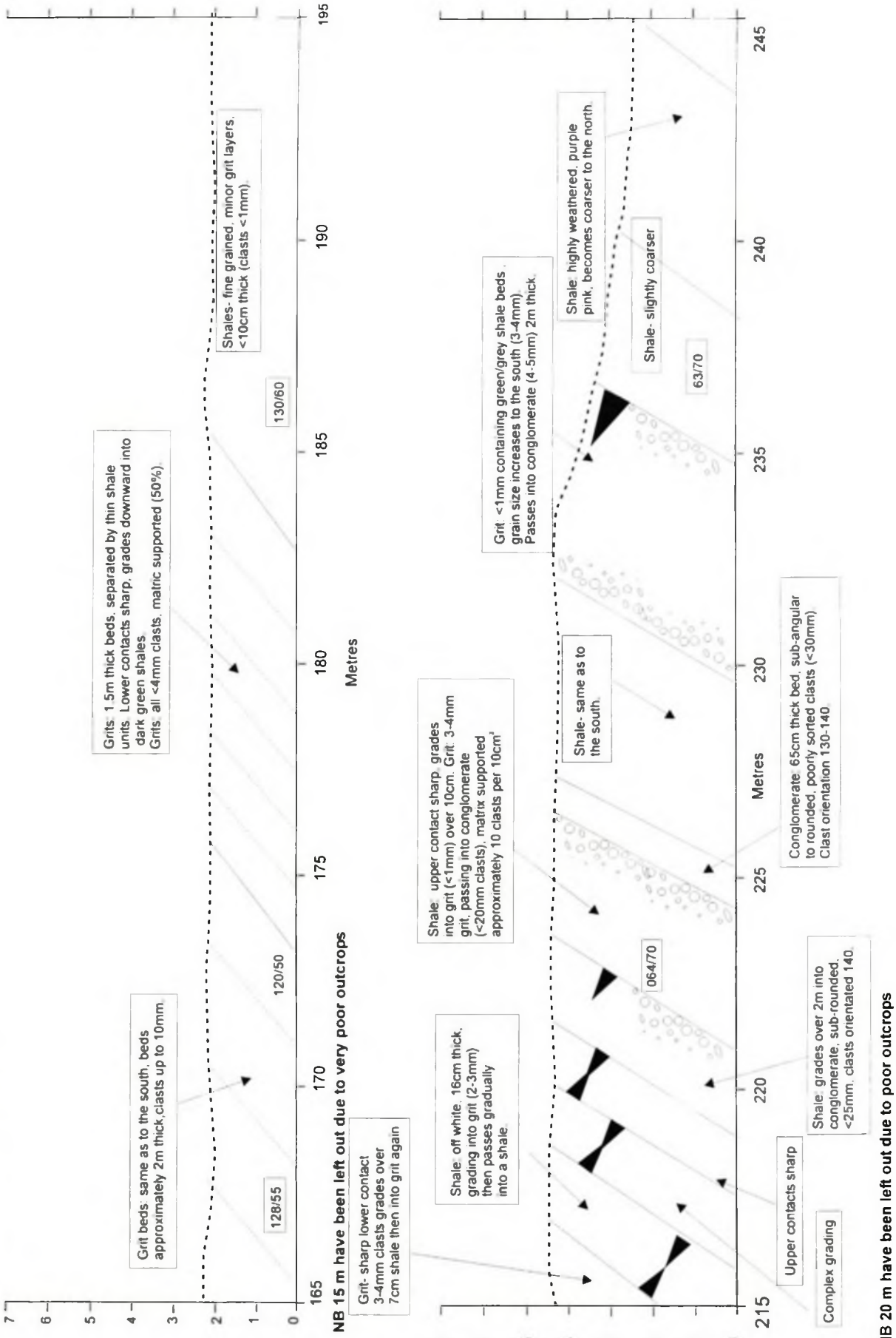

APPENDIX D, Figure 2. continued.

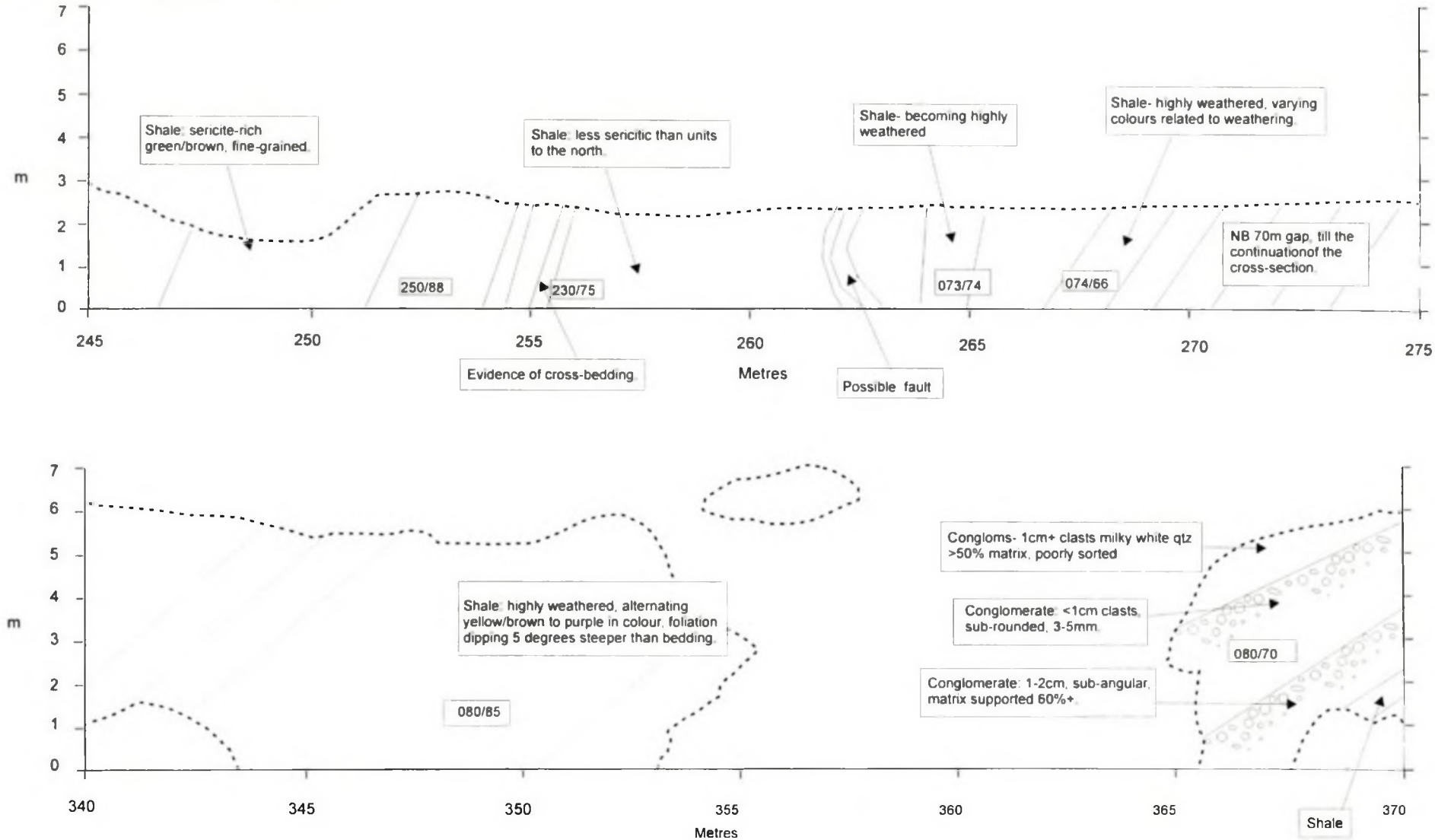

NB 65 m have been left out due to very poor outcrops

APPENDIX D, Figure 2. continued.

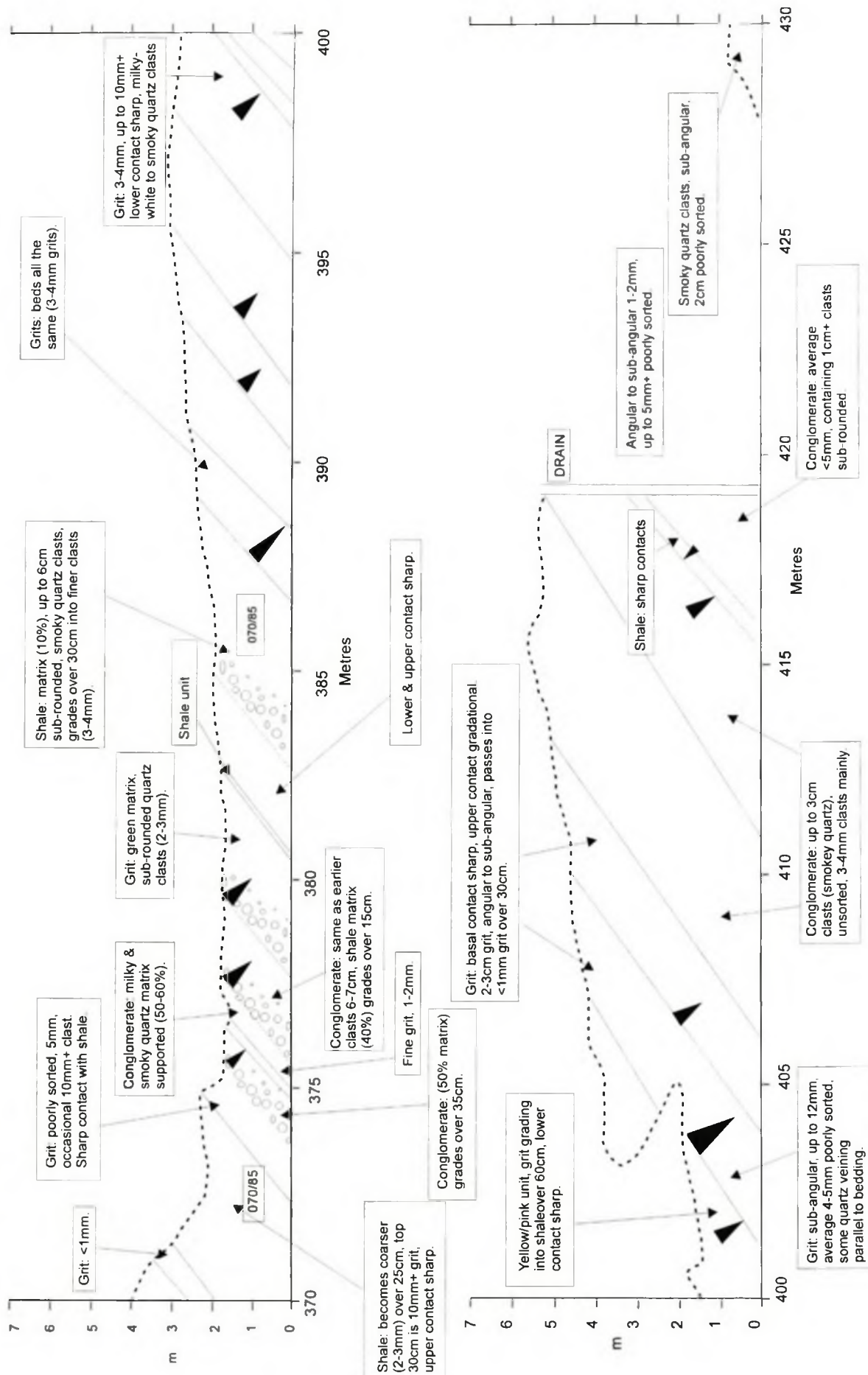

APPENDIX D, Figure 2. continued.

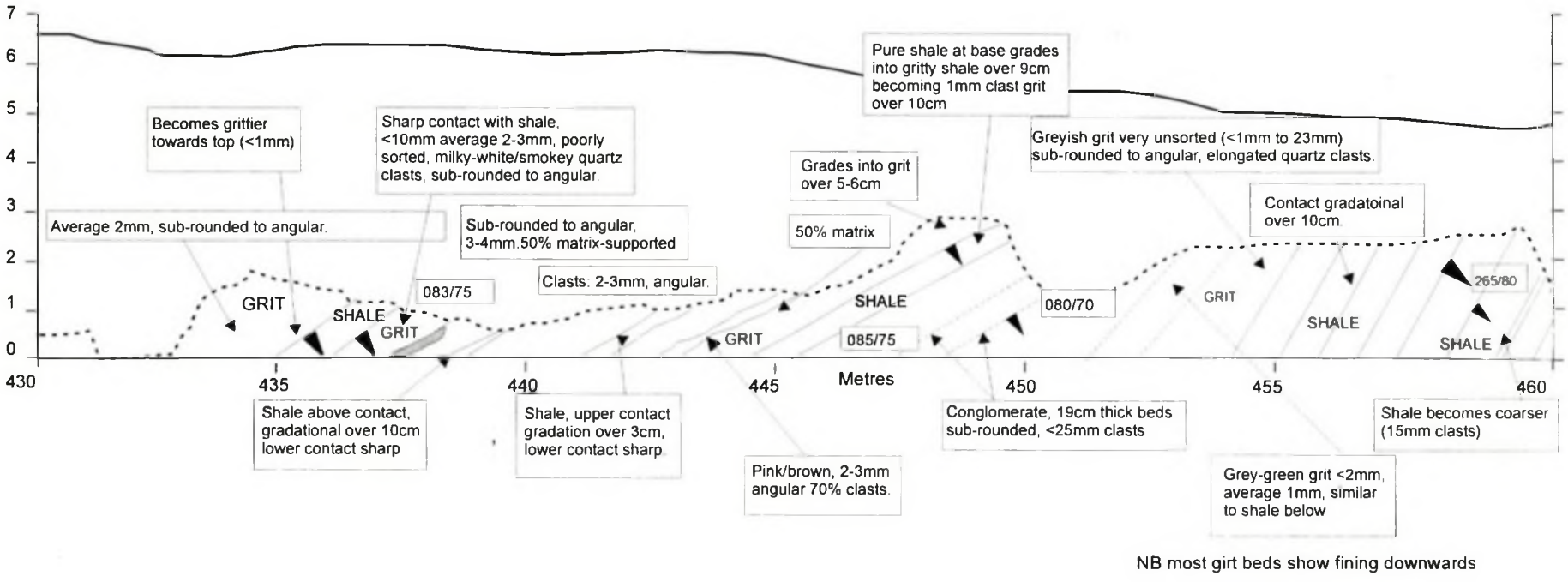

NB most girt beds show fining downwards